UNIVERSITY OF PARDUBICE
FACULTY OF CHEMICAL TECHNOLOGY

DOCTORAL THESIS

2024 Veerabhadragouda B. PATIL, M.Sc.

University of Pardubice

Faculty of Chemical Technology

Institute of Energetic Materials

Achieving balanced cocrystals of energetic materials *via* coagglomeration and their applications

Veerabhadragouda B. PATIL, M.Sc.

DOCTORAL THESIS

2024

Declaration

I declare that all the data presented in this Ph.D. thesis entitled "*Achieving balanced cocrystals of energetic materials via coagglomeration*" is from my own work. Most of the presented results have been published in several international journals and conferences, in whole or in part being co-authored with my supervisor, Prof. Dr. Svatopluk Zeman, DrSc., and some other colleagues, who have been mentioned in the acknowledgement of this thesis. The fundamental theories, statements, and referred data from the literature for this thesis are properly cited and completely listed at the end of each chapter.

I declare that my thesis is to comply with the rights and obligations arising from Act No. 121/2000 coll. Copyright Act. In particular, the University of Pardubice (UPCE) has the right to issue the license agreement for use of this document as the university's property under the law of § 60 paragraph 1 for the Copyright Act. In addition, if the use of this work would be provided to me or license for use of any another entity, the UPCE is entitled to require appropriate contributions from me towards the cost of the creation and publication of this thesis, according to the circumstances, until their actual amount has been covered.

I acknowledge that in accordance with § 47b of Act No. 111/1998 Coll., on universities and on the amendment and addition of other laws (the Act on Universities), as amended, and the directive of the University of Pardubice No. 7/2019 Rules for submission, publication, and formal editing of final thesis, as amended, the work will be published through the Digital Library of the UPCE.

Date:

Place: Pardubice (M.Sc. Veerabhadragouda B. PATIL)

Acknowledgements

*Ahoj, já jsem Veera…***!** *I am grateful to the Faculty of Chemical Technology, University of Pardubice, for giving me the opportunity to complete my PhD studies with an academic fellowship. I am happy to present acknowledgments to my PhD Supervisor and our Prof. Svatopluk Zeman, who clocked eighty-one years on Nov 4, 2023, continues to be serving the professor with great enthusiasm and vision. There are very few parallels in the world for his enormous contributions to Academia, Research, Innovation, Energetic Materials, Engineering, and Technology. It's remarkable that one person possesses all these qualities. How was it accomplished by him? His effervescent smile hasn't faded at all, and he continues to motivate everyone who spends time with him. He is an incredibly rare combination of leadership skills and academic brilliance with historic milestones, having set numerous records wherever he worked and in whatever role. From all walks of life, he has amassed a large network of friends and admirers.*

During PhD studies, I received good support from my professor with chronological planning, also during the COVID pandemic and the continuous uncertainty of lockdowns. His support was invaluable. I still remember the day I showed schemes of preparation for Coagglomerated crystals of attractive nitramines. He agreed immediately, given the green signal to carry on the work. It made me do faster and get more research outputs. Professor's tremendous Chemical Technological prospects and real-time industrial experience knowledge with my Basic Science and Materials Chemistry made our work acceptable in reputable journals. Also, the UEnM institute's, as well as the Chemical Technology Faculty's well-conditioned instrumental facility and availability of materials enough quantity/on time, helped us achieve successful technological prospective research outputs.

I am very thankful to all professors and colleagues who taught me to Ph.D. coursework exams successfully. So, once again, I am thankful to Prof. S. Zeman here for teaching Technology of Explosives. Prof. Jiří Málek and Dr. Roman Svoboda thermal analysis and calorimetry teachings. Prof. Jiří Pachman for teaching the subject of Physics of Explosion course, providing some important reference books and support in student administrative activities.

During the first year of studies, we traveled to the Ludwig Maximilian University of Munich in cooperation with Prof. Thomas M. Klapötke and Prof. K. Karaghiosoff to realize cocrystal single crystal analysis. I am very thankful to both Professors for their cooperation. Also, later, it motivated me to visit again during a second Erasmus+. I extend my thanks to Dr. Rafał Lewczuk from Łukasiewicz Research Network – Institute of Organic Industry, Warsaw, for giving me the opportunity to carry out the application part of my CACs as rocket propellant during the first Erasmus+.

I express special thanks to our collaborative professors/colleagues, Dr. Roman from physical chemistry, who strongly helped in thermal analysis. Dr. Petr Bělina from Dept. Inorganic chemistry for strong cooperation with PXRD and Particle size analysis. Dr. Jana Shánělová for providing a facility for bomb calorimetric analysis. Prof. W. Trzcinski from Military University Warsaw, for software support to calculate the detonation parameters of the CACs. Dr. Jhonathan for cooperation with XPS analysis of CACs. Dr. Rafał Lewczuk for providing the facility for carrying out the application part of CACs in rocket propellant. Dr. Mirek Novak from CETVYK for providing the facility to carry out the application part of CACs in the gun propellant. Also, Dr. Jiří Brus Czech Academia of Science for solid NMR facility and cooperation.

Apart from these academic research activities, daily routine research colleagues strongly cooperated and supported me. I am very thankful to Prof. Zdeněk Jalový, who introduced safety training and training on spectroscopic instruments with a nice explanation. I am thankful to Dr. Ondřej Vodochodský; for thorough explanations about instruments; also, both

colleagues showed me fluent use of instruments in a safer manner. I am thankful to Prof. Robert Matyáš, who helped with impact sensitivities measurements and always said positive words during the interaction. I am thankful to Dr. Vojtěch Pelikán, who always greeted me with "Namaste," for making me comfortable and helping me carry out impact and electric spark measurements. Extending warm thanks to Prof. Marcela for on-time, quick financial support for my research activities support. Also, I am very thankful to Prof. Miloš Ferjenčík for administrative and good suggestions during the PhD process.

Also, I am very thankful to my colleagues for providing a ground-level research facility, Ms. Monika Šubrtová for nice explanations for DTA, and Ms. Lenka Dubská for providing me with all the laboratory support. To Ms. Taťána Korpová for administrative support, travel allowance clearance on the international conferences and visiting studies, etc.

I am very grateful to our Indian colleagues/professors followed by, Prof. A. Venkataraman, from Gulbarga University, Kalaburagi introducing me to interdisciplinary materials science like nanomaterials, conductive polymers and energetic materials and their applications during GUG-PEL project. Also recommending me to PhD. My MSc project supervisor Prof. S. T. Nandibewoor, from Karnatak University Dharwad and MSc Summer research supervisor Scientist Dr. Kiran Sonawane from CSIR-NCL - National Chemical Laboratory, Pune for introducing analytical instrumentations and recommending me to PhD. I am also thankful to Prof. S. V. Ganachari, for continuing our leftover projects/ideas which are initiated during 2018-19, continuing collaboration with constant support which resulted in some good research articles. Also, Sheetal H. M. for constant support related to instrumentation technical guidance and research methodology. Vinuta Kamath helping in organic chemistry related queries, and Akanksha Sharma for literature crystal simulation queries, Satish Ture for detection studies of EMs queries. Also, thankful to colleagues Sunil Kumar M. R., Mounesh Kammar, Venkat Viswanath, Mahendra R. Leena Hublikar and all my Indian friends for their direct/indirect support. Also, I extend my thanks to my scholar colleagues/friends, Honza, Milan, Jarda, and Mirek, who helped me during the initial days of laboratory activities. Also, I thank all colleagues, Filiph, Ondra, and Petr, for their support.

My deepest thanks go out to my mother and brother. More specifically, I am heartily grateful to my loving mother, who has selflessly manifested her entire being for my growth. I couldn't have progressed to this level without their support, as she used to say, "Where there is will, there is way." Throughout my life, they have been my closest friends, and I will always be in love with them.

I also thank to my PhD committee members and other reviewers of my thesis, the Assoc. Prof. Robert Matyáš (chairman), Prof. Zeman Svatopluk, Prof. Michael Gozin, Prof. Konstantin Karaghiosof, Assoc. Prof. Zdeněk Jalový, Assoc. Prof. Jiří Pachman, Dr. Jan Jakubko, Prof. Stanislaw Cudziło, hoping for their helpful career advice and suggestions in general.

Herewith, I am wholeheartedly thankful to everyone who helped me directly or indirectly, to providing a nice environment and support to carry out my Doctoral research.

I dedicate this thesis to my mother, for her endless love and encouragement…!

Yours Sincerely,

Veerabhadragouda B. PATIL

Abstract

Earlier reported methods for cocrystallization of EMs especially nitramines are lacking with selectivity and scalability. When it comes to adoption to industrial scale production of energetic-energetic cocrystals (EECCs) it's more difficult. We made thorough literature survey and developed method of coagglomeration for attractive nitramines via solvent mediated slurry method; in which Co-agglomeration of the co-precipitated micro-particles of nitramines themselves or with polynitroarenes by the slurry method is a unique crystal engineering approach to modify the energetic properties of attractive nitramines like CL20, HMX, BCHMX, RDX etc. The properties and structural modification in the 60+ co-agglomerated crystals (CACs) newly prepared in our laboratory. There are notable variations in the crystal morphologies and packing of crystals, including key properties like relatively high density, melting point, impact sensitivity, and detonation properties. These CACs are in the overwhelming majority showing properties like co-crystals. Apart from these aspects, co-agglomeration provides a huge opportunity to tune the key properties and performance of existing energetic materials and is easy to scale-up for the industrial level. These preliminary results also suggest that chemical engineering factors are involved in the preparation of CACs, as in conventional crystallization. The optimization of them should be a matter of downstream technological research.

Abstrakt

Dříve uváděné metody pro kokrystalizaci EM, zejména nitraminů, postrádají selektivitu a škálovatelnost. Pokud jde o přijetí do průmyslové výroby energeticko-energetických kokrystalů (EECCs) je to obtížnější. Provedli jsme důkladný průzkum literatury a vyvinuli metodu koaglomerace pro atraktivní nitraminy pomocí suspenzní metody zprostředkované rozpouštědlem; ve kterém ko-aglomerace společně vysrážených mikročástic nitraminů samotných nebo s polynitroareny suspenzní metodou je unikátní krystalový inženýrský přístup modifikovat energetické vlastnosti atraktivních nitraminů jako CL20, HMX, BCHMX, RDX atd. a strukturní modifikace v 60+ koaglomerovaných krystalech (CAC) nově připravených v naší laboratoři. Tam jsou pozoruhodné variace v morfologiích krystalů a uspořádání krystalů, včetně klíčových vlastností, jako je relativní vysoká hustota, bod tání, rázová citlivost a detonační vlastnosti. Těchto CACů je v drtivé většině většina vykazuje vlastnosti jako ko-krystaly. Kromě těchto aspektů poskytuje koaglomerace obrovské možnost vyladit klíčové vlastnosti a výkon stávajících energetických materiálů a lze je snadno škálovat průmyslovou úroveň. Tyto předběžné výsledky také naznačují, že se na tom podílejí faktory chemického inženýrství příprava CAC jako při konvenční krystalizaci. Jejich optimalizace by měla být otázkou následný technologický výzkum.

Keywords

Nitramines; Co-agglomeration; Co-crystals; Impact sensitivity; Detonation parameters

Klíčová slova

Nitraminy; Ko-aglomerace; Ko-krystaly; Citlivost na náraz; Detonační parametry

Souhrn

Toto krátké shrnutí doktorské práce může sloužit jako odkaz na klíčové poznatky výzkum vysoce výkonných ko-krystalů energetických materiálů (EMs) pomocí škálovatelného ko-aglomeračního přístupu pro případné budoucí aplikace těchto ko-krystalů ve všech speciálních činnostech jak v civilních, tak vesmírných a vojenských oblastí.

Technika ko-krystalizace EMs má perspektivu širokého využití, nicméně řada studií je stále ve fázi výzkumu a některé kritické problémy zůstávají nevyřešeny. Ko-krystalizace je spolehlivý a nákladově efektivní přístup k ladění energetických vlastností stávajících EMs bez nutnosti syntézy nových molekul. Větší výzvou je škálovatelnost. Velkokapacitní výrobní metody mohou produkovat vysoce kvalitní krystaly, ale v tomto procesu může docházet i k nežádoucí nukleaci, která ztěžuje udržení rovnoměrné velikosti krystalů pro požadované aplikace. Získání energetických ko-krystalů (EECCs) s vhodnou hustotou energie (objemový obsah energie), bezpečností a výkonem pro danou aplikaci však zatím není jednoduché. V práci se píše o ko-aglomerátech (CACs), což jsou směsi ko-krystalů s přebytkem jednoho koformeru, v mnohých případech jsou izolovány „čisté“ ko-krystaly.

Na Ústavu energetických materiálů Fakulty chemicko-technologické Univerzity Pardubice jsme vyzkoušeli tvarovou a optimalizovanou metodu modifikace EM; nakonec jsme vyvinuli univerzální strategii s koagulací v rozpouštědle na bázi suspenze (v níž jsou koformery velmi málo rozpustné), která je přijatelnější z hlediska bezpečnosti a účinnější při ladění energeticky bezpečných parametrů a zároveň při kontrole jejich morfologie.

Tato metoda je prakticky inovativní ko-krystalizací v suspenzi, v literatuře obecně klasifikovanou jako "Slurry method", která ve srovnání s ko-krystalizací rozpouštědlovou výrazně zkracuje dobu zpracování a snižuje množství rozpouštědel. Poskytuje jemné ko-krystaly (prakticky mikro-ko-krystaly) velmi dobré kvality. Zajímavé jsou ko-krystaly cyklických nitraminů s 1,3-diamino- a 1,3,5-triamino-2,4,6-trinitrobenzenem (DATB a TATB) s δ-1,3,5,7-tetranitro-1,3,5,7-tetrazokanem (δ-HMX), přičemž TATB působí jako protispékavá přísada (pro molární poměr HMX/TATB 1,00/0,12 jsou IS = 50 J a vypočtená D = 9,3 km/s). Ko-krystaly cyklických nitraminů s cis-2,2',4,4',6,6'-hexanitrostilbenem (HNS) a 2,2',4,4',6,6'-hexanitroazobenzenem (HNAB) vykazuje vyšší odolnost proti nárazu než jejich čisté koformery, přičemž δ-HMX/cis-HNS při molárním poměru 1,00/0,11 má IS = 47 J (pro TNT je to 39,4 J) a vypočtenou D = 8,9 km/s. Ko-aglomerace stericky přeplněných nitraminů ε-CL20 a BCHMX poskytla produkt β-CL20/BCHMX s molárním poměrem 1,8/1,0, IS = 14,9 J a vypočtenou D = 9,4 km/s. Odolnost posledně jmenovaného produktu proti nárazu převyšuje odolnost jeho čistých koformerů, především BCHMX s IS 3 J. Vzájemný molární poměr koformerů a typ kontinuální fáze významně ovlivňují ko-aglomeraci. Protogenní rozpouštědla často poskytují lepší morfologii než aprotická prostředí, ale HNAB se v nich rozkládá (alkoholyzuje).

Ve studovaných typech ko-krystalů byl HMX přítomen v jeho δ-modifikaci, CL20 v jeho β-modifikaci a HNS v cis-konformaci. Prostorově podobnou orientací molekul δ-HMX a cis-HNS můžeme vysvětlit nízkou citlivost kokrystalu δ-HMX/cis-HNS pro molární poměr koformerů 1,00/0,11. Fenomén výbušných směsí s vyššími detonačními parametry, vypočtenými na základě procentuálního zastoupení složek (v porovnání s výpočetním výstupem CHEETAH), je pozorován u ko-krystalů s DATB a TATB, slabší pak u ko-krystalů s cis-HNS a HNAB. Opak byl zjištěn u ko-krystalů β-CL20/BCHMX. Koaglomerát β-HMX a 3,6-bis(1H-1,2,3,4-tetrazol-5-ylamino)-1,2,4,5-tetrazinu (BTATz) poskytl produkt s ko-krystalem α-HMX/BTATz, který v procese ko-krystalizacce v suspenzi s mícháním pomocí křížového míchadla vykazoval nejnižší citlivost (46 J) ze studovaných CACs tohoto typu; očekává se, že α-HMX/BTATz bude mít o něco lepší detonační energii než β-HMX (6097 oproti 5864 $J.g^{-1}$ CHEETAH kódem).

V oblasti předběžných aplikačních testů některých připravených ko-aglomerátů byla pozornost věnována propelantům. Byly tak připraveny a testovány vzorky raketových pohonných hmot HMX/BCHMX v AP/HTPB s nitraminy jednak ve formě CACs, jednak jako mechanické směsi a to ve třech složeních (10, 20 a 30 %) v

porovnáním se vzorky s aplikací jen čistého β-HMX v tomto kompozitu. Podobně byla testována směs RDX/BCHMX ve střelném pistolovém prachu (obdoba švýcarského výrobku ECL120). V případě CAC HMX/BCHMX se ukázala velmi dobrá morfologická kompatibilita, termochemické vlastnosti a při 20% podílu vykázaly optimální rychlost hoření ve srovnání s čistým HMX i fyzikálními směsmi. Také ve srovnání s dříve v literatuře uváděnými kompozitními pohonnými hmotami vykazovaly HMX/BCHMX CAC relativně dobré rychlosti hoření (7-9 mm.s-1). V případě pistolového paliva vykázal přídavek 2 % BCHMX do RDX/BCHMX CACs ve srovnání s čistými RDX kompozicemi pozitivní výsledky. Jeden z nejcitlivějších CL20/BHMX (mol. poměr 1,52:1,00 s IF = 1,2 J), použitý jako iniciační složka v elektrické rozbušce nevykazoval požadovanou hodnotu urychlovací schopnosti v dané konstrukci rozbušky. Nepodařilo se v rozbuškách otestovat kompozity α-HMX/polyanilín se značně sníženou citlivostí na náraz ale zvýšenou citlivostí k elektrické jiskře.

Z hlediska citlivosti k nárazu je zřejmé, že ve většině případů jsou nitraminové koformery stabilizovány proti této iniciaci. Molární poměr koformerů zde hraje klíčovou roli v proměnlivosti nárazové citlivosti kokrystalů, konkrétně u stericky stísněných CL20 a BCHMX, ale při molárním pomě 1:1,8 má tento ko-krystal větší resistenci vůči nárazu, jako čisté koformery. Také v případě HNS a HNAB se mírné změny molárních poměrů dosti promítaly do citlivosti na náraz. Stejně tak proces krystalizace během ko-precipitace - rychlé přidávání rozpouštědla nebo pomalé přidávání rozpouštědla, a co je důležitější, tvar míchadla - všechny faktory jsou dobře zdokumentovány.

Ze studií ko-aglomerátů pomocí DTA je zřejmé, že počátky i píky tepelného rozpadu CAC jsou trvale o něco nižší než u čistých nitraminů. Mechanismy, kterými koformery spolu vzájemně interagují, jsou plně v souladu s dosavadními poznatky v oboru energetických ko-krystalů a potvrzeny i námi získanými výstupy spektroskopických analýz, a ty mohou být příčinou nižší tepelné stability CACs ve srovnání s čistými nitraminy (zde se také ukazuje vliv smíšeného bodu tání, který odstraňuje stabilizační účinek krystalické mřížky). Zmíněné intermolekulární interakce mohou podporovat homolýzu vazeb --N-N-- u nitraminů a -N---O---H- u polynitroarenů s atomy vodíku v poloze gama vůči nitroskupině. K exotermickému rozkladu dochází v původním tepelném rozmezí polymorfního přechodu CL20, a to nejen v důsledku extrémního stupně kontaktu složek v kompozitu. Podobně rozklad komplexu s přenosem náboje α-HMX/polyanilín začíná také v teplotní oblasti jeho α - δ- přechodu (v obou případech pohyb molekul v krystalové mřížce při polymorfním přechodu poškozuje její stabilizační účinek). Iniciační reaktivita atraktivních nitraminů se obvykle zvyšuje po přidání molekul polynitrosloučenin do jejich krystalové mřížky, zejména u molekul, které jsou stericky stísněné. Tento efekt však lze zmírnit pečlivou volbou molárního poměru výsledných CAC, jak ukázala naše předchozí zjištění. Jako nejúčinnější "stabilizátor" pro tyto nitraminy se zatím ukázal TATB. Je zajímavé, že koformer cis-HNS má srovnatelný vliv na stabilizaci δ-HMX i když nejodolnější vzorek δ-HMX/cis-HNS (1,00/0,11 s IF = 47 J) měl mikroporézní strukturu. Z hlediska vlastností výbušiny je nejvýhodnější ko-aglomerát δ-HMX/TATB, jehož výkon je srovnatelný s čistým β-HMX.

Při řešení dílčích problémů disertační práce, v závislosti na druzích intermolekulárních interakcí a jejich vzájemných zastoupení ve studovaných ko-krystalech jsme nově popsali celou řadu vztahů výstupů spektroskopických měření na jedné straně a charakteristik iniciační reaktivity, výkonu a energetického obsahu CACs, na straně druhé, v tom jsou zahrnuty i výstupy XPS (vazebné energie) a kvantový výtěžek fluorescence polyanilinových komplexů s nitraminy.

Table of Contents

Abbreviations / Full forms of codes viii
List of Figures / Schemes x
List of Tables xv
Aim of the Study 1
Chapter 1 Introduction 3
1.1 Research background 4
1.2 Research & developments in cocrystallization of energetic materials 5
1.3 Preparation methods / techniques 6
1.3.1 Evaporation crystallization 6
1.3.2 Spray drying / vapour deposition technique 7
1.3.3 Slurry technique 7
1.3.4 Vacuum freeze drying 8
1.4 Components shaping cocrystals - Intermolecular interactions 9
1.4.1 Hydrogen bonding 10
1.4.2 π -Stacking (π-π & n-π) 11
1.4.3 van der Waals interactions 11
1.4.4 Packing of structures - layered stacking, chanal stacking, caged stacking 13
1.5 Thermochemical properties of cocrystals 14
1.5.1 Decomposition temperature 14
1.5.2 Heat of combustion and Enthalpy of formation($\Delta H_{form.}$) 15
1.5.3 Crystal density 17
1.6 Mechanical sensitivity of cocrystals – reaction towards external stimuli 17
1.6.1 Impact sensitivity (IS) 20
1.6.2 Friction sensitivity (FS) 21
1.6.3 Electrostatic spark discharge (ESD) 23
1.7 Detonation properties of cocrystals 24
1.8 Technological challenges in preparation of cocrystals of EMs – Current research problem. 26
References 27
Chapter 2 Materials and Methods 39
2.1 Materials 40
2.1.1 RDX: 40
2.1.2 HMX: 40

2.1.3 BCHMX: 40
2.1.4 RS-ε-HNIW/ CL-20: 40
2.1.5 DATB: 40
2.1.6 TATB: 40
2.1.7 HNAB: 40
2.1.8 HNS: 40
2.1.9 PANi: 40
2.1.10 BTATz: 40
2.2 Other inexplosive chemicals / Materials 43
2.3 Characterization Methods 43
2.3.1 Powder X-ray diffraction (PXRD): 43
2.3.2 Fourier transformation infra-red spectroscopy (FTIR): 44
2.3.3 Raman spectroscopy: 44
2.3.4 Densitometer (ρ): 44
2.3.5 High-performance liquid chromatography (HPLC): 44
2.3.6 Field emission scanning electron spectroscopy (FeSEM): 44
2.3.7 Elemental analyzer: 44
2.3.8 Particle size analyzer: 44
2.3.9 Differential thermal analysis (DTA): 44
2.3.10 Heat of combustion by Bomb calorimeter: 45
2.3.11 Differential thermal analysis (DSC): 45
2.3.12 Impact sensitivity by BAM fall hammer: 45
2.3.13 Electric spark sensitivity measurement: 46
2.3.14 Friction Sensitivity: 46
2.3.15 Hardness Test: 46
2.3.16 Ignition temperature: 46
2.3.17 Burn rate measurements: 47
2.4 Software / Computational Methods 48
2.4.1 FEST: 48
2.4.2 CHEETAH (Thermochemical calculations): 48
2.4.3 ICT-Thermodynamic code calculations: 48
2.4.4 CCDC & Mercury: 49
2.5 Preparation of co-crystals of attractive nitramines *via* Coagglomeration Method 49
2.6.2 Charging and pressing of detonator for CACs of CL20/BCHMX 52
2.6.3 The preparation of gunpowder 52

References 53
Chapter 3 Results and Discussions 57
3.1 Co-agglomerated crystals of 1,3-di- and 1,3,5-tri-amino-2,4,6-trinitrobenzenes with attractive cyclic nitramines 58
3.1.1 Background 59
3.1.2 Results 59
3.1.2.1 Morphology and particle size analysis 59
3.1.2.2 Powder X-Ray diffraction (PXRD) studies 61
3.1.2.3 Differential thermal analysis (DTA) 63
3.1.2.4 FTIR Spectroscopy 64
3.1.2.5 Raman spectroscopy 65
3.1.2.5 Thermochemical and explosive properties 68
3.1.3 Discussion 70
3.1.3.1 Co-agglomeration 70
3.1.3.2 Thermal analysis 71
3.1.3.3 Spectral examination 71
3.1.3.4 The energetic point of view 74
3.1.3.5 Impact sensitivity 75
3.1.3.6 Detonation parameters. 75
3.1.4 Summary 76
3.2 Coagglomerated crystals of 2,4,6,8,10,12-hexanitro-2,4,6,8,10,12-hewxaazaisowurtzitane (ε-CL-20) with cis-1,3,4,6-tetranitrooctahydroimidazo-[4,5-d]imidazole (BCHMX) 81
3.2.1 Background 82
3.2.2 Results and Discussion 82
3.2.2.1 Morphology and particle-size analysis 82
3.2.2.2 FTIR spectral studies 83
3.2.2.3 Raman spectral studies 86
3.2.2.4 Powder X-ray diffraction (PXRD) studies 89
3.2.2.5 Differential thermal analysis (DTA): 90
3.2.2.6 Compositions and thermochemical characteristics of mixed crystals 92
3.2.2.7. Impact-sensitivity data and calculated detonation parameters 92
3.2.2.8 Initiation reactivity of cyclic nitramines mixed crystals from the perspective of XPS and Hirshfield analysis 96
3.2.2.9 The Hirshfeld surface analysis of co-crystals 97
3.2.2.10 Initiation reactivity in terms of impact sensitivity 99

3.2.2.11 Initiation reactivity in terms of electric spark sensitivity 101
3.2.2.12 Initiation reactivity in terms of detonation velocity 102
3.2.2.13 The viewpoint of energy 104
3.2.2.14 Interesting relationships involving Raman and FTIR spectroscopy findings 105
3.2.2.14.1 Raman spectroscopy 105
3.2.2.14.2 FTIR Spectroscopy 106
3.2.3 Summary 107
References 108
3.3 Co-agglomerated crystals of 2,2',4,4',6,6'-hexanitro -stilbene /-azobenzene with attractive nitramines 113
3.3.1 Background 114
3.3.2 Results 114
3.3.2.1 Powder X-Ray diffraction (PXRD) studies: 114
3.3.2.2 Morphology and Particle size analysis 115
3.3.2.3 Differential thermal analysis (DTA) 119
3.3.2.4 FTIR Measurements 120
3.3.2.5 Raman Spectral studies: 122
3.3.2.6 Thermochemical and Explosive Properties 128
3.3.3 Discussions 128
3.3.3.1 Co-agglomeration 128
3.3.3.2. Thermal Analysis 129
3.3.3.3 Spectral Examination 129
3.3.3.4 The Energetic Point of View 132
3.3.3.5 Impact sensitivity 134
3.3.3.6 Detonation parameters 135
3.3.4 Summary 136
References 137
3.4 Composite crystals of polyaniline with attractive nitramines via coagglomeration 141
3.4.1 Background 142
3.4.2 Results 143
3.4.2.1 Powder X-Ray diffraction(PXRD) studies 143
3.4.3.2 Morphology and Particle size analysis 145
3.4.3.3 Differential thermal analysis(DTA) 146
3.4.3.4 FTIR Spectral studies 147
3.4.3.5 Raman Spectral studies: 149

3.4.3.6. Fluorescence studies 150
3.4.3.6 Thermochemical and Explosive Properties 151
3.4.4. Discussions 153
3.4.4.1 Co-agglomeration 153
3.4.4.2. Thermal Analysis 154
3.4.4.3 Spectral Examination 155
3.4.4.3.1 The N-N bond stretching vibrations 156
3.4.4.3.2 New unusual dependencies 157
3.4.4.3.3 Relationships derived from fluorescence measurements 159
3.4.4.4 Towards the electric spark and impact sensitivities, including shock influence 160
3.4.4.5 The Energetic Point of View 162
3.4.5. Summary 164
3.5 Co-agglomerated crystals of cyclic nitramines with the nitrogen rich 3,6-bis(1H-1,2,3,4-tetrazol-5-ylamino)-1,2,4,5-tetrazine (BTATz) 169
3.5.1 Background 170
3.5.2 Results 171
3.5.2.1 Powder X-Ray diffraction (PXRD) studies: 171
3.5.2.2 Morphology and Particle size analysis 173
3.5.2.3 Differential thermal analysis (DTA) 174
3.5.2.4 FTIR Spectral studies 176
3.5.2.5 Raman Spectral studies 178
3.5.2.6 Thermochemical and Explosive Properties 181
3.5.3 Discussions 184
3.5.3.1 Co-agglomeration 184
3.5.3.2. Thermal Analysis 185
3.5.3.3 Spectral Examination 185
3.5.3.4 The energetic point of view 188
3.5.3.5 Impact Sensitivity 190
3.5.3.6 Detonation parameters 191
3.5.4 Summary 192
Chapter 4 Applications of CACs 197
4.1 Application of HMX/BCHMX CACs in composite rocket propellant 198
4.1.1 Background 198
4.1.2 Results 199
4.1.2.1 Powder X-ray diffraction 199

4.1.2.2 Fourier transformation infra-red spectroscopy (FTIR) 200
4.1.2.3 Raman spectroscopy 201
4.1.2.4 Morphology and Particle size measurements 202
4.1.2.5 Thermal Analysis 205
4.1.2.6 Ignition/ Decomposition temperature 206
4.1.2.7 Vacuum stability test STABIL 207
4.1.2.8 Dynamic mechanical analysis (DMA-Tg) 207
4.1.2.9 Hardness Test 208
4.1.2.10 Friction and Impact sensitivities 208
4.1.2.11 Thermodynamic performance calculation 208
4.1.2.12 Burn rate measurements 209
4.1.3 Discussions 210
4.1.3.1 Co-agglomeration 210
4.1.3.2 Differential thermal analysis (DTA) 210
4.1.3.3 Ignition / Decomposition temperature 211
4.1.3.4 Vacuum stability test 212
4.1.3.5 Dynamic mechanical analysis (DMA-Tg) 212
4.1.3.6 Powder X-ray diffraction 214
4.1.3.7 Spectral Examination 214
4.1.3.8 Impact & Friction sensitivity, and Hardness test 215
4.1.3.9 Outputs of Thermodynamic performance calculation 216
4.1.3.10 Outputs of Burn rate measurements 216
4.1.3.11 Some important correlations 220
4.1.3.12 Relation between combustion and propulsion characteristics 224
4.2 A test of the initiation efficiency of CL20/BCHMX CACs 224
4.2.1 Detonators 224
4.2.2 A possible practical application of CL-20/BCHMX co-crystals 226
4.3 Intra-ballistic analysis of RDX/BCHMX CACs in the nitrocellulose gunpowder 226
4.3.2 Grain geometry analysis 226
4.3.3 Analysis of the samples 227
4.3.3 Basic ballistic properties of powder 227
4.3.4 Intra-ballistic analysis of powder samples 229
4.4 Futuristic applications of remaining CACs of attractive nitramines 231
4.4.1 DATB and TATB CACs: 231
4.4.2 HNS and HNAB CACs: 231

4.4.3 PANi CACs: 231
4.4.4 BTATZ CACs: 231
4.5 Summary 232
4.5.1 HMX/BCHMX CACs in composite rocket propellant 232
4.5.2 CL20/BCHMX CACs in detonators 233
4.5.3 RDX/BCHMX CACs in gun powder 233
4.5.4 Applications Remaining CACs 234
References 234
Chapter 5 Conclusion 241
5.1 CACs of attractive nitramines with selective coformers 243
5.1.1 CACs of attractive nitramines with DATB and TATB 243
5.1.2 CACs of CL20 and BCHMX 243
5.1.3 CACs of attractive nitramines with HNS and HNAB 244
5.1.4 CACs of attractive nitramines with PANi 244
5.1.5 CACs of attractive nitramines with BTATz 245
5.2 Particle size and morphology of CACs 246
5.3 Impact sensitivity 247
5.4 Explosive properties 249
5.5 Feasibility of co-agglomeration method 251
5.6 Applications of CACs 251
5.7 Concluding Remarks 252
References 254
LIST OF STUDENTS' PUBLISHED WORKS 257

Abbreviations / Full forms of codes

α, β, γ, ε and δ - HMX	Four polymorphic modifications of 1,3,5,7-tetranitro-1,3,5,7-tetrazocane
α, β, γ, ε and δ -CL20/HNIW	Four polymorphic modifications of 2,4,8,10,12-Hexanitro-2,4,8,10,12-hexaza-isowurtzitane
ΔH_f	Enthalpy of formation
Qc	Heat of combustion
P	Detonation pressure
D	Detonation velocity
E_{deton}	Energy of detonation,
Dv(50) & *Dv(90)*	50 & 90 % of the cumulative volume distribution of particles
E_{dr} *50 %* & E_{dr} *95%*	Impact sensitivity- drop energy 50% and 95% probabilities of initiation
° C / C	Celsius degree
K	Kelvin degree
MPa	Mega Pascal
Mg	Milligram
min	Minute(time)
ml / mL	Milliliter
T_g	Glass transition temperature
L	Large-scale
P	Co-precipitate
CCs	Cocrystals
CACs	Coagglomerated crystals
LOVA	Low vulnerability ammunition
PM / Phy Mix	Physical mixture
PXRD	Powder X-ray diffraction
FESEM	Field emission scanning electron microscopy
FTIR	Infra-red Raman spectroscopy
DTA	Differential thermal analysis
DSC	Differential scanning colorimetry
TGA	Thermogravimetric analysis
DMA	Dynamic mechanical analysis
VST	Vacuum Stability test
1, 4 DNI	1,4-dinitroimidazole
2, 4 DNI	2,4-dinitroimidazole
4, 5 MDNI	4,5-dinitro-1-methylimidazole
ADNP	4-amino-3,5-dinitropyrazole
AMTN	1-amino-3-methyl-1,2,3-triazoliumnitrate
ANPyO	2,6-diamino-3,5-dinitropyridine-1-oxide
AN	Ammonium nitrate
AP	Ammonium per chlorate
aTRz	Azo-bis-1,2,4-triazole
BCHMX	1,3,4,6-Tetranitrooctahydroimidazo-[4,5-d]imidazole
BTF	Benzotrifuroxane
BTNEN	1,2,4-Butanetriol trinitrate

CAM	ε-caprolactone monomer
CL20 /HNIW	2,4,6,8,10,12 - Hexanitro - 2,4,6,8,10,12 - hexaazaisowurtzitane
DADP	Diacetone diperoxide
DAF	3,4-diaminofurazan
DATB	1,3-Diamino-2,4,6-trinitrobenzene
DMF	Dimethyl formaldyhyde
DMSO	Dimethyl suifoxide
DNB	Dinitrobenzene
DNBT	5,5′-dinitro-2H,2H′-3,3′-bi-1,2,4-triazole
DNDAP	2,4-dinitro-2,4-diazapentane
DNI	dinitroimidazole
DNMT	1-methyl-3,5-dinitro-1,2,4-triazole
DNP	2,4-Dinitrophenol
DNT	1-Methyl-2,4-dinitrobenzene
FOX-7	1,1-diamino-2,2-dinitroethene
H_2O_2	Hydrogen peroxide
HMPT	hexamethylphosphoramide
HMX	1,3,5,7-Tetranitro-1,3,5,7-tetraazacyclooctane
HNAB	2,2’,4,4’,6,6’-Hexanitroazobenzene
HNTO	hydrazine 3-nitro-1,2,4-triazol-5-one
HNS	2,2’,4,4’,6,6’-Hexanitrostilbene
HTPB	Hydroxyl-terminated polybutadiene
MDNT	1-methyl-3,5-dinitro-1,2,4-triazole
MTNI	1-methyl-3,5-dinitro-1,2,4-imidazole
MTNP	1-methyl-3,4,5-trinitropyrazole
n-K6 or Keto-RDX	2-oxo-1,3,5-trinitro-1,3,5-triazacyclohexane, K6
NC	Nitrocellulose
NM	Nitromethane
NMP	N-methyl-2-pyrrolidone
N−O···H	Hydrogen bonding
NT	Nitrotoluene
NTO	3-nitro-1,2,4-triaole-5-one
PANi	Polyaniline
PETN	Pentaerythritol tetranitrate
PVAc	Polyvinyl acetate
RDX	1,3,5-Trinitro-1,3,5-triazacyclohexane
TATB	1,3,5-Triamino-2,4,6-trinitrobenzene
TATP	triacetone triperoxide
TCTNB	1,3,5- trichloro-2,4,6-trinitrobenzene
TEX	4,10-dinitro-2,6,8,12,-tetraoxa-4,10-diazasowurtzitane
TFAZ	7H-trifurazano[3,4-b:3′,4′-f:3″,4″-d]azepine
TMS	tetramethylene sulfone
TNAZ	1,3,3 - Trinitroazetidine
TNP	1,3,5-Trinitro-1,3-diazacyclohexane
TNT	2, 4, 6,-Trinitrotoluene

List of Figures / Schemes

Chapter 1. Introduction

Figure 1.1 a) Schematic of Cocrystals(CCs) of energetic materials; if coformer B is energetic its known as Energetic-Energetic Cocrystals (EECCs) and b) Multi-component solid forms inherently overlap with one another and in addition they can exhibit polymorphism; recreated from reference [4].....4

Figure 1.2. Schematic road map - evaluation of Cocrystals in attractive nitramines.....5

Figure 1.3 Schematic representation of different cocrystallization methods 9

Figure 1. 4 Schematic of the intra- and inter-layered intermolecular interactions. The thickness of the lines represents the strength of intermolecular interactions: the thicker line suggests stronger interactions (Recreated from Ref. [64]). 10

Figure 1.5 Schematic of coformers interactions in crystalline lattice one hydrogen containing energetic coformer acts as hydrogen donor and nonhydrogen containing energetic coformer hydrogen accepter with hydrogen bonding and intermolecular interactions(as shown in Figure X2) between both coformers forms EECCs (Recreated from Ref.[70]). 10

Figure 1.6 3D Single crystal XRD molecular structures of EECCs of nitramines, here, orange coloured bonds indicates pure hydrogen bonds whereas blue coloure bonds indicates electrostatic intermolecular short contacts developed between both coformers during cocrystallization. CL20/TNT[15]; CL20/BTF[16]; CL20/DNB[18]; BTF/DNB[87]; CL20/2,4 MDNI[22]; CL20/Pyrazine[27]; CL20/2,4 DNI[25] and 2CL20/HMX[48]. 12

Figure 1.7 Schematic of the principle of crystal packing-impact sensitivity relationship by π-stacked energetic crystals with few suitable examples. Third column, four arrows symbolize interlayer sliding directions (right/left and up/down) of inter layer sliding allowed (green), not allowed (red) and partially allowed (red/green) of four kinds stacking. The bottom plots show packing modes and inter/intramolecular potential (p)–sliding distance (d) dependencies of four kinds of stacking. α and β denote the sliding along left/right and back/front, respectively(Recreated from Refs.[88, 89]) 13

Figure 1.8 Schematic of thermal behaviour of the CCs – (i) heating of the nitramine-heat supply surround the surface of cocrystal surface; (ii) heat absorbed makes polymorphic change in nitramine crystal and coformer intermediate conversion; (iii) cracking of the nitramine crystal (for HMX, BCHMX and CL20 see in paper17); (iv) spontaneous decomposition and/or explosion[101]. 15

Figure 1.9 a) Schematic diagram of the phonon up-pumping theory: external stimuli excite mechanical energy transfer into doorway modes and then doorway modes up-pump to intramolecular vibrations, which cause initiation; and b) Schematic diagram of shock-induced detonation mechanism of energetic crystals (recreated from Ref. [132]) 21

Figure 1.10 Schematic of electron attack on the nitramine grouping producing an aza-radical and a nitrite anion (the first step in the nitramine electro-reduction)(recreated from Ref. [146]). 24

Chapter 2. Materials and Methods

Figure 2. 1 Energetic Materials used in CACs preparations a) RDX[10], b)HMX [11], c) BCHMX [2], d) DMNA [12], e) ε-CL20 [13], f) β-CL20 [14], g) DATB [15], h) TATB [16], i) HNAB [17], j) HNS [18], k) BTATZ [19] and l) PANi (E-indicates here nitramines forming charge transfer complex with PANi) [7].....43

Figure 2. 2 a) Schematic of gunpowder grain with dimensions and b) real enlarged image of powder grain sample S10.2.....53

Chapter 3. Results and Discussions

3.1 Co-agglomerated crystals of 1,3-di- and 1,3,5-tri-amino-2,4,6-trinitrobenzenes with attractive cyclic nitramines

Figure 3.1.1 FESEM images of cocrystals -Cp1: BCHMX/DATB, Cp2: BCHMX/DATB, Cp3: RDX/DATB, Cp4: δ-HMX/DATB, Cp5: β-CL-20/DATB, a & b: 32 HMX/TATB, c & d: 33 BCHMX/TATB, e & f: 34 CL-20/TATB and g & h: 35 RDX/TATB. 60

Figure 3.1.2 PXRD diffractograms of co-agglomerated crystals /co-crystals (CACs) Cp1: BCHMX/DATB, Cp2: BCHMX/DATB, Cp3: RDX/DATB, Cp4: δ-HMX/DATB, Cp5: β-CL-20/DATB, 32 HMX/TATB, 33 BCHMX/TATB, 34 CL-20/TATB and 35 RDX/TATB. 62

Figure 3.1.3 DTA thermograms of co-crystals a) S32 HMX/TATB, b) S33 BCHMX/TATB, c) S34 CL-20/TATB and d) S35 RDX/TATB. 64

Figure 3.1.4 A comparison of the lengths of the longest N-N bonds with the N-N bond stretching vibration (the C-N bond stretching for TATB) vibration of pure nitramines, their CACs; the N-N bond lengths were taken from the ORTEP views of the nitramines used in the CCDC database shown in Fig. 2.1 Chapter 2. Materials and methods. .68

Figure 3.1.5 The relationships between volume energy of detonation and spectroscopic characteristic stretching vibrations; a) asymmetric NO_2 stretching; b) symmetric N-O stretching. 71

Figure 3.1.6 The comparison of impact sensitivity of the energetic materials in the study with their spectroscopic characteristics: 72

Figure 3.1.7 The relationships between natural logarithm of impact sensitivity and: 74

Figure 3.1.8 Relationship between detonation velocity and crystal density of the nitramines and their CACs in this study 75

3.2 Coagglomerated crystals of 2,4,6,8,10,12-hexanitro-2,4,6,8,10,12-hewxaazaisowurtzitane (ε-CL-20) with cis-1,3,4,6-tetranitrooctahydroimidazo-[4,5-d]imidazole (BCHMX)

Figure 3.2.1 FESEM images of co-crystals and coformers according to the section 2.2: a) & b) CCs1; c) & d) CCs2; e) & f) S4; g) & h) S5; i & j) S4LVP; k & l) S4LV; m & n) S4LZP; o & p) S4LZ; q & r) of S5LVP; s & t) S5LV **Note: -** the samples labelled with "L" indicates the large-scale (amount ≥ 5 g) preparation of the respective samples series and "P" indicates co-precipitates of the respective samples before co-agglomeration. The morphology of the starting CL-20 and BCHMX does not play an important role here because both nitramines undergo co-precipitation, and the starting data are then the morphologies of the co-precipitates and specification of molar ratios of coformers see in Table 5. 84

Figure 3.2.2 Relationship between in-plane ring deformation vibrations and enthalpy of formation (taken from Table 5) 88

Figure 3.2.3 PXRD diffractograms of CCs/CACs and their coformers 90

Figure 3.2.4 DTA thermograms of a) BCHMX/CL-20 and all CACs and b) co-crystal 1 (CCs1) and co-crystal 2 (CCs2) 91

Figure 3.2.5 Semi-logarithmic relationships between impact sensitivity, expressed as drop energy (in J), and a) the difference in asymmetric $–NO_2$ stretching vibrations (the vibration in pure CL-20 minus those in CCs/CACs); b) voluminal energy of explosion 95

Figure 3.2. 6 A) The Hirshfeld analysis of the pure coformers with their three angle views: i) BCHMX [cell vol.: 249.56 A^3; area: 245 A^2] , ii) ε-CL20 [cell vol.: 345.24 A^3; area: 305.50 A^2] and iii) β-CL20 [cell vol.: 350.32 A^3; area: 300.0 A^2] and iv) TTAZ [cell vol.: 212.24 A^3; area: 207.23 A^2]; an analysis for the "dimer" of TTAZ (a local π-π stacking by the $–NO_2$ in position 3 of its molecule [1, 43]). 98

Figure 3.2.7 The relationships between the impact sensitivity, expressed as drop energy, and binding energies of the nitramines used in this study (the numbers in parentheses indicate the molar ratio of β-CL20/BCHMX): **a)** for the N 1s binding energy (N-NO_2) and **b)** for the O 1s binding energy (NO_2). 101

Figure 3.2.8 The relationships between the electric-spark sensitivity (here expressed as the energy of an electric spark) and binding energies of the nitramines under study: **a)** for N 1s binding energy and **b)** for O 1s binding energy. ...102

Figure 3.2.9 The relationships between the calculated detonation velocity and binding energy of the nitramines in the present study: **a)** for N 1s binding energy and **b)** for O 1s binding energy. 103

Figure 3.2.10 The relationships between the maximum crystal density (taken from Table 2) and the binding energy of the nitramines studied: **a)** for N 1s binding energy and **b)** for O 1s binding energy. 104

Figure 3.2.11 The relationships between the energetic content of the nitramines studies, expressed as the enthalpy of formation, ΔH_{form}, and binding energy (the data for TTAZ, whose molecule is not crowded, are outside the range used in this Fig., with its ΔH_{form} being 41 kJ mol^{-1} [60]): **a)** for N 1s binding energy and **b)** for O 1s binding energy. ...105

Figure 3.2.12 The semi-logarithmic relationship between the in-plane ring deformation vibrations and the O 1s binding energies of the nitramines studied (the required spectroscopic data have been taken and are also summarized in Chapter 2 Materials section). 106

Figure 3.2.13 The relationship between symmetric N-O stretching vibration and the N 1s binding energies of the nitramines studied (the spectroscopic data required have been taken and are also summarized in Chapter 2 Materials section). 107

3.3 Co-agglomerated crystals of 2,2',4,4',6,6'-hexanitro -stilbene /-azobenzene with attractive nitramines

Figure 3.3.1 PXRD diffractograms of CACs; 3 HMX/ HNS; 6 HMX/ HNS; 8 HMX/ HNS; 17 RDX/ HNS; 18 CL-20/ HNS; 19 BCHMX/ HNS; 20 RDX/ HNAB; 21 BCHMX/ HNAB; 22 CL-20/ HNAB; 31 HMX/ HNAB; 38 HMX/ HNAB and 39 CL-20/ HNAB 117

Figure 3.3.2 FESEM images of co-crystals a & b) 3 HMX/ HNS, c & d) 6 HMX/ HNS, e & f) 8 HMX/ HNS, g & h) 17 RDX/ HNS, i & j) 18 CL-20/ HNS and k & l) 19 BCHMX/ HNS; a2 & b2) 20 RDX/ HNAB; c2 & d2) 21 BCHMX/ HNAB; e2 & f2) 22 CL-20/ HNAB; g2 & h2) 31 HMX/ HNAB; i2 & j2) 38 HMX/ HNAB; k2 & l2) 39 CL-20/ HNAB 118

Figure 3.3.3 DTA thermograms of CACs S3) HMX/ HNS; S6 HMX/ HNS; S8 HMX/ HNS; S17 RDX/ HNS; S18 CL-20/ HNS; S19 BCHMX/ HNS; S20 RDX/ HNAB; S21 BCHMX/ HNAB; S22 CL-20/ HNAB; S31 HMX/ HNAB; S38 HMX/ HNAB and S39 CL-20/ HNAB.....121

Figure 3.3.4 A comparison of the lengths of the longest N—N bonds with this bond stretching vibration (the CN bond stretching for HNS and HNAB) of pure nitramines and their CACs. (the data placing in this Figure indicates the co-crystals existence); the N-N bond lengths were taken from the ORTEP views of the nitramines used in the CCDC database shown in Chapter 2. 130

Figure 3.3.5 The relationships of the impact sensitivities with spectroscopic stretching vibration characteristics of the CACs prepared: 130

Figure 3.3.6 The relationships between the FTIR symmetrical N-O stretching (cm^{-1}) and performance (voluminal energy of explosion) of the CACs prepared. 132

Figure 3.3.7 The semilogarithmic relationships between impact sensitivities and energy content (represented by enthalpy of formation) of the prepared CACs. 133

Figure 3.3.8 The mutual relationships between the energies of detonation calculated on the base of additive principle (i.e., on the percentage of components in the co-agglomerate) and those, calculated by CHEETAH code using experimental enthalpies of formation; in the Figure also data of CACs with DATB and TATB coformers are inserted (taken from papers [2, 3]). 134

Figure 3.3.9 Detonation parameters of CACs with pure nitramines used for synthesis 3 HMX/ HNS; 6 HMX/ HNS; 8 HMX/ HNS; 17 RDX/ HNS; 18 CL-20/ HNS; 19 BCHMX/ HNS; 20 RDX/ HNAB; 21 BCHMX/ HNAB; 22 CL-20/ HNAB; 31 HMX/ HNAB; 38 HMX/ HNAB and 39 CL-20/ HNAB 135

3.4 Composite crystals of polyaniline with attractive nitramines *via* coagglomeration

Figure 3.4.1 PXRD diffractograms of composites(CACs); 57 CL20/PANi; 58HMX/PANi; 59 BCHMX/PANi; 60 RDX/PANi 144

Figure 3.4.2 FESEM images of compositesa& b) 57CL20/ PANi; c & d) 58 HMX/PANi; e & f) 59 BCHMX/PANi; g & h) 60 RDX/PANi 145

Figure 3.4.3 DTA thermograms of cocrystals 57 CL20/ PANi; 58 HMX/PANi; 59 BCHMX/PANi; & 60 RDX/PANi 147

Figure 3.4.4 a) Normalized UV/vis absorption (blue), fluorescence excitation (red) and emission (black) spectra of PANi in DMSO; b) Fluorescence spectrum of pure PANi and their NAs-composites in DMSO 151

Figure 3.4.5 Dependences connected with the N-N bond stretching: 156

Figure 3.4.6 Dependences connected with the structural characteristics: 158

Figure 3.4.7 Dependences connected with the quantum yield of the studied NAs/PANi complexes: 160

Figure 3.4.8 Dependences connected with the FTIR outputs of nitro group in studied composites: 161

Figure 3.4.9 Dependences connected with the thermochemical aspects of the substances studied: 163

Scheme 3.4.1 Schematic representation of co-agglomerated - polyaniline composite crystals, the binding of attractive nitramines with PANi chain(recreated from earlier reported work [1–4]).....142

Scheme 3.4.2 Schematic representation of two kinds of CACs: 154

Scheme 3.4.3 Mesomeric effect in the nitramine- grouping 154

3.5 Co-agglomerated crystals of cyclic nitramines with the nitrogen rich 3,6-bis(1H-1,2,3,4-tetrazol-5-ylamino)-1,2,4,5-tetrazine (BTATz)

Figure 3.5.1 PXRD diffractograms of Coagglomerated crystals /cocrystals (CACs) 9) RDX/BTATz B1, 10) RDX/BTATz B2, 11) HMX/BTATz B1, 12) HMX/BTATz B2, 13) CL20/BTATz B1, 14) CL20/BTATz B2, 15) BCHMX/BTATz B1 and 16) BCHMX/BTATz B2 172

Figure 3.5.2 FESEM images of CACs, a) & b) 9 RDX/BTATz B1; c &d) 10 RDX/BTATz B2; e & f)11, HMX/BTATz B1; g &h) 12 HMX/BTATz B2; I & j) 13 CL20/BTATz B1; k & l) 14 CL20/BTATz B2; m & n) 15 BCHMX/BTATz B1 and o & p) 16 BCHMX/BTATz B2 174

Figure 3.5.3 DTA thermograms of cocrystals 9) RDX/BTATz B1, 10) RDX/BTATz B2, 11) HMX/BTATz B1, 12) HMX/BTATz B2, 13) CL20/BTATz B1, 14) CL20/BTATz B2, 15) BCHMX/BTATz B1 and 16) BCHMX/BTATz B2 175

Figure 3.5.4 FTIR spectrum of 9) RDX/BTATZ B1, 10) RDX/BTATZ B2, 11) HMX/BTATZ B1, 12) HMX/BTATZ B2, 13) CL20/BTATZ B1, 14) CL20/BTATZ B2, 15) BCHMX/BTATZ B1 and 16) BCHMX/BTATZ B2 177

Figure 3.5.5 Raman spectrum of 9) RDX/BTATZ B1, 10) RDX/BTATZ B2, 11) HMX/BTATZ B1, 12) HMX/BTATZ B2, 13) CL20/BTATZ B1, 14) CL20/BTATZ B2, 15) BCHMX/BTATZ B1 and 16) BCHMX/BTATZ B2 179

Figure 3.5.6 A comparison of the lengths of the longest N-N bonds with the N-N bond stretching vibration of pure nitramines, their CACs and BTATZ (triangular points are the co-crystals data); the N-N bond lengths are taken from the ORTEP molecular structures of the nitramines used in the CCDC database. 180

Figure 3.5.7 A comparison impact sensitivity, expressed as a drop (fall) energy for 50 % probability of initiation, with the characteristics of IR spectroscopy: 186

Figure 3.5.8 A comparison of the crystal density and FTIR C-H bond stretching of the studied nitramines and their CACs. 187

Figure 3.5.9 A comparison of energetic characteristic of the studied nitramines and their composites with their spectroscopic data: 189

Figure 3.5.10 The semilogarithmic relation between impact sensitivity and voluminal energy of detonation. 191

Figure 3.5.11 Relationship between detonation velocity, *D*, and maximal crystal density of the studied nitramines and their CACs. 191

Chapter 4. Applications CACs

4.1 Application of HMX/BCHMX CACs in composite rocket propellant

Figure 4.1.1 PXRD diffractogram of pure HMX, BCHMX, physical mixture and CACs 200

Figure 4.1.2 a) FTIR spectra of Physical mixture, CACs, HMX and BCHMX; b) Raman spectra of Physical mixture, CACs, HMX and BCHMX.....201

Figure 4.1.3 FESEM micrographs a & b) CACs and c & d) Phy Mix and images of propellant coarse cubes (P1 to P9) 200x with insert 300x at three different faces of propellant cubes. 205

Figure 4.1.4 Microscopic images of propellant coarse 205

Figure 4.1.5 Differential thermal thermograms of pure HMX, pure BCHMX, their physical mixture, their CACs, and propellant batches (P1 to P9) in comparison with ammonium perchlorate 207

Figure 4.1.6 Relationship between ignition temperature and heat of combustion of the studied propellants 212

Figure 4.1.7 Relationship between the T_g values and heats of combustion. 213

Figure 4.1.8 Relationship between heat of combustion vs a) impact & b) friction sensitivities of the studied propellants 216

Figure 4.1.9 Burning rate measurements of the HMX, HMX/BC Phy Mix and HMX/BCHMX CACs 219

Figure 4.1.10 Mutual logarithmic comparison of the impact sensitivity and the specific rate constant of thermal decomposition of the propellant. 221

Figure 4.1.11 a) Relationship between burning rate and heat of combustion of propellant: here line **D** correspond to mixtures with only HMX, line **B** is the best Series 2 with 20 % of nitramines, line **C** corresponds to Series 3 with 30 % of nitramines and line **A** is a hybrid one. It is very logical relationship. 222

Figure 4.1.12 Relationship between impact sensitivity and propellant burning rate: here, with the exception of Series 1 for the other ones, an increase in burn rate corresponds to a decrease in impact sensitivity. 222

Figure 4.1.13 Semilogarithmic relationship between burning rate and decomposition temperature (more complicated comparing with Fig. 4.6) 223

Figure 4.1.14 Semilogarithmic relationship between burning rate and hardness of propellant. 223

Figure 4.1.15 Mutual comparisons of burning rate and specific impulse 224

4.2 A test of the initiation efficiency of CL20/BCHMX CACs

Figure 4.2.1 a) An experimental setup for testing the initiation efficiency of CACs in detonators and b) a cross-sectional view of a detonator 225

Figure 4.2.2 The initiation efficiency determination of detonators with CACs as primers results of two tests for each weighed amount - the lead plates pictures. 225

4.3 Intra-ballistic analysis of RDX/BCHMX CACs in the nitrocellulose gunpowder

Figure 4.3.1 Pressure vs. time for samples S00, S10.1, S10.2 and S10.3. 228

Figure 4.3.2 Dynamic liveliness of S00, S10.1, S10.2 and S10.3 powders 228

Figure 4.3.3 Schematic Assembly of 7,62x39 cartridge with FMJ 8 g bullet. 230

Chapter 5. Conclusion

Figure 5.1 FESEM images with sample IDs top 3 highly impact insensitive left to right; A) HMX CACs, B) CL20 CACs, C) BCHMX CACs and D) RDX CACs. (images regenerated from Ref. [1–5]). For sample codes compositions shown in Chapter 2; Table 2.1 and their impact sensitivities results see respective chapter 3 sub-sections.....246

Figure 5.2 A comparative graphical representation of impact and electrical spark sensitivities(only in case of PANi CACs) [1–7]. 247

Figure 5.3 The semi-logarithmic relationships between the impact sensitivity and energy content (represented by the enthalpy of formation) of the CACs prepared (data taken from papers [1–7]).....248

Figure 5.4 Detonation parameters of CACs with pure nitramines used for preparation [1–7] (For sample codes details see caption Figure 5.2).....249

Figure 5.5 The mutual relationships between the energies of detonation calculated on the basis of the additive principle (i.e., the percentage of components in the co-agglomerates) and that calculated by CHEETAH code [16] using experimental enthalpies of formation (data taken from papers [1–7]).....250

Figure 5.6 The mutual relationships between the calculated detonation velocity for the maximal crystal density and this crystal density (data taken from papers [1–7]).....250

Scheme 5.1 General importance coagglomeration method over traditional cocrystallization methods 242

List of Tables

Chapter 1. Introduction

Table 1.1 EECCs of attractive nitramines using evaporation method.....6

Table 1.2 EECCs of attractive nitramines using spray drying method 7

Table 1.3 EECCs of attractive nitramines using slurry method 8

Table 1.4 Decomposition temperatures EECCs of attractive nitramines 16

Table 1.5 Thermochemical properties - EECCs of attractive nitramines.....18

Table 1.6 Sensitivities EECCs of attractive nitramines 22

Table 1.7 Detonation properties of EECCs of attractive nitramines 25

Chapter 2. Materials and Methods

Table 2.1 Solvent system in preparation of CACs of attractive nitramines 50

Table 2.2 Propellant composition with individual components [Sample codes].....52

Chapter 3. Results and Discussion

3.1 Co-agglomerated crystals of 1,3-di- and 1,3,5-tri-amino-2,4,6-trinitrobenzenes with attractive cyclic nitramines

Table 3.1.1 The particle size measurements results 60

Table 3.1.2 Summarized data from DTA thermograms of co-formers and co-crystals with visible melting points...63

Table 3.1.3 Summarized results of FTIR measurements 66

Table 3.1.4 Summarized results of Raman measurements.....67

Table 3.1.5 Molecular formulas, thermochemical properties, and maximum crystal densities of pure substances and their corresponding CACs 69

Table 3.1.6 Impact sensitivity and explosive properties of pure substances and corresponding CACs.....70

3.2 Coagglomerated crystals of 2,4,6,8,10,12-hexanitro-2,4,6,8,10,12-hewxaazaisowurtzitane (ε-CL-20) with cis-1,3,4,6-tetranitrooctahydroimidazo-[4,5-d]imidazole (BCHMX)

Table 3.2.1 Particle-size measurements of CL-20/BCHMX co-mixed crystals 85

Table 3.2.2 A summary of the results of FTIR measurements 85

Table 3.2.3 A summary of the results of Raman measurements.....87

Table 3.2.4 A summary of the data from DTA thermograms of coformers and CCs/CACs with their visible melting points. 91

Table 3.2.5 Molecular formulas, thermochemical properties, and crystal densities of pure substances and the corresponding CCs/CACs.....93

Table 3.2.6 The impact-sensitivity and detonation characteristics of pure substances and the corresponding CCs / CACs 94

3.3 Co-agglomerated crystals of 2,2',4,4',6,6'-hexanitro -stilbene /-azobenzene with attractive nitramines

Table 3.3.1 PXRD data for pure nitramines and CACs 115

Table 3.3.2 Particle size measurements of CACs 119

Table 3.3.3 Summarized data from DTA thermograms of coformers and co-crystals with their visible melting points. 120

Table 3.3.4 Summarized results of FTIR measurements 123

Table 3.3.5 Summarized results of Raman measurements.....124

Table 3.3.6 Molecular formulas, thermochemical properties, and maximal crystal densities of pure substances and corresponding CACs.....126

Table 3.3.7 Impact sensitivity and explosive properties of pure substances and corresponding CACs.....127

3.4 Composite crystals of polyaniline with attractive nitramines via coagglomeration

Table 3.4.1 PXRD data for pure nitramines and CACs 144

Table 3.4.2 Particle size measurements 145

Table 3.4.3 Summarized data from DTA thermograms of coformers and cocrystals with visible melting points....146

Table 3.4.4 Summarized results of FTIR measurements 148

Table 3.4.5 Summarized results of Raman measurements.....149

Table 3.4.6 Quantum yields of samples under study measured in DMSO.....150

Table 3.4.7 Molecular formulas, thermochemical properties, and maximal crystal densities of pure substances and corresponding CACs.....152

Table 3.4.8 Sensitivities and explosive properties of pure substances and corresponding CACs.....153

3.5 Co-agglomerated crystals of cyclic nitramines with the nitrogen rich 3,6-bis(1H-1,2,3,4-tetrazol-5-ylamino)-1,2,4,5-tetrazine (BTATz)

Table 3.5.1 PXRD data for pure nitramines and CACs 171

Table 3.5.2 Particle size measurements of BTATZ CACs.....173

Table 3.5.3 Summarized data from DTA thermograms of coformers and cocrystals with visible melting points....176

Table 3.5.4 Summarized results of FTIR measurements 178

Table 3.5.5 Summarized results of Raman measurements.....182

Table 3.5.6 Molecular formulas, thermochemical properties, and maximal crystal densities of pure substances and corresponding CACs.....183

Table 3.5.7 Impact sensitivity and explosive properties of pure substances and corresponding CACs 184

Chapter 4 Applications of CACs

4.1 Application of HMX/BCHMX CACs in composite rocket propellant

Table 4.1.1 PXRD data for pure nitramines and CACs 200

Table 4.1.2 Summarized results of FTIR measurements 201

Table 4.1.3 Summarized results of Raman measurements.....202

Table 4.1.4 Particle size measurements of CACs 203

Table 4.1.5 Summarized data from DTA thermograms of coformers and co-crystals with their visible melting points 206

Table 4.1.6 Properties of propellant samples 208

Table 4.1.7 Input characteristics of the propellant components required for calculation.....209

Table 4.1.8 Results of thermodynamic performance calculation of the studied propellants.....210

Table 4.1.9 Results of the 6 hours vacuum stability test at 120 C 213

Table 4.1.10 The burning rate of CACs propellants with comparison earlier literature reported works 95% confidence bounds for each fit parameter are also given. The fit parameters from the literature were either directly reported or calculated reported [5, 9, 10, 11] 218

4.2 A test of the initiation efficiency of CL20/BCHMX CACs (No Tables)

4.3 Intra-ballistic analysis of RDX/BCHMX CACs in the nitrocellulose gunpowder

Table 4.3.1 Thermochemical properties of gun powder grain samples 227

Table 4.3.2 Ballistic properties of gun powder grain samples 229

Table 4.3.3 Intra-ballistic analysis of powder samples 230

Table 4.3.4 The courses of individual intra-ballistic quantities of for both variants(as per Table 4.3.3) tests of powder mass in the 7.62x39 cartridge 230

Chapter 5 Conclusion (No Tables)

Aim of the Study

Indeed, essentially, cocrystallization is a credible, productive, and cost-effective way to tune the energetic properties of existing EMs instead of undergoing or switching to new molecule synthesis. However, the crystal engineering techniques reported in literature are fraught with challenges when comes to large scale preparations to employ defense and civil applications. The more important challenge here is scalability, when it comes to large scale preparation methods can give good quality of crystals, and at the same time they are possibly undergo nucleation and its complex maintain required application crystalline sizes.

Achieving effective energy-energetic cocrystals (EECCs) with holding their energy density/ bulk density, safety, and performance as required for the application is also challenging task. Especially come to their physiochemical with detonation properties it must be fulfilled their inherent high sensitivity and high reactivity contribution EECCs is leads to energy – safety contradiction, same time it needed to be stabilized.

Also, sometime during the preparation solubility of coformers generally leads to two kinds of crystals with recrystallization without undergoing cocrystallization. Similarly, morphology of EECCs end up with rod like or needle like structures which makes them incompetent to use in applications. There are still few barriers in this field's future, but there is no denying that cocrystallization technology will be crucial to the creation of the newest forms of EMs, pyrotechnics, and for propellants additives.

Keeping these all aspects the preparation of EECCs as per current applications requirement, is challenging and tedious endeavor; it made to us look into alternative optimized method or modification existing method which can be able to helpful in production of EECCs in large scale.

At Institute of Energetic Materials, Faculty of Chemical Technology, University of Pardubice we tried, created, and optimized method to modify the EMs finally developed universal strategy up with slurry based coagglomeration in solution state which is more compatible safety wise as well to more effective in tuning energy - safety parameters with controlling their morphology too. Obtained results discussed throughout this thesis.

Chapter 1 Introduction

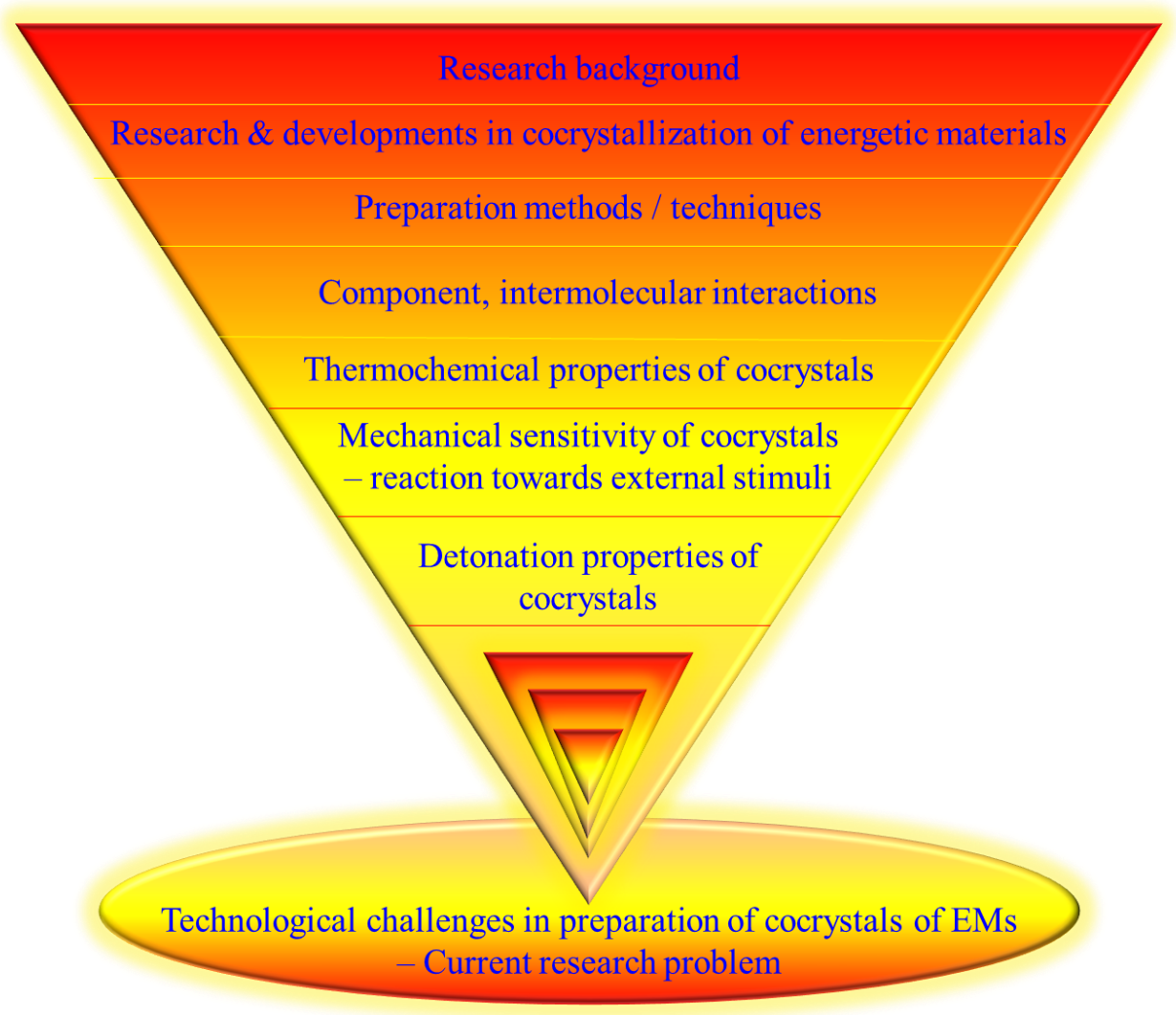

1. Introduction

1.1 Research background

The energetic materials (EMs - explosives, propellants, and pyrotechnics) are used widely for military as well as civil applications[1]. Researchers synthesized various EMs based on the requirements; however, synthetic methods are slowly reaching saturation. More attractive energetic materials exhibit inherits impact sensitivity. To overcome this property, there are several efforts made by researchers to achieve energy-safety balanced EMs. Several methods came into existence, like improved crystallization, coating with insensitive materials to modification of surface morphology and shapes of the crystals [2], mixing with energetic/non-energetic materials, polymer coating [3] cocrystallization(Figure 1 & 2) etc.

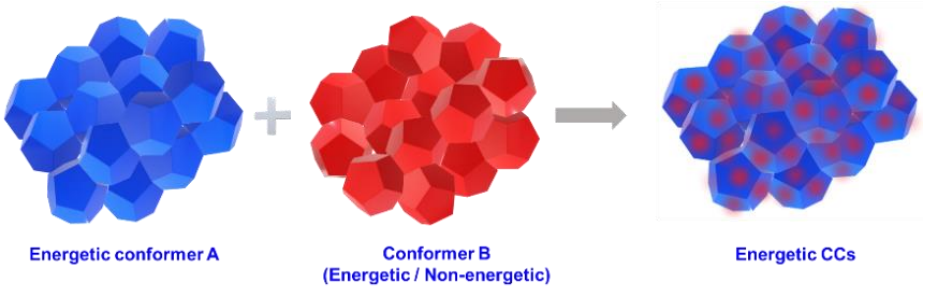

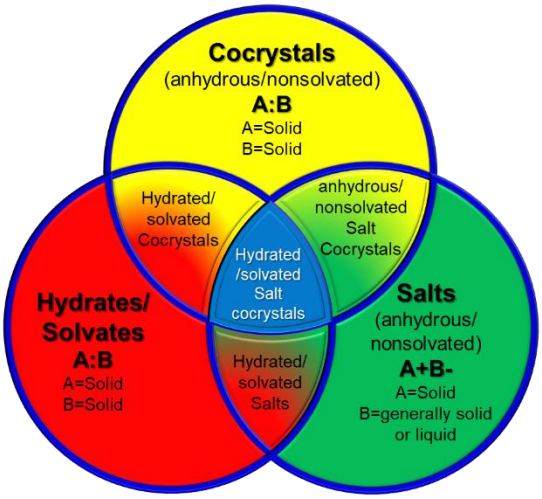

Figure 1.1 a) Schematic of Cocrystals(CCs) of energetic materials; if coformer B is energetic its known as Energetic-Energetic Cocrystals (EECCs) and b) Multi-component solid forms inherently overlap with one another and in addition they can exhibit polymorphism; recreated from reference [4]

These efforts continued; however, approaches slowly focused along with sensitivity, the key research components thermal stability and detonation properties of EMs [5]. Later, cocrystallization with energetic-energetic materials begins. Initially, it did not much grab the attention from researchers, but gradually from

2010 onwards, it became a hot topic for researchers from both scientific as well as technological points of view. We made efforts and made it compatible and easily scalable with a high-purity achievable approach, i.e., via coprecipitation followed by coagglomeration.

Hoping our research can be a reference to exploring high-performance cocrystals energetic materials in scalable approach in application in future application in all special activities of the space and military purposes [6]. Because there is plenty of potential in this approach that needs to be explored.

1.2 Research & developments in cocrystallization of energetic materials

The cocrystallization is beginning more attraction to researchers rather than synthesizing new materials as an alternative route in development of the novel properties with existing energetic materials [6, 7](Figure 1). This method also helps to alter the physical chemical as well as performance and strengthen safety of the EMs[7]. Its most promising method to develop excellent energetic materials as it can achieve a favorable balance between high energy and low sensitivity for the energetic materials by tuning their components and ratios [4, 6, 7].

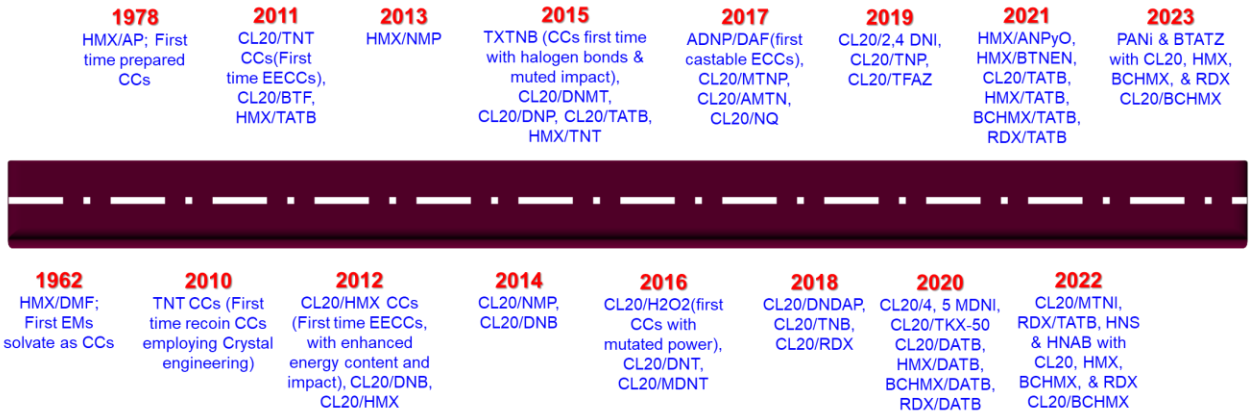

Figure 1.2. Schematic road map - evaluation of Cocrystals in attractive nitramines

Considering these aspects their huge research and development have been happening in cocrystallization of EMs, not only preparations there is huge research also happened in simulation to understand the intermolecular structural orientations and compatibility [7–9]. Cocrystallization of EMs mainly two ways one cocrystallization with non-energetic material and another is cocrystallization with energetic molecule. Further, confirmation of cocrystallization; if single crystal grown successfully characterization is easier and otherwise bit challenging [11]. There are different methods of preparations (discussed in section 1.3) which varies with thermochemical and instrumental conditions [12].

1.3 Preparation methods / techniques

1.3.1 Evaporation crystallization

Evaporation crystallization is the most commonly used method in cocrystallization, mainly used for development or to grow single crystals of cocrystals(Table 1). In this method complete crystallization was carried out via solvent allowed to slow evaporation. Selection of solvents is challenging in this method due to both conformers great difference in solubility[13]. The crystal free-growth shapes are not controllable in this method, yielded single crystals more beneficial to scientific studies than technological application viz. sometimes crystals appeared to be sharp needles possess mechanical sensitivity will be retained or increased(Table 1) [6, 11, 13]. In addition to this sometimes there might be formation of solvate usage of large amount of solvent, long time, larger crystals, these might cause low yield irregular shape and size etc. of cocrystals [12]. However, there are supplement methods were developed with this method to improve this method especially to do fast evaporation; still these problems are not avoidable completely especially there is chances of solvate formation, difficult to separate, and low yields, it creates uncertainty in feasibility to scale up production of CCs of EMs due to different shapes of EECCs (Table 1).

Table 1.1 EECCs of attractive nitramines using evaporation method

Sr No's	Cocrystal (A/B)	Solvent system	Particle size	Shape	Ref.
1	CL20/TNT	EtOH	< 500 μm	hexahedral cubicles	[15]
2	CL20/BTF	EtOH	NA	hexagonal elongated	[16]
3	CL20/TNT	EtAc/DMK/Toluene/ CH_2Cl_2	> 100 μm	NA	[17]
4	CL20/DNB	EtOH	> 100 μm	Block prism	[18]
4	CL20/MTNP	EtAc	> 100 μm	Irregular blocks	[19]
5	CL20/RDX	ACN	> 50 μm	Rods like	[20]
6	CL20/AMTN	EtOH/EtAc	> 100 μm	NA	[21]
7	CL-20/2,4-MDNI	EtOH	> 100 μm	hexahedral prism	[22]
8	CL-20/4,5-MDNI	EtOH	> 100 μm	broken rods like	
9	CL20/MTNP	EtOH	500 μm	Flattened square	[23]
10	CL20/HMX	DMK; DMK+H_2O	20 - 100 μm	Irregular	[24]
11	CL-20/1,4-DNI	EtAc	> 100 μm	Rods like	[25]
12	CL20/TNP	EtAc / DMK / CAN	NA	NA	[26]
13	CL-20/pyrazine	EtAc	> 100 μm	NA	[27]
14	CL-20/pyrazine	MeOH+EtAc	> 100 μm	NA	
15	CL20/4,5-MDNI	ACN	> 100 μm	Squared cubes	[28]
16	CL20/4,5-MDNI	EtOH	> 100 μm	Elongated cubes	
17	CL-20/TFAZ	H2O	1 mm	Chunk like	[29]
18	CL-20/MTNI	MeOH	> 100 μm	Irregular	[30]
19	CL-20/BTF	EtOH	> 100 μm	NA	[31]
20	DNP/DAF	H_2O	> 100 μm	Needle	[32]
21	DNP/DAF	H2O+30% H_2O_2	> 100 μm	Squared	[32]

1.3.2 Spray drying / vapour deposition technique

In this technique process coformer EMs dissolved selective solvents then dried into a powder form by spraying the liquid feed into a hot drying medium[33]. Recently, this technique is getting more attention from researchers to get nano sized cocrystals with equimolar distribution of crystals. This process is quicker and easier to get nanosized crystals, more details of the obtained crystal morphological properties shown in Table 2. However, the safety aspect of the cocrystals preparation mainly with large-scale of this process is not very compatible certainty due to possibly formation of flakes if crystals not dried completely (aspects of their sensitivity). Also, difficulty in designing spray nozzle, pressure maintenance and sometimes different masses of small droplets cannot be completely dispersed due to the uniform direction of draft and gravity, resulting in agglomeration when not completely dried. However, there are efforts are going to scale up this process due to it being a one step process and faster and continuity[32, 33] (as shown in Table 2).

Table 1.2 EECCs of attractive nitramines using spray drying method

Sr No's	Cocrystal (A/B)	Solvent system	Particle size	Shape	Ref.
1	HMX/AP n-K6/n-RDX	DMSO	30-300 microns	NA	[36]
2	Keto-RDX (2-oxo-1,3,5-trinitro-1,3,5-triazacyclohexane, K6)	DMK	82 nm	hexagonal flat crystals	[37]
3	HMX/TNT	DMK	50 - 200 nm	Spherical	[38]
4	CL-20/HMX CL-20/HMX	DMK DMK	50 -100 nm 100 Mm	Spherical	[39]
5	CL20/HMX	DMK	100 Mm	Spherical	[40]
6	CL20/HMX + PVAc	DMK	100 -1000 nm	Spherical	[41]
7	CL-20/DNDAP	MeAc	0.5 - 5 µm	Spherical	[42]
8	CL20/TNT	EtAc	200 nm	Irregular	[35]
9	CL20/DNB	BuOn	100 to 500 nm	Irregular	[35]
10	CL20/TNB	n-BuAc	200 to 600 nm	Irregular	[35]
12	CL-20/ 2,4-DNI	DMK	518.25 nm	Spherical beeds	[34]
13	CL-20/NQ	DMSO	> 50 µm	Spherical	[43]
14	CL20/HMX/DOS CL20/HMX/PVAc CL20/HMX/PVB	ACN	± 1 µm	Hallow networked flakes	[44]

1.3.3 Slurry technique

This technique is usually a solvent mediated one, both coformers dissolved in solution made them controlled evaporations of the solvent. Slurry forms initial stage later the dried cocrystals obtained which are controlled size and shape by means of the stirring process used and solvent addition variation etc. This method is easily adaptable to larger scale productions the compatible to scale up. This method both coformers undergo good reaction to each other in solvent medium with controlled size growth of the crystals. The risk of adulteration with external materials is low, as the technique involves only physical

bonding and the obtained cocrystals are also with structural homogeneity[45](as shown in Table 3). So, it also generally known as reaction cocrystallization and it has been extensively used as an efficient, straightforward cocrystallization screening method, but only few attempts at utilizing this method for scaled-up cocrystal production have been undertaken and none have realized its full potential by utilizing solid dosing and process analytical technology, semi batch reaction cocrystallization (SBRC) provided the first scale-up of high quality CL-20/HMX cocrystal (Table 3).

1.3.4 Vacuum freeze drying

In this process solution of EMs in which a completely frozen form is placed under a vacuum in order to remove solvents, allowing to sublimate i.e., the ice to change directly from a solid to a vapor without passing through a liquid phase so it also known as sublimation drying. This method is very helpful in achieving the ultrafine nano cocrystals of the EMs. In the vacuum freeze drying process, the solution was frozen quickly so that the process of particles of co-crystal growth and aggregation was very short which was helpful to form the nano-sized co-crystals [11, 41].

Table 1.3 EECCs of attractive nitramines using slurry method

Sr No's	Cocrystal (A/B)	Method used	Solvent system	Particle size	Shape	Ref.
1	HMX/TATB	SLM-Coprecipitation	DMSO/H_2O	20 - 30 μm	prismatic type microstructure without apparent crystal edges	[46]
2	CL20/TNT , CL20/HMX	SLM & EVM	Various organic solvents	100 μM	Hexagonal prismatic	[47]
3	CL20/HMX	SLM & EVM	Acetone & Acetone/propanol	>100 μM	Irregular Squared & pentagon	[48]
4	CL20/TNT	SLM-Coprecipitation	EtAc+Dextrin/H_2O	100 μM	Prism shaped with slightly smoothened edges	[38]
5	CL-20/DNMT	SLM-resonant acoustic mixing process	ACN	NA	Hexagonal	[49]
6	CL20/TATB	SLM-Coprecipitation	DMSO	>3–5 μm	Hexagonal irregular bulk crystals	[50]
7	CL20/HMX	SLM-Beed milling	H2O/PVA	< 200 nm	Squared cubes	[51]
8	CL20/MDNT	SLM-Solvent agitation	ACN	> 100 μm	NA	[52]
9	CL20/RDX	SLM-Ball milling	EtOH/H_2O	123.8 nm	Spherical	[53]
10	CL20/TNT	SLM-Ball milling	EtOH	100 μm	Regular hexahedral	[54]
11	CL20/HMX	SLM-resonant acoustic mixing process	DMK/Xylene/Dextrine	101 μm	diamond	[55]
12	CL-20/TNT	SLM -ball milling	EtOH	119.5 nm	Irregular spherical	[56]
13	HMX/ANPyO	SLM-Coprecipitation	DMSO/glyxol/H_2O	50−150 μm	irregular polyhedron	[57]
14	HMX/ANPyO	SLM-Coprecipitation	DMSO/glyxol/H_2O	50−150 μm	irregular polyhedron	[57]
14	HMX/BTNEN	SLM-Coprecipitation	DMK/CH_2Cl_2/hexane	NA	broken crystal	[58]
15	CL20/HMX	SLM- reaction crystallization	ACN	0.02 cm	cubic	[59]
16	CL-20/HMX	SLM-Coprecipitation	DMSO/H_2O	21.8 μm	cubic	[60]
17	RDX/TATB	SLM-Coprecipitation	distilled water	30 - 40 μm	Granules	[61]
18	CL-20/MTNP	Solvent agitation	EtOH/IPA	> 100 μm	Linear	[62]
19	HMX/NTO	Coprecipitation	H2O	> 100 μm	Granuls	[63]

This method slightly modified by eliminating freezing condition known as vacuum pyrolysis it basically antisolvent extraction from the cocrystal solution were then applied to remove the solvent molecules from the solvates [64]. In both methods the basic difference is vacuum drying based on water boiling point, vacuum freeze drying based on water melting point. In this method need to maintain the continuous high vacuum otherwise cocrystallization ends up with slurry and wet crystals.

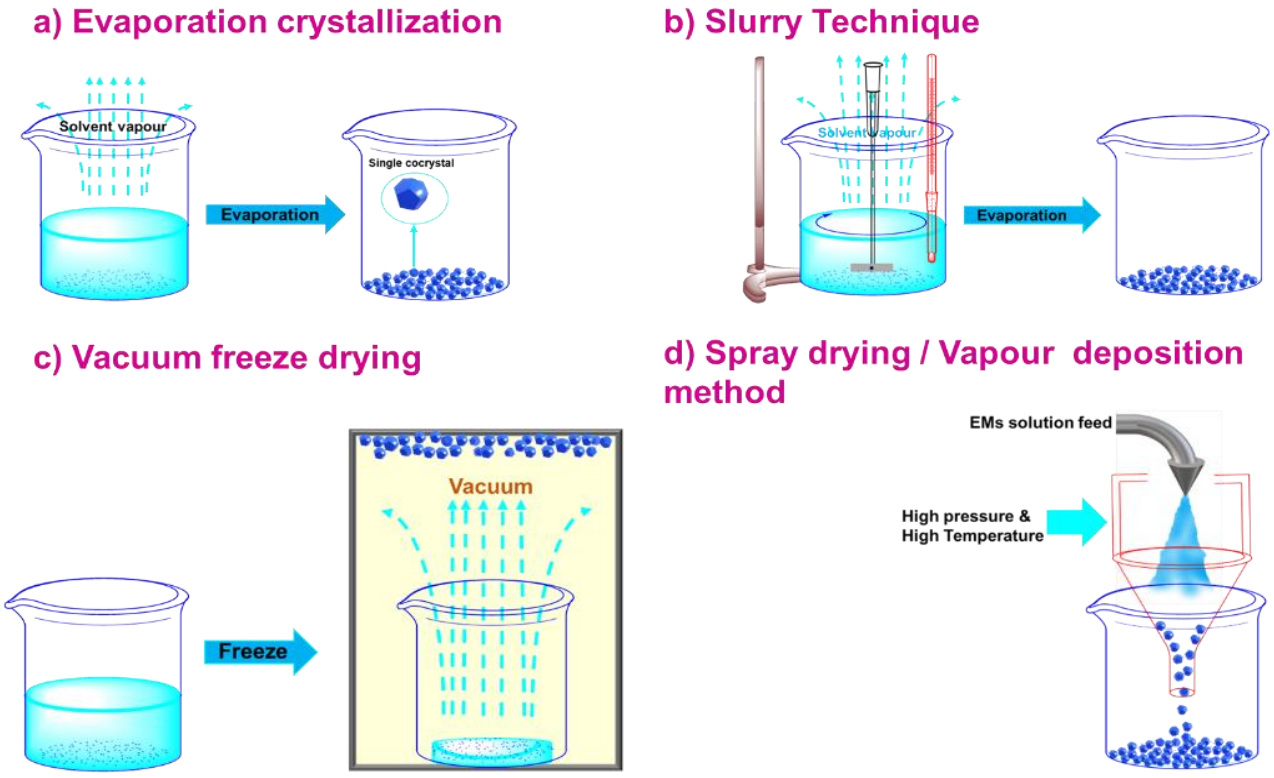

Figure 1.3 Schematic representation of different cocrystallization methods

1.4 Components shaping cocrystals - Intermolecular interactions

Usually, the individual coformers exhibits hydrogen bonding between them to form a stabilized crystal lattice. Further, several researchers found that in cocrystals the coformers connected by attractive intermolecular / interlayered electrostatic interactions[8](see Figure 4 [65]).

These interactions also help to stabilize both coformers in the single crystal lattice i.e., in cocrystal form. According to the component and structural types of the objects involved in the interactions, intermolecular interaction (noncovalent interaction) is divided into van der Waals interaction (dispersion interaction) and electrostatic interaction (Coulomb interaction). Chemically, they are also be referred to as hydrogen bonding (HB), halogen bonding, or stacking[5, 7, 60].

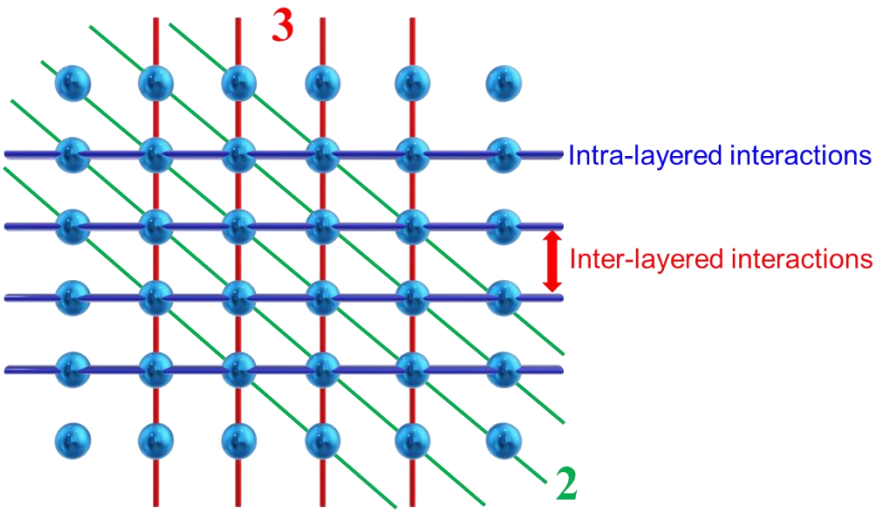

Figure 1. 4 Schematic of the intra- and inter-layered intermolecular interactions. The thickness of the lines represents the strength of intermolecular interactions: the thicker line suggests stronger interactions (Recreated from Ref. [64]).

1.4.1 Hydrogen bonding

When a molecule can act as a hydrogen bond donor, the hydrogen or hydrogens in question are characterized by relatively strongly positive molecular surface electrostatic potentials. Hydrogen bonding involves a donor and an acceptor containing an acidic hydrogen atom and an electronegative atom (N, O, F, etc.), respectively[67] (Figure 5). Hydrogen bonding consequently tends to be less directional than halogen bonding and other σ-hole interactions[68]. Hydrogen bonds can be classified based on their bond energy as weak, moderate, and strong[69]. However, in case energetic molecules are usually shortage of active hydrogen atoms and cannot form strong hydrogen bonds[68](See Figure 5 & 6).

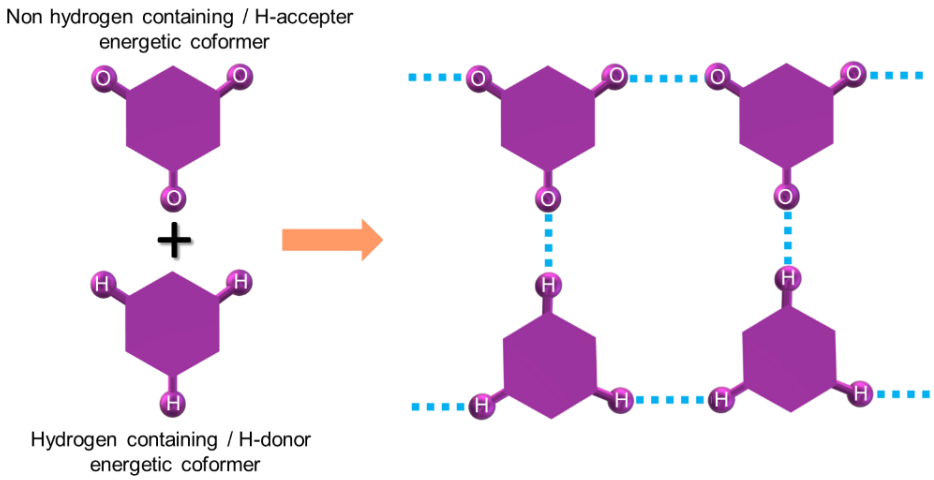

Figure 1.5 Schematic of coformers interactions in crystalline lattice one hydrogen containing energetic coformer acts as hydrogen donor and nonhydrogen containing energetic coformer hydrogen accepter with

hydrogen bonding and intermolecular interactions(as shown in Figure X2) between both coformers forms EECCs (Recreated from Ref.[70]).

Generally, strong hydrogen bonds are shorter, which strongly influences formation of stable cocrystal[71]. Not only in cocrystals, for example the complete nitration of the polyamino-arenes to its poly-nitro derivative like 1,3,5-triamino-2,4,6-trinitriobenzene (TATB) increases it chemical stability with formation of short intra- and inter-molecular H-bonding[72] (see Figure 7). Hydrogen bonds also have an obvious effect on trigger bond lengths when it undergoes cocrystallization for nitramine like HMX with MDNI[73]. In case of crowded molecule like CL-20 undergo cocrystallization with TNT, HMX, RDX, FOX-7, MDNT and TEX; primarily H-bonding formation take place -NO_2 bonds and hydrogen atoms via H · · · O or H · · · N bonds [61,62](See Figure 5 & 6). However, these H-bonding interactions in which are bonded to carbon atoms are not refereed to be hydrogen bonds, these interactions are the result of molecular packing[16](which discussed in detail section 1.4.5).

1.4.2 π -Stacking (π-π & n-π)

An intermolecular stacking between the two coformers is denoted as π-stacking if this interaction lone pair of one coformer with π-structure of other referred as n- π stacking and similarly if both π it denoted as π - π stacking. This stacking possesses a donor-accepter couple of both coformers. π -π stacking stronger, well studied whereas n -π stacking weaker and still needs to be studied actively, usually it occurs crystals stacked planar molecules with strong hydrogen doners and acceptors[5, 60, 70]. These stacking changes actively influence intermolecular arrangement and respond to stimuli via converting mechanical to intermolecular interaction energy which disperse throughout stacked layers of the EECCs - in ascending order; wavelike(layer-by-layer), crossed(caged), face-to-face (sandwich) and followed by mixed stackings[78], [79](see Figure 7). These π- stacking interactions between -NO_2 groups & aromatic rings, form herringbone-like structure via stacking groups[80]. Even though PETN, RDX, HMX, and CL-20 lack conjugated frames, their molecular stacking patterns can still be directly described using the stacking pattern of molecules that are in closer contact with one another[81].

1.4.3 van der Waals interactions

van der Waals forces one of kind of intermolecular interactions very different from the hydrogen bonds; which composed of polarization and charge transfer effects[69,70]. Normally, the distances of intermolecular forces (van der Waals interactions and HB) are in the range of 3.10–5.03 Å and 1.10–3.10 Å[84]. This interaction forces enhance bond lengths of N-NO_2 bond in EECCs interaction with aromatic coformer like DNT[85]. Also this interaction forces weaker cause frozen effect for coformers in EECCs (ΔEfrozen)[86]. Along with HBs these interactions play a key role in improving density of the EECCs.

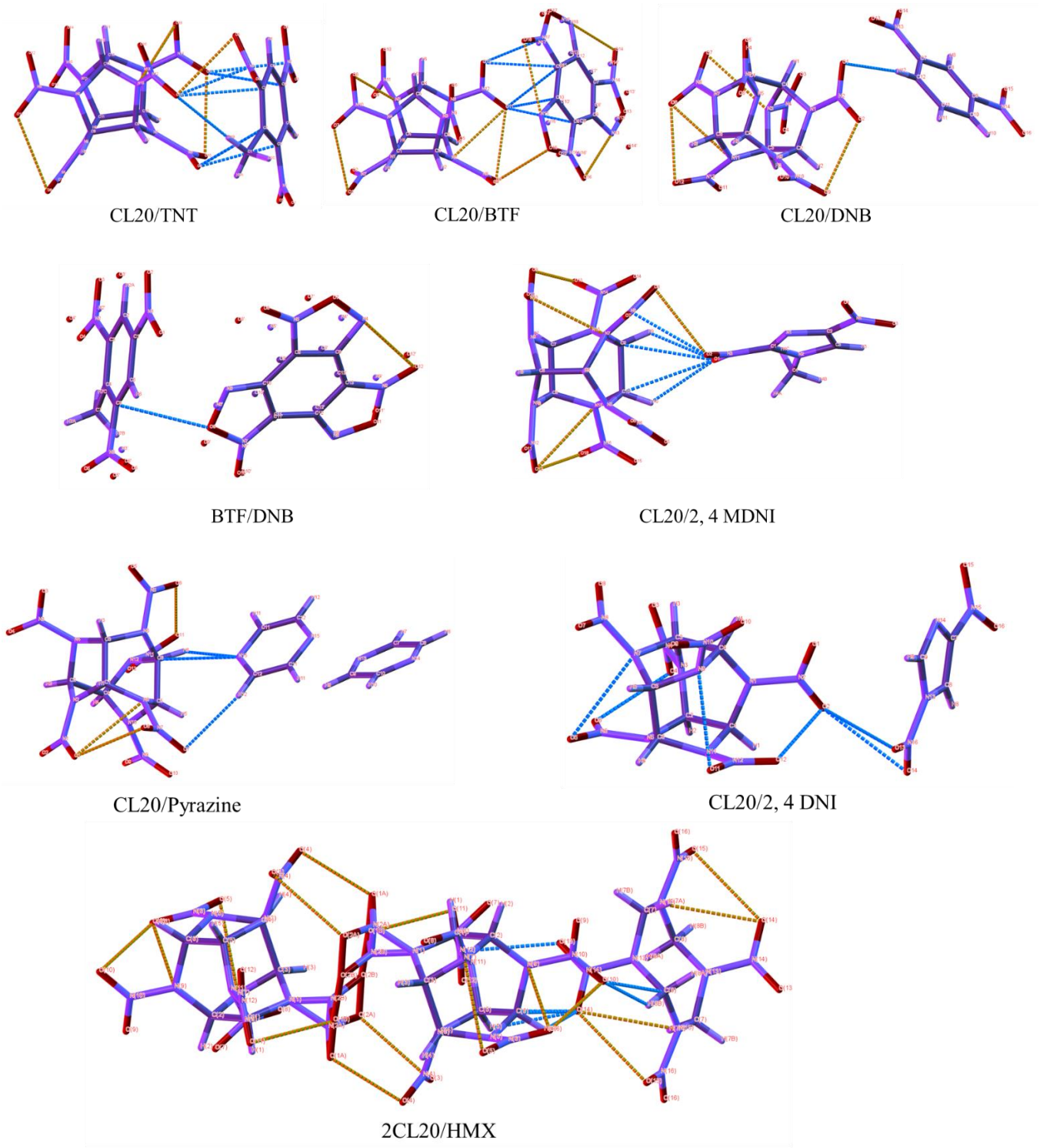

Figure 1.6 3D Single crystal XRD molecular structures of EECCs of nitramines, here, orange coloured bonds indicates pure hydrogen bonds whereas blue coloure bonds indicates electrostatic intermolecular short contacts developed between both coformers during cocrystallization. CL20/TNT[15]; CL20/BTF[16]; CL20/DNB[18]; BTF/DNB[87]; CL20/2,4 MDNI[22]; CL20/Pyrazine[27]; CL20/2,4 DNI[25] and 2CL20/HMX[48].

Van der Waals and weak steric intermolecular interactions may be the primary causes of the formation of CL-20/MTNP cocrystal as a typical example with high density. Even though hydrogen bonds are the strongest intermolecular interactions, and all others are much weaker, they all have a significant impact on the final physical properties[12].

1.4.4 Packing of structures - layered stacking, chanal stacking, caged stacking

Packing of structures plays an important role in defining sensitivity and performances of EECCs. The detonation properties, sensitivity, and other parameters of EMs are essentially determined by the packing configuration[88]. We first concentrate on the packing arrangements e.g., CL-20-based EECCs as examples, which have the same CL-20 component but various coformers[74,79].

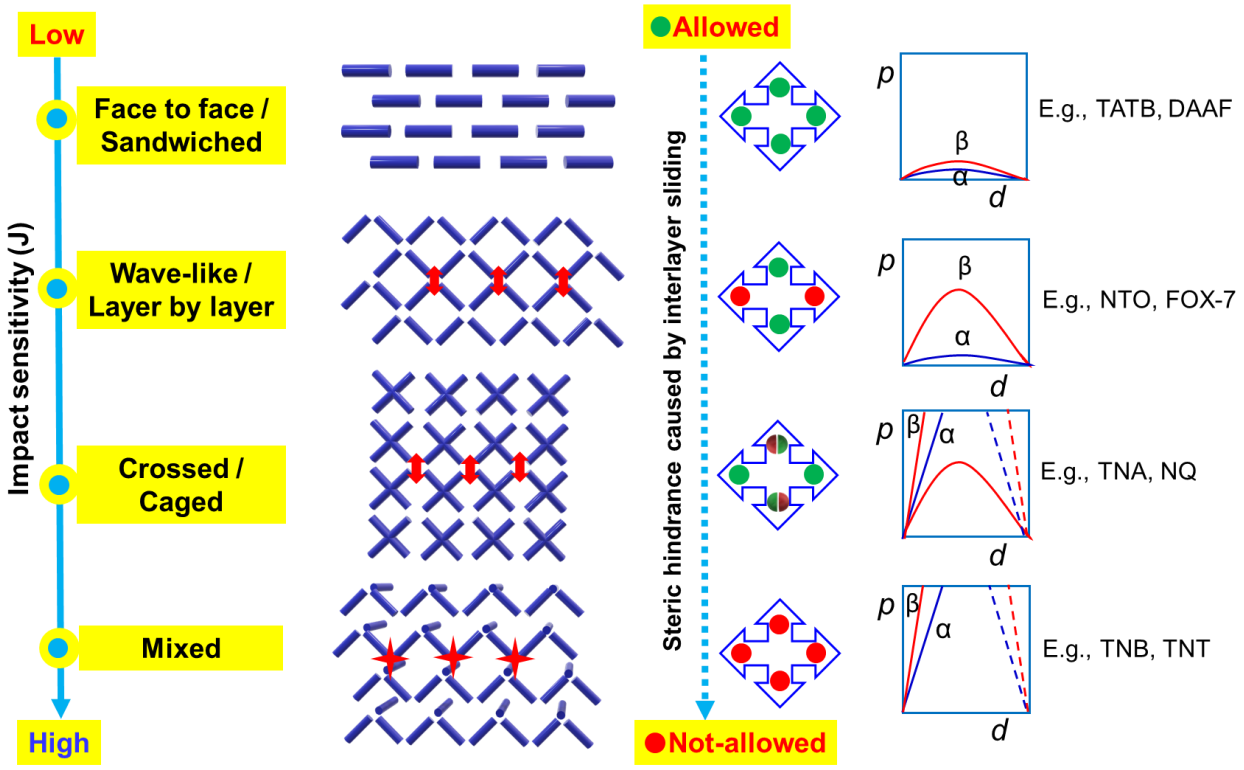

Figure 1.7 Schematic of the principle of crystal packing-impact sensitivity relationship by π-stacked energetic crystals with few suitable examples. Third column, four arrows symbolize interlayer sliding directions (right/left and up/down) of inter layer sliding allowed (green), not allowed (red) and partially allowed (red/green) of four kinds stacking. The bottom plots show packing modes and inter/intramolecular potential (p)–sliding distance (d) dependencies of four kinds of stacking. α and β denote the sliding along left/right and back/front, respectively(Recreated from Refs.[88, 89])

The strongest of these three intermolecular interactions, HB, strengthens crystal packing by enhancing interactions between component molecules, while stacking, especially face-to-face stacking, tends to reduce

the mechanical sensitivity of energetic crystals (see Figure 7). Halogen bonding is thought to be rare, but it can potentially alter the molecular stacking structure through cocrystallization[8]. Further layered packing is less sensitive[91] however if sheet-like or herring-bone lattice structures they are more sensitive similarly if its zig-zag packing makes more stable crystal lattice[80, 82]. A thorough examination using single crystal X-ray diffraction to analyze structural variables revealed the significance of weak interactions, particularly - interactions and hydrogen bonds in close packing[67]. It should be noted that packing efficiency, which may be confirmed by an analysis of packing coefficients, also adds to an EMs high density for e.g., ε-CL-20/TNT[5, 77, 84]. These are key intermolecular aspects of cocrystals briefly covered here that play an important role in crystal engineering; instead of creating new molecules with the desired properties, packing structures and physicochemical properties can be changed by manipulating existing molecules[79, 85].

1.5 Thermochemical properties of cocrystals

Thermal stability and sensitivity are our main concerns with regard to energy materials because inadequate thermal stabilities greatly restrict their application. A crucial factor in determining the thermal behavior and assessing the potential of energetic materials for real-world use is thermal analysis[94]. The cocrystal has exceptional thermal stability and a rapid rate of energy release, according to thermal studies and calculations of detonation characteristics[50]. The EECCs crystal packing and their lattice energy causes significant change in thermal behaviour[95]. Therefore, based on the observed thermal data it is differentiable as physical mixture and no clear differences in thermal stability were attributable to cocrystallization[96]. Same time significant significant inconsistence between impact sensitivity and thermal stability, or the high thermal stability does not essentially imply the low impact sensitivity[6].

1.5.1 Decomposition temperature

Continuing activity in the thermal stability needed to focus on decomposition temperatures of EECCs and compared with the pure coformer EMs. Because, it's also necessary to adopt new storage and transport conditions to avoid self-accelerating decomposition temperature(SADT)[97]. Usually, CCs exhibits decomposition at slightly lesser temperatures than that of pure coformers[30]. Some cases slight increase also takes place[98](see Figure 8). Overall the cocrystallization alters physicochemical behavior including melting and decomposition temperatures (5 – 10 C) based on intermolecular interactions and crystal packing[55](as shown in Table 4). It happens due to initial reactive products of the coformer A further reacts with coformer B heat will be carry forward and come contact with high temperature before leaving the crystal surface it makes initiation E.g., CL20/HMX[55]. However, cocrystals withstand the initial endothermic changes to a certain extent. Further detailed study of thermal behaviour at different heating

rates of EECCs found that decomposition temperature directly dependent on heating rate[30,89,90](See Figure 8).

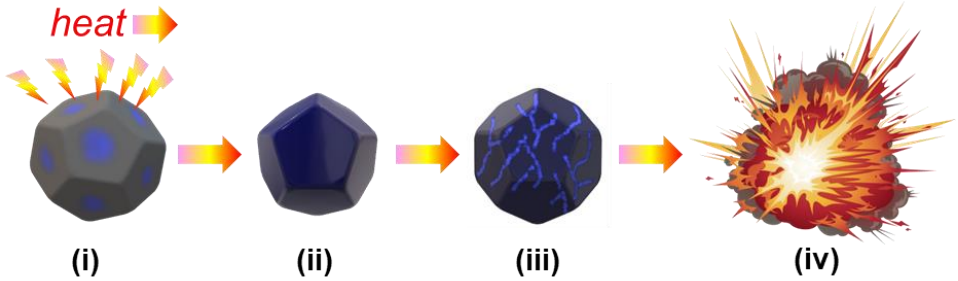

Figure 1.8 Schematic of thermal behaviour of the CCs – (i) heating of the nitramine-heat supply surround the surface of cocrystal surface; (ii) heat absorbed makes polymorphic change in nitramine crystal and coformer intermediate conversion; (iii) cracking of the nitramine crystal (for HMX, BCHMX and CL20 see in paper17); (iv) spontaneous decomposition and/or explosion[101].

The amount of decomposition products grows as the temperature rises during the thermal breakdown process, but the time to equilibrium and potential energy decrease[102]. Although, the decomposition temperature modified by certain extent selective cocrystallization with TATB is a type of explosive that is thermally stable and insensitive e.g., HMX/TATB [98].

1.5.2 Heat of combustion and Enthalpy of formation($\Delta H_{form.}$)

In order to evaluate the performance of the EECCs as part of application, enthalpy of formation($\Delta H_{form.}$) needed to calculate the on the basis of their heat of combustion measurements [103] and basis of obtained data it's possible to calculate thermochemical and detonation parameters using CHEETAH and Explo5 codes [104, 105](See Table 7). However, researchers more focused on scientific work in EECCs needed to be also technologically orientated. Usually, the mentioned calculations are carried out by using Hess law [106]. Heat release rate has a big importance for the combustion and mainly detonation performance of these EECCs; also dependents on stoichiometric ratio of coformers and reaction conditions [54, 100]. Enthalpy of formation, ΔH_{form}, indicates the energetic content EECCs; higher heat of combustion corresponds to the lower energetic content and the ΔH_{form} values with oxygen balance affect heat of detonation [13, 101]. It also follows, and confirmed, that there is a direct very good linear relationship between the heat of combustion and the experimental relative explosive strength of explosives [109]. Inert heating, thermal decomposition (or the beginning of gasification), main flame occurrence, secondary flame development, "snap-back," and establishment of steady-state combustion were all terms used to characterize the ignition process[110].

Table 1.4 Decomposition temperatures EECCs of attractive nitramines

Sr No's	Cocrystal	Decomposition Temp / °C	Technique used	Ref.
1	CL20/TNT	150	DSC	[15]
2	HMX/TATB	284.9	DSC	[46]
3	CL20/BTF	235	DSC-TG	[16]
4	CL20/HMX	240	DSC / Hot stage microscope	[111]
5	CL20/TNT	212	TGA-DSC	[17]
6	CL20/DNB	242	DSC-TG	[18]
7	CL-20/DNMT	NA	DSC	[49]
8	HMX/TATB	231.8 C	DSC-TG	[50]
9	n-K6/n-RDX	234	DSC	[37]
10	HMX/TNT	290	DSC	[38]
11	CL20/MDNT	NA	DSC	[52]
12	CL20/HMX	246.8	DSC	[40]
13	CL-20/NQ	229.3 & 257.4	DSC	[43]
14	CL20/MTNP	222	DSC	[19]
15	CL20/RDX	264.4 & 285.8	DSC	[20]
16	CL20/RDX	227	DSC	[53]
17	CL-20/2,4-MDNI	220	DSC	[22]
18	CL-20/4,5-MDNI	220	DSC	[22]
19	CL20/HMX	248	DSC	[55]
20	CL-20/DNDAP	214.2 & 243.7	DSC	[42]
21	CL-20/DNDAP	223.5 & 254.1	DSC	
22	CL20/TNP	230.1	DSC	[26]
23	RDX/TMS	244	TGA-DSC	[64]
24	RDX/HMPT	243.7	TGA-DSC	
25	CL20/4,5-MDNI	219	DSC	[112]
26	CL20/4,5-MDNI	222	DSC	
27	HMX/ANPyO	284.1	DSC	[57]
28	HMX/ANPyO	284.1	DSC	[57]
29	HMX/BTNEN	NA	DSC	[58]
30	CL-20/HMX	245.4	DSC	[60]
31	CL-20/BTF	224.1	DSC	[31]
32	DNP/DAF	211.5	TGA-DSC	[32]
33	RDX/TATB	244	DSC	[61]
34	CL-20/MTNP	133	TGA-DSC	[62]
35	HMX/NTO composite	223.75	TGA-DSC	[63]
36	NBA:AmTz, NBA:TATOT, NBA:NPTA & NBA:DAG	222, 239, 232, 310,	TGA-DSC	[113]
37	CL20/HMX/DOS	240	DSC	
38	CL20/HMX/PVAc	242	DSC	[44]
39	CL20/HMX/PVB	235	DSC	
40	TT/HNT	178	DSC	
41	TT/HDNT	251	DSC	[114]
42	TT/TNP	218	DSC	
43	HNTO/AN	NA	NA	[115]
44	TNB/1,4-DNI	84.4	DSC	[116]
45	TNB/DNMT	88.5	DSC	
46	CL-20/HMX/MF	246.5 to 250.8	NA	[117]

Combustion also depends on morphology of crystals, on porous RDX shown improved combustion properties [64]. Transition metal are commonly used as combustion catalysts, these compounds increase the efficiency of EM energy release [12]. Since more heterocycles can significantly increase the enthalpy of material formation, Since increasing heterocycles rings in molecule can significantly increase the enthalpy of formation, is also a assembling various nitrogen-rich heterocycles like pyrazole units a proven method in this area as shown in paper [118]. Recent research has looked into how thermal decomposition and combustion behavior of cocrystal are impacted by nonbonding interactions e.g., CL-20/HMX [55]. All these aspects helpful to build the groundwork for the industrial applications of EECCs by investigating their ignition and combustion mechanisms [12].

1.5.3 Crystal density

The most significant gains in energy density in the past 100 years have been achieved largely by increasing the physical crystal density of HEDMs by the use of more efficiently packed crystals with high crystal density [119]. However, excessive H atoms are disadvantageous to increase energy density because covalent H atoms usually have a lower mass density than O and N atoms, leading to a lower crystal packing density [70]. The density of the co-crystals prepared exceeds 99% of the theoretical maximum density of the starting nitramines [106]. The detonation rate of explosives is proportional to the density and thus the crystal packing of energetic materials [120] and some cases cocrystallization enhances density e.g., HMX/NTO [121] and BTF with different coformers [122]. Morphologically EECCs enhancement of crystal density indicates the decrease in explosive volume and number of cavities-defects which helpful gain detonation pressure [34, 46, 105]. Further, on other side the stacking conditions in crystal lattice of EECCs significantly contribute doing so [83] and density gained by these intermolecular interactions defined as cohesive energy density (CED) [124]. Also, crystals with p-π interactions shown good impact sensitivity with high energy density content e.g., CL20/TNT and other EECCs with CL20 [77, 93]. Generally, nitrogen rich EECCs have compact packing with strong binding strengths and packing coefficient which make them high density and energy content [92]. However cocrystals not always have higher density than their pure coformers as said before it also depends on crystal defects and morphology [125]. Overall, compared with pure EMs, EECCs have shown change physiochemical properties such as solubility, stability, and density [126].

1.6 Mechanical sensitivity of cocrystals – reaction towards external stimuli

The sensitivity of an energetic material is represented by the minimum amount of force (or energy) applied/required to an EMs that undergoes 50/50 probability of detonation from the point of view of physics of explosion. These tests key evaluation of safety handling of EECCs.

Table 1.5 Thermochemical properties - EECCs of attractive nitramines

No	Explosive Code design.	Molar ratio	Enthalpy of formation ΔH_f (kJ.mol^{-1})	Crystal Density (g.cm^{-3})	Ref
1	CL20/TNT	1:01	NA	1.84 -1.91	[15]
2	CL20/BTF	1:01	NA	1.918	[16]
3	CL20/HMX	2:01	NA	1.945	[111]
4	HMX/NMP	1:01	NA	1.571	[120]
5	CL20/TNT	1:01	NA	1.760	[127]
6	CL20/DNB	1:01	NA	1.880	[18]
7	CL20/TNT	1:01	NA	1.846	[18]
8	CL-20/DNMT	1:01	NA	1.920	[49]
9	HMX/TATB	8:01	NA	1.960	[41]
10	n-K6/n-RDX	1: 1 & 1: 2	NA	NA	[37]
11	HMX/TNT	2:1 & 3:1	NA	NA	[38]
12	CL20/HMX	2:01	NA	NA	[51]
13	CL20/MDNT	1:01	2166	1.883	[52]
14	CL-20/NQ	1:01	186.61 & 468.91	NA	[43]
15	CL20/MTNP	1:01	793.9	1.932	[19]
16	CL20/AMTN	1:01	NA	1.710	[21]
17	CL20/RDX	1:01	202.33	NA	[53]
18	CL-20/2,4-MDNI	1:01	NA	1.867	[22]
19	CL-20/4,5-MDNI	1:01	NA	1.882	[22]
20	CL20/TNT	1:01	NA	1.934	[54]
21	CL20/HMX	2:01	NA	1.961	[55]
22	CL-20/DNDAP	2:01	732	1.871	[42]
23	CL-20/ 2,4-DNI	1:01	-708	1.84 to 2.01	[34]
24	CL-20/1,4-DNI	1:01	NA	1.922	[25]
25	CL20/4,5-MDNI	1:03	NA	1.813	[112]
26	CL20/4,5-MDNI	1:01	NA	1.882	
27	HMX/ANPyO	4:01	582.4	1.940	[57]
28	HMX/ANPyO	8:01	582.4	1.920	[57]
29	HMX/BTNEN	2:01	NA	1.930	[58]
30	CL-20/TFAZ	1:01	1164.2	1.932	[29]
31	CL20/HMX	0.482-0.916 : 0.463-0.898	NA	1.954	[59]
32	CL-20/HMX	3:01	NA	1.955	[60]
33	NBA:AmTz, NBA:TATOT, NBA:NPTA & NBA:DAG	1:1, 1:2, 1:1, 1:1	NA	1.80; 1.71; 1.74; 1.76	[113]
34	CL20/HMX/DOS	Each category has five different proportions	−505 ± 13	NA	[44]
35	CL20/HMX/PVAc				
36	CL20/HMX/PVB				
37	TT/HNT	1:01	NA	1.492	[114]
38	TT/HDNT	2:01	NA	1.403	
39	TT/TNP	1:01	NA	1.703	
40	HNTO/AN	1:03	−505 ± 13	NA	[115]
41	TNB/1,4-DNI	1:01	NA	NA	[116]
42	TNB/DNMT	1:01	NA	NA	
43	CL-20/HMX/MF	2:01	NA	1.88 to 1.93	[117]
44	CL-20/MTNP	1:01	NA	NA	[62]
45	HMX/NTO composite	4.0:0.1	NA	NA	[63]
46	DNP/DAF	1:01	NA	1.68	[32]
47	DNP/DAF	1:01	NA	1.76	

Four sensitivities are generally reported for each EMs; Impact sensitivity (IS), friction sensitivity (FS), and electrostatic discharge (ESD) and sensitivity to shock wave (SSW) – the determination of the last one needs

a bigger amount of sample and relatively complicated equipment; therefore, it is not usually a part of the basic research in energetic materials. Classification of EMs is based upon the sensitivity; those sensitive to external stimuli primary explosives (IS ≤4 J; FS ≤ 10 N & ESD 0.002 - 0.020 J) while relatively insensitive secondary explosives (IS ≥4 J; FS ≥ 50N & ESD ≥ 0.1 J). Cocrystallization has shown significant effect in alteration of these sensitivities. Zeman et al studied thoroughly environmental conditions which are also responsible for sensitizing EMs [129, 130].

Molecular point of view, mechanical perturbation of intramolecular vibrations and intramolecular stretching due to initiation impulses (the latter gives rise to collective delocalized excitations – phonons) leads either to energy transfer vibrations to phonons (vibrational relaxation) or energy transfer from the phonons to vibrations (multiphonon up pumping) [131]. This disruption should go under extreme pressures and temperatures. Still, there is evidence that the first fragmentations of energetic molecules in initiation occur at conditions already milder than those prevailing at the front of the detonation wave and partially already before this front [130]. It is well-known that the phonon is one of the most important elementary excitations in solid systems as a gene related to the thermal properties and chemical stability of energetic materials, i.e., to the lattice stability, thermal properties, vibrational spectra, and initiation mechanisms Shown in Figure 1.9 [132].

The initiation of energetic materials by heat, impact, shock, friction, and electric spark should have a common mechanism of primary splitting of their molecules [133]. For the study of the listed types of the EMs initiation reactivity, the application of thermoanalytical methods is advantageous [133]. Thus, for cyclic nitramines and PBXs at their base a logarithmic relationship between impact energies and the zero-order isothermal decomposition rate constant has been described, according to which in the vast majority of cases an increasing value of this constant corresponds to an increase in the impact resistance of the investigated explosives (this relation is waiting for interpretation [130]. Similarly, the relationships between the activation energies of thermal decomposition of nitramines, on the one hand, and both the impact and friction sensitivities, on the other hand, are described [133].

In cocrystallization sensitivity of EECCs depends on the coformer EMs molecule selected to modify the targeted EMs, molar ratio, and their intermolecular interactions(Section 1.4), crystallization method(Section 1.3) as well as the obtained EECCs crystal morphology and are discussed briefly as follows (Table 6).

1.6.1 Impact sensitivity (IS)

The impact sensitivity determination primarily depends on many factors, especially the method of measurement and human error. According to theoretical and synthetic chemists, due to these aspects, corresponding outputs are not easy to correlate quantitatively with lattice parameters [129].

However, if the methodology for determining this sensitivity is strictly followed (the BAM method is predominant in the world [134], then for pure energetic materials there are logical semilogarithmic relationships of impact energies to characteristics of the pure EMs molecular structure, represented by the ^{13}C or ^{15}N NMR chemical shifts of the key atoms in reaction center of their molecules [109, 131]. In connection with the above, a linear relationship between the impact energy (impact sensitivity) and net charge of the most reactive nitro group of nitramines and polynitropolyphenylenes is also logically described [130].

The important relation of impact sensitivity to performance (volumetric explosive heat or detonation energy) or better to the energy content (enthalpy of formation or heat of combustion) of energetic materials. Licht's rule that high power is usually accompanied by increased sensitivity and that an insensitive explosive does not exhibit peak performance applies here (although there are numerous exceptions and also stated that this result is not yet supported by theory [133, 134].

In terms of the theory of Up-Pumping [131] (Figure 1.9a) there is a good correlation between the phonon vibration coupling model and the experimental impact and shock sensitivity of various secondary explosives. The more complex and denser the vibrational spectrum of the material, the greater the probability of phonon coupling with the oscillator, the faster the transfer of energy from the phonon manifold to the intramolecular vibration mode, and the more sensitive the energetic material [137].

Theoretically shear contact with surface of EECCs initiates thermal heat transfer detonation, however, practically there is significant difference between the thermal stability and impact sensitivity viz., high thermal stability does not necessarily indicates low impact sensitivity; both different characteristics depends on molecular stacking in crystal (cocrystal) [6]. The impact sensitivity of EECCs sometime “tun-on” or “turn off” depends, for e.g., HNIW/TNT [138] decreases 87% it impact with [127] and similarly in some cases of its increases [37]. Overall, in the majority of cases impact sensitivities of EECCs are decreased and this phenomenal change made cocrystallization interesting for researchers. It’s also confirmed that crystal packing-stacking pattern influence on impact; doing so π−π stacking play important role EECCs achieve low impact [5, 116].

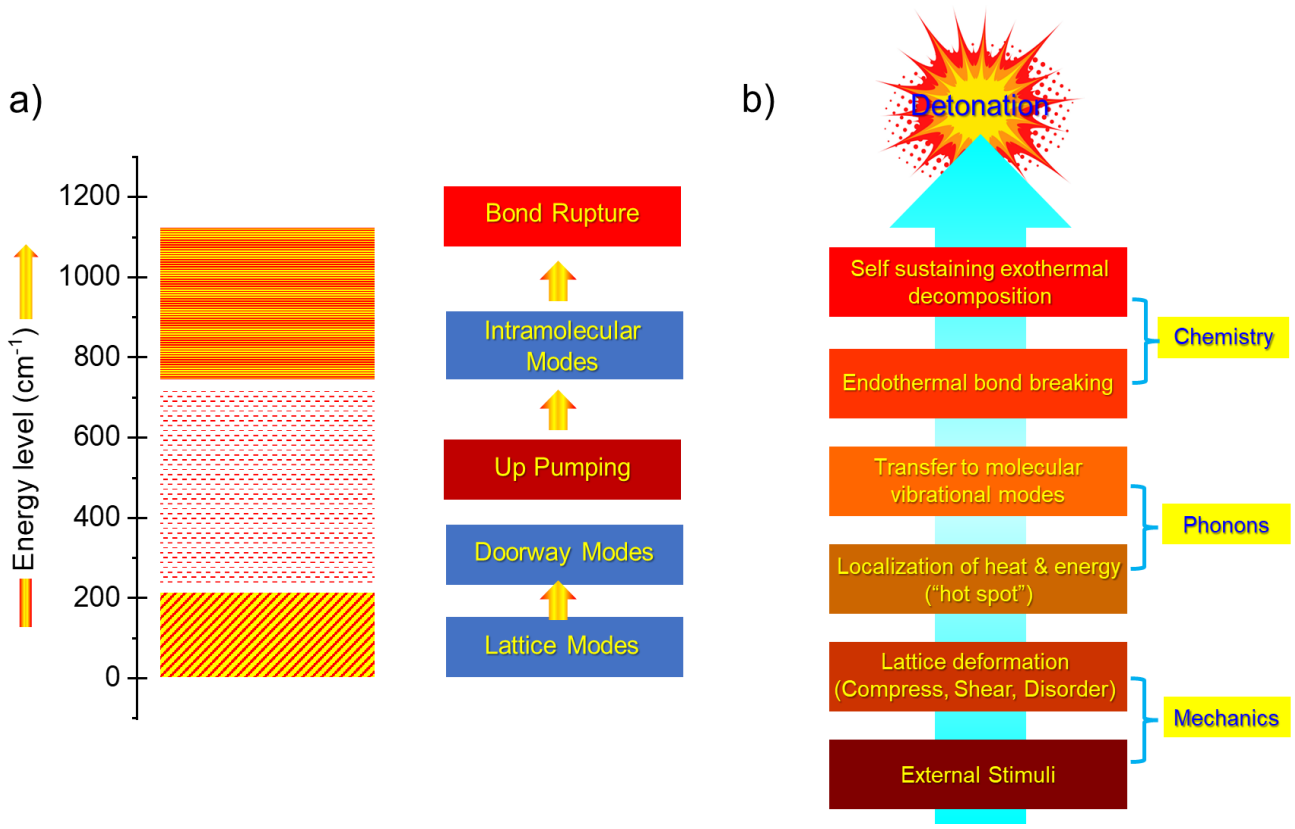

Figure 1.9 a) Schematic diagram of the phonon up-pumping theory: external stimuli excite mechanical energy transfer into doorway modes and then doorway modes up-pump to intramolecular vibrations, which cause initiation; and b) Schematic diagram of shock-induced detonation mechanism of energetic crystals (recreated from Ref. [132])

1.6.2 Friction sensitivity (FS)

FS measurement for EECCs, to note that that typical friction generated while handling these which potentially initiate detonation and must be needed for those EECCs IS closer to primary explosives and it highly dependent on equipment operator. Sometimes EMs are quite insensitive however they are more sensitive to friction especially energetic salts. FS is also dependent morphology and size of CCs for e.g., β HMX, nano-CCs [140]. HMX/CL20, CL20/RDX shown significant drop in impact and friction sensitivities [11, 42, 50]. Similarly, EMs with metal oxides like CuO, ZnO with HMX shown reduction in IS however enhancements in FS [98]. Like IS, FS for EECCs shown lower than their pure coformers which exhibited rich hydrogen bonds and π-π stacking [6].

Table 1.6 Sensitivities EECCs of attractive nitramines

Sr No	Energetic Cocrystals (ECCs)	Impact sensitivity (J)			Friction sensitivity (%)			Electric spark sensitivity			Ref.
	(A:B)	A	B	ECCs (A:B)	A	B	ECCs (A:B)	A	B	ECCs (A:B)	
1	CL20/TNT	13.54	NA	28.52	NA	NA	NA	NA	NA	NA	[15]
2	HMX/TATB	100 %	NA	10%	NA	NA	NA	NA	NA	NA	[46]
3	CL20/TNT, CL20/HMX	NA	NA	NA	NA	NA	NA	NA	NA	NA	[47]
4	CL20/HMX	1.42	NA	2.67	NA	NA	NA	NA	NA	NA	[111]
5	CL20/TNT	13	103	30	100	0	58	NA	NA	NA	[127]
6	CL20/DNB	NA	NA	9.212	NA	NA	NA	NA	NA	NA	[18]
7	CL20/TNT	NA	NA	6.86	NA	NA	NA	NA	NA	NA	[18]
8	CL20/DNMT	12.838	>49	12.495	72	252	120	20/20 @ 0.051J	20/20 @ 0.025J	20/20 @ 0.025J	[49]
9	HMX/TATB	2.25	3	3	NA	NA	NA	NA	NA	NA	[128]
10	n-K6/n-RDX	<1.56	2.05	3.03	72	180	168	0.158	0.359	0.246	[37]
11	HMX/TNT	4.802	36.652	15.215	NA	NA	NA	NA	NA	NA	[38]
12	CL20/MDNT	19.6	5.1352	4.998	72	128	120	20/20 @0.05J	20/20 @0.5J	20/20 @0.025 J	[52]
13	CL20/HMX	3.209	4.802	11.588	100	84	64	NA	NA	NA	[40]
14	CL20/HMX	NA	NA	>78.6	NA	NA	NA	NA	NA	NA	[41]
15	CL20/MTNP	4	24.5	6	94	240	180	272	253	276	[19]
16	CL20/RDX	13.6	49.8	29.4	100	80	80	NA	NA	NA	[20]
17	CL20/AMTN	3.43	25.24	10.54	NA	NA	NA	NA	NA	NA	[21]
18	CL20/RDX	7.35	20.408	25.2	100	74	56	NA	NA	NA	[53]
19	CL20/TNT	3.185	23.275	10535	100	49	38	NA	NA	NA	[54]
20	CL20/HMX	5.488	9.8	9.4	84-90	190-200	300-330	NA	NA	NA	[55]
21	CL-20/DNDAP	2.55	17.052	5.88	100	8	48	NA	NA	NA	[42]
22	CL20/TNT	4	15	7.5	NA	NA	NA	NA	NA	NA	[35]
23	CL20/DNB	4	39	9	NA	NA	NA	NA	NA	NA	[35]
24	CL20/TNB	4	14	8	NA	NA	NA	NA	NA	NA	[35]
25	CL-20/ 2,4-DNI	9.099	>49.01	29.57	120	>360	>360	NA	NA	NA	[34]
26	CL-20/1,4-DNI	2.5	14	10	NA	NA	NA	NA	NA	NA	[25]
27	CL-20/TNT	6.37	45.08	19.11	100%	4%	68%	NA	NA	NA	[56]
28	CL20/4,5-MDNI	2.5	34	16	NA	NA	NA	NA	NA	NA	[112]
29	CL20/4,5-MDNI	2.5	34	11	NA	NA	NA	NA	NA	NA	
30	HMX/ANPyO	4	24	8	NA	NA	NA	NA	NA	NA	[57]
31	HMX/ANPyO	4	24	10	NA	NA	NA	NA	NA	NA	[57]
32	CL-20/TFAZ	2.548	16.464	8.232	100%	4%	38%	NA	NA	NA	[29]
33	CL-20/HMX	10	NA	>20	80	144	168	NA	NA	NA	[60]
34	CL-20/MTNI	4	13	10	95	360	360	NA	NA	NA	[30]
35	RDX/TATB	6	NA	17.5	NA	NA	216	NA	NA	NA	[61]

Table 6. Continued…

Sr No	Energetic Cocrystals (ECCs)	Impact sensitivity (J)			Friction sensitivity (%)			Electric spark sensitivity			Ref
	(A:B)	A	B	ECCs (A:B)	A	B	ECCs (A:B)	A	B	ECCs (A:B)	
36	NBA:AmTz, NBA:TATOT, NBA:NPTA & NBA:DAG	NA	NA	>40 (All)	NA	NA	>360 (All)	NA	NA	NA	[113]
37	CL20/HMX/DOS	NA	NA	6.419-14.896	NA	NA	NA	NA	NA	NA	[44]
38	CL20/HMX/PVAc	NA	NA		NA	NA		NA	NA	NA	
39	CL20/HMX/PVB	NA	NA		NA	NA		NA	NA	NA	
40	1:1 TT/HNT	NA	NA	24	NA	NA	80	NA	NA	NA	
41	2:1 TT/HDNT	NA	NA	>40	NA	NA	168	NA	NA	NA	[114]
42	1:1 TT/TNP	NA	NA	32	NA	NA	112	NA	NA	NA	
43	HNTO/AN	NA	NA	NA	NA	NA	NA	NA	NA	NA	[115]
44	TNB/1,4-DNI	NA	14	18	NA	NA	NA	NA	NA	NA	[116]
45	TNB/DNMT	NA	20	22	NA	NA	NA	NA	NA	NA	
46	CL-20/HMX/MF	NA	NA	5 to 15	NA	NA	NA	NA	NA	NA	[117]
47	CL-20/MTNP	NA	NA	4 to 28	NA	NA	60 to 100	NA	NA	NA	[62]
48	HMX/NTO	NA	NA	44%	NA	NA	40%	NA	NA	NA	[63]
59	DNP/DAF	NA	NA	> 40	NA	NA	128	NA	NA	NA	[32]

1.6.3 Electrostatic spark discharge (ESD)

ESD measurement for EECCs based on requirement, to note that that typical static electricity build-up from everyday activities is in the range of a few millijoules and therefore could potentially initiate detonation and also realize their ESD initiation as technological applications. EECCs π-electrons excitation effectively causes ESD response, as IS and FS like π-stacking play significant role in ESD too [6].

Morphologically porous crystals with air gaps can be able to exhaust more energy of ESD spark, e.g., porous RDX and its effectively drops with decrease particle size [64]. In addition to researchers also studied detail the external electric field influence on the EECCs, found that -NO_2 groups triggering bond on the molecular surface field i.e., electric field gradually increases, the charge of the nitro group gradually increases, indicating that the sensitivity of the EECCs increases [67, 119]. Applied electric field the trigger the bond such way that the direction of applied positive electric field defined as N → NO_2 and same time applied negative electric field NO_2 → N [141] (See Figure 1.10). Keeping in mind the technological applications, sensitivity of EECCs is an significant standard to estimation the safety and it is mainly defined as the probability for these modified EMs to be exploded or ignited once subjected to external stimuli, including IS, FS, ESD, shock waves, high temperature, flame combustion etc. [142].

Decreasing the electric spark sensitivity (i.e. increasing the EES values), when the grain size of nitramines' crystals increases, confirms the idea by Auzanneau et al. [143] about the mechanism of spark energy transfer into the powdered reactive solid, i.e., in this case, to decrease the number of inter grain points in a volume

unit. However, there are also dislocations in the crystals that should have some effect on this type of energetic material initiation [142, 143].

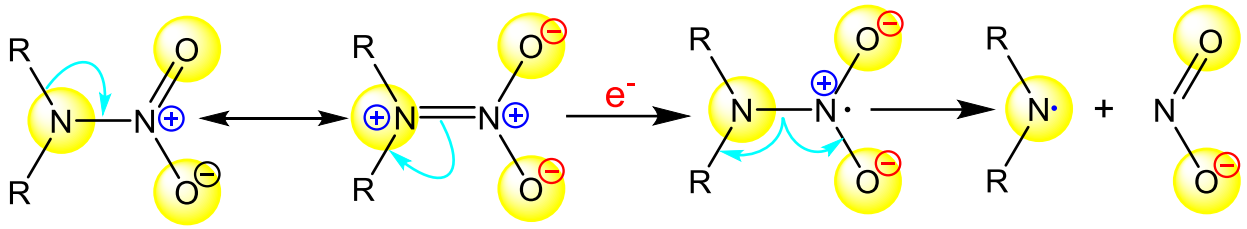

Figure 1.10 Schematic of electron attack on the nitramine grouping producing an aza-radical and a nitrite anion (the first step in the nitramine electro-reduction)(recreated from Ref. [146]).

1.7 Detonation properties of cocrystals

Detonation parameters detonation velocity (*D*), detonation pressure (*P*), and detonation energy (E) are key parameters to evaluate the performance of EECCs (Table 7). Once achieving safer in sensitive EECCs it needed to evaluate their performance to comply with of technological application suitability [119]. Initial assessment these parameters predicted software codes like CHEETAH and EXPLO5, using the JCZ3 equation of state [66, 121, 122]. and by Kamlet and Jacob equations approach [149]. This key parameter decides the EECCs alteration of their detonation power and effectiveness as like its initial coformers. D and P will be affected by cocrystallization, packing density of EECCs lower further it directly influences viz., higher density more promising EMs D and also it varies with molar ratios of the coformers chosen for EECCs preparations [64, 105].

However, the detonation velocities of mixture of the explosives would be generally higher than what would correspond to the percentage of the components in these mixtures [150] which often valid for EECCs also [109, 124, 125], in some cases these properties are increased [16]. Another way it can described it achieve safety and morphological suitability of EECCs needed to adjust with detonation properties slightly, however its negligible. It occurs due to the binding energy, trigger bond energy, trigger bond length, cohesive energy density of EECCs [153]. Earlier reported results showed that difference in detonation velocities between the EECCs and physical mix, the crystal structure and resultant coformer bond energy contribute to the observed difference in detonation velocities [104]. Also, researchers studied crystals orientation dependence, (0 1 0) crystal orientation is more stable, the binding energies of the three crystal orientations are (0 1 0) > (0 0 0) > (0 0 1) > (1 0 0). The detonation performance of PBXs will likely be compromised given the decrease in density and detonation characteristics [153].

Table 1.7 Detonation properties of EECCs of attractive nitramines

Sr No	Energetic Cocrystals (ECCs)	Detonation velocity, D (m s^{-1})			Detonation pressure, P (GPa)			Ref.
	(A:B)	A	B	ECCs (A:B)	A	B	ECCs (A:B)	
1	CL20/BTF	9385	8425	8969	44.9	34.3	39.1	[16]
2	CL20/TNT	8770	6712	8426	36.1	19.1	28.7	[127]
3	CL20/DNB	9386	5840	8434	45.09	14.18	34.07	[18]
4	CL20/TNT	9386	NA	8466	45.09	NA	33.8	[18]
5	CL20/MTNP	9406	8650	9347	44.6	33.7	40.5	[19]
6	CL20/AMTN	10117	7108	8863	NA	NA	NA	[21]
7	CL-20/2,4-MDNI	NA	NA	8839	NA	NA	34.82	[22]
8	CL-20/4,5-MDNI	NA	NA	8919	NA	NA	35.69	[22]
9	CL20/TNT	8426	6854	8631	NA	NA	NA	[54]
10	CL-20/DNDAP	9570	7430	8997	44.3	23.4	37.5	[42]
11	CL-20/TFAZ	9570	8416	9103	44.3	32.9	37.2	[29]
12	CL-20/ 2,4-DNI	9687	8136	9324	46	28.1	39.2	[34]
13	CL-20/1,4-DNI	NA	NA	9242	NA	NA	39.01	[25]
14	CL20/4,5-MDNI	9386	7455	8604	45.02	23.68	34.45	[112]
15	CL20/4,5-MDNI	9386	7455	8972	45.02	23.68	38.59	
16	HMX/ANPyO	9277	6810	9444	39.87	15.46	41.03	[25]
17	HMX/ANPyO	9277	6810	9387	39.87	15.46	40.44	[25]
18	HMX/BTNEN	8820	9460	9380	38.54	43.46	42.95	[58]
19	CL-20/TFAZ	9570	8416	9103	44.3	32.9	37.2	[29]
20	CL20/HMX	NA	NA	NA	NA	NA	NA	[59]
21	CL-20/HMX	NA	NA	NA	NA	NA	NA	[60]
22	CL-20/MTNI	9767	8360	9093	44.83	30.49	37.46	[30]
23	NBA:AmTz, NBA:TATOT, NBA:NPTA & NBA:DAG	NA	NA	7280; 7521; 6837; 7685	NA	NA	19.5; 19.7; 17.0; 20.9	[113]
24	1:1 TT/HNT	NA	NA	6091	NA	NA	NA	
25	2:1 TT/HDNT	NA	NA	5884	NA	NA	NA	[114]
26	1:1 TT/TNP	NA	NA	6903	NA	NA	NA	
27	HNTO/AN	NA	NA	NA	NA	NA	NA	[115]
28	TNB/1,4-DNI	7277	NA	7704	22.4	NA	26.08	[116]
29	TNB/DNMT	7277	NA	7709	22.4	NA	22.4	
30	CL-20/HMX/MF	NA	NA	9200 to 9250	NA	NA	NA	[117]
31	CL-20/MTNP	NA	NA	9347	NA	NA	40.5	[62]
32	HMX/NTO composite	NA	NA	NA	NA	NA	NA	[63]
33	DNP/DAF	NA	NA	NA	NA	NA	NA	[32]

In C-NO_2 linkages needs more energy to decompose and detonate than the N-NO_2 linkages [154], it needs taken care while selecting coformers all these facts to obtain better performing EECCs for military weapons as well as civil applications. Detonation velocity and detonation pressure are only weakly dependent upon the detonation heat released, it is typically the case for single-component explosives that a high heat of detonation is accompanied usually by a high sensitivity [69, 129]. In other words, increasing the fraction of

the EM coformer with the highest heat of detonation does not improve the detonation performance (P and D) for some EECCs [155].

So, overall, it directs our interest cocrystallization is attractive strategy to produce decreased sensitivities which helps to avoid accidental detonation with maintaining the detonation properties. However, these methodologies still hold some intriguing challenges when it comes to large scale synthesis and are discussed in next section

1.8 Technological challenges in preparation of cocrystals of EMs – Current research problem.

Despite the widespread use of the cocrystallization approach in the field of EMs, certain investigations are still in the exploratory phase, and as a result, some more difficult problems are awaiting solutions [11, 81]. In matter of fact, cocrystallization given credible productive and cost effective way to tuning energetic properties of existing EMs instead of undergoing or switching to new molecules synthesis. However, these crystal engineering techniques are fraught with challenges when comes to large preparation to employ defense and civil applications. Although as discussed in section 1.3, each method of preparation holds it clause and benefits, researchers in their open to read publications, are more focused on the scientific part with laboratory scale due to the EMs availability and their processing laboratory capacity.

The more important challenge here is scalability, when it comes to large scale synthesis methods can give good quality of crystals, and at the same time they are possibly undergo nucleation and its complex maintain required application crystalline sizes [52]. Achieving effective EECCs with holding their energy density/ bulk density, safety, and performance as required for the application is also challenging task [11, 90, 130]. Especially come to their physiochemical with detonation properties it must be fulfilled their inherent high sensitivity and high reactivity contribution EECCs is leads to energy – safety contradiction, same time it needed to be stabilized [47, 48, 126, 131]. Also, sometime during the preparation solubility of coformers generally leads to two kinds of crystals with recrystallization without undergoing cocrystallization [11]. Similarly, morphology of EECCs end up with rod like or needle like structures which makes them incompetent to use in applications [158]. There are still few barriers in this field's future, but there is no denying that cocrystallization technology will be crucial to the creation of the newest forms of EMs, pyrotechnics, and for propellants additives [91]. Keeping these all aspects the preparation of EECCs as per current applications requirement, is challenging and tedious endeavor; it made to us look into alternative optimized method or modification existing method which can be able to helpful in production of EECCs in large scale.

At Institute of Energetic Materials, University of Pardubice we tried created and optimized method to modify the EMs finally developed universal strategy up with slurry based coagglomeration in solution state which is more compatible safety wise as well to more effective in tuning energy – safety parameters with controlling their morphology too. Structure property relationships needed to address as point of EECCs with respect their conformers, it will play very crucial role as backup data and justification to scale up [80, 97]. The coagglomeration method (section 2) fulfilled all these challenges successfully developed around 50+ agglomerated crystals (CACs) which form EECCs, and some interesting results have been briefly presented in upcoming chapter 3.

References

[1] J. P. Agrawal, High Energy Materials: Propellants, Explosives and Pyrotechnics, 1st ed. Wiley, 2010. doi: 10.1002/9783527628803.

[2] Ahmed Ikhlas, Mohamed Elbeih, Adela Husarova, Svatopluk Zeman, "Method of preparation of ε-2,4,6,8,10,12-hexanitro-2,4,6,8,10,12-hexaazaisowurtzitane with reduced impact sensitivity," WO2013044891A1, Apr. 04, 2013

[3] T. Deplancke, O. Lame, F. Rousset, I. Aguili, R. Seguela, and G. Vigier, "Diffusion versus Cocrystallization of Very Long Polymer Chains at Interfaces: Experimental Study of Sintering of UHMWPE Nascent Powder," Macromolecules, vol. 47, no. 1, pp. 197–207, Jan. 2014, doi: 10.1021/ma402012f.

[4] S. Aitipamula et al., "Polymorphs, Salts, and Cocrystals: What's in a Name?," Crystal Growth & Design, vol. 12, no. 5, pp. 2147–2152, May 2012, doi: 10.1021/cg3002948.

[5] J. Bennion, A. McBain, S. Son, and A. Matzger, "Design and Synthesis of a Series of Nitrogen-Rich Energetic Cocrystals of 5,5 '-Dinitro-2H,2H '-3,3 '-bi-1,2,4-triazole (DNBT)," Crystal Growth & Design, vol. 15, no. 5, pp. 2545–2549, May 2015, doi: 10.1021/acs.cgd.5b00336.

[6] R. Bu, Y. Xiong, and C. Zhang, "pi-pi Stacking Contributing to the Low or Reduced Impact Sensitivity of Energetic Materials," Crystal Growth & Design, vol. 20, no. 5, pp. 2824–2841, May 2020, doi: 10.1021/acs.cgd.0c00367.

[7] J. Bennion and A. Matzger, "Development and Evolution of Energetic Cocrystals," Accounts of Chemical Research, vol. 54, no. 7, pp. 1699–1710, Apr. 2021, doi: 10.1021/acs.accounts.0c00830.

[8] G. Liu, S. Wei, and C. Zhang, "Review of the Intermolecular Interactions in Energetic Molecular Cocrystals," Crystal Growth & Design, vol. 20, no. 10, pp. 7065–7079, Oct. 2020, doi: 10.1021/acs.cgd.0c01097.

[9] C. Ren, H. Liu, X. Li, and L. Guo, "Decomposition mechanism scenarios of CL-20 co-crystals revealed by ReaxFF molecular dynamics: similarities and differences," Physical Chemistry Chemical Physics, vol. 22, no. 5, pp. 2827–2840, Feb. 2020, doi: 10.1039/c9cp06102a.

[10] R. Feng, S. Zhang, F. Ren, R. Gou, and L. Gao, "Theoretical insight into the binding energy and detonation performance of epsilon-, gamma-, beta-CL-20 cocrystals with beta-HMX, FOX-7, and DMF in different molar ratios, as well as electrostatic potential," Journal of Molecular Modeling, vol. 22, no. 6, Jun. 2016, doi: 10.1007/s00894-016-2998-9.

[11] R. Wiscons and A. Matzger, “Evaluation of the Appropriate Use of Characterization Methods for Differentiation between Cocrystals and Physical Mixtures in the Context of Energetic Materials,” Crystal Growth & Design, vol. 17, no. 2, pp. 901–906, Feb. 2017, doi: 10.1021/acs.cgd.6b01766.

[12] Z. Xue, B. Huang, H. Li, and Q. Yan, “Nitramine-Based Energetic Cocrystals with Improved Stability and Controlled Reactivity,” Crystal Growth & Design, vol. 20, no. 12, pp. 8124–8147, Dec. 2020, doi: 10.1021/acs.cgd.0c01122.

[13] N. Liu et al., “Rapid and High-Yielding Formation of CL-20/DNDAP Cocrystals via Self-Assembly in Slightly Soluble-Medium with Improved Sensitivity and Thermal Stability,” Propellants Explosives Pyrotechnics, vol. 44, no. 10, pp. 1242–1253, Oct. 2019, doi: 10.1002/prep.201900053.

[14] J. Zhang, J. Hooper, J. Zhang, and J. Shreeve, “Well-balanced energetic cocrystals of H5IO6/HIO3 achieved by a small acid-base gap,” Chemical Engineering Journal, vol. 405, Feb. 2021, doi: 10.1016/j.cej.2020.126623.

[15] O. Bolton and A. J. Matzger, “Improved Stability and Smart-Material Functionality Realized in an Energetic Cocrystal,” Angew. Chem. Int. Ed., vol. 50, no. 38, pp. 8960–8963, Sep. 2011, doi: 10.1002/anie.201104164.

[16] Z. Yang et al., “Characterization and Properties of a Novel Energetic–Energetic Cocrystal Explosive Composed of HNIW and BTF,” Crystal Growth & Design, vol. 12, no. 11, pp. 5155–5158, Nov. 2012, doi: 10.1021/cg300955q.

[17] S. M. Aldoshin et al., “Structure and properties of cocrystals of trinitrotoluene and 2,4,6,8,10,12-hexanitro-2,4,6,8,10,12-hexaazaisowurtzitane,” Russ Chem Bull, vol. 62, no. 6, pp. 1354–1360, Jun. 2013, doi: 10.1007/s11172-013-0192-0.

[18] Y. Wang et al., “A Novel Cocrystal Explosive of HNIW with Good Comprehensive Properties,” Propellants, Explosives, Pyrotechnics, vol. 39, no. 4, pp. 590–596, Aug. 2014, doi: 10.1002/prep.201300146.

[19] Q. Ma et al., “A novel multi-nitrogen 2,4,6,8,10,12-hexanitrohexaazaisowurtzitane-based energetic co-crystal with 1-methyl-3,4,5-trinitropyrazole as a donor: experimental and theoretical investigations of intermolecular interactions,” New Journal of Chemistry, vol. 41, no. 10, pp. 4165–4172, May 2017, doi: 10.1039/c6nj03976f.

[20] H. Gao et al., “Synthesis and Characterization of a New Co-Crystal Explosive with High Energy and Good Sensitivity,” Journal of Energetic Materials, pp. 1–9, Feb. 2017, doi: 10.1080/07370652.2017.1290712.

[21] X. Zhang et al., “A novel cocrystal composed of CL-20 and energetic ionic salt,” Chem. Commun., vol. 54, pp. 13268–13270, doi: https://doi.org/10.1039/C8CC06540C.

[22] Z. Yang et al., “Isomeric Cocrystals of CL-20: A Promising Strategy for Development of High-Performance Explosives,” Crystal Growth & Design, vol. 18, no. 11, pp. 6399–6403, Nov. 2018, doi: 10.1021/acs.cgd.8b01068.

[23] S. Zhu, S. Zhang, R. Gou, C. Wu, G. Han, and H. Jia, “Understanding the Effect of Solvent on the Growth and Crystal Morphology of MTNP/CL-20 Cocrystal Explosive: Experimental and Theoretical Studies,” Crystal Research and Technology, vol. 53, no. 4, p. 1700299, Apr. 2018, doi: 10.1002/crat.201700299.

[24] S. Sun et al., “Transitions from Separately Crystallized CL-20 and HMX to CL-20/HMX Cocrystal Based on Solvent Media,” Crystal Growth & Design, vol. 18, no. 1, pp. 77–84, Jan. 2018, doi: 10.1021/acs.cgd.7b00775.

[25] Y. Tan et al., “High Energy Explosive with Low Sensitivity: A New Energetic Cocrystal Based on CL-20 and 1,4-DNI,” Crystal Growth & Design, vol. 19, no. 8, pp. 4476–4482, Aug. 2019, doi: 10.1021/acs.cgd.9b00250.

[26] S. Sun et al., “Design, preparation, characterization and formation mechanism of a novel kinetic CL-20-based cocrystal,” Acta Crystallogr B Struct Sci Cryst Eng Mater, vol. 75, no. 3, pp. 310–317, Jun. 2019, doi: 10.1107/S2052520619002816.

[27] T. Fei, P. Lv, Y. Liu, C. He, C. Sun, and S. Pang, “Design and Synthesis of a Series of CL-20 Cocrystals: Six-Membered Symmetrical N-Heterocyclic Compounds as Effective Coformers,” Crystal Growth & Design, vol. 19, no. 5, pp. 2779–2784, May 2019, doi: 10.1021/acs.cgd.8b01923.

[28] Y. Liu, P. Lv, C. Sun, and S. Pang, “Syntheses, Crystal Structures, and Properties of Two Novel CL-20-based Cocrystals,” Zeitschrift fur Anorganische und Allgemeine Chemie, vol. 645, no. 8, pp. 656–662, Apr. 2019, doi: 10.1002/zaac.201900017.

[29] N. Liu, B. H. Duan, X. M. Lu, and B. Z. Wang, “Investigation of CL-20/TFAZ cocrystal: preparation, structure and performance,” J. Phys.: Conf. Ser., vol. 1721, no. 1, p. 012005, Jan. 2021, doi: 10.1088/1742-6596/1721/1/012005.

[30] P. Lian, L. Zhang, H. Su, J. Chen, L. Chen, and J. Wang, “A novel energetic cocrystal composed of CL-20 and 1-methyl-2,4,5-trinitroimidazole with high energy and low sensitivity,” Acta Crystallogr B Struct Sci Cryst Eng Mater, vol. 78, no. 2, pp. 133–139, Apr. 2022, doi: 10.1107/S2052520622000245.

[31] Y. Yin, J. Wang, J. Chen, J. Sun, and H. Sui, “Thermal Kinetics of Energetic CL-20/BTF Cocrystal Induced by Strong Intermolecular Coupling,” J. Phys. Chem. C, vol. 126, no. 19, pp. 8199–8207, May 2022, doi: 10.1021/acs.jpcc.1c05812.

[32] Q.-N. Tariq et al., “Synthesis, Performance, and Thermal Behavior of Two Insensitive 3,4-Dinitropyrazole-Based Energetic Cocrystals,” Crystal Growth & Design, vol. 23, no. 1, pp. 112–119, Jan. 2023, doi: 10.1021/acs.cgd.2c00809.

[33] B. Risse, D. Spitzer, F. Pessina, “Method For producing Cocrystals by means of Flash evaporation,” PCT/EP2015/065.335, Jan. 03, 2017

[34] J. Liu, Z. Yan, D. Chi, and L. Yang, “Synthesis of the microspheric cocrystal CL-20/2,4-DNI with high energy and low sensitivity by a spray-drying process,” New J. Chem., vol. 43, no. 44, pp. 17390–17394, 2019, doi: 10.1039/C9NJ04731J.

[35] C. Huang et al., “High-Yielding and Continuous Fabrication of Nanosized CL-20-Based Energetic Cocrystals via Electrospraying Deposition,” Crystal Growth & Design, vol. 18, no. 4, pp. 2121–2128, Apr. 2018, doi: 10.1021/acs.cgd.7b01568.

[36] M. L. Levinthal, “Propellant made with corystals of cyclotetramethyenetetramine and ammonium per chlorate,” 4086110, Apr. 25, 1978

[37] L. Blas, M. Klaumünzer, F. Pessina, S. Braun, and D. Spitzer, “Nanostructuring of Pure and Composite-Based K6 Formulations with Low Sensitivities,” Propellants, Explosives, Pyrotechnics, vol. 40, no. 6, pp. 938–944, Dec. 2015, doi: 10.1002/prep.201500187.

[38] H. Li, C. An, W. Guo, X. Geng, J. Wang, and W. Xu, “Preparation and Performance of Nano HMX/TNT Cocrystals,” Propellants Explosives Pyrotechnics, vol. 40, no. 5, pp. 652–658, Oct. 2015, doi: 10.1002/prep.201400175.

[39] D. Doblas, M. Rosenthal, M. Burghammer, D. Chernyshov, D. Spitzer, and D. Ivanov, “Smart Energetic Nanosized Co-Crystals: Exploring Fast Structure Formation and Decomposition,” Crystal Growth & Design, vol. 16, no. 1, pp. 432–439, Jan. 2016, doi: 10.1021/acs.cgd.5b01425.

[40] C. An, H. Li, B. Ye, and J. Wang, “Nano-CL-20/HMX Cocrystal Explosive for Significantly Reduced Mechanical Sensitivity,” Journal of Nanomaterials, vol. 2017, pp. 1–7, 2017, doi: 10.1155/2017/3791320.

[41] V. Stepanov, R. Damavarapu, R. Patel, H. Qiu, “Nanoscale cocrystalline explosives,” US9790137b1, Oct. 07, 2017

[42] N. Liu et al., “Preparation of CL-20/DNDAP cocrystals by a rapid and continuous spray drying method: an alternative to cocrystal formation,” CrystEngComm, vol. 20, no. 14, pp. 2060–2067, Apr. 2018, doi: 10.1039/c8ce00006a.

[43] H. Gao et al., “A Novel Method to Prepare Nano-sized CL-20/NQ Co-crystal: Vacuum Freeze Drying,” Propellants Explo Pyrotec, vol. 42, no. 8, pp. 889–895, Aug. 2017, doi: 10.1002/prep.201700006.

[44] Y. Li, B. Li, D. Zhang, and L. Xie, “Preparation and characterization of a series of high-energy and low-sensitivity composites with different desensitizers,” New J. Chem., vol. 46, no. 11, pp. 5218–5233, 2022, doi: 10.1039/D2NJ00285J.

[45] J. V. Viswanath et al., “Studies and Theoretical Optimization of CL-20 : RDX Cocrystal,” Prop., Explos., Pyrotech., vol. 44, no. 12, pp. 1570–1582, Dec. 2019, doi: 10.1002/prep.201900126.

[46] J. P. Shen et al., “Preparation and Characterization of a Novel Cocrystal Explosive,” Crystal Growth & Design, vol. 11, no. 5, pp. 1759–1765, May 2011, doi: 10.1021/cg1017032.

[47] Adam Matzger, Onas Bolton, “Crystalline explosive material,” US 2012/0305150 A1, Dec. 06, 2012

[48] O. Bolton, L. Simke, P. Pagoria, and A. Matzger, “High Power Explosive with Good Sensitivity: A 2:1 Cocrystal of CL-20:HMX,” Crystal Growth & Design, vol. 12, no. 9, pp. 4311–4314, Sep. 2012, doi: 10.1021/cg3010882.

[49] J. Salan, J. am Ende, S. R. Anderson, “CL-20:DNMT cocrystal crystal structure,” US 2015/0361056A1, US /0361056A1 2015

[50] H. Xu, X. Duan, H. Li, and C. Pei, “A novel high-energetic and good-sensitive cocrystal composed of CL-20 and TATB by a rapid solvent/non-solvent method,” RSC Advances, vol. 5, no. 116, pp. 95764–95770, 2015, doi: 10.1039/c5ra17578j.

[51] H. Qiu, R. B. Patel, R. S. Damavarapu, and V. Stepanov, “Nanoscale 2CL-20·HMX high explosive cocrystal synthesized by bead milling,” CrystEngComm, vol. 17, no. 22, pp. 4080–4083, 2015, doi: 10.1039/C5CE00489F.

[52] S. R. Anderson, P. Dubé, M. Krawiec, J. S. Salan, D. J. A. Ende, and P. Samuels, “Promising CL-20-Based Energetic Material by Cocrystallization,” Prop., Explos., Pyrotech., vol. 41, no. 5, pp. 783–788, Oct. 2016, doi: 10.1002/prep.201600065.

[53] X. Song, Y. Wang, S. Zhao, and F. Li, “Mechanochemical fabrication and properties of CL-20/RDX nano co/mixed crystals,” RSC Adv., vol. 8, no. 59, pp. 34126–34135, 2018, doi: 10.1039/C8RA04122A.

[54] Y. Liu, C. An, J. Luo, and J. Wang, “High-density HNIW/TNT cocrystal synthesized using a green chemical method,” Acta Crystallographica Section B-Structural Science Crystal Engineering and Materials, vol. 74, pp. 385–393, Aug. 2018, doi: 10.1107/S2052520618008442.

[55] M. Ghosh, A. K. Sikder, S. Banerjee, and R. G. Gonnade, “Studies on CL-20/HMX (2:1) Cocrystal: A New Preparation Method and Structural and Thermokinetic Analysis,” Crystal Growth & Design, vol. 18, no. 7, pp. 3781–3793, Jul. 2018, doi: 10.1021/acs.cgd.8b00015.

[56] Y. Hu et al., “Preparation and Characterization of Nano-CL-20/TNT Cocrystal Explosives by Mechanical Ball-Milling Method,” ACS Omega, vol. 5, no. 28, pp. 17761–17766, Jul. 2020, doi: 10.1021/acsomega.0c02426.

[57] Z. Xue et al., “Assembling of Hybrid Nano-sized HMX/ANPyO Cocrystals Intercalated with 2D High Nitrogen Materials,” Crystal Growth & Design, vol. 21, no. 8, pp. 4488–4499, Aug. 2021, doi: 10.1021/acs.cgd.1c00386.

[58] N. Zohari, F. Mohammadkhani, M. Montazeri, S. Roosta, S. Hosseini, and M. Zaree, “Synthesis and Characterization of a Novel Explosive HMX/BTNEN (2:1) Cocrystal,” Propellants Explosives Pyrotechnics, vol. 46, no. 2, pp. 329–333, Feb. 2021, doi: 10.1002/prep.202000202.

[59] D. Herrmannsdörfer and T. M. Klapötke, “Semibatch Reaction Crystallization for Scaled-Up Production of High-Quality CL-20/HMX Cocrystal: Efficient Because of Solid Dosing,” Crystal Growth & Design, vol. 21, no. 3, pp. 1708–1717, Mar. 2021, doi: 10.1021/acs.cgd.0c01611.

[60] L. Li, H. Ling, J. Tao, C. Pei, and X. Duan, “Microchannel-confined crystallization: shape-controlled continuous preparation of a high-quality CL-20/HMX cocrystal,” CrystEngComm, vol. 24, no. 8, pp. 1523–1528, 2022, doi: 10.1039/D1CE01524A.

[61] Y. Qu et al., “Interfacial engineered RDX/TATB energetic co-particles for enhanced safety performance and thermal stability,” Dalton Trans., vol. 51, no. 27, pp. 10527–10534, 2022, doi: 10.1039/D2DT01421A.

[62] F. Yang, Z. Yang, Q. Yu, G. Li, C. Zhao, and Y. Tian, “‘Thermal escape’ of MTNP: the phase separation of CL-20/MTNP cocrystals under long-term heating,” Phys. Chem. Chem. Phys., vol. 25, no. 9, pp. 6838–6846, 2023, doi: 10.1039/D2CP04822A.

[63] H. Zhao, G. Gu, J. Shen, X. Zhao, J. Wang, and G. Lan, “Preparation of Spherical HMX/DMF Solvates, Spherical HMX Particles, and HMX@NTO Composites: A Way to Reduce the Sensitivity of HMX,” ACS Omega, vol. 8, no. 15, pp. 14041–14046, Apr. 2023, doi: 10.1021/acsomega.3c00606.

[64] M. Yan et al., “Porous Cyclotrimethylenetrinitramine with Reduced Sensitivity Prepared by a Solvation–Desolvation Method,” Crystal Growth & Design, vol. 20, no. 8, pp. 5387–5394, Aug. 2020, doi: 10.1021/acs.cgd.0c00597.

[65] B. Tian, Y. Xiong, L. Chen, and C. Zhang, “Relationship between the crystal packing and impact sensitivity of energetic materials,” CrystEngComm, vol. 20, no. 6, pp. 837–848, 2018, doi: 10.1039/C7CE01914A.

[66] S. Li, R. Gou, and C. Zhang, “n−π Stacking in Energetic Crystals,” Crystal Growth & Design, vol. 22, no. 3, pp. 1991–2000, Mar. 2022, doi: 10.1021/acs.cgd.2c00034.

[67] J. Zhang et al., “Novel strategies for synthesizing energetic materials based on BTO with improved performances,” Dalton Transactions, vol. 48, no. 31, pp. 11848–11854, Aug. 2019, doi: 10.1039/c9dt02334h.

[68] P. Politzer and J. S. Murray, “Quantitative Analyses of Molecular Surface Electrostatic Potentials in Relation to Hydrogen Bonding and Co-Crystallization,” Crystal Growth & Design, vol. 15, no. 8, pp. 3767–3774, Aug. 2015, doi: 10.1021/acs.cgd.5b00419.

[69] Z. Ren, X. Chen, G. Yu, Y. Wang, B. Chen, and Z. Zhou, “Molecular simulation studies on the design of energetic ammonium dinitramide co-crystals for tuning hygroscopicity,” CrystEngComm, vol. 22, no. 31, pp. 5237–5244, 2020, doi: 10.1039/D0CE00602E.

[70] X. Wei, Y. Ma, X. Long, and C. Zhang, “A strategy developed from the observed energetic–energetic cocrystals of BTF: cocrystallizing and stabilizing energetic hydrogen-free molecules with hydrogenous energetic coformer molecules,” CrystEngComm, vol. 17, no. 37, pp. 7150–7159, 2015, doi: 10.1039/C5CE01355K.

[71] Y. Wei, F. Ren, W. Shi, and Q. Zhao, “Theoretical Insight into the Influences of Molecular Ratios on Stabilities and Mechanical Properties, Solvent Effect of HMX/FOX-7 Cocrystal Explosive,” Journal of Energetic Materials, vol. 34, no. 4, pp. 426–439, Oct. 2016, doi: 10.1080/07370652.2015.1115917.

[72] P. Vishnoi, M. Walawalkar, and R. Murugavel, “Containment of Polynitroaromatic Compounds in a Hydrogen Bonded Triarylbenzene Host,” Crystal Growth & Design, vol. 14, no. 11, pp. 5668–5673, Nov. 2014, doi: 10.1021/cg500948h.

[73] G. Han, R. Gou, F. Ren, S. Zhang, C. Wu, and S. Zhu, “Theoretical investigation into the influence of molar ratio on binding energy, mechanical property and detonation performance of 1,3,5,7-tetranitro-1,3,5,7-tetrazacyclo octane (HMX)/1-methyl-4,5-dinitroimidazole (MDNI) cocrystal explosive,” Computational and Theoretical Chemistry, vol. 1109, pp. 27–35, Jun. 2017, doi: 10.1016/j.comptc.2017.03.044.

[74] L. Hao et al., “Theoretical Study on CL-20-Based Cocrystal Energetic Compounds in an External Electric Field,” ACS Omega, vol. 5, no. 24, pp. 14767–14775, Jun. 2020, doi: 10.1021/acsomega.0c01643.

[75] P.-Y. Chen, L. Zhang, S.-G. Zhu, and G.-B. Cheng, “Intermolecular interactions, thermodynamic properties, crystal structure, and detonation performance of CL-20/TEX cocrystal explosive,” Can. J. Chem., vol. 93, no. 6, pp. 632–638, Jun. 2015, doi: 10.1139/cjc-2014-0433.

[76] G. Hang, W. Yu, T. Wang, J. Wang, and Z. Li, “Theoretical insights into effects of molar ratios on stabilities, mechanical properties and detonation performance of CL-20/RDX cocrystal explosives by molecular dynamics simulation,” Journal of Molecular Structure, vol. 1141, pp. 577–583, Aug. 2017, doi: 10.1016/j.molstruc.2017.03.126.

[77] R. Chen, A. Aquino, A. Sue, T. Niehaus, and H. Lischka, “Characterization of Charge Transfer in Excited States of Extended Clusters of pi-Stacked Donor and Acceptor Complexes in Lock-Arm Supramolecular Ordering,” Journal of Physical Chemistry A, vol. 123, no. 21, pp. 4532–4542, May 2019, doi: 10.1021/acs.jpca.9b02208.

[78] N. Şen, “Characterization and properties of a new energetic co-crystal composed of trinitrotoluene and 2,6-diaminotoluene,” Journal of Molecular Structure, vol. 1179, pp. 453–461, Mar. 2019, doi: 10.1016/j.molstruc.2018.11.013.

[79] Y. Liu, R. Gou, S. Zhang, Y.-H. Chen, M.-H. Chen, and Y.-B. Liu, “Effect of solvent mixture on the formation of CL-20/HMX cocrystal explosives,” J Mol Model, vol. 26, no. 1, p. 8, Jan. 2020, doi: 10.1007/s00894-019-4265-3.

[80] J. Bennion, L. Vogt, M. Tuckerman, and A. Matzger, “Isostructural Cocrystals of 1,3,5-Trinitrobenzene Assembled by Halogen Bonding,” Crystal Growth & Design, vol. 16, no. 8, pp. 4688–4693, Aug. 2016, doi: 10.1021/acs.cgd.6b00753.

[81] R. Bu, H. Li, and C. Zhang, “Polymorphic Transition in Traditional Energetic Materials: Influencing Factors and Effects on Structure, Property, and Performance,” Crystal Growth & Design, vol. 20, no. 5, pp. 3561–3576, May 2020, doi: 10.1021/acs.cgd.0c00233.

[82] Q. Zeng, Y. Ma, J. Li, and C. Zhang, “Energy decomposition of intermolecular interactions in energetic co-crystals,” CrystEngComm, vol. 19, no. 19, pp. 2687–2694, May 2017, doi: 10.1039/c6ce02373h.

[83] F. Lu et al., “Noncovalent Modification of 4,4′-Azo-1,2,4-triazole Backbone via Cocrystallization with Polynitroazoles,” Crystal Growth & Design, vol. 19, no. 12, pp. 7206–7216, Dec. 2019, doi: 10.1021/acs.cgd.9b01069.

[84] S. Zhu, J. Ji, and W. Zhu, “Intermolecular interactions, vibrational spectra, and detonation performance of CL -20/ TNT cocrystal,” J Chin Chem Soc, vol. 67, no. 10, pp. 1742–1752, Oct. 2020, doi: 10.1002/jccs.202000001.

[85] M. Sultan et al., “A complete thermal decomposition mechanism study of an energetic-energetic CL-20/DNT cocrystal at different extreme temperatures by using ReaxFF reactive molecular dynamics simulations,” Journal of Molecular Structure, vol. 1269, p. 133691, Dec. 2022, doi: 10.1016/j.molstruc.2022.133691.

[86] G. Liu et al., “Energetic Cocrystallization as the Most Significant Crystal Engineering Way to Create New Energetic Materials,” Crystal Growth & Design, vol. 22, no. 2, pp. 954–970, Feb. 2022, doi: 10.1021/acs.cgd.1c01090.

[87] Z. Yang, Y. Wang, J. Zhou, H. Li, H. Huang, and F. Nie, “Preparation and Performance of a BTF/DNB Cocrystal Explosive,” Propellants, Explosives, Pyrotechnics, vol. 39, no. 1, pp. 9–13, Feb. 2014, doi: 10.1002/prep.201300086.

[88] G. Liu, H. Li, R. Gou, and C. Zhang, “Packing Structures of CL-20-Based Cocrystals,” Crystal Growth & Design, vol. 18, no. 11, pp. 7065–7078, Nov. 2018, doi: 10.1021/acs.cgd.8b01228.

[89] Y. Ma, A. Zhang, C. Zhang, D. Jiang, Y. Zhu, and C. Zhang, “Crystal Packing of Low-Sensitivity and High-Energy Explosives,” Crystal Growth & Design, vol. 14, no. 9, pp. 4703–4713, Sep. 2014, doi: 10.1021/cg501048v.

[90] R. Bu, Y. Xiong, and C. Zhang, “π–π Stacking Contributing to the Low or Reduced Impact Sensitivity of Energetic Materials,” Crystal Growth & Design, vol. 20, no. 5, pp. 2824–2841, May 2020, doi: 10.1021/acs.cgd.0c00367.

[91] J. Zhang and J. Shreeve, “Time for pairing: cocrystals as advanced energetic materials,” Crystal Growth & Design, vol. 18, no. 33, pp. 6124–6133, 2016, doi: 10.1039/c6ce01239f.

[92] B. Duan, Y. Shu, N. Liu, B. Wang, X. Lu, and Y. Lu, “Direct insight into the formation driving force, sensitivity and detonation performance of the observed CL-20-based energetic cocrystals,” CrystEngComm, vol. 20, no. 38, pp. 5790–5800, Oct. 2018, doi: 10.1039/c8ce01132j.

[93] N. Şen, H. Dursun, K. S. Hope, H. Nazir, N. Acar, and O. Atakol, “Towards low-impact-sensitivity through crystal engineering: New energetic co-crystals formed between Picric acid, Trinitrotoluene and 9-Vinylanthracene,” Journal of Molecular Structure, vol. 1219, p. 128614, Nov. 2020, doi: 10.1016/j.molstruc.2020.128614.

[94] S. Hanafi et al., “Synthesis, characterization and thermal decomposition behavior of a novel HNTO/AN co-crystal as a promising rocket propellant oxidizer,” Chemical Engineering Journal, vol. 417, p. 128010, Aug. 2021, doi: 10.1016/j.cej.2020.128010.

[95] C. Guo et al., “Crystal structure and explosive performance of a new CL-20/caprolactam cocrystal,” Journal of Molecular Structure, vol. 1048, pp. 267–273, Sep. 2013, doi: 10.1016/j.molstruc.2013.05.025.

[96] C. J. Chapman and L. J. Groven, “Evaluation of a CL-20/TATB Energetic Co-crystal,” Prop., Explos., Pyrotech., vol. 44, no. 3, pp. 293–300, Mar. 2019, doi: 10.1002/prep.201800255.

[97] L. Zhao et al., “Kinetic model of thermal decomposition of CL-20/HMX co-crystal for thermal safety prediction,” Thermochimica Acta, vol. 674, pp. 44–51, Apr. 2019, doi: 10.1016/j.tca.2019.02.001.

[98] B. Huang, Z. Xue, X. Fu, and Q.-L. Yan, “Advanced crystalline energetic materials modified by coating/intercalation techniques,” Chemical Engineering Journal, vol. 417, p. 128044, Aug. 2021, doi: 10.1016/j.cej.2020.128044.

[99] D. Guo, Q. An, S. V. Zybin, W. A. Goddard Iii, F. Huang, and B. Tang, “The co-crystal of TNT/CL-20 leads to decreased sensitivity toward thermal decomposition from first principles based reactive molecular dynamics,” J. Mater. Chem. A, vol. 3, no. 10, pp. 5409–5419, 2015, doi: 10.1039/C4TA06858K.

[100] X. Wu, Z. Liu, and W. Zhu, “Conformational Changes and Decomposition Mechanisms of HMX-Based Cocrystal Explosives at High Temperatures,” J. Phys. Chem. C, vol. 124, no. 1, pp. 25–36, Jan. 2020, doi: 10.1021/acs.jpcc.9b08286.

[101] V. B. Patil, R. Svoboda, and S. Zeman, “Thermal studies on performance of DATB and TATB coagglomerated crystals,” no. 724, p. 179494, 2023, doi: https://doi.org/10.1016/j.tca.2023.179494.

[102] W. Pang, K. Wang, W. Zhang, L. T. De Luca, X. Fan and J. Li, “CL-20-Based Cocrystal Energetic aterials: Simulation, Preparation and Performance,” Molecules, vol. 25, no. 18, p. 4311, 2020, doi: https://doi.org/10.3390/molecules25184311.

[103] Z.-B. Zhang, T. Li, L. Yin, X. Yin, and J.-G. Zhang, “A novel insensitive cocrystal explosive BTO/ATZ: preparation and performance,” RSC Adv., vol. 6, no. 79, pp. 76075–76083, 2016, doi: 10.1039/C6RA14510H.

[104] V. S. Vuppuluri, P. J. Samuels, K. C. Caflin, I. E. Gunduz, and S. F. Son, “Detonation Performance Characterization of a Novel CL-20 Cocrystal Using Microwave Interferometry,” Prop., Explos., Pyrotech., vol. 43, no. 1, pp. 38–47, Jan. 2018, doi: 10.1002/prep.201700150.

[105] V. S. Vuppuluri, J. C. Bennion, R. A. Wiscons, I. E. Gunduz, A. J. Matzger, and S. F. Son, “Detonation Velocity Measurement of a Hydrogen Peroxide Solvate of CL-20,” Prop., Explos., Pyrotech., vol. 44, no. 3, pp. 313–318, Mar. 2019, doi: 10.1002/prep.201800202.

[106] V. B. Patil, K. Zalewski, J. Schuster, P. Belina, W. Trzcinski, and S. Zeman, “A new insight into the energetic co-agglomerate structures of attractive nitramines,” Chemical Engineering Journal, vol. 420, Sep. 2021, doi: 10.1016/j.cej.2021.130472.

[107] Q. Jia et al., “Low-temperature heat capacities, standard molar enthalpies of formation and detonation performance of two CL-20 cocrystal energetic materials,” Fluid Phase Equilibria, vol. 518, Aug. 2020, doi: 10.1016/j.fluid.2020.112638.

[108] C. Ren, X. Li, and L. Guo, “Chemical Insight on Decreased Sensitivity of CL-20/TNT Cocrystal Revealed by ReaxFF MD Simulations,” Journal of Chemical Information and Modeling, vol. 59, no. 5, pp. 2079–2092, May 2019, doi: 10.1021/acs.jcim.8b00952.

[109] S. Zeman, A. K. Hussein, M. Jungova, and A. Elbeih, “Effect of energy content of the nitraminic plastic bonded explosives on their performance and sensitivity characteristics,” Defence Technology, vol. 15, no. 4, pp. 488–494, Aug. 2019, doi: 10.1016/j.dt.2018.12.003.

[110] A. McBain, V. Vuppuluri, I. Gunduz, L. Groven, and S. Son, “Laser ignition of CL-20 (hexanitrohexaazaisowurtzitane) cocrystals,” Combustion and Flame, vol. 188, pp. 104–115, Feb. 2018, doi: 10.1016/j.combustflame.2017.09.017.

[111] O. Bolton, L. R. Simke, P. F. Pagoria, and A. J. Matzger, “High Power Explosive with Good Sensitivity: A 2:1 Cocrystal of CL-20:HMX,” Crystal Growth & Design, vol. 12, no. 9, pp. 4311–4314, Sep. 2012, doi: 10.1021/cg3010882.

[112] Y. Tan, Y. Liu, H. Wang, H. Li, F.Nie, and Z. Yang, “Different Stoichiometric Ratios Realized in Energetic−Energetic Cocrystals Based on CL-20 and 4,5-MDNI: A Smart Strategy to Tune Performance,” Cryst. Growth Des, vol. 20, pp. 3826–3833, 2020, doi: https://dx.doi.org/10.1021/acs.cgd.0c00138.

[113] A. K. Yadav, V. D. Ghule, and S. Dharavath, “Thermally Stable and Insensitive Energetic Cocrystals Comprising Nitrobarbituric Acid Coformers,” Crystal Growth & Design, vol. 23, no. 4, pp. 2826–2836, Apr. 2023, doi: 10.1021/acs.cgd.3c00016.

[114] P. Peng et al., “Improving the Stability of All-Carbon-Nitrated Azoles through Cocrystallization,” Crystal Growth & Design, vol. 22, no. 4, pp. 2158–2167, Apr. 2022, doi: 10.1021/acs.cgd.1c01237.

[115] A. Abdelaziz, A. Tarchoun, H. Boukeciat, and D. Trache, “Insight into the Thermodynamic Properties of Promising Energetic HNTO·AN Co-Crystal: Heat Capacity, Combustion Energy, and Formation Enthalpy,” Energies, vol. 15, no. 18, p. 6722, Sep. 2022, doi: 10.3390/en15186722.

[116] S. Qiao, J. Wang, Y. Yu, Y. Liu, Z. Yang, and H. Li, “Two novel TNB energetic cocrystals with low melting point: a potential strategy to construct melt cast explosive carriers,” CrystEngComm, vol. 24, no. 16, pp. 2948–2953, 2022, doi: 10.1039/D2CE00025C.

[117] B. Duan, X. Lu, H. Mo, B. Tan, B. Wang, and N. Liu, “Fabrication of CL-20/HMX Cocrystal@Melamine–Formaldehyde Resin Core–Shell Composites Featuring Enhanced Thermal and Safety Performance via In Situ Polymerization,” IJMS, vol. 23, no. 12, p. 6710, Jun. 2022, doi: 10.3390/ijms23126710.

[118] H. Wang et al., “Hydrogen bonding distribution and its effect on sensitivity of planar tricyclic polyazole energetic materials,” Chemical Engineering Journal, vol. 433, p. 134479, Apr. 2022, doi: 10.1016/j.cej.2021.134479.

[119] O. T. O’Sullivan and M. J. Zdilla, “Properties and Promise of Catenated Nitrogen Systems As High-Energy-Density Materials,” Chem. Rev., vol. 120, no. 12, pp. 5682–5744, Jun. 2020, doi: 10.1021/acs.chemrev.9b00804.

[120] H. Lin, S.-G. Zhu, L. Zhang, X.-H. Peng, and H.-Z. Li, “Synthesis and First Principles Investigation of HMX/NMP Cocrystal Explosive,” Journal of Energetic Materials, vol. 31, no. 4, pp. 261–272, Oct. 2013, doi: 10.1080/07370652.2012.716492.

[121] H. Lin, S.-G. Zhu, L. Zhang, X.-H. Peng, P.-Y. Chen, and H.-Z. Li, “Intermolecular interactions, thermodynamic properties, crystal structure, and detonation performance of HMX/NTO cocrystal explosive,” Int. J. Quantum Chem., vol. 113, no. 10, pp. 1591–1599, May 2013, doi: 10.1002/qua.24369.

[122] L. Zhang, S.-L. Jiang, Y. Yu, and J. Chen, “Revealing Solid Properties of High-energy-density Molecular Cocrystals from the Cooperation of Hydrogen Bonding and Molecular Polarizability,” Sci Rep, vol. 9, no. 1, p. 1257, Feb. 2019, doi: 10.1038/s41598-018-37500-y.

[123] H. Zhang et al., “Five Energetic Cocrystals of BTF by Intermolecular Hydrogen Bond and π-Stacking Interactions,” Crystal Growth & Design, vol. 13, no. 2, pp. 679–687, Feb. 2013, doi: 10.1021/cg301353f.

[124] X. Wu, Z. Liu, and W. Zhu, “External electric field induced conformational changes as a buffer to increase the stability of CL-20/HMX cocrystal and its pure components,” Materials Today Communications, vol. 26, p. 101696, Mar. 2021, doi: 10.1016/j.mtcomm.2020.101696.

[125] J.-H. Zhou, L. Zhao, L.-W. Shi, and Pei-Cheng Luo, “Two models to estimate the density of organic cocrystals,” RSC Adv., vol. 11, no. 20, pp. 12066–12073, 2021, doi: 10.1039/D0RA10241E.

[126] Q. Jia, J. Wang, S. Zhang, J. Zhang, N. Liu, and K. Kou, “Investigation of the solid–liquid ternary phase diagrams of 2HNIW·HMX cocrystal,” RSC Adv., vol. 11, no. 16, pp. 9542–9549, 2021, doi: 10.1039/D1RA00057H.

[127] Z. Yang, H. Li, H. Huang, X. Zhou, J. Li, and F. Nie, “Preparation and Performance of a HNIW/TNT Cocrystal Explosive,” Propellants, Explosives, Pyrotechnics, vol. 38, no. 4, pp. 495–501, Aug. 2013, doi: 10.1002/prep.201200093.

[128] H. Xu, X. Duan, H. Li, and C. Pei, “A novel high-energetic and good-sensitive cocrystal composed of CL-20 and TATB by a rapid solvent/non-solvent method,” RSC Adv., vol. 5, no. 116, pp. 95764–95770, 2015, doi: 10.1039/C5RA17578J.

[129] S. Zeman, “Sensitivities of High Energy Compounds,” in High Energy Density Materials, T. M. Klapötke, Ed., in Structure and Bonding. , Berlin, Heidelberg: Springer, 2007, pp. 195–271. doi: 10.1007/430_2006_052.

[130] S. Zeman, “The Chemical Micromechanism of Energetic Material Initiation,” in Nano and Micro-Scale Energetic Materials, John Wiley & Sons, Ltd, 2023, pp. 567–623. doi: 10.1002/9783527835348.ch19.

[131] D. D. Dlott, “Multi-phonon up-pumping in energetic materials,” in Overviews of Recent Research on Energetic Materials, vol. Volume 16, in Advanced Series in Physical Chemistry, no. Volume 16, vol. Volume 16. , WORLD SCIENTIFIC, 2005, pp. 303–333. doi: 10.1142/9789812775283_0010.

[132] W. Qian and C. Zhang, “Review of the phonon calculations for energetic crystals and their applications,” Energetic Materials Frontiers, vol. 2, no. 2, pp. 154–164, Jun. 2021, doi: 10.1016/j.enmf.2021.03.002.

[133] S. Zeman, “Characteristics of Thermal Decomposition of Energetic Materials in a Study of Their Initiation Reactivity,” in Handbook of Thermal Analysis and Calorimetry, vol. 6, Elsevier, 2018, pp. 573–612. doi: 10.1016/B978-0-444-64062-8.00006-1.

[134] M. Suceska, Test Methods for Explosives. Springer Science & Business Media, 2012.

[135] H.-H. Licht, “Performance and Sensitivity of Explosives,” Propellants Explos. Pyrotech, vol. 25, no. 3, pp. 126–132, Jun. 2000, doi: 10.1002/1521-4087(200006)25:3<126::AID-PREP126>3.0.CO;2-8.

[136] S. Zeman, and M. Jungová, “Sensitivity and Performance of Energetic Materials - Zeman - 2016 - Propellants, Explosives, Pyrotechnics - Wiley Online Library,” Apr. 2016, doi: https://doi.org/10.1002/prep.201500351.

[137] S.-Y. Bao, W. Zeng, F.-S. Liu, Z.-T. Liu, and Q.-J. Liu, “Theoretical relationship between vibrational properties and impact sensitivity of energetic materials from the phonon upon transition theory,” Chemical Physics, vol. 576, p. 112085, Jan. 2024, doi: 10.1016/j.chemphys.2023.112085.

[138] H.-C. Ren et al., “Intermolecular Vibration Energy Transfer Process in Two CL-20-Based Cocrystals Theoretically Revealed by Two-Dimensional Infrared Spectra,” Molecules, vol. 27, no. 7, p. 2153, Mar. 2022, doi: 10.3390/molecules27072153.

[139] C. Zhang, F. Jiao, and H. Li, “Crystal Engineering for Creating Low Sensitivity and Highly Energetic Materials,” Crystal Growth & Design, vol. 18, no. 10, pp. 5713–5726, Oct. 2018, doi: 10.1021/acs.cgd.8b00929.

[140] M. Gruhne, M. Lommel, M. Wurzenberger, T. Klapotke, and J. Stierstorfer, “Investigation of Ethylenedinitramine as a Versatile Building Block in Energetic Salts, Cocrystals, and Coordination Compounds,” Inorganic Chemistry, vol. 60, no. 7, pp. 4816–4828, Apr. 2021, doi: 10.1021/acs.inorgchem.0c03752.

[141] X. Xu et al., “Density functional theory study of CL-20/Nitroimidazoles energetic cocrystals in an external electric field,” Computational and Theoretical Chemistry, vol. 1209, p. 113607, Mar. 2022, doi: 10.1016/j.comptc.2022.113607.

[142] G. Hang, J. Wang, T. Wang, H. Shen, W. Yu, and R. Shen, “Theoretical investigations on stability, sensitivity, energetic performance, and mechanical properties of CL-20/TNAD cocrystal explosive by molecular dynamics method,” J Mol Model, vol. 28, no. 3, p. 58, Mar. 2022, doi: 10.1007/s00894-022-05049-3.

[143] M. Auzanneau and M. Roux, “Electric Spark and ESD Sensitivity of Reactive Solids (primary or secondary explosive, propellant, pyrotechnics). Part II: Energy transfer mechanisms and comprehensive study on E50,” Propellants, Explosives, Pyrotechnics, vol. 20, no. 2, pp. 96–101, 1995, doi: 10.1002/prep.19950200211.

[144] S. Zeman, V. Pelikan, and J. Majzlik, “Electric Spark Sensitivity of Nitramines. Part I. Aspects of Molecular Structure*),” Central European Journal of Energetic Materials, vol. 3(3), pp. 27–44, 2006.

[145] S. Zeman, V. Pelikan, and J. Majzlik, “Electric Spark Sensitivity of Nitramines. Part II. A Problem of ‘Hot Spots’*),” Central European Journal of Energetic Materials, vol. 3(3), pp. 45–51.

[146] S. Zeman and N. Liu, “A new look on the electric spark sensitivity of nitramines,” Defence Technology, vol. 16, no. 1, pp. 10–17, Feb. 2020, doi: 10.1016/j.dt.2019.06.023.

[147] Fried, L E., “CHEETAH 1.39 Users’ Manual UCRL-MA-117541.” CA: Lawrence Livermore National Laboratory., 1996.

[148] P. J. Liouville, “Sur la propagation des réactions chimiques dans les gaz,” vol. 2, no. 1906, pp. 5–86.

[149] M. J. Kamlet and S. J. Jacobs, “Chemistry of detonations. I. A simple method for calculating detonation properties of C–H–N–O explosives,” The Journal of Chemical Physics, vol. 48, no. 1, pp. 23–35, 1968.

[150] T. Urbanski, “On entropy and free energy of explosives (preliminary communication),” Bull. l’Academie Pol. Des Sci. s, Ser. Des Sci. Chim., vol. 28, pp. 511–513, 1980, doi: https://gallica.bnf.fr/ark:/12148/cb343830642/date1980.

[151] H. Lin, S.-G. Zhu, H.-Z. Li, and X.-H. Peng, “Structure and detonation performance of a novel HMX/LLM-105 cocrystal explosive,” J. Phys. Org. Chem., vol. 26, no. 11, pp. 898–907, Nov. 2013, doi: 10.1002/poc.3188.

[152] J.-T. Wu, J.-G. Zhang, T. Li, Z.-M. Li, and T.-L. Zhang, “A novel cocrystal explosive NTO/TZTN with good comprehensive properties,” RSC Adv., vol. 5, no. 36, pp. 28354–28359, 2015, doi: 10.1039/C5RA01124H.

[153] G.-Y. Hang, W.-L. Yu, T. Wang, and J.-T. Wang, “Theoretical investigations on structures, stability, energetic performance, sensitivity, and mechanical properties of CL-20/TNT/HMX cocrystal explosives by molecular dynamics simulation,” J Mol Model, vol. 25, no. 1, p. 10, Jan. 2019, doi: 10.1007/s00894-018-3887-1.

[154] Y. Sha and X. Zhang, “Impact sensitivity and moisture adsorption on the surface of CL-20/TNT cocrystal by molecular dynamics simulation,” Applied Surface Science, vol. 483, pp. 91–97, Jul. 2019, doi: 10.1016/j.apsusc.2019.03.231.

[155] K. Song, F. Ren, S. Zhang, and W. Shi, “Theoretical insights into the stabilities, detonation performance, and electrostatic potentials of cocrystals containing α- or β-HMX and TATB, FOX-7, NTO, or DMF in various molar ratios,” J Mol Model, vol. 22, no. 10, p. 249, Oct. 2016, doi: 10.1007/s00894-016-3111-0.

[156] M. Pakhnova, I. Kruglov, A. Yanilkin, and A. Oganov, “Search for stable cocrystals of energetic materials using the evolutionary algorithm USPEX,” Physical Chemistry Chemical Physics, vol. 22, no. 29, pp. 16822–16830, Aug. 2020, doi: 10.1039/d0cp03042b.

[157] C. B. Aakeröy, T. K. Wijethunga, and J. Desper, “Crystal Engineering of Energetic Materials: Co-crystals of Ethylenedinitramine (EDNA) with Modified Performance and Improved Chemical Stability,” Chem. Eur. J., vol. 21, no. 31, pp. 11029–11037, Jul. 2015, doi: 10.1002/chem.201501721.

[158] M. K. Bellas and A. J. Matzger, “Achieving Balanced Energetics through Cocrystallization,” Angew. Chem. Int. Ed., vol. 58, no. 48, pp. 17185–17188, Nov. 2019, doi: 10.1002/anie.201908709.

Chapter 2 Materials and Methods

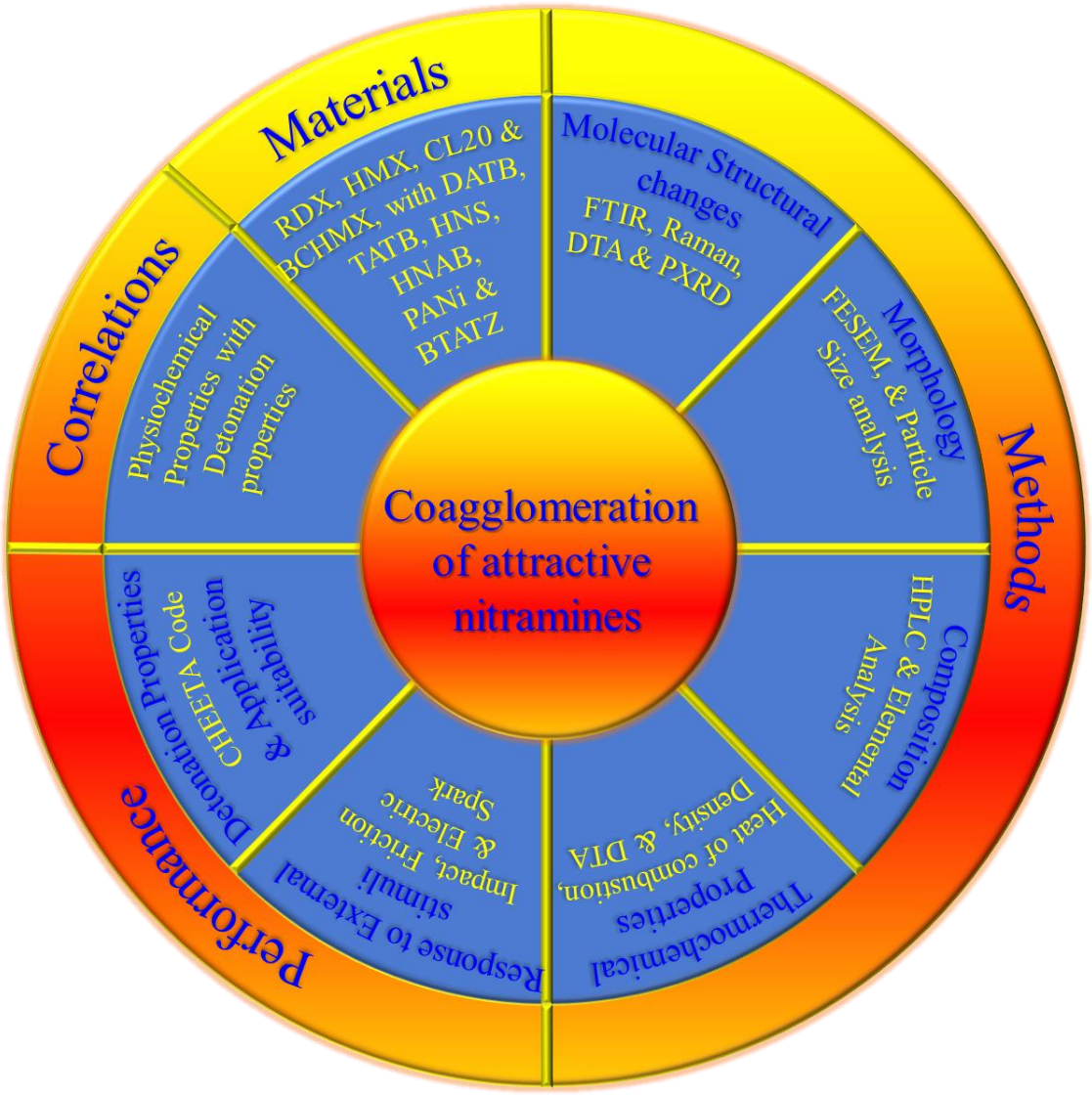

2.1 Materials

In recent years, nitramines (2.1.1 -2.1.4) have technically attracted researchers due to their potential detonation properties and their applications, so we named them “attractive nitramines”. However, plenty of applications of these nitramines can be achieved by slightly modifying their properties to attain a balanced form. So, we chose some thermally stable EMs (2.1.4 -2.1.11) as well as nonenergetic coformer like polyaniline (PANi) to achieve the required properties. All the nitramines and coformers molecular formulae are shown in Figure 1.

2.1.1 RDX: 1,3,5-Trinitro-1,3,5-triazinane was a product of its former producer, Chemko Strážske company (Eastern Slovakia).

2.1.2 HMX: ß-1,3,5,7-Tetranitro-1,3,5,7-tetrazocane was imported from the Russian Federation (with particle size close to Class 3).

2.1.3 BCHMX: cis-1,3,4,6-tetranitrooctahydroimidazo-[4,5-d]imidazole or bicyclo-HMX was indigenously prepared at our Institute of Energetic Materials, as reported in Ref. [1, 2]. It was recrystallized by acetone/heptane using the solvent/antisolvent technique.

2.1.4 RS-ε-HNIW/ CL-20: 2,4,6,8,10,12-hexanitro-2,4,6,8,10,12-hexaazaisowurtzitane was a product of the Explosia Pardubice pilot plant; it was converted into RS-ε-CL20 with reduced impact sensitivity of 9 J employing a patented method[3].

2.1.5 DATB: 1,3,5-Trinitrobenzene-2,4-diamine was prepared with a purity of 98 % by the amination of 1,3,5-trinitro-2,4-dichlorobenzene in a methanolic solution [4] (the impurities were entirely removed in the process of co-agglomeration).

2.1.6 TATB: 1,3,5-Trinitrobenzene-2,4,6-triamine was prepared with a purity of 98% by the amination of 1,3,5-trinitro-2,4,6-trichlorobenzene in a methanolic solution (the impurities were entirely removed in the process of coagglomeration)[5].

2.1.7 HNAB: 2,2',4,4',6,6'-hexanitroazobenzene was prepared at our Institute of Energetic Materials[6].

2.1.8 HNS: trans-2,2',4,4',6,6'-hexanitrostilbene was imported from the Russian Federation

2.1.9 PANi: polyaniline; It was prepared at the Institute of Energetic Materials, as reported in Refs.[7], [8].

2.1.10 BTATz: 3,6-bis(1h-1,2,3,4-tetrazol-5-ylamino)-1,2,4,5-tetrazine was indigenously prepared at our Institute of Energetic Materials[9].

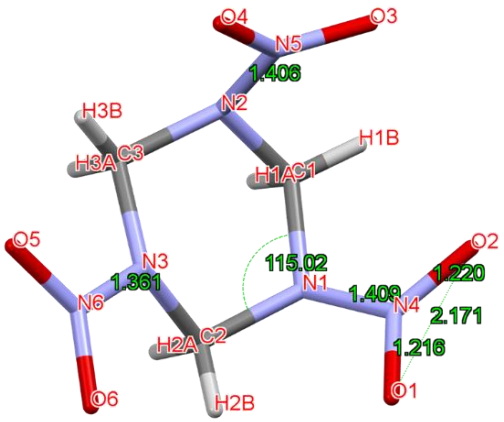

a) RDX

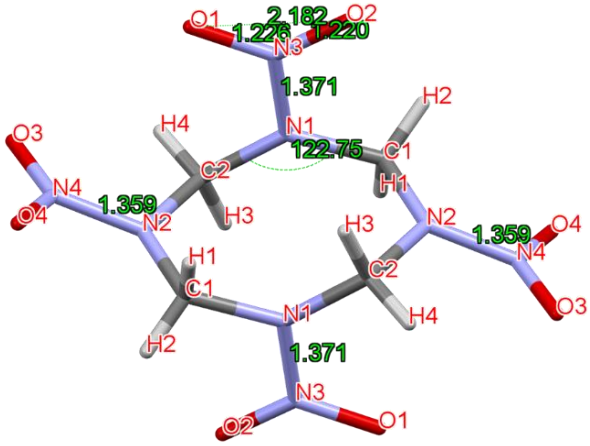

b) HMX

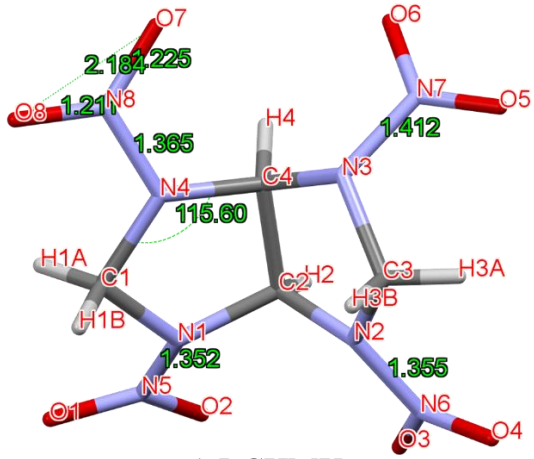

c) BCHMX

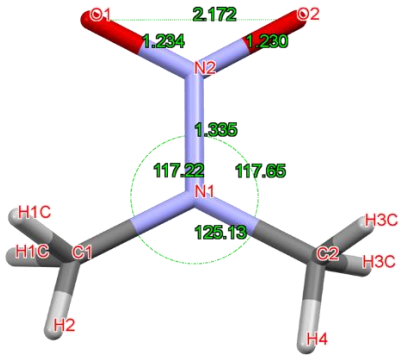

d) DMNA

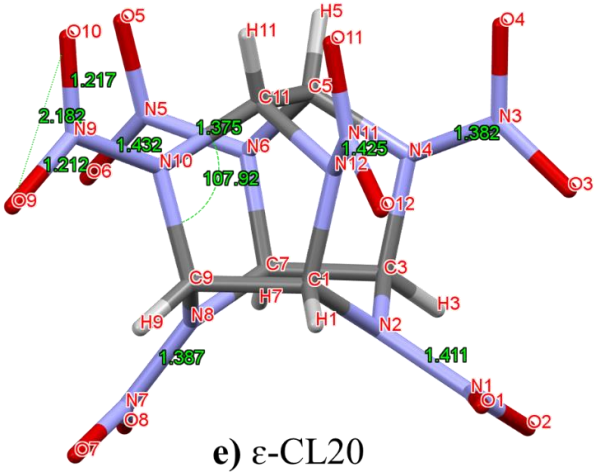

e) ε-CL20

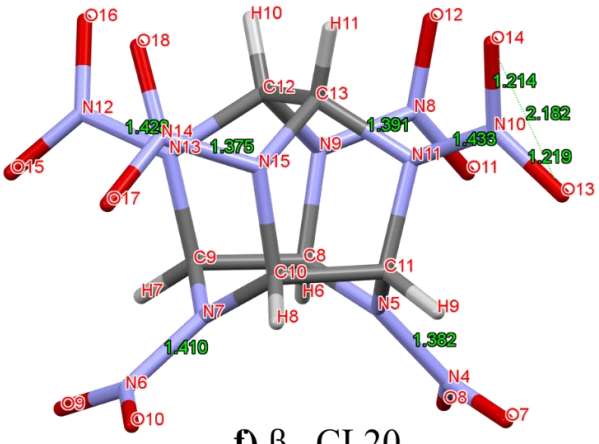

f) β –CL20

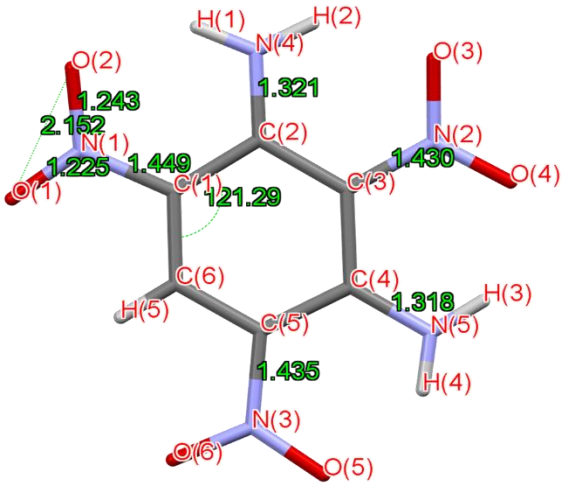

g) DATB

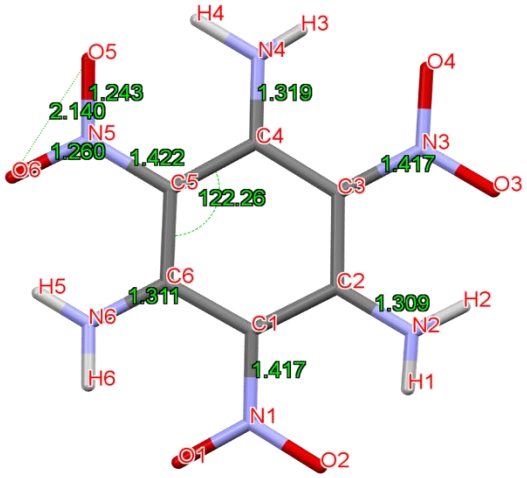

h) TATB

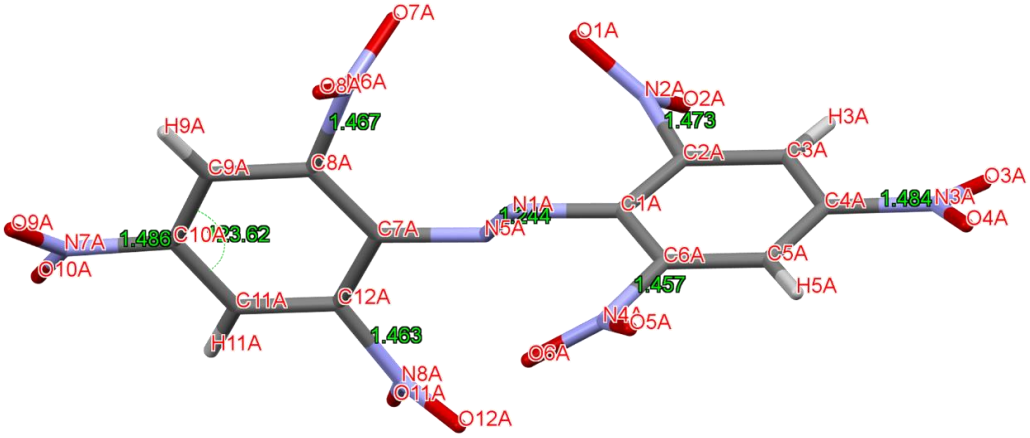

i) HNAB

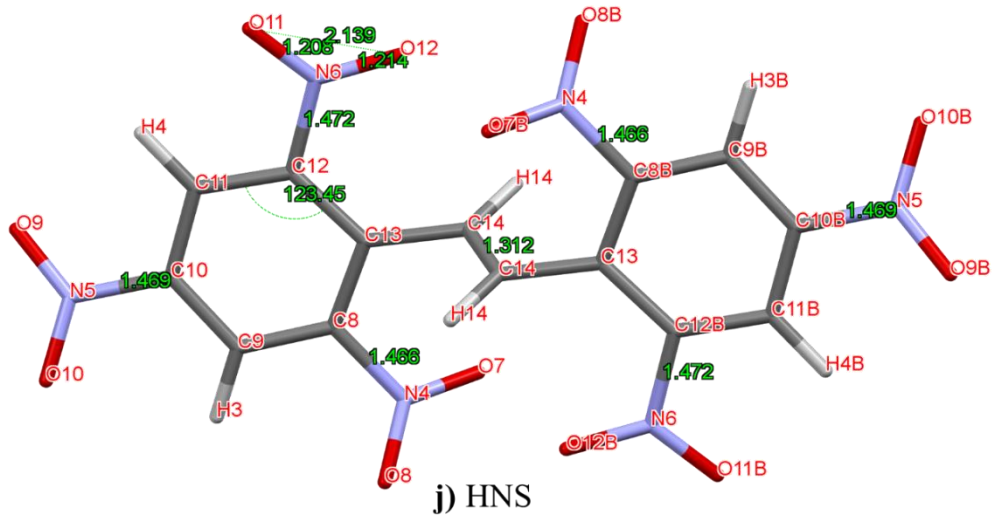

j) HNS

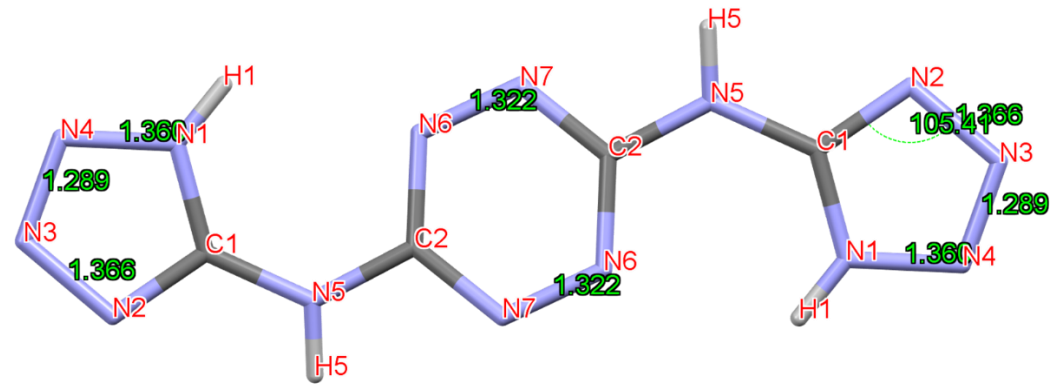

k) BTATZ

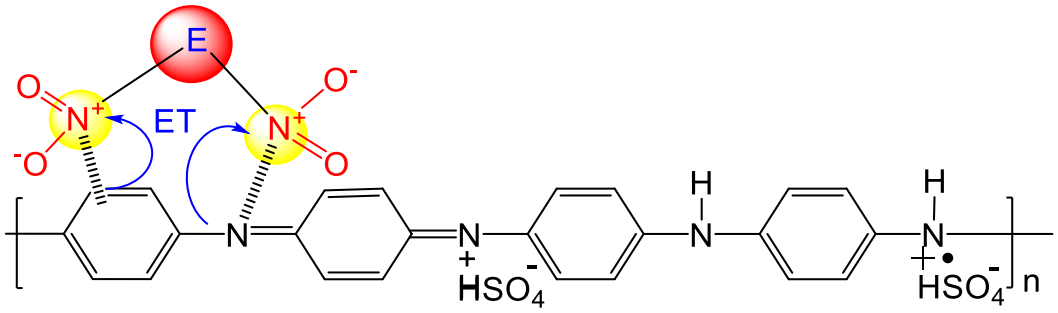

l) Emeraldine Salt form of PAnis

Figure 2. 1 Energetic Materials used in CACs preparations a) RDX[10], b)HMX [11], c) BCHMX [2], d) DMNA [12], e) ε-CL20 [13], f) β-CL20 [14], g) DATB [15], h) TATB [16], i) HNAB [17], j) HNS [18], k) BTATZ [19] and l) PANi (E-indicates here nitramines forming charge transfer complex with PANi) [7].

2.2 Other inexplosive chemicals / Materials

The other traditional chemicals like solvents and other materials were used as follows (their procurements). Acetone, butanol, chloroform, dimethyl sulfoxide, dimethyl formaldehyde, and dimethyl Pyrrolidone, ethanol, Ethyl-acetate, Ethyl-formate, Hexane, N-Methyl-2-pyrrolidone (all from Sigma Andrich). Similarly, HTPB (Island Pyrochemical Industries prod.), ammonium per chlorate-AP (Island Pyrochemical Industries prod.), alumina (Benda Lutz prod), dimethyl diisocyanate-DDI (Benda Lutz prod.), iron oxide nanoparticles-γ-Fe_2O_3 (product of the Military University of Technology in Warsaw), dioctyl adipate -ADO (Boryszew-Erg prod.), all the chemicals used without further purification.

2.3 Characterization Methods

2.3.1 Powder X-ray diffraction (PXRD): The powder X-ray diffraction data (PXRD) of the prepared samples were collected at room temperature with a Rigaku MiniFlex 600 powder diffractometer with Bragg–Brentano θ – 2θ geometry using CuK_α radiation (λ = 1.5418 Å, U = 40kV, I = 15 mA). The data

were scanned with an ultrafast Dtex Ultra detector over the angular range of 2–50° (2θ) with a step size of 0.02°.

2.3.2 Fourier transformation infra-red spectroscopy (FTIR): A Nicolet Protege 460 FTIR spectrometer was used to record the IR spectral measurements of the samples using the transmission technique.

2.3.3 Raman spectroscopy: Raman spectra were measured with Nicolet Is50 Raman, Thermo scientific, using an Ar laser (λ = 514.5 nm) and a semiconductor laser (λ= 785 nm). The maximum output power is 1.7 mW of the light spot of the Raman spectrometer, and the spectral resolution is 1 cm^{-1}.

PANi CACs shown higher laser sensitivity so these samples were measured at low laser power , by Thermo Scientific™ DXR3 Raman Microscope, employing an excitation laser source (wavelength of 785 nm & power 29 mV), 10x/0.25 objective and using 400 lines/mm grating (3378 to 49 cm^{-1}).

2.3.4 Densitometer (ρ): The density of the prepared co-crystals was measured by an AccuPyc II 1345 gas pycnometer. This technique is non-destructive as it uses the gas displacement method to measure volume.

2.3.5 High-performance liquid chromatography (HPLC): The chromatographic analysis was carried out in Agilent HPLC 1200 Series with DAD detector. To verify the purity and composition of CACs concentration HPLC analysis was carried out by taking 100 ppm of each sample solution, using mobile phase ACN:H_2O (60:40). Results are as follows for more details. Hypothetical formulas of CACs were calculated from the HPLC outputs. So, the number of nitrogen atoms in the formula of a given CAC is the same as in the nitramine that this CAC contains (i.e., for RDX 6, for BCHMX and HMX 8 and CL20 12).

2.3.6 Field emission scanning electron spectroscopy (FeSEM): The particle morphology, size distribution, crystal structure and composition analysis of the CACs and the conformers were examined using a MIRA3 LMH scanning electron microscope (Tescan, Czech Republic).

2.3.7 Elemental analyzer: Elemental analysis has been performed on Vario MICRO Cube (Elementar) in CHNS mode with calibration on sulfanilamide, using a 1 mg sample for this analysis; results with calculated empirical formulae were calculated.

2.3.8 Particle size analyzer: The particle morphology, size distribution, crystal structure and composition analysis of the CACS and the conformers were examined using a MIRA3 LMH scanning electron microscope (Tescan, Czech Republic).

2.3.9 Differential thermal analysis (DTA): A DTA 550 Ex apparatus (OZM Research, Czech Republic) was used for differential thermal analysis. The measurements were carried out at atmospheric pressure, with the tested sample in direct contact with the air. The sample (0.05g) was placed in a test tube made of

Simax glass, 5 mm in diameter and 50 mm long. The reference standard was 0.05g aluminum oxide. A linear heating rate of 5^{o}C min^{-1} was used.

2.3.10 Heat of combustion by Bomb calorimeter: Due to instrument maintenance, we used two instruments for measurements of heat of combustion of the CACs, as follows.

i) OZM MS-10A Calorimeter: The heat of combustion was measured with an MS-10A (OZM Research s.r.o.) calorimeter.

ii) IKA C 200 Bomb-type Calorimeter: The heat of combustion was measured with an IKA C 200 Bomb-type calorimeter. Both instruments bomb placing is different, however method of analysis is same only. The calorimeter was calibrated using benzoic acid. The increase of temperature in the calorimeter barrel could be converted into the heat of combustion. The enthalpy of formation was calculated according to Hess's law.

2.3.11 Differential thermal analysis (DSC): The DSC measurements of the pure nitramines and CACs were performed utilizing a heat-flow differential scanning calorimeter Q2000 DSC (TA Instruments, USA) equipped with a cooling accessory, auto lid, autosampler, and T-zero Technology. The samples of masses circa 0.5 – 1 mg were accurately weighed and hermetically sealed in low-mass aluminum pans. The decomposition kinetics were for each sample performed as simple heating scans in the approx. 50 – 350 °C temperature range (slightly corrected in a few individual cases) at heating rates 0.5, 1, 2, 3, 5, 7, 10 and 20 °C·min^{-1}. A tangential area-proportional baseline was used to subtract the thermokinetic background.

2.3.12 Impact sensitivity by BAM fall hammer: The impact sensitivity was determined by employing a standard impact tester with an exchangeable anvil (Julius Peters[11, 12]), with the amount of the tested substance being 40 mm^3 [19]; the detection was based on a sound effect [11,12]; drop hammers weighing 2 & 5 kg were used [19, 20, 21]. The new method/algorithm, called FEST [22] (an innovative method of probit analysis [22]), was utilized to determine the probability levels of the initiation. The obtained sensitivity was expressed as the drop energy, *Edr*, versus the percentage of initiation. The 50% (*Edr* 50 %) and 95% (*Edr* 95 %) probabilities of initiation are specified in this article.

For propellant samples the sensitivity was determined employing a standard impact tester with exchangeable anvil (Julius Peters [11, 12]), BAM BPH series tester make OZM research s. r. o. with the amount of the tested substance being 40 mm^3 [6]; the detection was based on sound effect; drop hammers of 5 kg weight were used [11, 12]. The method European standard PN-EN 13631-4 2003 [15, 16], was utilized to determine the probability levels of the initiation. The obtained sensitivity was expressed as the

drop energy, E_{dr}, versus the percentage of initiation. The 50% (E_{dr} 50 %) probabilities of initiation are specified in this method.

2.3.13 Electric spark sensitivity measurement: Instrumental setup used, and its spark gap are presented in papers [26, 27, 28]. The bottom electrode is a steel base with an attached screw as a leak electrode in the center. To this screw is attached a plastic cylinder with a cut for fastening a piece of flexible tubing of 5 mm height and 5 mm diameter serving as a container of the sample tested. The top electrode is a steel cylinder of conical shape with attached resistance wire protected by a plastic distance stop, which presses an Umafol lid to the flexible tubing. The capacity of the capacitors was chosen to allow measurements in the voltage interval from 8 to 14 kV. If the initiation was successful, the next measurement was made with a voltage lowered by 0.2 kV; if it was unsuccessful, the voltage was increased by the same value. We considered an initiation successful if the sample disappeared or the flexible tubing was torn. The measurements were made with each substance, and the results obtained utilizing the "Up and Down method".

2.3.14 Friction Sensitivity: The sensitivity of propellants to mechanical stimuli means the ability to undergo an explosive transformation under the influence of mechanical action (e.g., as a result of impact, shot). Friction sensitivity was tested in the Peters apparatus. The method European standard PN-EN 13631-4 2003 [25]; in which the force of pressure on two rubbing surfaces is changed (porcelain tile and porcelain stamp, between which the rectangular sample is placed). The pressing force is adjusted by moving the weight into the device. Sensitivity means the highest pressing force with no explosive transformation in six trials.

2.3.15 Hardness Test: The hardness of tested samples was measured using Shore A hardness tester as per standard ASTM D 2240 [29]. The method consists of measurement of the resistance posed by the sample when a needle of specific dimensions and shape is inserted into it. The test result is the average value of sic measurements.

2.3.16 Ignition temperature: The Ignition temperature has been measured by using differential thermal analysis (DTA) and heating the samples in the Wood's alloy method, as per polish working standard BN-76/6091-08 [12, 21]. The apparatus OZM Research DTA 551-Rez was used in the DTA method to measure temperature of Ignition. The rate of temperature increase was 5 °C/min and the weight of samples was 30-40 mg. Measurements were performed in the range of 30-400 °C. In Wood's alloy method, the temperature was measured by a simultaneous heating of three samples of each propellant at temperature increase rate equal to 5 °C/min and visual observation and assessment of propulsion changes. After preheating the alloy

to the temperature of 100 °C the test tubes with samples of the propellant (cubes of ca. 40 mg) inserted into it.

2.3.17 Burn rate measurements: Instrumental setup for Stojan Vessel for Burn rate Measurements

The dependence of the burning rate on pressure was measured using an SV2 (Stojan Vessel) closed vessel (OZM Research). ABSW software (OZM Research) was used to evaluate the measurement results; this evaluation is based on Eq. (1), [31] The uncertainty of the pressure measurement is within 0.5% as given by the manufacturer.

$$\mathbf{u(p)} = \left(\frac{\mathbf{e_0}}{(\mathbf{P_{max}} - \mathbf{P_z})}\right) * \left(\frac{\mathbf{dp}}{\mathbf{dt}}\right) \ldots\ldots\ldots\ldots\ldots\ldots (\mathbf{1})$$

Where
$\mathbf{e_0}$ is unit burning thickness of solid propellant grain
$\mathbf{P_{max}}$ is maximal pressure in closed bomb
$\mathbf{P_z}$ **i**s ignition pressure
$\left(\frac{\mathbf{dp}}{\mathbf{dt}}\right)$ is the pressure change as a function of time

2.3.18 Vacuum stability test STABIL: A modernized Czech vacuum stability test (STABIL 16-E STABIL VI apparatus [32], manufactured by OZM Research) was used; the original apparatus is described in Ref. [33] and used procedure of measurement was according to papers [34, 35]. The used STABIL methodology is compatible with the STANAG [36].

2.3.19 Glass transition temperature (T_g) by Artemis dynamic mechanical analysis (DMA-T_g): NETZSCH's DMA 242 E Artemis dynamic mechanical analysis (DMA) device was used to determine the mechanical properties of fuel samples. Fuel samples were bent in the dual cantilever mode, measuring 50.0 x 10.0 x 2.0 mm (fixing the samples at two ends). DMA analysis was carried out in an inert gas flow (nitrogen, 50 ml/min) at a temperature range of -120 to 30 °C with a temperature increase rate of 2 °C/min and a frequency of 1 Hz. The deformation has an amplitude of 20 µm. For every fuel sample, there were two measurements taken. The maximum of the loss modulus (E'') peak vs temperature was used to calculate the glass transition temperature. The average of the data is known as the glass transition temperature (T_g).

2.3.20 X-Ray photoelectron spectroscopy (XPS): The surface chemical composition of the mixed nitramine crystals was determined by X-ray photoelectron spectroscopy (XPS, ESCA2SR, Scienta-Omicron) using a monochromatic Al Kα (1486.7 eV) X-ray source operated at 200 W. The samples were fixed in sample holders with a carbon conductive adhesive tape. The measurements were carried out in an analysis chamber at a pressure below 5×10^{-9} mbar and in the fixed analyzer transmission (FAT) mode. The survey and high-resolution spectra were recorded at a pass energy of 150 and 50 eV, respectively. The

following sequence of spectra was recorded: survey spectrum, C 1s, O 1s, N 1s and C 1s again to verify the stability of the charge as a function of time. The surface-charge compensation of the samples was controlled by a charge neutralizer (CN 10). The binding-energy (BE) scale of the spectra was corrected taking the adventitious carbon at 284.8 eV as a reference. The data analysis was performed using a Shirley type background with the CasaXPS software (Casa Software Ltd) employing the elemental sensitivity factors provided by the manufacturer (Scofield's factors).

2.4 Software / Computational Methods

2.4.1 FEST: The new method/algorithm, called FEST [22] (innovative method of probit analysis [23]), was used to determine the probability levels of the initiation. The obtained sensitivity was expressed as the drop energy, E_{dr}, versus a percentage of initiation. The 50 % (E_{dr} 50 %) and 95 % (E_{dr} 95 %) probability of initiation are specified in this current work.

2.4.2 CHEETAH (Thermochemical calculations): The theoretical detonation parameters (detonation velocity D, detonation pressure P and detonation energy E_{det}) for the compositions tested as well as pure explosives were calculated using the CHEETAH code [37] with the BKWS set of parameters for the BKW (Becker-Kistiakowsky-Wilson) equation of state, that is, $\alpha = 0.5$, $\beta = 0.298$, $\kappa = 1050$, $\Theta = 6{,}620$ [38]. The detonation energy is a sum of mechanical and thermal energies released during the detonation process. Mechanical energy represents the amount of energy available to do mechanical work, and it is equal to the expansion work of detonation products and determined for the volume of detonation products corresponding to a pressure of 1 atm. In contrast, thermal energy is the heat in the detonation products under this pressure. For these calculations, the composition of detonation products was frozen at a temperature of 1800 K on the Isentrope beginning at the CJ point. The final thermal energy determined for all compositions and explosives was zero. The calculated detonation parameters for the compositions and the pure explosives are presented in the Tables.

In contrast, thermal energy is the heat in the detonation products at this pressure [39, 40]. For these calculations, the composition of detonation products was frozen at a temperature of 1800 K on the Isentrope beginning at the CJ point. The thermal energy determined for all compositions and explosives was zero.

2.4.3 ICT-Thermodynamic code calculations: The effect of the nitramines on the properties of the SHRP was determined with the ICT-Thermodynamic Code (version 1.00) program. The ICT-code uses mass action and mass balance expressions to calculate chemical equilibria. Thermodynamic equilibria can be estimated for constant pressure or volume conditions. The following settings were set to exclude gases with mole numbers smaller than 10-5; start temperature for iterations: 3000 K; step temperature iteration:

20 K; freeze-out temperature: 1500 K. It was assumed that the pressure in the engine chamber is 70 bar and gaseous products expand to a pressure of 1 bar, while the heat of combustion value was calculated for a pressure of 0.1 bar.

2.4.4 CCDC & Mercury: Crystal structure information had a vital role to play in understanding crystallization. The Cambridge Crystallographic Data Centre (CCDC) has included serving as a trustee and training several scientists partly originated from his view of nucleation as a process in which desolation mechanisms play a central role in the self-assembly journey of molecules in solution. Thus, the structural study of solvates could shed light on the transition states leading to anhydrous forms [41, 42].

To better understand the mutual interactions of component molecules in CACs, their spectral data are compared in the main text with characteristics of molecular crystals of these components taken from the CCDC crystal database [29, 30]. The ORTEP views of the used nitramines and all coformers were plotted using mercury and measured distances between the atoms in molecules [43, 45], which helped to understand structural predictions orientations and intermolecular modifications concerning H-bonding, π-π stackings, van der Waals interactions and other short connections in pure EMs and possibility of involvements in CACs [45].

2.3.21 Hirshfeld surface analysis: The Crystal Explorer 3.0 (version 17.5) software tool was utilized to examine Hirshfeld surfaces [46] and the corresponding 2D fingerprint plots [47]. In this paper, the measured specific chemical interactions of the pure coformers CL20 and BCHMX are visually represented. The Hirshfeld surfaces were systematically generated and analyzed based on their d_{norm} and shape-index features. The d_{norm} function exhibits a symmetry with respect to the distances from the nuclei inside and outside the Hirshfeld surfaces (d_i and d_e, respectively) to their corresponding van der Waals (vdW) radii. This symmetry facilitates the detection of significant regions involved in intermolecular interactions. This technique also makes it easier to find the crucial regions for these intermolecular interactions. The d_{norm} surfaces have been plotted using a predefined color scale, ranging from −0.086 au (red) to −0.605 Å au (blue). The shape-index characteristic relies on the local curvature of a surface and has been found to be highly successful in applications recognizing the planar characteristics of π-stacking arrangements [47, 48].

2.5 Preparation of co-crystals of attractive nitramines *via* Coagglomeration Method

As it was previously mentioned, also as stated in research problem the earlier reported traditional cocrystallization methods are lacking the scalability-industrial scale production to overcome this; from the traditional methods of co-crystallization, we developed an interesting “the slurry method” of EECCs preparation, i.e., co-agglomeration, which is based on:

Table 2.1 Solvent system in preparation of CACs of attractive nitramines

		Coagglomeration Process	
No	Code design.	i. Coprecipitation	ii. Coagglomeration
1	32 HMX/TATB	DMFA/water	CHF
2	33 BCHMX/TATB	DMFA/water	CHF
3	34 CL-20/TATB	DMFA/water	CHF
4	35 RDX/TATB	DMFA/water	CHF
5	Cp1 BCHMX/DATB	NMP/water	BuOH
6	Cp2 BCHMX/DATB	NMP/water + Surfactant	BuOH
7	Cp3 RDX/DATB	NMP/water	BuOH
8	Cp4 δ-HMX/DATB	DMSO/water	BuOH
9	Cp5 ß-CL-20/DATB	DMSO/water	BuOH
10	3 HMX/ HNS	DMSO/water	BuOH
11	6 HMX/ HNS	DMSO/water	BuOH
12	8 HMX/ HNS	DMSO/water	BuOH
13	17 RDX/ HNS	DMF/water/	CHF
14	18 CL-20/ HNS	DMF/water	CHF
15	19 BCHMX/ HNS	DMF/water	CHF
16	20 RDX/ HNAB	DMK/hexane	CHF
17	21 BCHMX/ HNAB	DMK/hexane	CHF
18	22 CL-20/ HNAB	DMK/hexane	CHF
19	31 HMX/ HNAB	DMK/hexane	CHF
20	38 HMX/ HNAB	DMK/hexane	CHF
21	39 CL-20/ HNAB	DMK/hexane	CHF
22	S4 CL20/BCHMX	DMSO/water	CHF
23	S4LV CL20/BCHMX	DMSO/water	CHF
24	S4LZ CL20/BCHMX	DMSO/water	CHF
25	S5 CL20/BCHMX	DMSO/water	BuOH
26	S5LV CL20/BCHMX	DMSO/water	BuOH
27	CCs 1 CL20/BCHMX*	Ethyl-acetate/hexane	NA
28	CCs 2 CL20/BCHMX*	Ethyl-formate/hexane	NA
29	57 CL20/ PANi	DMSO/water	CHF
20	58 HMX/PANi	DMSO/water	CHF
31	59 BCHMX/PANi	DMSO/water	CHF
32	60 RDX/PANIi	DMSO/water	CHF
33	9 RDX/BTATz B1	Dimethyl Pyralidone/Water	CHF
34	10 RDX/BTATz B2	Dimethyl Pyralidone/Water	CHF
35	11 HMX/BTATz B1	DMSO/Water	CHF
36	12 HMX/BTATz B2	DMSO/Water	CHF
37	13 CL20/BTATz B1	Dimethyl Pyralidone/Water	CHF
38	14 CL20/BTATz B2	Dimethyl Pyralidone/Water	CHF
39	15 BCHMX/BTATz B1	Dimethyl Pyralidone/Water	CHF
40	16 BCHMX/BTATz B2	Dimethyl Pyralidone/Water	CHF

Note: i) *CCs 1 & 2 CL20/BCHMX prepared by traditional coprecipitation method
ii) DATB CACs coprecipitation carried out employing water jet pump; remaining solution of nitramines mixed with vigorously stirring water as per principle of coagglomeration method

- Susceptibility mainly of the RDX and HMX nanoparticles to self-glomeration to sizes of 5-7 μm essentially immediately after preparation.
- Facilitating this self-glomeration (co-agglomeration) by the presence of a small amount of solvent in which the components are very slightly to minutely soluble.

The preparation of co-agglomerated crystals (CACs) with specific energetic coformers (shown Figure 2a to d) and the aforementioned attractive nitramines (shown Figure 2c to h) was conducted using a primarily two-step procedure [49].

- First step - the co-precipitates are prepared by employing the rapid solvent-antisolvent method. This method involves introducing a solution containing co-formers, which do not necessarily possess a defined crystallography and can be obtained directly from their production after stabilization (E.g., introducing water into the acetonic solution).

- Second step - Co-agglomeration strategy involves combining a small quantity of solvent with a co-precipitate, resulting in a well-mixed slurry (in which components exhibit low solubility in the solvent). Subsequently, the slurry is subjected to heating for a specific duration, reaching a temperature around the boiling point of the solvent.

Co-agglomerated crystals (CACs) of selected coformers using the above described technique, which consists primarily of two steps [49], in which 1 g of coformers (their molecular structures see in Figure 1g – l) together with 4 g of the respective nitramines (HMX, BCHMX, CL-20 and RDX – their molecular structures in Figure 2.1a – k)). The obtained CACs were dried, labeled, and then thoroughly analyzed using the analytical techniques described in section 2.3 for phase purity and morphology. Additionally, upon coagglomeration, underlying intermolecular interactions in both coformers were characterized.

2.6 Application of the CACs

2.6.1 Preparation of samples of propellants

Propellant compositions are prepared as per Table 2.2, each batch size 700 gm have been prepared. The mixing conditions 10 min in normal atmospheric and 15 min in vacuum conditions. For coarse AP it will be 10 and 30 mins followed by for HMX and for plasticizer mixing 5 and 10 min. Based on the received results. BCHMX suitability as physical mixture and CACs with HMX for the respective application can be

effectively evaluated in chapter 4. This can help design new combinations of nitramines for applications in propellants.

Table 2.2 Propellant composition with individual components [Sample codes]

Components / %	Series - I (10 %) [**P1**. **P4**. & **P7**]	Series – II (20 %) [**P2**. **P5** & **P8**]	Series – III (30 %) [**P3**. **P6**. & **P9**]
AP	56	46	36
HTPB	11	11	11
Al	18	18	18
HMX/ PhysMix / CACs	10	20	30
FeNPs	1.0	1.0	1.0
Plasticizer(DDI)	2.1	2.1	2.1
Curing Agent (ADO)	1.9	1.9	1.9
Total	100 %		

Here. CACs- co-agglomerates of HMX/BCHMX; PhysMix- HMX/BCHMX physical mixture;

2.6.2 Charging and pressing of detonator for CACs of CL20/BCHMX

The test of the initiation strength of coagglomerates (CACs) of CL20 with BCHMX was carried out according to standard [50] with weights from 51 to 300 mg of selected CACs, in aluminium shells of 7.5 mm diameter, with a pressure of 60 kg per pressing pin, with a secondary charge of 720 mg pentaerythritol tetranitrate (PETN), pressed by a pressure of 180 kg per pressing pin. The adjusted detonator was then placed on a 5 mm thick lead plate, and the detonator was initiated according to the standard procedure [21].

2.6.3 The preparation of gunpowder

This nitrocellulose GRADE C type I was phlegmatized with 30% alcohol. After submission to the homogenizer, it was kneaded. Sufficient mixed solvent was then added to the nitrocellulose to achieve the desired consistency. Subsequently, the desired amount of RDX moistened with ethanol was added to the gelatinized nitrocellulose. In such an amount that the resulting powder contained 10 % pure RDX - this sample was named S10.1. Sample S10.2 was similarly processed, containing 89 % NC and 10 % of the RDX/BCHMX Physical mixture. The last sample named S10.3, contained 89% NC and 10% KP RDX/BCHMX CACs. In addition, 1% diphenylamine was added to the samples as a chemical stabilizer.

Once the sample was mixed, the powder dough was transferred to a press, which was used to extrude the munitions blank through the selected matrix. The extruded powder strips were uncut to the desired size. The die allowed the extrusion of 1.5x0.34 mm strips. By cutting, the grain size was adjusted to 1.5x1.5x0.34

mm, Figure 2.2. The cut grains were dried. By soaking in water, the mixed solvent was removed to the normally required limit (assessed as volatile content). The powder samples were then dried and graphed.

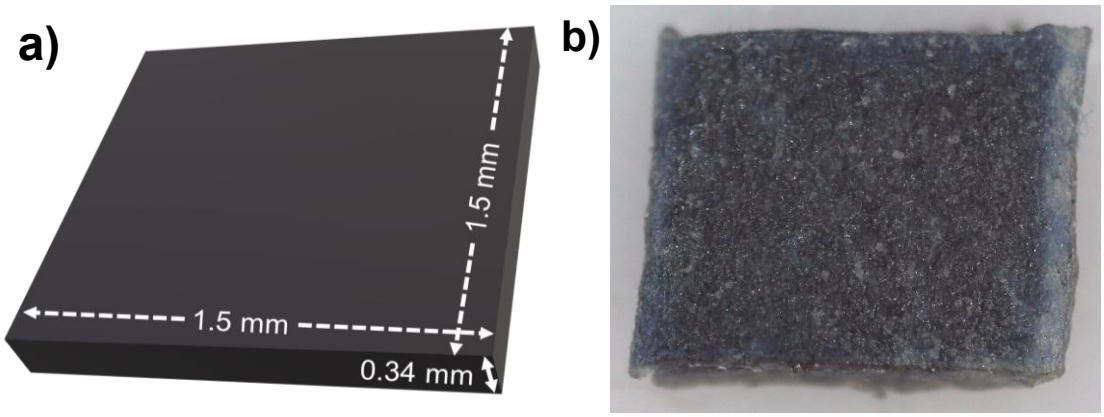

Figure 2. 2 a) Schematic of gunpowder grain with dimensions and b) real enlarged image of powder grain sample S10.2.

References

[1] D. Klasovitý, S. Zeman, A. Růžička, M. Jungová, and M. Roháč, "cis-1,3,4,6-Tetranitrooctahydroimidazo-[4,5-d]imidazole (BCHMX), its properties and initiation reactivity," Journal of Hazardous Materials, vol. 164, no. 2–3, pp. 954–961, May 2009, doi: 10.1016/j.jhazmat.2008.08.106.

[2] S. Zeman, A. K. Hussein, A. Elbeih, and M. Jungova, "cis-1,3,4,6-Tetranitrooctahydroimidazo-[4,5-d]imidazole (BCHMX) as a part of explosive mixtures," Defence Technology, vol. 14, no. 5, pp. 380–384, Oct. 2018, doi: 10.1016/j.dt.2018.04.002.

[3] A. Ikhlas, M. Elbeih, A. Husarova, S. Zeman, "Method of preparation of ε-2,4,6,8,10,12-hexanitro-2,4,6,8,10,12-hexaazaisowurtzitane with reduced impact sensitivity," WO2013044891A1, Apr. 04, 2013

[4] J. P. Agrawal, and R. D. Hodgson, Organic Chemistry of Explosives. John Wiley & Sons, Inc, 2007.

[5] M. E. H. K.G. Shipp, T.N. Hall, "No Title," Report 6225,U.S. Naval Ordnance Laboratory, White Oak, Silver Spring 1958, available as Report AD 307 213, NTIS Sprinfield, 1974, p. 6225, 1974.

[6] E. J. Graeber and B. Morosin, "The crystal structures of 2,2',4,4',6,6'-hexanitroazobenzene (HNAB), forms I and II," Acta Crystallogr B Struct Sci, vol. 30, no. 2, pp. 310–317, Feb. 1974, doi: 10.1107/S0567740874002731.

[7] V. B. Patil, M. Nadagouda, S. Ture, C. V. Yelamaggad, and V. Abbaraju, "Detection of energetic materials via polyaniline and its different modified forms," Polymers for Advanced Technologies, vol. 32, no. 12, pp. 4663–4677, Dec. 2021, doi: 10.1002/pat.5458.

[8] V. B. Patil, S. Ture, C. Yelamaggad, M. Nadagouda, and A. Venkataraman, "Turn-off Fluorescent Sensing of Energetic Materials using Protonic Acid doped Polyaniline: A Spectrochemical Mechanistic Approach,"

Zeitschrift fur Anorganische und Allgemeine Chemie, vol. 647, no. 4, pp. 331–340, Feb. 2021, doi: 10.1002/zaac.202000321.

[9] A. Saikia et al., “Synthesis and characterization of 3,6-bis(1H-1,2,3,4-tetrazol-5-ylamino)-1,2,4,5-tetrazine (BTATz): Novel high-nitrogen content insensitive high energy material,” Journal of Hazardous Materials, vol. 170, no. 1, pp. 306–313, Oct. 2009, doi: 10.1016/j.jhazmat.2009.04.095.

[10] P. Hakey, W. Ouellette, J. Zubieta, and T. Korter, “Redetermination of cyclo -trimethylenetrinitramine,” Acta Crystallogr E Struct Rep Online, vol. 64, no. 8, pp. o1428–o1428, Aug. 2008, doi: 10.1107/S1600536808019727.

[11] L. Zhang et al., “Experimental Study of the Crystal Habit of High Explosive Octahydro-1,3,5,7-tetranitro-1,3,5,7-tetrazocine (HMX) in Acetone and Dimethyl Sulfoxide,” Crystal Growth & Design, vol. 20, no. 10, pp. 6622–6628, Oct. 2020, doi: 10.1021/acs.cgd.0c00766.

[12] B. Krebs, J. Mandt, R. E. Cobbledick, and R. W. H. Small, “The structure of N,N-dimethylnitramine,” Acta Crystallogr B Struct Crystallogr Cryst Chem, vol. 35, no. 2, pp. 402–404, Feb. 1979, doi: 10.1107/S0567740879003630.

[13] N. B. Bolotina, M. J. Hardie, R. L. Speer Jr, and A. A. Pinkerton, “Energetic materials: variable-temperature crystal structures of γ- and ∈-HNIW polymorphs,” J Appl Crystallogr, vol. 37, no. 5, pp. 808–814, Oct. 2004, doi: 10.1107/S0021889804017832.

[14] O. Bolton and A. J. Matzger, “Improved Stability and Smart-Material Functionality Realized in an Energetic Cocrystal,” Angew. Chem. Int. Ed., vol. 50, no. 38, pp. 8960–8963, Sep. 2011, doi: 10.1002/anie.201104164.

[15] Y. Kohno et al., “Molecular Dynamics Studies of the Structural Change in 1,3-Diamino-2,4,6-trinitrobenzene (DATB) in the Crystalline State under High Pressure,” J. Phys. Chem. A, vol. 113, no. 11, pp. 2551–2560, Mar. 2009, doi: 10.1021/jp809240x.

[16] H. H. Cady and A. C. Larson, “The crystal structure of 1,3,5-triamino-2,4,6-trinitrobenzene,” Acta Cryst, vol. 18, no. 3, pp. 485–496, May 1965, doi: 10.1107/S0365110X6500107X.

[17] M. A. Rodriguez, C. F. Campana, A. D. Rae, E. Graeber, and B. Morosin, “Form III of 2,2′,4,4′,6,6′-hexanitroazobenzene (HNAB-III),” Acta Crystallogr C Cryst Struct Commun, vol. 61, no. 3, pp. o127–o130, Mar. 2005, doi: 10.1107/S0108270105000569.

[18] Y. Liu, L. Chen, J. Wang, J. Chen, J. Wang, and H. Pan, “The crystal structure and thermal decomposition kinetics of cis -hexanitrostilbene,” Acta Crystallogr B Struct Sci Cryst Eng Mater, vol. 77, no. 1, pp. 150–157, Feb. 2021, doi: 10.1107/S2052520620015371.

[19] G. Parvari et al., “Proposed Proton-Transfer Mechanism for the Initial Decomposition Steps of BTATz,” J. Phys. Chem. A, vol. 122, no. 27, pp. 5789–5798, Jul. 2018, doi: 10.1021/acs.jpca.7b12217.

[20] “Public Notice of Czech Mining Authority No. 246/1996 Collection of Czech Laws, Establishing more Detailed Conditions for Allowing Explosives, Explosive Objects and Aids into Use, and Their Testing, P 3200-3208.” Czech Mining Authority, Aug. 13, 1996.

[21] M. Suceska, Test Methods for Explosives. Springer, 2012.

[22] J. Selesovsky, V. Pelikan, J. Schuster, B. Janovský, and R. Matyáš, “FEST – New Procedure for Evaluation of Sensitivity Experiments,” Propellants, Explosives, Pyrotechnics, vol. 45, no. 11, pp. 1813–1818, 2020, doi: 10.1002/prep.202000120.

[23] J. Šelešovský, J. Pachmáň, “Probit Analysis – a Promising Tool for Evaluation of explosive’s sensititvity,” vol. 7, no. April, pp. 269–278, 2010.

[24] Directive 2014/28/EU, “Explosives for civil uses.” European Union, Apr. 20, 2016.

[25] The European standard 1363104, “Explosives for civil uses high explosives Part 4: Determination of sensitivity to impact.” 2002.

[26] Z. Kamenský, “Electric Spark Sensitivity of Polynitro Compounds; M.Sc. Thesis, University of Pardubice,” 1995.

[27] S. Zeman, Z. Kamenský, P. Valent, J. Jakubko, “On the Electrostatic Spark Sensitivity of Some Organic Polynitro Compounds, in: M. Roux (Ed.) [Proc.], Recueil des comunications ‘Journees d´etudes sur la sensibilité des composants et des substances énergét. á l´electricite statique’. Aussois,” pp. 197–206, May 1996.

[28] S. Zeman, P. Valenta, V. Zeman, Z. Kamenský, “Electric Spark Sensitivity of Polynitro Compounds: A Comparison of some Authors; Results, HanNeng CaiLiao,” vol. 6, pp. 118–122, 1998.

[29] “Standard Test Method for Rubber Property - Durometer Hardness. ASTM D2240-05; Annual Book of ASTM Standards.” 2005.

[30] F. Bogdan, B. Rafał, S. Wincenty, C. Michał, “Study of the effect of nitrated hydroxy-terminated polybutadiene (NHTPB) content on the properties of heterogeneous rocket propellant,” Cent. Eur. J. Energ. Mater., vol. 12, no. 4, pp. 841–854, 2015.

[31] S. P, “The Use of Low Pressure Closed Vessel and Rocket Motor for Measurements of Burning Rate of Rocket Solid Propellants,” in NTREM2009, Czech Republic: University of Pardubice, 2006, pp. 730–735.

[32] M. Krupka, “Devices and equipment for testing of energetic materials,” in New Trends in Research of Energetic Materials, Pardubice, Univ. Pardubice: Pardubice, Univ. Pardubice, Apr. 2001, p. 222.

[33] V. Kučera and B. Vetlický, “Investigation of the Decomposition Processes in Single-Base Propellants under vacuum using a minicomputer-controlled automated apparatus,” Propellants, Explosives, Pyrotechnics, vol. 10, no. 3, pp. 65–68, 1985, doi: 10.1002/prep.19850100303.

[34] S. Zeman, Š. Gazda, A. Štolcová, and A. Dimun, “Dependence on temperature of the results of the vacuum stability test for explosives,” Thermochimica Acta, vol. 247, no. 2, pp. 447–454, Dec. 1994, doi: 10.1016/0040-6031(94)80144-4.

[35] S. Zeman, A. Elbeih, A. Hussein, T. Elshenawy, M. Jungova, and Q. L. Yan, “A modified vacuum stability test in the study of initiation reactivity of nitramine explosives,” Thermochimica Acta, vol. 656, pp. 16–24, Oct. 2017, doi: 10.1016/j.tca.2017.08.006.

[36] NATO, “NATO - STANAG 4556 - Explosives: Vacuum Stability Test | GlobalSpec.” Belgium, Nov. 22, 1999. Accessed: Nov. 14, 2023. [Online]. Available: https://standards.globalspec.com/std/188120/STANAG%204556

[37] L E. Fried, “CHEETAH 1.39 Users’ Manual UCRL-MA-117541.” CA: Lawrence Livermore National Laboratory., 1996.

[38] M. L. Hobbs, and M. R. Baer, “Calibrating the BKW-EOS with a large products species base and measured C-J properties.,” in Proceedings of the 10th Symposium (International) on Detonation, 1993, pp. 409–418.

[39] W. C. Davis and W. Fickett, “DETONATION THEORY AND EXPERIMENT.,” pp 2-12 of Behaviour of Dense Media Under High Dynamic Pressures. New York, Gordon and Breach, 1968., Oct. 1969, Accessed: Aug. 15, 2021. [Online]. Available: https://www.osti.gov/biblio/4785669

[40] W. Ficket, and W. C. Davies, Detonation. Berkeley, CA: University of California Press, 1979.

[41] A. J. Cruz-Cabeza et al., “Can solvated intermediates inform us about nucleation pathways? The case of β- p ABA,” CrystEngComm, vol. 22, no. 43, pp. 7447–7459, 2020, doi: 10.1039/D0CE00970A.

[42] Y. Xiao, S. K. Tang, H. Hao, R. J. Davey, and T. Vetter, “Quantifying the Inherent Uncertainty Associated with Nucleation Rates Estimated from Induction Time Data Measured in Small Volumes,” Crystal Growth & Design, vol. 17, no. 5, pp. 2852–2863, May 2017, doi: 10.1021/acs.cgd.7b00372.

[43] I. J. Bruno et al., “New software for searching the Cambridge Structural Database and visualizing crystal structures,” Acta Crystallogr B Struct Sci, vol. 58, no. 3, pp. 389–397, Jun. 2002, doi: 10.1107/S0108768102003324.

[44] Cambridge Crystallographic Data Centre, Inc., One Boston Place, Suite 2600, Boston, MA 02108, and United States, “The Cambridge Crystallographic Data Centre (CCDC).” [Online]. Available: https://www.ccdc.cam.ac.uk/structures/

[45] C. F. Macrae et al., “Mercury 4.0 : from visualization to analysis, design and prediction,” J Appl Crystallogr, vol. 53, no. 1, pp. 226–235, Feb. 2020, doi: 10.1107/S1600576719014092.

[46] J. J. McKinnon, D. Jayatilaka, and M. A. Spackman, “Towards quantitative analysis of intermolecular interactions with Hirshfeld surfaces,” Chem. Commun., no. 37, p. 3814, 2007, doi: 10.1039/b704980c.

[47] J. J. McKinnon, M. A. Spackman, and A. S. Mitchell, “Novel tools for visualizing and exploring intermolecular interactions in molecular crystals,” Acta Crystallogr B Struct Sci, vol. 60, no. 6, pp. 627–668, Dec. 2004, doi: 10.1107/S0108768104020300.

[48] M. A. Spackman, M. J. Turner, M. J.J.J McKinnon, J. J. Wolff, S. K. Grimwood, DJPR Spackman, D . Jayatilaka, “Crystal Explorer 17.” Univ. West. Aust. [Online]. Available: . http://hirshfeldsurface.net

[49] V. B. Patil, K. Zalewski, J. Schuster, P. Belina, W. Trzcinski, and S. Zeman, “A new insight into the energetic co-agglomerate structures of attractive nitramines,” Chemical Engineering Journal, vol. 420, Sep. 2021, doi: 10.1016/j.cej.2021.130472.

Chapter 3 Results and Discussions

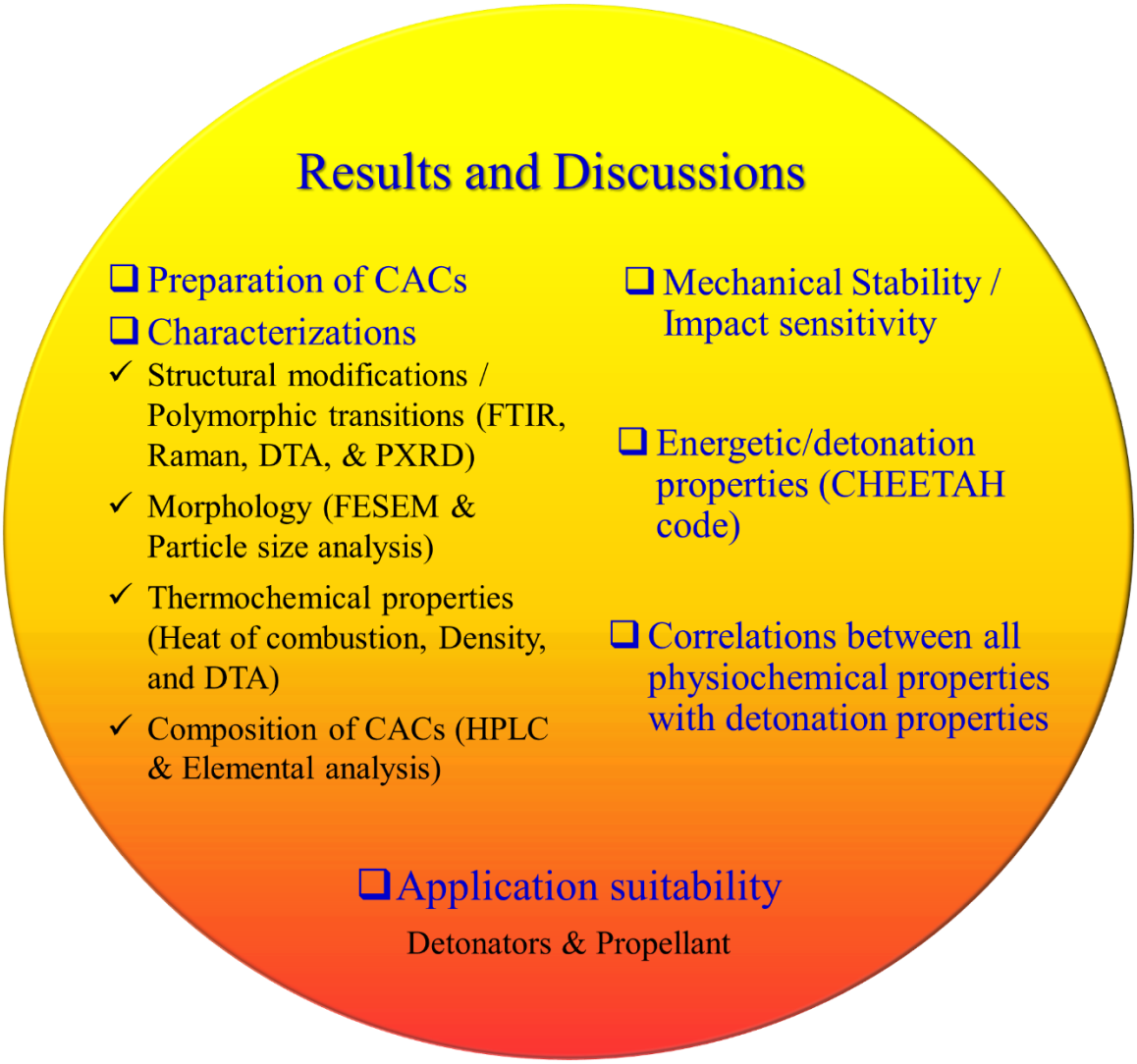

3.1 Co-agglomerated crystals of 1,3-di- and 1,3,5-tri-amino-2,4,6-trinitrobenzenes with attractive cyclic nitramines

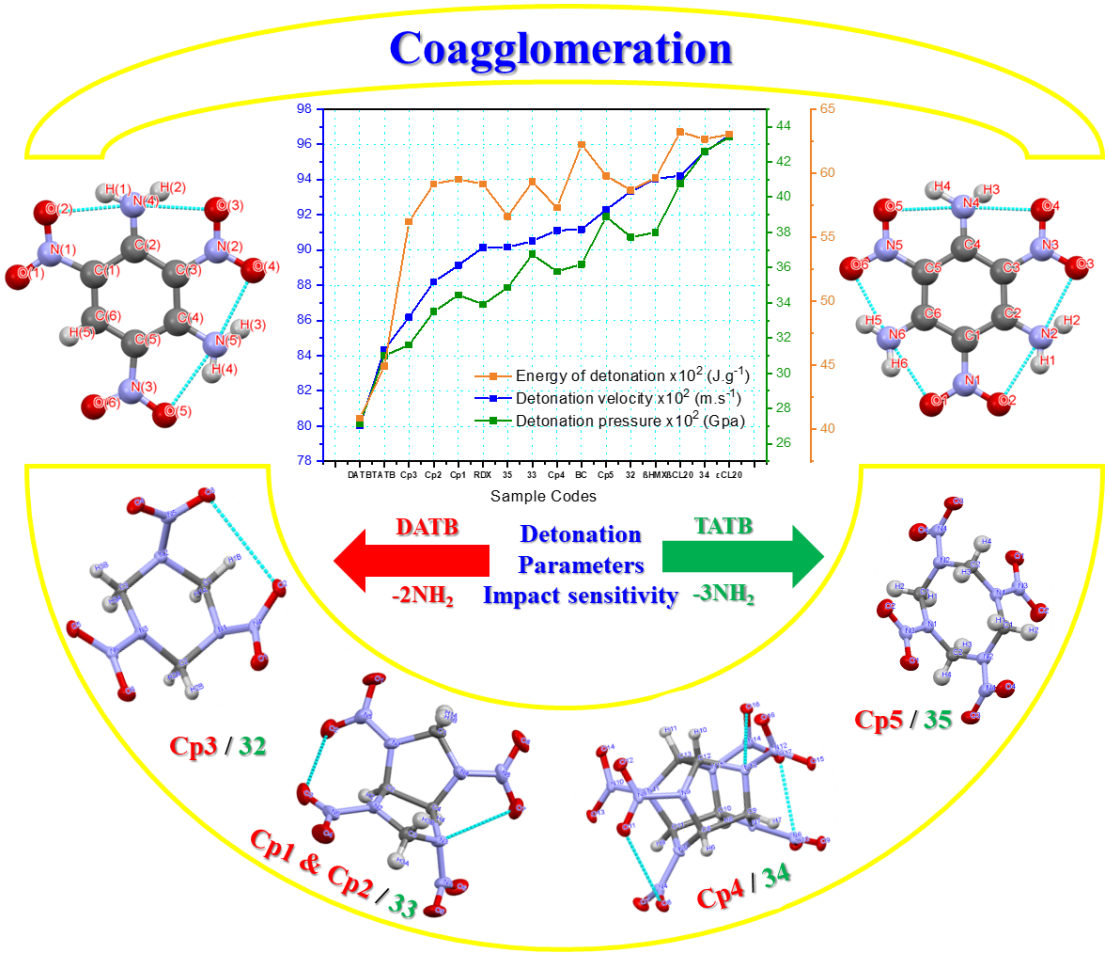

Published in…

Chemical Engineering Journal;
Vol. 420, 3, 2021, P 130472, DOI:10.1016/j.cej.2021.130472

Journal of Industrial and Engineering Chemistry;
Vol. 115, 25, 2022, P 135-146, DOI: 10.1016/j.jiec.2022.07.043

3.1.1 Background

The co-formers for the modification of technically suitable nitramines are the highly insensitive 1,3,5-triamino-2,4,6-trinitrobenzene (TATB) [1, 2] and 1,3-diamino-2,4,6-trinitrobenzene (DATB) [3] whose planar molecules form the planar nets with face to face and crossed stackings in their crystal lattices respectively [2]. Especially TATB, which is highly insoluble in the usual solvents. The positioning of these both in the crystal lattice of the nitramine creates the N-O---H hydrogen bonding between $-NO_2$ (nitramine) and $-NH_2$ (TATB) and π-π stacking. In addition, van der Waals force interactions [2, 4, 5] can be observed, potentially initiating the nitramine's reactivity. However, practical experience in this area was limited to CL-20 and HMX [6]. The other two nitramines, BCHMX and RDX, were left aside; thus, no comprehensive evaluation of the effect of TATB on the reactivity of these particular nitramines was carried out. In this work, we prepared co-agglomerates/co-crystals of these nitramines with TATB and DATB using a coagglomeration method. Firstly, we attempted DATB and then repeated it with the TATB [7, 8], the approximately planar molecules linked in its crystal by intermolecular hydrogen bonds into continuous chains [9]. The stabilizing effect of DATB was clearly evident but only in the case of its co-agglomeration with RDX and HMX [10]. To clarify the effect of polyamino-derivatives of 1,3,5-trinitrobenzene on the impact sensitivity of suitable nitramines in particular, presented here our results from the application of DATB and TATB cocrystals.

3.1.2 Results

3.1.2.1 Morphology and particle size analysis

Detailed morphology and particle size results are summarized in Table 3.1.1. All CACs pictured in Figure 3.1.1 (a-h). All the DATB CACs shown smoother edges with irregular shapes. Especially in case of the BCHMX/DATB slight sharp edges. Similarly in case of TATB CACs, show granular 'pop-corn'-like structures except for 32 HMX/TATB where the FESEM images (1a & 1b) show a 'rice grain'-like particle structure. In the case of 33 BCHMX/TATB, particles show slightly irregular shapes with slightly sharper edges (Figure 3.1.1c & 3.1.1d). All CACs, with the exception of 34 CL-20/TATB, exhibit slightly smaller particle sizes (Figure 3.1.1e & 3.1.1f). The case of 35 RDX/TATB (Figure 3.1.1g & 3.1.1h) shows similar characteristics. From the FESEM images it is also clear that the DATB and TATB particles shown uniform distribution on surface of nitramines in all cases. In all four cases, particles exhibit smooth surfaces. The presence of these active interactions between particles of both co-former nitramines helps enhance intermolecular interactions in the molecular crystals. These active interactions between the co-formers also help to achieve high density CACs [7].

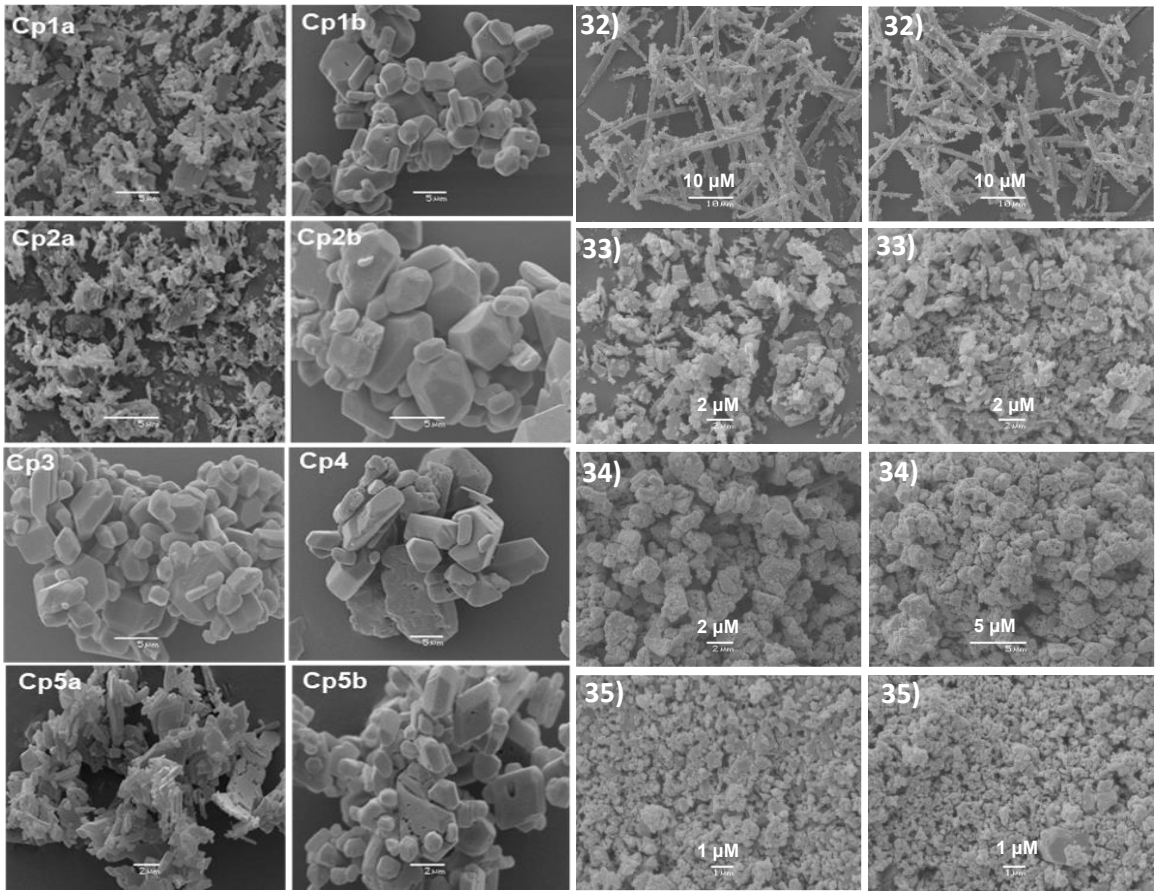

Figure 3.1.1 FESEM images of cocrystals -Cp1: BCHMX/DATB, Cp2: BCHMX/DATB, Cp3: RDX/DATB, Cp4: δ-HMX/DATB, Cp5: β-CL-20/DATB, a & b: 32 HMX/TATB, c & d: 33 BCHMX/TATB, e & f: 34 CL-20/TATB and g & h: 35 RDX/TATB.

Table 3.1.1 The particle size measurements results

Sr No's	Code design.	Surface area (m^2/kg)	Dv(50) µM	Dv(90) µM	Continous phase in agglomeration
1	32p HMX/TATB	2884	3.21	13.6	DMFA/water
2	32 HMX/TATB	3160	2.45	12.0	chloroform
3	33p BCHMX/TATB	3765	1.93	59.3	DMFA/water
4	33 BCHMX/TATB	3765	1.69	12.8	chloroform
5	34p CL-20/TATB	5551	1.82	3.91	DMFA/water
6	34 CL-20/TATB	5633	1.77	3.88	chloroform
7	35p RDX/TATB	4020	12.9	43.4	DMFA/water
8	35 RDX/TATB	4614	12.5	43.1	chloroform
9	BCHMX/DATB-Cp1	621.1	14.1	33.3	hot water[a]
10	BCHMX/DATB-Cp2	70.6	127.0	1809.0	hot water[a]
11	RDX/DATB-Cp3	433.5	23.4	53.3	n-butanol
12	δ-HMX/DATB-Cp4	665.7	12.1	23.6	n-butanol
13	ß-CL-20/DATB-Cp5	1779	22.6	58.1	n-butanol

Notes: a: co-agglomeration at 130 °C in autoclave for 24 hours without stirring [7]
p: after the sample codes indicates the co-precipitate sample (in DMFA/water) of that CAC

3.1.2.2 Powder X-Ray diffraction (PXRD) studies

The crystal phase changes were analyzed for both pure nitramines and CACs using the PXRD technique. The diffractograms of all CACs in comparison with their pure nitramine co-formers obtained at RT are shown in Figure 3.1.2. These help to understand the polymorphic structural modifications in CACs. The 2Θ values found were, respectively: for DATB 11.82º, 14.9º, 22.62º, 27.18º, and 41.4º, also with three intense peaks – at 20.16º, 24.94º and 29.98º; for TATB 27.32˚, 42.12˚, and 42.46˚ with three intense peaks observed at 28.06˚, 31.6 ˚ and 45.38˚; for BCHMX 15.70˚, 16.0˚, 19.74˚, 23.9˚, 30.02˚, 30.11˚, 32.51˚, 33.15˚ and 35.74˚, with three intense sharp peaks at 9.74˚, 12.65˚ and 23.57˚; for RDX 15.65˚, 16.01˚, 19.87˚, 24.12˚, 29.84˚, 30.11˚, 32.52˚, 33.15˚ and 35.65˚, with three intense peaks at 9.73˚, 12.65˚ and 23.59˚; for HMX 13.75˚, 19.48˚, 23.27˚, 25.55˚, 29.71˚, 30.74˚, 36.17˚ and 39.21˚, with five intense peaks at 14.61˚, 16.31˚, 24.45˚, 25.07˚ and 32.31˚, these peaks indicating β-polymorphic modification of HMX; for CL-20 11.88˚, 12.4˚, 17.64˚, 20.4˚, 24.7˚, 27.62˚, 28.78˚, 31.84˚, 32.98˚, 37.98˚, 44.44˚ and 45.38˚ with intense peaks at 14.3˚, 30.1˚, and 42.98˚. Similarly, CACs, the 2Θ values indicate that TATB interacts with co-forming EMs. For 32 HMX/TATB, 2Θ values were found at 13.9˚, 16.44˚, 19.52˚, 23.44˚, 24.6˚, 29.84˚, 32.44˚ with intense peaks at 14.78˚, 25.2˚, and 28.34. These intense peaks indicate that HMX is in its δ form. This crystal-phase change also occurred during the HMX/DATB formation. During interaction with DATB or TATB in the co-agglomeration process, β-HMX converted to its δ-modification [7]. For 33 BCHMX/TATB, the 2Θ values were 10.2˚, 16.38˚, 20.32˚, 24.62˚, 30.32˚, 32.96˚ with intense peaks at 13.12˚, 24.04˚ and 28.54˚. For 34 CL-20/TATB, the 2Θ values were 15.04˚, 17.54˚, 20.16˚, 22.62˚, 25.27˚, 27.52˚, 30.30˚, 33.26˚, 35.82˚, 38.12˚ with intense peaks at 12.12˚, 13.76˚, and 28.02˚ these latter peaks indicating the presence of β-CL-20 [11]. The same observation was found with CL-20/DATB where ϵ-CL-20, after interaction with DATB or TATB during co-agglomeration, converted to its β-modification. Similarly, for 35 RDX/TATB, 2Θ values were 13.08˚, 15.28˚, 17.82˚, 20.32˚, 21.92˚, 26.9˚, 29.24˚, 30.78˚, 32.28˚, 34.70˚ with intense peaks at 17.34˚, 25.36˚, and 28.3˚.These changes and shift diffraction angle indicate that, after the interaction, the β-HMX or ϵ-CL-20 co-formers with TATB and/or DATB, there is a modification/development of a new crystalline phase occurring in the final CACs, which may also be seen through polymorphic changes. Overall, the diffractograms of pure EMs with their CAC with both TATB and DATB were not identical. Small new peaks appeared for all the TATB and DATB CACs, creating a shift in the intense peaks with doublet formation in some of them. However, these variations show an important role adjustment of co-formers in CACs with new crystalline phases. These changes are also seen visually in the FESEM images of these CACs, which show different / modified crystal surfaces compared to the standard FESEM images of the pure EMs. These changes were further confirmed by employing FTIR and Raman techniques.

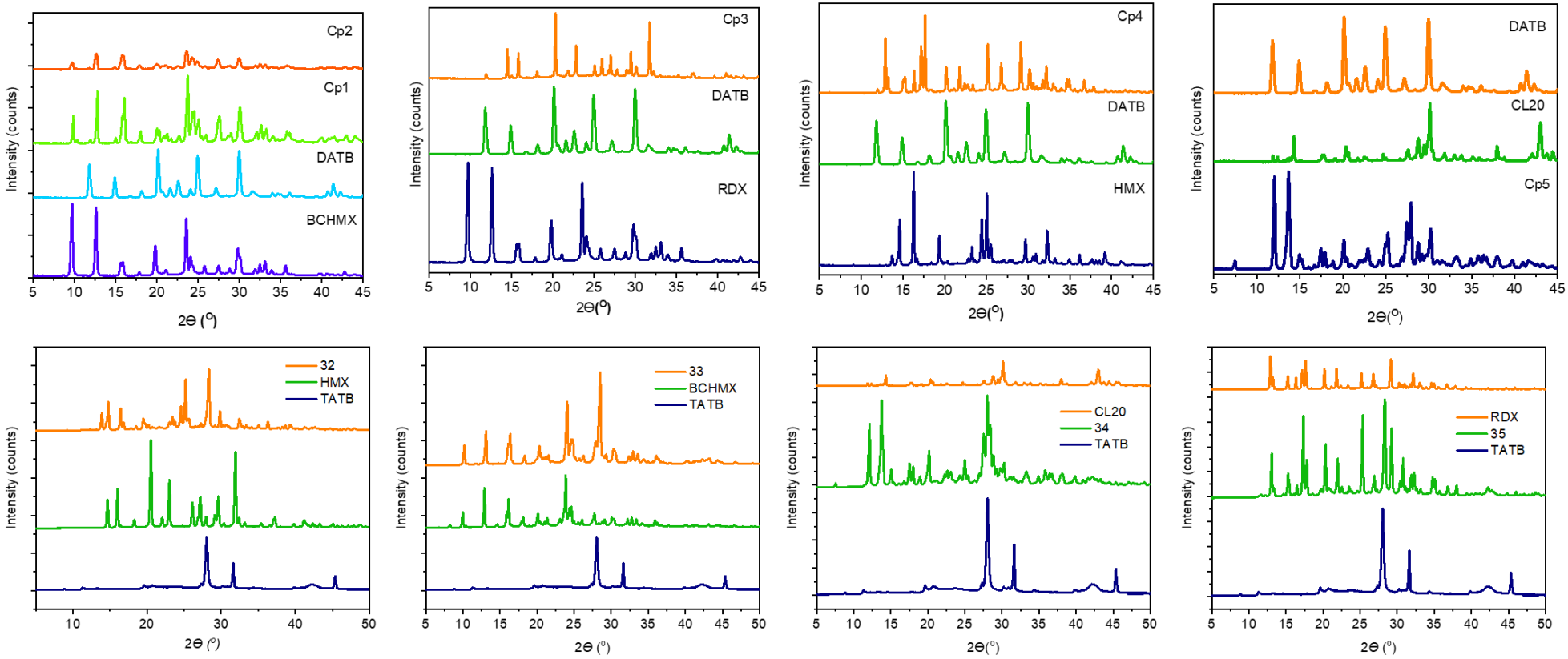

Figure 3.1.2 PXRD diffractograms of co-agglomerated crystals /co-crystals (CACs) Cp1: BCHMX/DATB, Cp2: BCHMX/DATB, Cp3: RDX/DATB, Cp4: δ-HMX/DATB, Cp5: β-CL-20/DATB, 32 HMX/TATB, 33 BCHMX/TATB, 34 CL-20/TATB and 35 RDX/TATB.

3.1.2.3 Differential thermal analysis (DTA)

The CACs' thermal behavior was analyzed using the DTA technique. Their thermograms of both DATB and TATB CACs are shown in Figure 3.1.3, with the details summarized in Table 3.1.2. Apart from these observations, all pure nitramines undergo polymorphic modifications in the resulting CACs when combined with TATB and DATB; both are arranged so that this polymorphic transition is restricted during the heat supply and undergoes melting directly, except with RDX in RDX/TATB. This was also observed with RDX/DATB. TATB apparently decomposes more readily in a solution of the RDX decomposition products (a loss of the stabilizing effect of the crystal lattice – for TATB [12] than in the other CACs studied here. In pure HMX, a polymorphic transition α to δ appeared, while a β to δ change in HMX/TATB is shown. Introducing TATB and DATB into the crystal lattice of nitramines generally produces a slightly negative influence on their thermal stability (in the sense of the exothermic peak position). In the case of the BCHMX, CL-20 and HMX CACs, this lowering of thermal stability is unambiguous for both the TATB and DATB co-formers, whereas for RDX it was observed only for DATB (with TATB increased stability of some +4.4°C was observed).

Table 3.1.2 Summarized data from DTA thermograms of co-formers and co-crystals with visible melting points.

Samples	Melting point / °C [Ref.]	Peaks of changes in DTA record / °C (with phase modifications)	
		Endothermic	Exothermic
ε-CL-20	240 decompn [13]	170 (ϵ - γ)	225 (γ - δ)
α-CL-20[a]	240 decompn [13]	175 (α–γ)	225 (γ–δ)
BCHMX	286 decompn[14]	--	224
β-HMX	--	190 (α – δ)	272
RDX	204	209	215
DATB	286	230; 290; 295	315; 330
TATB	--	320 [24]	357, 365
S32 δ- HMX/TATB	--	184 (β – δ)	268.85
S33 BCHMX/TATB	--	NA	225.01
S34 β-CL-20/TATB	--	NA	217.7
S35 RDX/TATB	--	206.18	219.4
Cp1 BCHMX/DATB	no melt[b]	--	227
Cp2 BCHMX/DATB	no melt[b]	--	231
Cp3 RDX/DATB	194 - 195	198	209
Cp4 δ-HMX/DATB	242 - 248	188[c]; 227[d]; 246[e] (β-δ)	249
Cp5 β-CL-20/DATB	212 - 218	176 (β-γ CL-20)	216

Note: Here, Cw- results obtained in current work; a) between 90° and 105°C very weak, elongated endotherm of the crystal-water evaporation; b) the sample does not melt - above 200°C it began to turn brown; c) a very small peak of the β-δ transition of HMX; d) the value of polymorphic transition of DATB; e) the value of the melting point of CAC;

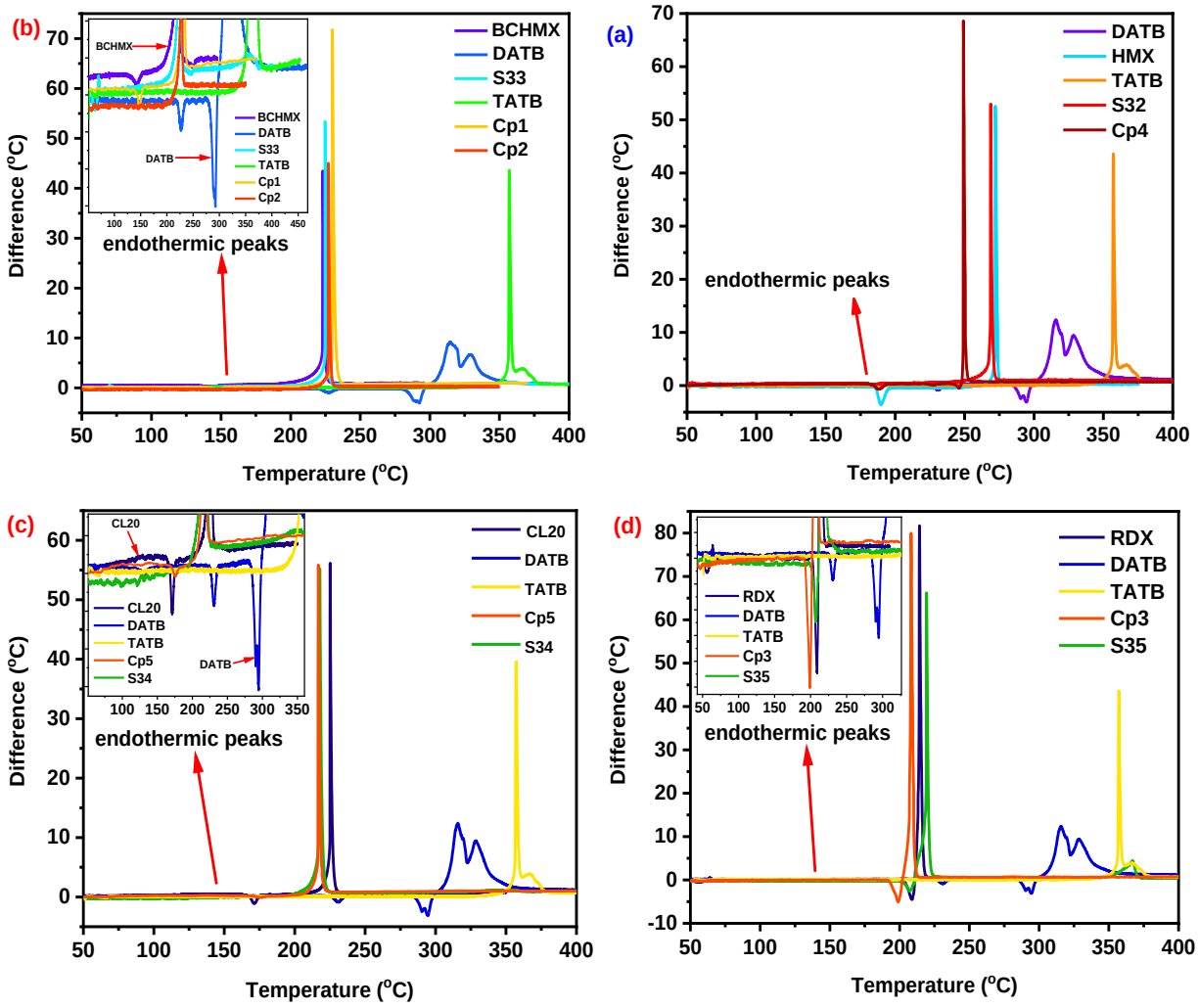

Figure 3.1.3 DTA thermograms of co-crystals a) S32 HMX/TATB, b) S33 BCHMX/TATB, c) S34 CL-20/TATB and d) S35 RDX/TATB.

In the case of pure CL-20, its thermal analysis showed ϵ to γ polymorphic transition, whereas in CL-20/TATB this change was restricted due to the presence of CL-20 already in its β form due to its active interaction with TATB. The polymorphic transitions of both CACs are already confirmed with PXRD, which is consistent with DTA results. The TATB decomposition curves in all thermograms in Figure 3.1.3 fully correspond to those from the literature because the di- and tri-amino derivatives of 1,3,5-trinitrobenzene typically have their exothermic peaks bifurcated [12, 15].

3.1.2.4 FTIR Spectroscopy

FTIR and Raman spectroscopy analysis carried out a detailed investigation of both co-formers intermolecular interactions in the co-agglomeration process. The FTIR stretching bending vibration details

are shown in Table 3, with the full-length spectra values, which shows the variations of these vibrations in pure nitramines and in their respective CACs. At 3500 cm^{-1}, all CACs showed a strong peak and, in the region of 3220-3320 cm^{-1}, showed smaller and sharper peaks that split into two bands. This indicates the formation of hydrogen bond-like interactions between both co-formers in CACs, which helps the latter attain stability. The asymmetric and symmetric stretching vibrations for the N-O group were observed in regions 1250 ± 70 and 1530 ± 30, respectively. The red shift in these wavenumbers, due to weak N-H---O interactions between co-formers, is a sign of the formation of hydrogen bonds. This was further seen in N-H and N-O stretching vibrations.

Similarly, at 3020 ± 50 cm^{-1}, C-H stretching vibrations are slightly split into two bands in CACs as doublet peaks with a slight shift at 3020 ± 55 cm^{-1}. In addition to these changes, the stretching vibrations 1315-1620 cm^{-1} showed observable changes. Also, the skeleton ring vibrations showed a predominant shift in CACs. The stretching vibrations in the TATB N-H and N-O bonds showed strong involvement in intermolecular interactions with nitramines in CACs. These changes might happen in two ways. One would be that the input of one co-former changes the molecular configuration (molecular skeleton) of the other one so that both enter into an optimum interaction with each other - in the case of CL-20/TATB, this would change ϵ-CL-20 to its β-polymorph. The second reason could be that a new stable CAC crystal lattice will be formed by modifying the configurations of both co-formers in the above sense and the formation of new mutual interactions between them.

3.1.2.5 Raman spectroscopy

CACs also showed noticeable shifts when submitted to Raman spectroscopy. The spectra stretching/bending vibrations are summarized in Table 3.1.4. All CACs exhibited asymmetric stretching vibration of the -ONO bond around 1590 ± 10 cm^{-1} and symmetric stretching of the $–NO_2$ bond at 1220 ± 50. Both these stretching vibrations indicate an interaction between the co-formers. This was followed by O-N-O deformation vibration observed at 832 and 840 cm^{-1} in 32 HMX/TATB and 34 CL-20/TATB, respectively, which clearly showed the presence of the δ-HMX and β-CL-20 in the respective CACs. These polymorphic modifications occurred so that both co-formers adjust into a single stable crystal lattice. Raman spectral observations are consistent with FTIR and PXRD analysis results.

Also, there will be a red shift in other vibrations, C-H bending, C-H, N-H and N-N bond stretching bands. The pure nitramines show noticeable shifts after interaction with TATB, which indicates that TATB enters into the nitramines crystal lattice and creates new intermolecular force interactions in the new crystal lattice thus formed. All these spectral observations indicate there will be weak intermolecular interactions between

Table 3.1.3 Summarized results of FTIR measurements

Assignments	CL-20	BCHMX	HMX	RDX	DATB	TATB	32	33	34	35	Cp1	Cp2	Cp3	Cp4	Cp5
I O-N-O-H-- structural bond	3042	3031	3671	--		3313, 3214	3318, 3218,	3317, 3217	3319, 3219	3315, 3216,	3280, 3386	3281 3388	3281 3387	3280 3386	3283 3390
C-H stretching	3042; 3017	3019	3052	3074, 3065, 3002		--	3049	3018	3052, 3024	3074	3015	3017	3074	3036	3024 3052
Symmetrical N-O stretching	1251, 1278	1216, 1231, 1262	1240, 1270	1262, 1231, 1216		1321	1248	1218, 1248	1218, 1255	1211, 1319	1233	1233	1210	1235	1253
Asymmetric N-O stretching	1562	1562	1539	1569		1549	1533	1529	1554	1567	1554	1553	1569 1590	1525	1598
C-N stretching [Amino group]	757	774	733, 763	737, 752, 779		716,	780, 763, 739	774, 742, 697	762, 748, 738	777, 751, 720, 696	779	779	780	781	781
C-N stretching [Nitro group]	1326	1326	1315	1309		1321	1317	1356	1326	1319, 1350	1356	1355	1352	1347	1326
Skeletal stretching [Ring]	1182; 1040	1137; 1084	1207, 1087	1216, 1037		1145, 1029,	1171	1169	1169	1168 1036	1137 1085	1137 1084	1036	1138 1086	1095 1047
Symmetric - NO_2 Stretching	1252, 1218 1280	1273 1209	1270, 1240,	1309, 1350		--	1210, 1248	1214, 1275	1228, 1255	1211, 1261	1274 1207	1272 1233 1205	1268 1209 1303	1259 1235	1263 1220
Asymmetric - NO_2 Stretching	1632, 1601, 1585, 1562	1603, 1554, 1526	1539	1529, 1569, 1588		1602, 1549	1603, 1533	1603, 1529, 1552	1600, 1554	1589, 1567, 1530	1588 1569 1529	1556 1600	1524 1568	1525	1598

Table 3.1.4 Summarized results of Raman measurements

Assignments	CL-20	BCHMX	HMX	RDX	DATB	TATB	32	33	34	35	Cp1	Cp2	Cp3	Cp4	Cp5
						3226	3227	3225	3228	3223	3020	3020	3075	3099 3037	3053 3033
–CH_2 stretching vibration	3052 3024	3020	--	--	--	-- --	3056 3049	-- 3020	3054 3024	3075 3045	2985	2985	2985	2993	2985
C–H stretching vibration		2992	--	--	--	2978 2985	2970	2985	2959	2948	2932	2931	3001	2942	2925
		2932					2985	2991	2985	2999		2856	2947	2856	2856
Asymmetric –NO_2 stretching vibration	1594	1606	--	--	1608	1603	1566	1607	1602	1598	1606	1606	1594	1609	
	1554	1557	--	--	1525	--	--	--	--	--	1526 1485	1526 1484	1571 1526 1484	1564 1526 1486	1526 1493 1486
C–H and –CH_2 deformation vibration	1326, 1280	1299	1315, 1270	1310, 1273	1362 1305	1319	1319, 1260	1319, 1260	1319	1318, 1272	1362 1305	1362 1305	1360 1305	1365 1306	1371 1360
Symmetric –NO_2 stretching vibration	1280, 1252	1273, 1264, 1240	1240, 1270	1217, 1273	1217	1220	1260, 1219	1221	1221, 1263	1272, 1220	1217	1218	1217 1571 1526	1217	1218
Asymmetric C–H stretching vibration	1164, 1182, 1137	1194, 1167	1207	1217	1161	1195, 1170, 1144	1194, 1170. 1144	1195, 1170, 1144	1195, 1170, 1143	1195, 1170, 1143	1161 1153	1153	1160 1153	1161	1161 1154 1140
N–N stretching vibration	1050, 1038, 1014, 984	967, 1058	1079, 952	1030	1034	1030	1030	1030	1030	1030	1035	1035	1034	1033	1040
C–C stretching vibration	1048	1058	1087	1085	909	--	1054	1062	1091	1064	909	908	943	951	908
Ring stretching vibration	979	967	939	943	--	--	930	967	988	943					
	935	906	904	--		--	946	953	961	--					
Ring deformation vibration	913	850	850	848	832	--	848	850	841	847	850	850	885	883	843
	881	906	--	885		883	881	882	883	883	832	832	832	832	832
–NO_2 deformation vibration	854 831	--	--	--	--	832	832	832	841	832	850	850	885	883	843
	819	--	--			--		809	833	--	777	777	777	777	777
	743	775	775	788	777	--	784	793	794	785	731	730	731	730	730
–NO_2 Wagging	737	750	750	757	731	701	741, 701	754, 702	700	701					

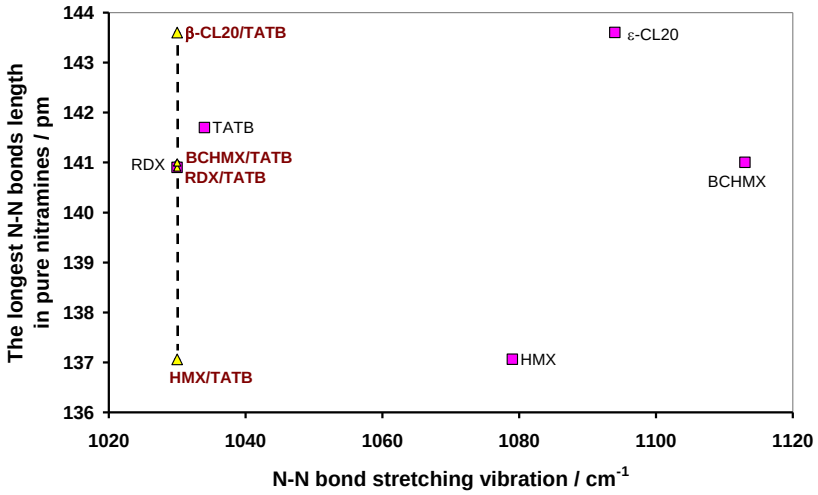

Figure 3.1.4 A comparison of the lengths of the longest N-N bonds with the N-N bond stretching vibration (the C-N bond stretching for TATB) vibration of pure nitramines, their CACs; the N-N bond lengths were taken from the ORTEP views of the nitramines used in the CCDC database shown in Fig. 2.1 Chapter 2. Materials and methods.

both co-formers such as hydrogen bonds and van der Waals force, etc. [1, 16, 17] and these observations indicate the formation of co-crystals during co-agglomeration. The graphical comparison of the length of the longest N-N bonds and their stretching vibrations (stretching of the C-N bond for TATB) in CACs and pure co-formers, given in Figure 3.1.4, corresponds very well with the aforementioned statement. This comparison again argues in favor of the formation of co-crystals in the process of co-agglomeration.

3.1.2.5 Thermochemical and explosive properties

The heat of combustion was determined by employing a bomb calorimeter. Taking the elemental analysis considered for molar ratios both co-formers in CACs), the enthalpy of formation was calculated employing Hess's law. The results obtained are summarized in Table 3.1.4.

Even though active stirring was applied during the co-agglomeration process, the co-agglomerated crystals obtained were larger and slightly non-uniform in shape and size (shown in Figure 3.1.1 FESEM images and Table 3.1.1), compared with their co-precipitated analogues. However, their densities exceeded those of pure nitramine co-formers, as can be seen from Table 3.1.4, especially in the case of the β-CL-20/TATB and δ-HMX/TATB CACs, which are closer to those for pure β-CL-20 and δ-HMX, respectively.

The theoretical detonation parameters (detonation velocity D, detonation pressure P and detonation energy E_{deton}) for the compositions tested, as well as pure explosives were calculated using the CHEETAH code [18] and are summarized in Table 3.1.6. The needed enthalpy of formation was calculated on the basis of Hess's law from the determined combustion heats and are presented in Table 3.1.6 taking needed data from Table 3.1.5.

Table 3.1.5 Molecular formulas, thermochemical properties, and maximum crystal densities of pure substances and their corresponding CACs

	Explosive				Heat of combustion		Enthalpy of formation		
No	Code design.	Molar ratio Nitram/ TATB	Formula	Mol. weight	Q_c ($J.g^{-1}$)	Ref	ΔH_f ($kJ.mol^{-1}$)	Ref	Crystal Density ($g.cm^{-3}$)
1	RDX	--	$C_3H_6N_6O_6$	222.14	9522	[19]	66.2	[19]	1.810
2	BCHMX	--	$C_4H_6N_8O_8$	294.17	9124	[19]	236.5	[19]	1.860
3	β-HMX	--	$C_4H_8N_8O_8$	296.18	9485	[19]	77.3	[19]	1.902
4	BCHMX	--	$C_4H_6N_8O_8$	294.17	9124	[19]	236.5	[19]	1.860
5	β-CL-20	--	$C_6H_6N_{12}O_{12}$	438.23	8327	[19]	421.74	[19]	1.985
6	ε-CL-20	--	$C_6H_6N_{12}O_{12}$	438,23	8311	[20]	397.80	[20]	2.044
7	TATB	--	$C_6H_6N_6O_6$	258.15	11927	[21]	-139.74	[21]	1.938
8	DATB	--	$C_6H_5N_5O_6$	243.14	11592	[21]	-101.3	[21]	1.838
9	32 HMX/TATB	1.00:0.12	$C_{4.33}H_{8.00}N_{8.00}O_{8.00}$	300.09	9720	Cw	68.80	Cw	1.909[d]
10	33 BCHMX/TATB	1.00:0.37	$C_{4.86}H_{4.86}N_{8.00}O_{8.00}$	303.33	9335	Cw	223.97	Cw	1.931[d]
11	34 CL-20/TATB	1.00:0.17	$C_{7.01}H_{7.01}N_{12.00}O_{12.00}$	451.35	8927	Cw	268.76	Cw	2.033[d]
12	35 RDX/TATB	1.00:0.28	$C_{3.65}H_{5.99}N_{6.00}O_{6.00}$	229.93	9660	Cw	39.12	Cw	1.869[d]
13	BCHMX/DATB-Cp1	4.20:1.00	$C_{4.72}H_{6.26}N_{8.00}O_{8.19}$	306.44	9627	Cw	197.37	Cw	1.851[e]
14	BCHMX/DATB-Cp2	3.90:1.00	$C_{4.76}H_{6.27}N_{8.000}O_{8.22}$	307.07	9579	Cw	171.46	Cw	1.831[e]
15	RDX/DATB-Cp3	3.90:1.00	$C_{3.66}H_{5.76}N_{6.00}O_{6.27}$	234.13	9919	Cw	58.33	Cw	1.793[e]
16	δ-HMX/DATB Cp4	3.70:1.00	$C_{4.79}H_{8.00}N_{8.00}O_{8.22}$	309.17	10002	Cw	63.10	Cw	1.885[e]
17	ß-CL-20/DATB-Cp5	2.20:1.00	$C_{7.36}H_{7.81}N_{12.00}O_{13.74}$	484.20	9272	Cw	318.22	Cw	1.981[e]

Note: Here, Cw- results obtained in current work;

The impact sensitivities of the CACs used in this study are shown in Table 3.1.6. In comparison with analogous results on CACs containing DATB, the expectation that the use of TATB is a significantly more suitable additive than DATB in reducing the mechanical sensitivity of cyclic nitramines was confirmed. The DATB co-former reduces this sensitivity only for RDX and HMX with approximately planar molecules and has the opposite effect for sterically hindered BCHMX and CL-20 molecules (see Table 3.1.6 and discussion in paper). By contrast, TATB has a very pronounced phlegmatizing effect on all nitramines studied here; in particular, in the case of CL-20, the addition of TATB does not act as an impurity, so the impact resistance of the corresponding CACs (15.4 J) is even higher than that of pure ε-CL-20 (13.2 J [22]). The difference between the effects of TATB and DATB was outlined in the introduction and lies in a difference in the arrangement of their molecules in the corresponding crystal lattices; the former forms planar sieves (crosslinking by strong hydrogen bonds - see in paper [23]), which turns out to be more favorable for the phlegmatization of cyclic nitramines, compared with the continuous chains of approximately planar molecules in the DATB crystals[9].

Table 3.1.6 Impact sensitivity and explosive properties of pure substances and corresponding CACs

Explosive		Impact sensitivity E_{dr}			Detonation velocity, D	Detonation pressure, P	Energy of detonation, E_{deton}	Additive value[a] of E_{deton}
Sr No	Code design.	E_{dr} 50 % (J)	Ref.	E_{dr} 95 % (J)	($m.s^{-1}$)	(Gpa)	($J.g^{-1}$)	($J.g^{-1}$)
1	RDX	5.6	[24]	--	9014	33.91	5915	--
2	BCHMX	3.0	[14]	--	9116	36.19	6223	--
3	ß-HMX	6.4	[24]	--	9404	38.00	5964	--
4	ß-CL-20	11.9[b]	[22]	--	9421	40.77	6320	--
5	ε-CL-20	13.2[b] 4.0 [c]	[22] [16]	--	9650	43.41	6303	--
6	DATB	78.5	[24]	--	8004	27.13	4086	--
7	TATB	112.0	[24]		8434	31.01	4492	--
8	32 HMX/TATB	50.0	Cw	98.3	9332	37.73	5867	5817
9	33 BCHMX/TATB	32.0	Cw	76.0	9051	36.75	5931	5798
10	34 CL-20/TATB	15.4	Cw	41.1	9556	42.60	6265	5788
11	35 RDX/TATB	46.7	Cw	71.5	9016	34.86	5662	5569
12	BCHMX/DATB-Cp1	3.4	Cw	8.8	8913	34.45	5952	5872
13	BCHMX/DATB-Cp2	2.9	Cw	6.0	8819	33.50	5915	5849
14	RDX/DATB-Cp3	9.7	Cw	20.0	8619	31.61	5621	5589
15	δ-HMX/DATB-Cp4	12.7	Cw	97.2	9111	35.78	5730	5630
16	ß-CL-20/DATB-Cp5	1.8	Cw	2.1	9229	38.88	5978	5869

Notes: a) the value calculated on the basis of the additive principle, i.e., percentage of components in the co-agglomerate;
b) the values for pure β-CL-20 and ε-CL-20, respectively;
c) the value for “common” (technical) quality ε-CL-20;

3.1.3 Discussion

3.1.3.1 Co-agglomeration

Data from particle size determinations show (in Table 3.1.1) that TATB in agglomeration acts as an anti-caking additive. In this case, the size of the specific surface area is more a grinding along with co-agglomeration (co-precipitates have smaller areas than "co-agglomerates"). It can also be seen from Table 3.1.1 that agglomeration in an aprotic medium, significantly finer CACs results in significantly higher surface areas than in a protogenic one. This may also be due to the DATB presence, which by not forming net links of its molecules in its crystal lattice (as is the case with TATB) may not act as an anti-caking additive. From Table 3.1.1 it can also be seen that co-precipitates with CL-20 show the least tendency to agglomerate in both these medium types.

3.1.3.2 Thermal analysis

As already mentioned, an important binding force in the CACs under study here is the N-O---H hydrogen bonding between -NO_2 (nitramine) and -NH_2 (TATB) [2, 5]. Although it has long been known that the presence of intra- and inter-molecular hydrogen bonds increases physical, thermal stability due to the stabilizing influence of the crystal lattice, such bonds are also able to increase the chemical, thermal reactivity, especially in solution [25, 26]. From Table 3.1.2, the increase in physical stability is not clearly visible, except perhaps some minor changes in the temperatures of the polymorphic transitions of HMX and CL-20 in the corresponding CACs. However, in the case of the peak temperatures of exothermic decomposition, there is already a clear decrease in their values for CACs compared to pure starting nitramines, as also mentioned above.

3.1.3.3 Spectral examination

The kinetic energy of the shock in compression during the detonation initiation is accumulated through translational-vibrational relaxation processes by translational and vibrational modes of molecular crystals of the material. This causes a considerable quasi-overheating (20000 to 40000 K [27, 28]), especially of vibration modes, and this is the beginning of the detonation initiation. Therefore, some outputs of measurement methods based on tracking vibrational modes correlate well with the performance, detonation, and sensitivity characteristics of CACs and CCs, and in the following, we extended some of these relations by CACs data with TATB content.

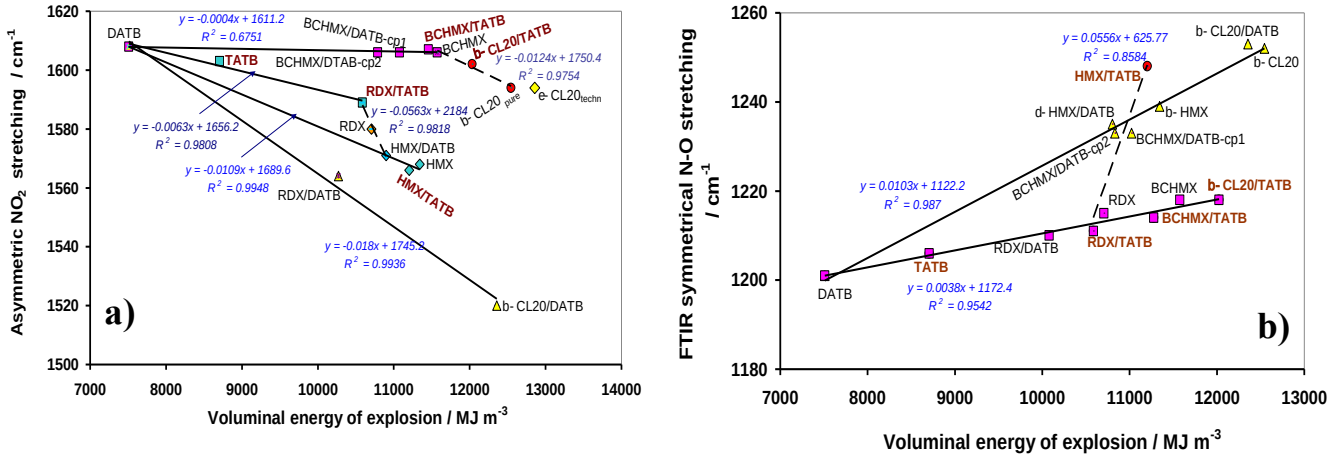

Figure 3.1.5 The relationships between volume energy of detonation and spectroscopic characteristic stretching vibrations; a) asymmetric NO_2 stretching; b) symmetric N-O stretching.

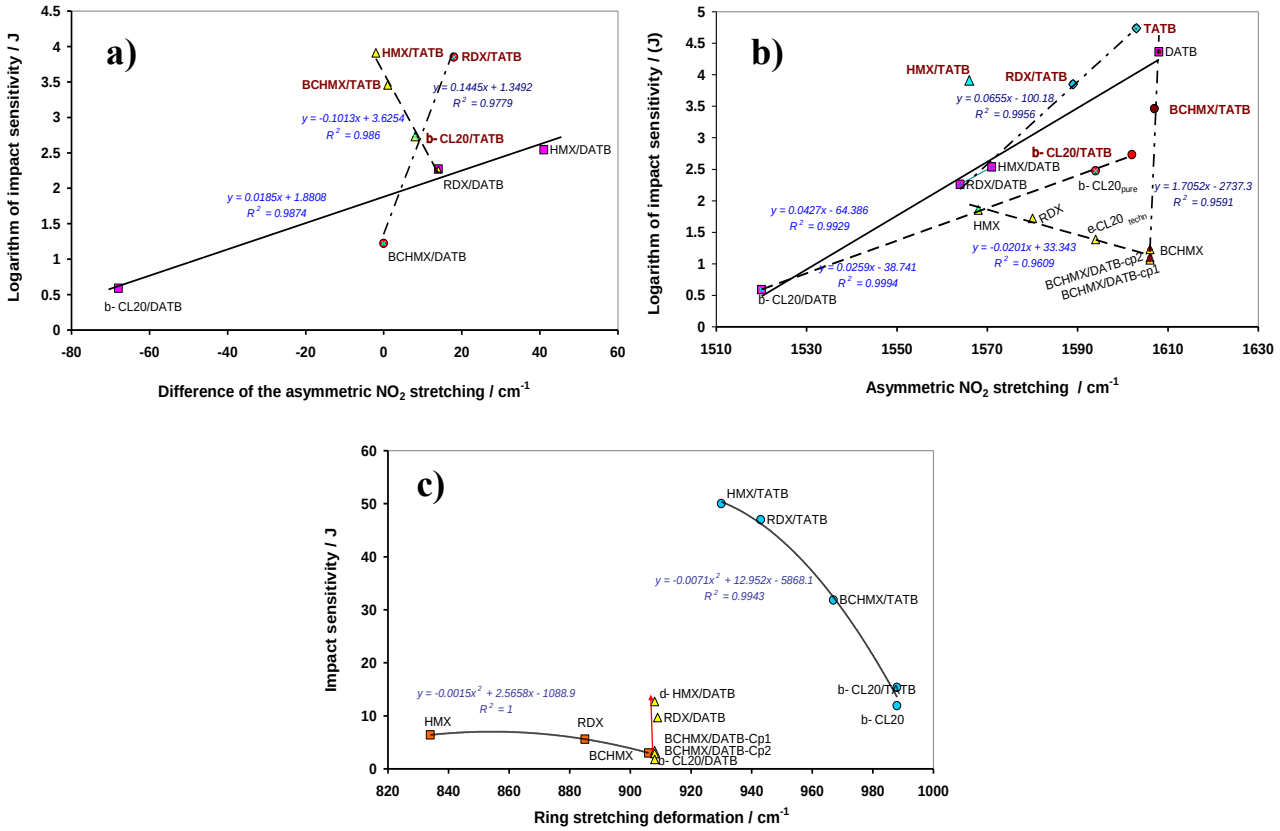

Figure 3.1.6 The comparison of impact sensitivity of the energetic materials in the study with their spectroscopic characteristics:

a) semilogarithmic relationship of impact sensitivity and difference between asymmetric NO_2 stretching vibration in pure nitramines and in their CACs;
b) semilogarithmic relationship between impact sensitivity and asymmetric NO_2 stretching vibrations;
c) graphical comparison of impact sensitivity and ring stretching deformation vibrations;

If we consider the definitional relationship between the vibrational frequency and the bond force constant (i.e., roughly the strength of the given bond) [29], then the relationship in Figure 3.1.5a should imply that the increasing performance of CACs here should correspond to a decrease in the strength of the internal NO_2 bonds involved in asymmetric stretching. Conversely, in the case of Figure 3.1.5b, the performance should be proportional to the strength of the N-O bond involved in symmetrical stretching vibration. In this context, it is worth remembering that the trigger bond of initiation in the nitramines under study and of their CACs is the N-NO_2 bond [14, 26, 28].

Figure 3.1.6a can be explained in a similar way to Figure 3.1.5b - as the difference between asymmetric NO_2 stretching vibrations of pure nitramines and those of their CACs increases, the trigger bond strength should increase, and thus, the impact sensitivity should decrease. But there is an exception - a dependence with a negative slope, i.e., the opposite effect of this increment, which is related to the presence of TATB

in CACs. As will be shown below, TATB, as opposed to DATB, has a specific effect on the behavior of the respective CACs. Also, the increasing strength of the trigger bond in terms of increasing values of asymmetric NO_2 stretching vibrations corresponds to a decrease in impact sensitivity in Figure 3.1.6b, again with one exception, which is somewhat reminiscent of the one from the "impact sensitivity - performance" dependency [30] (see also Figure 3.1.7); - technical data for ε-CL-20 (with an impact sensitivity of about 4 J) usually do not correlate in molecular-structural relationships [28, 30], so maybe here, the correlations are random. A graphical comparison of impact sensitivity and ring stretching deformation vibrations in Figure 3.1.6c somewhat resembles the graphical one in Figure 3.1.4. The presence of DATB in the crystal lattice of nitramine precipitates changes the ring stretching deformation practically to the same vibration value for all corresponding CACs, and the intrinsic impact sensitivity would then be determined by the intermolecular interactions of nitramines with DATB in the mixed crystal (four strong intra- and inter-molecular hydrogen bonding in DATB, van der Waals forces, π-stacking). These intermolecular interactions should be weaker than in the case of TATB, with six intra- and inter-molecular hydrogen bonds binding the TATB molecules into plane-like networks. The changes in ring stretching deformations for sterically crowded molecules are interesting: in BCHMX molecules, the introduction of DATB into their crystal lattice causes little change to these deformations, as does the introduction of TATB into the β-CL-20 molecule. It can also be seen from this comparison that the trend of impact sensitivity of CACs containing TATB somewhat resembles that for pure nitramines with a shift to higher values of deflection vibrations. It should also be noted that the impact sensitivity trends of CACs containing TATB in Figures 6a and 6b are quite similar to each other; the relatively strong influence of TATB on the vibrational modes of the molecules under study may therefore be the cause of the exception mentioned in Figure 3.1.6a (increasing the force constant of bonds should see an increase in the corresponding impact sensitivity. Although this is clearly evident in both Figures 3.1.6a and 3.1.6c, it is contrary to expectation). The increase in impact sensitivity can also be seen in Figure 3.1.6b in the order of the HMX/TATB, RDX/TATB and BCHMX/TATB series, with the asymmetric vibration values of their NO_2 groups increasing in the same sense. There is a fixed idea that the reactivity of energetic materials should increase as the bond length of the nitro group to its carrier (carbon, nitrogen or oxygen atom) increases, i.e., as the force constant of this bond decreases [31]. However, a simple comparison of the lengths of the longest N-N bonds of nitramines with their sensitivity to impact showed that this is not nearly so clear-cut and that this sensitivity decreases with increasing length of this bond, for example, in the order α-HMX, β-HMX, RDX and γ-CL-20 [32]. Only using the bond dissociation energy calculation by means of the UB3LYP/6-31G* method gave a somewhat acceptable and expected order of β-HMX, RDX, and ε-HNIW, with the exception of BCHMX, which has the lowest energy of the group of attractive nitramines, and lies outside of this series [32]. All experimentally found exceptions of the above type should be subjected to a detail analysis using quantum

chemistry methods (including similar exceptions to the Licht's rule [30, 33, 34] – increasing the explosive strength is usually accompanied by an increase in the sensitivity and therefore an insensitive explosive will not exhibit top explosive strength [34], here see for example Figure 3.1.7a).

3.1.3.4 The energetic point of view

This topic has already been partially mentioned in connection with Figure 3.1.5. It is primarily about the relationship between the performance or energy content of EMs and their impact sensitivity.

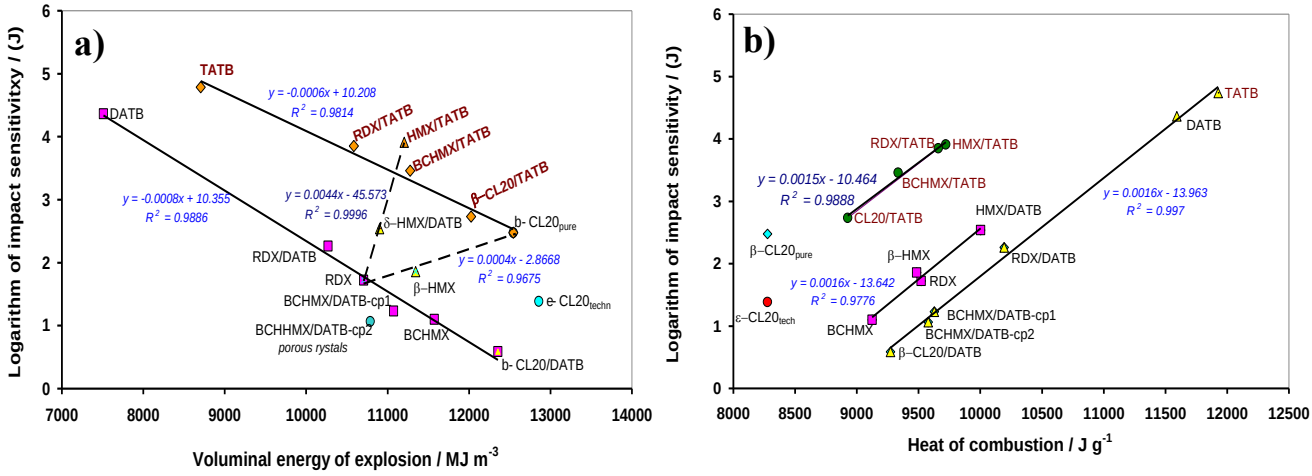

Figure 3.1.7 The relationships between natural logarithm of impact sensitivity and:

a) voluminal energy of detonation as a representative of performance;
b) heat of combustion as a representative of energy content;

Both of these cases are represented in Figure 3.1.7, which is based on Licht's rule [30, 33, 34], elaborated into semilogarithmic versions, represented by Figures 3.1.7a and 3.1.7b. Figure 3.1.7a presents the well-known relationship between impact sensitivity and voluminal heat of detonation, i.e., performance [30, 33]. The dependencies having positive slopes are exceptions to this rule and have not yet been explained (the rule itself also needs an extended explanation [30]). There is some similarity in these exceptions to those in some of the outputs from the spectroscopy work (section 4.3) as already mentioned.

The frequency of exceptions in relationships of this type is reduced if the performance is replaced by the energy content of the EMs, represented by the enthalpy of formation or heat of combustion [35, 36]. The latter case for the nitramines and their CACs studied here is represented by Figure 3.1.7b (the energetic content in this view increases from right to left) - thus, as the energy content of the EMs increases, their impact sensitivity increases (a slightly modified Licht's rule [34–36]).

3.1.3.5 Impact sensitivity

This issue has been essentially addressed in previous sections (i.e., 4.3 and 4.4). These show the dependence of such sensitivity on the molecular structure and energy content of the EMs. The quality of the crystals, as well as their size and shape, play a major role. However, "normal crystallization" under laboratory conditions usually results in products the sensitivity of which is comparable to the LANL database (see for example [24]]), as we have clearly demonstrated using ^{15}N NMR chemical shifts of polynitro compounds [37]. By using the NMR results, it is possible to describe a sensitivity relationship with the molecular structure of individual EMs (due to the reaction center in molecules) [30, 37]. Regarding the effect of crystal size, we found that, for grains from 20 to 200 μm in the HMX sieving fractions, the impact sensitivities change minutely and are consistent with the LANL data [37] (the same is true for the friction sensitivity of this HMX [38]]). The spherification of nitramine crystals will affect the impact sensitivity, as will the high incidence of defect-dislocations in their crystals (this may be a case of the "normal" CL-20 quality with impact sensitivity 2 - 4.6 J).

3.1.3.6 Detonation parameters.

It is clear from the summary in Table 3.1.6 that the detonation energies of the CACs under study are higher than would be expected from the percentages of the individual co-formers in the mixed crystals, which is consistent with the general observation [39].

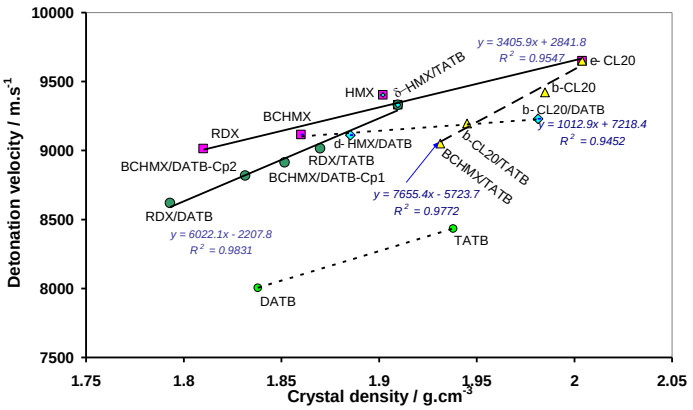

Figure 3.1.8 Relationship between detonation velocity and crystal density of the nitramines and their CACs in this study

Figure 3.1.8 shows the known relationship between detonation rate and density of nitramine crystals and their CACs. From this Figure and Table 3.1.6 it can be seen that incorporation of DATB or TATB into the crystal lattice of pure cyclic nitramines will indeed produce CACs with relatively high densities (especially in the case of TATB) but, with the exception of RDX/TATB and HMX/TATB, with reduced detonation

rates (this also depends on the proportion of these polynitroarenes in the CACs). From the application point of view, the most interesting appears to be HMX/TATB, which, in the formulation prepared here, has a slightly increased density with only slightly reduced parameters compared to pure HMX, while its impact resistance is extremely high (see Table 3.1.6, Figures 3.1.5 and 3.1.6).

3.1.4 Summary

The preparation of co-agglomerates (CACs) of nitramines with 1,3-diamino-2,4,6-trinitrobenzene (DATB), in comparison with the use of 1,3,5-triamino-2,4,6-trinitrobenzene (TATB) gives much finer results. Using differential thermal analysis (DTA), powder X-ray diffraction (PXRD), Fourier transform infrared spectroscopy (FTIR) and Raman studies confirmed that, similar to the DATB version, the use of TATB leads to the formation of co-crystals (CCs) with the nitramines RDX, β-HMX, BCHMX and ε-CL-20, in which HMX presents in its δ-form and CL-20 in its β-form. Whereas using DATB yielded CACs with a density of at most 99% of the theoretical density of the mixed crystal, the TATB CACs densities are higher than those using the pure nitramines (including β-CL-20). Logical relationships, described already for the DATB CACs, between some FTIR and Raman vibrational modes and parameters of initiation and detonation produced greater predictability after extending with the data for their TATB analogs. Detonation parameters of CACs containing DATB and TATB are logically lower than those of the starting nitramines. The detonation energies of these mixed crystals are higher than expected from the respective percentage of the co-formers.

References

[1] J. P. Shen et al., “Preparation and Characterization of a Novel Cocrystal Explosive,” Crystal Growth & Design, vol. 11, no. 5, pp. 1759–1765, May 2011, doi: 10.1021/cg1017032.

[2] H. Xu, X. Duan, H. Li, and C. Pei, “A novel high-energetic and good-sensitive cocrystal composed of CL-20 and TATB by a rapid solvent/non-solvent method,” RSC Advances, vol. 5, no. 116, pp. 95764–95770, 2015, doi: 10.1039/c5ra17578j.

[3] Y. Kohno et al., “Molecular Dynamics Studies of the Structural Change in 1,3-Diamino-2,4,6-trinitrobenzene (DATB) in the Crystalline State under High Pressure,” J. Phys. Chem. A, vol. 113, no. 11, pp. 2551–2560, Mar. 2009, doi: 10.1021/jp809240x.

[4] C. An H. Li, B. Ye, C. Xu, and J. Wang, “Preparation and Characterization of Ultrafine HMX/TATB Explosive Co-crystals,” Cent. Eur. J. Energ. Mater., vol. 14, no. 4, pp. 876–887, Dec. 2017, doi: 10.22211/cejem/77125.

[5] G. R. Desiraju, “Crystal and co-crystal,” CrystEngComm, vol. 5, no. 82, p. 466, 2003, doi: 10.1039/b313552g.

[6] X.-X. Zhang, Z.-J. Yang, F. Nie, and Q.-L. Yan, “Recent advances on the crystallization engineering of energetic materials,” Energetic Materials Frontiers, vol. 1, no. 3–4, pp. 141–156, Dec. 2020, doi: 10.1016/j.enmf.2020.12.004.

[7] V. B. Patil, K. Zalewski, J. Schuster, P. Belina, W. Trzcinski, and S. Zeman, “A new insight into the energetic co-agglomerate structures of attractive nitramines,” Chemical Engineering Journal, vol. 420, Sep. 2021, doi: 10.1016/j.cej.2021.130472.

[8] V. B. Patil, P. Bělina, W. A. Trzcinski, and S. Zeman, “Preparation and properties of co-mixed crystals of 1,3-di- and 1,3,5-tri-amino-2,4,6-trinitrobenzenes with attractive cyclic nitramines,” Journal of Industrial and Engineering Chemistry, vol. 115, pp. 135–146, Nov. 2022, doi: 10.1016/j.jiec.2022.07.043.

[9] J. R. Holden, “The structure of 1,3-diamino-2,4,6-trinitrobenzene, form I,” Acta Cryst, vol. 22, no. 4, pp. 545–550, Apr. 1967, doi: 10.1107/S0365110X67001100.

[10] C. Hou, Y. Zhang, Y. Chen, X. Jia, S. Zhang, and Y. Tan, “Fabrication of Ultra-Fine TATB/HMX Cocrystal Using a Compound Solvent,” PROPELLANTS EXPLOSIVES PYROTECHNICS, vol. 43, no. 9, pp. 916–922, Sep. 2018, doi: 10.1002/prep.201800004.

[11] D. S. Viswanath, T. K. Ghosh, and V. M. Boddu, Emerging Energetic Materials: Synthesis, Physicochemical, and Detonation Properties. Dordrecht: Springer Netherlands, 2018. doi: 10.1007/978-94-024-1201-7.

[12] S. Zeman, “The thermoanalytical study of some aminoderivatives of 1,3,5-trinitrobenzene,” Thermochimica Acta, vol. 216, pp. 157–168, Mar. 1993, doi: 10.1016/0040-6031(93)80389-R.

[13] D. S. Viswanath, T. K. Ghosh, and V. M. Boddu, “Hexanitrohexaazaisowurtzitane (HNIW, CL-20),” in Emerging Energetic Materials: Synthesis, Physicochemical, and Detonation Properties, D. S. Viswanath, T. K. Ghosh, and V. M. Boddu, Eds., Dordrecht: Springer Netherlands, 2018, pp. 59–100. doi: 10.1007/978-94-024-1201-7_2.

[14] D.Klasovitý, S. Zeman, “Process for preparing cis-1,3,4,6-tetranitrooctahydroimidazo-[4,5-d]imidazole (BCHMX),” Czech Pat. 302068, C07D 487/04, 2010

[15] H. Dong, R. Hu, P. Yao, S. Zhang, Thermograms of Energetic Materials. Beijing: China Academy Physical Science & Technology, 2002.

[16] J. Zhou et al., “Analysis of the structures and interactions between CL-20 and its formers,” JOURNAL OF MOLECULAR STRUCTURE, vol. 1207, May 2020, doi: 10.1016/j.molstruc.2020.127731.

[17] G. Liu et al., “Energetic Cocrystallization as the Most Significant Crystal Engineering Way to Create New Energetic Materials,” Crystal Growth & Design, vol. 22, no. 2, pp. 954–970, Feb. 2022, doi: 10.1021/acs.cgd.1c01090.

[18] Fried, L E., “CHEETAH 1.39 Users’ Manual UCRL-MA-117541.” CA: Lawrence Livermore National Laboratory., 1996.

[19] A. Elbeih, J. Pachman, S. Zeman, P. Vávra, W. A. Trzciński, and zbyněk Akštein, "Detonation Characteristics of Plastic Explosives Based on Attractive Nitramines with Polyisobutylene and Poly(methyl methacrylate) Binders," Journal of Energetic Materials, vol. 30, no. 4, pp. 358–371, Oct. 2012, doi: 10.1080/07370652.2011.585216.

[20] Fraunhofer Institut für Chemische Technologie, Pfinztal, Germany, 2004, "ICT Database of thermochemical values." 2004.

[21] P. E. Rouse, "Enthalpies of formation and calculated detonation properties of some thermally stable explosives," J. Chem. Eng. Data, vol. 21, no. 1, pp. 16–20, Jan. 1976, doi: 10.1021/je60068a026.

[22] Y. Ou, C. Wang, Z. Pan Z., B. Chen., "Sensitivity of hexanitrohexaazaisowurtzitane," HanNeng CaiLiao (Chinese J. Energ. Mater.), vol. 7, pp. 100–108, 1999.

[23] H. H. Cady and A. C. Larson, "The crystal structure of 1,3,5-triamino-2,4,6-trinitrobenzene," Acta Cryst, vol. 18, no. 3, pp. 485–496, May 1965, doi: 10.1107/S0365110X6500107X.

[24] C. B. Storm, J. R. Stine, and J. F. Kramer, "Sensitivity Relationships in Energetic Materials," Chemistry and Physics of Energetic Materials. Springer Netherlands, Dordrecht, pp. 605–639, 1990. [Online]. Available: https://doi.org/10.1007/978-94-009-2035-4_27

[25] S. Zeman, "Thermal stabilities of polynitroaromatic compounds and their derivatives," Thermochim. Acta, vol. 31, pp. 269–283, 1979.

[26] G.B. Manelis, G.M. Nazin, Yu.I. Rubtsov, V.,Strunin, Termicheskoe razlozhenie I goreniye vzryvchatykh veschestv i porokhov (Thermal Decomposition and Combustion of Explosives and Powders); English edition: Thermal Decomposition and Combustion of Explosives and Propellants. Izdat. Nauka, Moscow 1996, London and New York 2003: Taylor & Francis, 1996.

[27] V. Yu. Klimenko, "Multiprocess model of detonation (Version 3)," AIP Conference Proceedings, vol. 370, no. 1, pp. 361–364, May 1996, doi: 10.1063/1.50723.

[28] S. Zeman, "Sensitivities of High Energy Compounds," in High Energy Density Materials, vol. 125, T. M. Klapötke, Ed., in Structure and Bonding, vol. 125. , Berlin, Heidelberg: Springer Berlin Heidelberg, 2007, pp. 195–271. doi: 10.1007/430_2006_052.

[29] H. Kuhn, H.- D. Föfsterling, D. H. Waldeck, "Principles of Physical Chemistry, 2nd Edition | Wiley," Wiley.com. Accessed: Oct. 17, 2023. [Online]. Available: https://www.wiley.com/en-sg/Principles+of+Physical+Chemistry%2C+2nd+Edition-p-9780470089644

[30] S. Zeman, and M. Jungová, "Sensitivity and Performance of Energetic Materials - Zeman - 2016 - Propellants, Explosives, Pyrotechnics - Wiley Online Library," Apr. 2016, doi: https://doi.org/10.1002/prep.201500351.

[31] D. M. Byler, H. Susi, and W. C. Damert, "Relation between force constant and bond length for carbon—nitrogen bonds," Spectrochimica Acta Part A: Molecular Spectroscopy, vol. 43, no. 6, pp. 861–863, Jan. 1987, doi: 10.1016/0584-8539(87)80231-3.

[32] S. Zeman, T. Atalar, and A. Růžička, “N-N Bond Lengths and Initiation Reactivity of Nitramines,” Cent. Eur. J. Energ. Mater., vol. 17, no. 2, pp. 169–200, Jun. 2020, doi: 10.22211/cejem/122723.

[33] Z. Xue, B. Huang, H. Li, and Q. Yan, “Nitramine-Based Energetic Cocrystals with Improved Stability and Controlled Reactivity,” Crystal Growth & Design, vol. 20, no. 12, pp. 8124–8147, Dec. 2020, doi: 10.1021/acs.cgd.0c01122.

[34] H.-H. Licht, “Performance and Sensitivity of Explosives,” Propellants Explos. Pyrotech, vol. 25, no. 3, pp. 126–132, Jun. 2000, doi: 10.1002/1521-4087(200006)25:3<126::AID-PREP126>3.0.CO;2-8.

[35] S. Zeman, “Influence of the energy content and its outputs on sensitivity of polynitroarenes,” Journal of Energetic Materials, vol. 37, no. 4, pp. 445–458, Oct. 2019, doi: 10.1080/07370652.2019.1634159.

[36] S. Zeman, “The influence of energy content and its outputs on the impact sensitivity of high-nitrogen energetic materials,” Journal of Energetic Materials, vol. 40, no. 1, pp. 1–14, Jan. 2022, doi: 10.1080/07370652.2020.1822463.

[37] M. Jungová, S. Zeman, and Q.-L. Yan, “Recent Advances in the Study of the Initiation of Nitramines by Impact Using Their 15N NMR Chemical Shifts,” Central European Journal of Energetic Materials, 2014, Accessed: Oct. 17, 2023. [Online]. Available: https://www.semanticscholar.org/paper/Recent-Advances-in-the-Study-of-the-Initiation-of-Jungov%C3%A1-Zeman/1489ea424305a7fc2936ffbad2c5385790cb5e1c

[38] M. Jungova, S. Zeman, A. Husarova, “Friction Sensitivity of Nitramines. Part III: Comparison with Detonation Performance（英）,” Chinese J. Energet. Mater, vol. 19, no. 6, pp. 603–606, doi: 10.3969/j.issn.1006-9941.2011.06.003.

[39] T. Urbanski, “On entropy and free energy of explosives (preliminary communication),” Bull. l’Academie Pol. Des Sci. s, Ser. Des Sci. Chim., vol. 28, pp. 511–513, 1980, doi: https://gallica.bnf.fr/ark:/12148/cb343830642 /date1980.

3.2 Coagglomerated crystals of 2,4,6,8,10,12-hexanitro-2,4,6,8,10,12-hewxaazaisowurtzitane (ε-CL-20) with cis-1,3,4,6-tetranitrooctahydroimidazo-[4,5-d]imidazole (BCHMX)

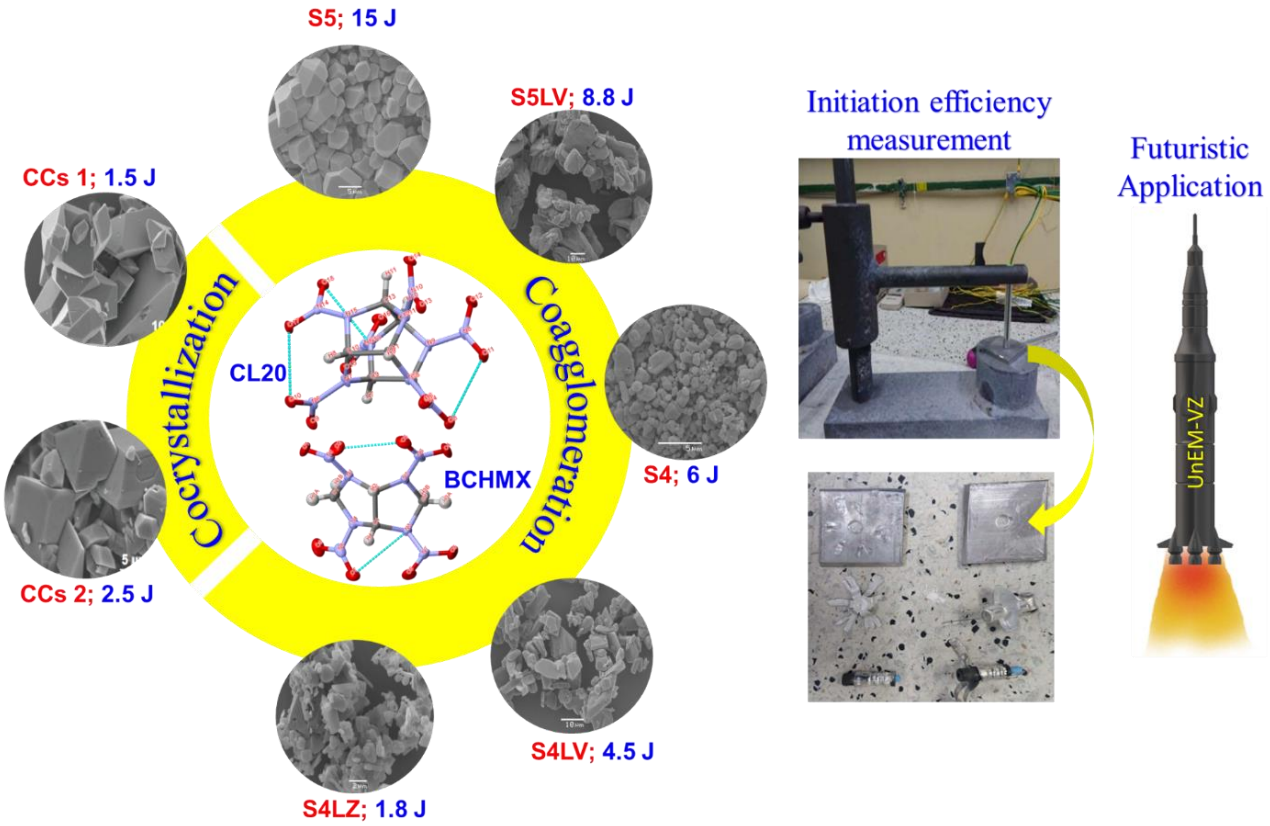

Published in
CrystEngComm, Vol. 24, 2022, P 7771-7785, RSC, DOI: 10.1039/d2ce00840h

3.2.1 Background

Traditional cocrystallization method works relatively well in approximately planar structures, for example, in the stabilization of the longest N-N bond in 1,3,5-trinitro-1,3,5-triazepane (TTAZ) [1], or in co-crystals of 1,3,5-trinitro-1,3,5-triazinane (RDX) or 1,3,5,7-tetranitro-1,3,5,7-tetrazocane (HMX) with 1,3,5-trinitrobenzene-2,4-diamine (DATB) [2, 3]. Still it could have a debatable effect in the mentioned co-crystals for nitramine molecules with an angularly shaped skeleton (cis-1,3,4,6-tetranitrooctahydroimidazo-[4,5-d]imidazole – BCHMX) or a globular skeleton (2,4,6,8,10,12-hexanitro-2,4,6,8,10,12-hexaazaisowurtzitane – CL-20) – for a corresponding discussion, see paper [2, 3]. It seems, however, that the mutual combination of these two molecular structures of nitramines could lead to CCs with increased sensitivity to mechanical stimuli, which could be important, for example, in the construction of detonators without classical primers ('green' detonators – the performance of these products, filled with BCHMX, is high [4]). Thus, this this work focuses on confirming or refuting these previous traditional assumptions. For the mentioned purpose, we use the preparation of the co-crystals and co-agglomerates of CL-20 with BCHMX, and we study their initiation reactivity. Nevertheless, both nitramines are also attractive fillers of propellants, which is a big topic. Therefore, we also need to pay broader attention to this area here.

3.2.2 Results and Discussion

3.2.2.1 Morphology and particle-size analysis

Surface morphological changes in co-agglomerated particles were probed by FESEM. All co-crystal images are shown in Figure 3.2.1 Interestingly, the particle shapes and sizes varied depending on the different solvent systems used for co-precipitation as well as co-agglomeration processes and depending on the method of addition of the same solvent systems. In the CCs1 co-crystal, the solvent system (ethyl acetate/n-heptane) influenced the development of particles with sharper edges, which then influenced the impact sensitivity. On the other hand, in the co-crystal where the solvent ethyl acetate had been replaced with ethyl formate, the surfaces of the particles were slightly smoothened, thus making the co-crystal more impact-resistant than the CCs1. Concerning the co-crystals obtained using the co-agglomeration method, both steps of FESEM images indicate that co-agglomeration helps aggregated particles to acquire defined shapes with smoother edges. For a clearer understanding of the crystal surface modifications in each sample, two FESEM images were included in Figure 3.2.1. Figures 3.2.1e, 3.2.1g and 3.2.1i show that the co-precipitated particles are more flattened with sharper edges, whereas Figures 3.2.1f, 3.2.1h and 3.2.1k indicate that the flattened crystals in co-precipitation acquire defined shapes with almost

smoothened surfaces. Figures 3.2.1e, 3.2.1g and 3.2.1i depict the same solvent system with fast (here 3.2.1e with 3.2.1g) and slow (here 3.2.1i) addition of an antisolvent (water) to the solution of both coformers in DMSO. The method of antisolvent addition affected the particle morphology. In both cases, the particles were also improved by co-agglomeration under the same conditions. This shows the important role of co-precipitation in the co-agglomeration process (see previously in paper [2, 3]). Similarly, with the solvent used for the co-agglomeration process, chloroform (Figures 3.2.1f and 3.2.1h) made the particles slightly smoother than butanol (Figure 3.2.1i). Nevertheless, both chloroform and butanol improved the particle shape in comparison with those in the corresponding co-precipitates, which indicates that both solvents in the co-agglomeration optimise the morphological characteristics of the particles and in n-butanol CACs attain a smaller surface area (see Table 3.2.1). The particle morphology, size distribution, crystal structure and composition of the CACS and the coformers were analysed using the Mastersizer 3000 laser diffraction system (Malvern Panalytical, UK); the particle-size distribution was evaluated using the Fraunhofer approximation; the results are summarised in Table 3.2.1.

3.2.2.2 FTIR spectral studies

FTIR analysis has been carried out to understand and shed light on the structural aspects of CACs and their co-crystal and co-agglomerate formers (Figure S1). The solvents have hardly affected the CACs structure, but they have had an impact on the morphology of co-crystals. These morphological changes are clearly visible in FESEM images and influence the sensitivity of co-crystals. In all co-crystals, N–O···H– peaks appear in the region of 3050 cm^{-1}; this hydrogen bonding improves the quality of co-crystals. In CACs, unlike in their coformers, crystal morphology is stabilized through phase transformation. The stretching vibrations of all coformers as well as those of individual CACs, are listed in detail in Table 3.2.2, and Figure S1 shows the full FTIR spectra of CACs (co-crystals). The symmetric stretching vibrations in all the O–N–O···H– of the EMs have been observed in the region of 3220–3330 cm^{-1}. Symmetric and asymmetric stretching of the N-O group has been observed in the regions of 1230±50 and 1570±10 cm^{-1}, respectively. The formation of the N–O···H– bond causes a slight red shift in wavenumbers, and it also helps to stabilize the co-crystals. The O–N–O···H– and N–O stretching vibrations in the co-crystals are caused by intermolecular forces of different directions, also facilitating the formation of a stable crystal lattice.

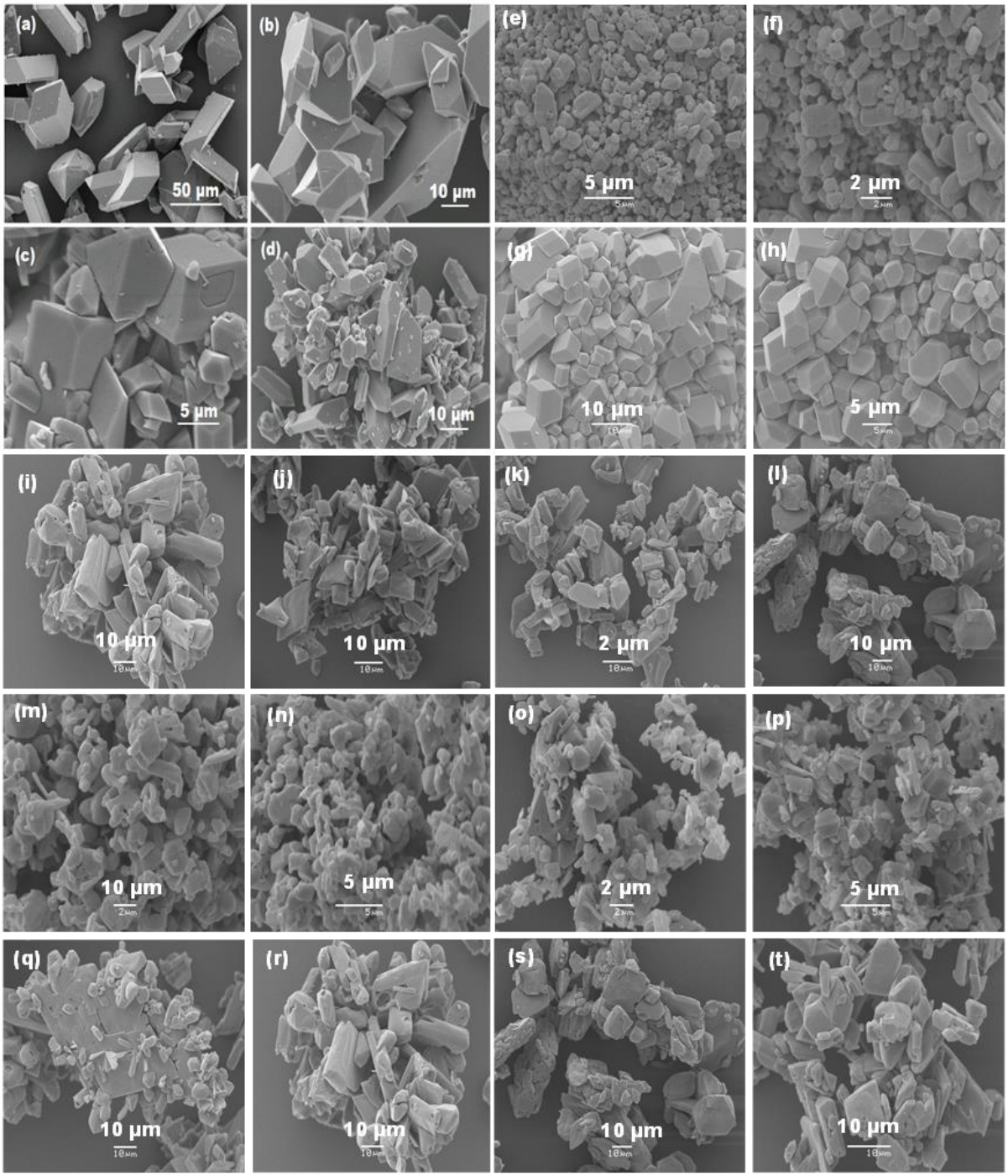

Figure 3.2.1 FESEM images of co-crystals and coformers according to the section 2.2: a) & b) CCs1; c) & d) CCs2; e) & f) S4; g) & h) S5; i & j) S4LVP; k & l) S4LV; m & n) S4LZP; o & p) S4LZ; q & r) of S5LVP; s & t) S5LV **Note: -** the samples labelled with "L" indicates the large-scale (amount ≥ 5 g) preparation of the respective samples series and "P" indicates co-precipitates of the respective samples before co-agglomeration. The morphology of the starting CL-20 and BCHMX does not play an important role here because both nitramines undergo co-precipitation, and the starting data are then the morphologies of the co-precipitates and specification of molar ratios of coformers see in Table 5.

These intermolecular hydrogen bonds and van der Waals forces of attraction exist between –N···H– hydrogen atoms of coformers. The stretching vibrations of the –N···H– and –N–O of EMs molecules prove the active involvement of the –N–O of BCHMX and CL-20 in the same crystal lattice.

Table 3.2.1 Particle-size measurements of CL-20/BCHMX co-mixed crystals

Particle-size analysis						Agglomeration medium
No.	Code design.	Surface area (m^2/kg)	D_v(10) μM	D_v(50) μM	D_v(90) μM	
1	CCs2	1106	2.44	16.9	64.8	ethylformate/hexane
2	S4	1468	1.42	15.4	65.2	chloroform
3	S5	1007	2.97	16.7	50.4	n-butanol
4	S4LVP	1462	2.23	8.42	17.9	
5	S4LV	861	3.62	16.3	58.8	chloroform
6	S4LZP	3273	0.798	3.15	9.14	
7	S4LZ	3171	0.811	3.22	9.48	chloroform
8	S5LVP	1098	3.17	10.6	31.3	
9	S5LV	927	3.39	15.6	37.5	n-butanol

Note: For the meaning of the symbols 'L' and 'P', see the Section 2.

Table 3.2.2 A summary of the results of FTIR measurements

Assignment	**CL-20**	**BCHMX**	**S4 ($CHCl_3$)**	**S5 (BuOH)**	**S4LV**	**S4LZ**	**S5LV**	**CCs1**	**CCs2**
O-N-O-H---- structural bond	3042	3020	3053	3052	3052	3052	3052	3038	3052
C-H stretching	3042, 3017	3019	3023	3022	3052, 3023	3052, 3023	3052, 3023	3052, 3018	3052, 3022
Symmetric N-O stretching	1252	1218	1209	1228	1210	1210	1210	--	1209
Asymmetric N-O stretching	1562	1562	1553	1554	1554	1554	1553	1556	1553
C-N stretching [amino group]	1632, 757	1603, 774	1601, 775	1601, 775	1601, 775, 747	1601, 775, 748	1601, 775, 741	1601, 775, 739	1602, 774, 742
C-N stretching [nitro group]	1326	1326	1386	1358	1326	1327	1326	1326	1325
Skeletal stretching [ring]	1182, 1040	1137, 1084	1166	1166	1166, 1050	1166, 1091	1166, 1081	1137, 1085	1166, 1085
Symmetric – NO_2 stretching	1252, 1218, 1280	1273, 1209	1228, 1257, 1209	1228, 1256, 1207	1228, 1255, 1210	1228, 1256, 1210	1228, 1255, 1210	1254	1259, 1209
Asymmetric – NO_2 stretching	1632, 1601, 1585, 1562	1554, 1526	1601, 1575, 1554, 1534	1601, 1575 1553	1601, 1576, 1554	1601, 1576, 1554	1601, 1576, 1554	1601, 1556,	1602, 1553, 1533

In addition, the –C–H stretching vibrations slightly split in the peak of 3020±50 cm^{-1} into two new doublet peaks. Similarly, significant changes caused by –C–N stretching vibrations have been observed in the region of 1325–1625 cm^{-1}. The stretching of the molecular skeleton ring observed at 1012–1210 cm^{-1} also indicates the formation of stabilised molecular hydrogen bonding to attain stabilized molecular structures of both coformers in the crystal lattice.

In contrast to the agglomerates of nitramines with DATB [2, 3], the changes in the FTIR spectra of the prepared CCs/CACs [2, 3], compared to the pure CL-20 and BCHMX in this work are relatively small (stronger –O···H–N– interactions are missing). Due to the mixed crystals of only two nitramine species, these changes are almost constant for all the prepared CCs/CACs (Table 3.2.2). The exception is the sample S5 with more significantly increased values of symmetric N–O stretching and of C–N stretching for the nitro group, and partially also the sample S4 with even more increased C–N stretching (S5 crystals are further characterized by unprecedented impact resistance, S4 crystals by good impact sensitivity – see paragraph 3.7).

3.2.2.3 Raman spectral studies

The Raman spectra of co-crystals detailed characteristics peaks of stretching vibrations are summarised in Table 3.2.3. Such coformer and CAC stretching vibrations as asymmetric –ONO stretching vibrations, which were observed at the levels of 760±20 cm^{-1}, are shifted to 725±50 cm^{-1} in all co-crystals. The symmetric and asymmetric -NO_2 stretching vibrations in co-crystals in the region of 1480–1610 cm^{-1} indicate the formation of an intermolecular hydrogen bond in the co-crystals. The spectral band of co-crystals at 281 cm^{-1} indicates that the CL-20 does not appear in the ε phase but in the α and β phases. A careful observation of other stretching vibration peaks clearly shows that the CL-20 is presented there in the β phase, except in co-crystal 1, which contains α and β mixed phases. Additional evidence for the presence of mixed phases is provided by the fact that two kinds of –NO_2 deformation are clearly visible with strong bands at 821 and 834 cm^{-1}. Moreover, the strong band at 282 cm^{-1}, which resulted from ring deformations, differentiates the modification β-CL-20 from ϵ-CL-20. Especially β-CL-20 shows a strong band of –NO_2 deformation vibrations at 841 cm^{-1}, whereas α-CL-20 at 821 cm^{-1} [5].

The CL-20 molecule has extended its NO_2-group deformations from 834 to 841 cm^{-1} to interact with the BCHMX. In addition, –O–N–O symmetric stretching has been observed in all co-crystals and coformers in the region of 1305–1320 cm^{-1}. In the case of both coformers, however, –C–H bending vibrations were clearly observable in the co-crystals at 1215±5 cm^{-1}. Furthermore, there are some distinguishing –N–N, –C–H and–O···H–N– stretching vibrations, summarised in Table 3.2.3.

Table 3.2.3 A summary of the results of Raman measurements

Assignment	CL-20	BCHMX	S4 ($CHCl_3$)	S5 (BuOH)	S4LV	S4LZ	S5LV	CCs 1	CCs 2
–CH_2 stretching vibration	3052, 3024	3020	3054, 3024	3054, 3024	3054, 3024	3054, 3024	3054, 3024	3046, 3020	3054, 3022
C–H stretching vibration		2992, 2932	2990, 2932	2991, 2931	2992, 2932	2992, 2932	2990, 2933	2992, 2933	2992, 2932
Asymmetric –NO_2 stretching vibration	1594, 1554	1606, 1557	1605, 1557	1604, 1557	1604, 1556	1604, 1557	1603, 1556	1607, 1558	1606, 1557
C–H and –CH_2 deformation vibration	1380, 1325	1337, 1299	1384, 1332	1384, 1332	1382, 1333	1382, 1332	1382, 1333	1381, 1334	1380, 1331
Symmetric –NO_2 stretching vibration	1250, 1228	1264, 1240	1264, 1231	1264, 1230	1264, 1230	1263, 1230	1264, 1230	1264, --	1265, 1230
Asymmetric C–H stretching vibration	1164	1194	1195	1165	1167	1163	1167	1193	1194
N–N stretching vibration	1094	1113	1093	1095	1093	1093	1093	1093	1097
C–C stretching vibration	1048	967	1047	1046	1050	1048	1050	1053	1053
Ring stretching vibration	988, 939	906	987, 962	988, 962	988, 961	988, 958	988, 961	908, 985	906, 988
Ring deformation vibration	902, 874	850	905, 843	905, 841	907, 849	904, 841	907, 840	908, 850	906, 834
–NO_2 deformation vibration	834	--	824	824	824	824	824	834, 821	850
–NO_2 wagging	795, 763, 737	775, 750	794, 750	794, 750	794, 794, 749	794, 750	794, 749	792, 750	834, 794, 750

All the spectral data from both FTIR and Raman spectra prove that co-crystals are formed in both co-crystallization and co-agglomeration processes. The β-CL-20 is metastable, which makes its isolated form extremely liable to polymorphic transition. It is evident from Table 3.2.3 that all the stretching vibrations (like the coformers undergoing ring and –NO_2 deformations) are actively involved in the formation of intermolecular hydrogen and van der Waals interaction bonds and stabilize the co-crystal lattice.

Nevertheless, the prominent broadband peaks of –O–N–O symmetric stretching and the second –NO_2 stretching have been observed with a red shift, which clearly indicates co-crystal formation in all cases.

Based on both structural and phase modifications, obtained by the FTIR, Raman and PXRD data, it is possible to propose the possible structures of CACs, shown in Chapter 2 Materials section.

From the observations presented here, it is worth pointing out the following facts:

-the asymmetric $–NO_2$ stretching vibrations of the prepared CCs/CACs are very close in value to those of pure BCHMX.

-the lower values of the symmetric $-NO_2$ stretching vibrations are practically identical to those of pure BCHMX, whereas the higher values of these vibrations are close to those of pure CL-20.

-the N–N stretching vibrations of the CCs/CACs prepared are very close to the same values of pure CL-20.

-the values of the asymmetric C–H vibrations for the samples S5, S4LV and S4LZ are almost identical to the same values of pure CL-20, and for the samples S4, CCs1 and CCs2 to the value of BCHMX.

-only the values of the stretching vibrations of the in-plane ring deformation are useful for inferring the molecular-structure dependence (see Figure 3.2.2).

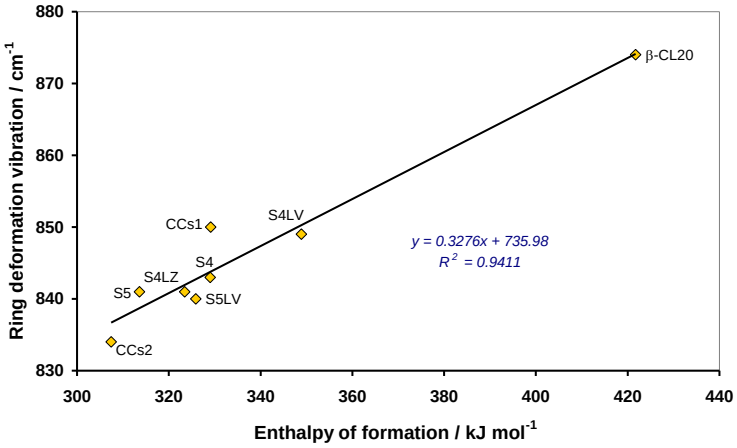

Figure 3.2.2 Relationship between in-plane ring deformation vibrations and enthalpy of formation (taken from Table 5)

Although the introduction of BCHMX molecules into the crystal lattice of CL-20 does not have a remarkable effect on most of the Raman spectroscopy output (as already mentioned in the key observations above), it is systematically manifested in the in-plane ring deformation vibrations in CCs/CACs. Since the sterically crowded molecules of both nitramines have different spatial arrangements and thus steric effects in the crystal lattice, there should also be differences in the bonding angles of the mentioned molecules, depending not only on the molar ratio of the components but also on the incorporation of the BCHMX molecules into the β-CL-20 crystal lattice. From the dependence of the magnitude of these vibrations on the energy content (here the enthalpies of formation) of the respective CACs, it is evident (Figure 3.2.2) that an increase in this content logically corresponds to an increase in the energy of the vibrational motion

(the translational-vibrational relaxation processes of the translational and vibrational modes of the molecular crystals play a decisive role in the initiation of detonation [6]. Detonation parameters are directly proportional to the energy content of EMs[7, 8]). Table 3.2.3 and Figure 3.2.2 not show the data of the in-plane ring deformation vibrations for pure BCHMX because its molecular skeleton cannot be interleaved with a plane; BCHMX might be represented by the data for CCs 2, with the molar ratio of β-CL-20/BCHMX being 0.63:1.00. Also based on a comparison of CL-20 and BCHMX crystal density (see Table 5), the dependence trend in Figure 3.2.2 is understandable (see a similar comparison and explanation of the physical and thermochemical properties of BCHMX with 1,3,5,7-tetranitro-1,3,5,7-tetrazocane, i.e., HMX[9]).

3.2.2.4 Powder X-ray diffraction (PXRD) studies

The phase purity of the coformers and co-crystals was confirmed by PXRD measurements (Figure 3.2.3) in the range of 0–50º, in which the ideal structural modifications had been observed. The following PXRD diffractogram changes have been observed for the coformers and co-crystals of BCHMX: 2Ɵ = 15.64º, 15.9º, 19.84º, 24.1º, 29.82º, 30.1º, 32.5º, 33.14º and 35.64º, with three intense sharp peaks at 9.72º, 12.64º and 23.58º. For RS ϵ-CL-20: 2Ɵ = 20.4, 20.70, 24.70, 27.62, 29.44, 30.48, 31.48, 37.98, 44.44 and 45.40, with intense peaks at 14.32º, 28.80º, 30.14º and 43.00º. For co-crystal 1 (CCs1): 2Ɵ = 12.48º, 13.26º, 15.30º, 17.76º, 23.04º and 24.30º, with intense peaks at 12.84º, 14.08º, 24.78 and 25.12º. These four prominent peaks indicate the presence of mixed α and β-CL-20 in this CCs1. For co-crystal 2 (CCs2): 2Ɵ = 15.14º, 16.22º, 2012º, 24.12º, 24.68º and 28.28º, with intense peaks at 12.92º, 13.64º, 15.92º and 23.92º. For co-crystal S4: 2Ɵ = 12.78º, 13.16º, 13.64º, 15.80º, 16.06º, 17.28º, 17.76º, 23.34º, 24.76º, 27.38º and 28.62º, with intense peaks at 11.88º, 13.48º, 13.66º, 19.96º and 27.76º. For S5: 2Ɵ = 12.76º, 13.06º, 14.74º, 16.04º, 17.26º, 17.74º, 22.86º, 23.74º, 24.76º, 27.24º, 28.62º, 29.04º and 29.98º, with intense peaks at 11.84º, 13.48º, 13.66º, 19.94º and 27.74º. For S4LV: 2Ɵ = 12.96º, 14.94º, 16.22º, 17.44º, 20.08º, 22.50º, 23.90º, 24.72º, 24.88º, 28.76º, 29.12º and 29.62º, with intense peaks at 12.02º, 13.66º, 20.08º, 27.38º, 27.90º and 30.16º. For S4LZ: 13.08º, 13.98º, 16.32º, 17.54º, 18.04º, 24.01º, 24.82º, 25.02º, 28.88º, 29.24º and 30.28º, with intense peaks at 12.12º, 13.78º, 20.20º, 27.54º and 28.00º. For S5LV: 2Ɵ = 12.9º, 14.9º, 16.16º, 17.40º, 17.86º, 22.48º, 23.86º, 24.36º, 24.68º, 24.84º, 28.72º, 29.62º and 30.14º, with intense peaks at 11.96º, 13.60º, 27.34º, 27.86º. The prominent peaks in these X-ray diffractograms indicate the presence of β-CL-20 in all these co-crystals except for CCs1, which has the mixed phase of α and β-CL-20.

The diffractograms of the pure coformers and co-crystals in Figure 3.2.5 are clearly mutually different, which indicates the formation of a new phase in co-crystallization and co-agglomeration. In addition, there are prominent changes and shifts in smaller peaks; some peaks exhibit doublet formation after co-crystallization.

However, these prominent changes might be a result of simultaneous co-crystallisation and possible formation of polycrystalline-type phases coexistence within it. These smaller crystals sometimes cause peak enlargement. Therefore, the mentioned diffractogram changes are most likely to emerge with a new phase in the co-crystal form; at the same time, the co-crystal may be stabilised by a polymorph of a coformer, in this work CL-20 (ε–β).

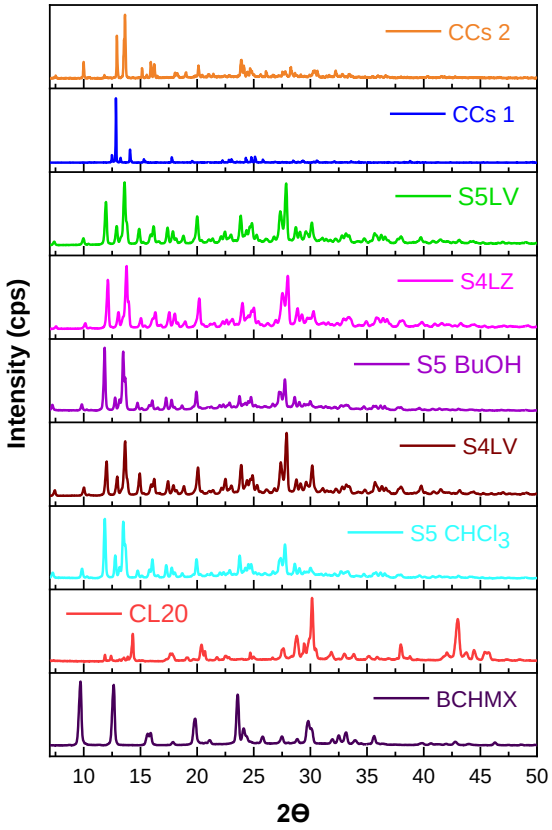

Figure 3.2.3 PXRD diffractograms of CCs/CACs and their coformers

3.2.2.5 Differential thermal analysis (DTA):

To understand the thermal stability of CCs/CACs in detail, the DTA analysis has been carried out for all samples reported in Table 4. These changes observed in CCs/CACs have been compared with their pure coformers (Table 4). This sheds light on the thermal modifications of the solid–solid phases of EMs in pure form as well as in their co-crystal forms [10, 11]. CL-20 shows an endothermic peak at 171 °C, resulting from the transition of ε to the γ polymorphic form, and an exothermic peak at 225 °C, indicating further changes towards decomposition of γ-CL-20[12, 13]. Similarly, the endothermic peak in BCHMX has been observed at 144 °C. BCHMX has enriched the β-CL-20 with the influence of the crystal lattice and, to

certain extent, restricted temperature-induced crystal modifications (T ± ΔT) (±50 °C); however, there is a decrease in the onsets of exothermic changes (up to 5 °C).

Table 3.2.4 A summary of the data from DTA thermograms of coformers and CCs/CACs with their visible melting points.

Sample	Melting point / °C	Peaks of changes in DTA records / °C (CL-20 phase modifications)	
		endothermic	exothermic
ε-CL-20	240 decompn[b]	170 (ε–γ)	225 (γ–δ)
α-CL-20[a]	240 decompn[b]	175 (α–γ)	225 (γ–δ)
BCHMX	286 decompn[c]	144	224
CCs 1	--	173.24 (α & β–γ)	222.01 (γ–δ)
CCs 2	--	196.31 (β–γ)	218.24 (γ–δ)
S4 ($CHCl_3$)	--	196.01 (β–γ)	214.04 (γ–δ)
S5 (BuOH)	--	200.01 (β–γ)	215.01 (γ–δ)
S4LV ($CHCl_3$)	--	193.75 (β–γ)	218.01 (γ–δ)
S4LZ ($CHCl_3$)	--	200.01 (β–γ)	212.75 (γ–δ)
S5LV (BuOH)	--	198.01 (β–γ)	220.40 (γ–δ)

Note: a) between 90 and 105 °C – a very weak, elongated endotherm of crystal-water evaporation; b) taken from Ref.[13]; c) taken from Ref.[14].

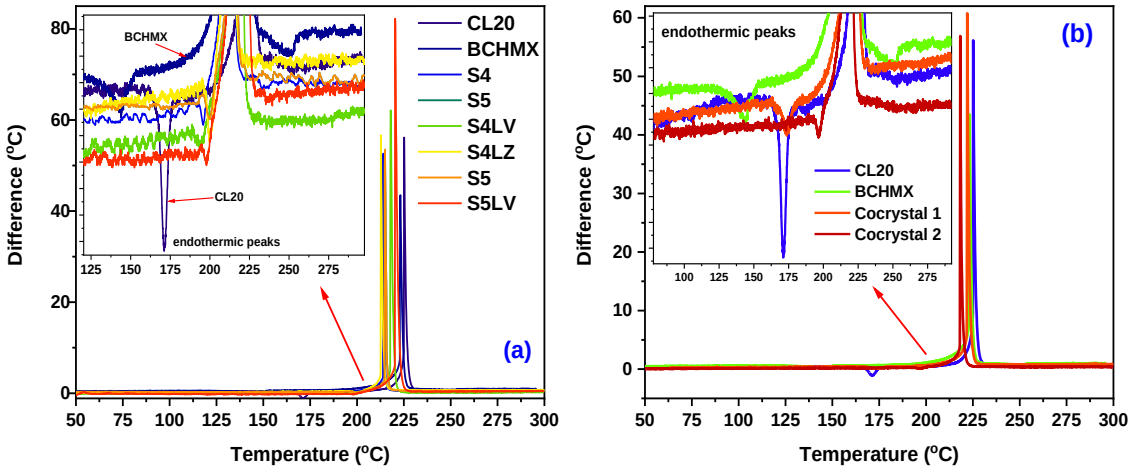

Figure 3.2.4 DTA thermograms of a) BCHMX/CL-20 and all CACs and b) co-crystal 1 (CCs1) and co-crystal 2 (CCs2)

The endothermic changes in the purest forms of both coformers then merge with the exothermic peaks. The polymorphic changes (in round brackets) vary in all co-crystal (± *ΔT*) (endothermic and exothermic) codes: co-crystal 1 (+2.3 and −3.01 °C), co-crystal 2 (+25.3 and −6.76 °C), S4 (+25.01 and −11 °C), S5 (+29 and −10 °C), S4LV (+23 and −7 °C), S4LZ (+29 and −12.25 °C) and S5 LV (+27 and −4.6 °C), and they have

affected their thermal stability. Specifically, the physical stability of these mixed crystals is slightly enhanced, but their chemical thermal stability is consistent with the general finding about the influence of impurities on the stability of CL-20, which means that it is reduced (see data in Table 4 and Figure 3.2.4).

3.2.2.6 Compositions and thermochemical characteristics of mixed crystals

As earlier mentioned, the hypothetical formulae of the CCs/CACs in Table 5 were calculated from the results of HPLC (shown in Chapter 2 Materials section). The data in this table show that co-agglomeration yields CACs/CCs with a crystal density of 99.5 % in comparison with the theoretically calculated value and of 99.6 % when compared with β-CL-20 crystal density. Co-crystallization (CCs1 and CCs2) has given similar results; only the density of the corresponding CCs is of 97.5 % in comparison with β-CL-20 due to the predominant content of BCHMX in these mixed crystals.

3.2.2.7. Impact-sensitivity data and calculated detonation parameters

Over the years of our attempts to prepare mixed BCHMX and CL-20 crystals by co-crystallization, we mostly obtained small crystals (unsuitable for molecular X-Ray applications) with high sensitivity, inhomogeneous in terms of co-crystal requirements. These problems are related to the spatial arrangement of the coformers – globular CL-20 and BCHMX with an angular and rigid molecular skeleton. In this study, we have included the two highest-quality products, CCs1 and CCs2. The former contains α- and β-CL-20, and it is also physically relatively inhomogeneous (as evident from Figures 2a and 2b); the high sensitivity of CCs1 is thus understandable (see Table 6).

While the detonation parameters of all the prepared CACs/CCS are in relatively close agreement, the impact sensitivity is strongly dependent on the molar ratio of coformers (shown in Table 5), on the quality of their crystal surface and on their morphology (shown in Figures 2 and 8a).

The data in Table 5 as well as in Table 4 (chemical thermal stability) show that in terms of stability, the co-agglomeration of CL-20 and BCHMX is much more advantageous, especially in the medium (i.e. in the continuous phase) of protogenic n-butanol, than in the case of aprotic chloroform (the selection of the continuous phase is crucial for the formation of the co-crystal also in the slurry method[15]). The use of n-butanol also yields CAC particles with a significantly smaller specific surface area (see Table 3.2.1). The molar ratio of coformers is important as well. These factors have a major influence on the (optimal) arrangement of molecules in the crystal lattice of the co-agglomerate and thus, on its sensitivity in general. What is surprising is the relatively high insensitivity of the sample S5 (the β-CL-20/BCHMX molar ratio of 1.8:1.0), which is higher than those of all the pure CL-20 polymorphic modifications (see Table 6).

Likewise, the impact sensitivity of the S5LV sample (the β-CL-20/BCHMX molar ratio of 1.6:1.0, prepared also in n-butanol) is good, below that of technical ε-CL-20 (of about 4 J – see Table 6).

The dependence of the type shown in Figure 3.2.5a was first described in paper [2, 3]. Its detailed explanation is difficult without molecular X-ray (the studied CCs/CACs cannot be prepared with a size above 0.1 mm). Nevertheless, it is undoubtedly related to the involvement of nitro groups in intermolecular interactions in CCs and to dislocations in their crystal lattices. The position of the data of the samples S4LV and S4LZ in this figure is undoubtedly a result of the disturbances of their crystals (their heterogeneity, as described in the paper [16]), prepared by agglomeration in chloroform (not a very suitable medium for these purposes). In the case of the data of the S4 and especially S5 samples, their symmetric N–O and C–N stretching vibrations (nitro groups) may imply stabilization by the interaction of the coformer molecules in the sense of local π-π stacking, like in the stabilization of the longest N–N bond in 1,3,5-trinitro-1,3,5-triazepane (TTAZ) [1] (this could be indicated in the S4 and S5 CACs by their IR outputs, mainly the Raman ones; in the case of S4, a certain role may also be played by asymmetric –C–H stretching vibrations):

Table 3.2.5 Molecular formulas, thermochemical properties, and crystal densities of pure substances and the corresponding CCs/CACs

Explosive				Heat of combustion		Enthalpy of formation		Crystal density ($g.cm^{-3}$)	
Code design.	Molar ratio of CL-20 / BCHMX	Formula	Mol. weight	Q_c ($J.g^{-1}$)	Ref.	ΔH_f ($kJ.mol^{-1}$)	Ref.	experim.	calcd.[b]
BCHMX	–	$C_4H_6N_8O_8$	294.17	9124	[17]	236.50	[17]	1.860	–
β-CL-20	–	$C_6H_6N_{12}O_{12}$	438.23	8327	[18]	421.74	[18]	1.985	–
ε-CL-20	–	$C_6H_6N_{12}O_{12}$	438.23	8311	[17]	397.80	[17]	2.044	–
S4	1.10:1.00	$C_{6.00}H_{7.23}N_{12.00}O_{12.00}$	439.44	8475	a	329.00	a	1.9620	1.9701
S4LV	1.53:1.00	$C_{6.00}H_{6.91}N_{12.00}O_{12.00}$	439.12	8446	a	348.87	a	1.9744	1.9841
S4LZ	1.52:1.00	$C_{6.04}H_{6.89}N_{12.00}O_{12.00}$	439.58	8379	a	323.47	a	1.9745	1.9839
S5	1.80:1.00	$C_{6.00}H_{6.78}N_{12.00}O_{12.00}$	438.99	8343	a	313.62	a	1.9761	1.9905
S5LV	1.57:1.00	$C_{5.99}H_{6.89}N_{12.00}O_{12.00}$	438.98	8318	a	325.89	a	1.9617	1.9852
CCs 1	0.60:1.00	$C_{6.03}H_{7.21}N_{12.00}O_{12.00}$	439.78	8447	a	329.13	a	1.9366	1.9425
CCs 2	0.63:1.00	$C_{6.00}H_{7.46}N_{12.00}O_{12.00}$	439.70	8655	a	307.45	a	1.9356	1.9448

Note: a) this paper; b) calculated on the basis of the additive principle

Table 3.2.6 The impact-sensitivity and detonation characteristics of pure substances and the corresponding CCs / CACs

Explosive		Impact sensitivity E_{dr}			Detonation velocity, D ($m.s^{-1}$)	Detonation pressure, P (GPa)	Energy of detonation, E_d ($J.g^{-1}$)	Additive value[a] of E_d ($J.g^{-1}$)
No	Code design.	E_{dr} 50 % (J)	E_{dr} 95 % (J)	Ref.				
1	BCHMX	3.0	-	[14]	9116	36.19	6223	--
2	α-CL-20	10.2	-	[19]	9307	39.37	6143	--
3	ß-CL-20	11.9	-	[19]	9421	40.77	6320	--
4	ε-CL-20	13.2[b] 4.0[c]	- -	[19]	9650	43.41	6303	--
5	S4	6.0	8.4	d	9373	39.65	6163	6273
6	S4LV	4.4	8.6	d	9410	40.20	6198	6279
7	S4LZ	1.2	4.9	d	9385	39.94	6136	6278
8	S5	14.9	38.5	d	9383	39.93	6123	6281
9	S5LV	8.7	20.8	d	9341	39.41	6143	6279
10	CCs1	1.5	-	d	9262	38.43	6139	6261
11	CCs2	2.5	-	d	9268	38.39	6113	6262

Note: a) the value calculated on the basis of the additive principle, i.e., the percentage of components in the co-agglomerate; b) the value for pure ε-CL-20; c) the value for the ε-CL-20 of 'common' (technical) quality; d) this paper respect to the crystal structure of CACs; b) a graphic overview of impact-sensitivity values; c) a graphical comparison of the detonation parameters.

In the formation of CL-20/BCHMX co-crystals, the Raman spectra show the formation of ≡C–H···O– hydrogen bonds between $–NO_2$ and $–CH_2$ groups [20]. A comparison of the positions of the S5 and S5LV data reveals the importance of the molar ratio of coformers in CACs; both of these samples are agglomerated in n-butanol but differ in the aforementioned ratio. The relations in Figure 3.2.5a suggest that the optimal (stoichiometric) molar ratio of CL-20 to BCHMX could be about 2:1. All of this is consistent with the results of the theoretical work of Feng et al. on the relationship between the molar ratio of the CL-20 polymorphs and other coformers (including HMX) on the one hand and the binding energy in the corresponding co-crystals on the other [21]; this energy is used as a scale factor indicating how strongly the molecule is attached to the crystal face [18, 19].

The well-known relationship between performance and impact sensitivity is represented here in Figure 3.2.5b [6, 8, 23, 24]. Roughly speaking, the indirectly proportional relationship between the performance and sensitivity of energetic materials has the characteristics of a general rule [8, 23] (in Figure 3.2.5b, this might be the case of the line 'S5-α-CL-20-S4-S4LZ'). However, there are exceptions to this rule, which have not been explained yet [8]. In nitramines, the opposite trend to this dependence has been observed for RDX, HMX and CL-20 [8], shown for CL-20 in Figure 3.2.5b. The course of dependences for CCs/CACs with a positive directive makes it appear as if CL-20 were 'transferring its exceptionality' to these products.

The difference in the partial dependence plots is primarily related to the impact sensitivity of the CACs, which, as earlier noted, strongly depends on the intrinsic crystal quality and the molar ratio of the coformers.

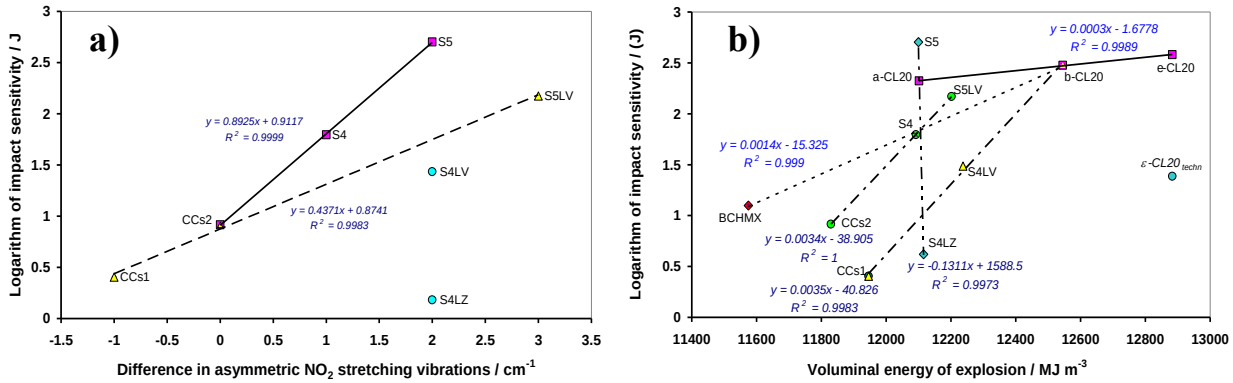

Figure 3.2.5 Semi-logarithmic relationships between impact sensitivity, expressed as drop energy (in J), and a) the difference in asymmetric $–NO_2$ stretching vibrations (the vibration in pure CL-20 minus those in CCs/CACs); b) voluminal energy of explosion

Nevertheless, the CL-20 of 'normal quality' (i.e., the impact sensitivity of around 4 J) and BCHMX do not belong to the mentioned exceptions [8]. Like in Figure 3.2.5a, the position of the data of the samples CCs1, CCs2, S4LZ and S4LV in Figure 3.2.5b is also undoubtedly caused by the disturbances of their crystals, co-agglomerated in chloroform. This is true regardless of the close correlations of their data with the corresponding sub-dependences in Figure 3.2.5b, each of which might connect the CACs/CCs data with a similar construction of their crystal lattice. Figure 3.2.5b also clearly shows that CACs with a CL-20/BCHMX molar ratio lower than 1.8 have higher impact sensitivity than the pure CL-20 modifications, and the products obtained by classical co-crystallization (CCs1 and CCs2) have it even higher than pure BCHMX. In paper [21], it is documented that for a β-CL-20/β-HMX co-crystal, the relationship of the molar ratio of these coformers to the binding energy should have a convex shape with a minimum for the molar ratio of 1:2 (thus a possible dual effect on the stability of this CC). Therefore, the surprisingly low impact-sensitivity value of the S5 sample (14.9 J) could be within expectations. Given the importance of this ratio demonstrated here, further theoretical but mainly practical research in this area is needed.

A new finding of this section is that the CACs studied have lower detonation energies than would be consistent with the percentage of individual coformers in these crystals. This is contrary to the general view about the detonation parameters of explosive mixtures [2, 3, 25]. Taking into account our findings about the detonation parameters of CACs based on DATB and nitramines [2, 3] and accepting the view opinion of Prof. Urbański on the possible role of entropy in these mixtures [25], we may, based on the Boltzmann–Planck microscopic definition of the entropy of a system [26], arrive at the following reasoning: CCs/CACs based on DATB/nitramine mixtures comprise coformers of substantially different chemical nature

(polynitroarenes versus nitramines) [2, 3]. However, our analogous CL-20/BCHMX CCs/CACs include mixtures of structurally different but chemically identical substances.

Therefore, the former group of CCs/CACs represents a much more disordered system (the detonation parameters are higher than those that have been calculated from the content of coformers in mixtures [2, 3]); in the latter, comprising nitramines, it is the opposite. In terms of the mentioned Boltzmann–Planck definition of entropy [26], i.e. on the basis of the logarithm of the physical probability of the state of a system, the number of the microscopic probabilities of the realisation of this macro state should be very different for the two mentioned groups of CCs/CACs.

3.2.2.8 Initiation reactivity of cyclic nitramines mixed crystals from the perspective of XPS and Hirshfield analysis

As earlier mentioned, the nitramines CL20 and BCHMX are crowded molecules (deformed valence angles) [27, 28], which is not the case of the TTAZ molecule [1] – this is evident from the corresponding ORTEP 3D structures of these nitramines, shown in Chapter 2 Materials section. This may be the main reason for the significant differences in the binding energies of the first two nitramines and their CACs to those of TTAZ. Unlike the others, TTAZ is a simple heterocyclic compound, having fewer N and O atoms, as a result of which the interaction in the electronic cloud of these elements is weaker. Consequently, the sorts appear with lower binding energy. The CACs studied in the present work are co-crystals formed between β-CL20 and BCHMX (with the exception of samples S5 and CCs1). It is well known that common intermolecular interactions, hydrogen bonds (HBs) and π-π-stacking, consolidate co-crystals as single-component energetic crystals [29, 30, 31]. The determination of the above-mentioned interactions in these CACs using molecular X-ray techniques is hampered by the very small size of their crystals (below 0.1 mm). By applying IR techniques (FTIR and Raman), we identified the formation of hydrogen bonds between $-NO_2$ and $-CH_2$ groups, as confirmed using XPS in the nanocrystals of 1,3,5-trinitro-1,3,5-triazinane (RDX) co-agglomerated with those of CL20 [20]. In the case of a similar hydrogen bond of the =N-H···O-N= type in the co-crystals of 1,3,5,7-tetranitro-1,3,5,7-tetrazocane (HMX) with 1,3,5-triamino-2,4.6-trinitrobenzene (TATB), the intermolecular interaction increased the HMX original binding energies of 405.5 eV (N 1s) and 532.6 eV (O 1s) to 406.7 eV and 533.2 eV, respectively [32].

Co-crystal (CCs) formation inherently leads to products with a more random intermolecular ordering and with lower variability in intermolecular interactions than the original pure EMs [30]. This increases the entropy and subsequently results in the formation of CCs, which could also affect photon emission (in this respect, it resembles the concept of high-entropy alloys [33]).

3.2.2.9 The Hirshfeld surface analysis of co-crystals

The intermolecular interactions in the pure conformers have been analyzed using the Hirshfeld-surface method [34, - 38]. The normalized contact distance (d_{norm}) is calculated based on the distances d_i and d_e from the surface to the nearest atom interior and exterior to the surface, respectively. In this study, both d_i and d_e were constrained to the range of 0–2.6 Å. The color mapping employed in this study is utilized to differentiate the varying levels of intensity across points. Specifically, the color red is used to represent high intensities, whereas the color blue marks low intensities. Hence, the observation of the spatial distribution of the points (d_i, d_e) and their corresponding frequencies on the surface helps in understanding the intensity of these interactions. The Hirshfeld surface areas obtained are illustrated for the pure conformers in Figure 3.2.6.

The red dots in the Hirshfeld analysis are actively involved in the intermolecular interactions along with interlayered interactions and help to reduce the sliding impact at the molecular level [39]. In the Hirshfeld analysis, β-CL20 showed more red dots than ε-CL20. This is also the reason why most of the energetic-energetic CL20 co-crystals are exhibited in the β-CL20, which is thus more cooperative in intra- as well as intermolecular interactions. At the same time, a comparison of the Hirshfeld surfaces of both forms of CL20 has indicated that the shape of the molecule involved in an energetic β-CL20 crystal resembles a block with a larger number of red dots on the block edge, with the crystal tending to slide easily along the molecular plane. Therefore, β-CL20 has larger numbers of these red dots dispersed in various orientations and exhibits increasingly difficult sliding with high, even forbidden, energy barriers, which may further contribute to the impact resistance of the CACs S4 and S5 (a correlation between intermolecular interactions and the sliding properties of a crystal has been found earlier [35]). Curvature analysis has shown that the curvature of the coformers affects their interactions. It further affects the geometry and strength of the intermolecular interactions, altering the energy landscape of the co-crystal lattice.

An earlier analysis has found that the intermolecular interactions of the main co-crystals are formed by –N···O–, –N···H–, O···O and –O···H– non-covalent contacts (Fig. 1A (i)). Especially the —O···O— interactions stabilize forces in the molecular crystal environment [40], whereas —N···H—, —N···O— and —O···H— are involved in more $NO_2\cdots\pi$-like interactions of π–π stacking [41]. In the current study, a mutual comparison of the β- and ε-forms of CL20 has shown that the intermolecular fingerprint plots of these interactions are more stable for the β-isomer (Fig. 1A (i)), which might be another reason for CL20 in its co-crystals with polynitro coformers exhibited as β-CL20.

Furthermore, the presence of a consistent arrangement of red and blue triangles inside a specific area of the shape-index surface can be identified as a distinctive feature of π-π stacking [42], as depicted in Figure 3.2.6 A (ii). The mapping of curvedness on the Hirshfeld surfaces ranges from red to blue, while the shape

index varies from red to blue (the maximum and minimum values given below the mapped images). The appropriate scale has been used to map the distance property of each pure coformer in order to optimize the information obtained and facilitate a direct comparison between related structures. The feature depicted in Figure 3.2.6 A (ii c) is manifested as a predominantly uniform green area on the surface of β-CL20, with contact distances being highly similar. The area of ε-CL20 is smaller than that of β-CL20, which explains why CL20 exists in the co-crystals of CL20/BCHMX in its β-CL20 form.

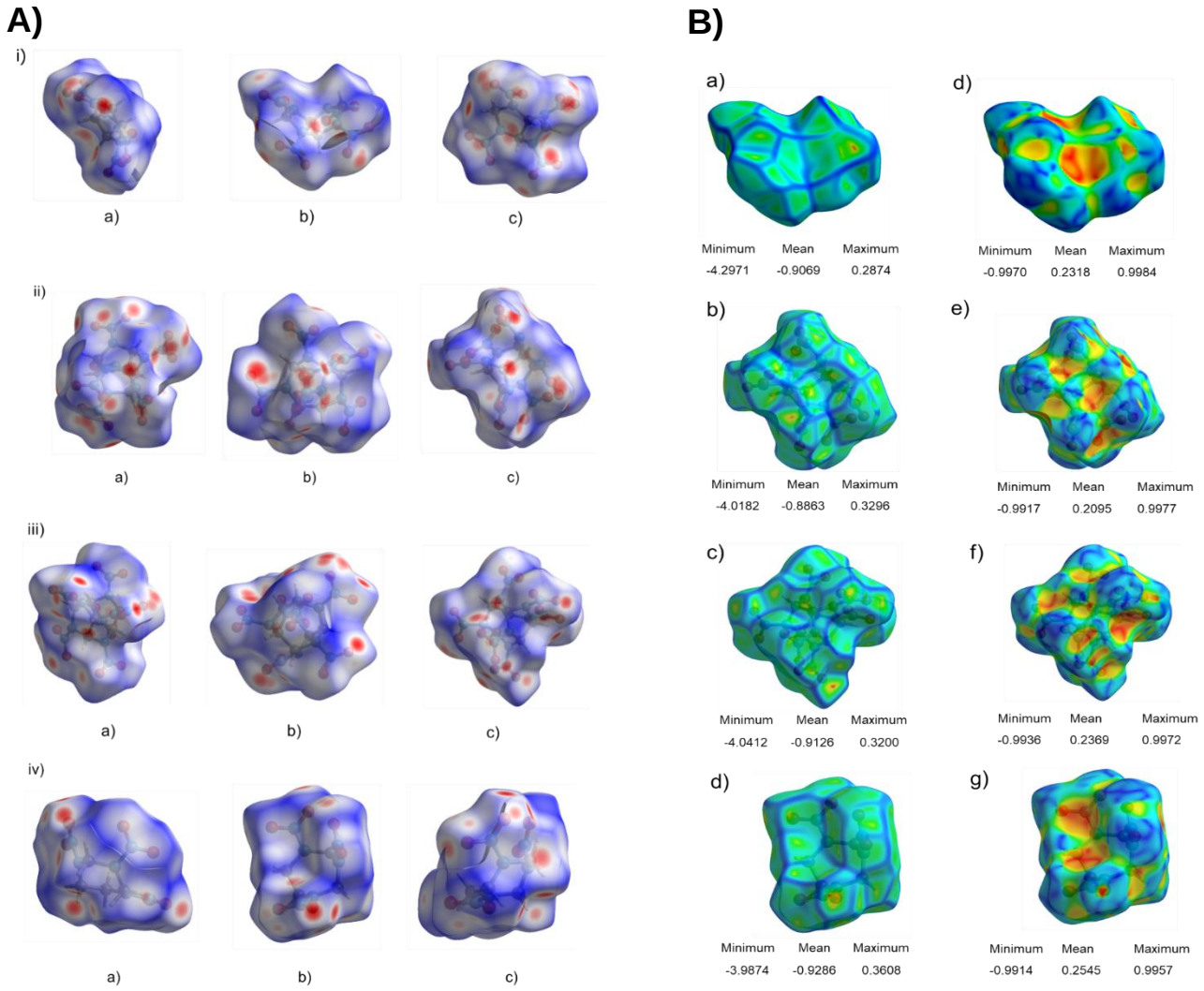

Figure 3.2. 6 A) The Hirshfeld analysis of the pure coformers with their three angle views: i) BCHMX [cell vol.: 249.56 A^3; area: 245 A^2] , ii) ε-CL20 [cell vol.: 345.24 A^3; area: 305.50 A^2] and iii) β-CL20 [cell vol.: 350.32 A^3; area: 300.0 A^2] and iv) TTAZ [cell vol.: 212.24 A^3; area: 207.23 A^2]; an analysis for the "dimer" of TTAZ (a local π-π stacking by the $–NO_2$ in position 3 of its molecule [1, 43]).

B) The curvedness plots of the pure coformers a) BCHMX, b) ε-CL20 and c) β-CL20 and d) TTAZ with the minimum, maximum and mean values, and the shape indices of e) BCHMX, f) ε-CL20, g) β-CL20 and h) TTAZ with the minimum, maximum and mean values [CIF files accessed from [42 - 46].

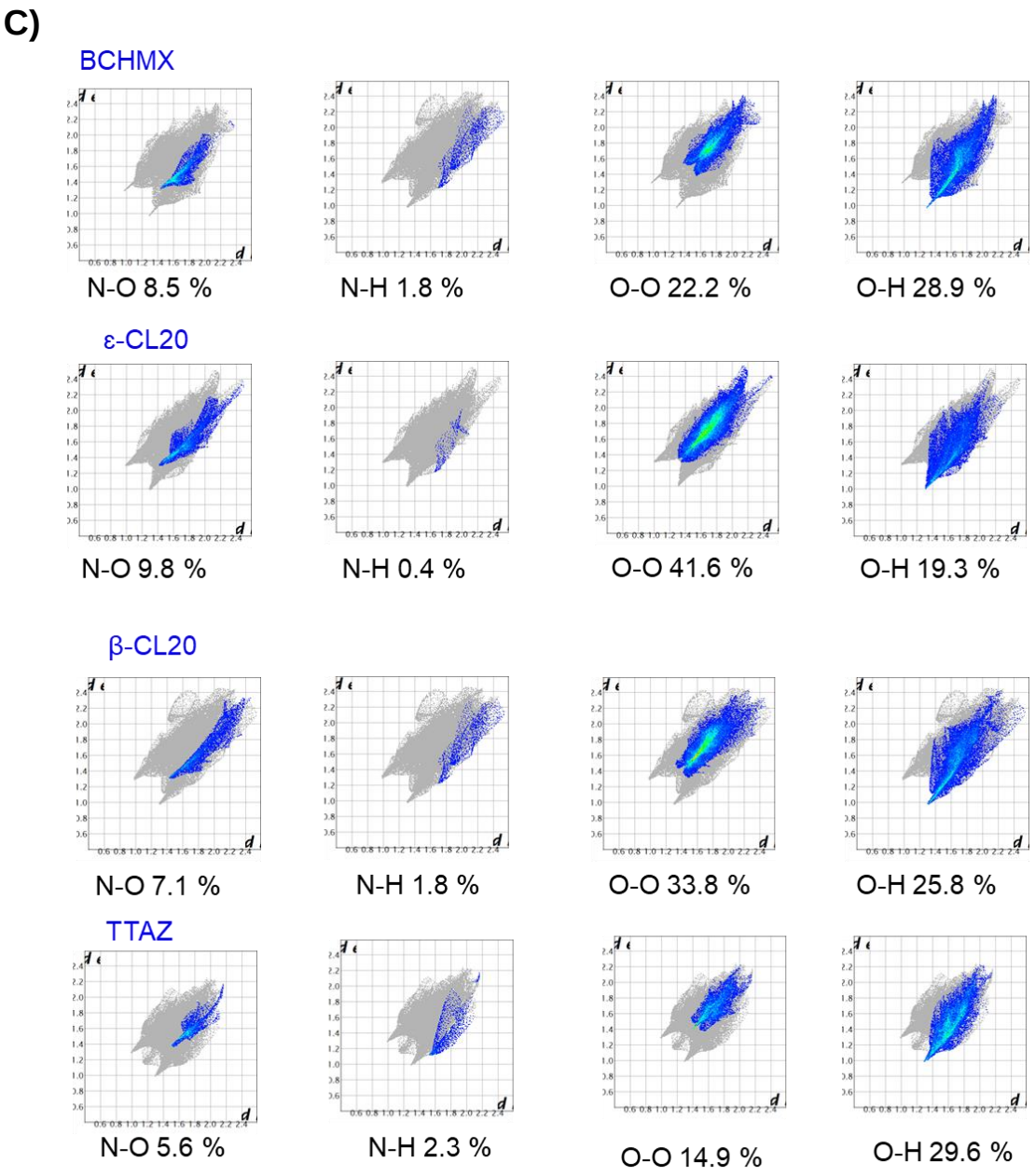

Figure 3.2.6 Contd…

C) The Hirshfeld analysis of the fingerprint plots of the coformers BCHMX, ε- & β-CL20, and TTAZ; the d_{norm} function exhibits symmetry in relation to the distances from the nuclei inside and outside the Hirshfeld surfaces (d_i and d_e, respectively) to their corresponding van der Waals (vdW) radii.

3.2.2.10 Initiation reactivity in terms of impact sensitivity

Impact sensitivity is expressed as the amount of the fall (or drop) energy, E_{dr}, needed for the initiation of the given EM with 50% probability [8, 47]. A semi-logarithmic relationship between this sensitivity and

the ^{15}N NMR chemical shift, δ, of the nitrogen atom in the most reactive nitramino group (the primary homolysis of the N-N bond [46]) has been described and explained. It is expressed by Eqn. 1 [8, 24, 43, 48, 49]:

$$\ln E_{dr} = \alpha.\delta + \beta. \quad (1)$$

From the δ values, it is the most convenient to use in this correlation the ^{15}N shifts of the aza-atoms of the mentioned nitramino group, because these chemical shifts, δ_N, are influenced by nitrogen hybridization, the size and conformation of the molecule, and the extent to which the nitrogen lone pair is involved in π-bonding with the $–NO_2$ group [50]. In the intermolecular interactions in the respective crystals, the role of the conformation and size of molecule is crucial in the achievement of a stable crystal lattice; therefore, these factors have a significant influence on the impact sensitivity.

Figure 3.2.7a shows the relationship between the impact sensitivity (expressed as drop energy) and the N 1s binding energies: With growing E_{bind}, the sensitivity values decrease, which is within expectations. The "TTAZ – β-CL20 – S5" straight line connects structurally very closely related substances (the skeleton of TTAZ forms a part of the β-CL20 globular skeleton, and this nitramine is the predominant component of the co-crystal S5). This line may also prove that the CACs S5 could be a co-crystal as discussed earlier. The rest of the CACs (mixtures of co-crystals with β-CL20) form a separate relationship; for molecular-structural reasons, pure nitramines, ε-CL20 and BCHMX, do not correlate with any of the lines.

A similar relationship between the impact sensitivity and O 1s binding energy is presented in Figure 3.2.7b. Oxygen atoms are concentrated on the surface of the nitraminic molecule and are directly involved in intermolecular interactions mainly through HBs, π-π stacking and van der Waals interactions (the presence of strong electron-withdrawing $–NO_2$ groups could be responsible for the formation of mainly HBs). Without the molecular X-ray, it is impossible to specify these interactions for the studied CACs accurately. The E_{bind} values here are should also be affected by the deformation of the valence angles in $-CH_2-N-CH_2-$ clusters, which feature the longest N-N bonds: The valence angles are 109.89° in BCHMX [14], 109.2° in for β-CL20 [28] and 107.98° in for ε-CL20 [30] in comparison with 124.6° in N,N-dimethylnitramine [51], which is taken as a standard (the ORTEP 3D structures of these nitramines are shown in Chapter 2, Materials and methods).

Figure 3.2.7b, compared to Figure 3.2.7a, thus reflects the deformations of the molecules and their intermolecular interactions through nitro groups rather than their similar molecular structures. The line with a positive slope in Figure 3.2.7b connects the data that, except for S4LZ and CCs1, show a correlation with another two dependence relations in this figure (see also Figure 3.2.13 and the related discussion); except for the CCs1 and ε-CL20, the samples are CACs with β-CL20/BCHMX molar ratios ranging from 1.52 to

1.57 (see also Figure 3.2.7b). Concerning another important mechanical sensitivity of the studied substances, i.e. friction sensitivity, there is also a semi-logarithmic relationship between it and impact sensitivity [43].

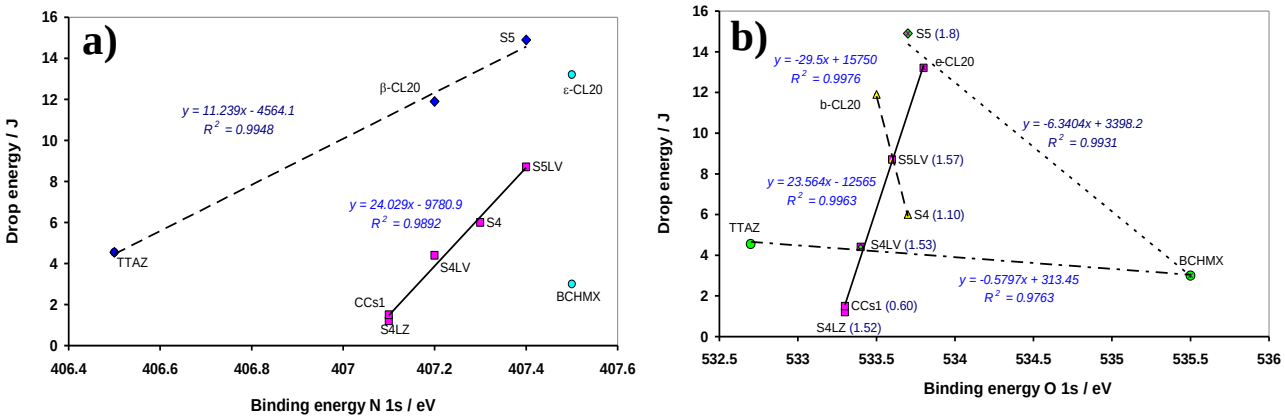

Figure 3.2.7 The relationships between the impact sensitivity, expressed as drop energy, and binding energies of the nitramines used in this study (the numbers in parentheses indicate the molar ratio of β-CL20/BCHMX): **a)** for the N 1s binding energy (N-NO_2) and **b)** for the O 1s binding energy (NO_2).

3.2.2.11 Initiation reactivity in terms of electric spark sensitivity

Electric-spark sensitivity is the energy of an electric spark that has a 50% probability of initiating the energetic material under investigation [52, 53]; the primary chemical step of this initiation is the addition of an electron to the nitramine group with the subsequent homolysis of the N-N bond c. The relationships between electric-spark sensitivity and binding energies are documented in Figure 3.2.8.

Here, the dependence of the N 1s E_{bind} (Figure 3.2.8a) shows the effect of the high molecular-structural similarity between the TTAZ, β- and ε-CL20 nitramines and influence of the sensitization of CL20 by the addition of BCHMX to it, which leads to CACs. In Figure 3.2.8b for the O 1s E_{bind}, the trend of Figure 3.2.8a, i.e. the increasing resistance of CACs to electric spark with increasing E_{bind}, is essentially maintained, which appears to be logical and thus confirms the mechanism of the primary step of the fission of the nitramine molecules by electric spark [52].

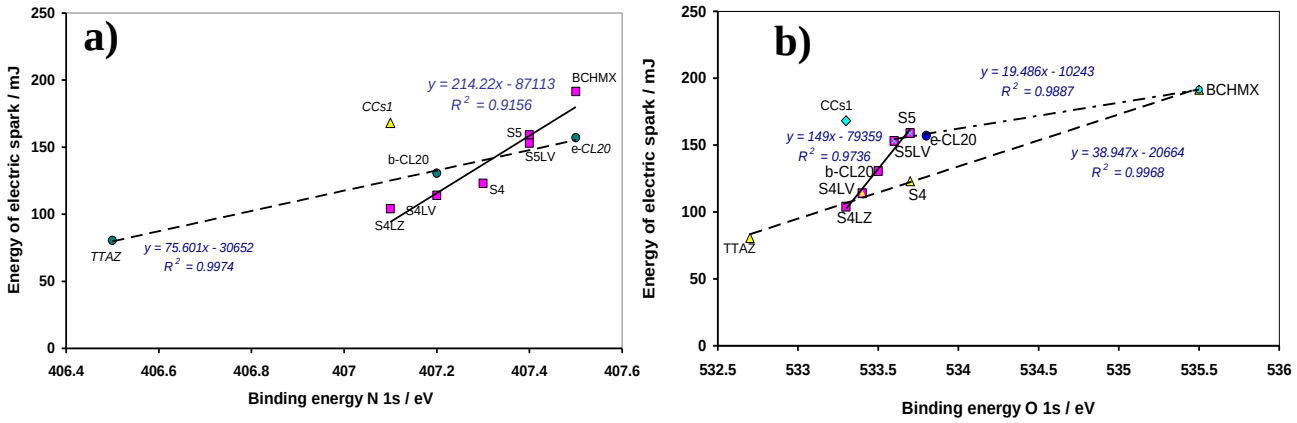

Figure 3.2.8 The relationships between the electric-spark sensitivity (here expressed as the energy of an electric spark) and binding energies of the nitramines under study: **a)** for N 1s binding energy and **b)** for O 1s binding energy.

3.2.2.12 Initiation reactivity in terms of detonation velocity

The explosion process of any explosive is defined by detonation velocity (*D*), detonation pressure (*P*) and the heat of explosion [8, 54], between which there are specific relationships [8]. The pressure effects (shock waves) are directly related to the initiation of this process, but the detonation velocities is more readily available experimentally. The XPS method and the information provided above led to the selection of the detonation rate as a representative for the initiation impulse in this case.

In terms of the physics of explosion, detonation is a hydrodynamic quantity [54]. In the perspective of classical reaction kinetics, detonation appears as a zero-order reaction [55, 56]; in this context, the relations between this zero-order rate and the reaction constants of both the zero-order and unimolecular thermal (uncatalyzed) decomposition of EMs have been described for example in [43, 55, 56].

A simple comparison of the binding energy with the detonation velocity, calculated for the maximum crystal density of the nitramines studied, is presented in Figure 3.2.8. The corresponding correlation for the E_{bind} N 1s (Figure 3.2.9a) again does not include BCHMX and ε-CL20 because of the emission of the internal-nitrogen aza- and nitro-atoms. However, the influence of the π-π stacking between the coformers molecules, in which nitro groups participates, is not to be excluded (this local stacking has been described for TTAZ crystals, where it stabilizes the longest N-N bond in position 3 [1, 43]). This relationship is much better captured by the application of the O 1s E_{bind} (Figure 3.2.9b), i.e. for the emission of photons from the oxygen atoms that directly participate in intermolecular interactions in the crystal via HBs.

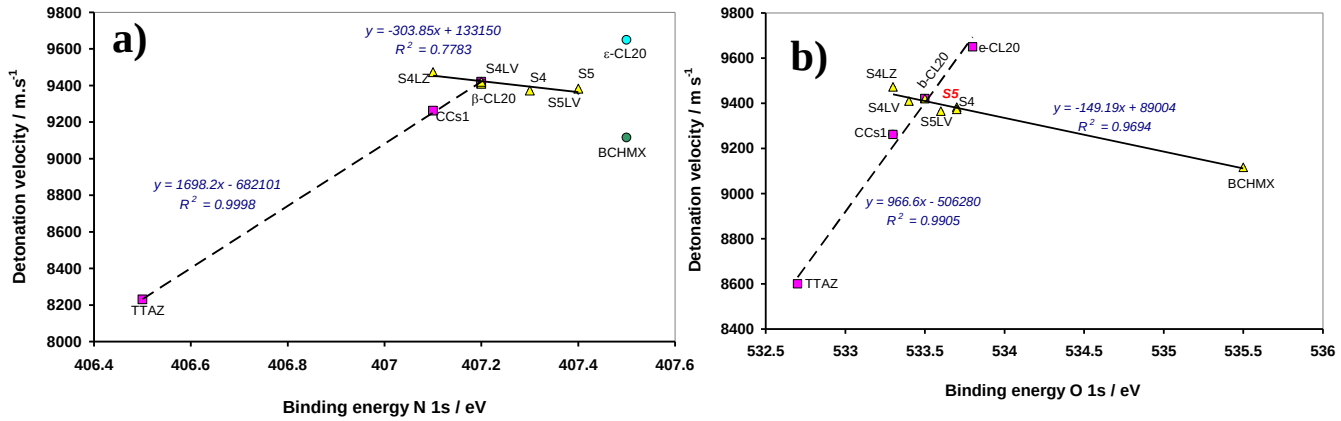

Figure 3.2.9 The relationships between the calculated detonation velocity and binding energy of the nitramines in the present study: **a)** for N 1s binding energy and **b)** for O 1s binding energy.

Whereas the lines in both parts of Figure 3.2.9 with positive slopes are related to pure nitramines and the co-crystal CCs1, and hence the relationship is within expectations, the dependence lines of the CACs have negative slopes. The introduction of the foreign, rigid and angular-shape BCHMX molecule [14] in a non-stoichiometric molar ratio into the CL20 crystal lattice should increase the disorder of the resulting mixture of CCs and β-CL20. The subsequent intermolecular interactions may lead to unfavorable packing structures (reduction in the packing coefficient), very important features in the crystal engineering of EMs [29, 31], which would immediately be manifested by a decrease in crystal density (see in Figure 3.2.10). If we also take into account the possibility of an increase in entropy upon CC formation [31], these assumptions should be reflected in the dependence lines with a negative slope in Figure 3.2.9 (which is not valid here for the data of pure nitramines for BCHMX). Our previous work [41] mentions the steric problem of the optimal placement of the BCHMX molecule in the crystal lattice, and thus its crystal density, as compared to its monocyclic analog HMX).

It is well known that there is a linear relationship between the detonation velocity of explosives and their density. Therefore, it comes as no surprise that there is a relationship between the maximum crystal density and the O 1s binding energy, with exactly the same division of the nitramines studied into subgroups as in the analogous detonation relationship (compare Figure 3.2.9b with Figure 3.2.10). This means that the same intermolecular interactions influence both the crystal density and the detonation initiation, which is logical. On the other hand, the emission from the internal-nitrogen atoms leads to a similar conclusion as in the case of Figure 3.2.9 (also see Figure 3.2.10), except for the group CCs1 – S4 – S5, which, in the sense of the trend in this relationship, exhibits the property of pure nitramines (CCs1 and S5 are demonstrably co-crystals, with their crystal lattices being better arranged than those of the other agglomerates).

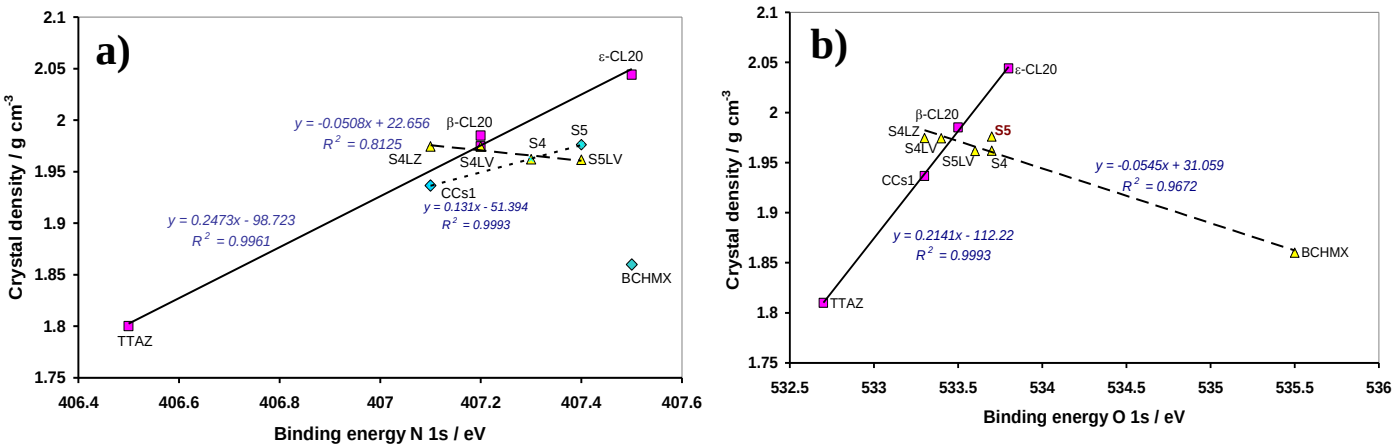

Figure 3.2.10 The relationships between the maximum crystal density (taken from Table 2) and the binding energy of the nitramines studied: **a)** for N 1s binding energy and **b)** for O 1s binding energy.

3.2.2.13 The viewpoint of energy

This aspect is related not only to the relative explosive strength of the explosives but also to their sensitivity and hence the safety of their handling [57]. A high performance and energy content of energetic materials are usually accompanied by an enhanced sensitivity, and insensitive explosives generally do not exhibit an optimum performance; it has been shown that this might be considered a general rule (Licht's rule), but this opinion has not yet been supported by a satisfactory theory [8, 43, 58].

Therefore, it is not without interest to understand the relationship between the energy content of the nitramines and the electron emissions from reaction centers of these nitro-compounds. For the nitramines in the present study, this is presented in Figure 3.2.11. The relationship suggested in Figure 3.2.11a for the N1s E_{bind} is consistent with similar relationships for impact sensitivity (Figure 3.2.7a), electric-spark sensitivity (Figure 3.2.8a) and, to some extent, also for detonation velocity (Figure 3.2.9a); specifically, with the decreasing values of E_{bind} (increasing ΔH_{form} values), the initiation reactivity of the investigated EMs increases.

The situation is more complicated in the case of the correlation with the O 1s E_{bind}: the oxygen atoms are directly involved in the intermolecular interaction in nitramines via the corresponding HBs [31–35]. It is known that hydrogen bonds increase physical stability and that they increase reactivity in general (they act in opposite directions) [58] - for an increase in the thermal reactivity of CACs due to HBs, see for example [57]. The above-mentioned increase in reactivity, depicted in Figure 3.2.7a, would be reflected in the dependence lines with a negative slope, which are consistent with the lines in Figure 3.2.11b.

Based on its relatively high impact sensitivity, lower thermal stability, and slightly lower thermal reactivity compared to CL20, BCHMX should be the most reactive of the CAC-forming coformers discussed in this study [56]), because it also has the most deformed valence angle -CH_2-N-CH_2- (as earlier mentioned) with a pyramidal arrangement of the nitrogen atom [59]. This could be a reason for the arrangement of BCHMX dependence lines in Figure 3.2.11b, i.e. their common point (intersection). In other words, BCHMX should be the bearer of reactivity for all the mixed crystals studied here.

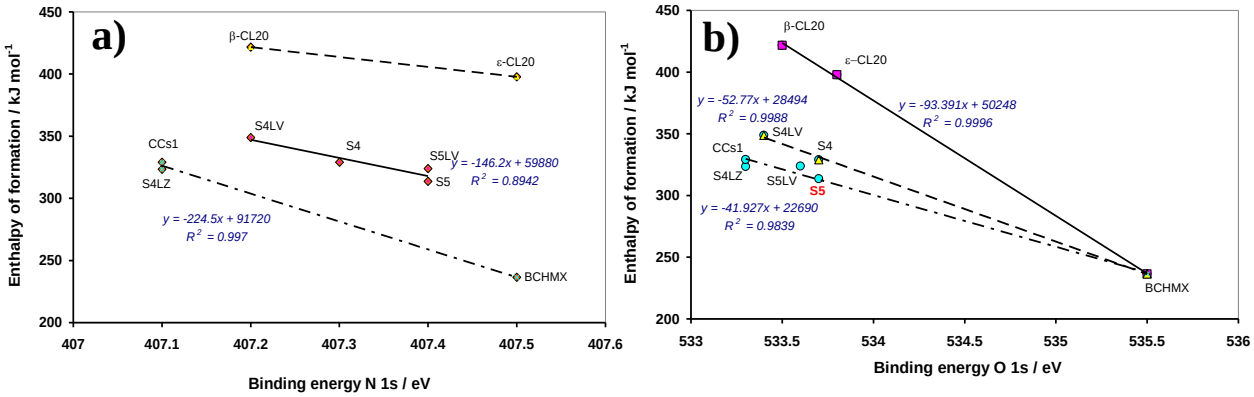

Figure 3.2.11 The relationships between the energetic content of the nitramines studies, expressed as the enthalpy of formation, ΔH_{form}, and binding energy (the data for TTAZ, whose molecule is not crowded, are outside the range used in this Fig., with its ΔH_{form} being 41 kJ mol^{-1} [60]): **a)** for N 1s binding energy and **b)** for O 1s binding energy.

Figure 3.2.8 also shows that the insertion of BCHMX into the crystal lattice of CL20 leads to a rather significant decrease in the energy content of the resulting CCs and CACs with a decrease in the E_{bind} values from BCHMX to CL20 (especially to its β-isomer). The decrease of E_{bind} is lower in the S5 sample, which also shows a higher resistance to impact than its coformers (see Figure 3.2.7) and the lowest sensitivity to electric spark among the CACs (see Figure 3.2.8).

3.2.2.14 Interesting relationships involving Raman and FTIR spectroscopy findings

Details of Raman and FTIR spectroscopy analyses along with their corresponding results have been taken from [15]; for more details, see also Chapter 2 Materials section.

3.2.2.14.1 Raman spectroscopy

As mentioned earlier, a directly proportional relationship between the in-plane ring deformation vibrations and the enthalpy of formation of the CCs and CACs under study was described. A similar approach to that applied in the case of the E_{bind} values in that work has revealed a semi-logarithmic relationship, which is shown in Figure 3.2.12. In this sense, only the O 1s E_{bind} values are correlated (the analogous N 1s E_{bidn} has provided no relationship). This relationship should be a manifestation of the existence of the interaction of

peripheral oxygen atoms (in the nitro groups) with the hydrogen atoms of methylene groups (part of the nitramine skeletons) in the neighboring molecules via intermolecular HBs. It is related to a certain molecular similarity in the crystal lattices starting from BCHMX and ending with the sample S5LV; this arrangement should be different from those in the samples S4LV, S4LZ and CCs1. In this context, it is worth recalling Figure 3.2.7a, where the impact-sensitivity data of these samples show a positive relationship with the O 1s E_{bind} values. These samples have the highest impact sensitivity of the nitramines studied and, with the exception of CCs1, a relatively high sensitivity to electric spark.

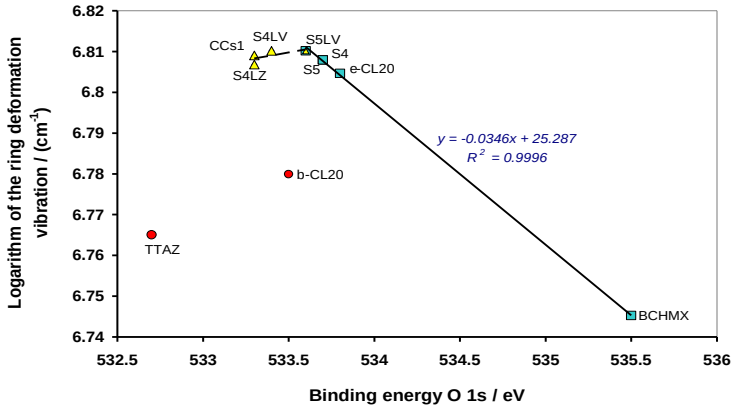

Figure 3.2.12 The semi-logarithmic relationship between the in-plane ring deformation vibrations and the O 1s binding energies of the nitramines studied (the required spectroscopic data have been taken and are also summarized in Chapter 2 Materials section).

3.2.2.14.2 FTIR Spectroscopy

The most interesting of the FTIR spectroscopy results are the symmetric N-O stretching vibration, whose relation to the N 1s E_{bind} is presented in Figure 3.2.13 (the application concerning the O 1s E_{bind} has not yielded satisfactory results). As mentioned earlier, the N 1s emissions are rather tightly coupled to the conformation and size of the molecule. On the other hand, the oxygen atom of the N-O group interacts with the neighboring molecules (via HBs), after which the whole nitro group can participate in π-π-stacking (e.g., in position 3 in the TTAZ molecule [1, 43]). This logically corresponds to the inversely proportional relationship of the N-O stretching vibration. E_{bind} N 1s in Figure 3.2.11 shows the relationship between the force constant of the N-O bond and this energy (for the relationship between the force constants of nitrogen-oxygen compounds and the frequencies of the corresponding N-O bond stretching, see [61]).

For these reasons, pure nitramines, and co-crystal S5 are again distinguished from other CACs in the sense of Figure 3.2.13. Therefore, this can be used as another auxiliary relationship to differentiate CCs from CACs.

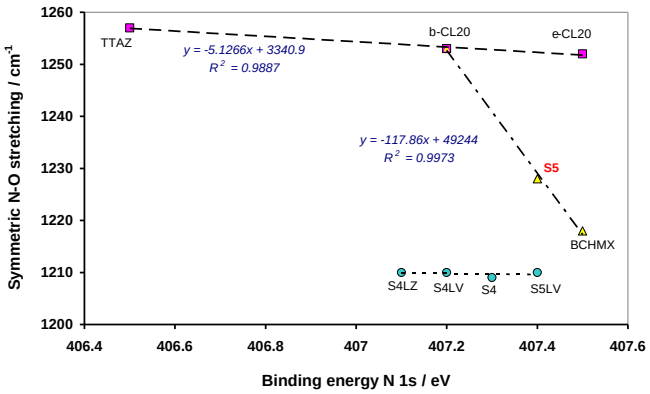

Figure 3.2.13 The relationship between symmetric N-O stretching vibration and the N 1s binding energies of the nitramines studied (the spectroscopic data required have been taken and are also summarized in Chapter 2 Materials section).

3.2.3 Summary

Producing ε-CL-20 and cis-1,3,4,6-tetranitrooctahydroimidazo-[4,5-d]imidazole co-crystallize is an extremely difficult process. Nonetheless, the co-precipitates (micro-co-particles) of the two nitramines produce excellent outcomes when they primarily agglomerate in protogenic medium—n-butanol, using the slurry method. In addition to the co-agglomeration medium, the molar ratio of the two components plays a significant role. This leads to a co-crystal with significantly lower impact sensitivity (14.9 J for the β-CL-20/BCHMX molar ratio = 1.8) compared to pure ε-CL-20 (13.2 J). This finding is not unexpected, considering previous research on the correlation between binding energies in CL-20 isomer co-crystals and the molar ratio of the coformers within them. One sample, obtained by classical co-crystallization, has both α- and β-modifications, while the PXRD analysis of the prepared CACs has revealed that CL-20 is present in them as its ß-modification. The use of Raman, FTIR, and PXRD techniques has demonstrated that CL-20/BCHMX mixed micro-co-particles aggregate to form mixed crystals, most of which exhibit co-crystal properties (CCs).

Also, XPS and Hirshfield analysis revealed that, in terms of co-crystal identification among CACs, interesting relationships have been found between binding energy and FTIR-spectroscopy results. The semi-logarithmic relationship of Raman ring deformation vibration with the O 1s E_{bind} confirms that intermolecular interactions in the crystals studied probably occur via HBs and highlights crystals with internal molecular arrangements different from CCs, BCHMX and ε-CL20. The Hirshfeld analysis of CL20 has shown more stable intermolecular fingerprint plots for its β-isomer than for its ε-analog, which might account for the stabilization of this particular nitramine in co-crystals with polynitro coformers in the β-CL20 polymorphic modification (in general, see [62]).

In addition, FTIR symmetric N-O stretching vibrations versus the N 1s E_{bind} values sharply distinguish the CCs and pure nitramines from the CACs. In both cases, both vibration and stretching increase with decreasing E_{bind} values. In most cases, the presence of CCs during co-agglomeration can be confirmed by the logical relationships between the heat of formation and ring-deformation vibrations (in plane), as well as between the impact sensitivity and the difference in the asymmetric –NO2 stretching vibrations in pure CL-20 and its CCs.

References

[1] S. Zeman, T. Atalar, and A. Růžička, "N-N Bond Lengths and Initiation Reactivity of Nitramines," Cent. Eur. J. Energ. Mater., vol. 17, no. 2, pp. 169–200, Jun. 2020, doi: 10.22211/cejem/122723.

[2] V. B. Patil, K. Zalewski, J. Schuster, P. Belina, W. Trzcinski, and S. Zeman, "A new insight into the energetic co-agglomerate structures of attractive nitramines," Chemical Engineering Journal, vol. 420, Sep. 2021, doi: 10.1016/j.cej.2021.130472.

[3] V. B. Patil, P. Bělina, W. A. Trzcinski, and S. Zeman, "Preparation and properties of co-mixed crystals of 1,3-di- and 1,3,5-tri-amino-2,4,6-trinitrobenzenes with attractive cyclic nitramines," Journal of Industrial and Engineering Chemistry, vol. 115, pp. 135–146, Nov. 2022, doi: 10.1016/j.jiec.2022.07.043.

[4] R. Lewczuk, P. Koślik, and J. Rećko, "Performance of BCHMX in Small Charges," Propellants, Explosives, Pyrotechnics, vol. 45, no. 4, pp. 581–586, 2020, doi: 10.1002/prep.201900315.

[5] M. Ghosh, S. Banerjee, M. A. S. Khan, N. Sikder, and A. K. Sikder, "Understanding metastable phase transformation during crystallization of RDX, HMX and CL-20: experimental and DFT studies," Phys. Chem. Chem. Phys., vol. 18, no. 34, pp. 23554–23571, Aug. 2016, doi: 10.1039/C6CP02185A.

[6] S. Zeman, "Sensitivities of High Energy Compounds," in High Energy Density Materials, vol. 125, T. M. Klapötke, Ed., in Structure and Bonding, vol. 125. , Berlin, Heidelberg: Springer Berlin Heidelberg, 2007, pp. 195–271. doi: 10.1007/430_2006_052.

[7] M. Jungova, S. Zeman, A. Husarova, "Friction Sensitivity of Nitramines. Part III: Comparison with Detonation Performance（英）," Chinese J. Energet. Mater, vol. 19, no. 6, pp. 603–606, doi: 10.3969/j.issn.1006-9941.2011.06.003.

[8] S. Zeman and M. Jungová, "Sensitivity and Performance of Energetic Materials," Propellants, Explosives, Pyrotechnics, vol. 41, no. 3, pp. 426–451, Jun. 2016, doi: 10.1002/prep.201500351.

[9] M. Ghosh, A. Sikder, S. Banerjee, M. Talawar, and N. Sikder, "Preparation of reduced sensitivity co-crystals of cyclic nitramines using spray flash evaporation," DEFENCE TECHNOLOGY, vol. 16, no. 1, pp. 188–200, Feb. 2020, doi: 10.1016/j.dt.2019.05.018.

[10] G. Yan et al., "Phase Retransformation and Void Evolution of Previously Heated HMX-Based Plastic-Bonded Explosive in Wet Air," J. Phys. Chem. C, vol. 121, no. 37, pp. 20426–20432, Sep. 2017, doi: 10.1021/acs.jpcc.7b04165.

[11] Z. G. Aliev et al., “Polymorphism of bimolecular crystals of CL-20 with tris[1,2,5]oxadiazolo[3,4-b:3′,4′-d:3″,4″-f]azepine-7-amine,” Russ Chem Bull, vol. 66, no. 4, pp. 694–701, Apr. 2017, doi: 10.1007/s11172-017-1794-8.

[12] D. S. Viswanath, T. K. Ghosh, and V. M. Boddu, “Properties of Insensitive Energetic Materials and Their Measurement,” in Emerging Energetic Materials: Synthesis, Physicochemical, and Detonation Properties, D. S. Viswanath, T. K. Ghosh, and V. M. Boddu, Eds., Dordrecht: Springer Netherlands, 2018, pp. 1–57. doi: 10.1007/978-94-024-1201-7_1.

[13] D. S. Viswanath, T. K. Ghosh, and V. M. Boddu, “Hexanitrohexaazaisowurtzitane (HNIW, CL-20),” in Emerging Energetic Materials: Synthesis, Physicochemical, and Detonation Properties, D. S. Viswanath, T. K. Ghosh, and V. M. Boddu, Eds., Dordrecht: Springer Netherlands, 2018, pp. 59–100. doi: 10.1007/978-94-024-1201-7_2.

[14] D. Klasovitý, S. Zeman, A. Růžička, M. Jungová, and M. Roháč, “cis-1,3,4,6-Tetranitrooctahydroimidazo-[4,5-d]imidazole (BCHMX), its properties and initiation reactivity,” Journal of Hazardous Materials, vol. 164, no. 2–3, pp. 954–961, 2009, doi: 10.1016/j.jhazmat.2008.08.106.

[15] Z. Xue, B. Huang, H. Li, and Q. Yan, “Nitramine-Based Energetic Cocrystals with Improved Stability and Controlled Reactivity,” Crystal Growth & Design, vol. 20, no. 12, pp. 8124–8147, Dec. 2020, doi: 10.1021/acs.cgd.0c01122.

[16] R. Wiscons and A. Matzger, “Evaluation of the Appropriate Use of Characterization Methods for Differentiation between Cocrystals and Physical Mixtures in the Context of Energetic Materials,” Crystal Growth & Design, vol. 17, no. 2, pp. 901–906, Feb. 2017, doi: 10.1021/acs.cgd.6b01766.

[17] A. Elbeih, J. Pachman, S. Zeman, P. Vávra, W. A. Trzciński, and zbyněk Akštein, “Detonation Characteristics of Plastic Explosives Based on Attractive Nitramines with Polyisobutylene and Poly(methyl methacrylate) Binders,” Journal of Energetic Materials, vol. 30, no. 4, pp. 358–371, Oct. 2012, doi: 10.1080/07370652.2011.585216.

[18] Fraunhofer Institut für Chemische Technologie, Pfinztal, Germany, 2004, “ICT Database of thermochemical values.” 2004.

[19] P. Z. and C. B. Ou Y., Wang C., “Sensitivity of hexanitrohexaazaisowurtzitane[J],” Chinese Journal of Energetic Materials(Hanneng Cailiao), vol. 7, pp. 100-108., 1999.

[20] X. Song, Y. Wang, S. Zhao, and F. Li, “Mechanochemical fabrication and properties of CL-20/RDX nano co/mixed crystals,” RSC Adv., vol. 8, no. 59, pp. 34126–34135, 2018, doi: 10.1039/C8RA04122A.

[21] R. Feng, S. Zhang, F. Ren, R. Gou, and L. Gao, “Theoretical insight into the binding energy and detonation performance of ε-, γ-, β-CL-20 cocrystals with β-HMX, FOX-7, and DMF in different molar ratios, as well as electrostatic potential,” J Mol Model, vol. 22, no. 6, p. 123, Jun. 2016, doi: 10.1007/s00894-016-2998-9.

[22] F. Shen, P. Lv, C. Sun, R. Zhang, and S. Pang, “The Crystal Structure and Morphology of 2,4,6,8,10,12-Hexanitro-2,4,6,8,10,12-hexaazaisowurtzitane (CL-20) p-Xylene Solvate: A Joint Experimental and Simulation Study,” Molecules, vol. 19, no. 11, Art. no. 11, Nov. 2014, doi: 10.3390/molecules191118574.

[23] H.-H. Licht, “Performance and Sensitivity of Explosives,” Propellants Explos. Pyrotech, vol. 25, no. 3, pp. 126–132, Jun. 2000, doi: 10.1002/1521-4087(200006)25:3<126::AID-PREP126>3.0.CO;2-8.

[24] M. Jungová, S. Zeman, and Q.-L. Yan, “Recent Advances in the Study of the Initiation of Nitramines by Impact Using Their 15N NMR Chemical Shifts,” Central European Journal of Energetic Materials, 2014.

[25] T. Urbański, “On Entropy and Free Energy of Explosives (preliminary communication)” Bull. l’Academie Pol. Des Sci. s, Ser. Des Sci. Chim., vol. 28, pp. 511–513, 1980, doi: https://gallica.bnf.fr/ark:/12148/cb343830642/date1980.

[26] Ruslan P. Ozerov and Anatoli A. Vorobyev, Physics for Chemists - 1st Edition. 2007. Accessed: Oct. 20, 2023. [Online]. Available: https://shop.elsevier.com/books/physics-for-chemists/ozerov/978-0-444-52830-8

[27] N. B. Bolotina, M. J. Hardie, R. L. Speer Jr, and A. A. Pinkerton, “Energetic materials: variable-temperature crystal structures of γ- and ∈-HNIW polymorphs,” J Appl Crystallogr, vol. 37, no. 5, pp. 808–814, Oct. 2004, doi: 10.1107/S0021889804017832.

[28] O. Bolton and A. J. Matzger, “Improved Stability and Smart-Material Functionality Realized in an Energetic Cocrystal,” Angew. Chem. Int. Ed., vol. 50, no. 38, pp. 8960–8963, Sep. 2011, doi: 10.1002/anie.201104164.

[29] R. Bu, Y. Xiong, and C. Zhang, “π–π Stacking Contributing to the Low or Reduced Impact Sensitivity of Energetic Materials,” Crystal Growth & Design, vol. 20, no. 5, pp. 2824–2841, May 2020, doi: 10.1021/acs.cgd.0c00367.

[30] G. Liu, S. Wei, and C. Zhang, “Review of the Intermolecular Interactions in Energetic Molecular Cocrystals,” Crystal Growth & Design, vol. 20, no. 10, pp. 7065–7079, Oct. 2020, doi: 10.1021/acs.cgd.0c01097.

[31] G. Liu et al., “Energetic Cocrystallization as the Most Significant Crystal Engineering Way to Create New Energetic Materials,” Crystal Growth & Design, vol. 22, no. 2, pp. 954–970, Feb. 2022, doi: 10.1021/acs.cgd.1c01090.

[32] J. P. Shen et al., “Preparation and Characterization of a Novel Cocrystal Explosive,” Crystal Growth & Design, vol. 11, no. 5, pp. 1759–1765, May 2011, doi: 10.1021/cg1017032.

[33] X. Xu et al., “Elemental Core Level Shift in High Entropy Alloy Nanoparticles via X-ray Photoelectron Spectroscopy Analysis and First-Principles Calculation,” ACS Nano, vol. 14, no. 12, pp. 17704–17712, Dec. 2020, doi: 10.1021/acsnano.0c09470.

[34] P. R. Spackman et al., “CrystalExplorer: a program for Hirshfeld surface analysis, visualization and quantitative analysis of molecular crystals,” J Appl Cryst, vol. 54, no. 3, pp. 1006–1011, Jun. 2021, doi: 10.1107/S1600576721002910.

[35] C. Zhang et al., “Intermolecular friction symbol derived from crystal information,” CrystEngComm, vol. 15, no. 34, pp. 6837–6844, Aug. 2013, doi: 10.1039/C3CE40817E.

[36] M. A. Spackman and P. G. Byrom, “A novel definition of a molecule in a crystal,” Chemical Physics Letters, vol. 267, no. 3–4, pp. 215–220, Mar. 1997, doi: 10.1016/S0009-2614(97)00100-0.

[37] M. A. Spackman and J. J. McKinnon, “Fingerprinting intermolecular interactions in molecular crystals,” CrystEngComm, vol. 4, no. 66, pp. 378–392, 2002, doi: 10.1039/B203191B.

[38] J. J. McKinnon, D. Jayatilaka, and M. A. Spackman, “Towards quantitative analysis of intermolecular interactions with Hirshfeld surfaces,” Chem. Commun., no. 37, pp. 3814–3816, Sep. 2007, doi: 10.1039/B704980C.

[39] B. Tian, Y. Xiong, L. Chen, and C. Zhang, “Relationship between the crystal packing and impact sensitivity of energetic materials,” CrystEngComm, vol. 20, no. 6, pp. 837–848, 2018, doi: 10.1039/C7CE01914A.

[40] N. Liu, B. H. Duan, X. M. Lu, and B. Z. Wang, “Investigation of CL-20/TFAZ cocrystal: preparation, structure and performance,” J. Phys.: Conf. Ser., vol. 1721, no. 1, p. 012005, Jan. 2021, doi: 10.1088/1742-6596/1721/1/012005.

[41] S. Zeman, A. K. Hussein, A. Elbeih, and M. Jungova, “cis-1,3,4,6-Tetranitrooctahydroimidazo-[4,5-d]imidazole (BCHMX) as a part of explosive mixtures,” Defence Technology, vol. 14, no. 5, pp. 380–384, Oct. 2018, doi: 10.1016/j.dt.2018.04.002.

[42] J. J. McKinnon, M. A. Spackman, and A. S. Mitchell, “Novel tools for visualizing and exploring intermolecular interactions in molecular crystals,” Acta Crystallogr B Struct Sci, vol. 60, no. 6, pp. 627–668, Dec. 2004, doi: 10.1107/S0108768104020300.

[43] S. Zeman, “The Chemical Micromechanism of Energetic Material Initiation,” in Nano and Micro-Scale Energetic Materials, John Wiley & Sons, Ltd, 2023, pp. 567–623. doi: 10.1002/9783527835348.ch19.

[44] D. Klasovitý, S. Zeman, “Process for preparing cis-1,3,4,6-tetranitrooctahydroimidazo-[4,5-d]imidazole (BCHMX),” Czech Pat. 302068, C07D 487/04, 2010

[45] F. J. Brockman, G. F. Wright, and D. C. Downing, “Nitrolysis of hexamethylenetetramine: iii. preparation of pure cyclonite,” Can. J. Res., vol. 27b, no. 5, pp. 469–474, May 1949, doi: 10.1139/cjr49b-049.

[46] T. Atalar, M. Jungová, and S. Zeman, “A New View of Relationships of the N–N Bond Dissociation Energies of Cyclic Nitramines. Part II. Relationships with Impact Sensitivity,” Journal of Energetic Materials, vol. 27, no. 3, pp. 200–216, Apr. 2009, doi: 10.1080/07370650802640366.

[47] Muhamed Sućeska, Test Methods for Explosives. Springer, 2012.

[48] S. Zeman, “Chapter 2 - A study of chemical micro-mechanisms of initiation of organic polynitro compounds,” in Theoretical and Computational Chemistry, vol. 13, P. Politzer and J. S. Murray, Eds., in Energetic Materials, vol. 13. , Elsevier, 2003, pp. 25–52. doi: 10.1016/S1380-7323(03)80023-7.

[49] S. Zeman, “Chapter 14 - Characteristics of Thermal Decomposition of Energetic Materials in a Study of Their Initiation Reactivity,” in Handbook of Thermal Analysis and Calorimetry, vol. 6, S. Vyazovkin, N. Koga, and C. Schick, Eds., in Recent Advances, Techniques and Applications, vol. 6. , Elsevier Science B.V., 2018, pp. 573–612. doi: 10.1016/B978-0-444-64062-8.00006-1.

[50] S. Bulusu, T. Axenrod, and J. R. Autera, “Application of 13C and 15N NMR spectroscopy to structural studies on nitramines,” Organic Magnetic Resonance, vol. 16, no. 1, pp. 52–56, 1981, doi: 10.1002/mrc.1270160114.

[51] B. Krebs, J. Mandt, R. E. Cobbledick, and R. W. H. Small, “The structure of N,N-dimethylnitramine,” Acta Crystallogr B Struct Crystallogr Cryst Chem, vol. 35, no. 2, pp. 402–404, Feb. 1979, doi: 10.1107/S0567740879003630.

[52] S. Zeman and N. Liu, “A new look on the electric spark sensitivity of nitramines,” Defence Technology, vol. 16, no. 1, pp. 10–17, Feb. 2020, doi: 10.1016/j.dt.2019.06.023.

[53] S. Zeman, “Electric Spark Sensitivity of Nitramines. Part I. Aspects of Molecular Structure*)”.

[54] A. N. Dremin, Toward Detonation Theory. Springer Science & Business Media, 1999.

[55] S. Zeman, Q.-L. Yan, and A. Elbeih, “Recent Advances in the Study of the Initiation of Energetic Materials Using the Characteristics of Their Thermal Decomposition Part II. Using Simple Differential Thermal Analysis,” p. 10.

[56] S. Zeman, A. Elbeih, A. Hussein, T. Elshenawy, M. Jungova, and Q. L. Yan, “A modified vacuum stability test in the study of initiation reactivity of nitramine explosives,” Thermochimica Acta, vol. 656, pp. 16–24, Oct. 2017, doi: 10.1016/j.tca.2017.08.006.

[57] V. B. Patil, R. Svoboda, and S. Zeman, “Towards the thermal reactivity and behavior of co-agglomerated crystals of DATB and TATB with attractive nitramines,” Thermochimica Acta, vol. 724, p. 179494, Jun. 2023, doi: 10.1016/j.tca.2023.179494.

[58] S. Zeman, “Thermal stabilities of polynitroaromatic compounds and their derivatives,” Thermochim. Acta, vol. 31, pp. 269–283, 1979.

[59] Y. Shu, B. L. Korsounskii, and G. M. Nazin, “The mechanism of thermal decomposition of secondary nitramines,” Russ. Chem. Rev., vol. 73, no. 3, pp. 293–307, May 2004, doi: 10.1070/RC2004v073n03ABEH000802.

[60] L. M. Kostikova, E. A. Miroshnichenko, and Y. Matyushin, “The energies of dissociation bonds and efficient energies of interaction in nitramines,” in Proc. 31st Int. Annual Conf. ICT, Karlsruhe, Germany, 2000, p. 50/1-50/11.

[61] N. B. H. Jonathan, “Relations between force constants, bond orders, bond lengths, and bond frequencies for some nitrogen-oxygen bonds,” Journal of Molecular Spectroscopy, vol. 4, no. 1, pp. 75–83, Jan. 1960, doi: 10.1016/0022-2852(60)90066-7.

[62] V. B. Patil, P. Bělina, W. A. Trzcinski, and S. Zeman, “Co-agglomerated crystals of 2,2′,4,4′,6,6′-hexanitro -stilbene/-azobenzene with attractive nitramines,” Chemical Engineering Journal, vol. 457, p. 141200, Feb. 2023, doi: 10.1016/j.cej.2022.141200.

3.3 Co-agglomerated crystals of 2,2',4,4',6,6'-hexanitro -stilbene /-azobenzene with attractive nitramines

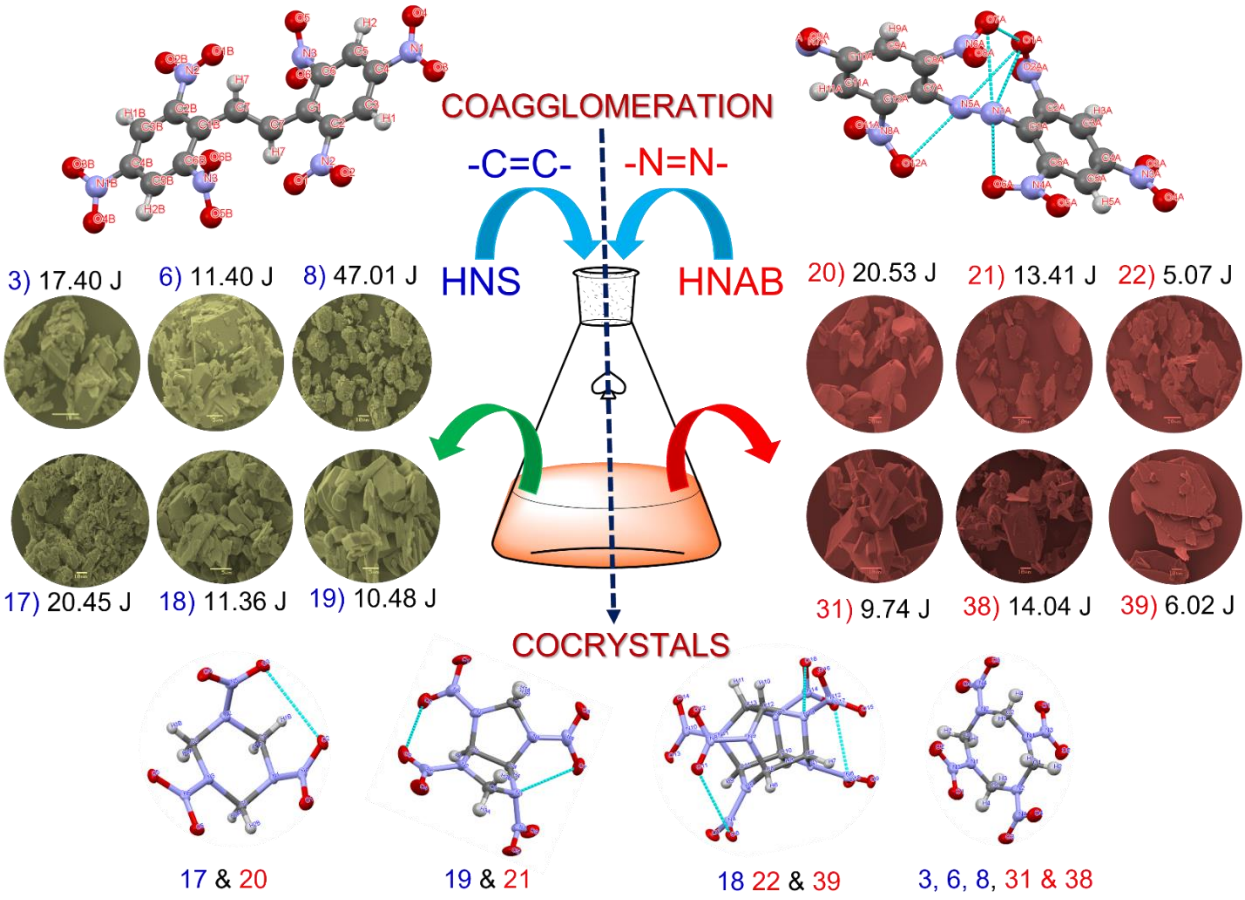

Published in

Journal of Chemical Engineering, Vol. 457, 1 P, 141200, DOI: 10.1016/j.cej.2022.141200

3.3.1 Background

A slightly more complicated way of reducing the sensitivity of nitramines is to add other, less sensitive explosives to them and incorporate all this into a polymer matrix, as in ternary blends, containing, for example, very sensitive BCHMX in mixture with low sensitive 2,4-diamino-1,3,5-trinitrobenzene (DATB) or 2,2',4,4',6,6'-hexanitroazobenzene (HNAB), bounded by styrene-butadiene rubber (SBR) [1]]. The effect of the addition of both these polynitroarenes on reducing the mechanical sensitivity of the resulting ternary plastic explosives is significant [1].

Crystal engineering replaces the mechanical mixture of nitramine with the low-sensitive EMs by the co-crystals by introducing another EM molecule into the crystal lattice of nitramines like DATB and TATB [2, 3], TNT [4], including own nitramines of a mutually distinct molecular structure [5], etc. However, co-crystals with TNT have low physical stability due to their low melting point. Much more stable in this respect is the 2,2',4,4',6,6'-hexanitrostilbene (HNS), produced from TNT [6]. It is, therefore, not without interest to see what effect this thermally stable polynitroarene may have on both the feasibility of preparing these co-crystals and their properties.

Speaking of HNS (crystallography see in [7, 8]), it is appropriate to mention the geometrically similar molecule HNAB (its crystallography see in [9, 10]). In the HNS crystal its molecule attains a good symmetry due to its linkages towards a layered arrangement with hydrogen bonds formation (by hydrogen atoms of benzene ring) followed by layers further connected by C-H---π (π - π) stacking with involvement of hydrogen atoms of the –C=C– bridge [11]. However, it's different in the case of HNAB which the molecule is balanced by more intermolecular interactions by nitrogen atoms of the –N=N– bridges with oxygen atoms in the N–O groupings of ortho-nitro groups [10]. However, there will be more possibility of interaction of π - π stacking after contact with molecules of other energetic materials in crystal lattice [11].

With reference to all here presented yet facts so we explore in this work the possibility of forming co-crystals (co-agglomerates) from attractive cyclic nitramines and both the aforementioned polynitroarenes, with a subsequent study of the utility properties of the resulting new EMs.

3.3.2 Results

3.3.2.1 Powder X-Ray diffraction (PXRD) studies:

After Surface morphological analysis to understand the crystallographic morphology, PXRD data of the HNS and HNAB CACs were collected. The obtained peak intensities 2Θ values are shown in Table 3.3.1, and the PXRD diffractograms are shown in Figure 3.3.1. These peak data are divided into two parts; normal and intense peaks. Once observing the 2Θ, we can see the crystal morphology of pure nitramines and their CACs with HNS and HNAB. To attain stability, the nitramines undergo phase transition during the co-

agglomeration process. This is observed by the peaks shifting and their intensities changes in Figure 3.3.2. These can be seen in an HMX CACs; its changed β to δ phase during the co-agglomeration (the same polymorphic change as it is in the case of the co-agglomeration of HMX with DATB, TATB [2, 3] and nitramines [5]). Whereas the CL-20 in its pure state was in the ϵ phase after co-agglomeration with HNS and HNAB, it changed to β (similarly it is the case of its co-agglomeration with DATB, TATB [2, 3] and nitramines [5]). These phase changes were further confirmed with thermal analysis by DTA, in which initial endothermic changes indicate the phase changes are overlays with the PXRD data. It shows that in 90% of cases of CL-20 co-crystals, it was observed that CL-20 was found to be in its β-phase; similarly, in the case of HMX, it was δ-phase. It indicates there will be co-crystals formation CACs. In another way, the particles of the co-crystals, along with the CACs detected, may also be of polycrystalline type.

Table 3.3.1 PXRD data for pure nitramines and CACs

Sr No	Code design.	2Θ values for intense peaks / ˚
1	ε-CL-20	14.30, 30.10, 42.98
2	β-CL-20	12.66, 13.86, 30.34
3	BCHMX	9.74, 12.65 and 23.57
4	β-HMX	14.61, 16.31, 24.45, 25.07, 32.31
5	δ-HMX	13.10, 17.02, 24.34
6	RDX	9.73, 12.65, 23.59
7	HNS	8.38, 16.84, 34.08, 24.18
8	HNAB	8.56, 17.40, 26.32
9	3 HMX/ HNS	14.48, 20.32, 22.82, 31.32
10	6 HMX/ HNS	14.52, 20.36, 22.90, 31.78
11	8 HMX/ HNS	14.48, 20.38, 22.88, 31.78
12	17 RDX/ HNS	17.30, 17.78, 25.30, 29.20
13	18 CL-20/ HNS	11.98, 13.62, 27.90
14	19 BCHMX/ HNS	9.98, 12.90, 16.18, 23.86
15	20 RDX/ HNAB	13.44, 27.02, 29.32
16	21 BCHMX/ HNAB	12.94, 21.42, 23.88
17	22 CL-20/ HNAB	8.72, 21.51, 33.22
18	31 HMX/ HNAB	20.50, 23.01, 29.62,
19	38 HMX/ HNAB	20.52, 23.01, 29.67, 31.88
20	39 CL-20/HNAB	8.76, 21.48, 23.32

3.3.2.2 Morphology and Particle size analysis

The morphological changes in CACs were analyzed using FESEM, and its influence on the CACs sizes was analyzed using particle size analysis techniques (shown in Figure 3.3.2 and Table 3.3.2). All CACs

showed irregular-shaped particles. In the case of HNS CACs, crystals penetrated each other, whereas, in the case of HNAB CACs, samples showed infirmity with layered structures. In the case of 3 HMX/ HNS and 6 HMX/ HNS, HNS crystals showed penetration in respective nitramines crystals with smoother surfaces, whereas 8 HMX/ HNS showed different crystals are like sugar cubes with uniform mixed with HMX with porosity also clearly visible. It is also interesting that porosity crystals were found to be smaller as compared to the other two HMX CACs with HNS. Then the 17 RDX/ HNS nitramines showed soft edges with the accumulation of HNS crystals, followed by the 18 CL-20/ HNS, showed uniform crystal distribution with slightly sharper edges. Next 19) BCHMX/ HNS showed slightly columnar crystals with uniform and smoother surface areas. Coming HNAB CACs, 21 BCHMX/ HNAB; 22 CL-20/ HNAB; and 39 CL-20/ HNAB are shown unique layered structured structures. This crystal is hexagonal in shape on the side of a larger surface area, with a uniform surface and sharp edges. These crystals are very soft and crystalline in physical observation. In the case of 20 RDX/ HNAB, these crystals are observed on segregated and uniform surfaces with smoother edges. This is followed by the case of 31 HMX/ HNAB crystals, which are found to have uniform surfaces, slightly porous, with broken edges. Similarly, in the case of 38 HMX/ HNAB also shows crystals with broken edges; however, crystals have a smoother surface here.

Overall, observations obtained from the FESEM images also showed that the HNS and HNAB particles showed uniform distribution in all cases. Except for the slight porosity and broken edges (especially in the case of 22 CL-20/ HNAB; 31 HMX/ HNAB; and 39 CL-20/ HNAB), all cases particles are observed with smoother surfaces with closed surfaces. The solvent used for co-agglomeration played a very important role in crystal morphology compared to the solvent used in the co-precipitation. These active interactions between the crystals show a strong influence formation of molecular crystals [11, 12]. These also helps crystals achieve/retain the higher density in CACs. As mentioned before, except for three CACs, these interactions strongly influence CACs to withstand the higher impact (i.e., impact sensitivity), which is discussed in the next part.

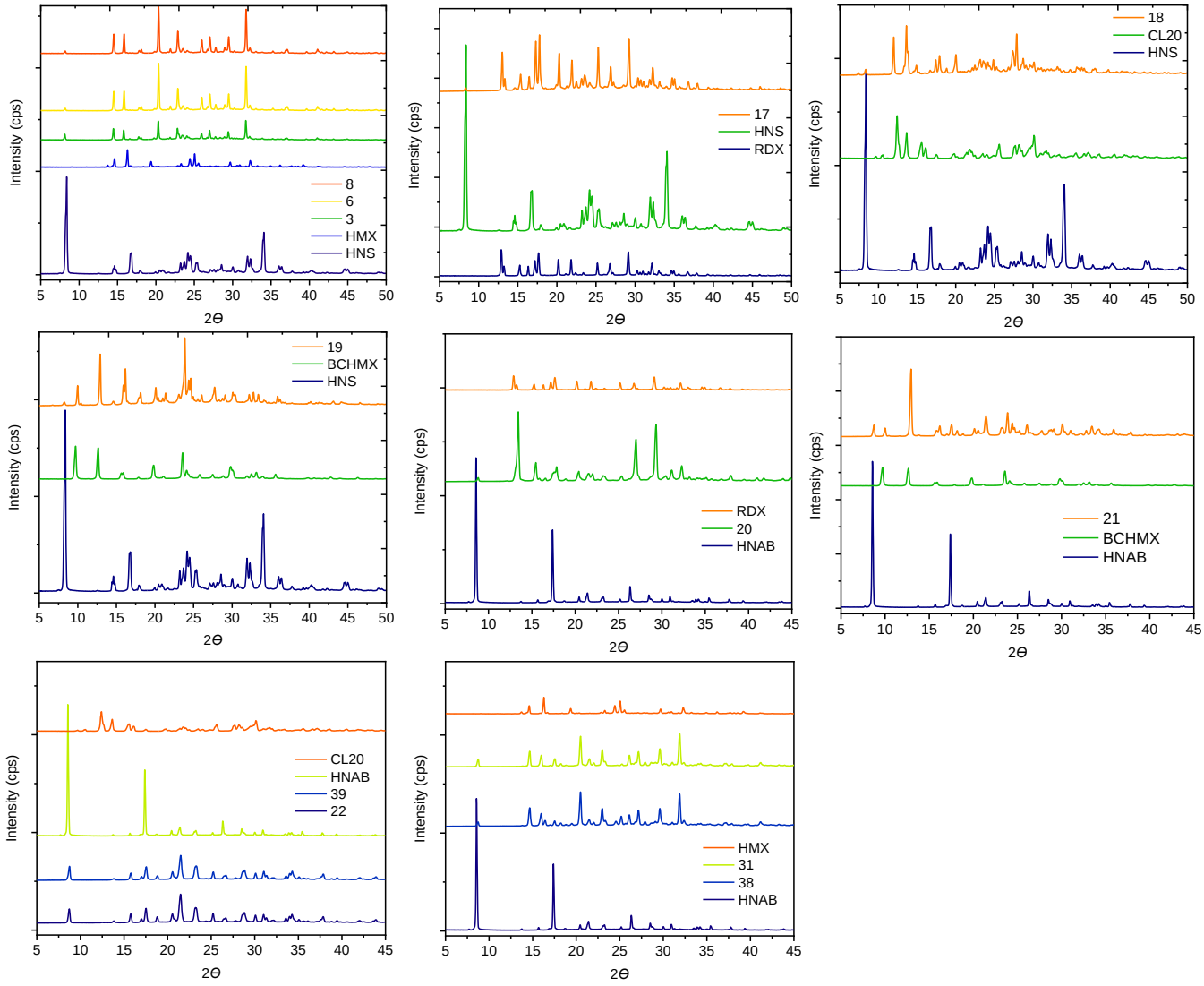

Figure 3.3.1 PXRD diffractograms of CACs; 3 HMX/ HNS; 6 HMX/ HNS; 8 HMX/ HNS; 17 RDX/ HNS; 18 CL-20/ HNS; 19 BCHMX/ HNS; 20 RDX/ HNAB; 21 BCHMX/ HNAB; 22 CL-20/ HNAB; 31 HMX/ HNAB; 38 HMX/ HNAB and 39 CL-20/ HNAB

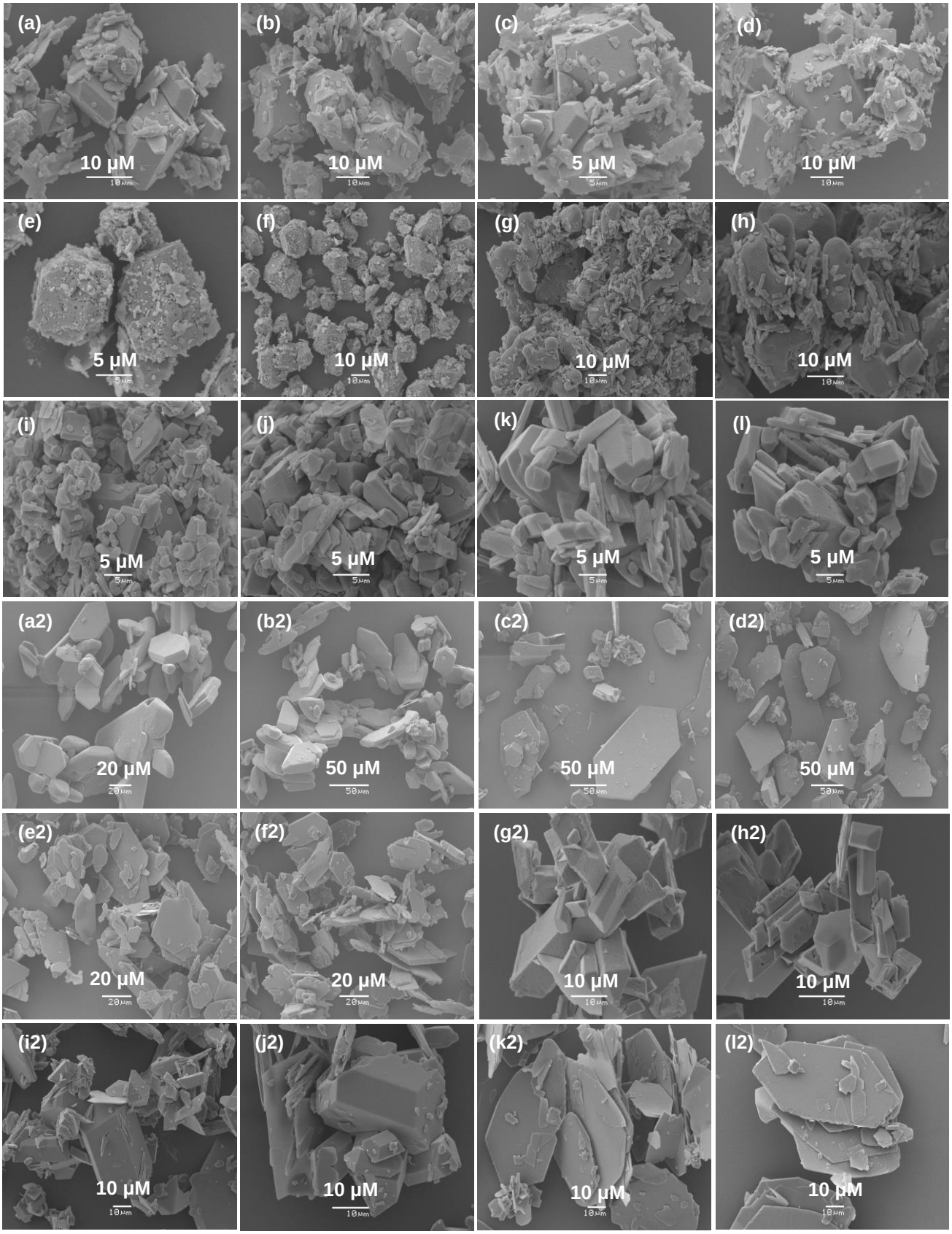

Figure 3.3.2 FESEM images of co-crystals a & b) 3 HMX/ HNS, c & d) 6 HMX/ HNS, e & f) 8 HMX/

HNS, g & h) 17 RDX/ HNS, i & j) 18 CL-20/ HNS and k & l) 19 BCHMX/ HNS; a2 & b2) 20 RDX/ HNAB; c2 & d2) 21 BCHMX/ HNAB; e2 & f2) 22 CL-20/ HNAB; g2 & h2) 31 HMX/ HNAB; i2 & j2) 38 HMX/ HNAB; k2 & l2) 39 CL-20/ HNAB

Table 3.3.2 Particle size measurements of CACs

Sr No	Code design.	Solvent system Sol / antisol / CASol	Particle size analysis			
			Surface area (m^2/kg)	Dv(10) μM	Dv(50) μM	Dv(90) μM
1	3 HMX/ HNS	DMSO / water / BuOH	1596	1.93	5.92	20.1
2	6 HMX/ HNS	DMSO / water / BuOH	1973	1.36	6.49	26.7
3	8 HMX/ HNS	DMSO / water / BuOH	1732	1.44	4.52	13.1
4	17 RDX/ HNS	DMF / water / CHF	2089	1.36	6.05	23.6
5	18 CL-20/ HNS	DMF / water / CHF	1772	1.49	8.76	34.2
6	19 BCHMX/ HNS	DMF / water / CHF	1547	1.79	6.87	20.2
7	20 RDX/ HNAB	DMK / hexane / CHF	441.3	10.1	27.2	54.8
8	21 BCHMX/ HNAB	DMK / hexane / CHF	629.4	5.59	19.8	61.8
9	22 CL-20/ HNAB	DMK / hexane / CHF	1056	3.35	10.8	25.1
10	31 HMX/ HNAB	DMK / hexane / CHF	912.4	3.98	15.8	41.9
11	38 HMX/ HNAB	DMK / hexane / CHF	792.0	4.30	15.8	62.9
12	39 CL-20/HNAB	DMK / hexane / CHF	872.9	3.78	12.3	33.0

Note: Sol -solvent; antisol – antisolvent; CASol – solvent used for co-agglomeration

3.3.2.3 Differential thermal analysis (DTA)

To understand the thermal properties of obtained CACs of HNAB and HNS analyzed employing the DTA technique, the obtained thermograms are shown in Figure 3.3.3, and the results are summarized in Table 3.3.4. As compared to targeted pure nitramines, their CACs showed a slight decrease in their thermal stability (± 5 - 15 C) (see exothermic peaks in Table 3). However, HNS and HNAB resist initial polymorphic changes in the CACs (see endothermic peaks in Table 3). As observed previously, RDX increased its thermal stability after undergoing co-agglomeration with DATB and TATB [2, 3]. The same thing is repeated in the case of HNS and HNAB. In the case of HMX, CACs with HNS stability was maintained as compared to CACs with HNAB. This stability effect was balanced here due to HMX polymorphic phase transition from β to δ in CACs.

Similarly, HMX shows the α- to δ- phase transition in its pure form. Next, in the case of RDX CACs with both HNS and HNAB, it was seen that overlapping of endothermic and exothermic peaks indicates that the RDX is undergoing sudden melting with changing to RDX solution form then followed by decomposition.

Table 3.3.3 Summarized data from DTA thermograms of coformers and co-crystals with their visible melting points.

Sample	Melting point / °C [Ref.]	Peaks of changes in DTA record / °C (CL-20 phase modifications)	
		endothermic	exothermic
ε-CL-20	240 decompn [12]	170 (ϵ - γ)	225 (γ)
BCHMX	286 decompn [13]	144	224
HMX	275 decompn [14]	190 (α – δ)	272
RDX	203.3-204.5 decompn [15]	209	215
HNS	312-314 decompn [16]	325.41	328.42; 335.25*; 340.80*
HNAB	222-223 [16]	134.63; 224.14	335.19; 347.79
3 HMX/ HNS	NA	196.54	268; 270.65
6 HMX/ HNS		192.65	267.21
8 HMX/ HNS		192.92	267.21
17 RDX/ HNS		205.85	221.15
18 CL-20/ HNS		NA	222.45
19 BCHMX/ HNS		NA	228.5
20 RDX/ HNAB		185.28; 198.23	216.19
21 BCHMX/ HNAB		152.04	215.12
22 CL-20/ HNAB		151.32, 223.78	335.36, 350.78*
31 HMX/ HNAB		203, 212.36	247.38, 257.66*
38 HMX/ HNAB		191.87, 215.10	249.50, 254.02*
39 CL-20/ HNAB		151.04; 225.28	341.14

*Tailing peaks

This is followed by in the case of CL-20 CACs; with HNS less stable than HNAB. In the case of the HNS CACs, endothermic changes are restricted and directly undergone in melting, as in the case of RDX CACs. At the same time, its CACs with HNAB showed improved thermal stability compared to its pure form. In all CACs of the CL-20, it was observed that there was a phase transition ϵ to β occurred. However, in the case of BCHMX, CACs with both stabilities were relatively maintained. It's interesting to see that the HNS molecular usually exhibits a *trans*-form to avoid steric hindrance and gain more stability. The pure HNS used was *trans*-form; it was converted into cis form during the co-agglomeration. It may be that CACs are intermolecularly connected with nitramines balanced with this *cis*- form of HNS [8].

3.3.2.4 FTIR Measurements

The previous analysis from PXRD and DTA data; observed that there would be an existence of intermolecular interaction between the HNS and HNAB with the attractive nitramines. To evaluate it, spectral studies were carried out with the help of FTIR and Raman spectroscopic techniques. This helps us with a detailed understanding of the intermolecular interactions of both coformers in the co-agglomeration process. The obtained FTIR stretching/bending vibrations data were summarized in Table 3.3.4, 1. in which the pure nitramines were compared with their CACs.

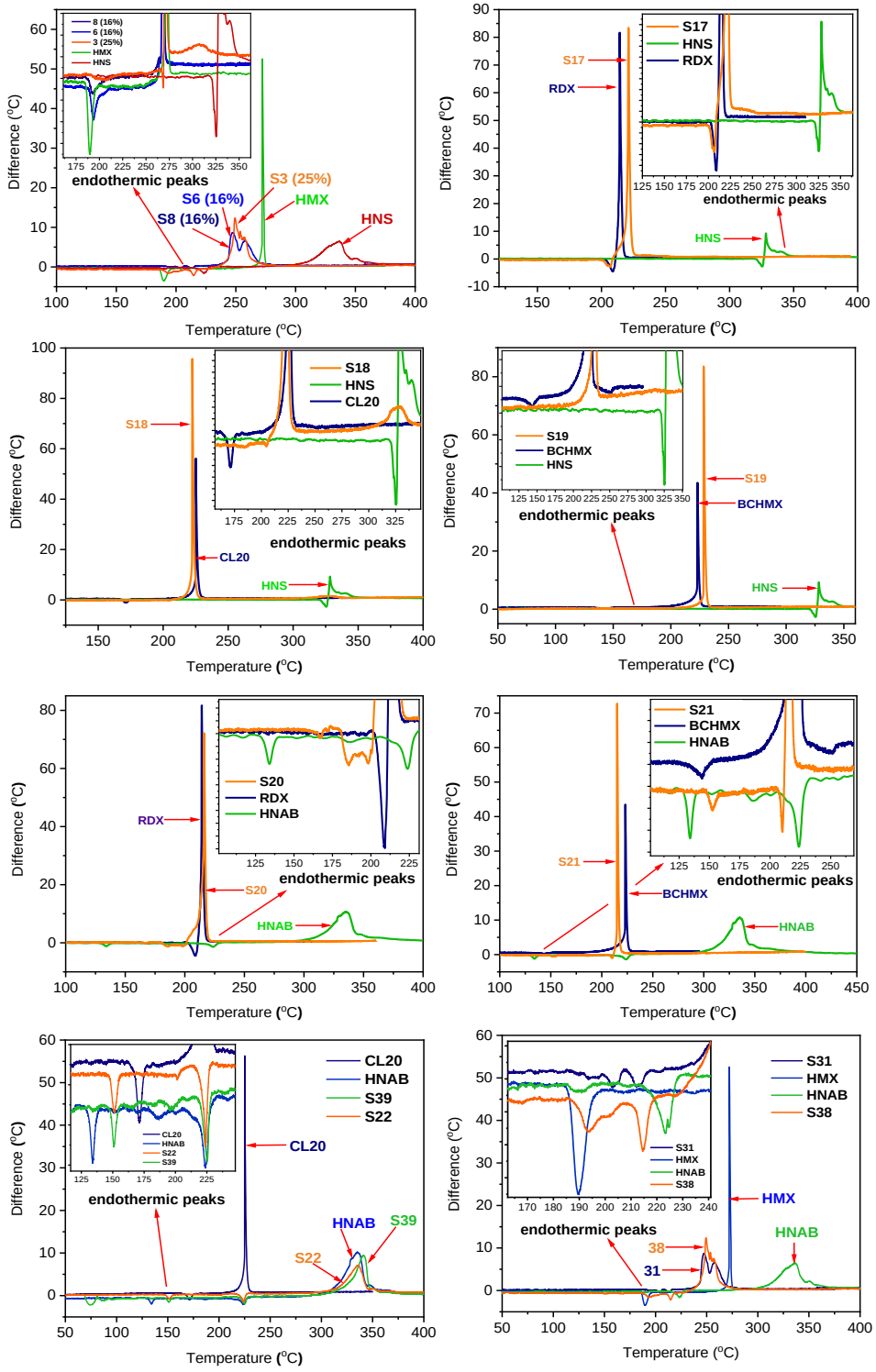

Figure 3.3.3 DTA thermograms of CACs S3) HMX/ HNS; S6 HMX/ HNS; S8 HMX/ HNS; S17 RDX/ HNS; S18 CL-20/ HNS; S19 BCHMX/ HNS; S20 RDX/ HNAB; S21 BCHMX/ HNAB; S22 CL-20/ HNAB; S31 HMX/ HNAB; S38 HMX/ HNAB and S39 CL-20/ HNAB

All the CACs were shown small shaper peaks at 3500 cm^{-1} and around 3220-3320 $cm^{-1,}$ indicates that there will be the formation of shorter contacts between both coformers like hydrogen bonds and π-π stacking kind interactions. It is further confirmed by observed peak shifts and stretching vibrations (Table 3.3.4). Mainly, symmetric and asymmetric vibrations were observed in pure and CACs around regions 1530 ± 30 and 1250 ± 70, respectively. The peak shifts of pure nitramines with their CACs found there will be a red shift in these regions, which indicates that there will be the formation of the –N–O···H– kind intermolecular interactions between both coformers. These changes strongly influence the CACs to attain the stability of the crystal lattice. Also, all other stretching vibrations were found to be observable changes. A C−H stretching vibration is splatted into two bands; this doublet peaks with a slightly shifted mode. Also, their skeleton ring stretching shown predominantly shifted in CACs; it indicates nitramines with HNAB and HNS structural orientation to adopt stable structure with intermolecular interactions. Likewise, HNS was changed into *trans*- to *cis*- form, CL-20 was changed from ϵ to β form and HMX from β to δ - polymorphs.

These changes made possible −N−O and −C−H bonds of HNS and HNAB involved mainly hydrogen bonds, wan der Waals forces of interactions and π-π stacking kind intermolecular interactions. As mentioned previously, these structural changes influenced CACs to attain stable crystal lattices [11, 12].

3.3.2.5 Raman Spectral studies:

A part of spectral studies to understand the intermolecular interactions exhibited in the HNS and HNAB CACs was further evaluated using Raman spectrum data. The obtained Raman spectrum stretching/bending vibrations were summarized in Table 3.3.5. A stretching vibration at 1590 ± 10 cm^{-1} of −ONO bond shows a shift in all CACs. Likewise, a symmetric starching of $-NO_2$ bond at 1220 ± 50 also showed observable shifts. This was followed by O−N−O deformation vibration at 832, and 840 cm^{-1} also showed Impactful shifts. The CL-20 in CACs showed β and HMX as δ-phases; in addition, the HNS were also converted from *trans*- form to *cis*- form during the co-agglomeration. This kind of flipping of the rings relatively helped in the formation of −C−H---π (π - π) stacking between the two benzene rings of HNS and HNAB with nitramines. These shifts are also clearly observable in −C−H bending, −C−H, −N−H and N−N bond stretching bands with redshift and other stretching vibrations, as shown in Table 3.3.5. The HNS and HNAB are actively involved in intermolecular interactions with the attractive nitramines.

All modifications and structural changes overlapped with the PXRD, FTIR, and DTA observations. These modifications appeared in the structural orientations that occurred during the co-agglomeration process. Due to these changes, which strongly helped coformers to CACs to gain stable crystal lattice, also indicate there might be H-bonding, von der Waals forces of interactions, and π-π stacking kind of intermolecular forces interactions occurred; this further leads towards formation of the co-crystals in CACs [17].

Table 3.3.4 Summarized results of FTIR measurements

Assignments	CL-20	BCHMX	HMX	RDX	HNAB	HNS	3 HMX/ HNS	6 HMX/ HNS	8 HMX/ HNS	17 RDX/ HNS	18 CL20/ HNS	19 BC/ HNS	20 RDX/ HNAB	21 BC / HNAB	22 CL20 / HNAB	31 HMX/ HNAB	38 HMX/ HNAB	39 CL20/ HNAB
O-N-O-H--structural bond	3042	3031	3671	--	3081	3010	3037	3037,	3037	3066	3024	3019	3090	3090	3090	3082	3091	3090
C-H stretching	3042; 3017	3019	3052	3074, 3065, 3002	2884	3099, 2880	3100	3100	3100	3075	3054	3099, 2880	3100	3100	3100	3074, 3100	3053, 3100	3100
Symmetrical N-O stretching	1252	1218	1240	1262, 1231, 1216	1195	1264,	1263, 1237, 1200	1261, 1237, 1200	1261, 1237, 1200	1263, 1231, 1216	1227, 1255	1209, 1264	1216, 1231, 1263	1197, 1283	1197, 1220,	1202, 1263	1198, 1258	1196, 1220
Asymmetrical N-O stretching	1562	1562	1539	1569	1536	1531	1531	1530	1530	1533, 1568	1537, 1552	1533	1530, 1565,	1534	1534	1537	1530	1535
C-N stretching [Amino group]	757	774	733, 763	737, 752, 779	733, 746, 762	714, 721, 740, 760, 781	714, 740, 759, 771, 780	714, , 741, 753, 759, 771	714, 741, 753, 759, 771	714, 723, 739, 752, 780	714, 739, 749, 762	714, 723, 741, 774	779, 751, 740, 722	777, 741, 721	720, 741, 768, 779	781, 759, 737, 727, 719	779, 760, 741, 722,	779, 768, 741, 720,
C-N stretching [Nitro group]	1326	1326	1315	1309	1339	1338	1343	1344	1344	1638, 1614	1638, 1614	1639, 1612	1311, 1346	1377, 1342	1341	1325, 1345	1316, 1344	1341
Skeletal stretching [Ring]	1182; 1040	1137; 1084	1207, 1087	1216, 1037	1195, 1082,	1180, 1084	1200, 1138, 1085	1200, 1138, 1085	1200, 1138, 1085	1216, 1085, 1038	1227, 1166, 1084, 1050	1539	1018, 1037, 1081	1081, 1136	1197, 1174, 1080	1202, 1139, 1086	1198, 1139, 1084	1196, 1174, 1080
Symmetric - NO2 Stretching	1252, 1218 1280	1273 1209	1270, 1240,	1309, 1350	1339	1338	1343, 1263, 1237	1344, 1261, 1226	1344, 1261, 1237	1388, 1366, 1346, 1310	1366, 1345, 1333 1302	1366, 1345, 1300	1216, 1231, 1263	1197, 1283,	1220	1263	1258	1220, 1196
Asymmetric - NO2 Stretching	1632, 1601, 1585, 1562	1603, 1554, 1526	1539	1529, 1569, 1588	1607, 1536	1531, 1600, 1617	1531, 1600, 1617	1530, 1600, 1617	1530, 1600, 1617	1273, 1216	1230, 1264	1238, 1264	1588, 1565, 1530	1603, 1534	1604, 1534	1552, 1537, 1516, 1613	1530, 1604	1535, 1604,

Table 3.3.5 Summarized results of Raman measurements

Assignments	CL-20	BCHMX	HMX	RDX	HNAB	HNS	3 HMX/ HNS	6 HMX/ HNS	8 HMX/ HNS	17 RDX/ HNS	18 CL20/ HNS	19 BC/ HNS	20 RDX / HNAB	21 BC / HNAB	22 CL20/ HNAB	31 HMX/ HNAB	38 HMX/ HNAB	39 CL20/ HNAB
					3226	3102	3102	3111	3101	3102	3102	3102	3130	3148	3269	3138	3138	3269
–CH_2 stretching vibration	3052	3020			--	3063	3063	3093	3064	3075	3054	3063	3099, 3075	3097	3097	3092, 3081	3092, 3081	3097
	3024				--	--	3028	3037, 3028	3038, 3028	3066, 3001	3035, 3026	3033, 3020	3066	3018	--	3037, 3028	3037, 3028	--
C–H stretching vibration		2992			2978 2985	--	2992	2992	2992	2948	2984	2933	2948, 2984,	2970, 2933	2985	2921	2921	2985
		2932				2917	2912	2926	2909	2907	2912	2992	3002	2985	--	2992	2992	--
Asymmetric –NO_2 stretching vibration	1594	1606			1603	1638, 1614	1638, 1614	1638, 1614	1638, 1614	1638, 1614	1638, 1614	1639, 1612	1608	1608	1608	1608	1608	1608
	1554	1557			--	1558, 1538	1538,	1558, 1568	1559, 1568	1594, 1572	1558, 1538	1539	1562, 1537	1561, 1537	1561, 1537	1561, 1535	1561, 1535	1561, 1537
C–H and –CH_2 deformation vibration	1326, 1280	1299	1315, 1270	1310, 1273	1319	1302, 1345, 1366	1309, 1349, 1366	1310, 1349, 1366	1366, 1349, 1309	1388, 1366, 1346, 1310	1366, 1345, 1333 1302	1366, 1345, 1300	1310	1318, 1352, 1368	1319, 1352, 1368	1310, 1267	1310, 1267	1319, 1352, 1368
Symmetric –NO_2 stretching vibration	1280, 1252	1273, 1264, 1240	1240, 1270	1217, 1273	1220	1264	1266, 1248,	1248,	1267, 1248	1273, 1216	1230, 1264	1238, 1264	1216, 1273	1205	1205, 1274	1204, 1248, 1267	1204, 1248, 1267	1205, 1274
Asymmetric C–H stretching vibration	1164, 1182, 1137	1194, 1167	1207	1217	1195, 1170, 1144	1182, 1206	1186, 1206	1208	1189, 1168.	1182,	1182, 1206	1113, 1206	1163, 1192, 1205. 1216	1192, 1162	1205, 1192, 1163	1192, 1164	1192, 1164	1205, 1192, 1163

N–N stretching vibration	1050, 1038, 1014, 984	967, 1058	1079, 952	1030	1030	989	952,	952,	951,	942, 1030	942, 989, 1046	942, 1056	944, 1032,	952,	958,	952	951	958
C–C stretching vibration	1048	1058	1087	1085	1082	1087	1087	1081	1087	1087	1088	1087	1083	1083	1083	1078	1083	1083
Ring stretching vibration	979	967	939	943	923	942	951	952	952	942	989	942	944	933	958	952	952	958
	935	906	904	--	939	927	927	931	927	927	958	969	933	955	955	952	952	955
Ring deformation vibration	913	850	850	848	823	842	834	834	834	848	842	850	885	850	825	825	825	825
	881	906	--	885	883	879	882	883	883	885	879	878	848	886	885	883	883	885
$-NO_2$ deformation vibration	854 831	--	--	--	832	826	834	834	834	848, 835	841	835	825	825	825	834	834	825
	819	--	--		823	--	--	--	--	826	826	826	--	--	--	--	--	--
	743	775	775	788	781	771	--	--	760	788	794	771	788	759	746	759	759	746
$-NO_2$ Wagging	737	750	750	757	701	744, 755	758	759,	720	756, 742, 722	756, 771, 717	755, 745,715	745 716, 705	746 704	716, 705	716, 705	716, 704	716, 705

Table 3.3.6 Molecular formulas, thermochemical properties, and maximal crystal densities of pure substances and corresponding CACs

	Explosive				Heat of combustion		Enthalpy of formation		Crystal Density ($g.cm^{-3}$)
No	Code design.	Molar ratio nitramines to HNS or HNAB*	Formula	Mol. weight	Q_c ($J.g^{-1}$)	Ref	ΔH_f ($kJ.mol^{-1}$)	Ref	
1	RDX	NA	$C_6H_6N_6O_{12}$	222.23	9522	[18]	66.20	[18]	1.810
2	BCHMX	NA	$C_4H_6N_4O_8$	292,01	9124	[18]	236.50	[18]	1.860
3	β-HMX	NA	$C_4H_8N_8O_8$	294.17	9485	[18]	77.30	[18]	1.902
4	δ-HMX	NA	$C_4H_8N_8O_8$	294.17	NA	NA	55.5 (82.03)	[19]	1.790
5	β-CL-20	NA	$C_6H_6N_{12}O_{12}$	438,19	8485	[20]	421.74	[20]	1.985
6	ε-CL-20	NA	$C_6H_6N_{12}O_{12}$	438.19	8311	[18]	397.80	[18]	2.044
7	HNS	NA	$C_{14}H_6N_6O_{12}$	450.23	11634	[18]	78.24	[18]	1.745
8	HNAB	NA	$C_{12}H_4N_8O_{12}$	452.21	5 583	[18]	284.09	[18]	1.799
9	3 HMX/ HNS	1.00:0.42	$C_{7.54}H_{8.00}N_{8.00}O_{9.93}$	369.56	10880	cw	77.64	cw	1.8730
10	6 HMX/ HNS	1.00:0.16	$C_{5.57}H_{8.00}N_{8.00}O_{8.85}$	328.60	10386	cw	72.78	cw	1.8820
11	8 HMX/ HNS	1.00:0.11	$C_{5.09}H_{7.96}N_{8.00}O_{8.57}$	318.32	10055	cw	73.55	cw	1.8778
12	17 RDX/ HNS	1.00:0.14	$C_{4.35}H_{6.00}N_{6.00}O_{6.73}$	250.02	10040	cw	68.10	cw	1.7824
13	18 CL-20/ HNS	1.00:0.61	$C_{11.14}H_{7.40}N_{12.00}O_{14.80}$	546.15	10444	cw	275.89	cw	1.9265
14	19 BCHMX/ HNS	1.00:0.25	$C_{5.89}H_{6.31}N_{8.00}O_{9.02}$	333.48	10087	cw	155.11	cw	1.8278
15	20 RDX/ HNAB	1.00:0.11	$C_{3.90}H_{5.79}N_{6.00}O_{6.00}$	242.32	10033	cw	78.10	cw	1.7831
16	21 BCHMX/ HNAB	1.00:0.34	$C_{6.44}H_{5.86}N_{8.00}O_{9.62}$	349.23	10138	cw	214.14	cw	1.8267
17	22 CL-20/ HNAB	1.00:0.46	$C_{8.81}H_{6.00}N_{12.00}O_{13.40}$	494.35	9504	cw	384.67	cw	1.7918
18	31 HMX/ HNAB	1.00:0.185	$C_{5.25}H_{7.37}N_{8.00}O_{8.62}$	320.46	10067	cw	119.90	cw	1.8467
19	38 HMX/ HNAB	1.00:0.180	$C_{5.22}H_{7.32}N_{8.00}O_{8.53}$	318.61	10046	cw	113.46	cw	1.8575
20	39 CL-20/ HNAB	1.00:0.37	$C_{8.37}H_{6.00}N_{12.00}O_{13.18}$	485.54	9260	cw	355.70	cw	1.9411

Note: *) in the weighed starting nitramines was a molar ratio of HNS and HNAB`

Table 3.3.7 Impact sensitivity and explosive properties of pure substances and corresponding CACs

Explosive		Impact sensitivity E_{dr}			Detonation velocity, D	Detonation pressure, P	Energy of detonation, E_{deton}	Additive value[a] of E_{deton}
Sr No	Code design.	E_{dr} 50 % (J)	Ref.	E_{dr} 95 % (J)	($m.s^{-1}$)	(Gpa)	($J.g^{-1}$)	($J.g^{-1}$)
1	RDX	5.6	[21]	NA	9014	33.91	5915	NA
2	BCHMX	3.0	[13]	NA	9116	36.19	6223	NA
3	ß-HMX	6.4	[21]	NA	9404	38.00	5964	NA
4	δ-HMX	~1	[20]	NA	8922	32.99	5879	NA
5	ß-CL-20	11.9[b]	[22]	NA	9421	40.77	6320	NA
6	ε-CL-20	13.2[b] 4.0 [c]	[22] [23]	NA	9650	43.41	6303	NA
7	HNS (form I)	11.5	cw	NA	7373	22.81	5015	NA
8	HNAB	8.6	[21]	NA	7744	26.12	5335	NA
9	3 HMX/HNS	17.4	cw	35.0	8685	33.03	5637	5592
10	6 HMX/HNS	11.4	cw	17.6	8927	34.45	5778	5773
11	8 HMX/HNS	47.0	cw	105.1	8982	34.73	5804	5819
12	17 RDX/HNS	20.4	cw	47.0	8572	30.95	5720	5717
13	18 CL-20/HNS	11.4	cw	18.6	8764	35.01	5961	5815
14	19 BCHMX/ HNS	10.5	cw	24.4	8622	32.13	5780	5891
15	20 RDX/ HNAB	20.5	cw	46.4	8671	31.66	5822	5807
16	21 BCHMX/ HNAB	13.4	cw	39.2	8568	32.01	5894	5918
17	22 CL-20/ HNAB	5.1	cw	11.4	8333	30.11	5791	6000
18	31 HMX/ HNAB	9.7	cw	34.8	8879	33.96	5842	5824
19	38 HMX/ HNAB	14.0	cw	37.5	8911	34.30	5817	5828
20	39 CL-20/ HNAB	6.0	cw	28.5	8921	36.17	5924	5786

Note: a) the value calculated on the basis of the additive principle, i.e., the percentage of components in the co-agglomerate; b) the value for pure ε-CL-20; c) the value for the ε-CL-20 of "common" (technical) quality; d) this paper.

3.3.2.6 Thermochemical and Explosive Properties

The heat of combustion of CACs and pure nitramines was considered for the calculation of thermochemical parameters. The heat of combustion of the obtained CACs was measured using a bomb calorimeter, and densities of all CACs were obtained using a densitometer. The composition of both coformers in each of the CACs was evaluated using HPLC data, in which the composition existence of both conformers in that particular CACs. From these data, the enthalpy of formation was calculated using Hess's law, and the obtained results were summarized in Table 3.3.6.

Although the irregular shapes of CACs particles obtained densities matched with polymorphic modified nitramines densities in CACs; i.e., in the case of the HMX CACs densities found closer to the δ-HMX whereas the CL-20 CACs it was β-CL-20. Further, the theoretical detonation parameters (detonation velocity, *D*, detonation pressure, *P*, and detonation energy, E_{deton}) for the tested explosives were calculated using the CHEETAH code [24]. The detonation energy is a sum of mechanical and thermal energies released during the detonation process. The mechanical energy is equal to the expansion work of detonation products and determined by the volume of detonation products corresponding to a pressure of 1 atm ($1.01325 \cdot 10^{-5}$ Pa), while the thermal energy is the heat in the detonation products under this pressure[20–22]. For these calculations, the composition of detonation products was frozen at a temperature of 1800 K on the Isentrope beginning at the CJ point.

3.3.3 Discussions

3.3.3.1 Co-agglomeration

As already mentioned, the co-agglomeration method applied by us is one of the types of co-crystallization (slurry method [4]). As such, it should be influenced by factors acting in the crystallization of EMs in general [28]. In our papers [2, 3, 5], we have not optimized this process but gained several insights. In the co-agglomeration process, even though applying intense stirring for an equal amount of time, particle sizes from each batch mutually varied; particle sizes and shapes were mainly influenced by the solvent used for co-agglomeration than the solvent system used for co-precipitation [2, 3, 5]. Application of protogenic n-butanol in the process led to particles with smaller specific surface areas of CACs than in the case of using of the aprotic chloroform continuous phase (see paper [2, 3, 5] and partially also Table 3.3.2). The polynitroarenes coformer has a relatively large influence on this specific surface: its size significantly increases TATB [2, 3] and quite significantly also HNS (see Table 3.3.2). The opposite effect is exhibited by DATB [2, 3] and especially by HNAB (see Table 3.3.2). These facts are related to the intensity of the involvement of polynitroarenes in the interaction with nitramines: besides the π-π staking it is in the case of TATB via hydrogen bonds —N–H….O–N— [2, 3, 24, 25], in the case of HNS bonds —N–O....H–C—

(from the ethylene bridge [7, 31]) and in the case of HNAB mainly this π-π staking [9, 10]. DATB, with a lower number of hydrogen bonds in its molecule [32] and its lower symmetry compared to TATB, has, as can be seen from Table 3.3.2, a "combined" effect of TATB and HNAB.

3.3.3.2. Thermal Analysis

The spectral observations show that there is the formation of ⎯N–O----H⎯ type short contacts like hydrogen bonding van der Waals forces of attractions. These occurred between mainly ⎯NO_2, ⎯N–N (nitramines) and ⎯CH, ⎯C–H---π (π - π) stacking with two benzene rings (of HNS and HNAB). These -intra and -intermolecular interactions increased the stability of the crystal lattice. Once CACs come in contact with heat, this intermolecular interaction gives a certain amount of stability to the CACs, which helps to withstand the initial polymorphic changes in the CACs. Once the temperature reaches near pure nitramine melting, sudden splitting of these interactions also responsible may generate excited species which are further evolved in the thermal reactivity of the CACs, but it does not seem that the thermal reactivity of CACs is increased compared to their pure nitramines (see Figure 3.3.3 and Table 3.3.3). For more exact examination a detailed kinetic study of the CACs thermal decomposition is needed.

3.3.3.3 Spectral Examination

As previously mentioned in sections, the intermolecular changes and orientation through translational-vibrational relaxation processes by translational and vibrational modes of molecular crystals of the material of the structure of coformers in the CACs formation can stabilize a new crystal lattice. This relates to a red shift in vibrations, C–H bending, C–H, and N–N bond stretching bands. The pure nitramines show noticeable shifts after interaction mainly with HNS, which indicates that HNS, but also HNAB, enter into the nitramines crystal lattice and create new intermolecular force interactions in the new crystal lattice thus formed. The existence of the corresponding weak intermolecular interactions here can be documented by the graphical comparison of the length of the longest N⎯N bonds and their stretching vibrations (stretching of the C–N bond for HNS and HNAB) in CACs and pure co-formers, given in Figure 3.3.4; it corresponds very well with the statement. This comparison should argue in favour of the formation of co-crystals in the process of co-agglomeration. Interestingly, in individual nitramines (mainly of HMX), after their entering in CACs, a change of their N–N bond stretching vibrations is nearly constant for both the HNS and HNAB coformers.

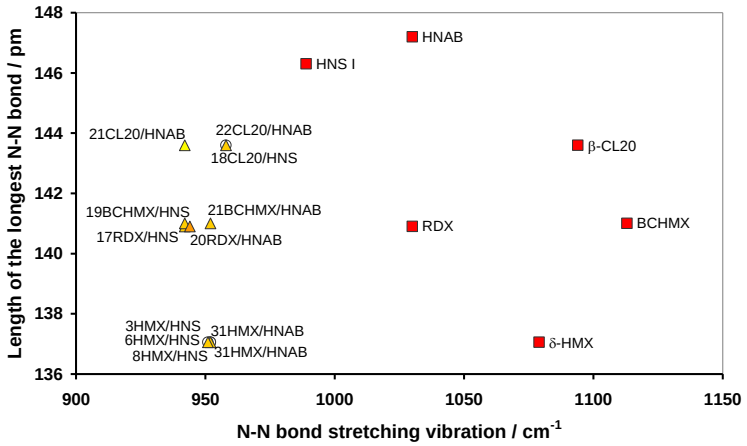

Figure 3.3.4 A comparison of the lengths of the longest N—N bonds with this bond stretching vibration (the CN bond stretching for HNS and HNAB) of pure nitramines and their CACs. (the data placing in this Figure indicates the co-crystals existence); the N-N bond lengths were taken from the ORTEP views of the nitramines used in the CCDC database shown in Chapter 2.

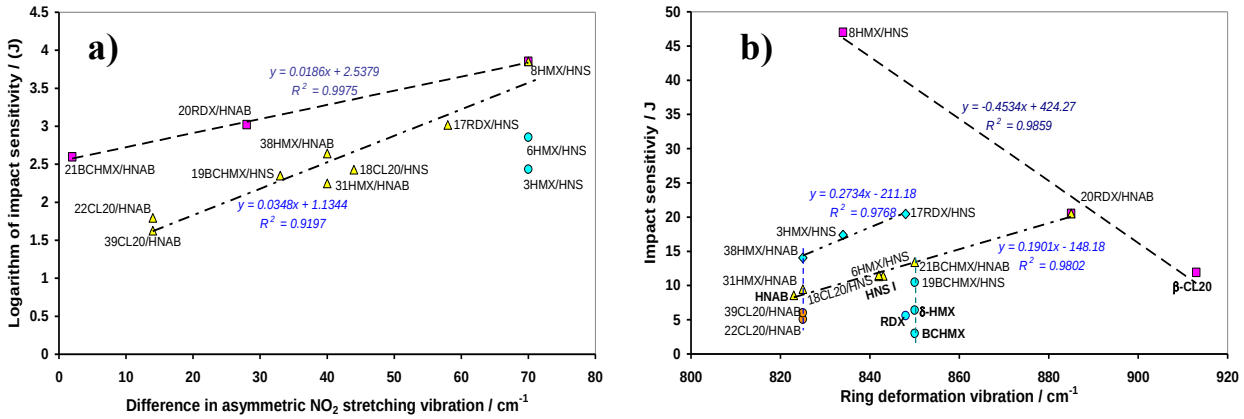

Figure 3.3.5 The relationships of the impact sensitivities with spectroscopic stretching vibration characteristics of the CACs prepared:

a) The natural logarithm of impact sensitivities (J) in relation to difference between asymmetric NO_2 stretching vibration in pure nitramine and in their CACs (cm^{-1});
b) Impact sensitivity (J) versus ring deformation vibration(cm^{-1})

Another verification of the close mutual interactions the HNS and HNAB molecules with those of the nitramines studied in their CACs is Figure 3.3.5a. If we consider the definitional relationship between the vibrational frequency and the bond force constant (i.e., roughly the strength of the given bond) [33] then this Figure should show imply that the increasing difference between the asymmetric NO_2 stretching vibrations in pure nitramines and their CACs corresponds to increase/decrease the strength of bonding of

this group in given nitramine (hereafter nitramine enter in close interaction with HNS or HNAB, respectively). Based on this assumption, the run of dependencies in Figure 3.3.5a is logical. As the bond strength of the nitro group in the nitramine grouping increases, the impact reactivity (sensitivity) decreases and vice versa.

The large relative difference in the influence of the individual coformers HNS and HNAB on the ring deformation vibrations of the respective CACs and thus on the impact reactivity is shown in Figure 3.3.5b. Particularly in the case of HMX, the molar ratio of coformers seems to play a large role in its CACs with HNS (in nitraminic CACs we have already encountered [5]). The three samples of this CACs type, the one 8 HMX/HNS with the lowest molar ratio (1.00/0.11) has unexpectedly high impact resistance, and in doing so, its SEM image does not look good (Figures 2e and 2f). Its crystals appear porous even though its crystal density value is not the lowest of the three HMX/HNS samples (see in Table 3.3.6). These three samples, CACs 6HMX/HNS looks the best visually (Figures 2c and 2d), and even though it is close in composition to CACs 8HMX/HNS, it has the highest densities of the three EMs (Table 3.3.6), its impact sensitivity is the lowest in this group of CACs. How is this possible? Chinese authors published a study of porous HNS, fabricated by supramolecular assembly and disaggregation [29, 30]. They obtained novel 3D porous micro/nano HNS microcrystalline clusters with hierarchical structure exhibit significantly different safety performance in contrast to that of raw HNS, ascribed to the well-organized hierarchical particles and porous structures [35]. By them published SEM images show a layered structure of their product in addition to pores [34]. Unfortunately, for impact sensitivity determination authors used the Chinese method [34] which is not compatible with the BAM method, thus also with our results (see Table 3.3.7). It may be that the 8 HMX/HNS sample is analogous to the aforementioned Chinese product, especially since CACs of similar composition, i.e., 6 HMX/HNS, with seemingly higher quality crystals (Figures 2c and 2d), higher density and higher ring strain vibration values, exhibit the highest impact sensitivity of the three HMX/HNS co-agglomerates discussed. The reason for these differences most likely lies in the influence of the preparation conditions of the co-precipitates on their quality and subsequently on co-agglomeration; we have so far paid only marginal attention to this problem in paper [2] (in co-agglomeration of BCHMX with DATB in a hot water under pressure).

Coformer HNAB enhances the sensitivity of CL-20 and, except perhaps for EMs 38HMX/HNAB and 20RDX/HNAB, does not contribute more significantly to the suppression of the sensitivity of the studied nitramines. The run of dependencies plot in Figure 3.3.5b with a positive slope is as expected (similar to Figure 3.3.5a). More points would be needed to fully explain the exception, i.e., negative dependence in Figure 3.3.5b; as Figures 3.3.2 and 3.3.5 with Table 3.3.6 logically show, not only bond strength but also

crystal (crystal lattice) quality and molar ratio of coformers co-determines impact sensitivity[36] and by these factors also are given a run of dependences the Figure 3.3.5b type.

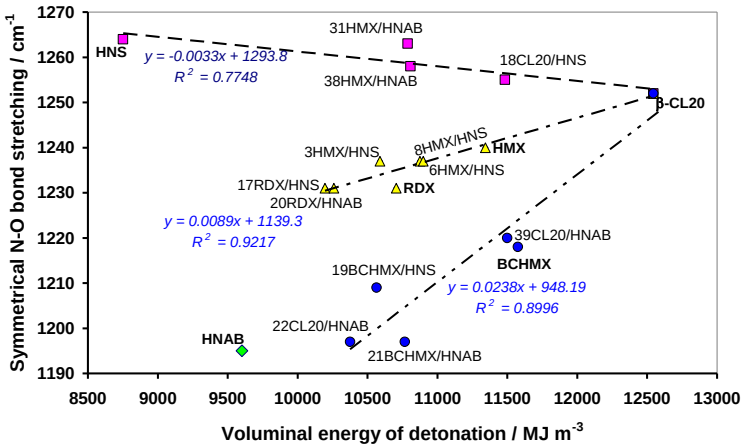

Figure 3.3.6 The relationships between the FTIR symmetrical N-O stretching (cm^{-1}) and performance (voluminal energy of explosion) of the CACs prepared.

If we use for the explanation of Figure 3.3.6 a similar approach, as it was in the case of Figure 3.3.5a, then the relationships with a positive slope here should imply that the increasing performance (voluminal energy of explosion) of CACs corresponds to an increase in the strength of the internal NO_2 bonds involved in symmetrical N—O stretching. A dependence with a negative slope could mean that a mode of the interaction of HMX and CL-20 with a given coformer leads to a slight decrease in the strength of the N—O bond with the raising of the performance. In this context, it is worth remembering that the trigger bond of initiation in the nitramines under study and of their CACs is the N–NO_2 bond [2, 3, 5, 13, 32]. It is here symptomatic that the data of all nitramines with distorted valence angles in the molecule (crowded molecules of BCHMX and CL-20) and their CACs (except 18 CL-20/HNS) are centered on the line "BCHMX - β-CL-20".

3.3.3.4 The Energetic Point of View

This topic has already been partially mentioned in connection with Figure 3.3.6. The relationship between sensitivity and performance is experimentally mostly based on Licht's rule: increasing the explosive strength is usually accompanied by an increase in the sensitivity, and therefore, an insensitive explosive will not exhibit top explosive strength [31, 33, 34]. By a further study of this problem was elaborated into a semilogarithmic version of this rule, in which performance was represented by voluminous energy of detonation [31, 35], and the last version substituted this performance by the energy content of the EMs molecules [2, 3, 36], and that is a case of Figure 3.3.7. The progression of the partial dependencies in this Figure is as expected (i.e., to Licht's rule) with the traditional exception for pure nitramines (RDX, HMX,

and CL-20), which occurs in all versions of this rule [31, 33, 34] and was not explained yet. Figure 3.3.7 clearly demonstrates that depending on the molar ratio of the coformers and, taking into account Figure 3.3.2, also the crystal quality of the co-agglomerates, CACs with higher impact resistance can be obtained as the pure starting coformers (see samples 8 HMX/HNS, RDX/HNS, RDX/HNAB, 3 HMX/HNS, RDX/HNAB and 38 HMX/HNAB).

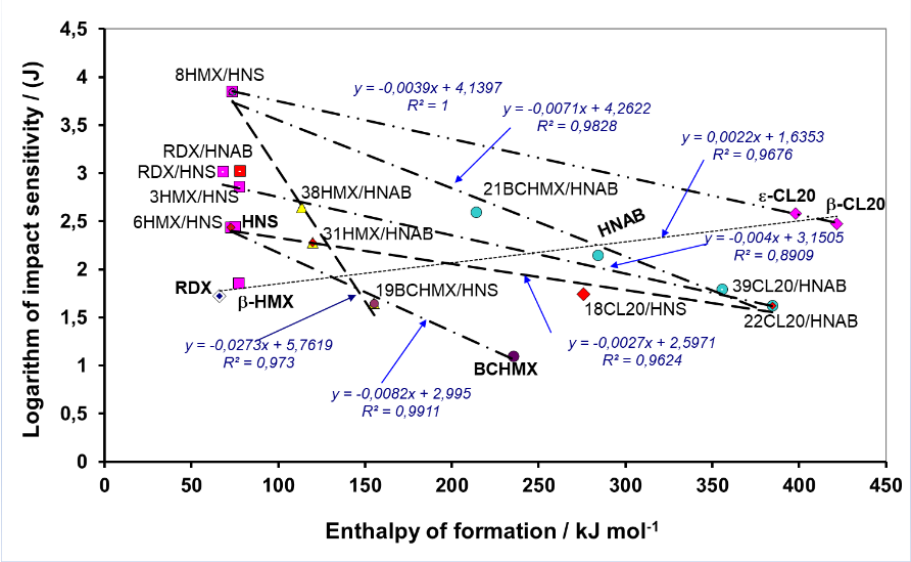

Figure 3.3.7 The semilogarithmic relationships between impact sensitivities and energy content (represented by enthalpy of formation) of the prepared CACs.

The dominant sample here is 8 HMX/HNS and of the polynitroarenes coformers it is HNS (see already discussion in section 3.3.3.3). In this context, it should be reminded that HMX is present in this CAC as its δ-modification with a crown conformation of its molecule (crystallographic study of δ-HMX see in [42]) and HNS in its cis-form (crystallographic study see in [8]). Both these forms of named coformers are quite compatible with each other spatially. Nitramines with deformed valence angles in the molecule (BCHMX, CL-20) form here CACs with higher impact sensitivity than pure RDX and HMX have.

Comparing impact sensitivities of CACs for both the HNS and HNAB coformers (see Figure 3.3.7) is possible to see that HNS shows greater stabilizing influence than the HNAB. It may be due to already mentioned better intermolecular interactions HNS with molecules of nitramines (mainly with HMX), and but also due to the —N=N— bridge in HNAB molecule acting as a "chemical hot spot" (the C—N=N bond should be a trigger one in the HNAB thermolysis [34, 38, 39]) as compared to bridge —CH=CH— in the HNS molecule (here the primary fission of HNS should go by a "trinitrotoluene mechanism" [32, 34]).

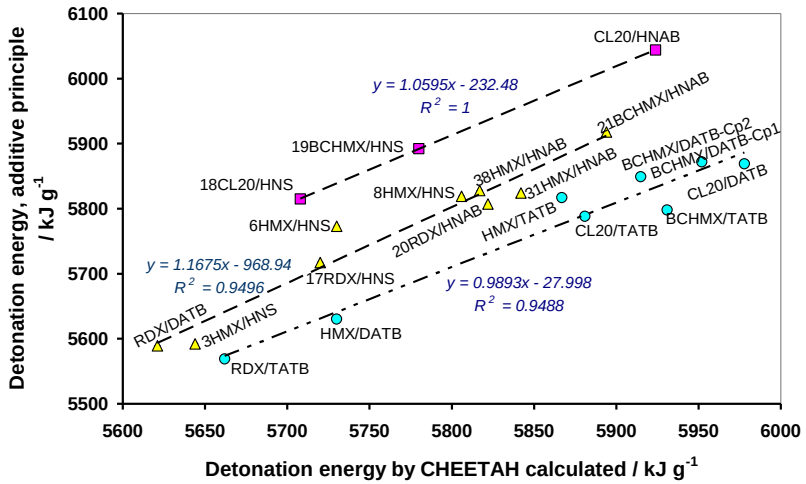

Figure 3.3.8 The mutual relationships between the energies of detonation calculated on the base of additive principle (i.e., on the percentage of components in the co-agglomerate) and those, calculated by CHEETAH code using experimental enthalpies of formation; in the Figure also data of CACs with DATB and TATB coformers are inserted (taken from papers [2, 3]).

From the fact, that the entropy of mixtures is higher than the sum of that of their individual components, Prof. Urbanski derived his consideration about reasons for higher detonation velocities of mixed explosives than would correspond to the percentage of components in this mixture [45]. In our recent papers [2, 3, 5], we have applied this reasoning to the detonation energy, specifically to the intercomparison of the values of this energy of CACs, obtained on the basis of the additive principle, and the values calculated with the CHEETAH code. Results for CACs with polynitroarenes coformers, are shown in Figure 3.3.8. The CHEETAH outputs here represent as if experimental data. As this Figure shows the lowest difference between both these methods of calculations is for CACs with content of the DATB and TATB coformers (taken from papers [2, 3]). For co-agglomerates based on BCHMX and CL-20 mixtures, whose data are not included in Figure 3.3.8, the situation is reversed - CHEETAH outputs have a lower value compared to the additive principle calculation.

3.3.3.5 Impact sensitivity

This issue has been largely addressed in previous sections (i.e., 3.3.3.3 and 3.3.3.4). These show the dependence of such sensitivity on the molecular structure (through the IR spectral characteristics) and energy content of the prepared CACs. The quality of the crystals, but also their size and shape, play a major role. Figure 3.3.2 shows that CACs with the HNAB content seems to be more quality comparing to the HNS analogues. However, their impact sensitivity is lower (perhaps with exception of 38HMX/HNAB and 21BCHMX/HNAB). As it was mentioned in Section 3.3.3.3, HNS crystals can exist in porous micro/nano HNS microcrystalline clusters, whose sensitivity is lower comparing "normal" HNS [34]; it could be

possible that sample 8 HMX/HNS here represents this cluster. This might be explained by an apparent variance with Physics of Explosion, i.e. that porous EMs have a lower sensitivity comparing than its high quality crystal. "Normal crystallization" under laboratory conditions usually results the EMs crystals, sensitivity of which is comparable to the Los Alamos Natl. Laboratory (LANL) data base (see for example [21]). Regarding the effect of crystal size, we found, for example, that for grains from 20 to 200 μm in the HMX sieving fractions, the impact sensitivities change minutely and are consistent with the LANL data [46] (the same is true for the friction sensitivity of this HMX [47]). Other situations, of course, are in the case of nanoparticles, for example nano-RDX was published impact sensitivity as far as 24 J [48], but it is not our case. Similarly, the spherification of nitramine crystals will affect the impact sensitivity, as will the high incidence of defect-dislocations in their crystals (this may be a case of the "normal" CL-20 quality with impact sensitivity 2 - 4.6 J[2]).

3.3.3.6 Detonation parameters

It is clear from the summary in Table 3.3.7, Figures 3.3.8 and 3.3.9 that the detonation energies of the CACs under study, calculated by CHEETAH code, are higher than would be expected from the percentages of the individual co-formers in the mixed crystals.

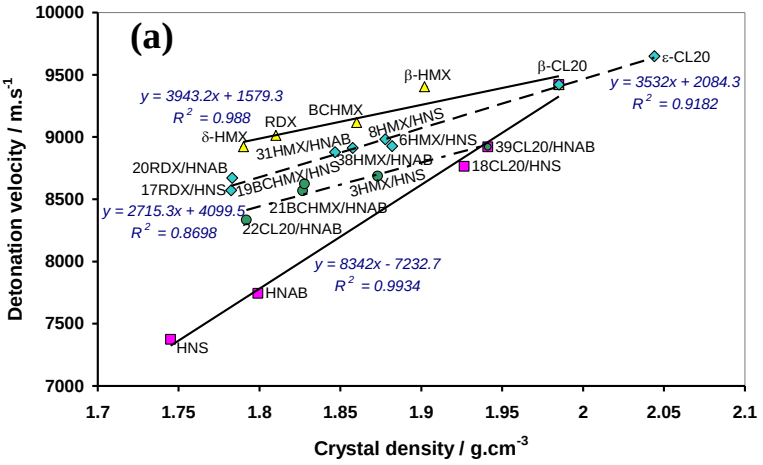

Figure 3.3.9 Detonation parameters of CACs with pure nitramines used for synthesis 3 HMX/ HNS; 6 HMX/ HNS; 8 HMX/ HNS; 17 RDX/ HNS; 18 CL-20/ HNS; 19 BCHMX/ HNS; 20 RDX/ HNAB; 21 BCHMX/ HNAB; 22 CL-20/ HNAB; 31 HMX/ HNAB; 38 HMX/ HNAB and 39 CL-20/ HNAB

This is consistent with the general observation [45] (see discussion in section 3.3.3.4). Figure 3.3.9a shows the known and in our case interesting relationship between detonation rate and density of nitramine crystals and their CACs. This Figure, PXRD, and spectroscopic data obtained here verified the presence of CL-20 in the CACs studied in its β-form. Figure 3.3.9a, together with Figure 3.3.7, confirms that sample

8HMX/HNS seems to be best from the series of CACs prepared and it from both the performance and sensitivity (it is similar as to CACs HMX/TATB from paper [3]).

For comparison, recently we dealt with a plastic explosive composed of 43.5% BCHMX, 43.5% HNAB (molar ratio 1.00/0.65), and of 13% SBR binder [8]. This explosive at a density of 1.59 $g.cm^{-3}$, exhibited an experimental detonation velocity of 7874 $m.s^{-1}$, a calculated detonation pressure of 23.5 GPa and an impact sensitivity of 25.1 J [8]. Its detonation parameters are logically considerably lower (due to the presence of inactive binder) than those of the CACs 21BCHMX/HNAB prepared here, with otherwise relatively close impact sensitivity (see in Table 3.3.7). Thus, the approach to desensitization of nitramines by co-agglomeration in the sense of this work appears to be much more effective than incorporating mechanical mixtures of nitramine/HNAB into the plastic matrix (it should be valid also be valid for the conformer HNS).

3.3.4 Summary

Co-precipitates (CPs) of trans-2,2',4,4',6,6'-hexanitrostilbene (HNS) and 2,2',4,4',6,6'-hexanitroazobenzene (HNAB) with the attractive nitramines, RDX, β-HMX, BCHMX and ε-CL-20 were prepared by the solvent/antisolvent technique with subsequent co-agglomeration (co-crystallization) of them in n-butanol or chloroform by the "slurry method". Co-agglomerates (CACs) with the HNS coformer were finer-grained than those with the HNAB one. CACs containing HNAB seem to be more perfect than CACs containing HNS. However, their impact sensitivity is generally lower; the dominant sample is HMX/HNS with a molar ratio of 1.00/0.11 and an impact sensitivity of 47 J, A study of these crystals surface morphology shows a micro-porous structure, which does not translate more significantly into crystal density. These CACs probably contain porous micro/nano HNS microcrystalline clusters (for pure HNS recently described [35]). Three other CACs (RDX/HNS; RDX/HNAB; BCHMX/HNAB) had higher impact resistance than that exhibited by their original pure coformers. For CL20, however, the entry of HNS or HNAB into its crystal lattice is destabilizes.

The dependencies of the impact sensitivity of the CACs studied to their energy content were specified, which shows beside awaited exceptions to Licht's rule for pure RDX, HMX and CL-20, unambiguously confirms the increase in impact sensitivity with energetic content of CACs. Detonation parameters of CACs containing HNS and HNAB are logically lower than those of the starting nitramines. The detonation energies of these co-crystals are higher than would correspond to the percentage of coformers in them; this difference is higher than in the case of analogous CACs with DATB and TATB coformers [3]. An interesting relation is between the detonation velocities of the CACs studied and their crystal densities - also this one confirms the presence of CL-20 in the CACs studied as its β-form.

References

[1] A. K. Hussein, S. Zeman, and A. Elbeih, “Cis-1,3,4,6-Tetranitrooctahydroimidazo-[4,5-d]Imidazole (BCHMX) as a Part of Low Sensitive Compositions based on DATB or HNAB,” *Propellants Explos. Pyrotech.*, vol. 46, no. 2, pp. 322–328, 2021, doi: 10.1002/prep.202000160.

[2] V. B. Patil, K. Zalewski, J. Schuster, P. Belina, W. Trzcinski, and S. Zeman, “A new insight into the energetic co-agglomerate structures of attractive nitramines,” *Chem. Eng. J.*, vol. 420, Sep. 2021, doi: 10.1016/j.cej.2021.130472.

[3] V. B. Patil, P. Bělina, W. A. Trzcinski, and S. Zeman, “Preparation and properties of co-mixed crystals of 1,3-di- and 1,3,5-tri-amino-2,4,6-trinitrobenzenes with attractive cyclic nitramines,” *J. Ind. Eng. Chem.*, vol. 115, pp. 135–146, Nov. 2022, doi: 10.1016/j.jiec.2022.07.043.

[4] Z. Xue, B. Huang, H. Li, and Q. Yan, “Nitramine-Based Energetic Cocrystals with Improved Stability and Controlled Reactivity,” *Cryst. Growth Des.*, vol. 20, no. 12, pp. 8124–8147, Dec. 2020, doi: 10.1021/acs.cgd.0c01122.

[5] V. B. Patil *et al.*, “Co-agglomerated crystals of cyclic nitramines with sterically crowded molecules,” *CrystEngComm*, p. 10.1039.D2CE00840H, 2022, doi: 10.1039/D2CE00840H.

[6] M. Szala and J. Sabatini, “2,4,6-Trinitrotoluene - A Useful Starting Compound in the Synthesis of Modern Energetic Compounds,” *Z. Für Anorg. Allg. Chem.*, vol. 644, Jan. 2018, doi: 10.1002/zaac.201700414.

[7] D. S. Viswanath, T. K. Ghosh, and V. M. Boddu, “Hexanitrostilbene (HNS),” in *Emerging Energetic Materials: Synthesis, Physicochemical, and Detonation Properties*, D. S. Viswanath, T. K. Ghosh, and V. M. Boddu, Eds., Dordrecht: Springer Netherlands, 2018, pp. 213–231. doi: 10.1007/978-94-024-1201-7_6.

[8] Y. Liu, L. Chen, J. Wang, J. Chen, J. Wang, and H. Pan, “The crystal structure and thermal decomposition kinetics of *cis* -hexanitrostilbene,” *Acta Crystallogr. Sect. B Struct. Sci. Cryst. Eng. Mater.*, vol. 77, no. 1, pp. 150–157, Feb. 2021, doi: 10.1107/S2052520620015371.

[9] E. J. Graeber and B. Morosin, “The crystal structures of 2,2’,4,4’,6,6’-hexanitroazobenzene (HNAB), forms I and II,” *Acta Crystallogr. B*, vol. 30, no. 2, pp. 310–317, Feb. 1974, doi: 10.1107/S0567740874002731.

[10] M. A. Rodriguez, C. F. Campana, A. D. Rae, E. Graeber, and B. Morosin, “Form III of 2,2′,4,4′,6,6′-hexanitroazobenzene (HNAB-III),” *Acta Crystallogr. C*, vol. 61, no. 3, pp. o127–o130, Mar. 2005, doi: 10.1107/S0108270105000569.

[11] Y. Liu *et al.*, “Three Energetic 2,2′,4,4′,6,6′-Hexanitrostilbene Cocrystals Regularly Constructed by H-bonding, π-Stacking, and van der Waals Interactions,” *Cryst. Growth Des.*, vol. 18, no. 4, pp. 1940–1943, Apr. 2018, doi: 10.1021/acs.cgd.8b00019.

[12] D. S. Viswanath, T. K. Ghosh, and V. M. Boddu, “Hexanitrohexaazaisowurtzitane (HNIW, CL-20),” in *Emerging Energetic Materials: Synthesis, Physicochemical, and Detonation Properties*, D. S. Viswanath, T. K. Ghosh, and V. M. Boddu, Eds., Dordrecht: Springer Netherlands, 2018, pp. 59–100. doi: 10.1007/978-94-024-1201-7_2.

[13] D. Klasovitý, S. Zeman, A. Růžička, M. Jungová, and M. Roháč, “cis-1,3,4,6-Tetranitrooctahydroimidazo-[4,5-d]imidazole (BCHMX), its properties and initiation reactivity,” *J. Hazard. Mater.*, vol. 164, no. 2–3, pp. 954–961, May 2009, doi: 10.1016/j.jhazmat.2008.08.106.

[14] E. Yu. Orlova, *Oktogen - termostoykoe vzryvchatoe veschestvo (Octogen - Thermostable Explosive)*. Moscow: Iydat. Nedra, 1975.

[15] S. Zeman, “Some predictions in the field of the physical thermal stability of nitramines,” *Thermochim. Acta*, vol. 302, no. 1, pp. 11–16, Oct. 1997, doi: 10.1016/S0040-6031(96)03101-2.

[16] S. Zeman, “Possibilities of applying the Piloyan method of determination of decomposition activation energies: Part III. Derivatives containing two picryl groups in the molecule, and melamine derivatives,” *J. Therm. Anal.*, vol. 19, no. 1, pp. 107–115, Aug. 1980, doi: 10.1007/BF01928436.

[17] G. Liu, S. Wei, and C. Zhang, “Review of the Intermolecular Interactions in Energetic Molecular Cocrystals,” *Cryst. Growth Des.*, vol. 20, no. 10, pp. 7065–7079, Oct. 2020, doi: 10.1021/acs.cgd.0c01097.

[18] P. E. Rouse, “Enthalpies of formation and calculated detonation properties of some thermally stable explosives,” *J. Chem. Eng. Data*, vol. 21, no. 1, pp. 16–20, Jan. 1976, doi: 10.1021/je60068a026.

[19] M. R. Manaa, “Determination of adiabatic ionization potentials and electron affinities of energetic molecules with the Gaussian-4 method,” *Chem. Phys. Lett.*, vol. 678, pp. 102–106, Jun. 2017, doi: 10.1016/j.cplett.2017.04.038.

[20] Fraunhofer Institut für Chemische Technologie, Pfinztal, Germany, 2004, “ICT Database of thermochemical values.” 2004.

[21] C. B. Storm, J. R. Stine, and J. F. Kramer, “Sensitivity Relationships in Energetic Materials,” *Chemistry and Physics of Energetic Materials*. Springer Netherlands, Dordrecht, pp. 605–639, 1990. [Online]. Available: https://doi.org/10.1007/978-94-009-2035-4_27

[22] Y. Ou, C. Wang, Z. Pan Z., B. Chen., “Sensitivity of hexanitrohexaazaisowurtzitane,” *HanNeng CaiLiao (Chinese J. Energ. Mater.)*, vol. 7, pp. 100–108, 1999.

[23] D. S. Viswanath, T. K. Ghosh, V. M. Boddu, *Emerging energetic materials: synthesis, physicochemical and detonation properties*. New York, NY: Springer Berlin Heidelberg, 2017.

[24] Fried, L E., “CHEETAH 1.39 Users’ Manual UCRL-MA-117541.” CA: Lawrence Livermore National Laboratory., 1996.

[25] Hobbs, M. L. and M. R. Baer, “Calibrating the BKW-EOS with a large products species base and measured C-J properties.,” in *Proceedings of the 10th Symposium (International) on Detonation*, 1993, pp. 409–418.

[26] W. C. Davis and W. Fickett, “DETONATION THEORY AND EXPERIMENT.,” *Pp 2-12 Behav. Dense Media High Dyn. Press. N. Y. Gordon Breach 1968*, Oct. 1969, Accessed: Aug. 15, 2021. [Online]. Available: https://www.osti.gov/biblio/4785669

[27] Ficket, W. and W. C. Davies, *Detonation*. Berkeley, CA: University of California Press, 1979.

[28] X.-X. Zhang, Z.-J. Yang, F. Nie, and Q.-L. Yan, “Recent advances on the crystallization engineering of energetic materials,” *Energ. Mater. Front.*, vol. 1, no. 3–4, pp. 141–156, Dec. 2020, doi: 10.1016/j.enmf.2020.12.004.

[29] H. H. Cady and A. C. Larson, “The crystal structure of 1,3,5-triamino-2,4,6-trinitrobenzene,” *Acta Crystallogr.*, vol. 18, no. 3, pp. 485–496, May 1965, doi: 10.1107/S0365110X6500107X.

[30] G. R. Desiraju, “Crystal and co-crystal,” *CrystEngComm*, vol. 5, no. 82, p. 466, 2003, doi: 10.1039/b313552g.

[31] X. Zhao, S. Huang, Y. Liu, J. Li, and W. Zhu, “Effects of Noncovalent Interactions on the Impact Sensitivity of HNS-Based Cocrystals: A DFT Study,” *Cryst. Growth Des.*, vol. 19, no. 2, pp. 756–767, Feb. 2019, doi: 10.1021/acs.cgd.8b01334.

[32] J. R. Holden, “The structure of 1,3-diamino-2,4,6-trinitrobenzene, form I,” *Acta Crystallogr.*, vol. 22, no. 4, pp. 545–550, Apr. 1967, doi: 10.1107/S0365110X67001100.

[33] H. Kuhn, H.-D. Försterling, and D. H. Waldeck, *Principles of Physical Chemistry, 2nd Edition*. Hoboken, New Jersey, 2009.

[34] M. Yan *et al.*, “Porous Cyclotrimethylenetrinitramine with Reduced Sensitivity Prepared by a Solvation–Desolvation Method,” *Cryst. Growth Des.*, vol. 20, no. 8, pp. 5387–5394, Aug. 2020, doi: 10.1021/acs.cgd.0c00597.

[35] H. Zhang *et al.*, “Three-dimensional hierarchical 2,2,4,4,6,6-hexanitrostilbene crystalline clusters prepared by controllable supramolecular assembly and deaggregation process,” *CrystEngComm*, vol. 18, no. 41, pp. 7940–7944, 2016, doi: 10.1039/C6CE01292B.

[36] S. Zeman, and M. Jungová, “Sensitivity and Performance of Energetic Materials - Zeman - 2016 - Propellants, Explosives, Pyrotechnics - Wiley Online Library,” Apr. 2016, doi: https://doi.org/10.1002/prep.201500351.

[37] G.B. Manelis, G.M. Nazin, Yu.I. Rubtsov, V.,Strunin, *Termicheskoe razlozhenie I goreniye vzryvchatykh veschestv i porokhov (Thermal Decomposition and Combustion of Explosives and Powders); English edition: Thermal Decomposition and Combustion of Explosives and Propellants*. Izdat. Nauka, Moscow 1996, London and New York 2003: Taylor & Francis, 1996.

[38] H.-H. Licht, “Performance and Sensitivity of Explosives,” *Propellants Explos. Pyrotech.*, vol. 25, no. 3, pp. 126–132, Jun. 2000, doi: 10.1002/1521-4087(200006)25:3<126::AID-PREP126>3.0.CO;2-8.

[39] S. Zeman, “Sensitivities of High Energy Compounds,” in *High Energy Density Materials*, T. M. Klapötke, Ed., in Structure and Bonding. , Berlin, Heidelberg: Springer, 2007, pp. 195–271. doi: 10.1007/430_2006_052.

[40] A. Elbeih, S. Zeman, M. Jungová, and P. Vávra, “Attractive Nitramines and Related PBXs,” *Propellants Explos. Pyrotech.*, vol. 38, no. 3, pp. 379–385, Jun. 2013, doi: 10.1002/prep.201200011.

[41] S. Zeman, “Influence of the energy content and its outputs on sensitivity of polynitroarenes,” *J. Energ. Mater.*, vol. 37, no. 4, pp. 445–458, Oct. 2019, doi: 10.1080/07370652.2019.1634159.

[42] R. E. Cobbledick and R. W. H. Small, “The crystal structure of the δ-form of 1,3,5,7-tetranitro-1,3,5,7-tetraazacyclooctane (δ-HMX),” *Acta Crystallogr. B*, vol. 30, no. 8, Art. no. 8, Aug. 1974, doi: 10.1107/S056774087400611X.

[43] S. Zeman, “Thermal stabilities of polynitroaromatic compounds and their derivatives,” *Thermochim Acta*, vol. 31, pp. 269–283, 1979.

[44] H., John C. and F. Jeffery S., “Thermal stabilities of hexanitroazobenzene (HNAB) and hexanitrobiphenyl (HMB),” Technical rept. AD0656572, Jun. 1967.

[45] T. Urbanski, “On entropy and free energy of explosives (preliminary communication),” *Bull. l’Academie Pol. Des Sci. s, Ser. Des Sci. Chim.*, vol. 28, pp. 511–513, 1980, doi: https://gallica.bnf.fr/ark:/12148/cb343830642 /date1980.

[46] M. Jungová, S. Zeman, and Q.-L. Yan, “Recent Advances in the Study of the Initiation of Nitramines by Impact Using Their 15N NMR Chemical Shifts,” *Cent. Eur. J. Energ. Mater.*, 2014.

[47] M. Jungová, and S. Zeman, “Friction Sensitivity of Nitramines. Part I: Comparison with Impact Sensitivity and Heat of Fusion,” no. 6, pp. 603–606, Apr. 2012.

[48] J. Liu, W. Jiang, Q. Yang, J. Song, G. Hao, and F. Li, “Study of nano-nitramine explosives: preparation, sensitivity and application,” *Def. Technol.*, vol. 10, no. 2, pp. 184–189, Jun. 2014, doi: 10.1016/j.dt.2014.04.002.

3.4 Composite crystals of polyaniline with attractive nitramines via coagglomeration

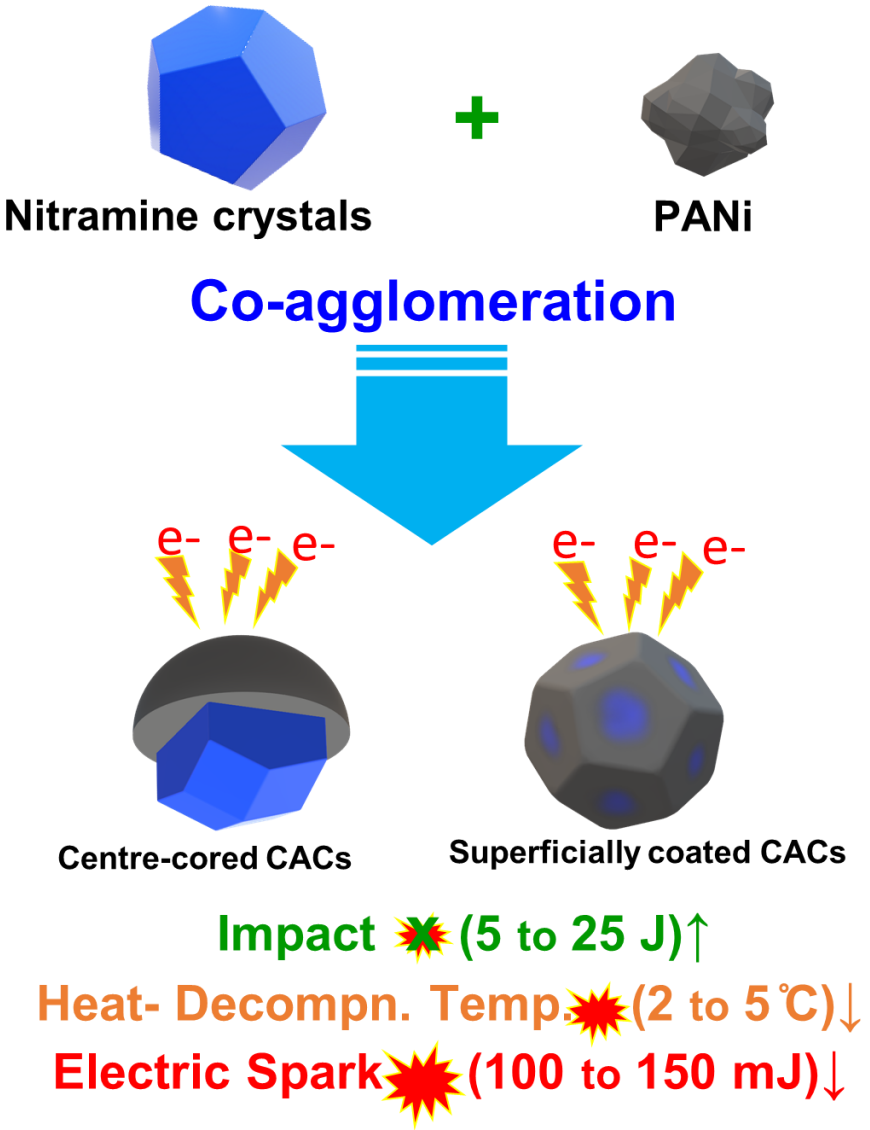

Published in

Advanced Composites and Hybrid Materials,
[under communication- peer review]

3.4.1 Background

The polyaniline shows certain fluorescence properties (it behaves as a fluorophore; see section 3.4.3.6). As recent works have shown, PANi forms the charge transfer complexes with polynitro compounds which act as fluorescent sensors and have utility for the quick trace spectrochemical detection of explosives. The structure of the mentioned complexes of nitramines with PANi (shown in Scheme 3.4.1) [1–4] indicates that they perhaps could have a beneficial effect on reducing the initiation reactivity of these polynitro compounds. Therefore, we devote attention to this possibility in this paper taking in account the utmost attractive cyclic nitramines 1,3,5-trinitro-1,3,5-triazinane (RDX), ß-1,3,5,7-tetranitro-1,3,5,7-tetrazocane (ß-HMX), ε-2,4,6,8,10,12-hexanitro-2,4,6,8,10,12-hexaazaisowurtzitane (ε-CL-20), and cis-1,3,4,6-tetranitrooctahydroimidazo-[4,5-d]imidazole (BCHMX or bicyclo-HMX) [5]. This work, also focus to verify the feasibility of co-agglomeration method [6] (slurry method of co-crystallization [6, 7]) for the preparation of the mixed crystals (composites) attractive nitramines with the non-explosive PANi-polymer. The above-mentioned is thus the subject of the present paper with a follow-up study of the explosive and stability properties of the nitramines/PANi complexes with an estimation of the possibility of their practical use as explosive fillings of various military and civilian usable objects.

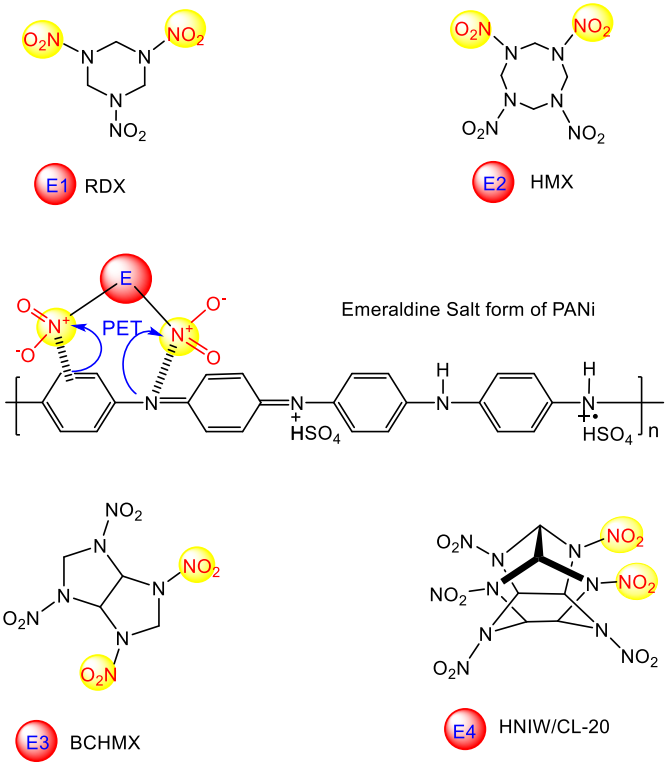

Scheme 3.4.1 Schematic representation of co-agglomerated - polyaniline composite crystals, the binding of attractive nitramines with PANi chain(recreated from earlier reported work [1–4])

3.4.2 Results

3.4.2.1 Powder X-Ray diffraction(PXRD) studies

Using PXRD technique the peak intense intensities 2Ɵ values were obtained which are summarised in Table 3.4.1, and documented by the PXRD diffractograms in Figure 3.4.1.The nitramines (NAs) with PANi undergo co-agglomeration - binding to PANi polymer chain (Scheme 3.4.1). Changes connected with it are clearly observable in PXRD diffractograms. Here NAs act as Lewis acids with electron withdrawing groups and easily bind electrons from the PANi chain (Scheme 3.4.1). This stabilizes the polymeric PANi-NAs chain. To attain this compactness in the polymeric chain, the polymorphic changes of some nitramines observed: ε-CL20 is converted into its β-modification during forming of the β-CL20/PANi composite, and β-HMX goes into its polymorphic α-modification and in this form, is stabilized in corresponding composite crystals α-HMX/PANi. In our earlier papers, HMX was stabilized in its co-agglomerated crystals (CACs) with polynitro arenes [8–10] and polynitramines [11] in the form of its δ-modification. It is a known fact, that CL20 in co-crystals with polynitro compounds is present mostly in its β-polymorph [12], while with the non-nitrated compounds, it enters into co-crystal lattice in its γ-modification; PANi seems in this sense a certain exception - as a non-nitrated (very low nitrogen content) polymer enhanced forming β-CL20 in the polymeric PANi-NAs chain.

These modifications changes are in a further text evaluated with DTA analysis, in which endothermic changes that occurred are matched with PXRD data. It shows the nitramines form the complexes formation with PANi with polycrystalline microparticles in other ways in comparison with classic co-crystals formation(in terms of intermolecular interactions),thus we may call them PANi doped with NAs. More broadly we here labelled as PANi-NAs composites. As is shown in section 3.4.1 and illustrated by Scheme 3.4.2, major two kinds of these composites crystals are formed.

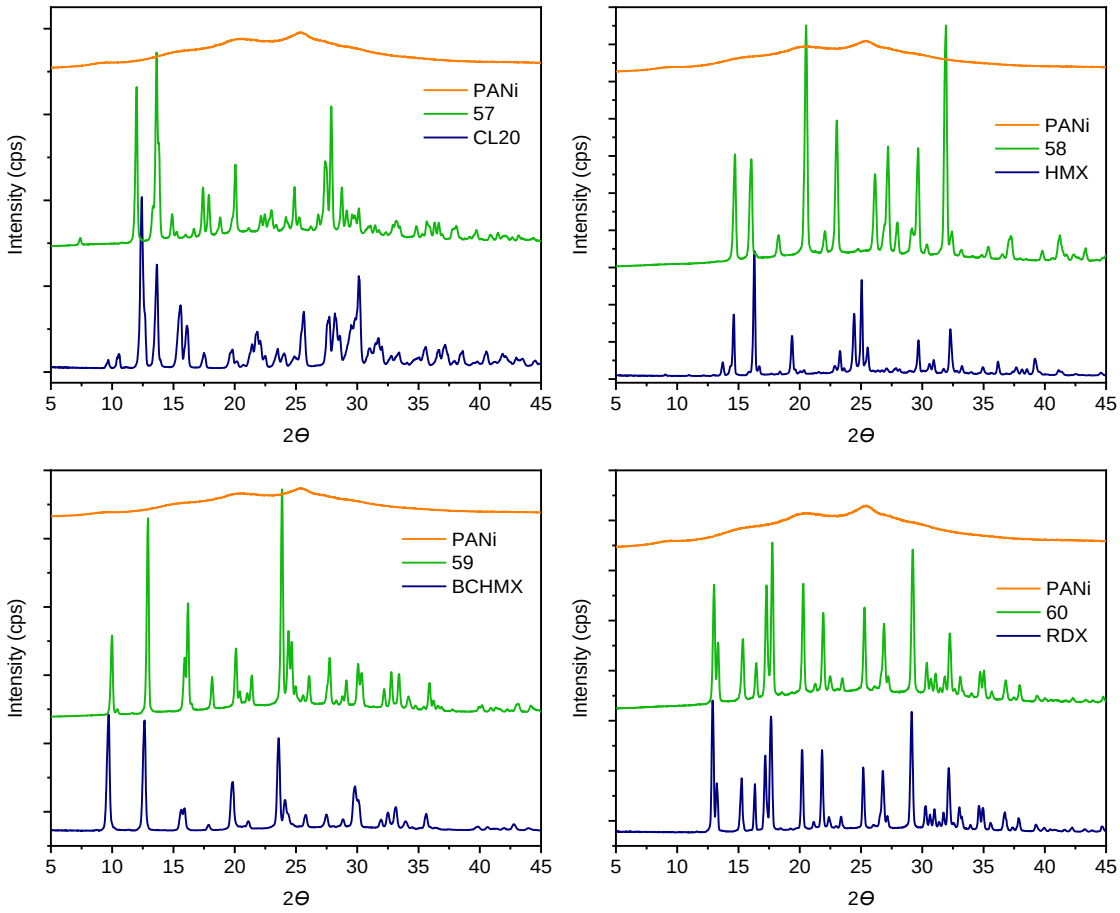

Figure 3.4.1 PXRD diffractograms of composites(CACs); 57 CL20/PANi; 58HMX/PANi; 59 BCHMX/PANi; 60 RDX/PANi

Table 3.4.1 PXRD data for pure nitramines and CACs

Sr No	Code design.	2Θ valuesfor intense peaks / °
1	ε-CL-20	14.30, 30.10, 42.98
2	β-CL-20	12.66, 13.86, 30.34
3	BCHMX	9.74, 12.65, 23.57
4	β-HMX	14.61, 16.31, 24.45, 25.07, 32.31
5	δ-HMX	13.10, 17.02, 24.34
6	RDX	9.73, 12.65, 23.59
7	PANI	20.50, 25.44
7	57 CL20/ PANI	11.98, 13.66, 20.06, 27.88
8	58 HMX/PANI	20.52, 27.20, 29.66, 31.94
9	59 BCHMX/PANI	9.98, 12.92, 16.18, 23.84
10	60 RDX/PANI	13.00, 17.28, 20.30, 29.22

The morphological changes in nitrmines crystals after binding with the polymeric chain of PANi were analyzed employing FESEM analysis. The obtained FESEM results were reported in Figure 3.4.2(a-h). It was found that CACs of CL20 and BCMHX were smoother spherical peanuts like structures. Whereas the in case of CACs of HMX and BCHMX its different smoother surfaced irregular sticks like crystals were found. The smothered surface is common in all NAs/PANi. It shows that PANi were coated on crystals and which made crystal edges smoother.

3.4.3.2 Morphology and Particle size analysis

It indicates there might be the formation of centre cored cocrystals with PANi. These smoothered surfaces can effectively be influenced the impact sensitivity tests, which made nitramines in CACs withstand higher drop energy (see Table 3.4.7).

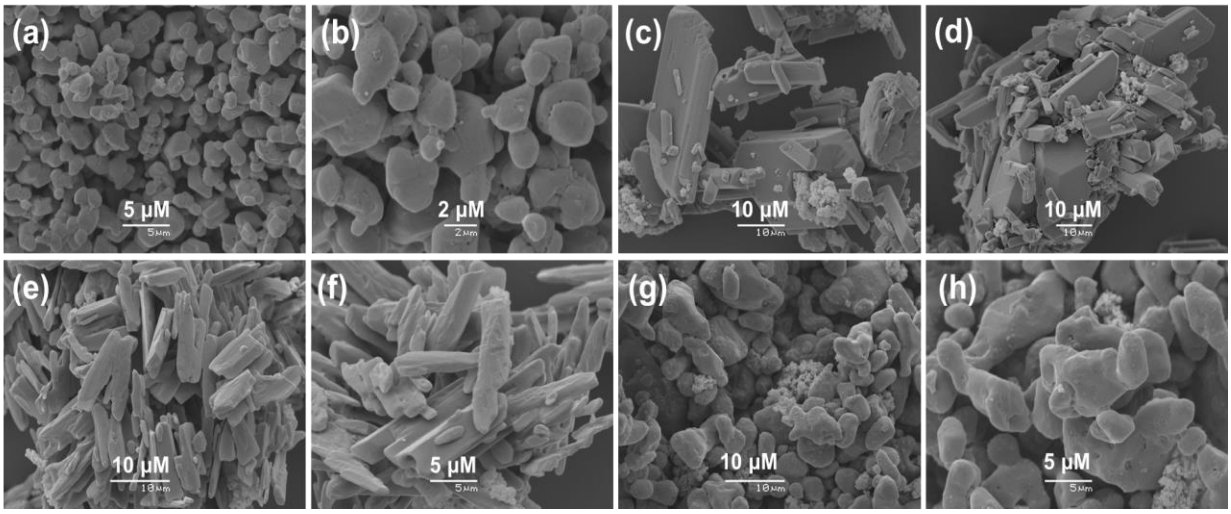

Figure 3.4.2 FESEM images of compositesa& b) 57CL20/ PANi; c & d) 58 HMX/PANi; e & f) 59 BCHMX/PANi; g & h) 60 RDX/PANi

Table 3.4.2 Particle size measurements

SrNo's	Code design.	Surface area (m^2/kg)	*Dv*(10) µM	*Dv*(50) µM	*Dv*(90) µM
1	57p CL20/ PANi	1740	1.59	6.89	25.6
2	57 CL20/ PANi	1764	1.76	6.79	40.5
3	58p HMX/PANi	724.5	4.11	18.2	51.2
4	58 HMX/PANi	788.6	3.89	18.7	80.6
5	59p BCHMX/PANi	1318	1.94	7.68	28.1
6	59 BCHMX/PANi	1233	2.06	8.35	40.1
7	60p RDX/PANi	774.5	4.07	15.6	83.8
8	60 RDX/PANi	1126	2.80	9.66	40.4

Note: Samples with "p" indicates samples obtained from first step of co-agglomeration i.e., co-precipitates

In addition to morphology, it is very important to analyze particle size and the NAs/PANi specific surface areas. As can be seen from Table 3.4.1, co-agglomeration of the NAs/PANi co-precipitates in chloroform leads to the largest increase in specific particle surface area for the RDX/PANi and β-HMX/PANi composites (RDX is known that its nanoparticles have the greatest propensity to a self-agglomeration [13]), this agglomeration is relatively small for β-CL20 and α-HMX analogues, and for BCHMX/PANi it is more of a grinding than agglomeration. Together with the surface morphology, these parameters also help NAs/PANi to resist higher droplet energy. Overall, it shows PANi acted as an effective phlegmatizer for selected attractive nitrmines (the effect of phlegamatiztion was shown in Scheme 3.4.2). Also, due to this core-centrered crystal affect the densities of CACs also maintained (see Table 3.4.7).

3.4.3.3 Differential thermal analysis(DTA)

The thermal stability of the composites prepared was evaluated employing the DTA [8, 11]. The obtained thermograms are shown in Figure 3.4.3, and the results are summarized in Table 3.4.2. PANi undergoes decomposition at 600 C. It is not important here; the main focus is on the thermal stability of its composites. From Figure 3.4.3 it can be seen that onsets of the CACs thermal decomposition are in all cases, lower than pure Nas. Logically also, peak temperatures of their exothermic decomposition are slightly decreased (see Table. 3).

Table 3.4.3 Summarized data from DTA thermograms of coformers and cocrystals with visible melting points.

Samples	Melting point / °C [Ref.]	Peaksofchanges in DTA record / °C(changeofmodification)	
		Endothermic	Exothermic
ε-CL-20	240 decompn [10]	170 (ϵ - γ)	225 (γ - δ)
α-CL-20	240 decompn [10]	175 (α–γ)	225 (γ–δ)
BCHMX	286 decompn [10]	--	224
α-HMX	--	189.6 (α – δ)	272
RDX	--	209	215
PANi		NA	243.25, 246.90, 251.36
57 CL20/ PANi	--	NA	218.92
58 HMX/PANi	--	179.4 (β – δ)	265.95
59 BCHMX/PANi	--	NA	218.53
60 RDX/PANi	--	NA	199.19, 217.56

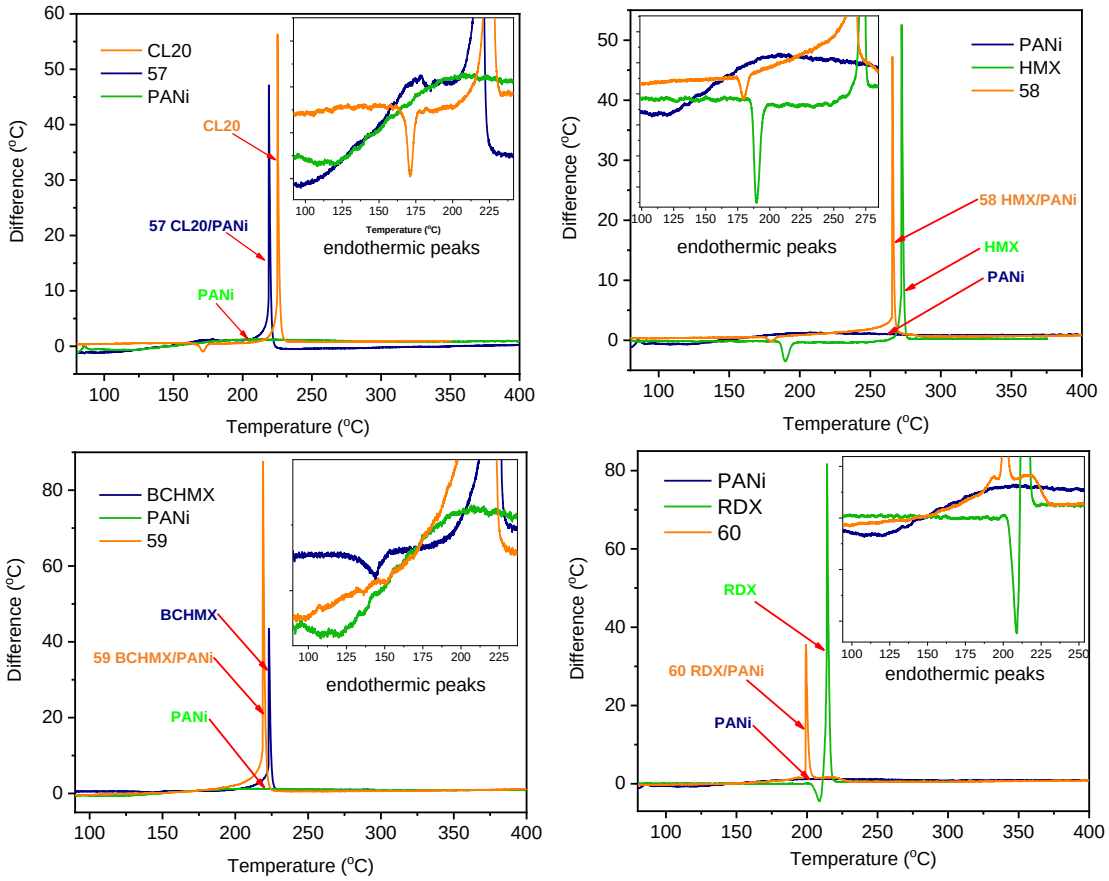

Figure 3.4.3 DTA thermograms of cocrystals 57 CL20/ PANi; 58 HMX/PANi; 59 BCHMX/PANi; & 60 RDX/PANi

It can be seen from Figure 3.4.3 that RDX, bonded on the PANi chain, began decomposing in a solid state of this complex, which is a big difference from thermolysis of its CACs with polynitro compounds [8–10]. The decrease in thermal stability of the composites compared to pure nitramines may be due to the mechanism of their interaction with the building units of the PANi chain, as shown in Scheme 3.4.1: the indicated mode of interaction should facilitate homolysis of the N-N bond and, in addition, hydrogen sulfate anions are present in the chain, i.e. acidic anions. The intensity of the interaction in the composite is so intense that exothermic decomposition appears in the original thermal range of the CL20 polymorphic transition. Similarly, in a composite with HMX, decomposition starts in the region of itsα – δ- transition.

3.4.3.4 FTIR Spectral studies

To further confirm the intermolecular interactions between PANi and nitramines, spectral studies were used in which FTIR showed some interesting results; characteristic peak shifts at the wavelengths were summarized in Table 3.4.1. These spectra are sufficiently optimal for the identification of peak shifts with

clear separations. The spectra showed absorption peaks in the wavelength region, i.e., 1480 ± 20 and 1565 ± 20 cm^{-1}, are characteristic of stretching vibrations of C=C quinoidal and benzenoid rings, respectively. Similarly, the peak lengths of polarons and quinoids indicate the presence of polaron and bipolaron ratios in the polymer chain [14] (based on the peak lengths, the ratios of polarons and bipolarons can be determined). If this ratio of polarons and bipolarons is equal to one, there will be an equilibrium between them; if not, there is no equilibrium. In this study, it was found that there is no equilibrium, so this means that there is a form of emerald salt PANi [2] that will further strongly influence the sensitivity to the electric spark (discussed in section 3.4.4.5).

Table 3.4.4 Summarized results of FTIR measurements

Assignments	PANi	57 CL20/ PANi	58 HMX/ PANi	59 BC / PANi	60 RDX/ PANi
N = Q = N Quinonoid (Q) unit stretching	1563	1594,	1525	1552	1568
N-B-N Benzenoid (B) unit stretching	1480	1490	1459	1471	1458
(C–N) stretchingofsecondaryaromatic amine	1290	1250	1259	1270	1262
(C–N) stretchingofprimaryaromatic amine	1237	1227	1236	1207	1231
Q = NH+–B or B–NH+• –B	1032	1093	1085	1084	1037
Gamma (C–H) (1,4-disubstituted unit) / Q unit deformation	879	874	871	860	880
HSO_4 ; $-SO_4^{2-}$	696	687	657	654	671
Symmetrical -NO_2 stretching	NA	1250	1259	1270	1262
Unsymmetrical -NO_2 stretching	NA	1553	1525	1529	1529
C-N stretching [Amino group]	NA	762	771	774	752
C-N stretching [Nitro group]	NA	1325	1324	1355	1349
Skeletalstretching [Ring]	NA	1163, 1093	1137, 1085	1135, 1084	1131, 1037
N-O symmetricstreching	NA	1251	1260	1272	1261

After undergoing co-agglomeration, a blue shift of these shifts has shown to be varied with individual nitramines; in CL20, due to its crowdedness (slightly repulsive influence with rings of the PANi chain), there might be interaction with PANi and with some surplus amount CL20 in mixture. Whereas the remaining nitramines, due to electrostatic attraction with short contacts, made bond elongation within polymeric chain in, which shown the red shift. These observations clearly indicated there will be rapid transition process in both rings (benzenoid & quinoid in PANi) after adding nitramines. This further influences the formation of PANi-NAs complex with electron transfer mechanism (Scheme 3.4.1). Also, significant changes occurred in C-N stretching of both primary and secondary aromatic amine groups.

Similarly, in bipolaronic B–NH+•–B peaks; in addition to these observations the nitramines significantly showed -NO_2 stretching vibrations. From DTA and PXRD data it is already known that CL20 changed its polymorphic form ε to β form, which more conveniently sits in a polymeric chain. However, CL20 might exhibit slight unbonded pure nitramine in this composite. Apart from this remaining the RDX and BCHMX also shown good compatibility with PANi. A peak observed at 675±20 cm^{-1} corresponds to bending vibration of -HSO_4^- group [15]. Which is further confirmed by the Raman spectrum.

3.4.3.5 Raman Spectral studies:

Raman spectra were measured by Thermo Scientific™ DXR3 Raman Microscope, employing an excitation laser source (wavelength of 785 nm & power 29 mV), 10x/0.25 objective and using 400 lines/mm grating (3378 to 49 cm^{-1}). The characteristic peak shifts were summarized in Table 3.4.2. However, the pure PANi and its composites found highly sensitive to laser power above 29 mV with 10x/0.25 grating(more details see Chapter 2), if it taken above this laser power Raman spectrum will show mainly two peaks which are polaronic charge carriers (-C-N·+)and -C=C stretching vibration of the semiquinoid ring [11 - 13].

Table 3.4.5 Summarized results of Raman measurements

Assignments	PANi	57 CL20/ PANi	58 HMX/ PANi	59 BC / PANi	60 RDX/ PANi
Phenazine-likecrosslinking	1703	1619	1620	1620	1669
C ~ C stretchingvibrationsofthesemiquinonoid unit	1592	1593	1598	1601	1591
N-H deformation in thesemiquinonoidstructures	1506	1504	1510	1509	1502
C~N+• stretchingvibrations in highlylocalizedpolarons	1376	1378	1376	1379	1380
C~N+• stretchingvibrationsofthesemiquinonecationradicals in delocalizedpolaronicStructures	1339	1332	1349	1339	1334
C–N stretching in benzenoid and quinonoidstructures	1232	1267	1267	1267	1269
C–H deformationvibrationof a quinonoid unit	1169	1170	1172	1174	1169
The benzene unit deformation in theemeraldine salt	809	805	881	850	846
Phenazine-likecrosslinking	575	579	597	578	575
Out-of-plane unit deformations in theemeraldine base	413	414	413	416	414
Asymmetric –NO_2stretchingvibration	NA	1570, 1593	1578, 1598	1567, 1597	1560, 1591
Symmetric –NO_2 stretchingvibration	NA	1285, 1267	1267, 1248	1267, 1259	1269, 1250
–NO_2deformationvibration	NA	841, 805	844, 806	848, 803	882, 805
–NO_2Wagging	NA	737, 718	735, 719	735, 715	732, 715
-N-N- bond streching	NA	1169	1170	1172	1171

Its main observation which differentiates from FTIR in which Raman spectrum polaron interactions are observable [11].In the current study, it's important to see the measured interactions between the nitramines and PANi chain. So, we took spectrum lower laser peaks with optimum peak separation. A small peak appearance at 185±10 indicates PANi presence in emeraldine salt form II and which also indicates the presence of the -HSO_4^- anion [15]. This indicates from both FTIR and Raman sulphuric content in pure PANi as well as CACs; which is further confirmed by elemental analysis(see Table 3.4.7). FTIR benzenoid and quinoid peaks showed significant variations, which can be seen from the characteristic peak shifts summarized in Table 3.4.2.

3.4.3.6. Fluorescence studies

Fluorescence measurements were carried out to determine the influence of the charge transfer complex formation in the CACs (NAs/PANi – see Scheme 3.4.1) on their properties. Outputs of these measurements in a solution of DMSO are presented in Figure 3.4.4. In this Figure. the first absorption band at 630 nm is probably a mixture of n-π* and π-π* transitions and absorption band at 340 nm corresponds to π-π* transition [1–4].

From Figure 3.4.4b it clearly shown that the NAs-PANi complex formation leads to fluorescence decreases [1–4]. But there will still be a small amount of free moiety of PANi, which shows that there will be free electrons delocalization in polymer chain and linkage between the NAs-PANi easy access to external electric charges; these are the main reasons for the electrical spark sensitivity of CACs (see Table 3.4.4.7 and Section 3.4.4.4). The further structural changes were confirmed by quantum yield analysis (Figures 3.4.4, 3.4.6b, 3.4.7c, 3.4.8a, 3.4.8b, and 3.4.9a).

Similar behaviour was also found in the case of samples 57, 58, 59 and 60. Quantum yields related to the absorption band at 340 nm are summarized in Table 3.4.6. It is a known fact that quantum yield increases if a non-fluorescent molecule bound to a fluorescent molecule.

Table 3.4.6 Quantum yields of samples under study measured in DMSO

Sample	Quantum Yield (qFl)
PANi	$(2.5+/-0.3)\times10^{-3}$
57	$(2.2+/-0.2)\times10^{-3}$
58	$(3.8+/-0.4)\times10^{-3}$
59	$(4.3+/-0.5)\times10^{-3}$
60	$(4.4+/-0.4)\times10^{-3}$

The binding between the NAs-PANi makes the increase in the quantum yield, it can be explained by Lippart equation [16]. That nonfluorescent binder (NAs) bounded with fluorescent material (PANi) changes

quantum yield it due to excited / delocalizing electrons are absorbed by NAs (via NAs-PANi linkage), which causes non radiative decay (Knr) in complex [16].

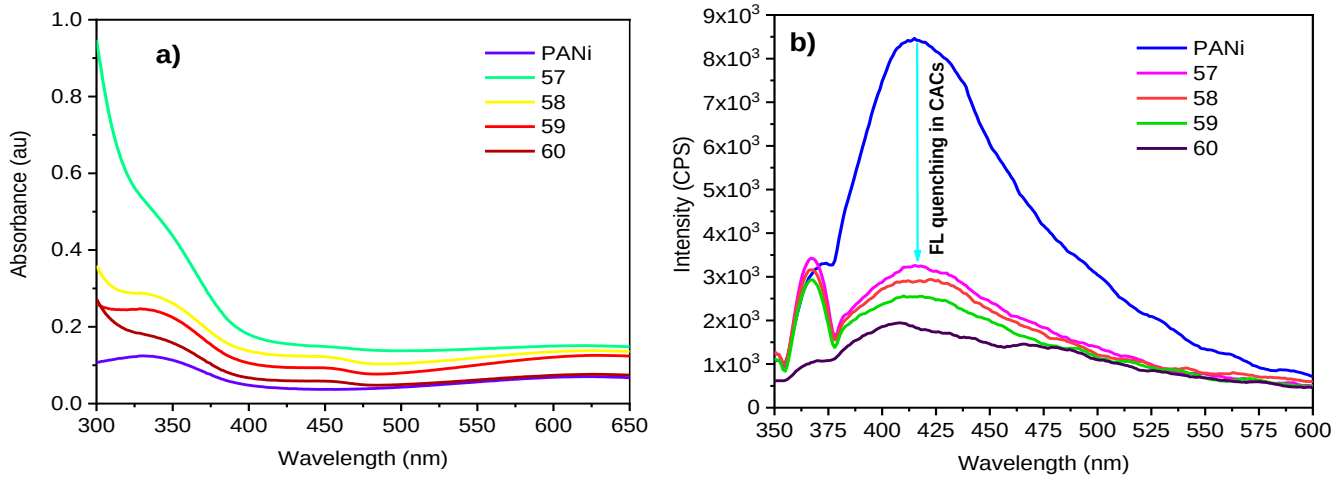

Figure 3.4.4 a) Normalized UV/vis absorption (blue), fluorescence excitation (red) and emission (black) spectra of PANi in DMSO; b) Fluorescence spectrum of pure PANi and their NAs-composites in DMSO

3.4.3.6 Thermochemical and Explosive Properties

The heat of combustions of pure nitramines and their PANi-composites were considered for the calculation of thermochemical parameters. The density was obtained experimentally from the densitometer, and the composition of composites from elemental analysis. From help Hess's law and using these data, calculated enthalpy of formation and obtained results were summarized in Table 3.4.7. The density of PANi is relatively low compared to the nitramines; after undergoing the treatment of it by Nas, the composites produced are with interesting arrangements (Scheme 3.4.3), which had crystals with relatively close or in some cases slightly higher density with pure nitramines (it is with respect to polymorph transition of ε to β in CL20 and β to α in HMX).

After obtaining all these data, they were utilized for detonation properties calculations using the CHEETA code [17]. Some of the mechanical and thermal energy was collectively considered as detonation energy here. The volume of detonation products considered to a pressure of 1 atm determined the mechanical energy, which is equal to the expansion work of the detonation products, and the thermal energy, which is the heat in the detonation products under this pressure[18–20]. Other conditions, temperature 1800 K on the Isentrope beginning at the CJ point, and composition of detonation products at this temperature conditions are considered for calculations.

Further next important part is the impact and electric spark sensitivities of the studied CACs; the first one was determined by means of the standard impact tester (Julius Peters [21]) with an exchangeable anvil, the amount of tested substance being 50 mm^3 and used drop hammer of 2 kg, as it was already described in our previous paper [11]. To determination of the electric spark sensitivity [22] the device was used with the electrodes in direct contact with the sample(the ESZ 2000 MIL apparatus of the company OZM Research).

Table 3.4.7 Molecular formulas, thermochemical properties, and maximal crystal densities of pure substances and corresponding CACs

No	Explosive				Heat of combustion[a]		Enthalpy of formation		Crystal density
	Code design.	NA/ PANi	Formula[b]	Mol. weight	Q_c ($J.g^{-1}$)	Ref	ΔH_f ($kJ.mol^{-1}$)	Ref	($g.cm^{-3}$)
1	RDX	--	$C_3H_6N_6O_6$	222.14	9522	[22]	66.2	[22]	1.810
2	BCHMX	--	$C_4H_6N_8O_8$	294.17	9124	[22]	236.5	[22]	1.860
3	α-HMX	--	$C_4H_8N_8O_8$	296.18		[22]	75.02	[22]	1.839
4	β-HMX	--	$C_4H_8N_8O_8$	296.18	9485	[22]	77.3	[22]	1.902
5	ε-CL20	--	$C_6H_6N_{12}O_{12}$	438,23	8311	[22]	397.80	[22]	2.044
6	β-CL20	--	$C_6H_6N_{12}O_{12}$	438.23	8327	[23]	421.74	[23]	1.985
7	PANi	--	$([C_6H_4NH]_2[C_6H_4N]_2)_n$ $C_{6.00}H_{6.33}N_{0.98}O_{2.00}S_{0.14}$	95800[24] 128.64	24497	[Cw]	158.57	[Cw]	1.5022
8	57 CL20/ PANi	--	$C_{10..66}H_{11.01}N_{12.00}O_{14.62}S_{0.17}$	546.59	11240	[Cw]	321.47	[Cw]	1.9691
9	58 HMX/PANi		$C_{6.66}H_{10.16}N_{8.00}O_{9.02}S_{0.13}$	354.58	11979	[Cw]	31.19	[Cw]	1.8967
10	59 BCHMX/PANi		$C_{6.35}H_{8.00}N_{8.00}O_{8.82}S_{0.05}$	333.40	11245	[Cw]	89.21	[Cw]	1.8916
11	60 RDX/PANIi		$C_{5.09}H_{8.60}N_{6.00}O_{6.71}S_{0.08}$	263.72	12379	[Cw]	6.17	[Cw]	1.8295

Note: Here, Cw- results obtained in current work;

The results of both these mentioned test methods are summarized in Table 3.4.7. It is interesting and important that due to morphological changes (Figures 3.4.4 and 3.4.7a, Scheme 3.4.2) in CACs, the presence of PANi causes their better resistance to impact; other hand, due to their conducting properties these NAs/PANi composites show higher electrical sensitivity. PANi thus acts as passage for electrons transfer to reaction centers of nitramine molecules (their addition at nitro groups [22]), makes composites more electric spark sensitive than their pure forms.

Table 3.4.8 Sensitivities and explosive properties of pure substances and corresponding CACs

	Explosive	Impact sensitivity E_{dr}			Electric spark sensitivity	Detonation velocity	Detonation pressure	Energy of detonation,	Additive Value
No	Code design.	E_{dr} 50 % (J)	Ref.	E_{dr} 95 % (J)	E_{ES} (mJ)	D ($m.s^{-1}$)	P (GPa)	E_{deton} ($J.g^{-1}$)	E_{deton} ($J.g^{-1}$)
1	RDX	5.6	[10]	--	147.7	9014	33.91	5915	--
2	BCHMX	3.0	[10]	--	191.4	9116	36.19	6223	--
3	α-HMX	1.9	[10]	--		9126	35.05	5904	--
4	ß-HMX	6.4	[10]	--	160.0	9404	38.00	5964	--
5	ε-CL-20	13.2[a] 4.1 [b]	[10]	--	157.0	9650	43.41	6303	--
6	ß-CL-20	11.9	[10]	--	130.6	9421	40.77	6320	--
7	PANI	50.0	Cw	108.0	35.6	6813	16.61	4845	--
8	57 CL20/ PANi	17.4	Cw	33.4	40.9	9025	38.05	5971	6136
9	58 HMX/PANi	31.0	Cw	87.2	37.9	8890	35.30	5597	5876
10	59 BCHMX/PANi	22.3	Cw	55.9	23.2	8836	34.58	5638	5908
11	60 RDX/PANi	21.4	Cw	31.1	44.9	8744	33.26	5544	5805

Note: a) the value for pure ε-CL-20;
b) the value for "common" (technical) quality of ε-CL-20;

3.4.4. Discussions

3.4.4.1 Co-agglomeration

The attempt of co-agglomeration was preceded by the preparation of mixed microparticles by co-precipitation from a common solution. The intense stirring actively influenced the particles size and surface area of the NAs/PANi composites in both these processes (see Table 3.4.2). However, a real and mild co-agglomeration was observed only in the case of BCHMX/PANi; in the other mixed co-precipitates, there was an increase in the specific surface area after the co-agglomeration operation. This was further confirmed by analyzing the particles sizes of the co-precipitates and final composites (see Table 3.4.2). Thus, although we refer here to "co-agglomeration", then as an applied process (to maintain continuity with our previous publications [8–11]), it results in composite micro-particles. The obtained results are summarized in Table 3.4.2. The co-agglomeration process also showed improvements in the surface morphology of the CACs, which was observed from the FESEM analysis in all cases of crystals showed smothered surfaces. FESEM images show two major kinds of crystals, which centre-cored one and another coated, which made nitramine crystals edges smoother (Scheme 3.4.2). As exceptional case β-CL20/PANi centre-cored crystals PANi unequally distributed average crystals.

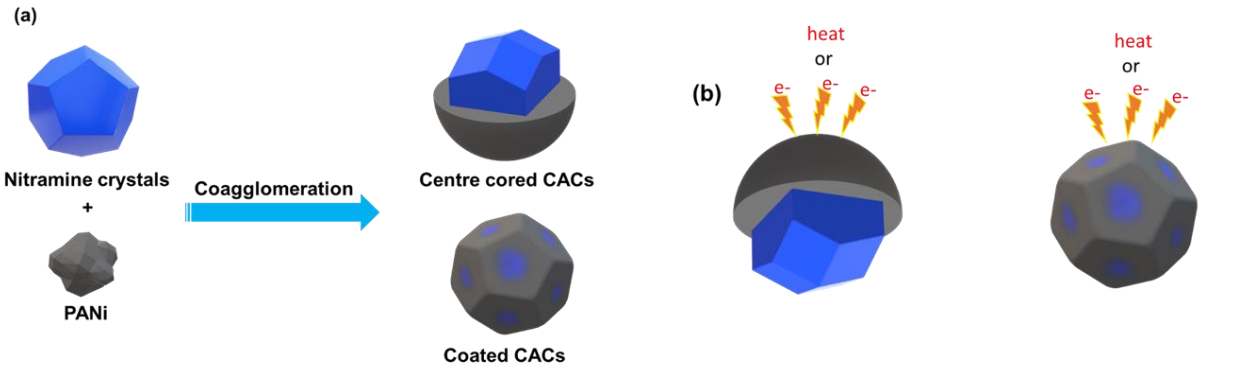

Scheme 3.4.2 Schematic representation of two kinds of CACs:

a) the nitramine centre cored crystals with surrounded by PANi and PANi superficially coated which made smoother edges of nitramine CACs;

b) both these partial Schemes with the indicates action of heat (during DTA measurements) and electron (during electrical spark sensitivity measurements) tansfer to composites.

3.4.4.2. Thermal Analysis

As mentioned, the interaction of the nitramine molecules with the building units of the polyaniline chain in the sense of Scheme 3.4.1 leads to their thermal destabilization. This could be explained as follows: this interaction of the π-electron system or the free electron pair of aniline nitrogen (complexes with the charge transfer) with the nitro group counteracts the mesomeric effect (Scheme 3.4.3) in the nitramine- grouping by reducing the charge deficiency on the nitrogen atom of the nitro group (the balance is then shifted to the left side and the N-N bond should be thus weakened).

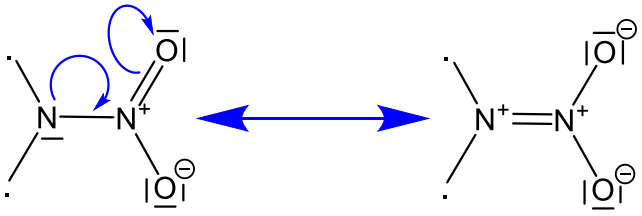

Scheme 3.4.3 Mesomeric effect in the nitramine- grouping

The morphological changes, connected with formation of the complexes with charge transfer, effectively influenced thermal analysis of the composites prepared (Table 3.4.2 and Figure 3.4.3). Considering the structure of these complexes (Schemes 3.4.1 and 3.4.2) and corresponding morphological changes (section 3.4.3.2), the heat transfer will take place first through the PANi chain with following transfer on the nitramine molecule.

3.4.4.3 Spectral Examination

In spectral observations viz., stretching, bending vibrations and vibrational modes of PANi are more dominated due to composites of the NAs crystals shielded by PANi (Scheme 3.4.2). From the spectral characterizations, it is known that nitramines are bonded with the polymeric chain with electro-force of attraction with the formation of short contacts with the benzenoid ring, quinoid units and polarons. These bond formations take place during the "co-agglomeration". Applied heat helped electron enriched PANi to attach with electron deficient nitro groups of nitramines. Except in the case of the β-CL20/PANi complex, the remaining composites found more possibilities of complex formation (see Scheme 3.4.2). Additionally, PANi and all its composites prepared were found to be laser sensitive; so, to avoid their ignition during analysis, the least power (29 mV with 10x/0.25 grating) laser power was used.

Both FTIR and Raman stretching vibrations are overlying each other and thus verify that there is a complex with charge transfer formation in the PANi CACs. The thermal electrons transfer during “co-agglomeration” leads to complex formation is explained with the help of molecular orbital theory (MOT); in which here PANi (P*) acts as electron donors whereas the nitramines (NAs) act as electron deficient species; during coagglomeration, these electronically charges species makes momentarily excited complex (P+.NM-) [1–4]. The exception is the β-CL20/PANi composite because of the presence of a high number of nitro groups in the molecule, bonded at the globular and crowded 2,4,6,8,10,12-hexaazaisovurtzitane skeleton, with internal interactions between these nitro groups make the β-CL20 molecule not goodly accessible to PANi chain mainly from the steric reasons.

The higher moiety electrons at aza-nitrogen atoms in the CL20 nitramino-groupings might attribute inductive effect to decrease affinity of nitro nitrogen atoms (see Scheme 3.4.2) to π-electrons from PANi (see Scheme 3.4.1). It ought to lower in the driving force for the charge transfer. A bigger part of the CL20 molecule should be balanced by internal π-π stacking; its short contacts in crystal lattice should stay partially, and thus, some amount of physical mixture is formed of β-CL20 with PANi in composite. These real facts influence its thermochemical, detonation and sensibility properties (energetic properties were discussed in section 3.4.4.4). From the FTIR analysis it was also found that there is an $-HSO_4^-$ peak at 675±20 cm^{-1}, which is a small amount present here, which further confirmed with elemental analysis, found that there is 0.02 – 4.00 % of sulphur content and higher level of oxygen. Each analysis indicates presence of Sulphur in the form of $-HSO_4^-$, which further balanced the complete PANi chain. This anion also helps here to remove the π-π stacking which makes electron mobility easier due to this electron density increases in polymeric chain which further utilized in the interaction with the nitramines forming complexes-composites. It also enhances the physical properties like processability, solubility and electrical conductivity of PANi as well as its NAs-composites. As polymer directed applications like using for sensor

activity based on electrical conductivity and fluorescence this property is good [1–4]. However, for corresponding composites it made relatively electrical spark sensitive than the pure NAs have (see section 3.4.4.5).

3.4.4.3.1 The N-N bond stretching vibrations

The first step in verification of co-crystal formation in our recent papers [8–11] consisted in comparing the lengths of the longest N-N bonds with the N-N ones stretching vibrations. For our PANi complexes, this approach is presented by Figure 3.4.5a. Here, in the first approximation, these bond lengths in pure nitramines were applied for the corresponding PANi composites.

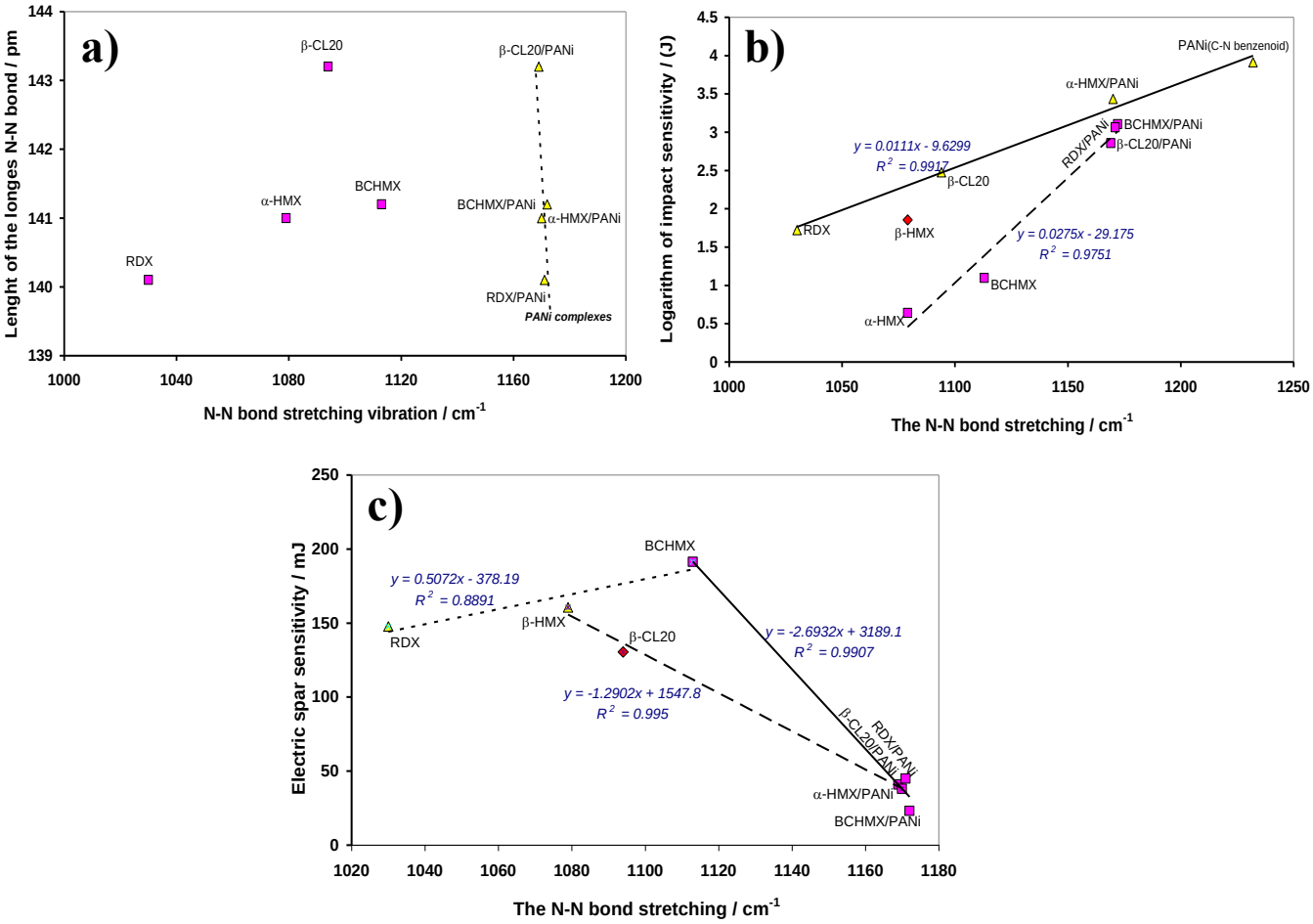

Figure 3.4.5 Dependences connected with the N-N bond stretching:

a) A comparison of the lengths of the longest N–N bonds and the stretching vibrations of these bonds of pure nitramines and their composites with PANi (the data placement in this Figure indicates the existence complexes with charge transfer in the sense of Scheme 3.4.1); the N–N bond lengths have been taken from the ORTEP views of the nitramines used in the CCDC database.

b) Semilogarithmic correlation with impact sensitivity, expressed as a drop energy for 50 % probability of initiation (for PANi is used C-N bond stretching in benzenoid and quinonoid structures);
c) Correlation with the electric spark sensitivity, taken here as an energy of spark, needed for 50 % probability of initiation.

It is understandable that due to forming of the charge transfer complex of nitramines with PANi the N-N bond lengths should be changed due to the negative influencing of mesomeric equilibrium (Scheme 3.4.3) in nitraminic grouping (because of the changes in the force ratios in the crystal lattice of nitramines). Similarly, as it was in co-crystals [8–11], this Figure 3.4.5a shows a large difference between pure nitramines and their NAs/PANi (more precisely their composites). But comparing this Figure with the similar ones in our recent papers [8–11] it can be seen the difference of the PANi composites from CACs of the co-crystal type; while in our case the values of N-N bond stretching of composites lie in the range of 1169-1172 cm^{-1}, in the case of co-crystals of the studied nitramines it was of 940-1040 cm^{-1}. The reason for this difference is the difference in the decisive intermolecular interactions in the mixed crystals of both groups of mixed crystals, which is reflected in the thermochemical, explosive and sensitivity properties of the composites (as already mentioned).

In the process of the nitramines initiation, it is primarily the N-N bond that is homolyzed [25, 26]. In this context, the semilogarithmic relationship between impact sensitivity and N-N bond stretching is understandable (Figure 3.4.5b): if we consider the definitional relationship between the vibrational frequency and the bond force constant (i.e., roughly the strength of the given bond) [27] then the relationship in Figure 3.4.5b should imply that the increasing this strength should correspond to decreasing of impact sensitivity, which correspond to reality. The fact that β-HMX data do not correlate here and α-HMX data do, also corresponds to reality (the latter named is present in the corresponding PANi complex).Similarly, Figure 3.4.5c could be perhaps discussed for pure nitramines. However, the initiation by the electric spark is related to the addition of an electron at the nitro group [22], and the N-N bond could function here as a conductor of the inductive effect. The formation of the PANi complex, however, is related to a sharp increase in electric spark sensitivity, perhaps due to the "good transporter" of electrons into the NAs reaction center through the conducting PANi chains. Why the position of the β-CL20 data suggests opposite it may be related to the complicated structure of its PANi complex (see already above).

3.4.4.3.2 New unusual dependencies

Interesting are the dependencies, presented by Figure3.4.6, that are not possible to consider for CACs of the co-crystal nature [8–11]. Thus Figure 3.4.6a presents the proportional influence of the deformation vibrations of the structural building units of PANi chain on the resistance against impact of the studied nitramines PANi complexes. While β-CL20 reduces these deformations somewhat compared to the same

ones of the pure PANi, the remaining nitramines show a more pronounced opposite effect. The effect of CL20 is undoubtedly due to the aforementioned special structure of its complex with PANi, the RDX, BCHMX and HMX behaviour then due to interaction with polyaniline as shown in Scheme 3.4.1. The intensity of this interaction can be assessed by fluorescence measurements: as the fluorescence of the PANi/NAs complex increases, the intensity of interactions between molecules of its coformers decreases (the opposite is true for quantum yield) [1–4]; in Figure 3.4.6a this intensity thus should decrease in series of the RDX-BCHMX-HMX/complexes, CL20 is an exception, as already mentioned.

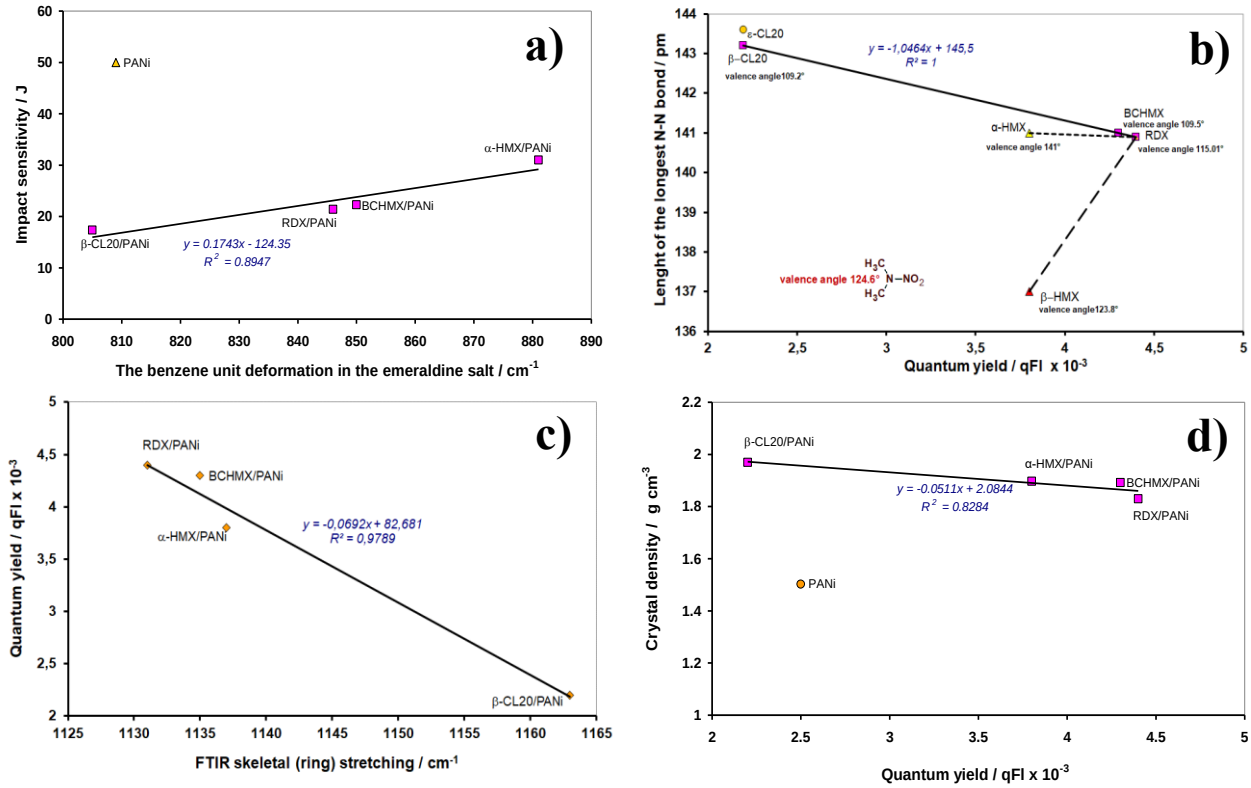

Figure 3.4.6 Dependences connected with the structural characteristics:

a) relationship between impact sensitivity (expressed as an drop energy in J) and the benzene unit deformation in the emeraldine salt;
b) relationship between length of the longest N-N bond and quantum yield from the fluorescence measurements (PANi complexes are indicated only by pure nitramine codes, dimethyl nitramine is presented as a standard for valence angles) – values of the N-N bonds length and valence angles.
c) relationship between quantum yield from fluorescence measurements and FTIR skeletal (ring) stretching;
d) relationship between crystal density NAs/PANi complexes and their quantum yields.

If the photons are emitted from the nitramine grouping –N–NO_2 of nitramine, then its electron configuration understandably has a large influence on it, which in the first approximation in Figure 3.4.6bcan be

represented by the length of the longest N-N bond (trigger bond) and a notice of valence angle –CH_2–N–CH_2–, connected with this bond.

Considering those angles, compared to the valence angle of dimethyl nitramine (taking it as a standard), it can be seen that all nitramines (except β-HMX) have crowded molecules (even RDX, corresponding to its reactivity compared to β-HMX).Stabilizing the highly sensitive α-HMX by converting it into a PANi complex makes it a very attractive low impact-sensitive explosive whose data in Figure 3.4.6c lie logically close to the dependence for the other NAs/PANi. The order of the NAs/PANi complexes in this Figure already corresponds to the order of the quantum yields found, i.e. the order of the intensity of the intermolecular interactions of the coformers of the studied complexes (the weakest for β-CL20, strongest for RDX). The aforementioned emission order is also very well captured by Figure 3.4.6c, i.e. the decrease in photon emission with increasing FTIR skeletal stretching (that stretching increases with increasing steric crowding of nitramines molecules).The logical linear relationship between quantum yield and crystal density, presented in Figure 3.4.6d, is also related to the above, i.e. to the electron configuration on nitramine grouping; this configuration is the result of the spatial arrangement and overall electron structure of the NA molecule, which has a major influence on method of its placement in the crystal lattice and thus on the density of the crystal.

3.4.4.3.3 Relationships derived from fluorescence measurements

Already, it was mentioned in the discussion of Figure 3.4.6 - this is the quantum yield, i.e., according to the IUPAC definition [28], the number of certain events per photon absorbed by the system. In the discussion of the above mentioned Figure., it was stated that the electron configuration on the nitramino grouping (trigger grouping) has a fundamently influence on the photon emission, which gives the quantum yield. Figure 3.4.7 shows further interesting relationships between quantum yields and the characteristics of the NAs/PANi complexes.

The dependence in Figure 3.4.7a confirms that the detonation characteristics are related to the electronic configuration of the ground state and the steric conditions, both these in the reaction center of the molecule [26, 29, 30]. Similarly, can be said for impact sensitivity in Figure 3.4.7b, but here data of the CL20 complex outside of the relationship is due to weakest mutual interaction of coformers (and thus different reactivity), as was already mentioned. No form of linear relationship could be found for the electric spark sensitivity (Figure 3.4.7c); as noted already above, the primary step in this initiation is the addition of an electron at the nitro group [22], i.e., the attack only on a part of the nitramino grouping and it might be reason this un-linearity. The difference in the correlation (uncorrelation) of the β-CL20/PANi data in each part of Figure 3.4.7 also lies in the strength of the initiation - that is, shock in detonation versus impact and spark in the

other two. It appears that these kinds of outputs from fluorescence measurements could be used to study the primary processes of initiation of energetic materials in the sense of the physical organic chemistry approaches [26, 30].

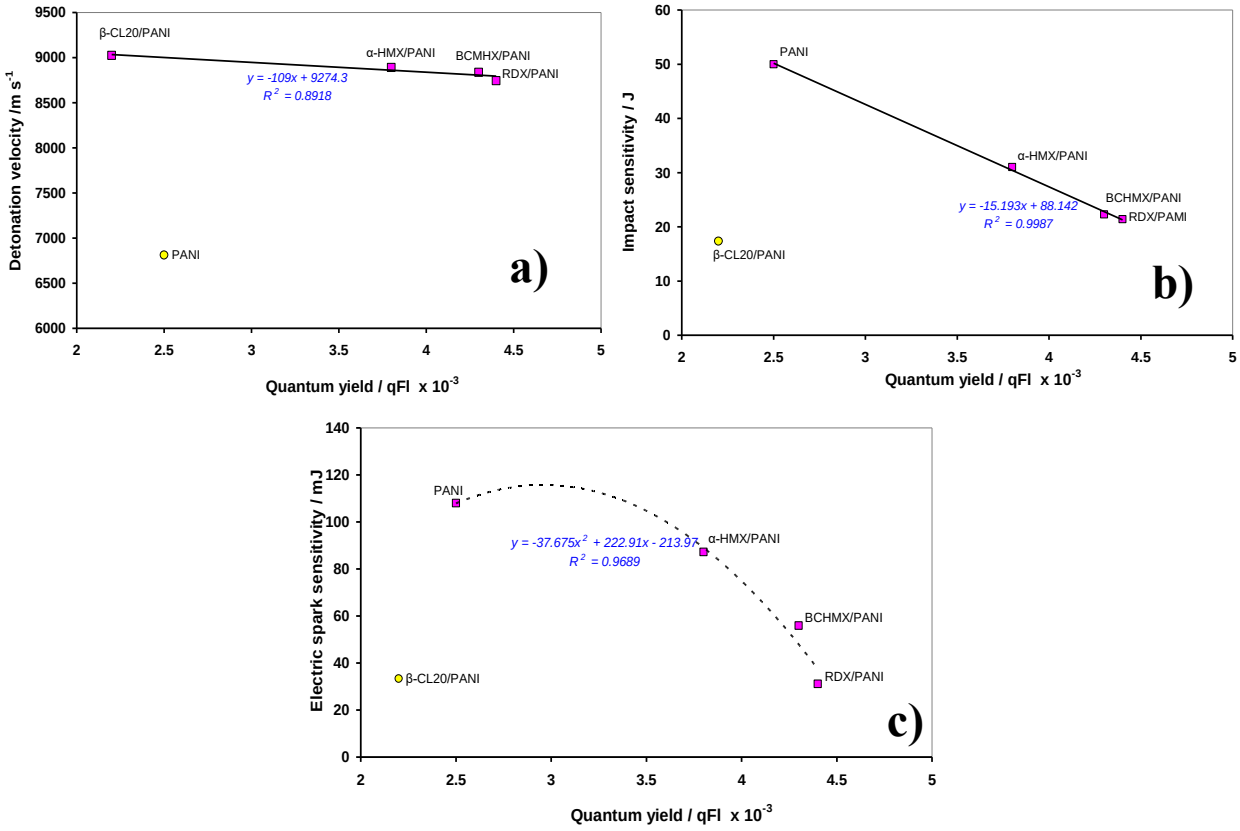

Figure 3.4.7 Dependences connected with the quantum yield of the studied NAs/PANi complexes:

a) relationship between detonation velocity and quantum yield;
b) relationship between impact sensitivity, expressed as a drop energy (in J), and quantum yield;
c) relationship electric spark sensitivity and quantum yields.

3.4.4.4 Towards the electric spark and impact sensitivities, including shock influence

As shown at Scheme 3.4.2, that there are two kinds of crystal arrangements of the PANi composites (verified by the spectroscopic and morphological analysis). Fall hammer dropping stress should be initially transferred to PANi layer, by which it can be partially absorbed, once it reaches to NAs it will lesser effect. In both cases of crystal arrangements, the PANi thus acted as effective phlegmatizer, with which HMX shows good compatibility, followed by BCHMX, RDX, and CL20. One from the first study of impact sensitivities in crystalline explosives, using the Raman vibrational spectra was published by Mc Nesby and Coffey [31]; their approach, through construct vibrational energy level diagrams, led to a model designed

to calculate the rate of energy transfer from phonon and near-phonon vibrational energy levels to higher energy vibrational levels. Unlike them we seek to correlate this sensitivity directly with the outputs of Raman and FTIR spectroscopy, as is presented in [8–11] and here in Figures. 3.4.5b and 3.4.6a, extended newly by output of fluorescence measurements (Figure 3.4.7b). Our goal is to search and confirm trigger bonds. It has already been pointed out in the discussion of Figure 3.4.5a that due to the difference in the crucial intermolecular interactions in PANi composite crystals and co-crystals with polynitro coformers (the last ones see in [8–11]), the assortment of direct relationships of both the Raman and FTIR outputs with characteristics of these composites initiation is somewhat limited.

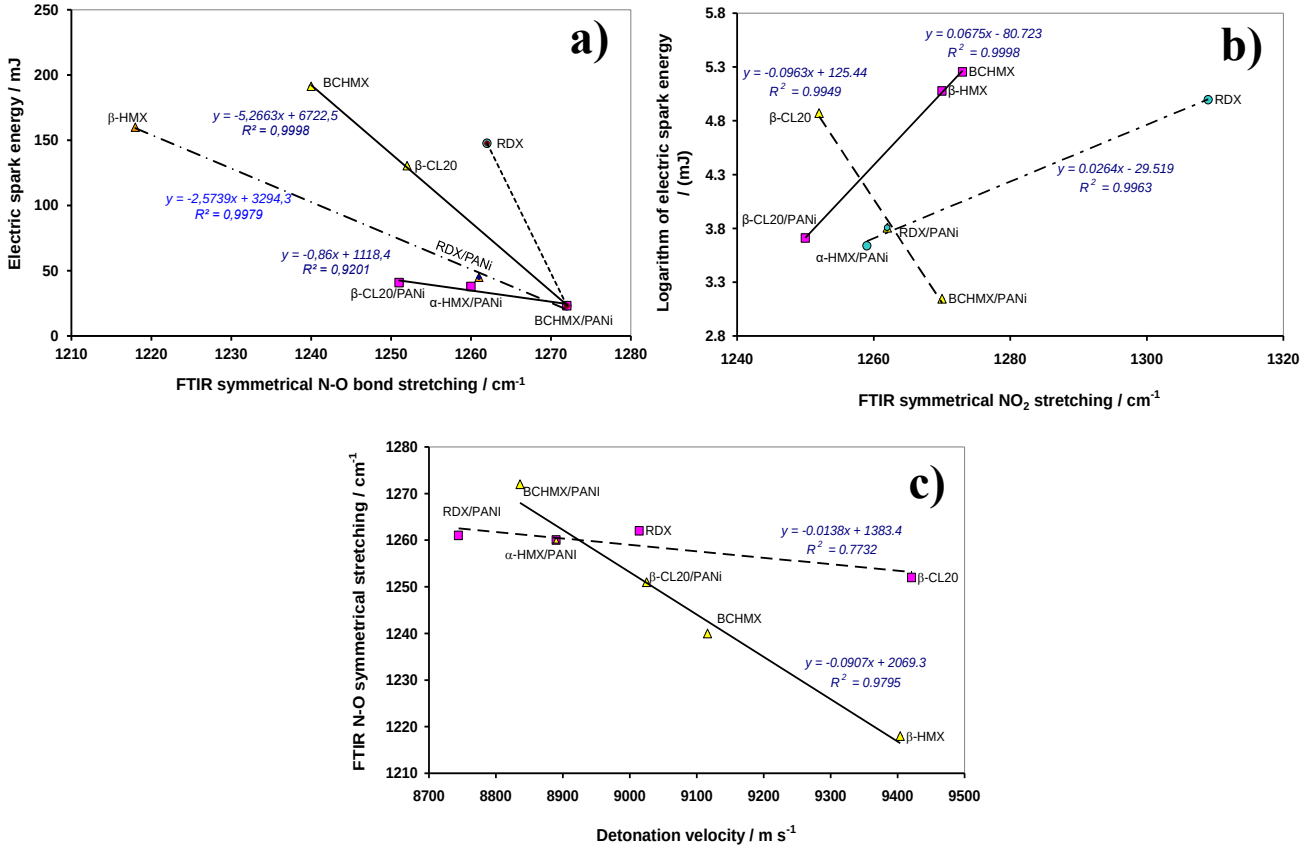

Figure 3.4.8 Dependences connected with the FTIR outputs of nitro group in studied composites:

a) relationship between energy of the electric spark (needed for 50 % probability of initiation) and FTIR symmetrical N-O bond stretching;
b) semilogarithmic relationship between energy of the electric spark (needed for 50 % probability of initiation) and FTIR symmetrical NO_2 stretching;
c) relationship between the FTIR symmetrical N-O bond stretching and detonation velocity.

The mode of interaction of electrically conductive PANi with NAs molecules (see Scheme 3.4.1) allows perfect electron transport from the electric discharge into the reaction centers of nitramino groupings, i.e., to nitro groups. In addition, presence of the -HSO_4anions in PANi enhances its electrical conductivity [1–4] (see section 3.4.4.5). The same group gives stability and processibility to PANi when comes its physical stability and storage, including of its composites.

It is in connection with the attack of the electron on the nitro group, as a primary step of initiation, that Figures. 3.4.8a and 3.4.8b might be of interest. In the first case, according to the proposed mechanism of electron entry at the nitro group [22], the enhancement of the N-O bond (see already a bond force constant in 4.3.1) should facilitate the homolysis of the N-NO_2 bond, i.e., the dependence in Figure 3.4.8a should essentially correspond to the said assumption. On the other hand, Figure 3.4.8a should represent the stabilization of the NO_2 group against electron addition for partial relations with positive slope. The introduction of sterically crowded beta-CL20 and BCHMX molecules into the PANi composites does not change their stretching much (compared to the same for HMX and RDX) thus in the case of negative slope dependence, the geometrical details of the respective PANi complexes with charge transfer should also play a role. As far as the effect of the shock on the initiation of the studied composites is concerned, this could be presented in a first approximation by Figure 3.4.8c: again taking into account the force constant of the bond, it can be stated that the detonation rate of the respective nitramine or its composite increases with the decrease of the N-O bond strength (an opposite situation in electric spark initiation according to Figure 3.4.8a) and, as it was shown in Figure 3.4.7a, with decreasing of electrons emission in the fluorescence measuring.

3.4.4.5 The Energetic Point of View

The detonation parameters of PANi in Table 3.4.8 may be somewhat surprising; this polymer is an energetic material with very slow exothermic decomposition (see Table 3.4.3 and paper[32]), whose thermochemical characteristics, elemental composition and density (all these data in Table 3.4.7), when inserted into the CHEETAH code, will give the values shown. However, this does not mean that PANi is a powerful explosive, but the possibility of its detonation in a larger charge diameter and with a very powerful initiation exists.

It is a well-known fact that the mixing of two explosives results in a mixture that usually has a higher detonation rate than would correspond to the percentage of components in this mixture (it is valid also for certain from inert admixtures) [33]. Prof. Urbanski explains these increases in values by the increase in entropy of the resulting mixture due to components entering in it [33]. For this kind of evaluation we have used energies of detonation, E_{deton} (see in Table 3.4.8, here additive value of E_{deton}) [8–11]. Compared to nitraminic co-crystals with polynitroaromatic coformers [8–10], the effect of the increase in these

"percentage" (additive) E_{deton} values, due to the PANi composite formation, is more pronounced (for the case of only nitramine coformers this effect is opposite [11]).

The inverse relationship between the performance [29, 34] and/or energy content [35, 36, 37] of explosives and their sensitivity has already been mentioned (Licht's rule [34]). How this situation looks in the case of the composites studied here is shown in Figure 3.4.9

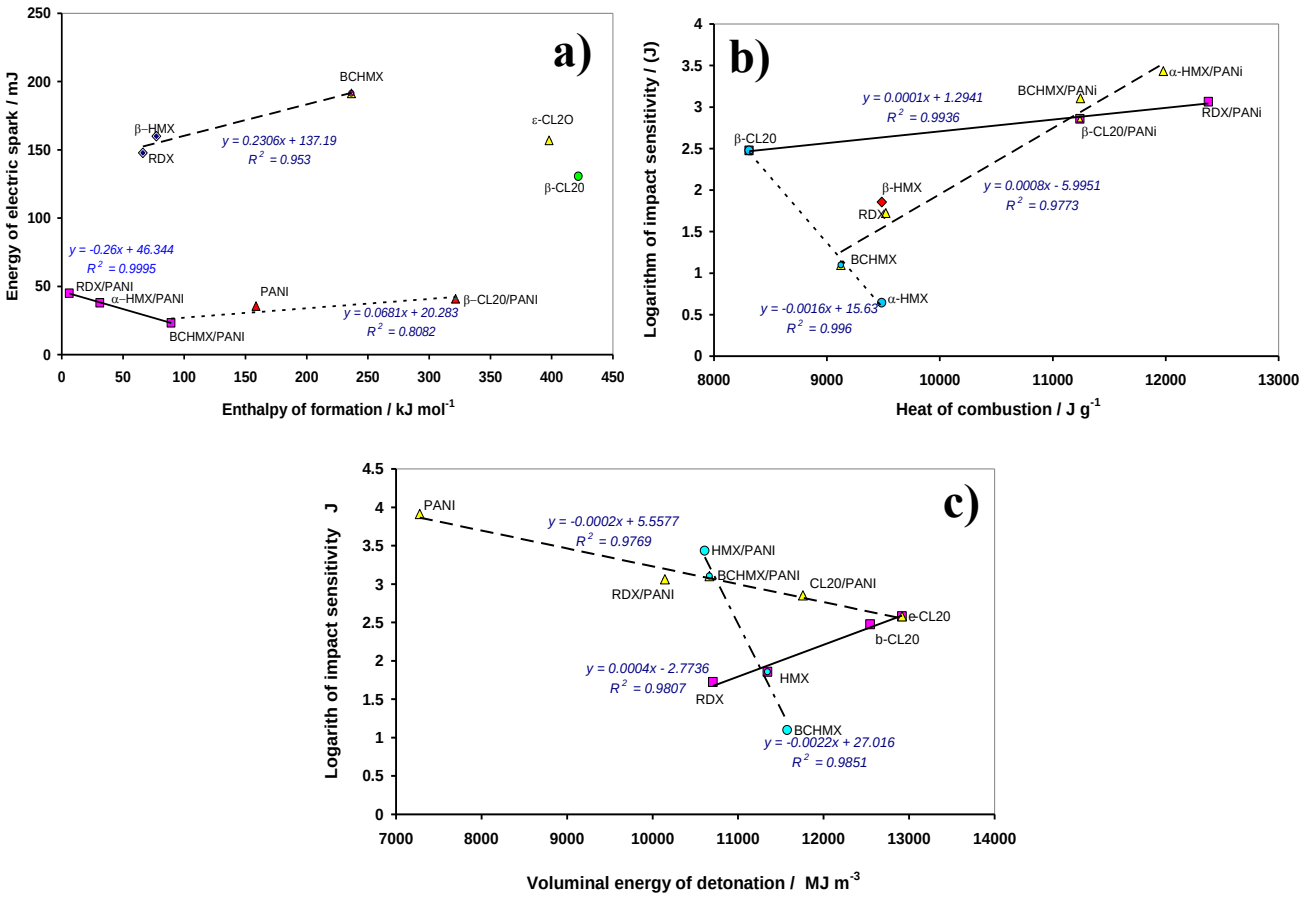

Figure 3.4.9 Dependences connected with the thermochemical aspects of the substances studied:

a) relationship between energy of electric spark (needed for 50 % probability of initiation) and enthalpy of formation of the nitramines and their composites studied;
b) semilogarithmic relationship between impact sensitivity (expressed as drop energy in J) and heat of combustion of the nitramines and their composites studied;
c) semilogarithmic relationship between impact sensitivity (expressed as drop energy in J) and voluminal energy of detonation of the nitramines and their composites studied.

It should be prefaced that pure cyclic nitramines (with save of BCHMX) make an exception to the above-mentioned Licht's rule [29, 34], as can be seen in all the illustrations of Figure 3.4.9. This exception is still waiting for scientific explanation. The sensitivity to electrical spark versus to enthalpy of formation (Figure

3.4.9a) [35, 36] corresponds within expectations, with some exception for β-CL20/PANi, whose specific structure has already been mentioned above and which might by a reason of this expectation. It is quite possible that during the initiation of the composites, the PANi itself is simultaneously attacked by the discharge. It is perhaps worth mentioning here that in nitramines the energy of the electric spark is semilogarithmically proportional to the length of the longest N-N bonding their molecules [22] (with this may also be connected the position of the β-CL20/PANi data in Figure 3.4.9a).

The relationship between impact sensitivity and energy content can be presented in a semilogarithmic version by Figure 3.4.8b: here the energy content, represented by heat of combustion [35], increases from the right to the left of this Figure. and, except for pure nitramines β-CL20, BCHMX, α-HMX, is in full agreement with Licht's rule. The same is possible about Figure 3.4.8c [29, 34].

3.4.5. Summary

Composite micro-particles of electrically conductive polyaniline (PANi) with attractive cyclic nitramines RDX, HMX, BCHMX and CL20 were prepared by co-precipitation from a mixed solution and subsequent co-agglomeration of the resulting coprecipitates. These composites are essentially charge transfer complexes, which is related to their somewhat lower thermal stability compared to the starting nitramines. The powder X-ray diffraction results showed changes in polymorph modifications in CL20 (from ε to β) and HMX (from β to α) during this preparation which was also confirmed with the spectral and differential thermal analysis techniques. FESEM images in all composite micro-crystals showed smothered surfaces and two major kinds of crystals which centre-cored one and another superficially coated which made the nitramine crystals edges rounded. This method of coating nitramine microcrystals significantly reduces their impact sensitivity, especially HMX (to 31 J from the original of 6.4 J), which is present in the composite in its α-modification, which is in its pure state extremely sensitive to impact (1.9 J).

Among the spectral outputs of the study of the prepared composites, the FTIR symmetrical NO_2 and N-O bond stretching, the N-N bond stretching and new quantum yield from fluorescence application are logically related to their initiation reactivity (i.e., impact and electric spark sensitivities), relating to the nitraminic components of composites. However, a relationship was also found and explained between impact sensitivity and the benzene unit deformation in the emeraldine salt of PANi chains and linear logical relationships between detonation rates and both the FTIR symmetric N-O bond stretching and quantum yield. The known effect of increasing the detonation parameters of explosives mixtures, compared to those calculated for their percentage representation in the mixture, is greater for the PANi composites than for conventional co-crystals. The interesting sensitivity characteristics of the PANi composites, and their easy preparation, should determine their potential use as a part of different initiators for various charges.

References

[1] V. B. Patil, S. Ture, C. Yelamaggad, M. Nadagouda, and A. Venkataraman, “Turn-off Fluorescent Sensing of Energetic Materials using Protonic Acid doped Polyaniline: A Spectrochemical Mechanistic Approach,” Z. Anorg. Allg. Chem., vol. 647, no. 4, pp. 331–340, Feb. 2021, doi: 10.1002/zaac.202000321.

[2] V. B. Patil, M. Nadagouda, S. Ture, C. Yelamaggad, and V. Abbaraju, “Detection of energetic materials via polyaniline and its different modified forms,” Polym. Adv. Technol., vol. 32, no. 12, pp. 4663–4677, Dec. 2021, doi: 10.1002/pat.5458.

[3] S. Ture, S. Pattathil, V. B. Patil, C. Yelamaggad, R. Martinez-Manez, and V. Abbaraju, “Synthesis and fluorescence sensing of energetic materials using benzenesulfonic acid-doped polyaniline,” J. Mater. Sci.-Mater. Electron., doi: 10.1007/s10854-021-06537-7.

[4] S. Ture, V. B. Patil, C. Yelamaggad, R. Martinez-Manez, and V. Abbaraju, “Understanding of mechanistic perspective in sensing of energetic nitro compounds through spectroscopic and electrochemical studies,” J. Appl. Polym. Sci., vol. 138, no. 32, Aug. 2021, doi: 10.1002/app.50776.

[5] Y. Wang, W. Jiang, X. Song, G. Deng, and F. Li, “Insensitive HMX (Octahydro-1,3,5,7-tetranitro-1,3,5,7-tetrazocine) Nanocrystals Fabricated by High-Yield, Low-Cost Mechanical Milling,” Cent. Eur. J. Energ. Mater., vol. Vol. 10, no. 2, 2013.

[6] M. L. Cheney et al., “Effects of Crystal Form on Solubility and Pharmacokinetics: A Crystal Engineering Case Study of Lamotrigine,” Cryst. Growth Des., vol. 10, no. 1, pp. 394–405, Jan. 2010, doi: 10.1021/cg901010v.

[7] Z. Xue, B. Huang, H. Li, and Q. Yan, “Nitramine-Based Energetic Cocrystals with Improved Stability and Controlled Reactivity,” Cryst. Growth Des., vol. 20, no. 12, pp. 8124–8147, Dec. 2020, doi: 10.1021/acs.cgd.0c01122.

[8] V. Patil, K. Zalewski, J. Schuster, P. Belina, W. Trzcinski, and S. Zeman, “A new insight into the energetic co-agglomerate structures of attractive nitramines,” Chem. Eng. J., vol. 420, Sep. 2021, doi: 10.1016/j.cej.2021.130472.

[9] V. B. Patil, P. Bělina, W. A. Trzcinski, and S. Zeman, “Preparation and properties of co-mixed crystals of 1,3-di- and 1,3,5-tri-amino-2,4,6-trinitrobenzenes with attractive cyclic nitramines,” J. Ind. Eng. Chem., vol. 115, pp. 135–146, Nov. 2022, doi: 10.1016/j.jiec.2022.07.043.

[10] V. B. Patil, P. Bělina, W. A. Trzcinski, and S. Zeman, “Co-agglomerated crystals of 2,2′,4,4′,6,6′-hexanitro - stilbene/-azobenzene with attractive nitramines,” Chem. Eng. J., vol. 457, p. 141200, Feb. 2023, doi: 10.1016/j.cej.2022.141200.

[11] V. B. Patil et al., “Co-agglomerated crystals of cyclic nitramines with sterically crowded molecules,” CrystEngComm, p. 10.1039.D2CE00840H, 2022, doi: 10.1039/D2CE00840H.

[12] G. Liu, H. Li, R. Gou, and C. Zhang, “Packing Structures of CL-20-Based Cocrystals,” Cryst. Growth Des., vol. 18, no. 11, pp. 7065–7078, Nov. 2018, doi: 10.1021/acs.cgd.8b01228.

[13] H. R. Pouretedal, S. Damiri, and A. Zandi, “Study the operating conditions on agglomeration of RDX particles in anti-solvent crystallization by using statistical optimization,” Def. Technol., vol. 15, no. 2, pp. 233–240, Apr. 2019, doi: 10.1016/j.dt.2018.09.007.

[14] I. Yu. Sapurina and M. A. Shishov, “Oxidative Polymerization of Aniline: Molecular Synthesis of Polyaniline and the Formation of Supramolecular Structures,” in New Polymers for Special Applications, A. De Souza Gomes, Ed., InTech, 2012. doi: 10.5772/48758.

[15] Ph. Colomban, S. Folch, and A. Gruger, “Vibrational Study of Short-Range Order and Structure of Polyaniline Bases and Salts,” Macromolecules, vol. 32, no. 9, pp. 3080–3092, May 1999, doi: 10.1021/ma981018l.

[16] J. R. Lakowicz, Ed., “Solvent and Environmental Effects,” in Principles of Fluorescence Spectroscopy, Boston, MA: Springer US, 2006, pp. 205–235. doi: 10.1007/978-0-387-46312-4_6.

[17] Fried, L E., “CHEETAH 1.39 Users’ Manual UCRL-MA-117541.” CA: Lawrence Livermore National Laboratory., 1996.

[18] Hobbs, M. L. and M. R. Baer, “Calibrating the BKW-EOS with a large products species base and measured C-J properties.,” in Proceedings of the 10th Symposium (International) on Detonation, 1993, pp. 409–418.

[19] Ficket, W. and W. C. Davies, Detonation. Berkeley, CA: University of California Press, 1979.

[20] W. C. Davis and W. Fickett, “DETONATION THEORY AND EXPERIMENT.,” Pp 2-12 Behav. Dense Media High Dyn. Press. N. Y. Gordon Breach 1968, Oct. 1969, Accessed: Aug. 14, 2021. [Online]. Available: https://www.osti.gov/biblio/4785669

[21] Muhamed Sućeska, Test Methods for Explosives. Springer, 2012.

[22] S. Zeman and N. Liu, “A new look on the electric spark sensitivity of nitramines,” Def. Technol., vol. 16, no. 1, pp. 10–17, Feb. 2020, doi: 10.1016/j.dt.2019.06.023.

[23] Fraunhofer Institut für Chemische Technologie, Pfinztal, Germany, 2004, “ICT Database of thermochemical values.” 2004.

[24] H. S. Kolla, S. P. Surwade, X. Zhang, A. G. MacDiarmid, and S. K. Manohar, “Absolute Molecular Weight of Polyaniline,” J. Am. Chem. Soc., vol. 127, no. 48, pp. 16770–16771, Dec. 2005, doi: 10.1021/ja055327k.

[25] G. B. Manelis, Thermal Decomposition and Combustion of Explosives and Propellants. London: CRC Press, 2014. doi: 10.1201/9781482288261.

[26] S. Zeman, “Characteristics of Thermal Decomposition of Energetic Materials in a Study of Their Initiation Reactivity,” in Handbook of Thermal Analysis and Calorimetry, vol. 6, Elsevier, 2018, pp. 573–612. doi: 10.1016/B978-0-444-64062-8.00006-1.

[27] S. Kaya, C. Kaya, I. B. Obot, and N. Islam, “A novel method for the calculation of bond stretching force constants of diatomic molecules,” Spectrochim. Acta. A. Mol. Biomol. Spectrosc., vol. 154, pp. 103–107, Feb. 2016, doi: 10.1016/j.saa.2015.10.030.

[28] V. Gold, Ed., The IUPAC Compendium of Chemical Terminology: The Gold Book, 4th ed. Research Triangle Park, NC: International Union of Pure and Applied Chemistry (IUPAC), 2019. doi: 10.1351/goldbook.

[29] S. Zeman and M. Jungová, “Sensitivity and Performance of Energetic Materials,” Propellants Explos. Pyrotech., vol. 41, no. 3, pp. 426–451, Jun. 2016, doi: 10.1002/prep.201500351.

[30] S. Zeman, “The Chemical Micromechanism of Energetic Material Initiation,” in Nano and Micro-Scale Energetic Materials, John Wiley & Sons, Ltd, 2023, pp. 567–623. doi: 10.1002/9783527835348.ch19.

[31] K. L. McNesby and C. S. Coffey, “Spectroscopic Determination of Impact Sensitivities of Explosives,” J. Phys. Chem. B, vol. 101, no. 16, pp. 3097–3104, Apr. 1997, doi: 10.1021/jp961771l.

[32] V. B. Patil, R. Svoboda, P. Belina, and S. Zeman, “Thermal studies of attractive nitramines/polyaniline composite crystals prepared via co-agglomeration,” presented at the NTREM, University of Pardubice, Apr. 2023.

[33] T. Urbanski, “On entropy and free energy of explosives (preliminary communication),” Bull. l’Academie Pol. Des Sci. s, Ser. Des Sci. Chim., vol. 28, pp. 511–513, 1980, doi: https://gallica.bnf.fr/ark:/12148/cb343830642/date1980.

[34] H.-H. Licht, “Performance and Sensitivity of Explosives,” Propellants Explos. Pyrotech., vol. 25, no. 3, pp. 126–132, Jun. 2000, doi: 10.1002/1521-4087(200006)25:3<126::AID-PREP126>3.0.CO;2-8.

[35] S. Zeman, “The influence of energy content and its outputs on the impact sensitivity of high-nitrogen energetic materials, Journal of Energetic Materials,” Journal of Energetic Materials, vol. 40:, no. 1, pp. 1–14, 2022, doi: 10.1080/07370652.2020.1822463.

[36] S. Zeman, “Influence of the energy content and its outputs on sensitivity of polynitroarenes,” J. Energ. Mater., vol. 37, no. 4, pp. 445–458, Oct. 2019, doi: 10.1080/07370652.2019.1634159.

[37] S. Zeman, A. K. Hussein, M. Jungova, and A. Elbeih, “Effect of energy content of the nitraminic plastic bonded explosives on their performance and sensitivity characteristics,” Def. Technol., vol. 15, no. 4, pp. 488–494, Aug. 2019, doi: 10.1016/j.dt.2018.12.003.

3.5 Co-agglomerated crystals of cyclic nitramines with the nitrogen rich 3,6-bis(1H-1,2,3,4-tetrazol-5-ylamino)-1,2,4,5-tetrazine (BTATz)

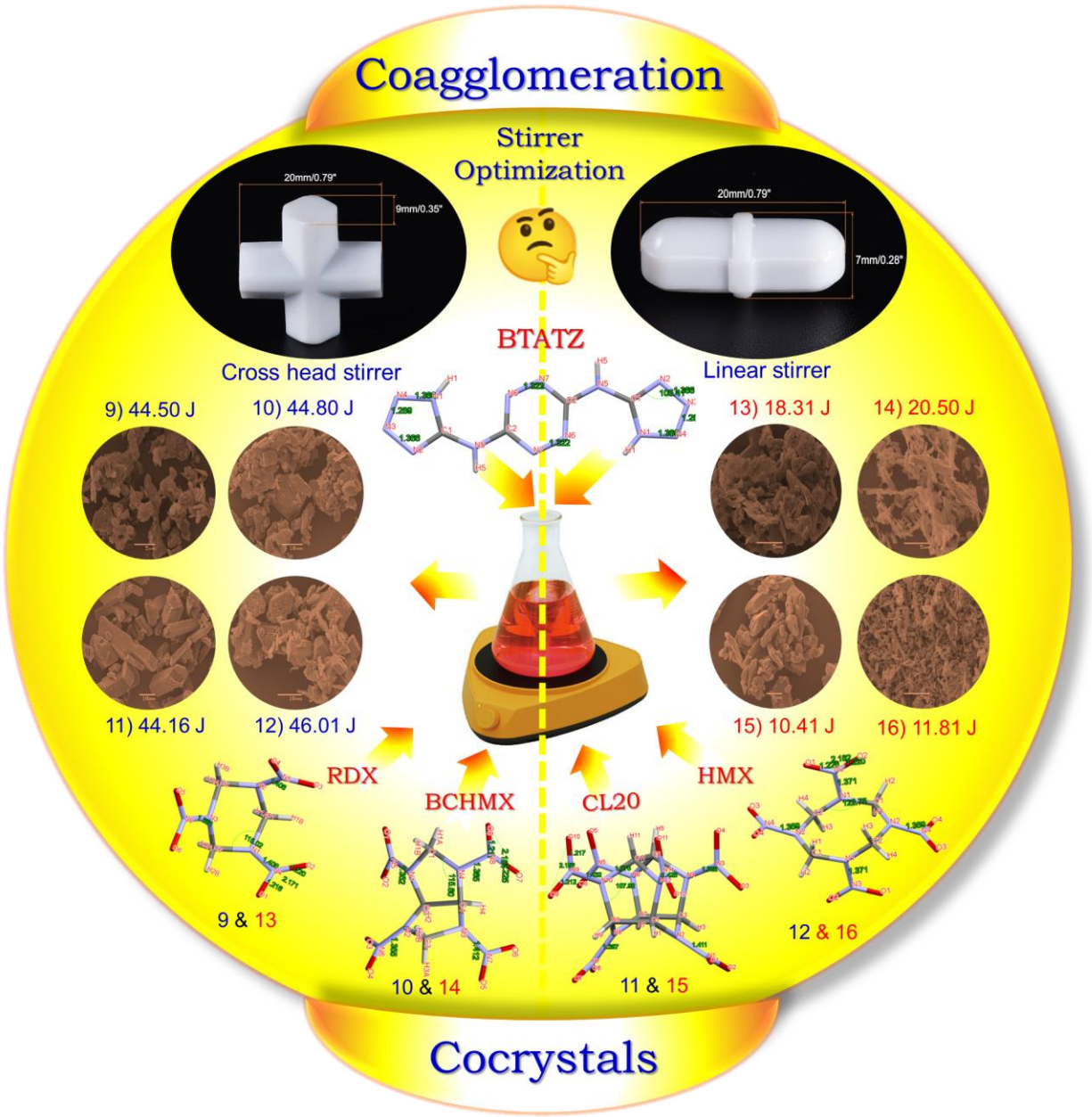

Published in

Chemical Engineering Journal, Vol. 483, 2024, P, 149029, DOI: 10.1016/j.cej.2024.149029

3.5.1 Background

The high nitrogen materials based very interesting are on the s-tetrazine, here namely 3,6-bis(1H-1,2,3,4-tetrazol-5-ylamino)-s-tetrazine (BTATz) [1–3]. BTATz is a strong candidate for phlegmatization of technically appealing cyclic nitramines because, as will be demonstrated here later, it has good explosive qualities and is exceedingly insensitive to impact; these nitramines are cis-1,3,4,6-tetranitrooctahydroimidazo-[4,5-d]imidazole (BCHMX or bicyclo-HMX), ε-2,4,6,8,10,12-hexanitro-2,4,6,8,10,12-hexaazaisowurtzitane(ε-CL-20), ß-1,3,5,7-tetranitro-1,3,5,7-tetrazocane (ß-HMX), and 1,3,5-trinitro-1,3,5-triazinane (RDX) [4].

To reduce the inherent sensitivity of these nitramines, in addition to traditional phlegmatization with polymeric materials [4–7], in some cases also, cocrystallization with suitable energetic materials or, more recently, coagglomeration with suitable coformers can be used. However, both of these mentioned crystal engineering approaches, may not lead to improved properties over the starting coformers (the case of the CL20/TNT cocrystal [8]). Still, by appropriately choosing the molar ratio of the coformers, their molecular structure and the kind of continual phase of the process, remarkably positive results can be obtained [9–13]. Examples of the successes mentioned can be energetic coagglomerates/cocrystals. Examples of the successes mentioned can be energetic coagglomerates/cocrystals of the HMX/TATB & RDX/TATB [10], CL20/BCHMX [11], HMX/HNS[12], CL20/FOX-7 [14], etc. (coagglomerates represent co-mixtures of the own cocrystals with one from the coformers [9–13]).

As far as BTATz is concerned, it has unique molecular structural features for the cocrystals because it contents and allows the formation of =N–H….N– interactions ranging from bridging amines to terminal tetrazoles rings, i.e., both the inter- and intra-molecular hydrogen bonding dominates in its crystals packing arrangement of its structure. BTATz exhibits edge-to-face geometries and sheets stacked vertically and high thermal stability [15]. It shows the effective cocrystal formation with the nonenergetic materials [15, 16]; earlier results have shown that the electrostatic potential plays a key role in the crystallization of BTATz with coformers and suggests that the more polar molecules of the energetic materials may be needed for successful cocrystallization with this high-nitrogen energetic material. At the same time, BTATz lacks solubility in common solvents, and thus it needs to choose a more selective solvent [15]. Earlier results from the BTATz cocrystallization showed its bigger compatibility with energetic materials like K-6 (2-oxo-1,3,5-trinitro-1,3,5-triazinane), LLM-107 (1,4,5,7-tetranitro-1,4,5,7-tetraazabicyclo[4.3.0] nonan-6-one - TNPDU), and NTO (5-nitro-1,2,4 triazol-3one) etc. [15, 17]. The application of BTATz as a coformer also brings a significant reduction in the sensitivity of the resulting cocrystal, and the effect of its density on those of this product is not negligible [15, 17]. The energetic cocrystals of BTATz are as yet very poorly

understood. Therefore, not without interest what effect this high nitrogen material will have on the properties of the technically attractive cyclic nitramines and is the focus of this work.

3.5.2 Results

3.5.2.1 Powder X-Ray diffraction (PXRD) studies:

To understand intriguing changes in crystal morphologies and crystalline phase PXRD and FESEM analysis were carried out. The observed results from PXRD at room temperature are summarized in Table 3.5.1 and corresponding diffractograms in Figure 3.5.1. The RDX values of 2Ɵ are 15.65º, 15.90º, 19.85º, 24.10º, 29.83º, 30.10º, 32.50º, 33.15º and 35.64º, 8º. For HMX are 13.71º, 19.37º, 23.27º, 25.55º, 29.71º, 30.94º, 36.19º and 39.20º. For BCHMX 2Ɵ values are 15.65º, 15.90º, 19.85º, 24.1º, 29.81º, 30.10º, 32.51º, 33.15º and 35.64º. For ε- CL20: 11.88º, 12.40º, 17.64º, 20.40º, 24.70º, 27.62º, 28.78º, 31.84º, 32.98º, 37.98º, 44.44º, 45.38º. Similarly, for BTATZ 13.22º, 15.26º, 16.34º, 17.20º, 30.28º, 31, 32.16º, 34.94º, 36.74º.

Table 3.5.1 PXRD data for pure nitramines and CACs

Sr No	Code design	2Ɵ values for intense peaks / ˚
1	ε-CL-20	14.30, 30.10, 42.98
2	β-CL-20	12.66, 13.86, 30.34
3	BCHMX	9.74, 12.65 and 23.57
4	β-HMX	14.61, 16.31, 24.45, 25.07, 32.31
5	δ-HMX	13.10, 17.02, 24.34
6	α-HMX	20.52, 27.20, 29.66, 31.94
7	BTATZ	12.88, 17.66, 20.18, 21.82, 25.18, 26.78, 29.14
7	**9)** RDX/BTATz B1	12.88, 17.66, 20.18, 21.82, 25.18, 29.14
8	**10)** RDX/BTATz B2	13.02, 17.78, 20.30, 21.94, 25.30, 29.22
9	**11)** HMX/BTATz B1	14.60, 20.46, 22.94, 31.82
10	**12)** HMX/BTATz B2	14.60, 20.46, 22.96, 31.84
11	**13)** CL20/BTATz B1	12.02, 13.66, 20.08, 27.92
12	**14)** CL20/BTATz B2	12.02, 13.66, 20.08, 27.93
13	**15)** BCHMX/BTATz B1	12.94, 16.18, 23.88, 27.74
14	**16)** BCHMX/BTATz B2	12.64, 16.15, 23.58, 29.82

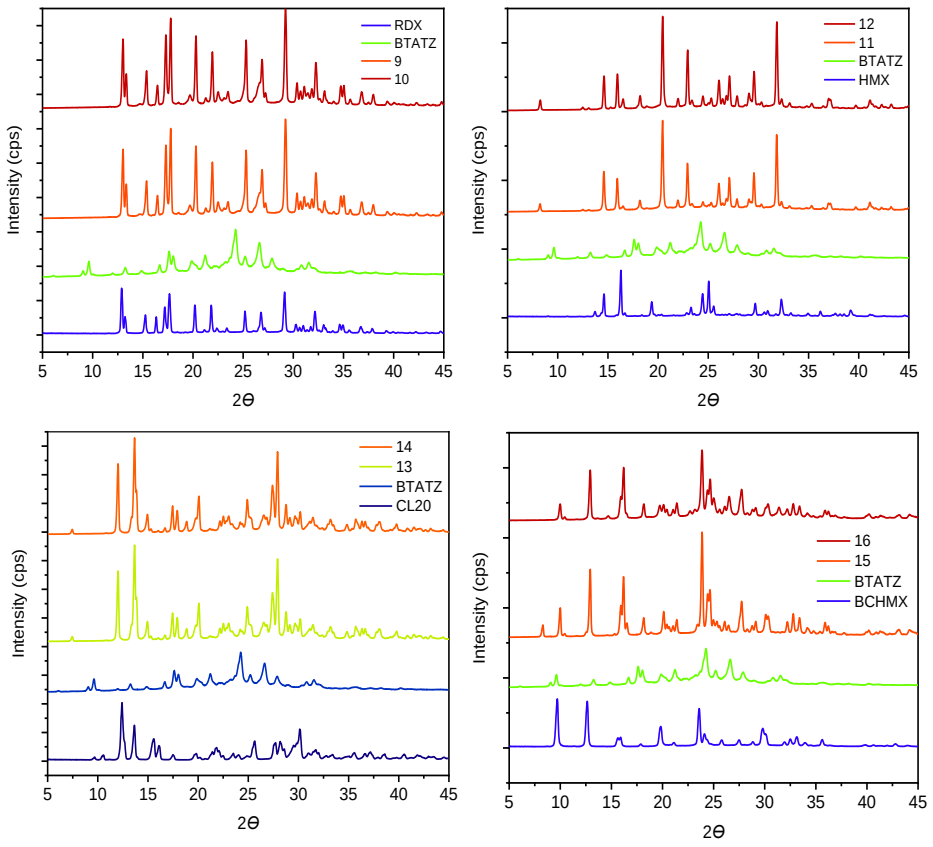

Figure 3.5.1 PXRD diffractograms of Coagglomerated crystals /cocrystals (CACs) 9) RDX/BTATz B1, 10) RDX/BTATz B2, 11) HMX/BTATz B1, 12) HMX/BTATz B2, 13) CL20/BTATz B1, 14) CL20/BTATz B2, 15) BCHMX/BTATz B1 and 16) BCHMX/BTATz B2

Coming to effect of the coagglomeration effect on the obtained CACs showed effective polymorphic changes in nitramines to amend the crystal lattice of the BTATZ. In RDX/BTATz-1: 13.22º, 15.26º, 16.34º, 17.20º, 26.78º, 30.28º, 32.16º, 34.62º and in B2: 13.34º, 15.38º, 16.46º, 17.30º, 26.64º, 26.88º, 30.38º, 31.10º, 31.84º, 32.24º, 35.04º. HMX/BTATz B1: 15.94º, 26.06º, 27.10º, 29.56º and B2: 15.94º, 26.08º, 27.12º, 29.56º, in both batches HMX converted from β to α modification. CL20/BTATz B1: 13.86º, 14.96º, 17.46º, 17.92º, 24.90º, 26.56º, 27.42º, 28.78º, 30.18º and B2: 13.66º, 14.96º, 17.47º, 17.92º, 20.08º, 24.90º, 26.56º, 27.42º, 28.78º, 30.18º in both batches CL20 converted from ε to β modification. BCHMX/BTATz B1: 10.0º, 15.92º, 20.12º, 24.42º, 30.12º, 30.32º, 32.8º and in B2: 9.72º, 15.96º, 19.84º, 30.10º, 30.82º, 33.14º. More convenient form, the remaining main intense peaks were mentioned in tabulated form in Table 3.5.1.

Overall, all the CACs show different polymorphic crystalline phases compared with their pure forms of nitramines, with the appearance of new peaks in PXRD diffractograms, some new doublet formation and new intense as well as small intense peaks. These all clearly show that active intermolecular interactions

occur between the attractive nitramines and BTATz. It further suggests changes in the cocrystal characteristics. In particular, in the case of HMX, it appears that BTATz stabilizes metastable α-HMX in the respective CACs, which may be due to the crystal arrangement of HMX in the BTATz interspace.

3.5.2.2 Morphology and Particle size analysis

The morphology and particle size analysis were conducted to assess the effect of coagglomeration (instrumental details mentioned in Supplementary information S2.1). From the morphological studies it was found that CACs contain generally irregular shapes and microcrystals. In the case of both RDX batches, crystals have round-shaped edges. Whereas in the case of both HMX batches their crystals are definite shapes with slightly porous surface and with smoothened crystal edges. In the case of CL20 samples, batch B1 differs from batch B2; the first one with round-edged crystals and batch B2 was found to be more like rice grains with smaller sized needle-shaped crystals. In the BCHMX batch, B1 was found irregularly round shaped edged crystals, and in batch B2, the totally different smaller rice grain shaped smaller broken needle-shaped crystals.

Particle size analysis showed a clear difference in both batches of all nitrmines: in the CACs, batches B1 found bigger crystals, whereas, in the CACs, batches B2 (except in the case of HMX, where practically remain the same particle size) showed the decrease in crystals sizes with an upsurge specific surface area [Dv(50) values are 3 -12 μM and surface are 1200 to 2400 m^2 kg^{-1}].

Table 3.5.2 Particle size measurements of BTATZ CACs

				Particle size analysis			
No	Code design.	Continous Phase	CA Phase	Surface area (m^2/kg)	*Dv*(10) μM	*Dv*(50) μM	*Dv*(90) μM
1	**9** RDX/BTATz B1	DMP/H_2O	CHF	1544	1.68	7.79	20.30
2	**10** RDX/BTATz B2	DMP/ H_2O	CHF	2399	1.14	3.95	16.80
3	**11** HMX/BTATz B1	DMSO/ H_2O	CHF/IPA	1034	4.21	12.8	29.50
4	**12** HMX/BTATz B2	DMSO/ H_2O	CHF/IPA	1237	2.89	12.2	25.01
5	**13** CL20/BTATz B1	DMP/ H_2O	CHF	1311	2.88	16.2	32.10
6	**14** CL20/BTATz B2	DMP/ H_2O	CHF	3154	1.01	2.97	6.55
7	**15** BCHMX/BTATz B1	DMP/ H_2O	CHF	1517	1.73	7.49	16.90
8	**16** BCHMX/BTATz B2	DMP/ H_2O	CHF	2377	1.10	4.52	11.50

Note: DMP - Dimethyl Pyrolidone; CHF- Chloroform, & IPA-Isopropanol and CA- phase coagglomeration solvent

Thus, the cross stirrer (batches B2) could be a better option for coagglomeration than the linear one (batches B1) in terms of crystal morphology and surface area. A survey of the studied samples with detailed analysis

is shown in Table 3.5.2. It can also seen from SEM images of HMX CACs totally different (Figure 3.5.2e - h) from the other CACs.

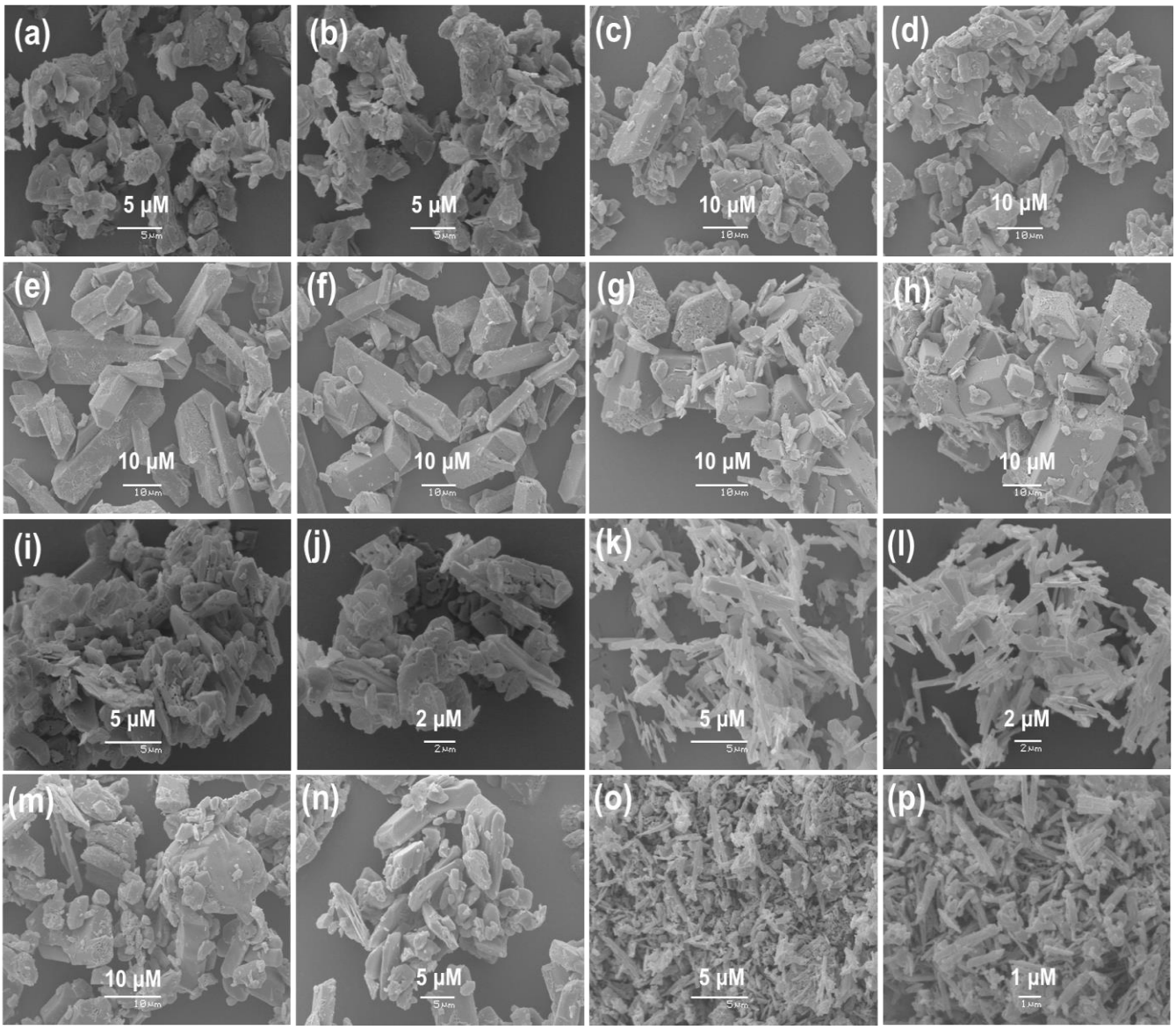

Figure 3.5.2 FESEM images of CACs, a) & b) 9 RDX/BTATz B1; c &d) 10 RDX/BTATz B2; e & f)11, HMX/BTATz B1; g &h) 12 HMX/BTATz B2; I & j) 13 CL20/BTATz B1; k & l) 14 CL20/BTATz B2; m & n) 15 BCHMX/BTATz B1 and o & p) 16 BCHMX/BTATz B2

3.5.2.3 Differential thermal analysis (DTA)

The characteristic thermograms obtained from DTA analysis (experimental details mentioned in Supplementary information S2.8) are shown in Figure 3.5.3, and exothermic and endothermic changes are tabulated in Table 3.5.3.

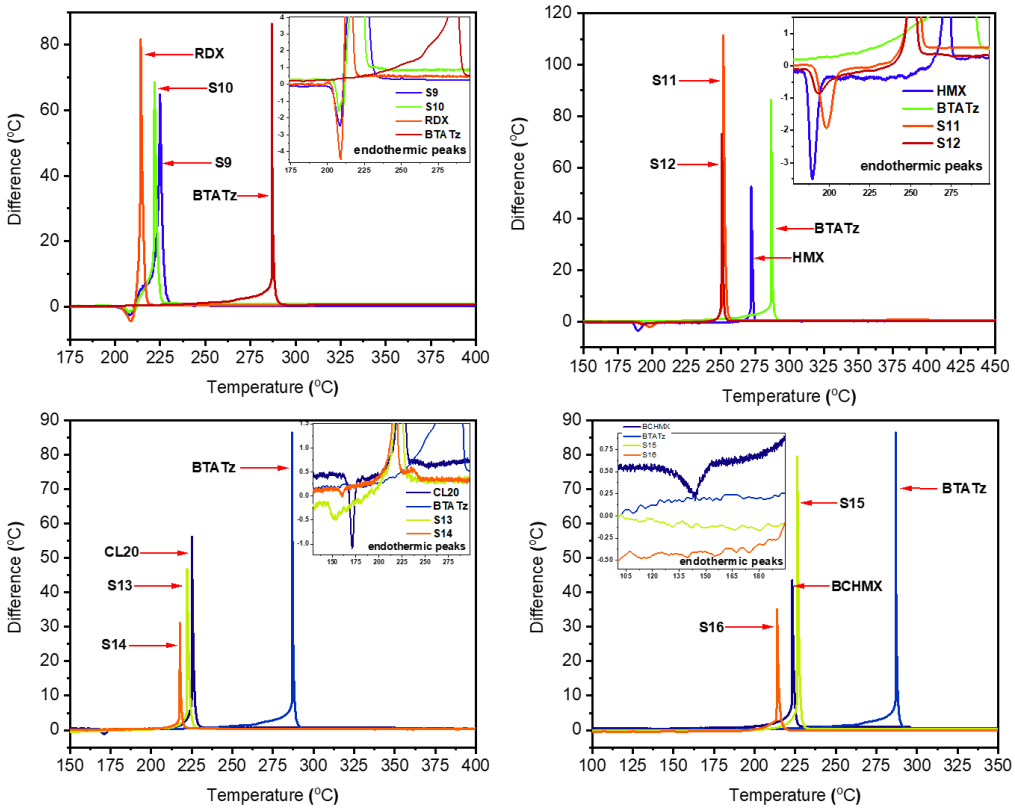

Figure 3.5.3 DTA thermograms of cocrystals 9) RDX/BTATz B1, 10) RDX/BTATz B2, 11) HMX/BTATz B1, 12) HMX/BTATz B2, 13) CL20/BTATz B1, 14) CL20/BTATz B2, 15) BCHMX/BTATz B1 and 16) BCHMX/BTATz B2

The thermograms of CACs are compared with the pure coformers in Figure 3.5.3, and thermal changes are evaluated. The endothermic changes showed that the nitramines polymorphic state in CACs slightly restricts the phase transition. Similarly, the exothermic changes showed ± 2 to 20 °C variation (differences w r t pure nitramines shown in brackets). BTATz is a very thermally stable energetic material [15]. However, after undergoing coagglomeration with nitramines, corresponding CACs showed early decomposition and observed key thermal changes (see Figure 3.5.3). Compared to the net state, RDX is stabilized in its CACs, HMX is more destabilized, CL20 is clearly destabilized, and BCHMX is slightly stabilized in B1 quality and destabilized in B2 quality.

That is, the intermolecular interactions of the coformers (specifically hydrogen bonding, van Der Waals interactions, and π-π stacking) changed in type, intensity, and mutual proportional representation after the entry of nitramines into CAC. Moreover, especially in the case of BCHMX, this documents the influence of chemical engineering parameters on the results of the "slurry cocrystallization".

Table 3.5.3 Summarized data from DTA thermograms of coformers and cocrystals with visible melting points.

Samples	Melting point / ºC [Ref.]	Peaks of changes in DTA record / ºC (with phase modifications)		Ref
		Endothermic	Exothermic	
ε-CL-20	240 decompn [12]	170 (ϵ - γ)	225 (γ - δ)	[12]
α-CL-20	240 decompn [12]	175 (α–γ)	225 (γ–δ)	[12]
BCHMX	286 decompn [12]	--	224	[12]
β-HMX	--	190 (α – δ)	272	[12]
RDX	204	209	215	[12]
BTATz	--	NA	286.81	[Cw]
9 RDX/BTATz B1	--	209.25	224.99 (+9)	[Cw]
10 RDX/BTATz B2	--	207.78, 211.90	222.32 (+11)	[Cw]
11 HMX/BTATz B1	--	199.34	251.97 (-20)	[Cw]
12 HMX/BTATz B2	--	193.19	250.81 (-21)	[Cw]
13 CL20/BTATz B1	--	152.74	222.32 (-2.7)	[Cw]
14 CL20/BTATz B2	--	160.08	217.96 (-7)	[Cw]
15 BCHMX/BTATz B1	--	NA	226.37 (+2.4)	[Cw]
16 BCHMX/BTATz B2	--	NA	213.85 (-10.15)	[Cw]

Note: Here, Cw- results obtained in current work;

3.5.2.4 FTIR Spectral studies

Intermolecular interactions between the coformer BTATz and nitramines are possible to predict on the basis of their bending and stretching vibrational changes in FTIR and Raman spectral studies. The key stretching and bending vibrations are tabularized in Table 3.5.4. BTATz bridging amines to terminal tetrazole rings and located on an inversion center with =NH···N– interactions, also edge-to-face stacking provides more space to geometries; additionally acts as a strong hydrogen donor to the studied nitramines [15]. These structural aspects make changes in CACs can be seen in spectra. A change in stretching of O−N−O---H– structural bond shows that the intramolecular hydrogen bonds switch to the intermolecular hydrogen bonds in the crystal lattice of CACs BTATz with the studied nitramines.

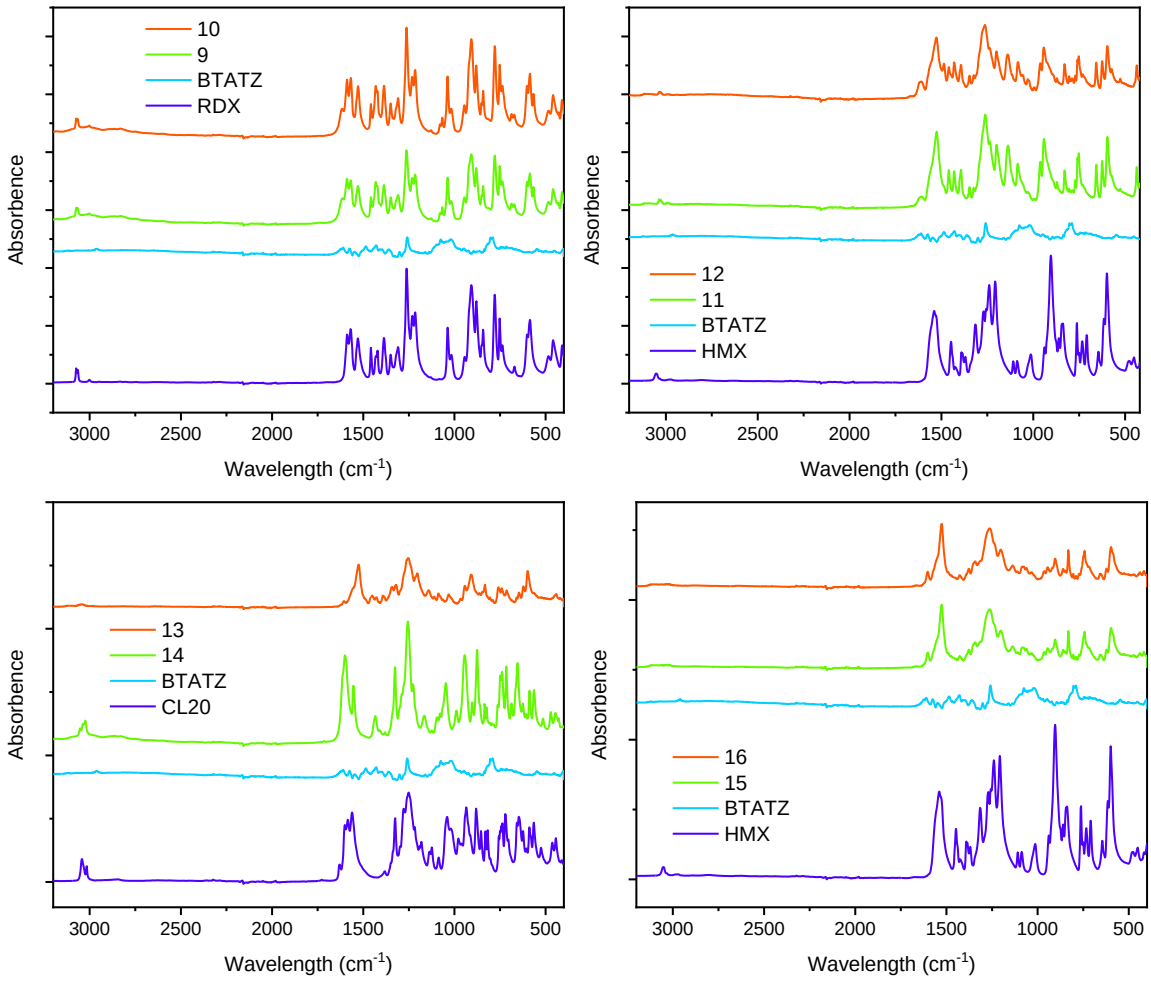

Figure 3.5.4 FTIR spectrum of 9) RDX/BTATZ B1, 10) RDX/BTATZ B2, 11) HMX/BTATZ B1, 12) HMX/BTATZ B2, 13) CL20/BTATZ B1, 14) CL20/BTATZ B2, 15) BCHMX/BTATZ B1 and 16) BCHMX/BTATZ B2

Similarly, the main stretching, like symmetric and unsymmetric -NO_2 stretching vibrations observed at 1230±50 and 1570±10 cm^{-1}, respectively, also shows effective changes. In addition, the same changes are also shown in ring stretching and C-H stretching vibrations. All these changes lead to stabilizing the crystal lattice of CACs through intermolecular interactions oriented in different order. Correspondingly, in the region of 1030–1200 cm^{-1}, the stretching vibrations of the skeleton rings are shifted in the new CACs, which indicates that the rings are stabilized by intermolecular hydrogen bonding.

3.5.2.5 Raman Spectral studies

Table 3.5.4 Summarized results of FTIR measurements

Assignments	CL-20	BCHMX	HMX	RDX	BTATZ	9	10	11	12	13	14	15	16
O-N-O-H-- structural bond	3042	3031	3671	3074	3121	3074	3074	3036	3036	3043	3052	3031	3032
C-H stretching	3042; 3017	3019	3052	3065, 3002	2962,	3066	3066	3027	2992	3016	3024	3018	3018
Symmetrical N-O stretching	1252	1218	1240	1262, 1231, 1216	*	1263, 1309	1263, 1309	1261, 1237	1263, 1237	1253,	1255,	1264	1273
Unsymmetrical N-O stretching	1562	1562	1539	1569	1575, 1547	1589, 1569	1589, 1568	1608	1610	1563, 1602	1554, 1600	1526, 1603	1531, 1603
C-N stretching [Amino group]	757	774	733, 763	737, 752, 779	790, 745, 715	779, 752, 737	779, 752, 737	771, 759, 752	771, 759, 752	721, 756, 743	716, 749, 738	772, 742, --	774, 742,
C-N stretching [Nitro group]	1326	1326	1315	1309	1301	1386	1386	1325, 1347	1325, 1347	1326, 1353	1326, 1380	1377, 1342,	1376, 1356,
Skeletal stretching [Ring]	1182; 1040	1137; 1084	1207, 1087	1216, 1037	1075	1215, 1067	1216, 1038	1137	1139	1124, 1084	1125, 1047	1137 1078, 1061, 1034	1136 1080, 1067, 1044
Symmetric - NO_2 Stretching	1252, 1218 1280	1273 1209	1270, 1240,	1309, 1350	1301, 1361	1231, 1263, 1215	1232, 1263, 1216	1237, 1261, 1200	1237, 1263, 1200	1219, 1253, 1278	1228, 1255,	1264 1202	1273, 1208
Asymmetric - NO_2 Stretching	1632, 1601, 1585, 1562	1603, 1554, 1526	1539	1529, 1569, 1588	1547*, 1575*, 1610*, 1623*	1614, 1589, 1569, 1529	1616, 1589, 1568, 1528	1608, 1526	1610, 1527	1602, 1563, 1586	1600, 1554,	1603, 1526,	1603, 1531, 1551

Note: * The ring structure (above 1320 cm^{-1}), absent in pure BTATZ molecules with centre of symmetry (1500 -1600 cm^{-1}).

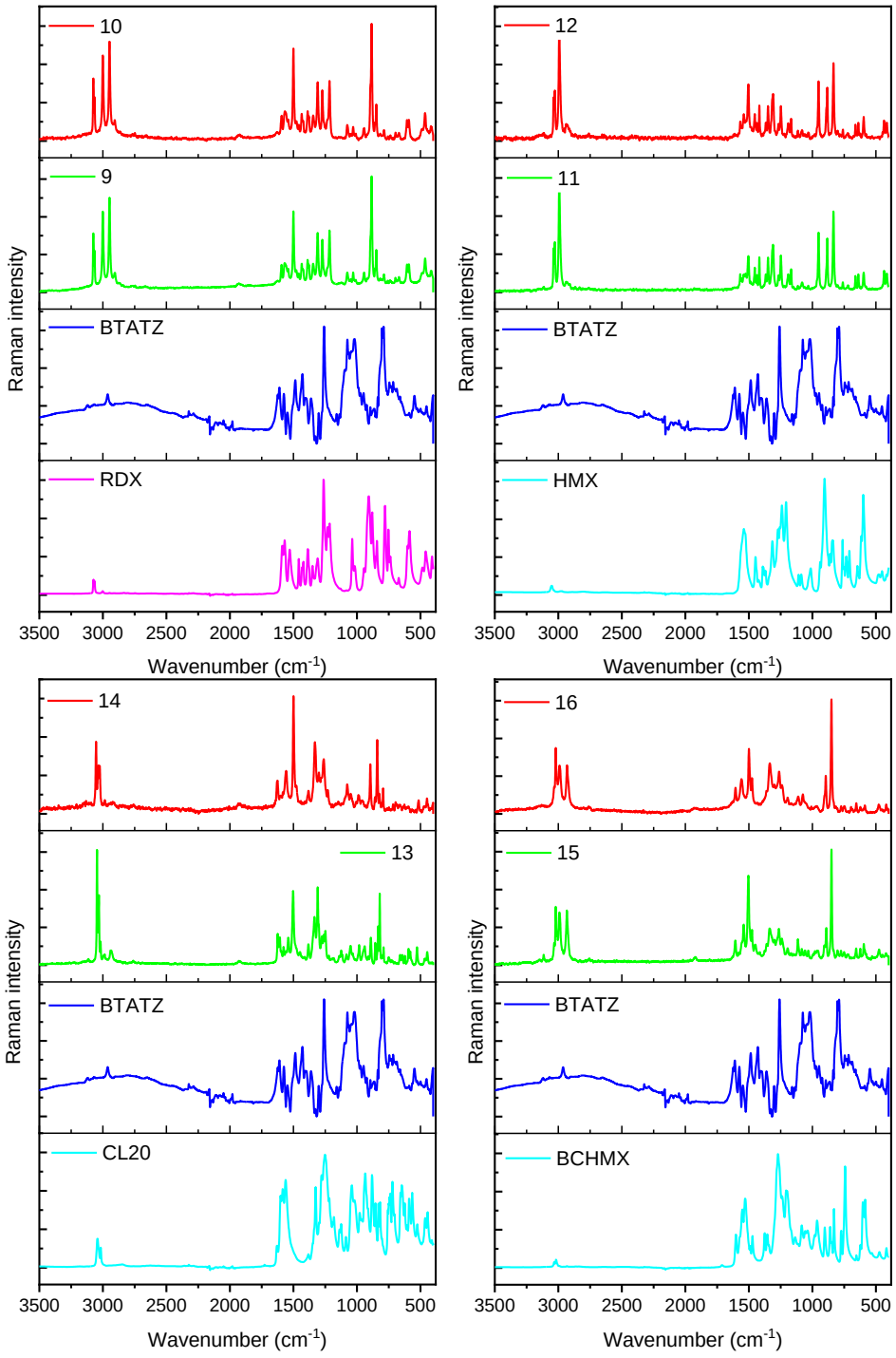

Figure 3.5.5 Raman spectrum of 9) RDX/BTATZ B1, 10) RDX/BTATZ B2, 11) HMX/BTATZ B1, 12) HMX/BTATZ B2, 13) CL20/BTATZ B1, 14) CL20/BTATZ B2, 15) BCHMX/BTATZ B1 and 16) BCHMX/BTATZ B2

The Raman spectral study of CACs of BTATz showed distinct changes in stretching vibrations compared to the original NAs. The Raman spectral study of CACs of BTATz showed distinct changes in stretching vibrations compared to the original NAs. As mentioned earlier, special characteristics of BTATz (see section 3.5.3.4) effects can be seen in Raman spectral stretching vibrations, asymmetric –ONO stretching vibration band at 760±10 cm^{-1} is shifted to 730±55 cm^{-1}, in which can see all CACs. An asymmetric and symmetric stretching of -NO_2 groups observed at 1480–1600 and 1250 – 1280 cm^{-1}, respectively; there is differential changes are observed as compared to the pure coformers, which indicates there is a formation of intermolecular interactions in CACs between the BTATZ and cyclic nitramines. The CACs of the CL20 spectrum show a band around 280 cm^{-1}. Its β polymorphic modifications were created during coagglomeration from all amounts of entered ε-CL20. The β-CL-20 and α-HMX show O-NO bending vibrations around 838 and 834 cm^{-1}, respectively. In the region of 1304 –1320 cm^{-1}, the O-N-O symmetric stretching was observed in all the CACs, compared to the pure starting NAs. Observed bands at 1210±5 cm^{-1} originated from C-H bending vibrations, and the ones at 1010±30 cm^{-1} show N-N stretching vibrations; these changes indicate the active involvement of BTATZ in CACs formation.

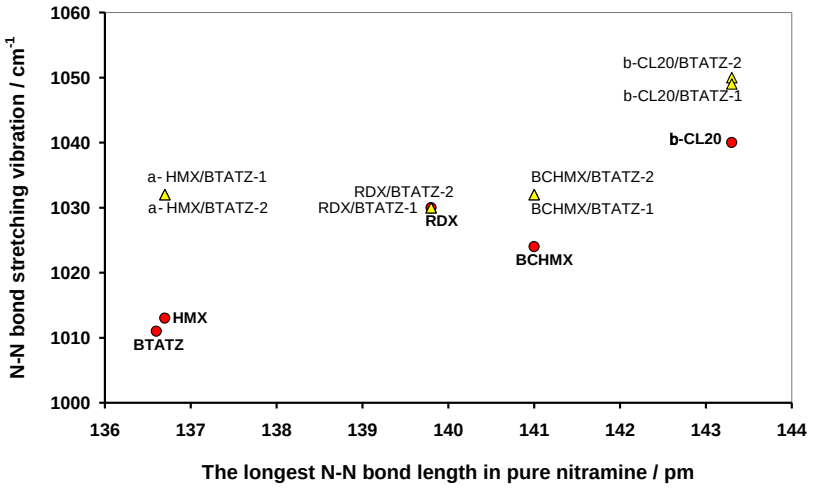

Figure 3.5.6 A comparison of the lengths of the longest N-N bonds with the N-N bond stretching vibration of pure nitramines, their CACs and BTATZ (triangular points are the co-crystals data); the N-N bond lengths are taken from the ORTEP molecular structures of the nitramines used in the CCDC database.

These distinct changes in mentioned characteristics of CACs, as compared to their coformers, indicate strong intermolecular and interlayered interactions. BTATz shows sandwich-type stacking [15], which helps to align the nitramines easily, as observed in the other stretching vibrations in Table 3.5.5. The effect of the formation of BTATz coagglomerates/co-crystals on the change in N-N bond stretching vibration is graphically documented in Figure 3.5.6; a zero change in this vibration is noted for RDX, which, however, has a similar behaviour in its interactions also with other coformers [9–13]. Overall, as per outputs of the

realized FTIR and Raman spectral analysis (also in our recent papers [9–13]) it strongly shows that there are cocrystals formation during coagglomeration.

From the spectral studies, it is clear that strong and complementary intermolecular interactions favor cocrystallization. However, other elements, such as each of the coformers molecular shape and lattice energy, can also have an impact on the outcome.

3.5.2.6 Thermochemical and Explosive Properties

The heat of combustion of pure nitramines and their BTATZ CACs was considered for the calculation of thermochemical parameters. Density was measured using a gas pycnometer, and the composition of the CACs was obtained from elemental analysis. The enthalpy of formation was calculated using these data and Hess's law. The results obtained are summarized in Table 3.5.6. The densities of the BTATZ CACs are relatively high compared to the nitramines (shown in Table 3.5.6), in some cases, slightly higher ones than pure nitramines (this might be due to polymorphic transitions and consequent by strong and complementary intermolecular interactions of the morphologically changed coformers). As mentioned earlier, the data were utilized for detonation property calculations using the CHEETA code [18]. Corresponding results are summarized in Table 3.5.7.

Table 3.5.5 Summarized results of Raman measurements

Assignments	CL-20	BCHMX	HMX	RDX	BTATZ	9	10	11	12	13	14	15	16
					3245	--	--	--	--	--	--	3115	--
–CH_2 stretching vibration	3052	3020	-	-	3003	3075	3075			3046	3054	3032	--
	3024				3146	3065	3065	3037	3037	3031	3035	3020	3020
C–H stretching vibration		2992	-	-	2921	3000,	3000,	3027,	3028,	3018	3025	2991	2990
					2856	2948	2948	2992	2992				
		2932			2805	2905	2905	--	--	2986	2984	2932	2931
Asymmetric –NO_2 stretching vibration	1594	1606	1568	1580-1485	--	1593,	1593,	1568	1568	1624, 1607	1557, 1626	1606,	1605,
	1554	1557	-	-	1560*	1567	1568	1541	1540	1503, 1577	1500	1504, 1541	1499, 1559
C–H and –CH_2 deformation vibration	1326,	1299	1315, 1270	1310, 1273	1339	1378, 1345	1378, 1344	1367, 1349	1367, 1349	1335, 1382	1331, 1382	1299, 1337,	1298, 1335,
Symmetric –NO_2 stretching vibration	1280, 1252	1273, 1264, 1240	1240, 1270	1217, 1273	*	1273, 1216	1273, 1216	1267, 1248	1267, 1248	1309, 1276, 1262, 1248	1299, 1261, 1230,	1264, 1240	1262, 1240
Asymmetric C–H stretching vibration	1164, 1182, 1137	1194, 1167	1207	1217	1117, 1138, 1156	1076	1076	1190, 1168, 1114,	1190, 1167, 1115,	1124, 1183, 1114	1147, 1191	1194, 1114	1195, 1111
N–N stretching vibration	1040, 1018, 979	1024	1013	1030	1011	1030	1030	1032	1032	1050	1049	1032	1008
C–C stretching vibration	1048	1058	1087	1085	1077	1048	1047	1081	1082	1082	1077	1059	1075
Ring stretching vibration	979	967	939	943	963	--	--	--	--	983	989	--	--
	935	906	904	--	895	944	943	952	952	--	--	--	--
Ring deformation vibration	913	850	850	848	963	848	848	834	834	939	938	961	968
	881	906	--	885	895	885	885	883	883	891	895	890	895
–NO_2 deformation vibration	854 831	--	--	--	804	816	816	834	834	856	858	850	850
	819	--	--	--	--	--	--	--	--	833, 821	841, 823	--	--
	743	775	775	788	777	788	787	760	780, 760	790, 803	794, 804	775, 750	7754 750
–NO_2 Wagging	737	750	750	757	716	758, 739, 695	755, 738, 696	720 661	721 661	790	794	716	695

Note: * The ring structure (1320-1495 cm^{-1}), absent in pure BTATZ molecules with centre of symmetry (1500-1600 cm^{-1})

Note: * The ring structure (1320-1495 cm^{-1}), absent in pure BTATZ molecules with centre of symmetry (1500-1600 cm^{-1})

Table 3.5.6 Molecular formulas, thermochemical properties, and maximal crystal densities of pure substances and corresponding CACs

Explosive					Heat of combustion		Enthalpy of formation		
No	Code design.	Molar ratio Nitram/ BTATZ	Formula	Mol. weight	Q_c ($J.g^{-1}$)	Ref	ΔH_f ($kJ.mol^{-1}$)	Ref	Crystal Density ($g.cm^{-3}$)
1	RDX	--	$C_3H_6N_6O_6$	222.14	9522	[12]	66.20	[12]	1.810
2	BCHMX	--	$C_4H_6N_8O_8$	294.17	9124	[12]	236.50	[12]	1.860
3	α-HMX	--	$C_4H_8N_8O_8$	296.18			75.02	[19]	1.839
4	β-HMX	--	$C_4H_8N_8O_8$	296.18	9485	[12]	77.30	[12]	1.902
5	β-CL20	--	$C_6H_6N_{12}O_{12}$	438.23	8327	[12]	421.74	[12]	1.985
6	ε-CL20	--	$C_6H_6N_{12}O_{12}$	438,23	8311	[12]	397.80	[12]	2.044
7	BTATZ	--	$C_4H_4N_{14}$	248.16	12048	[CW]	842.10	[CW]	1.7178
8	**9** RDX/BTATz B1	1.00:0.20	$C_{2.84}H_{5.16}N_{6.00}O_{4.81}$	200.27	9625	[CW]	72.37	[CW]	1.8562
9	**10** RDX/BTATz B2	1.00:0.21	$C_{2.92}H_{5.38}N_{6.00}O_{5.21}$	207.95	9546	[CW]	66.50	[CW]	1.8634
10	**11** HMX/BTATz B1	1.00:0.29	$C_{4.36}H_{8.03}N_{8.00}O_{7.80}$	297.28	10229	[CW]	176.54	[CW]	1.8835
11	**12** HMX/BTATz B2	1.00:0.28	$C_{4.45}H_{7.77}N_{8.00}O_{7.00}$	285.47	10993	[CW]	276.62	[CW]	1.8555
12	**13** CL20/BTATz B1	1.00:0.45	$C_{6.71}H_{6.92}N_{12.00}O_{10.58}$	424.95	9952	[CW]	524.14	[CW]	1.9692
13	**14** CL20/BTATz B2	1.00:0.40	$C_{5.66}H_{6.18}N_{12.00}O_{10.13}$	404.40	8787	[CW]	711.54	[CW]	2.0041
14	**15** BCHMX/BTATz B1	1.00:0.27	$C_{4.35}H_{6.02}N_{8.00}O_{6.64}$	276.59	10177	[CW]	241.96	[CW]	1.8341
15	**16** BCHMX/BTATz B2	1.00:0.24	$C_{4.87}H_{8.46}N_{8.00}O_{9.13}$	238.64	9975	[CW]	287.28	[CW]	1.8697

Note: Here, Cw- results obtained in current work; calculation of hypothetical formulas of the CACs prepared from the elemental analysis.

Another important issue is the impact sensitivity of the CACs studied; it was determined utilizing a standard impact tester (Julius Peters [20]) with exchangeable anvil, with the amount of the tested substance being 50 mm^3 and the drop hammer used to weigh 5 kg, as earlier described in our previous papers [9–13] . Results for both the 50 and 95 % probability of initiation are summarized in Table 3.5.7.

Table 3.5.7 Impact sensitivity and explosive properties of pure substances and corresponding CACs

Explosive		Impact sensitivity E_{dr}			Detonation velocity, D	Detonation pressure, P	Energy of detonation, E_{deton}
Sr No	Code design.	E_{dr} 50 % (J)	Ref.	E_{dr} 95 % (J)	($m.s^{-1}$)	(Gpa)	($J.g^{-1}$)
1	RDX	5.6	[12]	--	9014	33.91	5915
2	BCHMX	3.0	[12]	--	9116	36.19	6223
3	α-HMX	1.9	[21]	--	9126	35.05	5904
4	ß-HMX	6.4	[12]	--	9404	38.00	5964
5	ß-CL-20	11.9	[12]	--	9421	40.77	6320
6	ε-CL-20	13.2[a] 4.0 [b]	[12] [22]	--	9650	43.41	6303
7	BTATZ	78.50	[CW]	93.62	7291	20.41	3695
8	**9** RDX/BTATz B1	44.50	[CW]	71.41	8974	34.08	5478
9	**10** RDX/BTATz B2	44.80	[CW]	69.10	9063	34.93	5627
10	**11** HMX/BTATz B1	44.16	[CW]	64.60	9305	37.45	6098
11	**12** HMX/BTATz B2	46.01	[CW]	51.95	9167	36.17	6097
12	**13** CL20/BTATz B1	18.31	[CW]	46.72	9290	39.40	61.51
13	**14** CL20/BTATz B2	20.50	[CW]	25.06	9643	43.30	6633
14	**15** BCHMX/BTATz B1	10.41	[CW]	20.01	8810	33.25	5755
15	**16** BCHMX/BTATz B2	11.81	[CW]	18.06	8857	33.78	5497

Note: a) the value for pure ε-CL-20 [28];
b) the value for "common" (technical) quality of ε-CL-20;

3.5.3 Discussions

3.5.3.1 Co-agglomeration

Coagglomeration realized as the slurry method, emerged as a more effective technique to prepare cocrystals of cyclic nitramines [9–13]; earlier results showed output crystals found interesting properties in thermochemical as well as detonation properties [9–13]. Preliminary semi-plant trials have shown suitability for large-scale preparations with needed technological optimization (preparation coagglomerate RDX/BCHMX for a gun-powder [23]). Intial coprecipitation evolves some bonding between both coformers and subsequently undergoes coagglomeration, predominantly increasing the crystal sizes and surface area uniformity. The aprotic solvent (chloroform) used in coagglomeration has shown good suitability for the coagglomeration process. The earlier polynitroarene coformers showed relatively higher influence on the specific surface areas and particle sizes of CACs significantly increasesed, especially with 1,3,5-triamino-2,4,6-trinitrobenzene (TATB) [10] and significantly also 2,2',4,4',6,6'-hexanitrostilbene (HNS)[12]. The opposite effect is exhibited by 1,3-diamino-2,4,6-trinitrobenzene (DATB) [11] and especially by 2,2',4,4',6,6'-hexanitroazobenzene (HNAB) [12]. Comparing these previous results with those of BTATZ, especially using the crossed (+) stirrer, shows

predominantly higher values (Table 3.5.2). These properties are influenced by supramolecular interactions occurring between both coformers. Especially in the case of TATB [24] and BTATZ [25] showed similar kinds of (face-to-face) stacking interactions, which further helps to incorporate with cyclic nitramines in a crystal lattice. This space is more in the case of BTATZ due to two tetrazole units linked through the sym-tetrazine bridge with cis symmetry order. It further influences not only the crystal quality but also improves of resistance of CACs to the impact.

3.5.3.2. Thermal Analysis

Except for RDX the CACs of other nitramines showed decreased thermal signatures compared to their pure coformers despite the BTATZ being thermally stable energetic molecule. It is logical and it has also been proved in earlier cases of the nitraminic CACs with TATB and DATB [9, 10]. The above shows that there are active intermolecular interactions between BTATZ and the studied nitramines. It is also proven from spectral studies in which van der Waals forces of attraction (which occur mainly between —NO_2, —N–N (nitramines), —N–O----H— type hydrogen bonding, and —CH), and —C–H---π (π - π) stacking with two triazole rings of BTATZ. It acts as a strong hydrogen donor, making these intra and intermolecular interactions stronger and more efficient [15]. The BTATZ thermal decomposition begins by proton transfer [26] and its acidic nature thus may reduce the thermal stability of BTATZ incorporated nitramines mainly in the temperature range over 200°C (see Figure 3.5.3). Taking the exothermic peaks temperatures from Table 3.5.3 (and Figure 3.5.3) it can be seen, except for RDX (decomposing from the very beginning in the liquid state), other nitramines in their BTATZ composites show a decline in these temperatures, this is most pronounced with HMX.

3.5.3.3 Spectral Examination

Spectral (FTIR & Raman) studies showed active interactions between the studied nitramines and BTATZ. These interactions influenced the properties of CACs and clearly implies that there is cocrystal formation during the coagglomeration (see Figure 3.5.6 and section 3.5.3.4 & 3.5.3.5) - resulting from coagglomerates (CACs). However, there are mixtures of these cocrystals, with an excess of one from the coformer (our experience from our recent papers, for example [11]). The stretching vibrations in coagglomerates showed distinguishable shifts viz., N-N (Figure 3.5.6) & C-H stretching, C-H bending with redshifts compared to their pure nitramines (Table 3.5.6 and 3.5.5): for RDX, these changes are almost zero, HMX has the largest increase in N-N stretching vibration of among the nitramines studied, CL20 has a little and BCHMX has a minor decrease in FTIR C-H stretching, all upon transition to the respective agglomerates. In terms of ring deformation, again for RDX, there is almost zero, a large increase for BCHMX, a slight decrease for HMX and a slight increase in the respective values for CL20 as it transitions in the BTATZ complex. Among the other functional groups that may be involved in intermolecular interactions, one should point out the FTIR symmetric N-O stretching, where after the transition to coagglomerates, there is a large increase in values for BCHMX, then a smaller,

approximately equal increase for RDX and HMX, and a very small increase for CL20. The switching of intramolecular and intermolecular interactions causes these changes. In all cases, it is mainly the formation and strengthening of intermolecular hydrogen bonds, in HMX and especially in RDX-complexes, perhaps also π-π stacking (see structural schematic S5f in Supplementary information). Sterically problematic here is the intermolecular interaction of BTATZ with the angularly shaped BCHMX molecule. It can be clearly seen that the PXRD diffractograms show the polymorphic changes in the crystal lattices of nitramines after they are entering in the BTATZ crystal lattice (specifically, the transition of beta-HMX to its alpha-isomer, which may be associated here with the largest change in the N-N bond and C-H stretching in its BTATZ coagglomerates). All these intra/intermolecular interactions help to stabilize the newly formed nitramine/BTATZ crystal lattice.

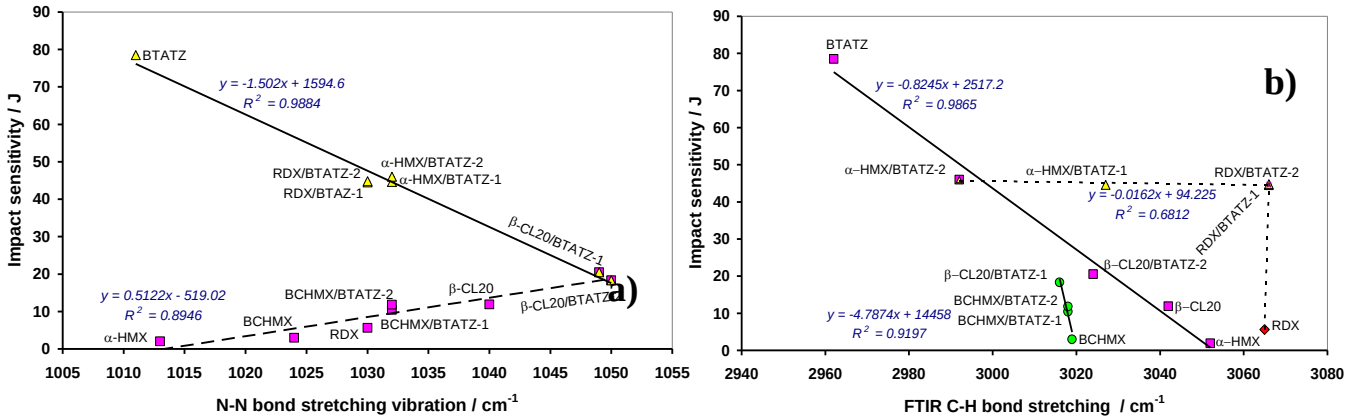

Figure 3.5.7 A comparison impact sensitivity, expressed as a drop (fall) energy for 50 % probability of initiation, with the characteristics of IR spectroscopy:

a) with the Raman N-N bond stretching vibration;
b) with the FTIR C-H bond stretching;

Regarding the mentioned N-N bonds, they are well known to be a triggering element in the initiation of nitramines [25, 26]; in this context, we found an interesting relationship between their stretching vibration and the impact sensitivity of the studied nitramines and their composites, which is shown in Figure 3.5.7. Given the definitional relationship between the oscillation frequency and the bond force constant (i.e., roughly the force of a given bond) [29], the relationship in this figure for the negative slope dependence is contrary to expectation, with the composites in question, however, being more impact resistant than their pure nitramine coformers.

On this contrary could perhaps be expanded the findings of Li et al. [30], who linked the known discrepancy between the performance and stability of EMs to a property of crystal packing, specifically interspecies interactions, could be expanded upon in relation to this discrepancy; here, the issue is the initiation reactivity, which is nevertheless closely linked to stability [27]. A straight line in Figure 3.5.7

with a positive slope is as expected in earlier results, i.e., it decreases in impact sensitivity as the N-N bond force constant increases.

Here, however, attention should be paid to the established idea that the reactivity of energetic materials should increase with increasing bond length of the nitro group to its carrier (carbon, nitrogen, or oxygen atom), i.e., with decreasing force constant of this bond [31]. However, a simple comparison of the lengths of the longest N-N bonds of nitramines with their impact sensitivity showed that this is far from being as simple as it might seem [32]; some discrepancies, that fall under the previously mentioned findings of Li et al. [30].

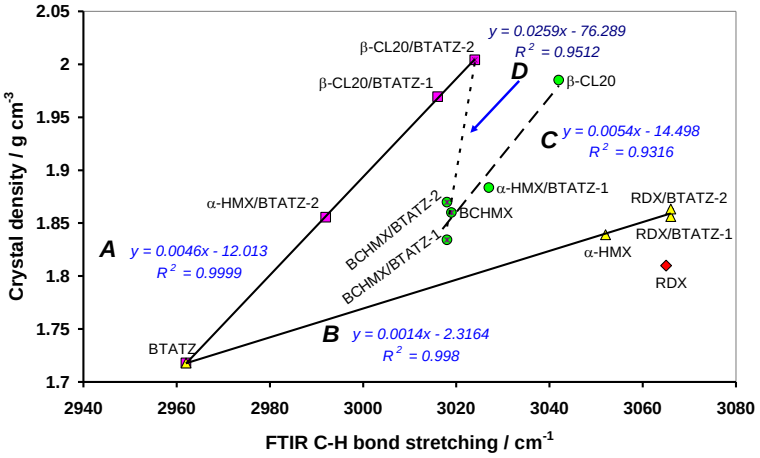

Figure 3.5.8 A comparison of the crystal density and FTIR C-H bond stretching of the studied nitramines and their CACs.

A similar vibrational dependence of the C-H bond stretching (Figure 3.5.7b) could perhaps indicate the intensity of the involvement of individual nitramine molecules in intermolecular interactions with BTATZ. This is mainly related to intermolecular hydrogen bonds (HB), which are usually found in low-energy and shock-insensitive molecules [31, 32]. From this perspective, then, the solid straight line in Figure 3.5.7b should correspond to the dominant interaction via hydrogen bonds in crystals (BTATZ has in its molecule two acidic hydrogen atoms). For CACs with HMX and especially RDX, a different kind of interaction, such as π-π-staking and wan der Waals forces, might dominate, which is related to the spatial similarity of HMX and especially RDX molecules with the spatial conformation of the tetrazine unit of BTATZ.

The sterically crowded molecules and their CACs, except for CL20/BTATZ-2 with higher BTATZ abundance, have their relationship for HB interaction in Figure 3.5.7b (this should come into consideration precisely because of the spatial conformation of CL20 and BCHMX.

The interactions utilizing the HBs have an effect on the packing coefficient, i.e., they should also be reflected in the crystal density [34], which is supported by Figure 3.5.8 (here, a decrease in the C-H bond stretching should correspond to an increase in the intensity of the HB interactions). Figure 3.5.8,

it can be seen that, except for the HMX coagglomerates, CACs of batches B2 have a higher density than those of batches B1, and Table 3.5.6 and Figure 3.5.7a also have higher resistance against impact. There should be a higher abundance of HBs in the CACs crystals of line A in Figure 3.5.6 compared to the default CL210 and HMX. The HMX CAC B1 batch might have a perfect crystal lattice arrangement with a lower proportion of the HB interaction compared to its batch B1. Line D represents the relation for crowded nitramines with the observation that the effect of HB on intermolecular interactions in coagglomerates of BCHMX should not differ from those in BCHMX itself. In RDX/BTATZ crystals, the influence of HB on the intermolecular interaction should be the smallest from the studied CACs due to certain spatial similarities of the s-tetrazine and s-triazocane skeletons, π-π-staking could dominate in them.

3.5.3.4 The energetic point of view

A general property of EM is the energy content, which has a direct influence on the initiation reactivity of these materials [6, 25, 26, 28, 33, 34]. This is only one aspect of the initiation of EMs; the other one is a mode of transfer of the initiation pulse to the reaction center of the EMs molecule.

In the modern contributions to the theory of the detonation initiation, a number of authors are concerned with the transfer of vibrational energy, i.e., the transformation of low-frequency crystal lattice vibrations (acoustic phonons) upon impact or shock action on EMs to high-frequency vibrations (vibrons) with subsequent spontaneous localization of vibrational energy in explosophore groups [25, 35, 36].

In this context, it is interesting to verify of whether there is any relation between the FTIR characteristics of the nitramine composites (i.e., explosive carriers) to the energy contents (heat of combustion and enthalpy of formation [26, 33, 34]), however, also to the energy outputs (energy or heat of explosion [6, 33, 34]) of the studied samples. These aspects with highlighted mutual comparisons are shown in Figure 3.5.7.

The relationship between N-N bond stretching vibrations and voluminous detonation energy in Figure 3.5.7a is directly proportional (increasing values of the bond force constants of these bonds corresponds to a performance increase studovaných EMs). The division into a group of pure nitramines and a group of their composites is logical; the spatial similarity of the RDX molecule to the BTATZ tetrazine unit causes the data for this nitramine to be placed close to the line for the composites.

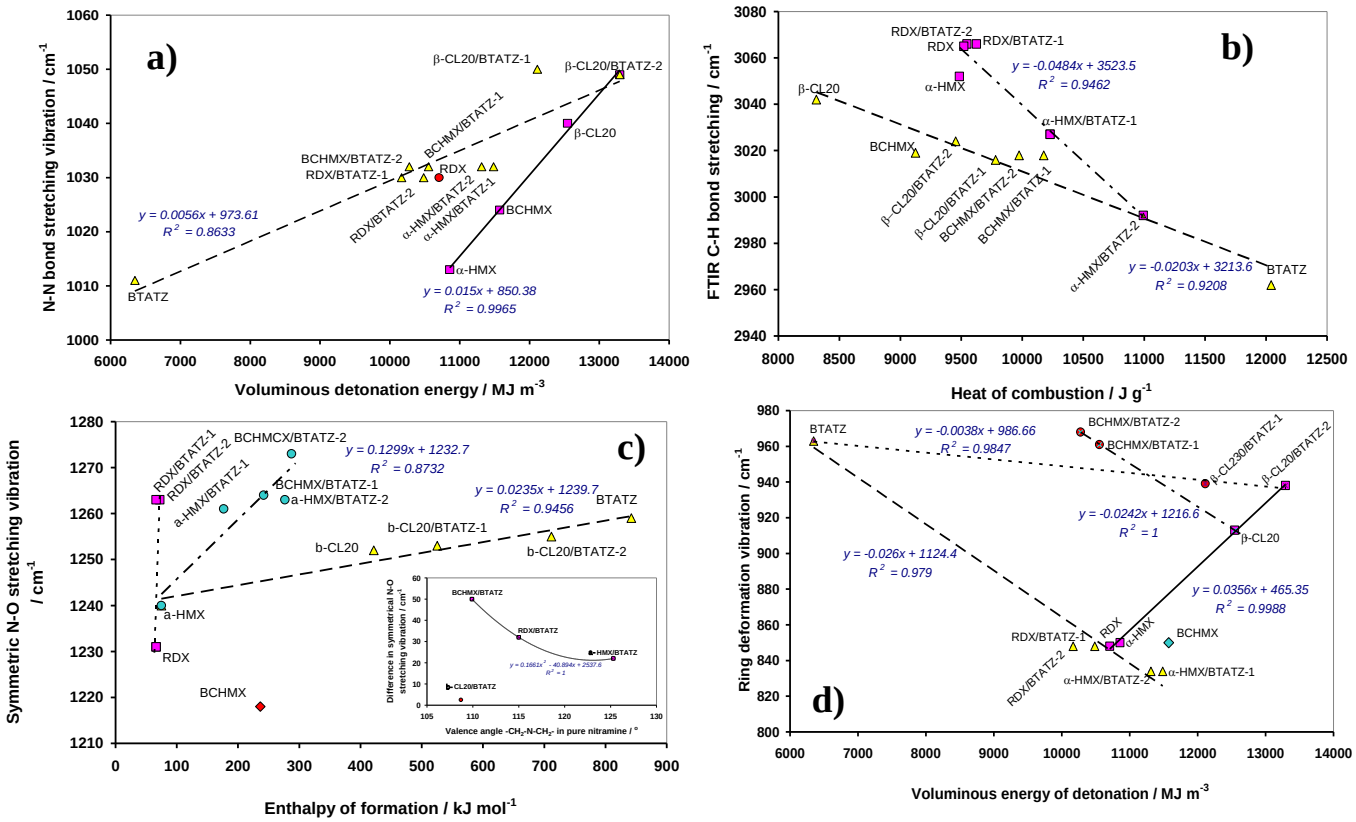

Figure 3.5.9 A comparison of energetic characteristic of the studied nitramines and their composites with their spectroscopic data:

a) Relationship between the N-N bond stretching vibrations and voluminous detonation energy (performance);
b) Mutual comparison of the FTIR C-H stretching vibrations with heat of combustion (energy content);
c) Mutual comparison of the symmetric N-O stretching vibrations with enthalpy of formation (energy content), data for BTATZ might correspond to N-C vibration. Inserted is there a graphic mutual comparison of the difference between symmetrical N-O stretching vibrations of CACs and pure nitramines with valence angles-CH_2-N-CH_2-, which correspond to the longest N-N bond;
d) Mutual comparison of the ring deformation vibrations with voluminous detonation energy (performance);

A similar trend can be seen in Figure 3.5.9b, where the FTIR vibration of C-H in stretching is compared with the heat of combustion (an increasing value of the C-H coupling force constant corresponds to a decrease in the heat of combustion or to the raising in enthalpy of formation or performance). The splitting of the EMs studied here into a group containing RDX and HMX and a group containing nitramines with crowded molecules is logical. In the former group, π-π-stacking is likely to be involved in the intermolecular interaction of the coformers with the possibility of the hydrogen intermolecular bonds, mainly in the case of HMX. The dominant intermolecular interaction via hydrogen bonds could be in the case of coagglomerates with BCHMX and especially CL20 contents.

According to Figure 3.5.9c, presenting the relation of symmetric N-O stretching vibrations to the enthalpies of formation, the group of EMs studied is divided into three subgroups (coagglomerates CL20, then BCHMX and HMX and separately RDX). In all cases, increasing values of the enthalpy formation correspond to an increase in the N-O bond force constant. In view of the reported results of the study by Li et al. (interspecies interactions) [30], it is interesting to compare the differences of these N-O symmetryc stretching vibrations (values for CACs minus those of pure nitramines) with the magnitudes of the —CH_2—N—CH_2— valence angles corresponding to the longest N-N bonds in pure nitramines - the order of the nitramines, the lengths of the longest N-N bonds, and their corresponding valence angles are given below: BCHMX (1.412 Å, 109.9° [7]), RDX (1.409 Å, 115.0° [39]), α-HMX (1.366 Å, 119.6° [21]), β-HMX (1.371 Å, 122.9° [40]) and separately β-CL20 (1.433 Å, 108.7° [41]). Mutual comparison mentioned differences and valence angles see on inserted graphic comparison in Figure 3.5.9c: this demonstrates how changes in the conformation of molecules after entry into coagglomerates contribute to their energetics and their performance.

In the case of the intercomparison of ring deformation vibration and voluminous energy of detonation (Figure 3.5.9d), the studied EMs are divided into the RDX and HMX groups, the group containing crowded molecules and the one of pure starting nitramines. In the first two groups, a decrease in the values of these vibrations corresponds to an increased in the performation The opposite is the case for the pure nitramines, similar to Figures 3.5.9a and 3.5.9a. In the context of a run of the dependences for pure starting nitramines in Figures 3.5.9a, 3.5.7a and 3.5.9d, it is worth mentioning here an exception to Licht's rule (original paper [42]), what is a decrease in sensitivity with increasing performance [6, 26] (or energy content [35]) of these nitramines, which is still not explained [6, 26]. The facts in Figures 3.5.8 and 3.5.9 are consistent with the idea, as mentioned earlier, of EM initiation by the transfer of kinetic energy of impact or shock to the reaction center of the molecule via low-frequency acoustic phonon vibrations subsequently transformed into vibrons [26, 36].

3.5.3.5 Impact Sensitivity

This was tentatively discussed in the case of Figure 3.5.9, where, in particular, Figure 3.5.9b allows one to consider the nature of the intermolecular interactions in the crystals of the CACs and nitramines studied, on which impact sensitivity largely depends. The well-known semilogarithmic dependence between this sensitivity and bulk detonation energy is as expected in the case of the studied nitramines. Again, the exception to Licht's rule for pure nitramines is seen here (see in [6, 26]). In addition to the mentioned intermolecular interactions, the large and insensitive molecule BTATZ should also act as the nitramines phlegmatizer; according to the impact sensitivity data in Table 3.5.6, this should be mainly true for nitramines with crowded molecules (CL20 and BCHMX).

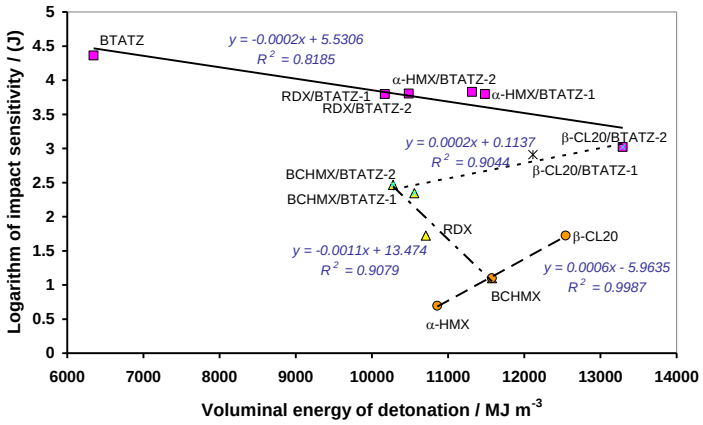

Figure 3.5.10 The semilogarithmic relation between impact sensitivity and voluminal energy of detonation.

3.5.3.6 Detonation parameters

For assessment of the influence of BTATZ on the detonation parameters of the corresponding CACs, Figure 3.5.11 presents the well-known relation between detonation velocity, D, and loading density (here, the maximum values of crystal density) [43]. According to Figure 3.5.11, the group of nitramines and their CACs are divided into three subgroups. Interestingly, these are the pure starting nitramines and, both the CACs of HMX/BTATZ (group A); both HMX/BTATZ should have higher *D* values than α-HMX. The remaining CACs are the next group except CL20/BTATZ-2 (group B). Well, the last is group C. This Figure also confirms that CL20 is present in its β-form in the corresponding CACs. Figure 3.5.11 also shows the previously mentioned fact that the coagglomerates of batches B1 have lower crystal densities than the products of batches B2, which is very important from the point of view of performance-prepared CACs.

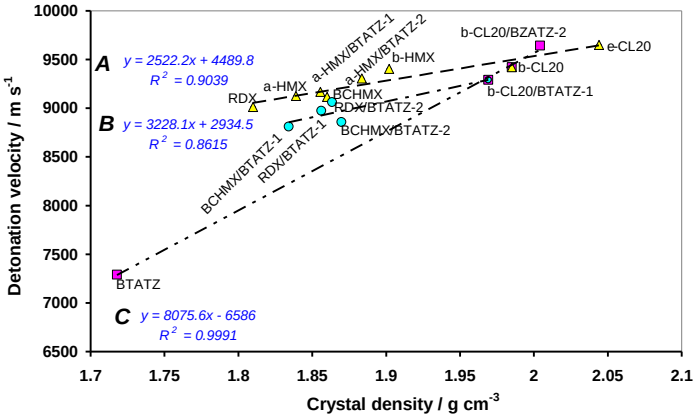

Figure 3.5.11 Relationship between detonation velocity, *D*, and maximal crystal density of the studied nitramines and their CACs.

A synoptic summary of the results of the sensitivity study and the explosive characteristics of the composites and nitramine composites. The CACs with the best application characteristics are α-

HMX/BTATZ-2 (with sample code 12), which has a higher detonation velocity and significantly higher impact resistance than α-HMX alone and slightly exceeds β-HMX in detonation energy.

3.5.4 Summary

Co-precipitates (CP) of 3,6-bis(1H-1,2,3,4-tetrazol-5-ylamino)-s-tetrazine (BTATZ) with cyclic nitramines RDX, β-HMX, BCHMX and ε-CL-20, prepared by solvent/antisolvent technique, were subsequently coagglomerated (slurry cocrystallization) mainly in chloroform parallelly in batches with a linear stirrer (- B1) and a cross stirrer (+ B2); the B2 approach yielding better crystal morphology, quality of surface and higher density. The resulting coagglomerates (CACs) logically exhibit slightly reduced thermal stability compared to pure nitramines, with the exception of the RDX CACs, which decompose in the liquid state from the beginning. Thorough CACs characterization of CACs using Powder X-ray diffraction (PXRD), Fourier transform infrared spectroscopy (FTIR) and Raman showed that the sandwich structure of the BTATZ crystal is optimal for entry into its lattice of RDX molecules (the best spatial compatibility), slightly less optimal of the HMX one, difficult for the angularly shaped BCHMX molecule, and more difficult entry for the globular CL20 molecule. This spatial compatibility of coformers is then related to the mutual representation of species and the intensity of intermolecular interactions (mainly π-π stacking and hydrogen bonding) in the resulting CACs, which also influences their impact sensitivity and crystal density. This all follows on newfound relationships between N-N bond stretching vibrations, FTIR C-H bond stretching in CACs on the one hand, and their impact sensitivity, crystal density, voluminous detonation energy (Q.ρ), the heat of combustion and enthalpy of formation, on the other. Also, a relationship between the ring deformation vibrations and the Q.ρ values, together with the relations described above for the N-N and C-H bonds stretching, corresponds to the idea of initiation of the energetic materials by the transfer of kinetic energy of a shock or impact to the reaction center of the molecule via low-frequency acoustic phonon vibrations subsequently transformed into vibrons and then localized in explosophore groupings.

References

[1] D. E. Chavez, M. A. Hiskey, and D. L. Naud, “Tetrazine Explosives,” Propellants, Explosives, Pyrotechnics, vol. 29, no. 4, pp. 209–215, Aug. 2004, doi: 10.1002/prep.200400050.

[2] A. Saikia et al., “Synthesis and characterization of 3,6-bis(1H-1,2,3,4-tetrazol-5-ylamino)-1,2,4,5-tetrazine (BTATz): Novel high-nitrogen content insensitive high energy material,” Journal of Hazardous Materials, vol. 170, no. 1, pp. 306–313, Oct. 2009, doi: 10.1016/j.jhazmat.2009.04.095.

[3] C. Yongjin and B. Shuhong, “High Energy Density Material (HEDM) - Progress in Research Azine Energetic Compounds,” Johnson Matthey Technology Review, vol. 63, no. 1, pp. 51–72, Jan. 2019, doi: 10.1595/205651319X15421043166627.

[4] A. Elbeih, S. Zeman, M. Jungová, and P. Vávra, “Attractive Nitramines and Related PBXs,” Propellants, Explosives, Pyrotechnics, vol. 38, no. 3, pp. 379–385, Jun. 2013, doi: 10.1002/prep.201200011.

[5] A. I. M. Elbeih, A. Husarova, and S. Zeman, “Method of preparation of epsilon-2,4,6,8,10,12-hexanitro-2,4,6,8,10,12-hexaazaisowurtzitane with reduced impact sensitivity,” US9227981B2, Jan. 05, 2016 Accessed: Oct. 20, 2023. [Online]. Available: https://patents.google.com/patent/US9227981B2/en

[6] S. Zeman and M. Jungová, “Sensitivity and Performance of Energetic Materials,” Propellants, Explosives, Pyrotechnics, vol. 41, no. 3, pp. 426–451, Jun. 2016, doi: 10.1002/prep.201500351.

[7] S. Zeman, A. K. Hussein, A. Elbeih, and M. Jungova, “cis-1,3,4,6-Tetranitrooctahydroimidazo-[4,5-d]imidazole (BCHMX) as a part of explosive mixtures,” Defence Technology, vol. 14, no. 5, pp. 380–384, Oct. 2018, doi: 10.1016/j.dt.2018.04.002.

[8] Z. W. Yang, Y. L. Zhang,; H. Z. Li, X. Q. Zhou,; F. D. Nie, J. S. Li, H. Huang, , “Preparation, structure and properties of CL-20/TNT cocrystal,” Chinese Journal Energetic Materials, vol. 20, no. 6, 2012, doi: 10.3969/j.issn.1006-9941.2012.06.003.

[9] V. B. Patil, K. Zalewski, J. Schuster, P. Belina, W. Trzcinski, and S. Zeman, “A new insight into the energetic co-agglomerate structures of attractive nitramines,” Chemical Engineering Journal, vol. 420, Sep. 2021, doi: 10.1016/j.cej.2021.130472.

[10] V. B. Patil, P. Bělina, W. A. Trzcinski, and S. Zeman, “Preparation and properties of co-mixed crystals of 1,3-di- and 1,3,5-tri-amino-2,4,6-trinitrobenzenes with attractive cyclic nitramines,” Journal of Industrial and Engineering Chemistry, vol. 115, pp. 135–146, Nov. 2022, doi: 10.1016/j.jiec.2022.07.043.

[11] V. B. Patil et al., “Co-agglomerated crystals of cyclic nitramines with sterically crowded molecules,” CrystEngComm, p. 10.1039.D2CE00840H, 2022, doi: 10.1039/D2CE00840H.

[12] V. B. Patil, P. Bělina, W. A. Trzcinski, and S. Zeman, “Co-agglomerated crystals of 2,2′,4,4′,6,6′-hexanitro -stilbene/-azobenzene with attractive nitramines,” Chemical Engineering Journal, vol. 457, p. 141200, Feb. 2023, doi: 10.1016/j.cej.2022.141200.

[13] V. B. Patil, O. Machalický, P. Bělina, R. Svoboda, W. A. Trzcinski, S. Zeman, “Co-agglomerated -polyaniline omposite crystals of attractive nitramines -manuscript under communication,” Langmuir ACS, 2023, doi: NA.

[14] Z. Xue, B. Huang, H. Li, and Q. Yan, “Nitramine-Based Energetic Cocrystals with Improved Stability and Controlled Reactivity,” Crystal Growth & Design, vol. 20, no. 12, pp. 8124–8147, Dec. 2020, doi: 10.1021/acs.cgd.0c01122.

[15] R. V. Kent, R. A. Wiscons, P. Sharon, D. Grinstein, A. A. Frimer, and A. J. Matzger, “Cocrystal Engineering of a High Nitrogen Energetic Material,” Crystal Growth & Design, vol. 18, no. 1, pp. 219–224, Jan. 2018, doi: 10.1021/acs.cgd.7b01126.

[16] G. Liu et al., “Energetic Cocrystallization as the Most Significant Crystal Engineering Way to Create New Energetic Materials,” Crystal Growth & Design, vol. 22, no. 2, pp. 954–970, Feb. 2022, doi: 10.1021/acs.cgd.1c01090.

[17] K. Wang, X. Zhao, and W. Zhu, “Application of Molecular Electrostatic Potential Surface to Predict Supramolecular Synthons for RDX/Solvent Cocrystals,” Crystal Research and Technology, vol. 54, no. 12, p. 1900171, Dec. 2019, doi: 10.1002/crat.201900171.

[18] Fried, L E., “CHEETAH 1.39 Users’ Manual UCRL-MA-117541.” CA: Lawrence Livermore National Laboratory., 1996.

[19] Fraunhofer Institut für Chemische Technologie, Pfinztal, Germany, 2004, “ICT Database of thermochemical values.” 2004.

[20] M. Suceska, Test Methods for Explosives. Springer Science & Business Media, 2012.

[21] H. H. Cady, A. C. Larson, and D. T. Cromer, “The crystal structure of α-HMX and a refinement of the structure of β-HMX,” Acta Cryst, vol. 16, no. 7, pp. 617–623, Jul. 1963, doi: 10.1107/S0365110X63001651.

[22] P. Z. and C. B. Ou Y., Wang C., “Sensitivity of hexanitrohexaazaisowurtzitane[J],” Chinese Journal of Energetic Materials(Hanneng Cailiao), vol. 7, pp. 100-108., 1999.

[23] M. Novák, “Ověření vlivu bicyklo-HMX na parametry prachu s obsahem RDX (Verification of the bicyclo-HMX effect on the RDX gunpowder parameters), The final project of the licensing study,” Univ. Pardubice, Feb. 2022.

[24] C. Zhang, B. Kang, X. Cao, and B. Xiang, “Why is the crystal shape of TATB is so similar to its molecular shape? Understanding by only its root molecule,” J Mol Model, vol. 18, no. 5, pp. 2247–2256, May 2012, doi: 10.1007/s00894-011-1245-7.

[25] D. Wang, K. Wang, and W. Zhu, “Theoretical insights into the roles of intermolecular interactions in BTATz-based solvate cocrystals,” Struct Chem, vol. 34, no. 5, pp. 1685–1697, Oct. 2023, doi: 10.1007/s11224-022-02084-x.

[26] G. Parvari et al., “Proposed Proton-Transfer Mechanism for the Initial Decomposition Steps of BTATz,” J. Phys. Chem. A, vol. 122, no. 27, pp. 5789–5798, Jul. 2018, doi: 10.1021/acs.jpca.7b12217.

[27] S. Zeman, “Characteristics of Thermal Decomposition of Energetic Materials in a Study of Their Initiation Reactivity,” in Handbook of Thermal Analysis and Calorimetry, vol. 6, Elsevier, 2018, pp. 573–612. doi: 10.1016/B978-0-444-64062-8.00006-1.

[28] S. Zeman, “The Chemical Micromechanism of Energetic Material Initiation,” in Nano and Micro-Scale Energetic Materials, John Wiley & Sons, Ltd, 2023, pp. 567–623. doi: 10.1002/9783527835348.ch19.

[29] H. Kuhn, H.- D. Föfsterling, D. H. Waldeck, “Principles of Physical Chemistry, 2nd Edition | Wiley,” Wiley.com. Accessed: Oct. 17, 2023. [Online]. Available: https://www.wiley.com/en-sg/Principles+of+Physical+Chemistry%2C+2nd+Edition-p-9780470089644

[30] C. Li et al., “Strategies for Achieving Balance between Detonation Performance and Crystal Stability of High-Energy-Density Materials,” iScience, vol. 23, no. 3, p. 100944, Mar. 2020, doi: 10.1016/j.isci.2020.100944.

[31] D. M. Byler, H. Susi, and W. C. Damert, “Relation between force constant and bond length for carbon—nitrogen bonds,” Spectrochimica Acta Part A: Molecular Spectroscopy, vol. 43, no. 6, pp. 861–863, Jan. 1987, doi: 10.1016/0584-8539(87)80231-3.

[32] S. Zeman, T. Atalar, and A. Růžička, “N-N Bond Lengths and Initiation Reactivity of Nitramines,” Cent. Eur. J. Energ. Mater., vol. 17, no. 2, pp. 169–200, Jun. 2020, doi: 10.22211/cejem/122723.

[33] R. Bu, Y. Xiong, X. Wei, H. Li, and C. Zhang, “Hydrogen Bonding in CHON-Containing Energetic Crystals: A Review,” Crystal Growth & Design, vol. 19, no. 10, pp. 5981–5997, Oct. 2019, doi: 10.1021/acs.cgd.9b00853.

[34] F. Bao, Y. Xiong, R. Peng, and C. Zhang, “Molecular Packing Density Coefficient Contradiction of High-Density Energetic Compounds and a Strategy to Achieve High Packing Density,” Crystal Growth & Design, vol. 22, no. 5, pp. 3252–3263, May 2022, doi: 10.1021/acs.cgd.2c00091.

[35] S. Zeman, A. K. Hussein, M. Jungova, and A. Elbeih, “Effect of energy content of the nitraminic plastic bonded explosives on their performance and sensitivity characteristics,” Defence Technology, vol. 15, no. 4, pp. 488–494, Aug. 2019, doi: 10.1016/j.dt.2018.12.003.

[36] S. Zeman, “Influence of the energy content and its outputs on sensitivity of polynitroarenes,” Journal of Energetic Materials, vol. 37, no. 4, pp. 445–458, Oct. 2019, doi: 10.1080/07370652.2019.1634159.

[37] X. Hong, J. R. Hill, and D. D. Dlott, “Vibrational Energy Transfer in High Explosives: Nitromethane,” MRS Online Proceedings Library, vol. 418, no. 1, pp. 357–362, Dec. 1995, doi: 10.1557/PROC-418-357.

[38] S. Zeman, “Sensitivities of High Energy Compounds,” in High Energy Density Materials, T. M. Klapötke, Ed., in Structure and Bonding. , Berlin, Heidelberg: Springer, 2007, pp. 195–271. doi: 10.1007/430_2006_052.

[39] P. Hakey, W. Ouellette, J. Zubieta, and T. Korter, “Redetermination of cyclo -trimethylenetrinitramine,” Acta Crystallogr E Struct Rep Online, vol. 64, no. 8, pp. o1428–o1428, Aug. 2008, doi: 10.1107/S1600536808019727.

[40] J. Ji, K. Wang, and W. Zhu, “Prediction of the crystal structure and properties of energetic LLM -105:oxidant cocrystals: A theoretical study,” J Chinese Chemical Soc, vol. 69, no. 4, pp. 618–629, Apr. 2022, doi: 10.1002/jccs.202200031.

[41] O. Bolton and A. J. Matzger, “Improved Stability and Smart-Material Functionality Realized in an Energetic Cocrystal,” Angew. Chem. Int. Ed., vol. 50, no. 38, pp. 8960–8963, Sep. 2011, doi: 10.1002/anie.201104164.

[42] H.-H. Licht, “Performance and Sensitivity of Explosives,” Propellants Explos. Pyrotech, vol. 25, no. 3, pp. 126–132, Jun. 2000, doi: 10.1002/1521-4087(200006)25:3<126::AID-PREP126>3.0.CO;2-8.

[43] P. W. Cooper, “Introduction to Detonation Physics,” in Explosive Effects and Applications, J. A. Zukas and W. P. Walters, Eds., in High-Pressure Shock Compression of Condensed Matter. , New York, NY: Springer, 1998, pp. 115–135. doi: 10.1007/978-1-4612-0589-0_4.

Chapter 4 Applications of CACs

4.1 Application of HMX/BCHMX CACs in composite rocket propellant

4.1.1 Background

Currently, the most popular type of solid rocket propellant is a mixture of metallic fuel which has been powdered and finely divided inorganic oxidizer contained in an elastomeric binder. The work aims to develop a low-sensitivity, high-energy oxidizer for solid rocket propellants with increased energy. It has to be affordable and simple to produce, and it should enhance the characteristics and energy content of the rocket propellants. The ammonium perchlorate in the typically standard formulations for solid propellants can be replaced with the new oxidizer.

In the past, HMX was employed in double base propellant window bombs with different percentages of 20 to 60%. Because it contained more carbonaceous material than AP/CMDB, it burned very slowly [1]. Additionally, RDX replacement of 10–30% in AP-based propellant was tested, and the results showed a good effect in enhancing burn rate with smaller particle size [2]. These efforts persisted in advancing additional crucial propellant ignition performance factors in line with technology demands [3]. Subsequently, RDX was used in substitute of HMX in LOVA-gun propellant, which proved to be more resistant to impact and other mechanical characteristics while also boosting ignition temperature [4]. Researchers found the HMX more attractive, the deeper researchers came out. Influences of particle size of HMX studied; At low pressure, burning rates declined with particle diameter, while at high pressure they barely changed. HMX concentration, particle diameter, and pressure dominated particle size effects assessment [5]. In later years, research concentrated more on the sensitivity and energetic performance of cocrystals, which led to their usage as propellant. When crystal CL20/HMX (2:1) was introduced to polyether solid rocket propellant, the influence on the breakdown behavior was examined. It was discovered that this resulted in improved mechanical and thermal properties, although the qualities were still similar to their physical mixture [6].

In the same way, HNTO/AN cocrystal was also used and proven to be a possible oxidizer for composite propellant [7]. An efficient metal oxide burn rate modifier can prevent intercalated HMX, which was found to have a high energy content and a decreased burn rate in another investigation on the propellants performance as a function of particle morphology [8]. CL-20 is a chemical with a high explosive potential that is more suited for low-signature rocket and gun propellant applications than HMX. However, because of polymorphic transition, impacts from the combustion surface, and weakens agglomeration during the process, it occasionally appears to be incompatible with coagglomeration with AP [9]. Recent study shown the HMX is more and more effective with reduced particle size[10]. Enhancing the combustion rate of solid propellants can be achieved with the use of ultrafine explosive particles. Although research on crystals for use in propellants and explosives is still in its early stages,

there may be future uses for them. Overall, the coagglomeration process produces crystals with smaller particle sizes to meet all of these requirements [11–14].

According to a report by Sinditsky et al. on BCHMX combustion, it burns faster and exhibits superior vacuum burning properties than HMX. Nitramines compounds having pyramidal nitro groups break down more quickly than those having planar nitro groups. HMX has a higher surface burning temperature than BCHMX, although having the same structural chemistry. Burning behavior of the BCHMX molecule changes at 10 MPa due to substantial changes in the molecule's electrical properties and crystal structure [15–17]. Technical solutions for the application of BCHMX in propellants are yet to appear in the open literature. There is currently hardly a published technical solution for the use of BCHMX in propellants.

The structural and molecular specificity of BCHMX, along with its related thermochemical properties, make it particularly well-suited for the design of heterogeneous propellants that exhibit good combustion characteristics even at sub atmospheric pressures, according to sporadic studies on the combustion of BCHMX and mixtures containing it [18]. Also known fact that CL120 gunpowder contains a mixture of BCHMX and RDX as the active component at a ratio of about 8 mol of RDX to 1 mol of BCHMX [19].

It turns out that BCHMX structural-molecular specificity [20, 21] and related thermochemical properties [21] may make it especially well-suited for designing heterogeneous propellants that perform well during combustion, even at sub atmospheric pressures. According to an initial attempt, the RDX/BCHMX coagglomerate is marginally more effective than a mechanical mixture when added to gunpowder. It appears that BCHMX is made in Russia and by the Swiss Nitrochemie Wimmis AG to modify HMX rocket fuels. In this work, propellant batches were created, and their effects were examined using HMX and its admixture with BCHMX at varying composition percentages (10, 20, and 30%).

4.1.2 Results

4.1.2.1 Powder X-ray diffraction

The undergone polymorphic changes in the CACs of HMX/BCHMX and their Physical mixture(Phy Mix) analyzed employing the PXRD technique. The obtained intense 2Ɵ values peaks were shown in Table 4.1.1 incoparision with the pure NMs and diaffractogrms in Figure 4.1.1. Both coformers shown the polymorphic stability after undergoing coagglomeration, with HMX tranfered into α to β polymorphic state after interaction with the BCHMX whereas in physical mixture it remains same. It indicates there will interaction between he both coformers in the form of weak hydrogen and von der waals kinds of interactions, which further caused changes in the polymoprhic changes in HMX. Which

leads to cocrystls formation during the coagglomeration process. The coagglomeration further influenced in morphological chages obtained uniform sized crystals, which further analyzed employing FESEM and particle size analysis.

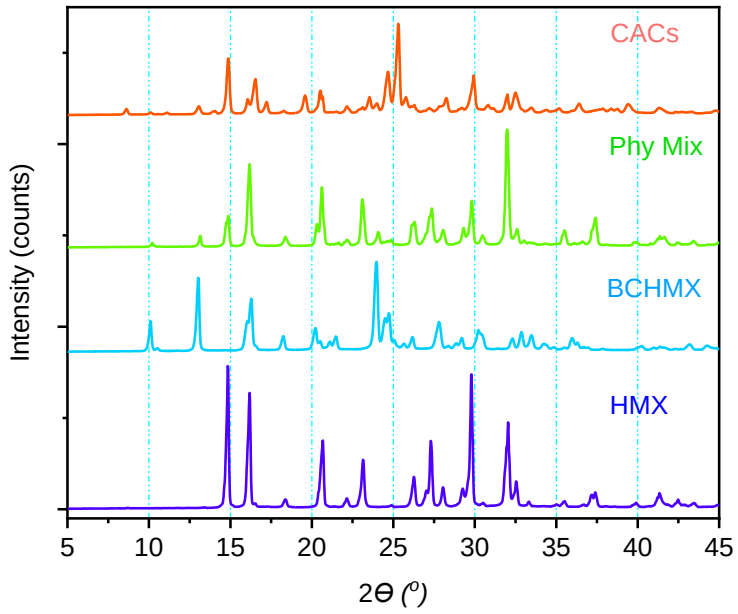

Figure 4.1.1 PXRD diffractogram of pure HMX, BCHMX, physical mixture and CACs

Table 4.1.1 PXRD data for pure nitramines and CACs

Sr No	Code design.	2Θ values for intense peaks / ˚
1	BCHMX	9.74, 12.65, 23.57
2	β-HMX	14.61, 16.31, 24.45, 25.07, 32.31
3	δ-HMX	13.10, 17.02, 24.34
4	HMX/BCHMX Phy Mix	14.86, 16.18, 20.6, 23.08, 27.36, 29.80, 31.98
5	HMX/BCHMX CACs	14.86, 16.54, 20.52, 24.66, 25.30, 29.92, 32.48

4.1.2.2 Fourier transformation infra-red spectroscopy (FTIR)

FTIR spectral analysis was carried out to understand intermolecular stretching vibrations occurred during coagglomeration for instrumental details see Chapter 2 section 2.2.2 and for spectra Figure 4.1.2a. To differentiate the Phy Mix and CACs, intermolecular interactions between both nitramine coformers analyzed using FTIR and Raman spectral studies. The FTIR studies shown interesting results which are summarized in Table 4.1.2 and FTIR spectrums in. From the obtained FTIR spectrum it is optimum enough to identify the intermolecular changes in the CACs with respect to Phy Mix and pure NMs.

Table 4.1.2 Summarized results of FTIR measurements

Assignments	BCHMX	HMX	HMX/BCHMX Phy Mix	HMX/BCHMX CACs
O-N-O-H-- structural bond | C-H stretching	3031 3019	3671 3052	-- 3036	3054 3049
Symmetrical N-O stretching	1218	1240	1237, 1261	1210, 1248
Asymmetrical N-O stretching	1562	1539	1527	1534, 1656
C-N stretching [Amino group]	774	733, 763	751, 772	763, 739, 713
C-N stretching [Nitro group]	1326	1315	1347	1369, 1392
Skeletal stretching [Ring]	1137; 1084	1207, 1087	1086, 1138, 1200	1087, 1108, 114, 1210
Symmetric -NO_2 Stretching	1273 1209	1270, 1240,	1237, 1261	1248, 1257
Asymmetric -NO_2 Stretching	1603, 1554, 1526	1539	1527, 1602	1534, 1603, 1656

4.1.2.3 Raman spectroscopy

Raman spectral measurements for CACs and Phy Mix of HM and BCHMX were measured, obtained results summarized in the Table 4.1.3, and spectra Figure 4.1.2b & instrumental details in Chapter 2 section 2.2.3. Asymmetric stretching vibration at 1560 ± 5 cm^{-1} of −ONO bond shows a shift in CACs. Likewise, a symmetric starching of $-NO_2$ bond at 1215 ± 50 cm^{-1} also showed observable shifts.

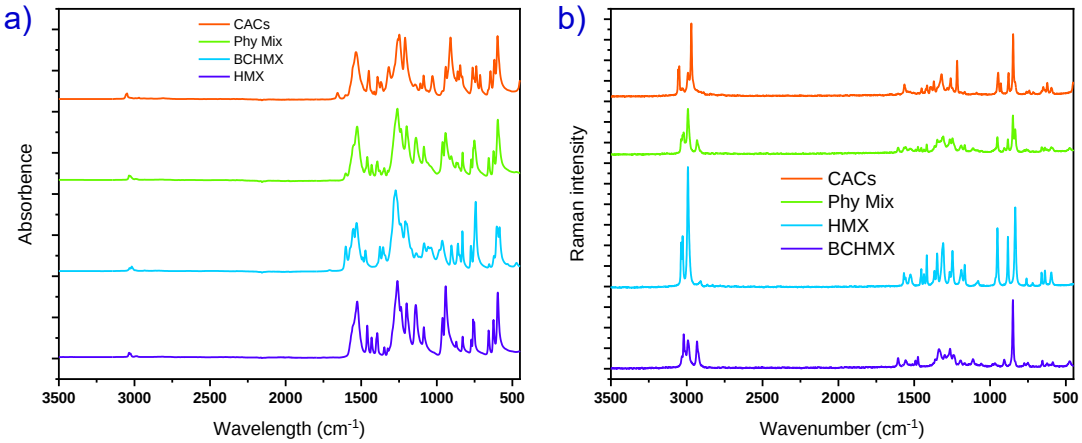

Figure 4.1.2 a) FTIR spectra of Physical mixture, CACs, HMX and BCHMX; b) Raman spectra of Physical mixture, CACs, HMX and BCHMX

Similarly, followed by O−N−O deformation vibration at 832, and 850 cm^{-1} also showed Impactful shifts. In addition, there are also clearly observable in −C−H bending, −C−H, −N−H and N−N bond stretching bands with redshift and other stretching vibrations, as shown in Table 4.1.3. These shifts are relatively differentiable from the Phy Mix. It indicates that both coformers actively involved in intermolecular interactions.

Table 4.1.3 Summarized results of Raman measurements

Assignments	BCHMX	HMX	HMX/BCHMX Phy Mix	HMX/BCHMX CACs
$–CH_2$ stretching vibration	3020	3037	3037	3037
C–H stretching vibration	2992	2992	2992	2992, 2970
	2932	--	2932	--
Asymmetric $–NO_2$ stretching vibration	1606	--	1606	1607
	1557	1568	1567	1564
-C–H and $–CH_2$ deformation vibration	1299	1315, 1270	1309, 1265, 1248	1320
Symmetric $–NO_2$ stretching vibration	1273, 1264, 1240	1248, 1266	1214, 1265	1217, 1260, 1282
Asymmetric C–H stretching vibration	1194, 1167	1189	1191, 1167	1167
N–N stretching vibration	967, 1058	1079, 951	1058	947
C–C stretching vibration	1058		1083	1089
Ring stretching vibration	967	882	882	878
	906	834	834	929
Ring deformation vibration	850	--	849	848
	906	--	906	878
$–NO_2$ deformation vibration	--	--	--	848
	--	--	--	760
$–NO_2$ Wagging	775	760	774	752
	750	719	760, 750	715

4.1.2.4 Morphology and Particle size measurements

The morphological changes after coagglomeration and propellant samples analyzed to understand, their surface morphology employing FESEM and Microscope (instrumental details see chapter 2 sections 2.2.6 & 2.2.8). The CACs crystal size and surface area were analyzed using particle size analysis. The particle size analysis clears that coagglomeration enhanced the specific surface area, decrease in particle sizes with uniform crystals. This enhancement in specific surface plays a very important role in propellant coarses. To understand the effect of all three kinds of propellant with three different concentrations; the propellant sample was prepared for FESEM and Microscope analysis by cutting into 3 mm cubes, the surface analyzed on corner, edge, and surface of these cubes to understand the hetergeneous mixture arrangement in the propellant. FESEM images of CACs and Phy Mix are shown in Figure 4.1.3a-d.

From both microscopic (Figure 4.1.4) and FESEM images; all propellant showed good distributions of ingredients in HTPB polymer moiety. Nitramines shining crystals distributions are clearly seen microscope images. There is Slight surface damage is visible in images due to cutting of samples into cubes took extra care done with sharp cutting table knife, still it's obvious in micro level they can be seen. Comparing with all three sets in pure HMX propellant surface crystals distribution good, with increasing amount there is not much effect on surface morphology slightly hardened (section 3.8

hardness test), it might be due to the crystals arranged using polymer moiety with less gaps between them with increasing the amount content (10 -30%). Similarly, in Phy Mix (P4 to P6) the two kinds of crystals impressions can be seen clearly on propellant surface. Whereas in CACs the distributions are more organized as compare both pure and Phy Mix, sample getting more quickly charged with electron beam, images taken quickly. These distributions happened due to uniform particles size with enhanced surface area after undergoing coagglomeration. In addition, this property of CACs uniform distribution made more "perfect mesh" type structure which unable to enter needle of hardness test and behaves "flexural rubbery" nature to impact and friction resistant of propellant (P7 to P9).

Table 4.1.4 Particle size measurements of CACs

Sr No	Code design.	Particle size analysis			
		Surface area (m^2/kg)	*Dv*(10) μM	*Dv*(50) μM	*Dv*(90) μM
1	HMX/BCHMX Phy Mix	780.8	3.19	27.6	90.9
2	HMX/BCHMX CACs	904.3	2.70	21.3	97.9

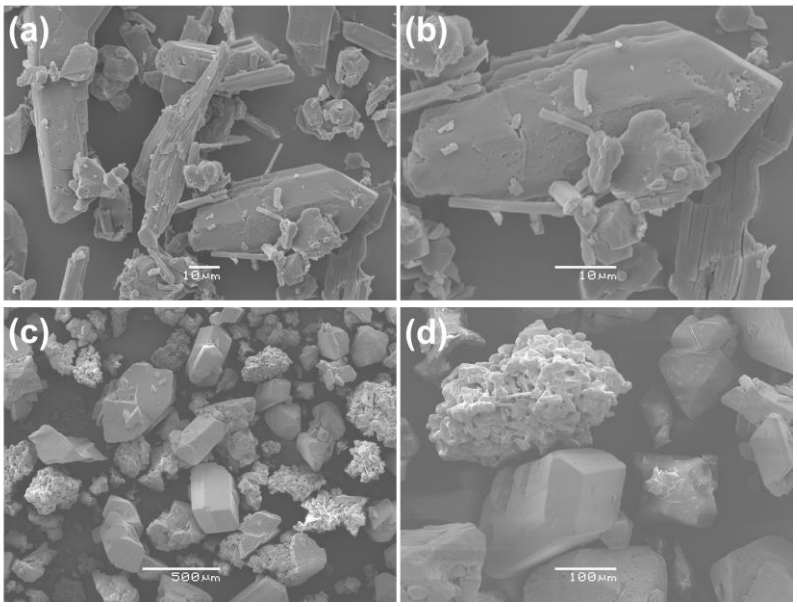

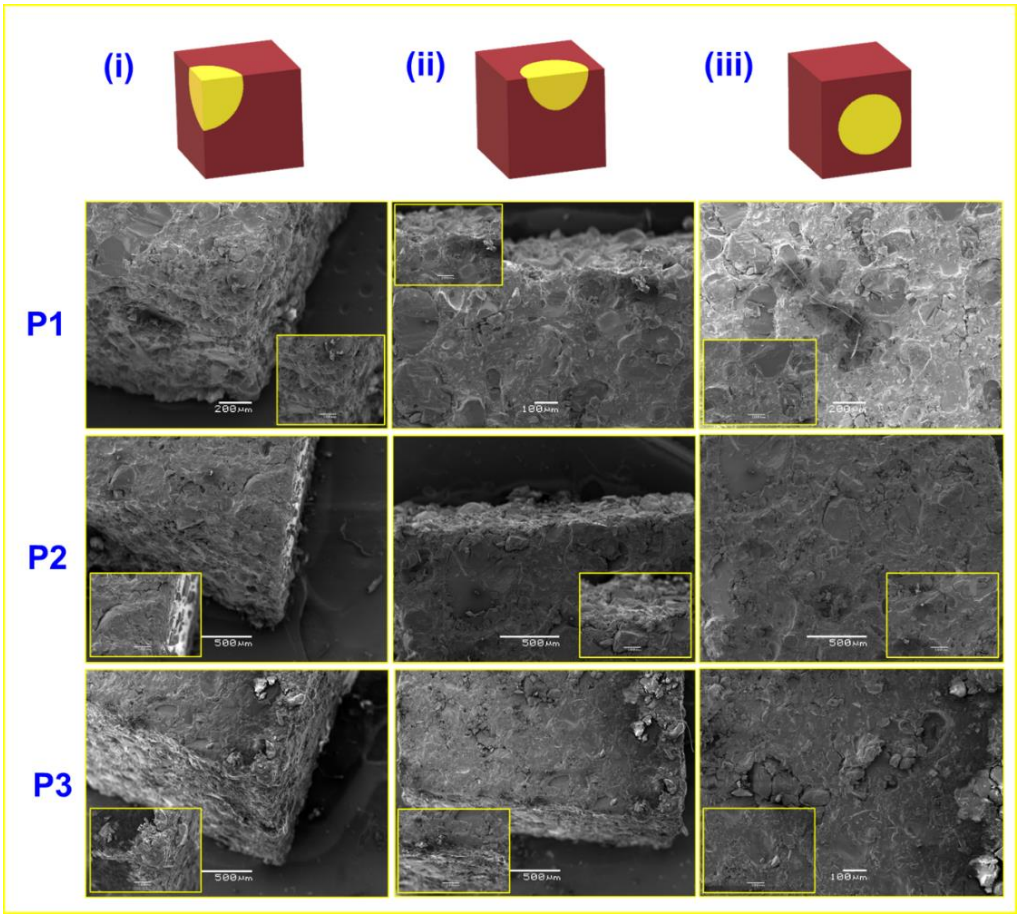
(i)
(ii)
(iii)
P1
P2
P3

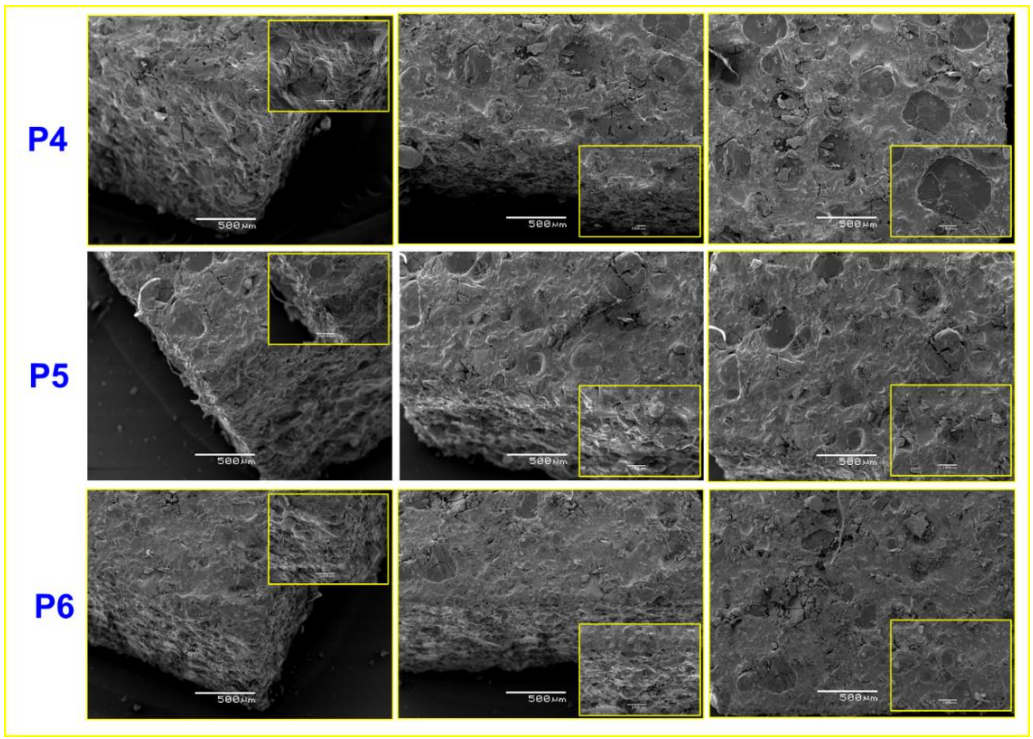
P4
P5
P6

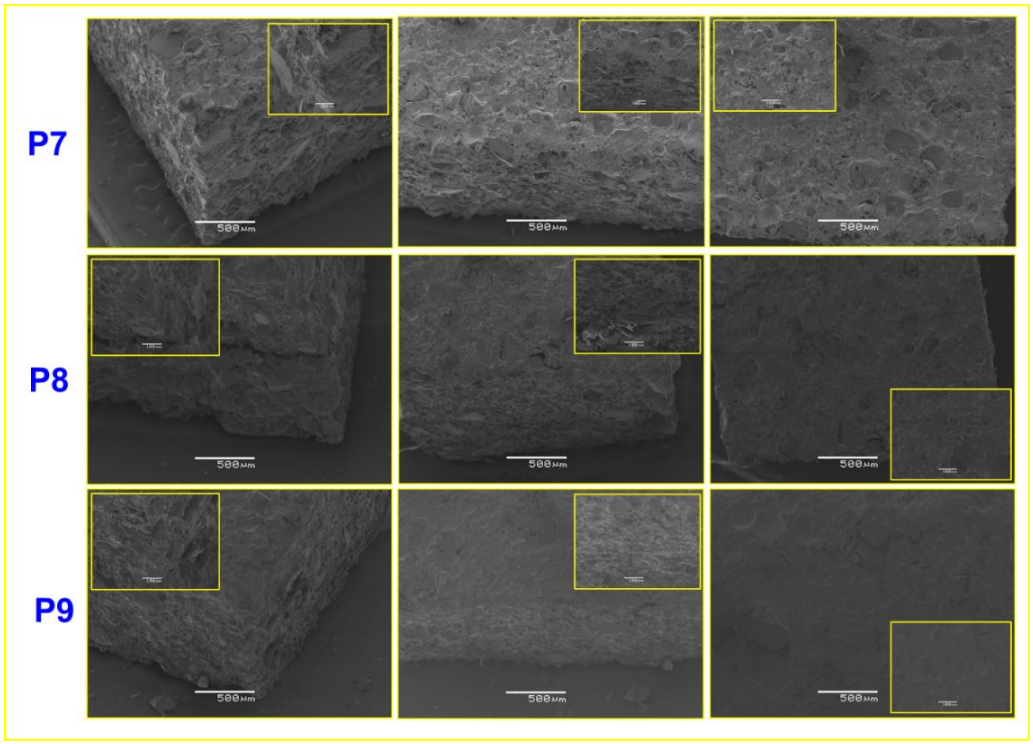

Figure 4.1.3 FESEM micrographs a & b) CACs and c & d) Phy Mix and images of propellant coarse cubes (P1 to P9) 200x with insert 300x at three different faces of propellant cubes.

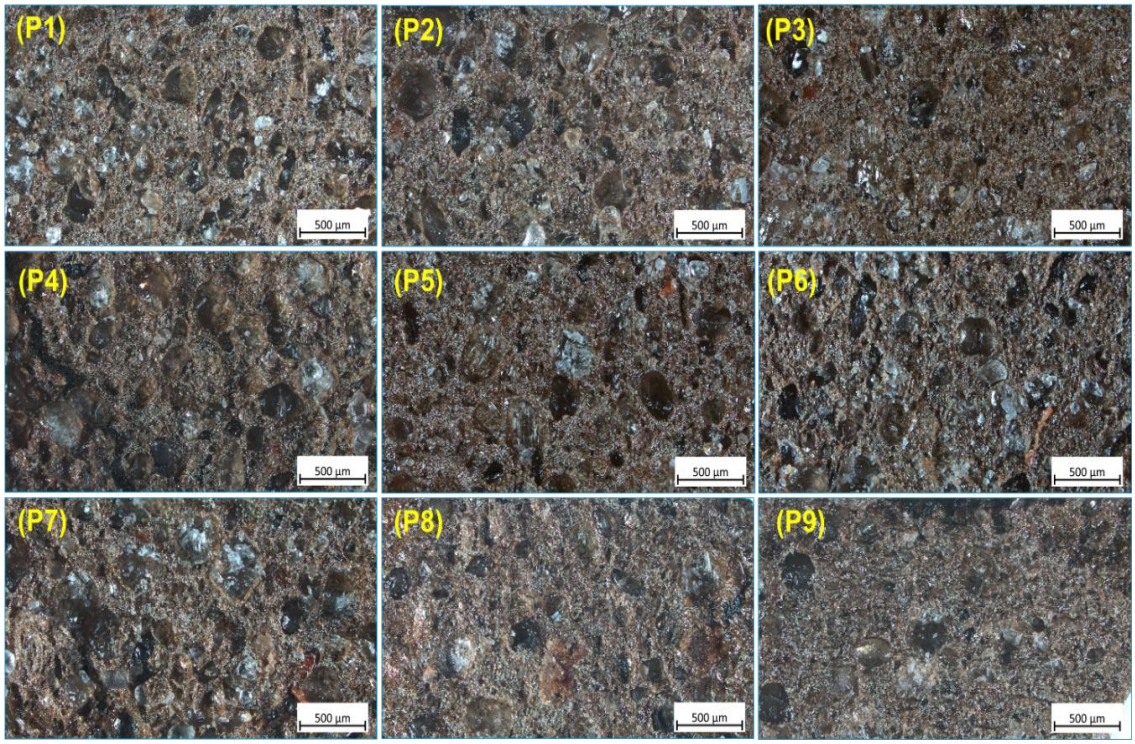

Figure 4.1.4 Microscopic images of propellant coarse

4.1.2.5 Thermal Analysis

The thermal stability and effect of three types of propellant thermal decomposition studied employing DTA analysis (instrumental details see Chapter 2 section 2.2.9). The obtained thermograms shown in

shown in Figure 4.1.5 and characteristic changes summarized in Table 4.1.5. The key active ingredients of the propellant were analyzed first to understand their effect as part of the composite propellant constituents.

All kinds of propellants shown decomposition between the decomposition temperature of BCHMX and HMX except P1 and P4. Similarly, the nitramine content decreases in the decomposition temperature observed. It is also observed in the manual decomposition temperature observations also (section 3.6 and Table 4.1.6) The first kind (P1-P3) of propellant which includes energy content enhancer with pure HMX, in 10 % concentration not shown any synergic effect on the propellant decomposition, whereas the increase in the concentration to 20 and 30 % it shown more effective. Undergone decomposition at one time.

Table 4.1.5 Summarized data from DTA thermograms of coformers and co-crystals with their visible melting points

Sample	Melting point / °C [Ref.]	Peaks of changes in DTA record / °C (phase modifications)	
		endothermic	exothermic
BCHMX	286 Decompn [14]	144	224
HMX	NA	190 (α – δ)	272
Ammonium perchlorate	NA	250	325*, 465
HMX/BCHMX Phy Mix	NA	172	232
HMX/BCHMX CACs	NA	NA	230
P1	NA	NA	240*, 271*, 343
P2	NA	NA	237
P3	NA	NA	235
P4	NA	NA	264
P5	NA	NA	225
P6	NA	NA	220
P7	NA	NA	228
P8	NA	NA	225
P9	NA	NA	217

Note: Ψ) Decomposition temperatures of all samples measured by peters apparatus at room temperature (20.1 ˚C) by visual observation of fire formation; *Minor exothermic peaks

4.1.2.6 Ignition/ Decomposition temperature

The ignition temperatures of all samples measured by peters apparatus at room temperature (20.1 C) observed results shown in Table 4.1.6 (for instrumental details see chapter 2 section 2.2.16). Decomposition temperature varied with the percentage of nitramines content; variation is shown not much difference relatively closer (±5 C). In the propellant samples with pure HMX compared with the physical mixture and CACs, CACs have shown a slightly higher decomposition temperature(±0.5 – 1 C). However, in comparison with pure HMX, both the physical mixture and CACs have shown relatively bigger difference (±10 C), it due to the addition of BCHMX, which undergoes decomposition around 224 C.

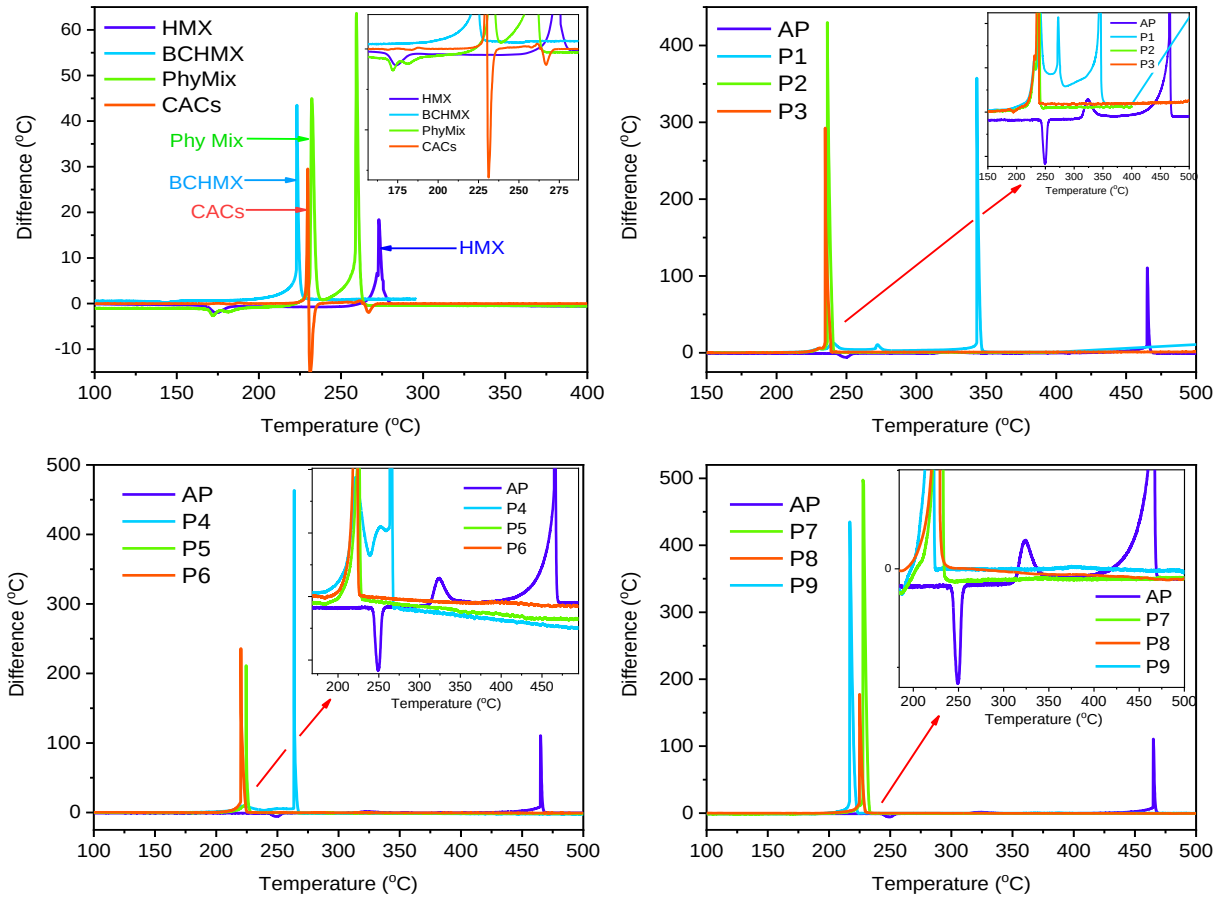

Figure 4.1.5 Differential thermal thermograms of pure HMX, pure BCHMX, their physical mixture, their CACs, and propellant batches (P1 to P9) in comparison with ammonium perchlorate

4.1.2.7 Vacuum stability test STABIL

A modernized Czech vacuum stability test (STABIL 16-E STABIL VI apparatus instrumental details shown in Chapter 2 section 2.2.18). The output of the isothermal measurement is both the time dependence and the final volume of gaseous products after 40 hours of exposure at 120 °C in both these approaches. In the first case, the lines were obtained by linearizing each curve for an isothermal exposure of 60 - 360 min, the data of which are given in Table 4.1.8; the slopes of these lines, k, correspond to the reaction rate of evolution of gaseous products in a zero-order reaction [22–24] - this k values thus represents a specific rate constant (here the values of k are in kPa $g^{-1}min^{-1}$).

4.1.2.8 Dynamic mechanical analysis (DMA-*Tg*)

The glass transition temperature, T_g, is a phenomenon of amorphous polymers. At this temperature, polymers undergo a transition from glassy to rubbery state. It is an important feature of polymer behavior. This information is often used for quality control, predicting product performance, and informing processing conditions or heat history. For our purposes in this work, TA's Dynamic Mechanical Analyzer, for instrumental details see Chapter 2 section 2.2.19 and the obtained results are mentioned in Table 4.1.6.

4.1.2.9 Hardness Test

After curing the propellant samples, hardness is measured, and the mean of six trials at the different surface spots has been considered for the hardiness of the sample; observed results are shown in Table 4.1.6 and for instrumental details see Chapter 2 section 2.2.15. In all samples, the insertion of nitramines has increased the hardness of the propellant samples. The pure HMX made the propellant softer compared to the physical mixture of HMX/BCHMX and their CACs.

4.1.2.10 Friction and Impact sensitivities

To understand the response to external mechanical stimuli of propellant samples - friction and impact sensitivity tests have been carried out(for instrumental details for instrumental details see Chapter 2 section 2.2.12 & 2.2.14). The observed results are shown in Table 4.1.6. As observed in the hardness test, the property further influenced the friction sensitivity test.

Table 4.1.6 Properties of propellant samples

Sample codes	Hardness [°ShA]	Impact sensitivity $D_{50\%}$ [J]	Friction sensitivity [N]	DMA T_g [°C]	Ignition temperature [C]
P1	32.45	17.15	160	-78,5	239.9
P2	32.95	17.15	160	-77,75	239.4
P3	36.56	14.70	120	-78,35	234.6*
P4	34.65	12.25	120	-78,65	223.6
P5	35.65	9.80	120	-78,30	218.9
P6	37.30	9.80	80	-78,65	221.6*
P7	43.05	17.15	160	-78,25	224.9
P8	46.25	14.70	160	-78,65	219.8
P9	47.17	12.25	120	-78,20	221.4*

Note: *burnt with intense propulsion flame

Both samples with pure HMX and CACs are shown the same. Whereas the physical mixture showed a higher impact sensitivity, it may be due to the irregular particle size initiating friction.

4.1.2.11 Thermodynamic performance calculation

Thermodynamic performance calculations were applied with the ICT thermodynamic code and data base developed by Volk and Bathelt [26, 27]. The calculated parameters for an expansion ratio of 70:1 for the studied formulations is compiled in Table 4.1.8 together with the calculated reaction products at nozzle. For combustion calorimetry instrumental & Thermodynamic code details Chapter 2 section 2.2.10 & 2.3.3.

4.1.2.12 Burn rate measurements

The samples were in the shape of rectangular blocks with a thickness ranging between 5.5 and 7.5 mm. The weight of the used samples was in the range of 12–15 g. The thickness measurement deviation is no more than 0.1 mm. The sides of the samples were wrapped with three layers of textile tape as insulation to ensure burning on only two sides. The uneven surface of the cured propellant sample was cut away to achieve a flat surface. The propellant sample was ignited using 1.5 g of black powder and loosely poured onto the sample. A minimum of two shots were performed for the measurement of each composition. The pressure exponent was determined for a pressure range of 4.5 – 14 MPa using ABSW software. The burning rates were evaluated over a pressure range of 4 – 14 MPa.

Table 4.1.7 Input characteristics of the propellant components required for calculation

	ΔH_{form} (kJ mole^{-1})	Density (g cm^{-3})	Oxygen balance (%)	Molecular weight
Ammonium Perchlorate	-295.77	1.95	34.04	117.4891
Iron oxide	-824.25	5.24	10.02	159.6922
HMX	84.01	1.901	-21.61	296.1551
Physical Mixture-PM (8 HMX:1 BCHMX wt. parts)	107.59	1.881**	-21.10	296.055
CACs (8 HMX:1 BCHMX wt. parts)*	108.10	1.817**	-21.10	296.055
Dioctyl adipate (DOA)	-1215.03	0.925	-263.37	370.5665
Dimethyl diisocyanate (DDI)	-872.79	0.872	-298.81	588.9905
HTPB	-52.58	0.93	-311.28	140.3973
Aluminum	0.0	2.702	-88.95	26.9815

Note: *) hypothetical formula CAC is $C_{4.01}H_{7.77}N_{8.00}O_{8.00}$
**) experimental value from this chapter

Table 4.1.8 Results of thermodynamic performance calculation of the studied propellants

Properties	P1	P2	P3	P4	P5	P6	P7	P8	P9
Heat of formation (kJ kg^{-1})	-1567.62	-1287.51	-1007.4	-1559.63	-1271.53	-983.43	-1559.63	-1271.53	-983.43
Oxygen balance (%)	-44.53	-50.09	-55.66	-44.47	-49.97	-55.48	-44.47	-49.97	-55.48
Density (g cm^{-3})	1.751	1.748	1.745	1.749	1.743	1.738	1.749	1.743	1.738
Specific impulse (s)	263.7	260.7	258.4	263.7	261.1	258.6	263.7	261.1	258.6
Heat of explosion (J g^{-1})	6488.2	6577.6	6667.2	6495.6	6592.6	6689.8	6495.6	6592.6	6689.8
Heat of explosion (cal g^{-1})	1550.7	1572.1	1593.5	1552.5	1575.7	1598.9	1552.5	1575.7	1598.9
Heat of explosion (J g^{-1}) (water gaseous)	6361.5	6456.4	6551.6	6369.2	6471.8	6574.7	6369.2	6471.8	6574.7
Heat of explosion (cal g^{-1}) (water gas.)	1520.4	1543.1	1565.9	1522.3	1546.8	1571.4	1522.3	1546.8	1571.4

4.1.3 Discussions

4.1.3.1 Co-agglomeration

The uniform sized microcrystals CACs of HMX/BCHMX obtained employing coagglomeration method. Usually, the surface area enhancements take place after undergoing coagglomeration [28, 29]. Coagglomeration feasible also for sterically crowed molecules, to get energy safety balanced CACs [28]. Its further confirmed with properties of physical mixture of both EMs. Found that the CACs are established uniform sized, well distributed, with softened edges microcrystals as compared to physical mixture. The intense stirring during coagglomeration is responsible for these key changes in CACs. CACs further analyzed particles size(see Table 4.1.4) and for morphological changes FESEM analysis. The CACs showed an increase in surface area and interesting morphological changes. FESEM images clearly observable the porous crystals of raw HMX disappeared after coagglomeration.

4.1.3.2 Differential thermal analysis (DTA)

The active interactions between both EMs further influenced their thermal properties. The CACs and their physical mixture comparison showed that the CACs undergo one step clear decomposition. Both physical mixture (PM) and CACs have exothermic peaks somewhat shifted to higher temperatures compared to the same of the pure BCHMX, but the decomposition peak of HMX in PM is lower placed than that of this pure nitramine. This behavior of CACs in particular is consistent with the results of spectral monitoring of

these mixed crystals (Section 2.1.1.2), i.e., with the nature of the mutual intermolecular interactions of both the conformers (see also in [12]). It is mainly visible in the third kind (P7-P9) where the CACs contributed to more effective changes in decompositions around 218 ± 10 °C for all three concentrations in contrast to the rest of samples kinds (P1-P8).

For pure AP, an endothermic peak is observed at about 250 °C, which is assigned to the crystallographic transition of AP from orthorhombic to cubic [29]. By further heating, AP underwent two complicated decomposition stages [30], i.e., a low temperature stage at 329.3 °C and a high temperature stage at 435.5 °C, which are followed by two exothermic peaks. The mentioned changes of AP during heating are clearly shown by Figure 4.1.5.

The synergistic effect of AP on the decomposition and combustion of HMX [31] is clearly evident in the decomposition curve of the propellants P1 (with 10% HMX) and P4 (with 10% PM), which starts in the temperature region of the polymorphic transition of AP and is folded from three exothermic peaks (see Figure 4.1.5). At higher nitramine contents in the samples, and also in P7 with 10% CACs, this effect no longer appears. This also implies that AP should not have a more significant effect on the decomposition of BCHMX. Both the HTPB/AP and HTPB/HMX thermal decompositions are divided into two stages with some amount of carbon residue [32]. Compared with the HTPB/AP mixture, more HTPB and HMX take part in this decomposition and hydrocarbons containing primary amine are produced. Considering these changes, in the third kind (P7-P9) the CACs showed more effective changes in decompositions for all three concentrations. It may be due to the intermolecular interactions between the HMX and BCHMX make them bind each other in fact after going to several hours propellant mixture mixing and secondly their enhanced surface area makes them uniform distribution in propellant coarse. Which makes the CACs thermal behaviour propellant with CACs different than other two kinds of the propellant.

4.1.3.3 Ignition / Decomposition temperature

The initiation reactivity of EMs is related to their energy content, which can be represented by the enthalpy of formation but also by the heat of combustion [24, 25, 34]. It should be noted that as the AP content of the propellant decreases, the heat of combustion increases and thus the explosion temperature decreases (see Table 4.1.6) and also that one from the characteristics of the initiation reactivity is ignition temperature; this temperature should be related to the heat of combustion, which is presented by Figure 4.1.6; here line P1-P2-P3 corresponds to expectation (increasing content of HMX leads to increased reactivity). This Figure 4.1.6 also shows that the admixture of BCHMX increased the thermal reactivity of samples containing PM and CACs relatively significantly, especially in the case of samples P5 and P8, between which there is quite a big difference in the Qc values. Also, the increasing Qc values of the samples in the order P3-P6-P9 (they

contain of 30 % wt. nitramines) are related to problem of the precisely definition of thermodynamic state of final products of combustion (mainly of amount of the chlorine acidic derivatives)[35], the composite of which might perhaps influence by the effect of AP on the combustion of HMX and HTBP (see paper [32]) even in an oxygen atmosphere (in any case presence of BCHMX changes decomposition of these propellants, as was already mentioned in section 4.3.1).

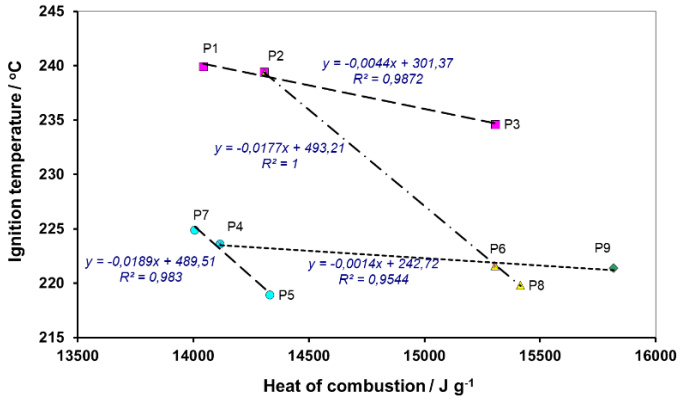

Figure 4.1.6 Relationship between ignition temperature and heat of combustion of the studied propellants

4.1.3.4 Vacuum stability test

As shown in Table 4.1.9, the reproducibility of the selected approach to the VST application is not the best in the PM 30% case, in comparison, for example, with the Russian Manometric Method (see [1, 2, 3]). Table 4.1.9, obtained by other VST thermoanalytical methods, shows a decrease in specific rate constants with the increase in nitramine content, except in the case of 30% of PM. In particular, the linearization of the decomposition curves for propellants obtained these values. In pure HMX propellants, the lower specific rate constant might be due to well crystal distribution over propellant coarse; similarly, in the case of CACs, after coagglomeration, crystal sizes were unified and made well distributed. However, whereas PM might be due to two kinds of crystal, different sizes of HMX and BCHMX are not well distributed, so the specific rate constant is higher in all PM propellants (P4 to P6) [39]. It also shows that CACs are thermally behaving like pure HMX as a single molecule, which means that there will be good interactions between the HMX and BCHMX via intermolecular interactions.

4.1.3.5 Dynamic mechanical analysis (DMA-*Tg*)

From the results of the T_g values determination in Table 4.1.6, they appear to be essentially the same for all propellant samples. However, if we considered the possible influence of the solid contents of the HTPB matrix on the rheology of the respective mixtures and the already mentioned possible problem with the precise definition of thermodynamic state of combustion products in the combustion calorimetry (see in

4.3.2), then there could be a relationship between T_g values and heats of combustion, which is confirmed by Figure 4.1.7.

Table 4.1.9 Results of the 6 hours vacuum stability test at 120 C

Sample	Equation of linearization		
	Slope k (kPa g^{-1} min^{-1})	intercept (kPa)	R^2
PM	0.0010	0.3526	0.9605
	0.0011	0.3373	0.9585
CACs	0.0006	0.2872	0.7556
	0.0005	0.1391	0.9447
P1	0.0006	0.1556	0.9509
	0.0005	0.1298	0.8918
P2	0.0002	0.4990	0.8850
	0.0003	0.3309	0.8944
P3	0.0006	0.3849	0.9395
	0.0005	0.1971	0.9675
P4	0.0011	0.5763	0.9868
	0.0008	0.1748	0.9717
P5	0.0014	0.5011	0.9880
	0.0010	0.3537	0.9694
P6	0.0009	0.3473	0.9748
	0.0014	0.2944	0.9769
P7	0.0005	0.0149	0.9864
	0.0002	0.6334	0.9672
P8	0.0011	0.9688	0.9885
	0.0008	1.2734	0.9685
P9	0.0015	0.1646	0.9732
	0.0010	0.3110	0.9820

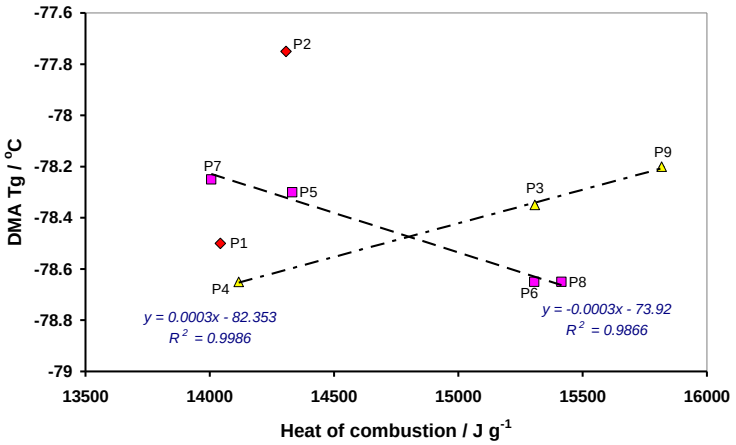

Figure 4.1.7 Relationship between the T_g values and heats of combustion.

Explaining the dependencies in Figure 4.1.7 is also difficult because the specific surfaces of the AP and other solid components are not known. However, a partial judgment can be made samples containing 10

and 20% of HMX (P1 and P2) are not compatible in the sense of Figure 4.1.7. with the other two groups of propellants produced by the dependencies found. In terms of the T_g values, samples P4 (10 % PM), P6 (30 % PM) and P8 (20 % CACs) seem to be the best.

4.1.3.6 Powder X-ray diffraction

The PXRD diffractograms (see Figure 4..1.1 and Table 4.1) indicate a new crystal phase, whereby HMX is tranformed from α into β polymorphic state after interaction with the BCHMX whereas in physical mixture it remains original α-HMX. It indicates there will interaction between both these coformers in CACs by form of the weak hydrogen and van der Waals kinds of interactions. which further caused changes the mentioned polymoprhic changes in HMX. This forms conditions for cocrystls formation during the co-agglomeration process also with influence in morphological chages obtained uniform sized crystals.

4.1.3.7 Spectral Examination

The interaction between both coformers EMs was evaluated by employing spectral analysis; by Raman and FTIR methods. Stretching and bending observations obtained by these studies clears the interactions between them. All the listed stretching vibrations in Table 4.1.2 & 4.1.3; clarify that CACs are not the physical mixture of both coformers, which purely present in the form of new crystal phase nature. Peak for O-N-O-H-- structural bond was absence in the Phy Mix it clearly sharp enough in the CACs it indicates presence of hydrogen bond kind weak interactions between both coformers in CACs. From PXRD results its shown that HMX changed polymorphic transition from α to β, it is clearly visible here too. This cocrystal nature of CACs was also identified from the PXRD peaks shifting, in which the PXRD diffractograms indicate new crystal phase. Overall, considering all potential peak shifts, the FTIR spectrum shows there are interactions between both coformers, totally different from Phy Mix which further indicates the cocrystals.

From earlier studies – spectral observations key horse role identifies the cocrystal formation carried out by comparing their longest N-N bond lengths and N-N bond stretching vibrations[11–14]. Considering the BCHMX and HMX EMs earlier CACs interesting correlations. It is clearly observable that; this bond length and stretching vibration differ from the pure EMs, also from the Phy Mix. Its showed the active intermolecular interactions between both coformer EMs. These stretching vibrations further compared with CACs mechanical properties like impact and friction initiations in which shown interesting logical correlations. This relation is important because during the intuition of EMs, initially all the N-N bonds harmonize [36–38].

All these PXRD, FTIR, and Raman measurements were overlaid with all shifts and structural changes. The structural orientations that developed throughout the co-agglomeration process. The creation of co-crystals in CACs is further aided by these structural modifications, which greatly assisted coformers to CACs in gaining a stable crystal lattice and also suggest that H-bonding, van der Waals forces of interactions, and - stacking type of intermolecular forces interactions may have taken place.

4.1.3.8 Impact & Friction sensitivity, and Hardness test

Hardness studies of propellant coarse indicated that physical mixture hardness is not much varied compared to pure HMX, it may be due to both particles BCHMX and HMX are distributed randomly in propellant coarse. It also indicates the composition of HMX is more and more dependent on it rather than BCHMX. Whereas the CACs distribution is ordered way, it is bound very tightly in the propellant coarse. Again, in CACs propellants hardness does not stiffness; its closed and tightened arrangement were observed. The propellant has a rubbery nature in both the physical mixture and CACs. However, the CACs with uniform crystal shapes and structures make the propellant tightly organized coarse. Further studies of impact and friction sensitivities of propellant coarse, CACs have shown friction sensitivity relatively close to pure HMX. In friction sensitivity tests, CACs have shown better than the physical mixture. Coming to the impact sensitivity test, a similar trend continues in samples with a physical mixture showing higher impact sensitivity. The pure HMX physical mixture showed higher, possibly due to free BCHMX crystals. Whereas in case CACs are less sensitive, it may be because uniform crystals are distributed uniformly ordered in propellant coarse.

As can be seen from Table 4.1.6, the sensitivity to mechanical stimuli of the prepared propellants is mainly influenced by the nature and amount of nitramines incorporated into them; while in the case of pure HMX its content in the mixture does not contribute significantly to this sensitivity (with perhaps of exception of 30 % wt. content), the opposite is true for PM and CACs. PM has a negative effect on both sensitivities, CACs only on the impact sensitivity. Unlike similar mixtures in paper [14], where the AP/HTPB propellant matrix significantly increases the sensitivity of the mixed HMX and BCHMX, in our case this matrix acts as a phlegmatizer.

From the point of view of safety in the production, handling, and storage of these propellants, it is quite important to know the relationship between their sensitivity and performance, or rather energy content. This relationship is experimentally mostly based on Licht's rule [42]: increasing the explosive strength is usually accompanied by an increase in the sensitivity and therefore an insensitive explosive will not exhibit top explosive strength [24, 25, 34, 39].

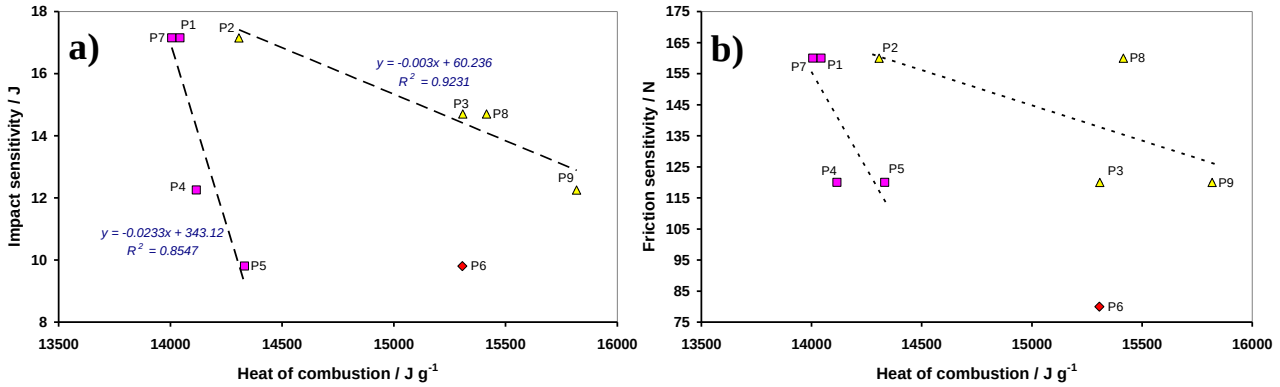

Figure 4.1.8 Relationship between heat of combustion vs a) impact & b) friction sensitivities of the studied propellants

However, there are exceptions to Licht's rule, which, like the rule itself [42], have not yet been scientifically explained [24, 25, 34]. These include the dependencies in Figures 4.6 and 4.7, where the hazard of each sample is related to the increasing nitramine content of the mixture, while the heat of explosion in this sense decreases (see Table 4.1.6). The steeper dependency in Figure 4.1.8 associates samples with content of 10% nitramine and one with 20% PM (P5) the second one associates samples with 20% and 30% nitramine. The data for P6 (30 % of nitramine) do not correlate with either line, the heterogeneity of PM negatively affected its impact sensitivity (influence of the hot spots). In a similar sense, the study samples were divided on the basis of their sensitivity to friction, only the variance of the values of these sensitivities is larger, which is understandable in this case for heterogeneous mixtures.

4.1.3.9 Outputs of Thermodynamic performance calculation

Thermodynamic performance calculations were applied with the ICT thermodynamic code and data base developed by Volk and Bathelt [26, 27]. The calculated parameters for an expansion ratio of 70:1 for the studied formulations is compiled in Table 4.1.8 together with the calculated reaction products at nozzle. For combustion calorimetry instrumental & Thermodynamic code details Chapter 2 section 2.2.10 & 2.3.3.

4.1.3.10 Outputs of Burn rate measurements

The specification of a propellant; the burning characteristic of a particular composition depends only on the chamber pressure and the beginning temperature of the propellant. For rocket motors, the form known as Saint-Robert's or Veille's law is chosen, since combustion pressures rarely reach 2000 psia (13.8 MPa) [43].

$$r = aP^n \quad (P < 2000 \text{ psia}) \ldots\ldots\ldots (1)$$

Where, a - is a constant dependent upon the propellant and the initial temperature, P- pressure and n - is pressure exponent.

High pressure exponent means that n is higher than 0.6 and standard motors pressure exponent lower than 1 [44].

In general, a reduced burning rate may lead to a slower burning process and a lower flame temperature. The linear burning rate is the rate, r, at which the burning surface recedes along the normal to the surface [45]. in present study considered 4-14 MPa (see Figure 4.1.9). The burning rate was calculated using just the linear section of the burn. At this pressure, deconsolidated burning was seen, which would account for the faster burning rate. Furthermore, Table 4.1.10 displays the Saint Robert's law burning rate fit parameters with 95% confidence ranges for each of the study's materials reported in literature with current CACs propellant for comparisons [46].

Chemical equilibrium calculations in literature indicate that although the burning rate behavior was expected, it is most likely not the result of an increase in the internal flame temperature. On the other hand, PLIF analysis of the same structure of these materials showed that the burning rate behavior can be explained by a modification in the chemical kinetics. The burning rate increases as the reaction zone gets closer to the surface because more heat flux is transported into the condensed phase material. This was demonstrated clearly by the fact that the materials with higher burning rates also had CN zones closer to the surface [46].

Earlier studies showed insertion of cocrystals in solid rocket propellant coarse. Burning rate data of each material were compared to those of the coformers described in the literature. HMX/CL-20 cocrystal and physical mixture burning rate compared to pure HMX and CL-20. [5, 9, 10, 11]. The burning rate of the HMX/CL-20 mixture and cocrystal was similar to that of CL-20, notwithstanding the difference in burning rates between the two. The TNT/CL-20 cocrystal burned between its coformers, but the HMX/CL-20 cocrystal and CL-20/HP solvate burned like CL-20[46]. Present study it clear that the CACs compared to pure HMX higher burning rates. Moderately larger and uniform particles are typically preferred over nano or submicron explosive particles due to their low critical diameter, high burning rate, and detonation rate [47]. When it comes to increasing the rate at which solid propellants burn, ultrafine explosive particles have an advantage over bigger ones [7, 8] which is well achieved in case of CACs.

Table 4.1.10 The burning rate of CACs propellants with comparison earlier literature reported works 95% confidence bounds for each fit parameter are also given. The fit parameters from the literature were either directly reported or calculated reported [5, 9, 10, 11]

Sr No.	Compound	Amount (%)	Pressure range (Mpa)	Pressure exponant - n	Burning rate (mm/sec)	REF
1	AN/Crown ether AN–Benzo-18-crown-6 (B18C6)	0.2	0.50 to 7.00	0.62	0.59	[45]
2	HMX/CL-20 CC	NA	0.69-13.80	0.782	2.35	[46]
3	HMX/CL-20 PM	NA	0.69-13.80	0.771	2.1	[46]
4	TNT/CL-20 CC	NA	0.69-13.80	0.767	1.25	[46]
5	TNT/CL-20 PM	NA	0.69-13.00	0.955	1.44	[46]
6	CL-20/HP Solvate	NA	1.38to6.89	0.774	2.26	[46]
7	HMX/AP Composite	NA	0.69 to 13.80	0.668	1.68	[46]
8	HMX/AP Coarse PM	NA	0.69 to 13.80	0.697	1.38	[46]
9	HMX/AP Fine PM	NA	0.69 to 13.80	0.642	1.83	[46]
10	TNT	NA	3.45 to 13.80	0.803	0.4	[46]
11	HMX, Atwood et al.	NA	0.69 to 10.30	0.816	1.14	[46]
12	HMX, Sinditskii et al	NA	0.2 to 10.00	0.81	1.19	[46]
13	CL 20, Atwood et al.	NA	0.69 to 10.30	0.744	2.21	[46]
14	CL 20, Yang et al.	NA	3.00 to 9.00	0.846	25.1	[46]
15	TNT, Kondrikov et al.	NA	5.00 to 58.00	0.422	0.49	[46]
28	AP /AN CCs	AN (28-68) AN (28) AP (constant)	1.00 to 7.00	(0.55 to 0.70 ±0.05)	5.00 to 6.00	[53]
29	HMX	55 to 80%	0.40 to 10.00	0.50 - 0.90	0.50 to 7.00	[5]
30	FOX7/RDX-BuNENA - 1	FOX7 (5 to 50) RDX (0)	0.5 -14	NIL	NIL	[54]
31	FOX7/RDX-BuNENA - 2	FOX7 (5 to 30) RDX (20)	0.5 -14	0.86	5.44	[54]
32	FOX7/RDX-BuNENA - 3	FOX7 (20) RDX (10 to 30)	0.5 -14	93	5.4	[54]
33	DB Matrix/RDX	(88/22)	0.5 -14	NA	8.6 to 10.6	[54]
34	DB Matrix/RDX/Al	(85/12/3)	0.5 -14	NA	9.2 to 10.7	[54]
35	DB Matrix/RDX/AP/$ZrSiO_3$	(80/12/6/2)	0.5 -14	NA	9.8 to 11.5	[54]
36	DB Matrix/RDX/AP/Al	(79/12/6/3)	0.5 -14	NA	10.4 to 12.5	[54]
37	DB Matrix/RDX/AP	(79/12/9)	0.5 -14	NA	10.4 to 11.7	[54]
38	HMX	10 - 30	4.00 to 14.00	0.6 – 0.9	4.50 – 8.00	[55]
39	BCHMX	10 - 30	4.00 to 14.00	0.65 – 0.8	4.50 – 8.00	[55]
40	P1	10	4.00 to 14.00	0.45	6.65	[CW]
41	P2	20	4.00 to 14.00	0.5	6.73	[CW]
42	P3	30	4.00 to 14.00	0.55	6.81	[CW]
43	P4	10	4.00 to 14.00	0.51	7.77	[CW]
44	P5	20	4.00 to 14.00	0.52	7.35	[CW]
45	P6	30	4.00 to 14.00	0.56	6.78	[CW]
46	P7	10	4.00 to 14.00	0.53	8.09	[CW]
47	P8	20	4.00 to 14.00	0.5	9.07	[CW]
48	P9	30	4.00 to 14.00	0.53	7.64	[CW]

Note; CW-Results of current work; Sr No. 38 to 48 considered burn rates at standard pressure 6.89 MPa at range 4-14 MPa

Also, true that according to [46], particle size significantly affects the burning rate of physical combinations, with coarser mixtures burning slower than finer ones. Which might also be a major factor in the CACs. Similarly, study showed CL-20/HP solvate burned at a rate similar to Atwood et al.[52] with two differences

[46]. A cocrystal or physical mixture burning rate is not an average of the coformers. Pressure affected each materials burning rate. Higher flame temperatures were projected to accelerate burning. This finding matched these materials burning rate characteristics. Changes in resulting flame structure significantly impact burning rate. Although the ne physical mixture burned at a similar pace to the physical mixture crystals, it may burn faster at lower pressures; these observations overlays with earlier finding [46]. These studies also showed, All HMX/AP compounds burned faster than HMX or AP alone, and particle size affected burning rate. The cocrystal and physical composition of TNT/CL-20 burned at a rate between CL-20 and TNT, unlike HMX/CL-20. CL-20 predominated in these materials because its physical mixture and cocrystal burning rates were similar [46]. Similarly in the present study, the cocrystals burning rate resulted in a significantly different pressure exponent (n) than the physical combination. The physical mixtures burning rate also dependence on pressure may be segmented by pressure. Collecting data at this pressure skews the pattern of burning rate. Except at low pressures, reported CL-20/HP solvate burned similarly to CL-20 [46].

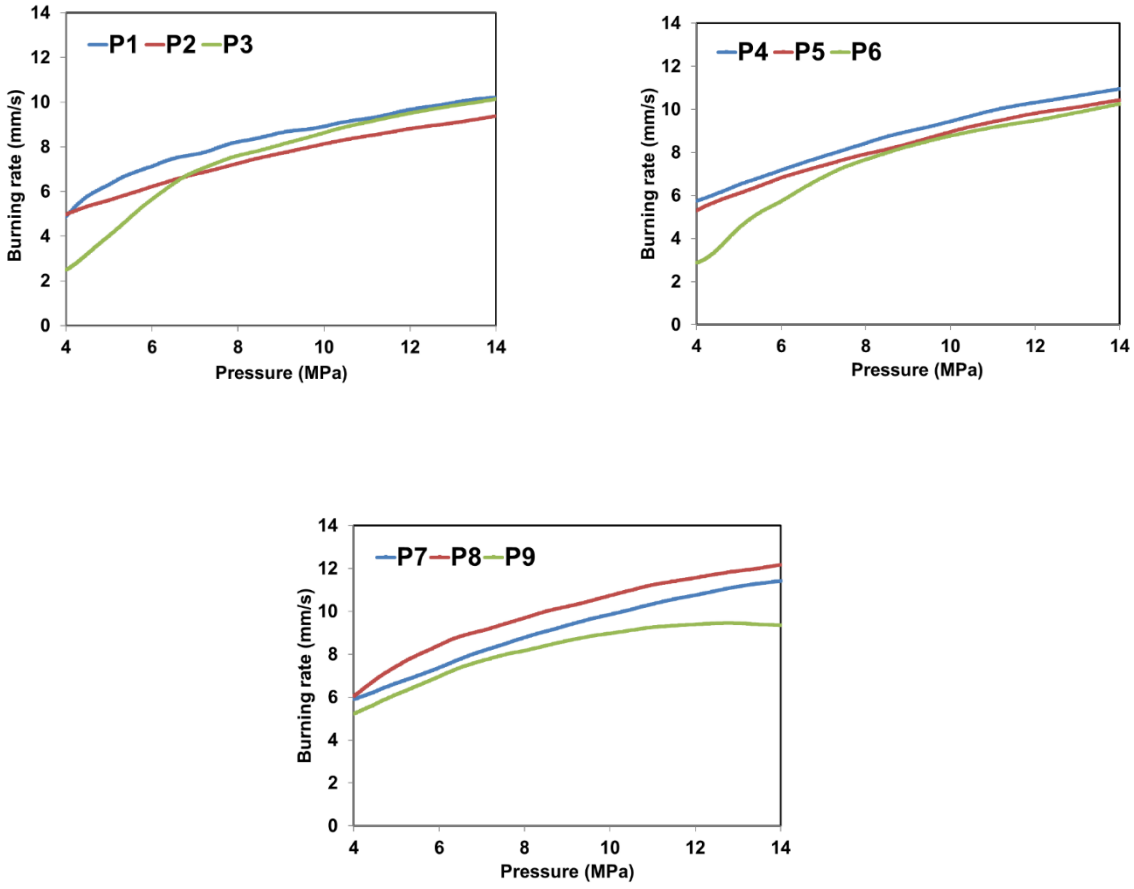

Figure 4.1.9 Burning rate measurements of the HMX, HMX/BC Phy Mix and HMX/BCHMX CACs

The results showed that the performance of coformers does not predict the performance of the final mixture or cocrystal. Varying the structure drastically impacts the burning rate. This may be owing to TNT's poor oxygen balance and the significant difference in burning rates between TNT and CL-20. However, the physical combination and TNT/CL-20 cocrystal burned below CL-20 between coformers [46].

Present study(as shown burning rate curves Figure 4.1.9), all the three concentrations varied the burning rates where 30% shown drop, it also clears 20% of insertion of the nitramine content might be optimum. However, 20% of CACs shown higher burning rate compared to both pure HMX and physical mixture. As per earlier observation about the cocrystals and their physical mixture influence on burn rate seen that dependent on particle size, as earlier discussed CACs shown better particle size (see section 4.1.2.4) and surface morphology in propellant coarse. It further helped uniform distribution/burning flame in CACs surface compared to physical mixture and pure HMX. As a matter of fact, CACs during coagglomeration attained the uniform particle size and surface, it makes them spread over the propellant coarse. Also, study reveals the addition of BCHMX and its influence on propellant performance, it can be seen that BCHMX increased burn rate both physical mixture and CACs compared to pure HMX.

Present study shown better burning rates compared earlier studies and same time also it not possible to comparison with earlier literature when it comes to burn rate because burning rates depend on so many factors, however in current propellant composition CACs shown overall better performance.

4.1.3.11 Some important correlations

Basically, these are the relationships of thermochemical parameters to the reactivity characteristics of the investigated samples of propellant, here specifically heat of combustion and enthalpy of formation, on the one hand, and rate constants of zero order thermal decomposition (specific rate constant), impact sensitivity and burning rate, on the other.

The logarithmic relationship between impact sensitivity and specific rate constants has already been described [53] and logically presents an increase in impact sensitivity with increasing values of this constant; in our case, this relationship is represented by Figure 4.1.10: here, physical mixtures (PM) have a negative effect on the impact sensitivity also incorporated in the propellant (see mainly line B), but increasing the CAC content in the propellant has a similar logically effect - although the latter case is not very significant.

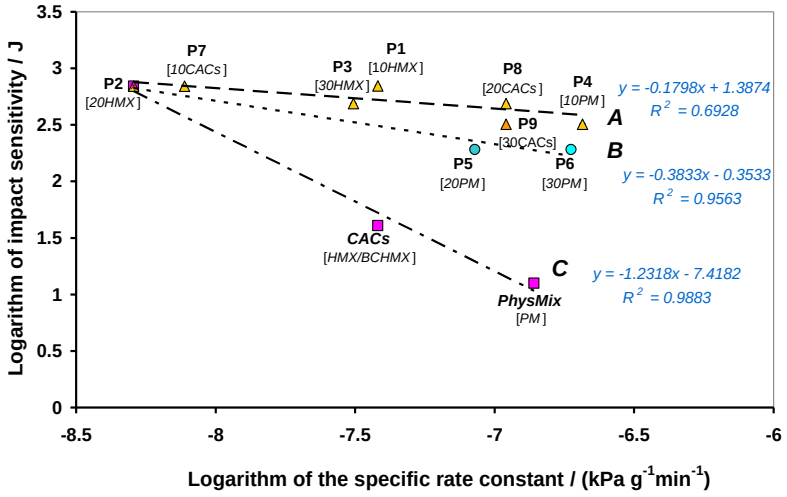

Figure 4.1.10 Mutual logarithmic comparison of the impact sensitivity and the specific rate constant of thermal decomposition of the propellant.

As with other energetic materials, an increase in the energy content of the propellant corresponds to an increase in its initiation reactivity, as already shown in Figures 4.7 and 4.9 and now also in Figure 4.1.11b. Here while crystalline CAC is more resistant to this decomposition compared to the physical mixture of crystals, its incorporation into propellant increases its activity (with exception of sample P7), which is most pronounced for sample P9. In the case of Fig. 10a this is only the case for samples group A, the small change in the enthalpy of formation for group B has a significant effect on the burning rate and for the remaining groups D and C the change in burning is not so significant. The composition of Group B samples thus provides the most suitable thermochemical parameters for propellant burning

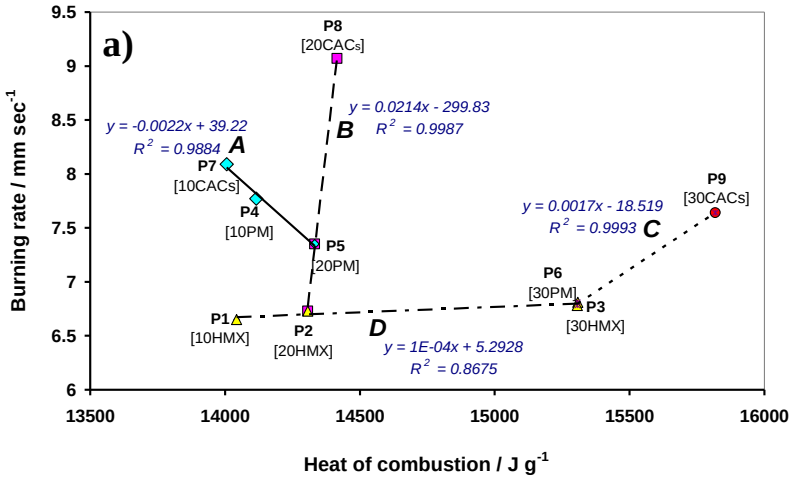

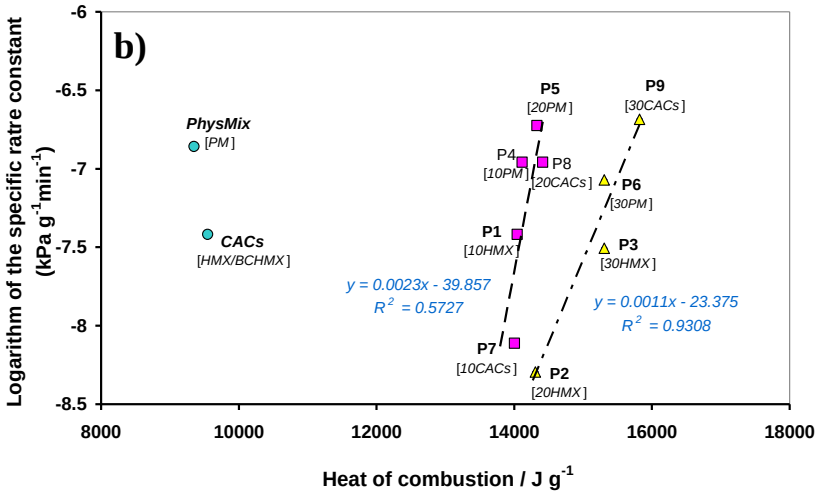

Figure 4.1.11 a) Relationship between burning rate and heat of combustion of propellant: here line **D** correspond to mixtures with only HMX, line **B** is the best Series 2 with 20 % of nitramines, line **C** corresponds to Series 3 with 30 % of nitramines and line **A** is a hybrid one. It is very logical relationship.

b) Semi-logarithmic dependence of the specific rate constants of thermal decomposition and heat of combustion;

The correlation between the characteristics of the reactivities, here impact sensitivity and burning rate, is presented in Figure 4.1.12. For a line with a negative slope, it seems logical that both the sensitivity and burning rate increase with increasing HMX content in the propellant. The relationship for propellants with a mixture of nitramines fundamentally differs from the former - in the field of explosives this would be reminiscent Licht's rule.

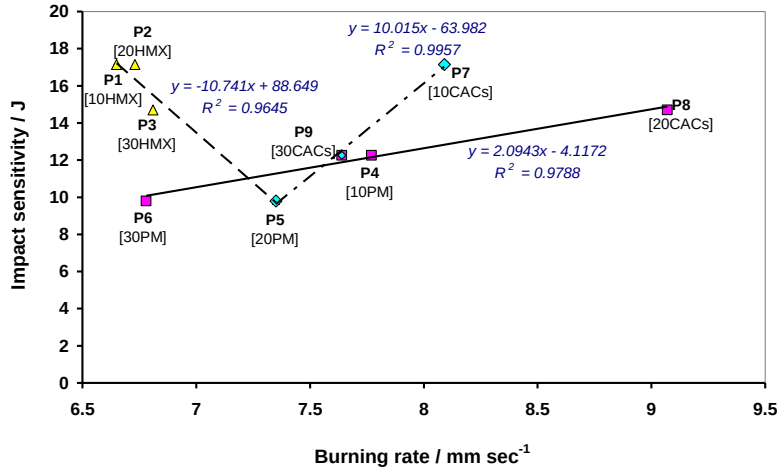

Figure 4.1.12 Relationship between impact sensitivity and propellant burning rate: here, with the exception of Series 1 for the other ones, an increase in burn rate corresponds to a decrease in impact sensitivity.

Figure 4.1.13 significantly separates the samples with both 30% pure HMX and 30% PM (Group C) from the other samples studied. The composition of group B is identical to that of the same group in Figure 4.1.14, so in both cases the hardness of the propellant could play certain role; but otherwise, the slope of this line is logical - decreasing ignition temperature corresponds to the increasing burning rate.

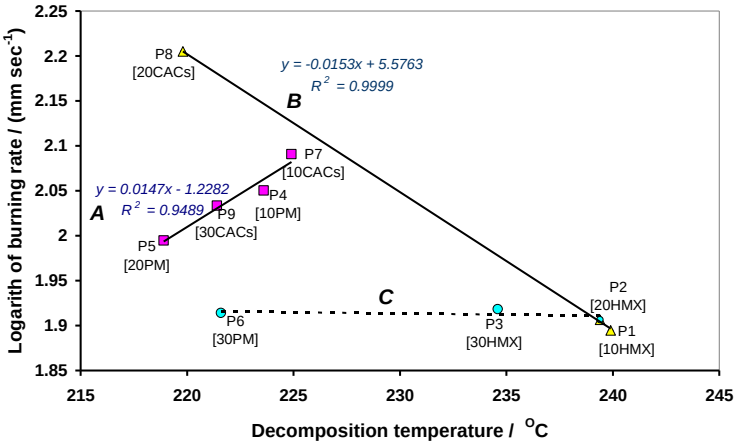

Figure 4.1.13 Semilogarithmic relationship between burning rate and decomposition temperature (more complicated comparing with Fig. 4.6)

The semilogarithmic relationship between burning rate and hardness of propellant in Fig. 4.14 is very interesting. It documents the disadvantage of using a mechanical mixture of nitramines (PM) (with increasing amounts of PM, the hardness of the propellant increases, but the burn rate decreases). A 30% nitramines content is also disadvantageous; 10 and 20% CACs are suitable for further development of the problem (a number of samples around P8 have already proven to be the most advantageous in Fig. 10a).

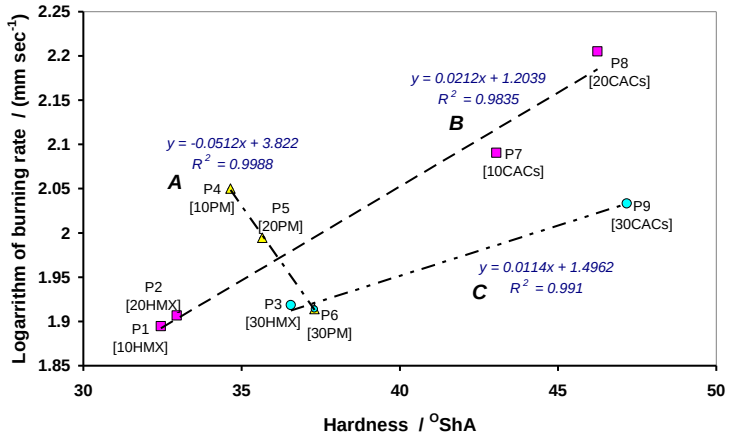

Figure 4.1.14 Semilogarithmic relationship between burning rate and hardness of propellant.

4.1.3.12 Relation between combustion and propulsion characteristics

The correlation of burn rate and specific impulse in Figure 4.1.15 shows both the known decrease in impulse with the degree of AP nitramine replacement and the significantly positive effect of CAC on burn rate. This comparison looks like a linear dependence, but for hybrid rocket propulsion it has a polynomial shape [57] - the authors of the cited paper cite as the novelty of their study the formulation of this polynomial relationship between combustion and propulsion characteristics because there was no correlation between them. They stated that although their relationship cannot be used extensively, it can be used as a conditional equation [57].

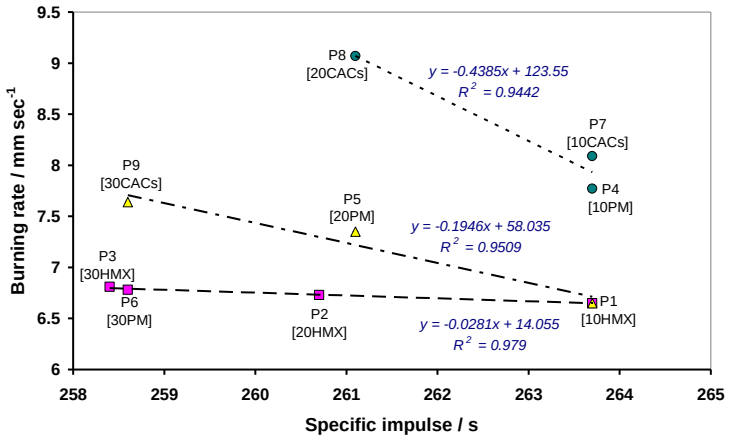

Figure 4.1.15 Mutual comparisons of burning rate and specific impulse

4.2 A test of the initiation efficiency of CL20/BCHMX CACs

The detailed characterizations and properties of these CACs see chapter 3.2. After seeing their interesting properties, they employed as additives in detonator and detailed performance study as follows.

4.2.1 Detonators

The impact sensitivity of lead azide, used in detonators, is between 1.37 and 1.96 J according to paper[58] (unrealistic values up to 4 J are given in the handbook [41]). This sensitivity is comparable with that of mainly in CACs S4LZ (1.2 J) while the sensitivity of S4LV (4.5 J) with the value in the handbook [41]. The samples S4LZ, S4LV and S5LV were tested for initiation efficiency by the detonator manufacturer, Austin Detonator in Vsetín, in accordance with the Public Notice of the Czech Mining Authority [60] (see the experimental setup in Figure 4.2.1).

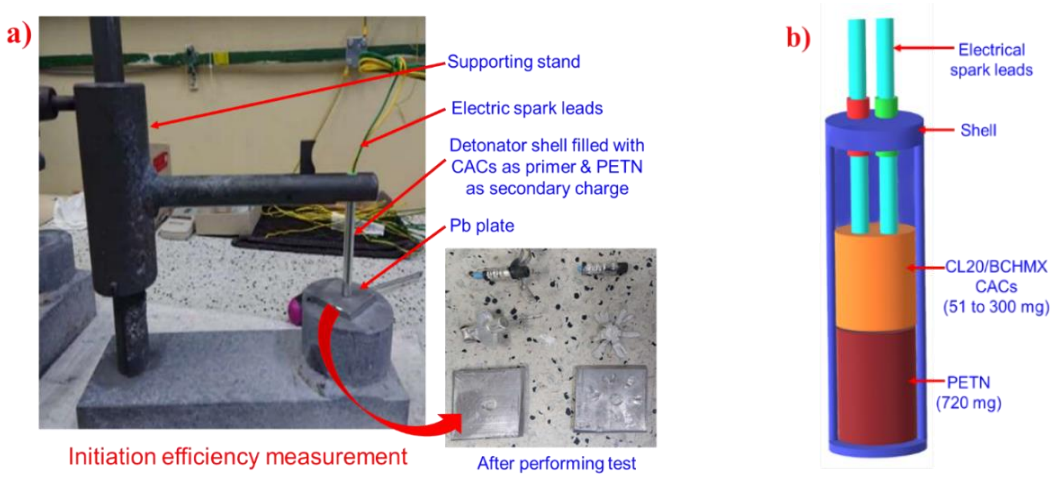

Figure 4.2.1 a) An experimental setup for testing the initiation efficiency of CACs in detonators and b) a cross-sectional view of a detonator

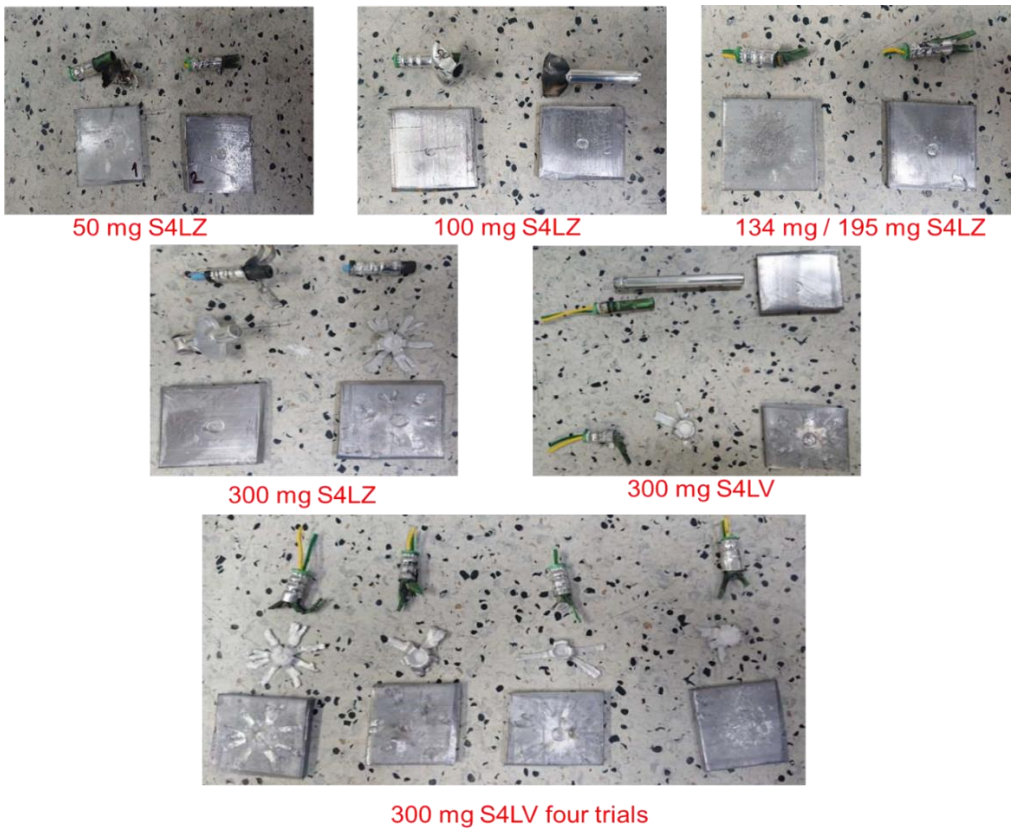

Figure 4.2.2 The initiation efficiency determination of detonators with CACs as primers results of two tests for each weighed amount - the lead plates pictures.

At such high weights, the pressure in the closed fuse system greatly increased because of the combustion gases. In most cases, the pressure thus made the fuse rupture, and no remnants of the detonated PETN were found. Figure 4.2.1 shows the measurement setup and the result of two tests with an amount of S4LZ from

50 to 300 mg sample weight: in neither of these two tests, the initiation of the secondary charge of the detonator occurred with a charge. In all cases, the aluminium tubes were ruptured, and PETN residues were found; the lead plates were not punctured effectively.

None of the three CACs tested exhibited acceleration capabilities in the given detonator design (7.5-mm-diameter Al shell NE620-301-8, with 2 x 0.36 g pentaerythritol tetranitrate – PETN as a secondary filler). For the best-performing and most sensitive sample S4LZ, the loading was gradually upgraded from 50 to 300 mg, whereas the compacting pressure for the explosives was left at 60 kg / pin. The other two samples, S4LV and S5LV, were then tested for initiation potency only at the maximum shot of 300 mg.

4.2.2 A possible practical application of CL-20/BCHMX co-crystals

ε-CL-20 and BCHMX have proved to be ideal propellant components. Despite a significant problem with the morphological instability of ε-CL-20 [44, 45], its application is already fairly well studied in this area [63]. Based on the data in, β-CL-20, present in the prepared CACs/CCs, seems to be morphologically stable in these mixed crystals. The burning of BCHMX and mixtures with its content has been the subject of several publications (for example papers [15–17, 47]; however, the application of BCHMX is still needed to explore in this area). Nevertheless, the structural and molecular specificities of BCHMX and its associated thermochemical characteristics [21] have been shown to be particularly suitable for the design of heterogeneous propellants with good combustion characteristics even under sub-atmospheric pressures [65], for example in the sense of CL-20/HMX co-crystals [66]. And indeed, as indicated by the mentioned literature [21, 48, 49] and unpublished data on military technology, this BCHMX nitramine is very important for application in propellants (see, for example, the ECL120 gunpowder from Nitrochemie Wimmis AG), which is also confirmed by our preliminary results from this area[19].

4.3 Intra-ballistic analysis of RDX/BCHMX CACs in the nitrocellulose gunpowder

The RDX/BCHMX CACs (at CETVYK, s. r. o. CZ » 0.5 Kg batch) prepared and characterized during Mirek license study the final results summarized Section 2.6.3.

4.3.2 Grain geometry analysis

Internal ballistics deals with the movement of the projectile in the gun barrel due to the pressure of the powder gases produced by the combustion of the ammunition. The course of the shot is quite complex. Therefore, we observe only the basic chemical and physical phenomena occurring during the shot, e.g., the increment of the amount of gases and the change of their state, the balance of energy, the movement of the

projectile, etc. The fundamental one is the ignition of powder gases, which is assumed to ignite all grains over the entire surface at one time, which is a simplifying assumption and more complex in a real situation. The intensity of the ignition can affect the combustion of the powder mass in the charge.

4.3.3 Analysis of the samples

The prepared samples are further subjected to a basic check of safety, quality, and performance parameters. The powder mass sensitivity was determined in the same manner as the KP RDX and BCHMX sensitivity, instrument details see Chapter 2. The results of the drop sensitivity and friction sensitivity tests are shown in Table 4.3.1.

Table 4.3.1 Thermochemical properties of gun powder grain samples

Samples	Friction sensitivity [N]	Impact Sensitivity [J]	Heat of explosion [kJ.kg^{-1}]	Water [%]	Volatiles [%]
S00	160	2	3903	1,15	0,80
S10.1 RDX	160	3	4234	1,45	0,31
S10.2 RDX/BCHMX Phy Mix	160	3	4178	1,45	0,41
S10.3 RDX/BCHMX CACs	160	3	4224	1,15	0,22

The heat of explosion of the individual samples determined (Table 4.3.1). It is very interesting that the values of the heat of explosion, which almost correlate with the theoretical values, are not affected by the by BCHMX. On the contrary, a decrease of less than 2% is evident for sample S10.2 compared to sample S10.1 where only RDX is present. It is possible that the recrystallization process of RDX and BCHMX affected the nature of the individual crystals, which had a positive effect on the result of the heat of explosion of the propellant.

4.3.3 Basic ballistic properties of powder

The basic ballistic and safety properties of powder are verified in a ballistic bomb. This is a closed container in which a certain amount of powder burns. This quantity is standardized for most measurements e.g., STANAG 4115 for a charge density of 0.2 g.cm^{-3}. The burning of the powder produces powder gases which increase the pressure in the container. By increasing the pressure in the container, the combustion of a given filling is accelerated. Based on the result of the measurement of the pressure waveform of the powder gases of Figure 4.3.1, it is possible to determine the combustion process with respect to the geometry of the grain, its surface treatment, and other characteristics. The combustion is characterized by the powder gas pressure waveform p, the maximum pressure pm, the total powder gas pressure impulse I_k and the derivative of the

powder gas pressure waveform in time d_p. Also, the dynamic powder liveliness is determined, which reflects the burn-off behaviour of the powder grain on the relative burned thickness and is determined on the basis of the pressure increment d_p normalized by the maximum pressure pmax Figure 4.3.2.

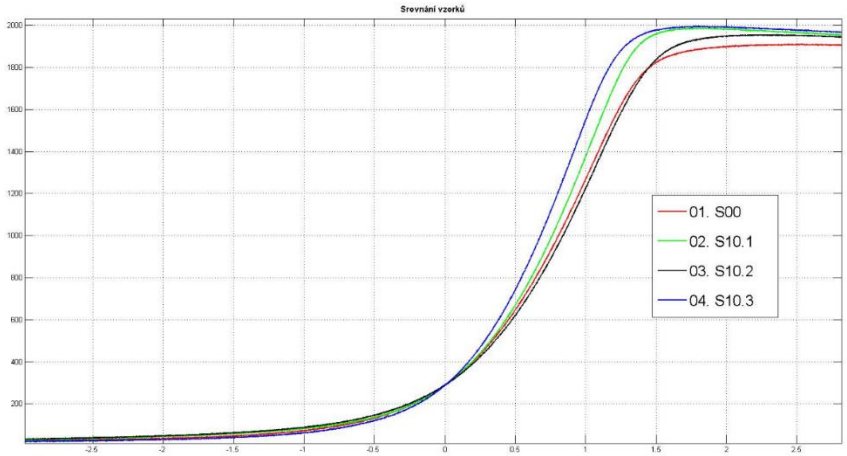

Figure 4.3.1 Pressure vs. time for samples S00, S10.1, S10.2 and S10.3.

The measured values also allowed the determination of other powder characteristics that are necessary for the assessment of gunpowder performance. The measurements in the ballistic bomb determined the specific energy of the powder f and the metalum of the powder α, which are important input values for the intra-ballistic calculation. The values are given in Table 4.3.2 and compared with the measured heat of explosion Q_v. Comparing the values in the table it is clear that the powder with the largest f (force) value is sample S10.3, in which CP RDX and BCHMX are mixed, so it is the sample with the largest potential.

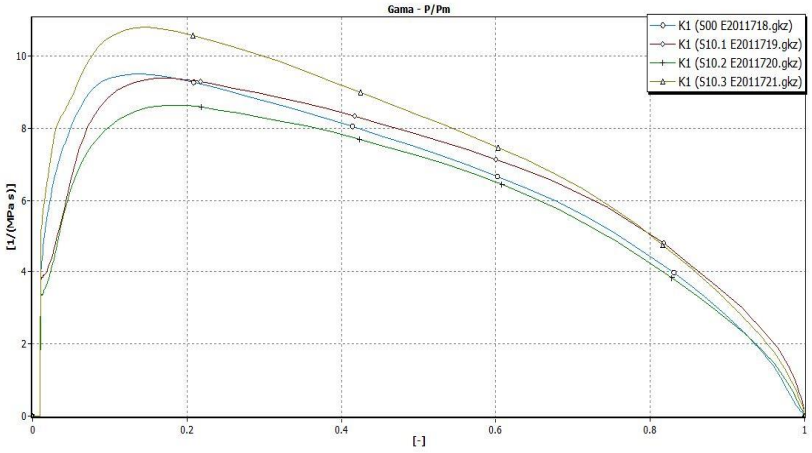

Figure 4.3.2 Dynamic liveliness of S00, S10.1, S10.2 and S10.3 powders

This finding is very interesting as the coagglomeration process of RDX and BCHMX was not successful. Nevertheless, this explosive processing probably had a positive effect on the specific energy of the powder.

Table 4.3.2 Ballistic properties of gun powder grain samples

Samples	p_m [MPa]	I_k [kPa.s]	dp [kPa.s^{-1}]	f [MJ.kg^{-1}]	Q_v [kJ.kg^{-1}]
S00	189.6	141.0	145.7	0.9914	3903
S10.1	197.1	139.6	170.8	0.9813	4234
S10.2	193.9	153.4	148.1	0.9943	4178
S10.3	198.0	124.0	178.5	1.0108	4224

For sample S10.1 it is clear that, on the contrary, the specific energy of powder has decreased to the lowest value, probably due to the addition of RDX, although the heat of explosion is the highest for this sample. Some works [67] mentioned this fact, that the addition of RDX or HMX can cause a decrease in the burning rate and nitramine behaves in some cases as an inert component (due to the real burning regime of RDX). The experiments in the mentioned work were performed at low pressures around 10-20 MPa, so it could be assumed that at pressures common for ammunition, the burning of RDX would be in a better regime. Better results can probably be achieved with higher concentrations of RDX in the ammunition (ECL powder). It may be significant that, based on these results, it may be possible to influence the burning of RDX or HMX in the powder mass by adding a small amount of BCHMX.

4.3.4 Intra-ballistic analysis of powder samples

With a comprehensive analysis of the powder grain and ballistic characteristics obtained from a ballistic bomb, it is possible to proceed to an intra-ballistic calculation. By this simulation, it is possible to search for pre-existing munitions that are suitable for the propellants in question by successive iterative calculations. The algorithm of Prof. Kusák [68] was used for the intra-ballistic calculation. By specifying the parameters and successively testing suitable ammunition assemblies, a 7.62x39 cartridge with 8 g bullet as shown in Figure 4.3.3.

For this charge, several calculations were performed to compare the powder samples with each other under different conditions, shown Table 4.3.3. All powder samples loading ω was adjusted so that the resulting maximum pressures correlate with the operating pressure of this hub (350 MPa) and second trial (ii) comparative study conducted different way, in which weight of powder samples kept constant all the samples. However, the S10.3 burned 100% compared to other samples in both trials. In addition to the maximum pressures, the table also gives the projectile velocity $v_ú$, which is essential information on the effectiveness of the entire ballistic system. Another important figure is the percentage of powder charge burned when the projectile leaves the barrel. This figure is also indicative of, for example, the economic yield of the propellant

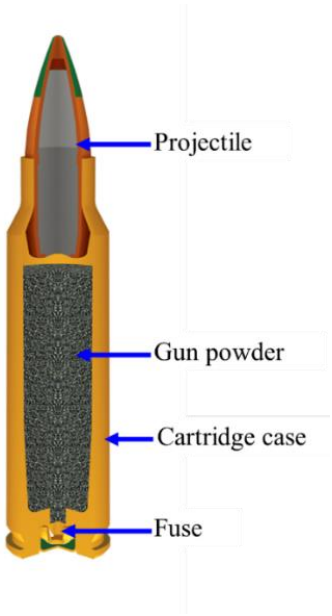

Figure 4.3.3 Schematic Assembly of 7,62x39 cartridge with FMJ 8 g bullet.

Table 4.3.3 Intra-ballistic analysis of powder samples

Samples	p_m [MPa]	$v_ú$ [m.s^{-1}]	ω [g]	Percentage of Gunpowder burned [%]
S00	i) 351.7	733.0	1.678	96.9
	ii) 229.3	654.3	1.506	87.0
S10.1	i) 351.9	723.5	1.603	96.8
	ii) 264.8	673.1	1.506	90.4
S10.2	i) 351.1	738.7	1.727	89.8
	ii) 201.8	632.8	1.506	77.6
S10.3	i) 351.4	753.8	1.506	100
	ii) 351.4	753.8	1.506	100

Table 4.3.4 The courses of individual intra-ballistic quantities of for both variants(as per Table 4.3.3) tests of powder mass in the 7.62x39 cartridge

Projectile	Recommended weights / size				Maximum weights / size						Stellar & Bellot
FMJ 8.0g 123 gr	Weights taken		Velocity V5		Weights taken		Velocity V5		Pressure		No. 2907
	In grams	Grain size	ms^{-1}	FPS	In grams	Grain size	ms^{-1}	FPS	Bar	PSI	Charge length
S053	1.50	23.1	715	2345	1.62	25.0	765	2509	3490	50600	56.00 mm
D063	1.50	23.1	730	2394	1.65	25.5	770	2526	3520	51100	

The courses of individual intra-ballistic further tested in for both powder mass trials in the 7.62x39 cartridge. In Table 4.3.4, which is extracted from the manual for LOVEX powder reloading of Explosia Inc., the values for the 7.62x39 cartridge. For the calculation, the same bullet assembly with a total length of 56 mm and a barrel length of 600 mm was used. The difference between the velocities according to the intra-ballistic calculation and the value from the reloading manual is due to the different locations of bullet velocity measurements. In the intra-ballistic calculation this is the value at the muzzle measured at 5 m from the muzzle is shown in Table 4.3.4. The additional effect of the powder gases, which accelerated the projectile, has already taken effect. It is clear, however, that the projectile has been flying inertia since the end of the additional gas effect and therefore its velocity has been gradually decreasing. Therefore, the velocity of the projectiles is slightly different.

4.4 Futuristic applications of remaining CACs of attractive nitramines

The remaining co-crystals can be used as replacement of their earlier purest forms applications apart from that basis of their interesting current gained properties in cocrystallization, they can be employed in various applications as follows;

4.4.1 DATB and TATB CACs:

These CACs are suitable for fillers in insensitive ammunition, especially the more selective ones are HMX/TATB and RDX/TATB.

4.4.2 HNS and HNAB CACs:

These CACs are suitable for ammunition, secondary fillers of detonators for deep holes with perforation of casting of metal pipes, especially the more suitable one is HMX/HNS.

4.4.3 PANi CACs:

These CACs are more suitable for secondary fillers of detonators charges and air bag initiators. Overall, more suitable for which application required impact insensitive and same time required to have spark sensitivity like electrical detonators and pyrotechnic goods mainly for spacecrafts.

4.4.4 BTATZ CACs:

The cyclic nitramines CACs with nitrogen rich BTATZ as a coformer are exergonic and could provide energy for self-propagating reactions for spacecrafts, making them ideal combination for propulsion applications, also ammunition and special charges.

4.5 Summary

4.5.1 HMX/BCHMX CACs in composite rocket propellant

Coagglomerated crystals (CACs) of and Physical mixture (PM) HMX/BCHMX were prepared, thoroughly characterized. The pure HMX (P1-P3) and these both [PM (P4-P6) & CACs (P7-P9)] are employed in composite rocket propellant separately (P1-P3; P4-P6 & P7-P9) at different proportions (10 – 30%). The experimental results obtained from PXRD, FTIR, Raman, and DTA analyses provide compelling evidence of robust intra- and intermolecular interactions between the coformers in the CACs. These findings unequivocally demonstrate the formation of cocrystals. In order to assess the impact of CACs on the properties of propellant particles, a comprehensive characterization was conducted. The results revealed significant enhancements in the performance of propellant particles when CACs were incorporated. The examination of morphology and particle size indicates that CACs exhibit consistent sizes, well-distributed characteristics, and possess microcrystal edges that have undergone softening. This results in a homogeneous distribution over the propellant coarse, which is compared to a physical mixture. The location of these particles has a significant impact on thermal characterization. Specifically, in the third category (P7-P9), the carbonaceous aerosol composites (CACs) exhibited more pronounced variations in decomposition for all three concentrations. In the thermal decomposition test, it was shown that both CACs and PM exhibited higher reactivity compared to batches containing pure HMX. This can be attributed to the reduction in ammonium perchlorate (AP) content and the greater reactivity of the binder-cured HMX with BCHMX. Moreover, the response of prepared propellants to mechanical stimuli is mostly determined by the composition and concentration of nitramines present inside them. The sensitivity of the combination is not significantly affected by the amount of pure HMX, with the exception of when it reaches a weight percentage of 30%. However, the sensitivity is influenced by the presence of PM and CACs. The use of CACs exclusively influences the sensitivity to impact, but the application of PM has a dual effect by negatively impacting both sensitivity to impact and another factor. The correlation between the sensitivity of these propellants and their performance, as well as their energy content, plays a pivotal role in ensuring safety during their manufacturing, handling, and storage processes. The experimental correlation is predominantly grounded on Licht's rule[42]. The measurement of burn rates has been conducted, revealing conflicting findings. Subsequently, we proceeded to verify and adjust the instrument, ultimately identifying instrumental errors. Consequently, we have chosen to exclude these errors from the present analysis. Upon careful evaluation of the many enhancements in propellant composition, it is evident that the CACs exhibit superior qualities compared to the other two categories.

4.5.2 CL20/BCHMX CACs in detonators

In the same way, the utilization of sensitive CACs is used in detonators. In order to assess their capacity for commencement. The utilization of the most sensitive CACs (1.2 J) as a detonator primer in this particular detonator design did not demonstrate the necessary acceleration capabilities. However, a thorough examination of existing literature reveals that co-crystals containing CACs and co-crystals of this nature possess potential benefits for usage in propellants due to the morphological stability of β-CL-20 within these co-mixed crystals.

4.5.3 RDX/BCHMX CACs in gun powder

The earlier results of this work showed that the use of nitramines in ammunition is of legitimate interest. By nitramines can be qualitatively substituted for nitroglycerin in some binary powders. For example, sample S10.3 can be tentatively compared with the measured results in Table 4.3.4 for the two-component powder D063 of the same charge and barrel length. The measured values on the samples also show that the use of only 10% of the amount of RDX as an additive in the propellant does not lead to an increase in specific energy of the powder with respect to plain nitrocellulose. For comparison, the calculation of the theoretically achievable projectile velocity and powder gas pressure was used, according to the intra-ballistic model of Prof. Kusák [2, 3] based on data from measurements made in a ballistic bomb.

A comparison of the calculated characteristics of samples S00 and S10.1 is given in Table 4.3.4. In S10.1, although a smaller weighting of 0.075 g is used due to the consolidation of pressure to the same level, where not only the pressure but also the percentage of the burnt charge are approximately the same, the value of the projectile velocity is lower by 10 $m.s^{-1}$ in sample S10.1. This means that the addition of RDX alone in this amount does not show any benefit on the propellant performance. On the contrary, it proved to be counterproductive. A likely explanation is the burning process of RDX particles during the powder function. Better results could be achieved by a higher concentration of RDX in the powder, such as in ECl powders, or by a suitable combustion moderator.

The computational model suggests that the aforementioned RDX deficiency in the powder mass can be corrected by adding 2 % BCHMX. This very small addition of BCHMX not only compensated for the decrease in values, but also slightly increased them, despite the fact that a larger weighting is used, and a smaller amount of powder mass is burned at the shot than in samples S00 and S10.1. The values of sample S10.2 are shown in Table 4.3.3 & 4.3.4. If the entire amount of powder in the barrel is not burned at the shot, it can be assumed that a more significant flash-off occurs in front of the barrel due to the afterburning of some grains. This phenomenon is almost unacceptable in military ammunition.

Sample S10.3 can be best evaluated, where the same amount of RDX and BCHMX is present as in sample S10.2, but the nitramines here have undergone a technological procedure for the formation of coprecipitates. Although it has been shown that the KP preparation process has not been completely successful, nevertheless the results of the calculation of achievable values of the projectile velocity and powder gas pressure in the 7.62x39 cartridge assembly of this propellant are the best.

Thus, it can be stated with a certain degree of uncertainty that cis-1,3,4,6-tetranitrooctahydro[4,5-d]imidazole (BCHMX) has an unquestionable positive effect on the combustion of a powder mass containing RDX even in a relatively small two per cent quantity. It would also be useful to demonstrate whether this powder is stable at other operating temperatures and whether the ballistic values of the ammunition are significantly affected by these temperature fluctuations. It is also necessary to validate the results of the theoretical calculations for the 7.62x39 mm cartridge with real bullet assemblies.

4.5.4 Applications Remaining CACs

The individual coformers chosen for preparation of CACs of attractive nitramines, the futuristic applications are addressed basis of their interesting characteristic thermochemical and energetic properties. Especially, PANi and BTATZ CACs are ideal combinations space craft carrier separate loads and initiating next stage by PANi CACs. PANi CACs are better as initiators and BTATZ CACs as main propulsion part. Also, PANi CACs can be used as catapulting charges with combination of other CACs as main charges i.e., application of electromagnetic launch technology in the field of missile.

References

[1] E. Cohen-Nir, “Combustion characteristics of advanced nitramine-based propellants,” Symposium (International) on Combustion, vol. 18, no. 1, pp. 195–206, 1981, doi: 10.1016/S0082-0784(81)80024-0.

[2] W. Klöhn and S. Eisele, “Nitramine Solid Rocket Propellants with Reduced Signature,” Propellants, Explosives, Pyrotechnics, vol. 12, no. 3, pp. 71–77, Jun. 1987, doi: 10.1002/prep.19870120303.

[3] M. H. Alexander et al., “Nitramine propellant ignition and combustion research,” Progress in Energy and Combustion Science, vol. 17, no. 4, pp. 263–296, Jan. 1991, doi: 10.1016/0360-1285(91)90005-8.

[4] R. R. Sanghavi, P. J. Kamale, M. A. R. Shaikh, S. D. Shelar, K. S. Kumar, and A. Singh, “HMX based enhanced energy LOVA gun propellant,” Journal of Hazardous Materials, vol. 143, no. 1–2, pp. 532–534, May 2007, doi: 10.1016/j.jhazmat.2006.09.087.

[5] T. Naya and M. Kohga, “Influences of particle size and content of HMX on burning characteristics of HMX-based propellant,” Aerospace Science and Technology, vol. 27, no. 1, pp. 209–215, Jun. 2013, doi: 10.1016/j.ast.2012.08.012.

[6] S. Zhou, F. Wu, G. Tang, Y. Wang, and A. Pang, “Effects of 2CL-20/HMX cocrystals on the thermal decomposition behavior and combustion properties of polyether solid propellants,” Energetic Materials Frontiers, vol. 2, no. 2, pp. 96–104, Jun. 2021, doi: 10.1016/j.enmf.2021.03.003.

[7] S. Hanafi et al., “Synthesis, characterization and thermal decomposition behavior of a novel HNTO/AN co-crystal as a promising rocket propellant oxidizer,” Chemical Engineering Journal, vol. 417, p. 128010, Aug. 2021, doi: 10.1016/j.cej.2020.128010.

[8] Z. Wang, Z.-H. Xue, K.-J. Meng, X.-X. Zhang, and Q.-L. Yan, “Decomposition and combustion of HTPB-based composite propellants containing intercalated HMX crystals with desired high energy but low burn rate,” Fuel, vol. 321, p. 124067, Aug. 2022, doi: 10.1016/j.fuel.2022.124067.

[9] X. Lv et al., “Effects of Ammonium Perchlorate and CL-20 on Agglomeration Characteristics of Solid High-Energy Propellants,” Energies, vol. 15, no. 20, p. 7545, Oct. 2022, doi: 10.3390/en15207545.

[10] D. Gou, Z. Fan, S. Wu, P. Liu, G. He, and W. Ao, “The role of HMX particle size in the combustion and agglomeration of HTPB-based propellant,” Aerospace Science and Technology, p. 108170, Feb. 2023, doi: 10.1016/j.ast.2023.108170.

[11] V. B. Patil, K. Zalewski, J. Schuster, P. Belina, W. Trzcinski, and S. Zeman, “A new insight into the energetic co-agglomerate structures of attractive nitramines,” Chemical Engineering Journal, vol. 420, Sep. 2021, doi: 10.1016/j.cej.2021.130472.

[12] V. B. Patil et al., “Co-agglomerated crystals of cyclic nitramines with sterically crowded molecules,” CrystEngComm, p. 10.1039.D2CE00840H, 2022, doi: 10.1039/D2CE00840H.

[13] V. B. Patil, P. Bělina, W. A. Trzcinski, and S. Zeman, “Preparation and properties of co-mixed crystals of 1,3-di- and 1,3,5-tri-amino-2,4,6-trinitrobenzenes with attractive cyclic nitramines,” Journal of Industrial and Engineering Chemistry, vol. 115, pp. 135–146, Nov. 2022, doi: 10.1016/j.jiec.2022.07.043.

[14] V. B. Patil, P. Bělina, W. A. Trzcinski, and S. Zeman, “Co-agglomerated crystals of 2,2′,4,4′,6,6′-hexanitro - stilbene/-azobenzene with attractive nitramines,” Chemical Engineering Journal, vol. 457, p. 141200, Feb. 2023, doi: 10.1016/j.cej.2022.141200.

[15] V. P. Sinditskii, V. Y. Egorshev, and M. V. Berezin, “Study on combustion of new energetic nitramines.” 2001.

[16] V. Sinditskii, V. Egorshev, M. Berezin, V. Serushkin, S. Filatov, and A. Chernyi, “Combustion mechanism of nitro ester binders with nitramines,” Combustion, Explosion, and Shock Waves, vol. 48, pp. 163–176, Mar. 2012, doi: 10.1134/S0010508212020062.

[17] V. Sinditskii et al., “Evaluation of decomposition kinetics of energetic materials in the combustion wave,” Thermochimica Acta, vol. 496, pp. 1–12, Dec. 2009, doi: 10.1016/j.tca.2009.07.004.

[18] L. Qiu, W.-H. Zhu, J.-J. Xiao, and H.-M. Xiao, “Theoretical Studies of Solid Bicyclo-HMX: Effects of Hydrostatic Pressure and Temperature,” J. Phys. Chem. B, vol. 112, no. 13, pp. 3882–3893, Apr. 2008, doi: 10.1021/jp070863f.

[19] M. Novák, “Ověření vlivu bicyklo-HMX na parametry prachu s obsahem RDX (Verification of the bicyclo-HMX effect on the RDX gunpowder parameters), The final project of the licensing study,” Univ. Pardubice, Feb. 2022.

[20] D. Klasovitý, S. Zeman, A. Růžička, M. Jungová, and M. Roháč, “cis-1,3,4,6-Tetranitrooctahydroimidazo-[4,5-d]imidazole (BCHMX), its properties and initiation reactivity,” Journal of Hazardous Materials, vol. 164, no. 2–3, pp. 954–961, May 2009, doi: 10.1016/j.jhazmat.2008.08.106.

[21] S. Zeman, A. K. Hussein, A. Elbeih, and M. Jungova, “cis-1,3,4,6-Tetranitrooctahydroimidazo-[4,5-d]imidazole (BCHMX) as a part of explosive mixtures,” Defence Technology, vol. 14, no. 5, pp. 380–384, Oct. 2018, doi: 10.1016/j.dt.2018.04.002.

[22] S. Zeman, “Characteristics of Thermal Decomposition of Energetic Materials in a Study of Their Initiation Reactivity,” in Handbook of Thermal Analysis and Calorimetry, vol. 6, Elsevier, 2018, pp. 573–612. doi: 10.1016/B978-0-444-64062-8.00006-1.

[23] S. Zeman, “The Chemical Micromechanism of Energetic Material Initiation,” in Nano and Micro-Scale Energetic Materials, John Wiley & Sons, Ltd, 2023, pp. 567–623. doi: 10.1002/9783527835348.ch19.

[24] S. Vyazovkin, N. Koga, and C. Shick, “Handbook of thermal analysis and calorimetry: recent advances, techniques and applications. Volume 6 Volume 6.” 2018.

[25] S. Kelzenberg, P. B. Kempa, S. Wurster, M. Herrmann, and T. S. Fischer, “New Version Of The ICT-Thermodynamic Code”.

[26] Fraunhofer Institut für Chemische Technologie, Pfinztal, Germany, 2004, “ICT Database of thermochemical values.” 2004.

[27] S. Zeman, A. Růžička, J. Moncol, Q.-L. Yan, J. Šelešovský, and K. Dudek, “Crystal structure and thermal behaviors of the tetrapotassium salt of octahydroimidazo-[4,5-d]imidazol-1,3,4,6-tetrasulfonic acid (TACOS-K),” J Therm Anal Calorim, vol. 126, no. 2, pp. 391–397, Nov. 2016, doi: 10.1007/s10973-016-5528-1.

[28] A. Elbeih et al., “Enhancing the explosive characteristics of a Semtex explosive by involving admixtures of BCHMX and HMX,” Defence Technology, vol. 16, no. 2, pp. 487–492, 2020, doi: 10.1016/j.dt.2019.05.012.

[29] M. Rajić and M. Sućeska, “Study of Thermal Decomposition Kinetics of Low-temperature Reaction of Ammonium Perchlorate by Isothermal TG,” Journal of Thermal Analysis and Calorimetry, vol. 63, no. 2, pp. 375–386, Feb. 2000, doi: 10.1023/A:1010136308310.

[30] J. Zhi et al., “Thermalbehavior of ammonium perchlorate and metal powders of different grades,” J Therm Anal Calorim, vol. 85, no. 2, pp. 315–320, Aug. 2006, doi: 10.1007/s10973-005-7035-7.

[31] A. N. Pivkina et al., “Synergistic Effect of Ammonium Perchlorate on HMX: From Thermal Analysis to Combustion,” in Chemical Rocket Propulsion: A Comprehensive Survey of Energetic Materials, L. T. De Luca, T. Shimada, V. P. Sinditskii, and M. Calabro, Eds., in Springer Aerospace Technology. , Cham: Springer International Publishing, 2017, pp. 365–381. doi: 10.1007/978-3-319-27748-6_15.

[32] Y. Wang, L. Liu, L. Xiao, and Z. Wang, “Thermal decomposition of HTPB/AP and HTPB/HMX mixtures with low content of oxidizer,” J Therm Anal Calorim, vol. 119, no. 3, pp. 1673–1678, Mar. 2015, doi: 10.1007/s10973-014-4324-z.

[33] W. Pang, L. T. DeLuca “Nano and Micro-Scale Energetic Materials | Wiley Online Books.” Accessed: Oct. 31, 2023. [Online]. doi:10.1002/9783527835348

[34] S. Zeman, A. K. Hussein, M. Jungova, and A. Elbeih, “Effect of energy content of the nitraminic plastic bonded explosives on their performance and sensitivity characteristics,” Defence Technology, vol. 15, no. 4, pp. 488–494, Aug. 2019, doi: 10.1016/j.dt.2018.12.003.

[35] W. N. Hubbard, J. W. Knowlton, and H. M. Huffman, “Combustion Calorimetry of Organic Chlorine Compounds. Heats of Combustion of Chlorobenzene, the Dichlorobenzenes and o- and p-Chloroethylbenzene,” J. Phys. Chem., vol. 58, no. 5, pp. 396–402, May 1954, doi: 10.1021/j150515a004.

[36] Yu. Y. Maksimov, “Termicheskoe razlozheniye geksogena I oktogena (Thermal de composition of hexogen and octogen),” Tr. - Mosk. Khim.-Tekhnol. Inst. im. D. I. Mendeleeva; (USSR), vol. 53, pp. 73–84, 1967.

[37] R. S. Stepanov, L. A. Kruglyakova, and A. M. Astakhov, “Kinetics of thermal decomposition of some nitramines with two condensed quinary cycles,” Zh. Obsh. Khim, vol. 76, p. 2063, 2006.

[38] Q.-L. Yan, S. Zeman, A. Elbeih, and Z. Akstein, “The Influence of the Semtex Matrix on the Thermal Behavior and Decomposition Kinetics of Cyclic Nitramines,” Central European Journal of Energetic Materials, vol. 10, pp. 509–528, Nov. 2013.

[39] S. Zeman, A. Elbeih, A. Hussein, T. Elshenawy, M. Jungova, and Q. L. Yan, “A modified vacuum stability test in the study of initiation reactivity of nitramine explosives,” Thermochimica Acta, vol. 656, pp. 16–24, Oct. 2017, doi: 10.1016/j.tca.2017.08.006.

[40] V. Kučera and B. Vetlický, “Investigation of the Decomposition Processes in Single-Base Propellants under vacuum using a minicomputer-controlled automated apparatus,” Propellants, Explosives, Pyrotechnics, vol. 10, no. 3, pp. 65–68, 1985, doi: 10.1002/prep.19850100303.

[41] S. Zeman, Š. Gazda, A. Štolcová, and A. Dimun, “Dependence on temperature of the results of the vacuum stability test for explosives,” Thermochimica Acta, vol. 247, no. 2, pp. 447–454, Dec. 1994, doi: 10.1016/0040-6031(94)80144-4.

[42] H.-H. Licht, “Performance and Sensitivity of Explosives,” Propellants Explos. Pyrotech, vol. 25, no. 3, pp. 126–132, Jun. 2000, doi: 10.1002/1521-4087(200006)25:3<126::AID-PREP126>3.0.CO;2-8.

[43] Sarner Stanley F.: F Propellant Chemistry. by, | Boojum and Snark Books, 1st ed., vol. 1. Reinhold Publishing, New York, 1966.

[44] K. Menke, J. Böhnlein-Mauß, and H. Schubert, “Characteristic Properties of AN/GAP-Propellants,” Propellants, Explosives, Pyrotechnics, vol. 21, no. 3, pp. 139–145, 1996, doi: 10.1002/prep.19960210306.

[45] T. Lee et al., “Stabilization and spheroidization of ammonium nitrate: Co-crystallization with crown ethers and spherical crystallization by solvent screening,” Chemical Engineering Journal, vol. 225, pp. 809–817, Jun. 2013, doi: 10.1016/j.cej.2013.04.002.

[46] M. Ruesch et al., “Burning rate and flame structure of cocrystals of CL-20 and a polycrystalline composite crystal of HMX/AP,” COMBUSTION AND FLAME, vol. 219, pp. 129–135, Sep. 2020, doi: 10.1016/j.combustflame.2020.04.009.

[47] H. Li, C. An, W. Guo, X. Geng, J. Wang, and W. Xu, “Preparation and Performance of Nano HMX/TNT Cocrystals,” Propellants Explosives Pyrotechnics, vol. 40, no. 5, pp. 652–658, Oct. 2015, doi: 10.1002/prep.201400175.

[48] C. An, H. Li, B. Ye, and J. Wang, “Nano-CL-20/HMX Cocrystal Explosive for Significantly Reduced Mechanical Sensitivity,” Journal of Nanomaterials, vol. 2017, pp. 1–7, 2017, doi: 10.1155/2017/3791320.

[49] T. Naya and M. Kohga, “Influences of particle size and content of RDX on burning characteristics of RDX-based propellant,” Aerospace Science and Technology, vol. 32, no. 1, pp. 26–34, Jan. 2014, doi: 10.1016/j.ast.2013.12.004.

[50] V. P. Sinditskii, V. Yu. Egorshev, M. V. Berezin, and V. V. Serushkin, “Mechanism of HMX combustion in a wide range of pressures,” Combust Explos Shock Waves, vol. 45, no. 4, pp. 461–477, Jul. 2009, doi: 10.1007/s10573-009-0057-x.

[51] A. I. Atwood et al., “Burning Rate of Solid Propellant Ingredients, Part 1: Pressure and Initial Temperature Effects,” Journal of Propulsion and Power, vol. 15, no. 6, pp. 740–747, Nov. 1999, doi: 10.2514/2.5522.

[52] R. Yang, H. An, and H. Tan, “Combustion and thermal decomposition of HNIW and HTPB/HNIW propellants with additives,” Combustion and Flame, vol. 135, no. 4, pp. 463–473, Dec. 2003, doi: 10.1016/j.combustflame.2003.08.008.

[53] D. Signoriello et al., “Solid propellants based on AN/AP co-crystals for green space access”.

[54] T. L. Jensen, E. Unneberg, and T. E. Kristensen, “Smokeless GAP-RDX Composite Rocket Propellants Containing Diaminodinitroethylene (FOX-7),” Propellants, Explosives, Pyrotechnics, vol. 42, no. 4, pp. 381–385, 2017, doi: 10.1002/prep.201600278.

[55] F. Sazeček, O. Vodochodský, R. Matyáš, P. Stojan, J. Zigmund, and J. Pachman, “Bicyclo-HMX as an Energetic Additive for Composite Propellants,” Journal of Propulsion and Power, vol. 39, no. 4, pp. 626–631, Jul. 2023, doi: 10.2514/1.B38977.

[56] S. Zeman, “Chapter 14 - Characteristics of Thermal Decomposition of Energetic Materials in a Study of Their Initiation Reactivity,” in Handbook of Thermal Analysis and Calorimetry, vol. 6, S. Vyazovkin, N. Koga, and C. Schick, Eds., in Recent Advances, Techniques and Applications, vol. 6. , Elsevier Science B.V., 2018, pp. 573–612. doi: 10.1016/B978-0-444-64062-8.00006-1.

[57] R. Sunil, A. Virkar, M. V. Kumar, I. Krishnamoorthy, and V. Malhotra, “Combustion and propulsive characteristics of potential hybrid rocket propellant,” IOP Conf. Ser.: Mater. Sci. Eng., vol. 912, no. 4, p. 042023, Aug. 2020, doi: 10.1088/1757-899X/912/4/042023.

[58] L Mertz, Zeitschrift für das gesamte Schiess- und Sprengstoffwesen, vol. 23. J. F. Lehmann., 1928.

[59] F. Shen, P. Lv, C. Sun, R. Zhang, and S. Pang, “The Crystal Structure and Morphology of 2,4,6,8,10,12-Hexanitro-2,4,6,8,10,12-hexaazaisowurtzitane (CL-20) p-Xylene Solvate: A Joint Experimental and Simulation Study,” Molecules, vol. 19, no. 11, Art. no. 11, Nov. 2014, doi: 10.3390/molecules191118574.

[60] “Public Notice of Czech Mining Authority No. 246/1996 Collection of Czech Laws, Establishing more Detailed Conditions for Allowing Explosives, Explosive Objects and Aids into Use, and Their Testing, P 3200-3208.” Czech Mining Authority, Aug. 13, 1996.

[61] S. A. Torry and A. V. Cunliffe, “Polymorphism and solubility of CL in plasticizers and polymers,” presented at the 31st Interanational Annual Conference, ICT, Karlsruhe, Germany: ICT, Jun. 2000, p. 107/1-107/12.

[62] V. Pelikán, S. Zeman, Q. L. Yan, M. Erben, A. Elbeih, and Z. Akštein, “Concerning the Shock Sensitivity of Cyclic Nitramines Incorporated into a Polyisobutylene Matrix*)”.

[63] U. R. Nair, R. Sivabalan, G. M. Gore, M. Geetha, S. N. Asthana, and H. Singh, “Hexanitrohexaazaisowurtzitane (CL-20) and CL-20-based formulations (review),” Combust Explos Shock Waves, vol. 41, no. 2, pp. 121–132, Mar. 2005, doi: 10.1007/s10573-005-0014-2.

[64] V. Sinditskii, V. Y. Egorshev, V. V. Serushkin, S. A. Filatov, and A. N. Chernyi, “Combustion mechanism of energetic binders with nitramines,” IJEMCP, vol. 11, no. 5, 2012, doi: 10.1615/IntJEnergeticMaterialsChemProp.2013005557.

[65] V. P. Sinditskij, V. Y. Egorshev, and M. V. Berezin, “Energetic materials: ignition, combustion and detonation : 32nd International Annual Conference of ICT,” in Internationale Jahrestagung. Karlsruhe, Germany: Fraunhofer-Institut für Chemische Technologie, Jul. 2001.

[66] Z. Wu et al., “Application and Properties of CL-20/HMX Cocrystal in Composite Modified Double Base Propellants,” Propellants, Explosives, Pyrotechnics, vol. 45, no. 1, pp. 92–100, 2020, doi: 10.1002/prep.201900245.

[67] V. Sinditskii, V. Egorshev, V. Serushkin, S. Filatov, and A. Chernyi, “Combustion mechanism of energetic binders with nitramines,” International Journal of Energetic Materials and Chemical Propulsion, vol. 11, pp. 427–449, Jan. 2012, doi: 10.1615/IntJEnergeticMaterialsChemProp.2013005557.

[68] Kusák Jan, “Matematický model vnitřní balistiky.” Czech Republic, 2010.

[69] Kusák, J. and V. Řebíček, “Charbonnier’s combustion function. In: Proceedings of VVU-ZVS, III,” in VP RVVT and Subdivision of ČSVTS at ZVS-VVU, Brno, 1981, pp. 61–81.

Chapter 5 Conclusion

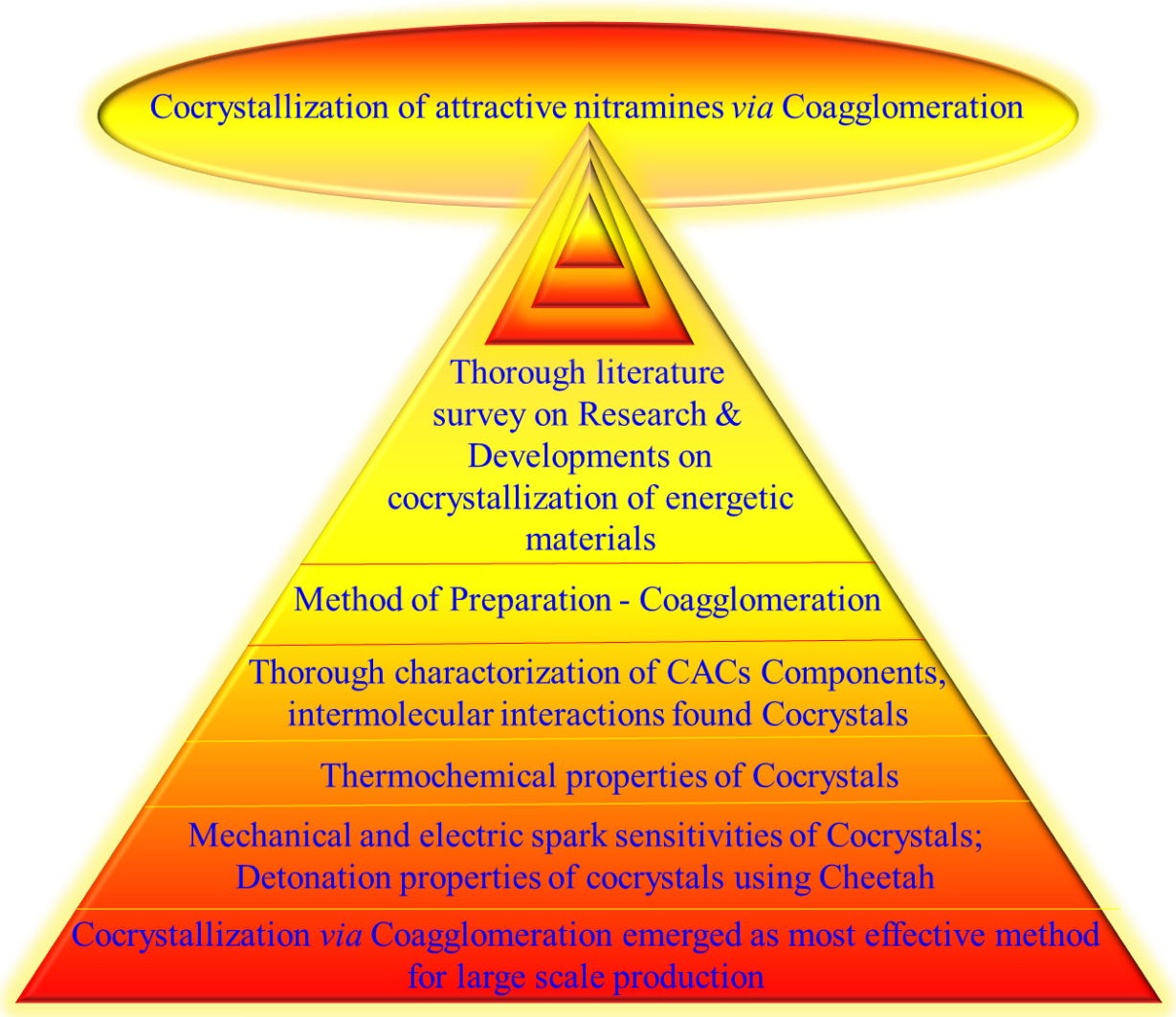

5. Conclusion

Current research thesis entitled “Achieving cocrystals of the attractive nitramines via coagglomeration”. We made our best efforts fulfilling the current requirements of energy-safety contradiction. On the bases known fact proclivity of nanoparticles of some nitramines to agglomerate - mainly 1,3,5-trinitro-1,3,5-triazinane (RDX) and 1,3,5,7-tetranitro-1,3,5,7-tetrazocane (HMX). Chosen attractive nitramines(NMs) for the study viz., ε-2,4,6,8,10,12-hexanitro-2,4,6,8,10,12- hexaazaisowurtzitane (ε-CL-20), cis-1,3,4,6-tetranitrooctahydroimidazo-[4,5-d]imidazole (BCHMX or bicyclo-HMX), ß-1,3,5,7-tetranitro-1,3,5,7-tetrazocane (ß-HMX), and 1,3,5- trinitro-1,3,5-triazinane (RDX), successfully modified their properties works are published in esteemed journals. The current paper summarizes the success of the journey and the output of the coagglomeration process and obtained coagglomerated crystals properties discussed in brief [1–7].

Most of the methods reported till today in modification properties of these NMs, still they have drawback as well as their undeniable advantages, such as higher amounts of solvents, long preparation times for cocrystals, quantitative limitations, or the impossibility of application to certain types of coformers (Scheme 5.1). In our approach, we made improvement of the known fact of easy agglomeration of nano- and micro-particles of HEMs. The co-agglomeration is essentially co-crystallization in suspension (“slurry method”), in our embodiment in an aprotic or protogenic solvent in which the coformers have low solubility. Process involves the initial mixture of the coformers was obtained by precipitation from their common solution by anti-solvent.

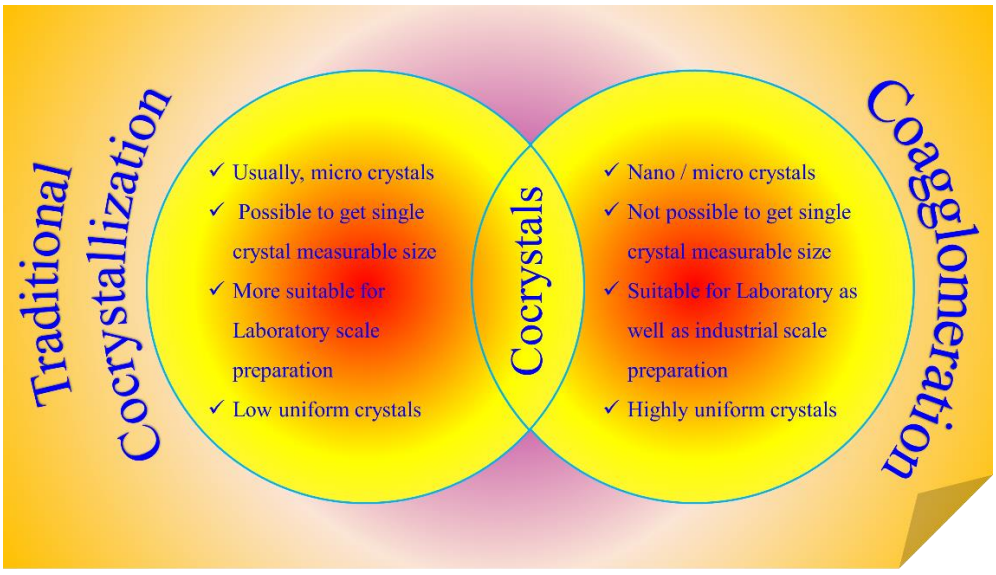

Scheme 5.1 General importance coagglomeration method over traditional cocrystallization methods

By this route we obtained co-agglomerated crystals (CACs) of the attractive nitramines CL20, HMX, BCHMX and RDX not only with polynitroarenes and between nitramines with sterically hindered molecules, i.e., CL20 and BCHMX, but also with electrically conducting polyaniline (PANi). Important key findings are briefly listed below [1–7].

5.1 CACs of attractive nitramines with selective coformers

5.1.1 CACs of attractive nitramines with DATB and TATB

Both 1,3-diamino-2,4,6-trinitrobenzene (DATB) and 1,3,5-triamino-1,3,5-trinitro benzene (TATB) lead to the formation of co-agglomerates (CACs) with the nitramines, in which HMX presents in its δ-form and CL-20 in its β-form [1, 2]; the δ-HMX stabilization in these CACs is particularly interesting, since the lifetime of this pure isomer is only 12 hours [8]. Whereas using DATB yielded CACs with a density of at most 99 % of the theoretical density of the mixed crystal, the TATB CACs densities are higher than those using the pure nitramines (including β-CL-20). The sensitivity is quite strongly reduced in the TATB CACs (15 – 50 J) compared to their DATB analogues (4 – 12 J). Detonation parameters of CACs containing DATB and TATB are logically lower than those of the starting nitramines. The detonation energies of these mixed crystals are higher than would be expected from the respective percentage of the co-formers. The most interesting of the CACs studied appears to be HMX/TATB (D = 9332 $m.s^{-1}$) which in the formulation used here, has a slightly increased density (ρ = 1.909 g.cm-3) with only slightly reduced detonation parameters compared to pure HMX (ρ = 1.902 g.cm-3, D = 9404 m.s-1), while its impact resistance is extremely high (50 J). This CACs, together with RDX/TATB co-agglomerate, could be suitable filler for ammunition objects with high vulnerability resistance.

5.1.2 CACs of CL20 and BCHMX

The CACs of sterically crowded molecules CL20/BCHMX took long time efforts finally stabilized form obtained [3], here most important things are used medium of co-agglomeration and the molar ratio of coformers. This can yield a co-crystal with clearly lower impact sensitivity (14.9 J for the β-CL-20/BCHMX molar ratio = 1.8) than that of pure ε-CL-20 (13.2 J) and of pure BCHMX (3 J). The density of the studied co-agglomerates (CACs) achieves 99.5 % of the theoretically calculated ones and the density of the coformers at the molar ratios used reaches 99.6 % of the β-CL-20 crystal density. The CACs has shown that CL-20 is present in them as its ß-modification; in one sample, obtained by classical co-crystallization, have both α- and β-modifications.

The CACs studied have lower detonation energies than would be consistent with the percentage of individual coformers in these crystals; this is a new finding, which does not correspond to the general view

about the detonation parameters of explosive mixtures. The application of the most sensitive CACs (1.2 J) as a detonator primer did not exhibit the required acceleration capabilities in the given detonator design. However, a comparison with literature data shows that the CACs and CCs of this type could have advantageous applications in propellants because β-CL-20 is morphologically stable in these co-mixed crystals.

5.1.3 CACs of attractive nitramines with HNS and HNAB

The CACs with the 2,2',4,4',6,6'-hexanitro-2,2',4,4',6,6'-stilbene (HNS) coformer are finer grained than those with the 2,2',4,4',6,6'-hexanitro- 2,2',4,4',6,6'- azobenzene (HNAB) one. CACs containing HNAB seem to be more perfect than CACs containing HNS [4]. However, impact sensitivity of the second mentioned ones is generally lower; the dominant sample is HMX/HNS with the molar ratio of 1.00/0.11 and the impact sensitivity of 47 J. The study of the surface morphology of these crystals has shown their microporous structure, which is not significantly reflected into their crystal density. These CACs probably contain porous micro/nano crystalline clusters of HNS (for the pure HNS recently similar structure described in [9]). Three other CACs (RDX/HNS, RDX/HNAB and BCHMX/HNAB) had higher impact resistance than that exhibited by their original pure coformers. For CL20, however, the entry of HNS or HNAB into its crystal lattice is destabilizing.

In these CACs the HMX is present in its δ-form, CL-20 in its β-form and the trans-HNS molecule changes its conformation to cis-form. On the basis of FTIR and Raman spectral studies shown there are more intense intermolecular interaction between HNS and nitramines (especially through the hydrogen bonds formed by the hydrogen atoms of the –CH=CH– bridge) and in the case of δ-HMX also thanks to its spatial compatibility with cis-HNS molecules. The most interesting CAC from those studied appears to be the already-mentioned HMX/HNS with the molar ratio of 1.00/0.11 and the microporous structure of its crystals, whose calculated detonation velocity is of 8.98 $km.s^{-1}$ for $\rho = 1.8778$ $g.cm^{-3}$ (compare with 9.40 $km.s^{-1}$ for β- HMX). The combination of HMX and HNS molecules thus appears to be advantageous. The CACs studied, with the exception of the ones containing CL-20, may be applied as secondary fillers of special detonators and, after the verification of their pressability, also as fillers of various ammunition objects.

5.1.4 CACs of attractive nitramines with PANi

After successfully preparing the CACs of the Energetic-Energetic molecules category, coagglomeration extended to check feasibility of the method nonenergetic polymeric moiety with these attractive nitramines [5]. Obtained results are interesting with polyaniline (PANi), which shown effective influence in these

attractive nitramines. As usual the polymorphic changes observed exhibited α-HMX and β-CL20 after interacting with polymer chain. These attractive nitramines formed a charge transfer complex with PANi chain [10, 11], its interesting changes further confirmed by fluorescence quenching and quantum yield. In crystalline form the PANi moiety coated on surface of the nitramines crystals which further leads to thermal, mechanical/impact stability in corresponding CACs, however due to conductive nature PANi electric they are spark sensitive. In all these nitramine complexes showed an increased sensitivity to electrical spark, especially BCHMX/PANi of 23.2 mJ and α-HMX/PANi of 37.9 mJ. From the point of view of performance in the studied nitramines is more interesting RDX/PANi complex (D = 8744 $m.s^{-1}$) with a slightly increased density (ρ = 1.8295 $g.cm^{-3}$), slightly reduced calculated detonation parameters compared to pure RDX (ρ = 1.810 $g.cm^{-3}$, D = 9014 $m.s^{-1}$), with also a good impact resistance of 21 J. The most resistant against impact is α-HMX/PANi (31.01 J), followed by remaining CACs. These PANi coagglomerates could be suitable primary components for electrical initiators.

5.1.5 CACs of attractive nitramines with BTATz

Keeping in mind all previous successful CACs this time prepared CACs of selected attractive nitramines with nitrogen rich BTATz, found quite interesting results. Also, in this work stirrer selection was optimized by carrying coagglomeration with two kinds of shaped stirrers like “linear(-)” and “crossed ones(+)”. Its interesting see that Crossed stirrer given predominant improvements in crystal quality, thermochemical as well as detonation properties. The PXRD, FTIR and Raman studies confirmed, the new relationships were found between N-N bond stretching vibrations, FTIR C-H bond stretching in CACs on the one hand, and their impact sensitivity, crystal density, voluminous detonation energy (Q.ρ), heat of combustion and enthalpy of formation on the other. These facts, together with the relation between the ring deformation vibrations and the Q.ρ values, correspond to the idea about the method of the energetic materials initiation by impact and shock.

The stabilization of HMX in the corresponding CACs as its α-modification, which is highly sensitive in the pure state (1.9 J). The coagglomerate of α-HMX with BTATz, obtained by coagglomeration under mixing by cross stirrer, was found to be the least sensitive (46 J) from the studied CACs and should have a detonation energy slightly better than that of β-HMX (6097 against 5864 $J.g^{-1}$). Similarly, during the coagglomeration process, the ε-CL20 was converted to its β-modification in CL20/BTATZ. The cyclic nitramines CACs with nitrogen-rich BTATZ as a coformer are exergonic and could provide energy for self-propagating reactions, making them ideal combination for propulsion applications.

5.2 Particle size and morphology of CACs

Particles size analysis of CACs shown the effect of co-agglomeration for attractive nitramines with enhancements in their surface areas. For understand influence both co-precipitation and co-agglomeration some samples particle analysis for co-precipitates also carried followed by final product CACs. Regarding the size of the CACs determined size and specific surface area, especially for nitramines with sterically crowded molecules, i.e., BCHMX and CL20, there is only a slight increase of its value during the agglomeration process; the spatial compatibility of the angular molecule BCHMX and the globular one β-CL20 have to be logically quite limited [6].

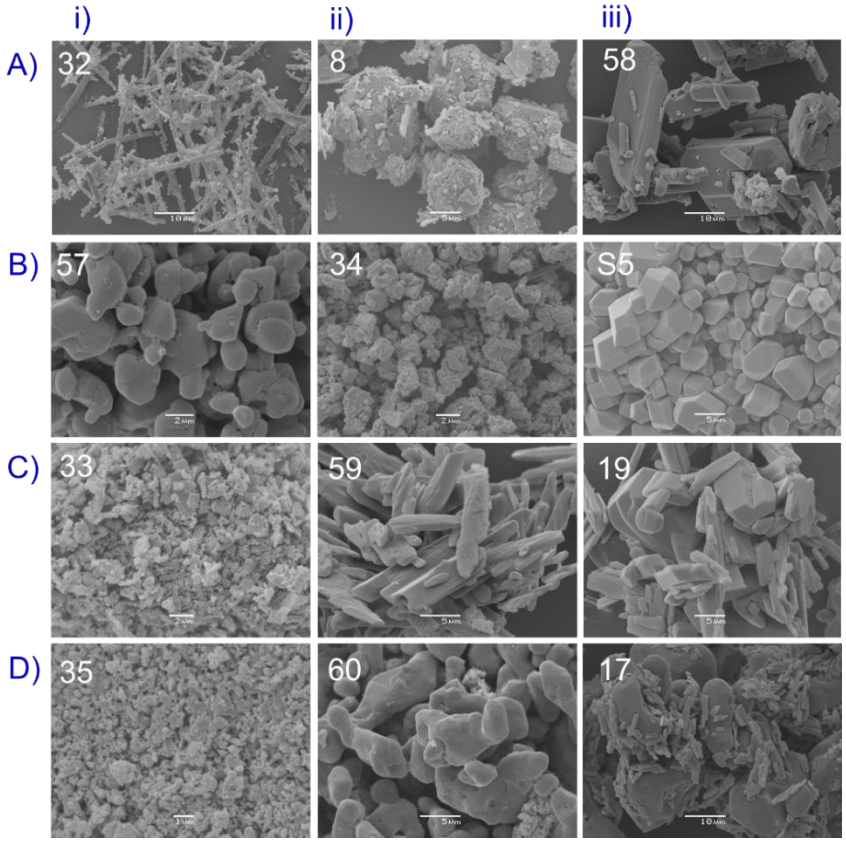

Figure 5.1 FESEM images with sample IDs top 3 highly impact insensitive left to right; A) HMX CACs, B) CL20 CACs, C) BCHMX CACs and D) RDX CACs. (images regenerated from Ref. [1–5]). For sample codes compositions shown in Chapter 2; Table 2.1 and their impact sensitivities results see respective chapter 3 sub-sections.

The CACs of RDX and HMX co-agglomerate well, which is within expectations. Of the polynitroaromatic coformers, co-agglomeration is most strongly suppressed by TATB, which is also logical (due to relatively strong non-covalent bonds of the N-O---H-N type [1–7]). In terms of SEM-based crystal quality assessment, the best CACs were β-CL20/BCHMX with a molar ratio of 1.8 components (also in terms of impact

sensitivity) [3], followed by nitramine co-agglomerates with HNAB [4]. On the other hand, in the case of a δ-HMX/HNS co-agglomerate with a molar ratio of 1.00/0.42, which is demonstrably microporous (see Figs. 2a and 2b) without significant reflect into their crystal density [4]; these microporous structure are caused by HNS crystal morphology [9].

5.3 Impact sensitivity

The well-known observation of Dr. Licht [12] that high performance explosives usually have high sensitivity was developed over time into a semilogarithmic relationship [13] between impact sensitivity and the energy content of explosives, represented by the enthalpy of formation which is presented by Figures 5.4 & 5.5.

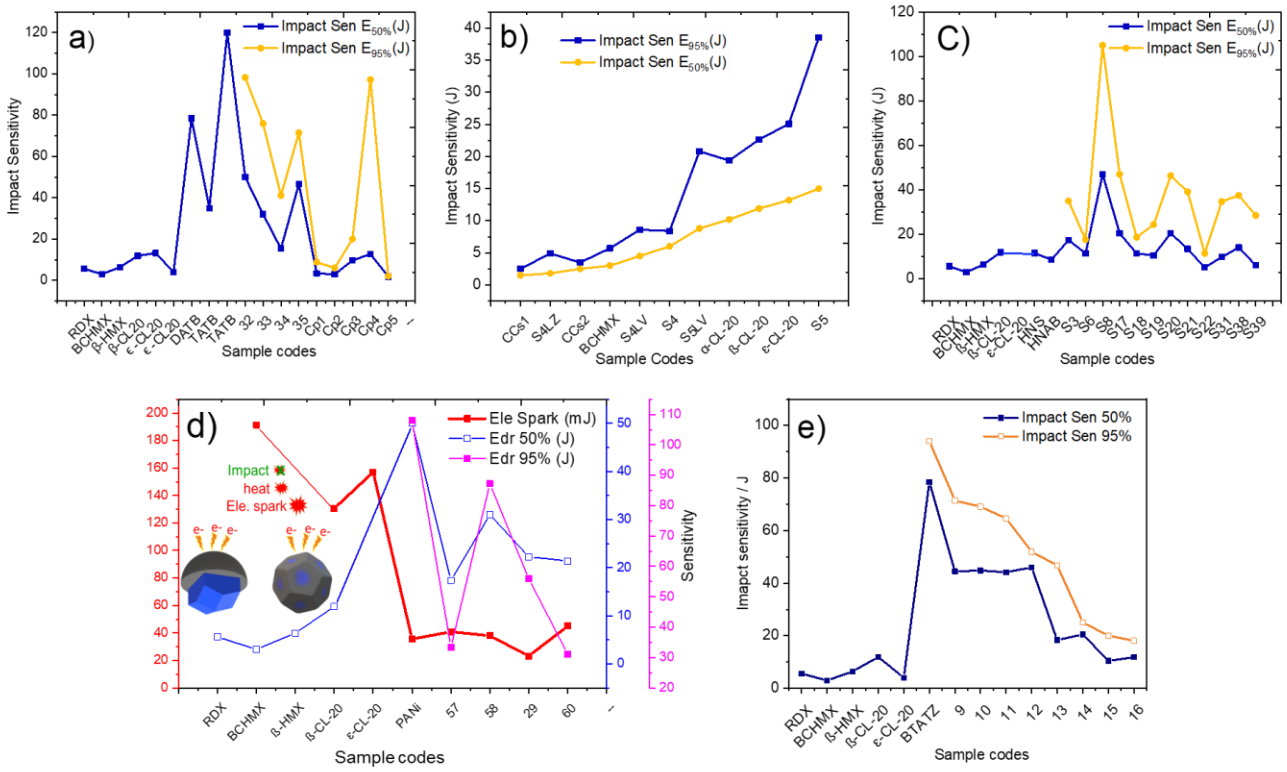

Figure 5.2 A comparative graphical representation of impact and electrical spark sensitivities(only in case of PANi CACs) [1–7].

CACs of DATB and TATB: BCHMX/DATB (Cp1); BCHMX/DATB (Cp2); RDX/DATB (Cp3) ; δ-HMX/ DATB (Cp4); β-CL-20/DATB (Cp5); δ-HMX/TATB (32); BCHMX/TATB (33); β-CL-20/TATB (34); RDX/TATB (35).
CACs of CL20/BCHMX: CCs1 [0.60/1.00]; CCs2 [0.63/1.00]; S4 [1.10/1.00]; S5 [1.80/1.00]; S4LV [1.53/1.00]; S4LZ [1.52/1.00]; S5LV [1.57/1.00].

CACs of HNS and HNAB: 3 HMX/HNS; 6 HMX/HNS; 8 HMX/HNS; 17 RDX/HNS; 18 CL-20/HNS; 19 BCHMX/HNS; 20 RDX/HNAB; 21 BCHMX/HNAB; 22 CL-20/HNAB; 31 HMX/HNAB; 38 HMX/HNAB; & 39 CL-20/HNAB.
CACs of BTATz: 9) RDX/BTATz B1, 10) RDX/BTATz B2, 11) HMX/BTATz B1, 12) HMX/BTATz B2, 13) CL20/BTATz B1, 14) CL20/BTATz B2, 15) BCHMX/BTATz B1 and 16) BCHMX/BTATz B2
CACs of PANi: 57 CL20/ PANi, 58 HMX/PANi, 59 BCHMX/PANi and 60 RDX/PANi

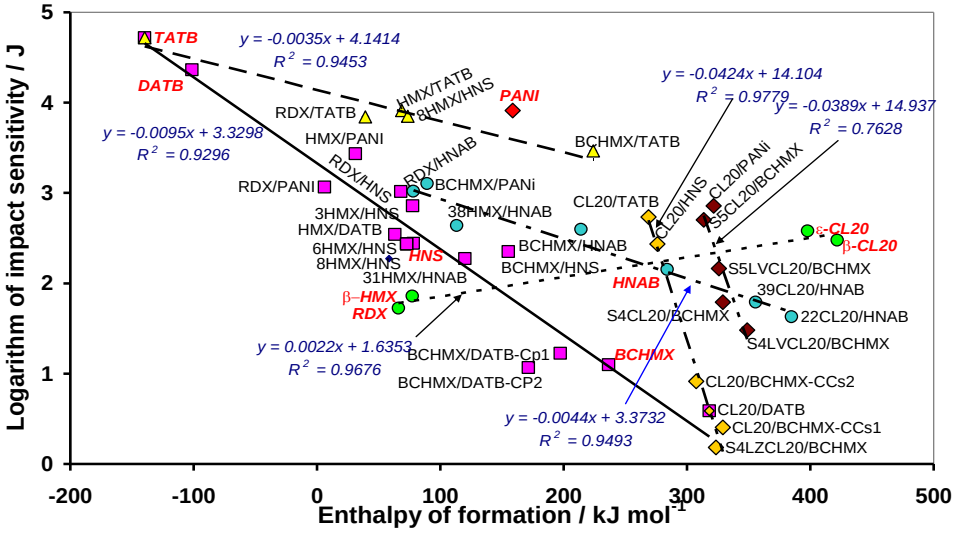

Figure 5.3 The semi-logarithmic relationships between the impact sensitivity and energy content (represented by the enthalpy of formation) of the CACs prepared (data taken from papers [1–7]).

It can be seen that the stabilizing effect of incorporating TATB into the HMX crystal lattice (32 HMX/TATB) can practically match with the same effect of HNS (8 HMX/HNS). In doing so, both types of CACs, in terms of the FESEM image (Figure 5.1), give the impression of imperfect crystals. This interesting effect is still waiting for explanation. It may be due to flexible crystal formation which are resisting impact becoming pallet. The flow of dependencies in Figure 5.3 is consistent with Licht's rule, except that there is a known, as yet unexplained exception for pure RDX, HMX and CL20 [14].

The importance of the molar ratio of coformers in CACs is best documented on the CL20/BCHMX cocrystals (samples of CL20/BCHMX); the introduction of foreign molecules into the crystal lattice of CL20 tends to destabilize this nitramine (except perhaps for TATB and DATB), but in the case of the BCHMX coformer and for a molar ratio of 1.8/1.0, ECCs with surprisingly high resistance to impact can be obtained (sample S5, it in comparison with impact sensitivity of ε-CL20 and BCHMX).

5.4 Explosive properties

Researchers in the field of energetic cocrystals do not mention the well-known fact that the mixing of two explosives results in a mixture that usually has a higher detonation rate than would correspond to the percentage of components in this mixture [15].

The detonation energies were compared (E_{deton}) in the studies in this sense [1–7], which is summarized in Figures 5.4, 5.5 & 5.6. Here, group A presents data of the brisant explosives (mostly CL20 and partly BCHMX) with the smallest effect of the increase in E_{deton} values for the CACs, group B of co-agglomerates of RDX and HMX with coformers, having larger increases in these values, and the largest ever such effect is observed for group C with the PANi coformer.

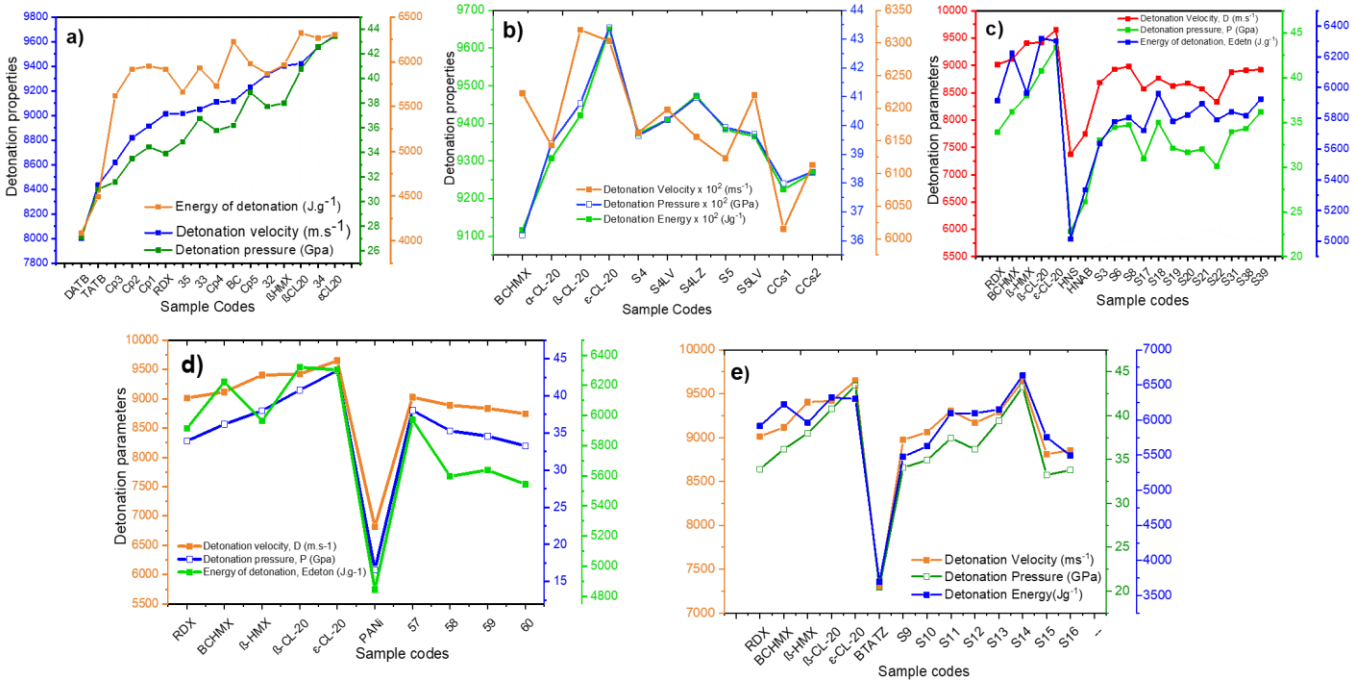

Figure 5.4 Detonation parameters of CACs with pure nitramines used for preparation [1–7] (For sample codes details see caption Figure 5.2)

All dependencies seem to intersect in a common intersection formed by the data of CL20/BCHMX nitramine CACs. For these nitraminic CACs alone, the effect of the mixture is opposite. Prof. Urbanski stated that these increases in values by the increase in entropy of the components entering the mixture [15]. For the nitraminic CACs, explained the decrease in the E_{deton} values for their CACs by the decrease in entropy in the mixture of admittedly molecularly-structurally mutually different but chemically uniform coformers [3].

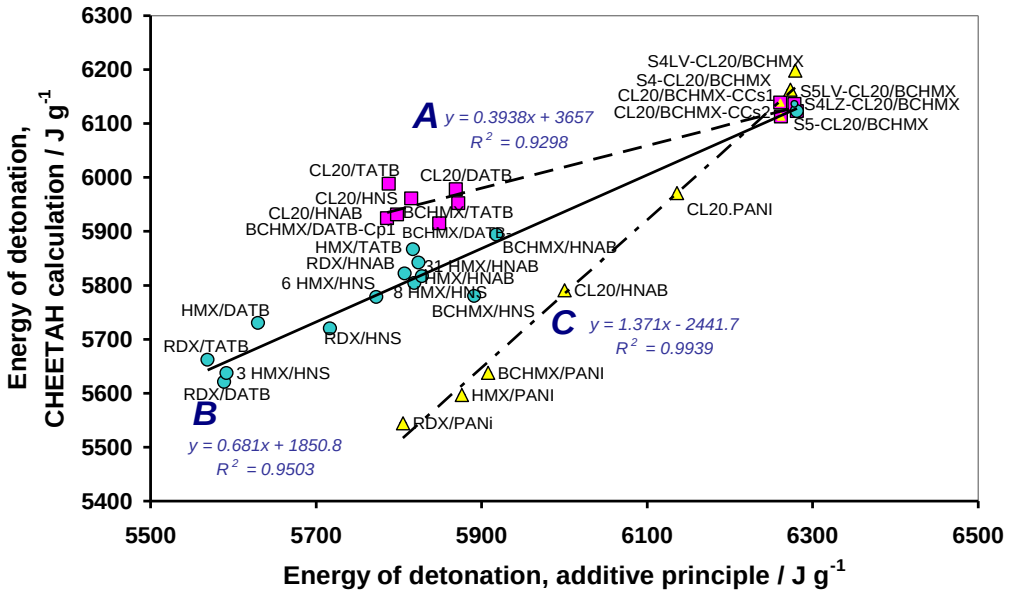

Figure 5.5 The mutual relationships between the energies of detonation calculated on the basis of the additive principle (i.e., the percentage of components in the co-agglomerates) and that calculated by CHEETAH code [16] using experimental enthalpies of formation (data taken from papers [1–7]).

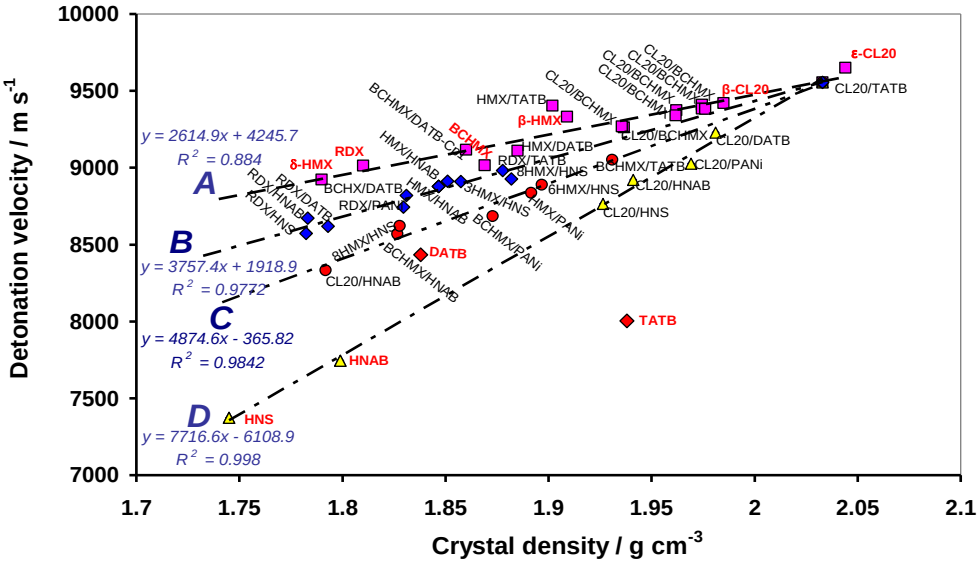

Figure 5.6 The mutual relationships between the calculated detonation velocity for the maximal crystal density and this crystal density (data taken from papers [1–7]).

The well-known relationship between detonation velocities and charge densities of explosives is presented in Figure 5.8. Here again, the set of CACs studied by us breaks down into group A of mostly pure nitramines (highly brisant explosives), into groups B and C of RDX, BCHMX and HMX co-agglomerates and into group C, formed by pure HNAB and HNS and also by CACs with CL20 content, in which

coformers HNS, HNAB, PANi and DTAB significantly reduce the detonation rate. It is possible to see here, that HMX/TATB (32 HMX/TATB) with high resistance against impact should have detonation velocity near those of pure β-HMX. Another highly resistant against impact CAC, i. e. δ-HMX/cis-HNS (8 HMX/HNS) is close to pure RDX in this sense.

5.5 Feasibility of co-agglomeration method

As shown by our results so far [1–7], the introduction of polynitro compound molecules into the crystal lattice of attractive nitramines usually leads to an increase in their initiation reactivity mainly for those with crowded molecules, but this can be partially eliminated by selection of the molar ratio in the resulting CAC. So far, the most effective "stabilizer" of these nitramines logically turns out to be TATB. Surprisingly, the coformer cis-HNS has a similar effect on the stabilization of δ-HMX (here also the molar ratio of the coformers plays a major role), where, moreover, the microporosity of cis-HNS in the final CACs shown positive effect towards impact. From an explosives property point of view, the δ-HMX/TATB co-agglomerate is the most advantageous, approaching pure β-HMX in its performance. Similarly, the best co-agglomerate δ-HMX/cis-HNS, which is, however, in its performance closed logically to pure RDX.

Preparation of co-crystals by co-agglomeration (by "slurry method" co-crystallization) appears to be very interesting, giving products relatively high crystal density. It does not require initial coformers of defined granulometry - it is possible to apply components directly from their production after isolation from the reaction mixtures of their preparation and subsequent stabilization. Purification of coformers can take place in solution as part of their co-precipitation. These preliminary results of ours also suggest that chemical engineering factors are involved in the preparation of CACs, as in conventional crystallization. With technical technological optimization this method is employable industrial scale cocrystal productions, it’s also evaluated and shown in initial stage preparations (1 to 2 Kg) in next section 5.10.

5.6 Applications of CACs

All the prepared CACs shown interesting Energy – Safety balanced characteristics. To further evaluate their application suitability three different types of applications we tried in current work. Along with this for remaining CACs, based on their characteristic properties the futuristic application suitability proposed in Chapter 4. Firstly HMX/BCHMX CACs (2 Kg) prepared in LRN-IPO, Poland; during ERASMUS+ visit was employed in the composite rocket propellant found tremendous all properties propellant coarse. CACs propellants (P7, P8 & P9) showed relatively good burning rates (7- 9 $mm.s^{-1}$) compared earlier studies, especially propellant P8 with 20% CACs content showed highest burning rate (9.07 $mm.s^{-1}$) and propellant composition of CACs shown overall better performance in morphologically and other thermochemical

properties. Overall, CACs shown more suitability than pure HMX and HMX/BCHMX compositions. Secondly, CL20/BCHMX CACs higher sensitive one to electric spark were employed in the detonator initiation ability analyzed and found not suitable. It implies that these are more suitable for insensitive ammunition like propellant. In third application, RDX/BCHMX CACs (1 Kg) preparation transferred to company CETVYK, s. r. o. CZ; as license study and are employed gun propellant found improvements, as compared to earlier traditional composition. Remaining CACs the futuristic applications are recommendation basis of experience and obtained key characteristics of the CACs. So, overall, all CACs shown more application suitability and coagglomeration method employable to industrial scale preparations.

5.7 Concluding Remarks

The contributions of this dissertation are both new applications of proven spectroscopic methods and the development of a new procedure for the preparation of cocrystals in the form of microparticles. The prepared coagglomerates/co-crystals were characterized using instrumental analysis techniques, such as PXRD, FTIR, and Raman spectroscopy; the results in all cases found results are fully consistent with the current insights of the types of intermolecular interactions in crystals and relative changes in properties that occur in these kinds of cocrystals. The discovery of significant correlations between the FTIR and Raman outputs and the initiation reactivity characteristics are correlated to each other. The successful usage of XPS (here binding energies) for coagglomerates/co-crystals of nitramines with crowded molecules and fluorescence quenching (here relative quantum yields) for PANi nitramine complexes to explain the initiation reactivity of coagglomerates is a completely new approach that has not yet been published in the global literature on energetic materials.

Key findings on the cocrystals of interest are presented below [1–7] are listed below.

- This method is practically an innovated co-crystallization in suspension, generally classified in the literature as the "Slurry method", which considerably reduces the processing time and decreases the quantity of solvents compared to a solvent co-crystallization. It provides fine co-crystals of very good quality [17, 18].
- Among the co-crystals of attractive cyclic nitramines with 1,3-diamino- and 1,3,5-triamino-2,4,6-trinitrobenzene, the ones with δ-HMX are very interesting, with a surprising result for coformer TATB with molar ratio 1.00/0.12 (IS = 50 J, calculated D = 9.3 kms^{-1}); however, TATB behaves here as an anticaking additive [1, 2].
- Among the co-crystals of cyclic nitramines with cis-2,2’,4,4’,6,6’-hexanitrostilbene (HNS) and 2’,4,4’,6,6’-hexanitroazobenzene (HNAB), δ-HMX/cis-HNS with a molar ratio of 1.00/0.11 and IS =

47 J (TNT has of 36.4 J) with calculated D = 8.9 kms^{-1} stands out surprisingly; the impact resistance of this product far exceeds that one of both its coformers [4].

- The attempted co-agglomeration of sterically crowded nitramines ε-CL20 and BCHMX also resulted in a surprisingly good β-CL20/BCHMX product with a molar ratio of 1.8/1.0, IS = 14.9 J and calculated D = 9.4 kms^{-1}; also, here its impact resistance exceeds that one of both its coformers (mainly of BCHMX with IS of 3 J) [3].
- The molar ratio of the coformers and the choice of the continuous phase play a very important role in this co-agglomeration - the proteogenic one usually gives a better morphology than the aprotic medium; however, HNAB undergoes decomposition in the proteogenic solvent.
- In all co-crystal types studied, HMX was specified in its δ-modification, CL20 in its β-modification and HNS in its cis-conformation; it is the spatially similar orientation of the δ-HMX and cis-HNS molecules that could be one of the reasons for the surprisingly low sensitivity of the δ-HMX/cis-HNS co-crystal for the molar ratio of coformers 1.00/0.11.
- The polyaniline (PANi) given a unique combination of CACs in which they are impact insensitive (+5 to 25 J) and electric spark (-100 to 150 mJ) and laser (29 mV with 10x/0.25 grating) sensitive, with relatively better physiochemical properties and detonation properties. Especially HMX (impact sensitivity 31 J from original of 6.4 J), which is present in the composite in its α-modification, which is in its pure state extremely sensitive to impact (1.9 J).
- BTATz CACs were prepared in two batch series using both linear and cross stirrers, with the cross stirrer giving very good results. Overall improvements in thermochemical as well as morphological properties are consistent. The impact insensitive (+5 to 45 J) with higher density. The highly insensitive sensitive CACs (46 J) among the ones studied was the α-HMX(1.9 J) with BTATz, which was produced by cross stirrer. It is expected to have a slightly better detonation energy than β-HMX (6097 against 5864 $J.g^{-1}$). Likewise, CL20/BTATZ converted the ε-CL20 to its β-modification during the coagglomeration process[19].
- The very well-known phenomenon of higher detonation parameters of explosives mixtures compared to their parameters, calculated on the basis of the percentage of components in the mixture, is valid for co-crystals with DATB and TATB, for co-crystals containing cis-HNS and HNAB there is not such a significant difference, and the opposite finding was found for cocrystals β-CL20/BCHMX.

References

[1] V. B. Patil, K. Zalewski, J. Schuster, P. Belina, W. Trzcinski, and S. Zeman, "A new insight into the energetic co-agglomerate structures of attractive nitramines," Chemical Engineering Journal, vol. 420, Sep. 2021, doi: 10.1016/j.cej.2021.130472.

[2] V. B. Patil, P. Bělina, W. A. Trzcinski, and S. Zeman, "Preparation and properties of co-mixed crystals of 1,3-di- and 1,3,5-tri-amino-2,4,6-trinitrobenzenes with attractive cyclic nitramines," Journal of Industrial and Engineering Chemistry, vol. 115, pp. 135–146, Nov. 2022, doi: 10.1016/j.jiec.2022.07.043.

[3] V. B. Patil et al., "Co-agglomerated crystals of cyclic nitramines with sterically crowded molecules," CrystEngComm, p. 10.1039.D2CE00840H, 2022, doi: 10.1039/D2CE00840H.

[4] V. B. Patil, P. Bělina, W. A. Trzcinski, and S. Zeman, "Co-agglomerated crystals of 2,2′,4,4′,6,6′-hexanitro -stilbene/-azobenzene with attractive nitramines," Chemical Engineering Journal, vol. 457, p. 141200, Feb. 2023, doi: 10.1016/j.cej.2022.141200.

[5] V. B. Patil, O. Machalický, P. Bělina, R. Svoboda, W. A. Trzcinski, S. Zeman, "Co-agglomerated - polyaniline omposite crystals of attractive nitramines -manuscript under communication".

[6] V. B. Patil, R. Svoboda, and S. Zeman, "Thermal studies on performance of DATB and TATB coagglomerated crystals," no. 724, p. 179494, 2023, doi: https://doi.org/10.1016/j.tca.2023.179494.

[7] M. Novák, "Ověření vlivu bicyklo-HMX na parametry prachu s obsahem RDX (Verification of the bicyclo-HMX effect on the RDX gunpowder parameters), The final project of the licensing study," Univ. Pardubice, Feb. 2022.

[8] R. E. Cobbledick and R. W. H. Small, "The crystal structure of the δ-form of 1,3,5,7-tetranitro-1,3,5,7-tetraazacyclooctane (δ-HMX)," Acta Cryst B, vol. 30, no. 8, Art. no. 8, Aug. 1974, doi: 10.1107/S056774087400611X.

[9] H. Zhang et al., "Three-dimensional hierarchical 2,2,4,4,6,6-hexanitrostilbene crystalline clusters prepared by controllable supramolecular assembly and deaggregation process," CrystEngComm, vol. 18, no. 41, pp. 7940–7944, 2016, doi: 10.1039/C6CE01292B.

[10] V. B. Patil, S. Ture, C. Yelamaggad, M. Nadagouda, and A. Venkataraman, "Turn-off Fluorescent Sensing of Energetic Materials using Protonic Acid doped Polyaniline: A Spectrochemical Mechanistic Approach," Zeitschrift fur Anorganische und Allgemeine Chemie, vol. 647, no. 4, pp. 331–340, Feb. 2021, doi: 10.1002/zaac.202000321.

[11] V. B. Patil, M. Nadagouda, S. Ture, C. Yelamaggad, and V. Abbaraju, "Detection of energetic materials via polyaniline and its different modified forms," Polymers for Advanced Technologies, vol. 32, no. 12, pp. 4663–4677, Dec. 2021, doi: 10.1002/pat.5458.

[12] H.-H. Licht, "Performance and Sensitivity of Explosives," Propellants Explos. Pyrotech, vol. 25, no. 3, pp. 126–132, Jun. 2000, doi: 10.1002/1521-4087(200006)25:3<126::AID-PREP126>3.0.CO;2-8.

[13] S. Zeman, "The influence of energy content and its outputs on the impact sensitivity of high-nitrogen energetic materials, Journal of Energetic Materials," Journal of Energetic Materials, vol. 40:, no. 1, pp. 1–14, 2022, doi: 10.1080/07370652.2020.1822463.

[14] S. Zeman and M. Jungová, “Sensitivity and Performance of Energetic Materials,” Propellants, Explosives, Pyrotechnics, vol. 41, no. 3, pp. 426–451, Jun. 2016, doi: 10.1002/prep.201500351.

[15] T. Urbanski, “On entropy and free energy of explosives (preliminary communication),” Bull. l’Academie Pol. Des Sci. s, Ser. Des Sci. Chim., vol. 28, pp. 511–513, 1980, doi: https://gallica.bnf.fr/ark:/12148/cb343830642 /date1980.

[16] Fried, L E., “CHEETAH 1.39 Users’ Manual UCRL-MA-117541.” CA: Lawrence Livermore National Laboratory., 1996.

[17] V. B. Patil and S. Zeman, “Successful journey in preparation of the energy-safety balanced cocrystals of attractive nitramines via coagglomeration,” in EUROPYRO2023, Saint Malo: International Pyrotechanic Society, Sep. 2023, pp. 87–99.

[18] V. B Patil and S. Zeman, “Novel approach for preparation of the energy-safety balanced cocrystals of attractive nitramines via coagglomeration,” in HEMCE2024, Thiruvananthapuram: HEMSI with ISRO & DRDO, Feb. 2024.

[19] V. B. Patil, P. Bělina, W. A. Trzcinski, and S. Zeman, “Co-agglomerated crystals of cyclic nitramines with the nitrogen rich 3,6-bis(1H-1,2,3,4-tetrazol-5-ylamino)-1,2,4,5-tetrazine (BTATz),” Chemical Engineering Journal, vol. 483, p. 149029, Mar. 2024, doi: 10.1016/j.cej.2024.149029.

LIST OF STUDENTS' PUBLISHED WORKS

➢ Research articles published in international peer-reviewed journals

1) Novel approach for preparation of the energy-safety balanced cocrystals of attractive nitramines *via* coagglomeration V. B. Patil, S. Zeman, FirePhysChem, **2024**, DOI: https://doi.org/10.1016/j.fpc.2024.03.003

2) Initiation reactivity of cyclic nitramines mixed crystals from the perspective of XPS application, V. B. Patil, J. R. Pereira, S Zeman, Preprint-Research Square, **2024**, DOI: https://doi.org/10.21203/rs.3.rs-3857166/v1

3) Co-agglomerated crystals of cyclic nitramines with the nitrogen rich 3,6-bis(1H-1,2,3,4-tetrazol-5-ylamino)-1,2,4,5-tetrazine (BTATz); V. B. Patil, W. A. Trzciński, P. Bělina, S. Zeman, Chemical Engineering Journal, DOI: https://doi.org/10.1016/j.cej.2024.149029, **2024**; 149029, 483(1) Q1, IF : 15.1

4) Towards the thermal reactivity and behavior of co-mixed crystals of DATB and TATB with attractive nitramines, V. B. Patil, R. Svoboda, S. Zeman, Thermochemica Acta, DOI: https://doi.org/10.1016/j.tca.2023. **2023**, 179494; 724, 179494; Q2, IF : 3.5

5) Co-agglomerated crystals of 2,2',4,4',6,6'-hexanitro -stilbene /-azobenzene with attractive nitramines; V. B. Patil, W. A. Trzciński, P. Bělina, S. Zeman, Journal of Chemical Engineering, DOI: https://doi.org/10.1016/j.cej.2022.141200; **2023**, 457(1), 141200; Q1, IF : 15.1

6) Co-agglomerated crystals of cyclic Nitramines with Sterically Crowded Molecules, V. B. Patil, Q. L. Yan, W. A. Trzciński, P. Bělina, J. Shánělová, T. Musil, S. Zeman, CrystEngChem, RSC, DOI: https://doi.org/10.1039/d2ce00840h; **2022**, 24, 7771-7785; Q1, IF : 3.1

7) Preparation and properties of co-mixed crystals of 1,3-di- and 1,3,5-tri-amino-2,4,6-trinitrobenzenes with attractive cyclic nitramines, V. B. Patil, W. A. Trzciński, P. Bělina, S. Zeman, Journal of Industrial and Engineering Chemistry, DOI: https://doi.org/10.1016/j.jiec.2022.07.043, **2022**, 115(25), 135-146; Q1, IF : 6.1

8) A new insight into the energetic co-agglomerate structures of attractive nitramines, V. B. Patil, K. Zalewski, J. Schuster, P. Bělina, W. A. Trzciński, S. Zeman; Chemical Engineering Journal; DOI: https://doi.org/10.1016/j.cej.2021.130472; **2021**, 420(3), 130472; Q1, IF : 15.1

➢ Research articles under communication / preparations

9) Coagglomerated-Polyaniline composite crystals of attractive nitramines, V B. Patil, O Machalický, P Bělina, R Svoboda, W. A. Trzciński, P. Bělina, S. Zeman, [Advanced composites, and Hybrid Materials, Under review]

10) Initiation Reactivity of Cyclic Nitramines Mixed Crystals from the Perspective of XPS Application, V. B. Patil, R-P, Jhonatan S. Zeman, [Defense Technology, under communication]

11) Towards to some published misconceptions about TNT and ε-CL20, S. Zeman, V. B. Patil,

[FirePhysChem, Under review]

12) Technological frontiers in cocrystallization of four attractive cyclic nitramines, V. B. Patil, S. Zeman [Chemical Engineering Journal, Manuscript under communication]

13) Application of BCHMX/HMX CACs in composite rocket propellant [Manuscript under preparation]

➢ Research articles in international conference proceedings

• Poster presentations at conferences

1) Innovative coagglomeration method for producing the energy-safety balanced cocrystals of attractive nitramines; V. B. Patil, S. Zeman, NTREM2024; organized by Institute of Energetic Materials, Faculty of Chemical Technology, University of Pardubice, Pardubice Czech Republic in April **2024**.

2) Coagglomerated Crystals of Attractive Nitramines in Nitrocellulose Gunpowder: A Technological Application; M. Novak, V. B. Patil, L. Velehradský, K. Kubát, S. Zeman, NTREM2024; organized by Institute of Energetic Materials, Faculty of Chemical Technology, University of Pardubice, Pardubice Czech Republic in April **2024**.

3) Thermal studies of attractive nitramines/polyaniline composite crystals prepared via co-agglomeration; V. B. Patil, R Svoboda, P Bělina, S Zeman, NTREM2023; organized by Institute of Energetic Materials, Faculty of Chemical Technology, University of Pardubice, Pardubice Czech Republic in April **2023**.

4) Preparation and emphasized study of TATB/nitramines co-mixed crystals via coagglomeration method, V. B. Patil, P Bělina , S Zeman, 24th New Trends in Energetic Materials (NTREM 2022), organized by Institute of Energetic Materials, Faculty of Chemical Technology, University of Pardubice, Pardubice Czech Republic on April 6 - 8, **2022**. Received BEST POSTER PRIZE.

5) A new insight into the energetic co-agglomerate structures of attractive nitramines; V. B. Patil, K. Zalewski, J. Schuster, P. Bělina, W. A. Trzciński, and S. Zeman, Nobel laureate s&t seminar series 11th India-Japan Science And Technology Seminar, (Virtual Conference); This was co-organized by Sree Chitra Tirunal Institute for Medical Sciences & Technology (Dept. of Science and Technology, Govt. of India) and Indian JSPS Alumni Association (IJAA) on 6-7 December **2021**.

• Oral presentations at conferences

6) Novel approach for preparation of the energy-safety balanced cocrystals of attractive nitramines via coagglomeration, V. B. Patil, S. Zeman, 14th International High Energy Materials Conference & Exhibits (HEMCE-2024), organized by High energy materials society of India in collaboration with Indian Space Research Organization (ISRO) & Defense Research & Development Organization (DRDO), INDIA; February 1-3, **2024**; Vikram Sarabhai Space Centre, Thiruvananthapuram, Kerala, INDIA, Received BEST ORAL PRESENTATION prize.

7) Successful journey in preparation of the energy-safety balanced cocrystals of attractive nitramines via coagglomeration, V. B. Patil, S. Zeman, 46th International Pyrotechnical Society Seminar, EUROPYRO2023, September 11-14, **2023**, Saint Malo, FRANCE.

8) Thermal studies on performance of DATB and TATB coagglomerated crystals, V B Patil, R Svoboda, S Zeman, 13th International High Energy Materials Conference and Exhibits (HEMCE-2022), organized by High energy materials society of India in collaboration with TRBL, Development Organization (DRDO) Chandigarh, May 26-28, **2022**, Chandigarh, INDIA.